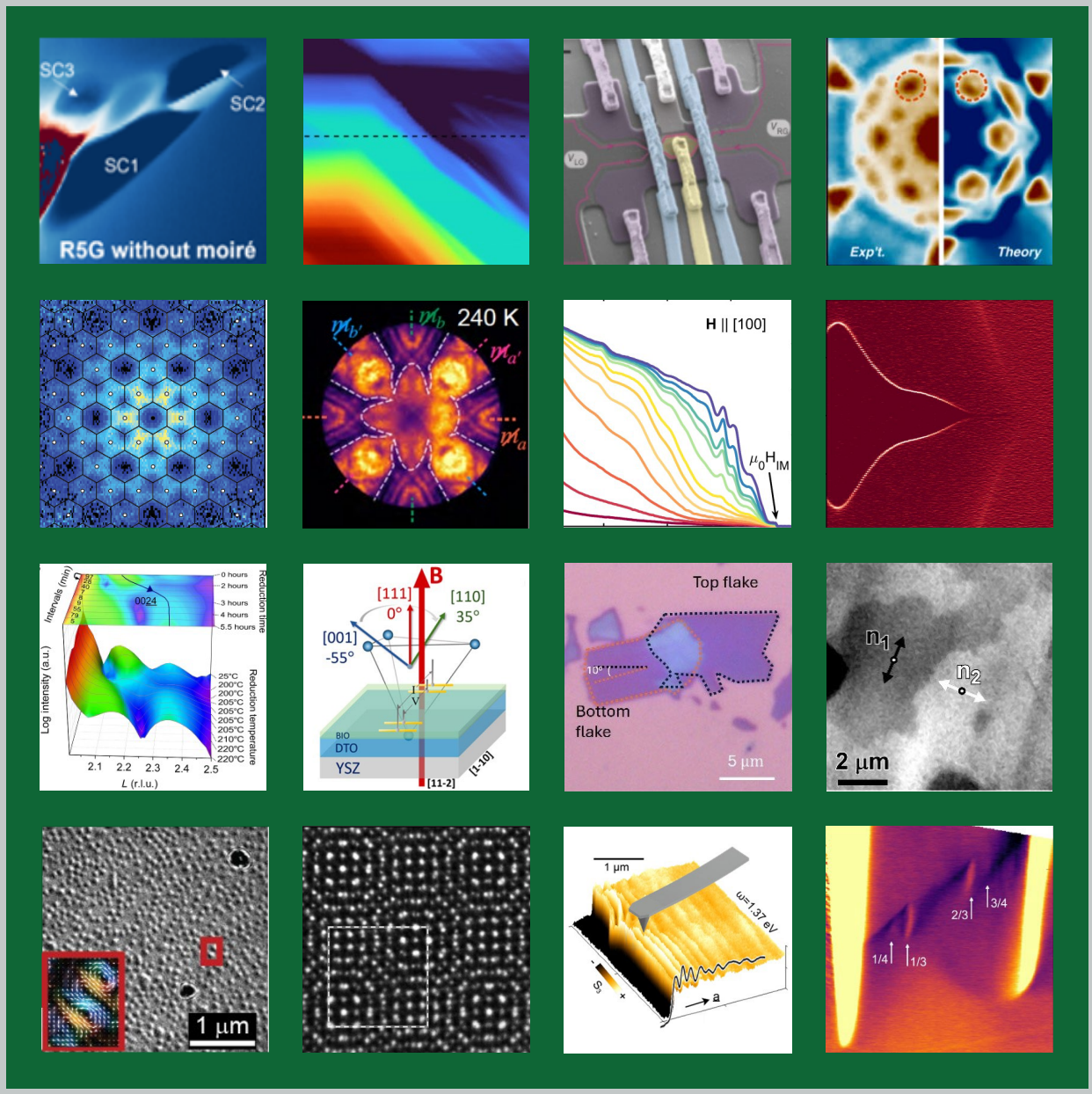
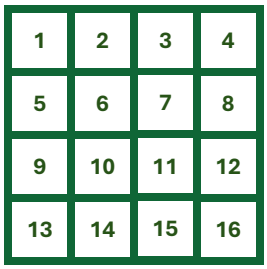
2025 Experimental Condensed Matter Physics Principal Investigators' Meeting

September 9-11, 2025

Program and Abstracts







1. Long Ju, *Fractional Quantum Anomalous Hall Effect and Chiral Superconductivity in Rhombohedral Graphene*, Phase diagram without moiré superlattice effect, exhibiting superconductivity.
2. Nai P. Ong et al., *Quantum Point Contact and Shot Noise in Monolayer Graphene*, The transmission map of a quantum point contact on monolayer graphene measured at 0.3 K and B = 13 T.
3. Philip Kim, *Emergent Quasiparticles in Graphene Heterostructure*, False color image of a representative graphene device depicting an interference measurement with a single edge channel.
4. Xavier Roy, Abhay Pasupathy, *Two Dimensional Heavy Fermions in the van der Waals Metal CeSiI*,Simulated (right) and measured (left) Fermi surface quasiparticle interference spectroscopy of CeSiI.
5. Rob J. McQueeney et al., D. Vaknin, *Magnetic Interactions and Excitations in Quantum Materials*, Localized chiral quasiparticle (black arrows) identified by the momentum dependence of the neutron scattering data for TbMn6Sn6 over an energy range from 130-150 meV.
6. Judy J. Cha, Eun-Ah Kim, *Defect-mediated charge density wave transition*, Ferro-axial CDW in RTe3 large-angle convergent beam electron diffraction patterns show all mirror symmetry breaking at 240 K.
7. Neil Harrison et al., *Science of 100 tesla: The reverse quantum limit and its implications for unconventional quantum oscillations in YbB12*, Quantum oscillations in the Kondo insulator YbB12 using high magnetic field measurements supported by the Science of 100T BES project.
8. Sergey Frolov, *Definitive Majorana Zero Modes in Optimized Hybrid Nanowires*, Sn-InAs nanowire Josephson junction sustains high supercurrents (500 nA) to large magnetic fields (>1T).
9. Anand Bhattacharya et al., Digital Synthesis: *A pathway to novel states of condensed matter*, Map of specular rods measured for the 1-unit-cell-thick film at different temperatures in the CaH2 reducing environment.
10. Haidong Zhou, *Probing ice-rule-breaking transition in Dy2Ti2O7 thin film by proximitized transport and magnetic torque*, Schematic diagram of the Bi2Ir2O7/Dy2Ti2O7 bilayer on the YSZ substrate and the proximitized transport measurement configuration.
11. Jifa Tian, Brian M. Leonard, University of Wyoming, *Growth, Anisotropy and Unconventional Superconductivity of 2M-WS2*,Optical image of a 2M-WS2/2M-WS2 junction.
12. Fengyuan Yang, *Electrical Switching and Antiferromagnetic Domain Imaging of LaFeO3 Epitaxial Thin Films*, X-ray Magnetic Linear Dichroism Photoemission Electron Microscopy images of antiferromagnetic domains of Pt(2 nm)/LaFeO3(3 nm).
13. Luis Balicas, Understanding and Harvesting Topological Transport in Centrosymmetric Layered Ferromagnets and Their Heterostructures, Lorentz transmission electron microscopy image revealing Neel skyrmions at room temperature.
14. Chang-Beom Eom, *Twisted oxide membrane interface by local atomic registry design*, Atomic-scale HAADF image of moiré supercell for 10.4°-twisted STO bilayer.
15. Dmitri N. Basov, *Good Plasmons in a Bad Metal*, Room-temperature near-field amplitude image of a 32 nm MoOCl2 microcrystal showing ultra-low-loss propagation of hyperbolic plasmon polaritons along the a-axis. Black line is an averaged line profile.
16. Raymond Ashoori, *Penetration-Capacitance Measurements and Noise Spectroscopies of Rhombohedral Multilayer and Twisted Bilayer Graphene*, Comparison of charge density waves and the potential Wigner crystal in moiré pentalayer rhombohedral-stacked graphene between filling factors $\nu = 0$ and 1. While both states have a high resistance in transport, the WC displays negative compressibility in the capacitance data.

FOREWORD

This book contains abstracts for presentations made at the 2025 Experimental Condensed Matter Physics (ECMP) Principal Investigators' Meeting sponsored by the Materials Sciences and Engineering Division of the US Department of Energy, Office of Basic Energy Sciences (DOE-BES). This biennial meeting convenes scientists supported within ECMP by the DOE-BES to present the latest, most significant, and most exciting accomplishments and proposed future research directions of their BES supported projects. The meeting also affords PIs in the program an opportunity to see the full range of research currently being supported. We hope the meeting fosters a collegial environment to 1) stimulate the discussion of new ideas and 2) provide unique opportunities to develop or strengthen collaborations among PIs. In addition, the meeting provides valuable feedback to DOE-BES in its assessment of the state of the program and in identifying future programmatic directions. The meeting was attended in person by approximately 100 ECMP supported scientists.

The ECMP program supports research that advances our fundamental understanding of the quantum physics governing the electronic structure of complex solid materials and will allow us to achieve new materials functionalities through manipulation and control of collective excitations and quasiparticles. ECMP funds studies of novel magnetic, ferroelectric, charge ordering, nonlinear optical, superconducting, and topological properties known to emerge from the interplay of various interactions and degrees of freedom, as well as away from equilibrium in transient or metastable states. ECMP supports design, synthesis, and characterization of material systems whose electronic properties derive from quantum effects and cannot be described by classical paradigms. Projects aim at achieving fundamental understanding of key principles that might provide the foundation for transformational quantum technologies (topological quantum computing, sensing, or transduction) and/or next-generation, energy-efficient microelectronics (quantum magnonics, spintronics, and non-von Neumann electronic circuit elements). The program also supports research to reduce or eliminate critical materials and minerals while maintaining functionality for energy technologies.

The meeting was held in a hybrid format and organized into ten oral sessions and two poster sessions covering the range of research activities supported by the program. All presentations were given by in-person participants and all lunches and dinners featured keynote presentations. Dinner on day 2 featured a 1-hour panel composed by experts in experimental, computational, and theoretical aspects of AL/ML methods for science titled "The Future of AI/ML in Condensed Matter Physics Experiments". We want to thank the panel moderator Ivan Schuller and all panelists for their valuable insights and for contributing to an important discussion within the ECMP community. Co-chairs for the meeting were Liuyan Zhao (University of Michigan) and Matthew Brahlek (Oak Ridge National Laboratory). To these two we express our sincere appreciation for their invaluable help in organizing the meeting. We also want to gratefully acknowledge the excellent support provided by Ms. Stephanie Fox, Ms. April Ward, and Mr. Kutter Craig of the Oak Ridge Institute for Science and Education and by Ms. Kerry Hochberger of BES, for their efforts in organizing the meeting.

Drs. Claudia Cantoni and Tim Mewes
Program Managers, Condensed Matter and Materials Physics
Division of Materials Sciences and Engineering
Basic Energy Science

Table of Contents

Agendas 1

Tuesday, September 9, 2025 2
Wednesday, September 10, 2025 4
Thursday , September 11, 2025 6
Poster Session 1 7
Poster Session 2 8

Abstracts 9

Tuesday, September 9, 2025 10

Fractional Quantum Anomalous Hall Effect and Chiral Superconductivity in Rhombohedral Graphene 11

Long Ju

Superconductivity and spin-canting in trilayer graphene 16

Andrea Young

Fractional electronic states can be mysteriously robust 18

David Goldhaber-Gordon, Marc Kastner, Aaron Sharpe,and Andrew Mannix

Hetero-orbital two-component fractional quantum Hall effect in bilayer graphene 22

Jun Zhu

Symmetry Breaking in Two Dimensional Flat-band Systems for Spin, Charge and Cooper Pair Transport 24

Chun Ning (Jeanie) Lau and Marc Bockrath

Probing electronic and topological properties in 2D atomic crystals and their heterostuctures 28

Eva Y. Andrei

Quantum Point Contact and Shot Noise in Monolayer Graphene 34

Sangwoo Sim, Nicholas P. Quirk, Yue Tang, Sanfeng Wu, and N. P. Ong

Charge, Spin, and Thermal Transport in Nanostructured Quantum Materials: Quantum Coherence of Heavy Fermion Quasiparticles 36

Douglas Natelson

Symmetries, Interactions and Correlation Effects in Carbon Nanostructures 41

Gleb Finkelstein

Mechanical Resonant Sensing of Spin Texture Dynamics in a 2D Antiferromagnet 46

Xiao-Xiao Zhang

Broken Symmetries for Control of Electrically-Generated Spin Currents and Torques 49

Daniel C. Ralph

Low-Field Regime of Magnon Transport in PLD-Grown YIG Films 54

James Analytis54

Magnetometry Studies of Quantum Correlated Topological Materials in Intense Magnetic Fields 59

Lu Li

Correlated Quantum Materials 64

Michael A. McGuire, Andrew F. May, Brenden R. Ortiz, Jiaqiang Yan, David Mandrus

Magnetic Interactions and Excitations in Quantum Materials (MIEQM) 69

L. Ke, R. J. McQueeney, A. Sapkota, T. J. Slade, B. G. Ueland, and D. Vaknin

Two Dimensional Heavy Fermions in the van der Waals Metal CeSiI 74

Xavier Roy and Abhay Pasupathsy

Defect-mediated charge density wave transition 79

Judy J. Cha

Prediction, Design, and Synthesis of New Magnetic Nitrides 84

Sage Bauers

Geometrically frustrated magnets with exotic Archimedean lattices 89

Tai Kong

Wednesday, September 10, 2025 92

Unconventional Superconductivity in Magnetic Rare-Earth Doped Nickelate Thin Films 93

Charles H. Ahn

Emerging Materials 98

Daniel Phelan, John F. Mitchell, Ulrich Welp, and Nirmal Ghimire

Correlated Materials – Synthesis and Physical Properties 103

I. R. Fisher

Cuprate strange metals as a quantum critical phase with linearly running power law exponent 108

Dan Dessau

Magneto-optical Study of Correlated Electron Materials in High Magnetic Fields 113

Dmitry Smirnov and Zhigang Jiang

Control of antiferromagnetic order using voltage, current and temperature 117

Ivan K. Schuller

Ferroelectric Polarization Control of Metal-Insulator Transition and Magnetism in Ultrathin $SrIrO_3$..... 122

Xia Hong and Tula Paudel

Probing ice-rule-breaking transition in $Dy_2Ti_2O_7$ thin film by proximitized transport and magnetic torque 125

Haidong Zhou and Jian Liu

Single Spin Relaxation in a Fire/Ice Magnet 130

Arthur P. Ramirez

Epitaxially-Imposed Control of Chiral Transport Phenomena..... 132

Matthew Brahlek

Weyl fermions meet magnetic monopoles: a quantum encounter..... 136

Jak Chakhalian

Synthesis and Characterization of 2D Weyl Semimetals in Epitaxial Bismuthene 138

Guang Bian

Investigating the Interplay of Quantum Geometry, Magnetism, and Superconductivity in Topological Materials 140

Ni Ni

Harnessing Topological Surface States in Dirac Semimetal α-Sn Thin Films 145

Mingzhong Wu

Impact of Electric Field and Crystal Structure on Anisotropic Superconductivity in Few-Layer T′ Structured TMDs..... 148

Daniel Rhodes and Xiaofeng Qian

Growth, Anisotropy and Unconventional Superconductivity of 2M-WS_2 154

Jifa Tian

g-Factor–Enhanced Upper Critical Field in Superconducting $PdTe_2$ due to Quantum Confinement..... 158

Badih A. Assaf, Yi-Ting Hsu, Xiaolong Liu, and Xinyu Liu

Thursday, September 11, 2025.....161

Good Plasmons in a Bad Metal..... 162

D.N. Basov

Indirect excitons in heterostructures 166

Leonid Butov

Exploring Topological Interfacial Superconductivity in Quantum Anomalous Hall/Iron Chalcogenide Heterostructures 170

Cui-Zu Chang

Ultrafast Control of Topological Transport in Quantum Materials..... 174

James McIver

Enabling hollow core fibers for Brillouin light scattering and control of magnetic excitations at cryogenic temperatures..... 179

Dmytro Bozhko

Penetration-Capacitance Measurements and Noise Spectroscopies of Rhombohedral Multilayer and Twisted Bilayer Graphene..... 184

Raymond Ashoori

Topology and molecular arrangement in low-dimensional magnetic materials..... 188

Claudia Ojeda-Aristizabal

Van der Waals Heterostructures: Novel Materials and Emerging Phenomena..... 194

Feng Wang, Michael Crommie, Alessandra Lanzara, Steven Louie, Zi Q. Qiu, Archana Raja, and Mike Zaletel

Optical sensing and melting of Wigner crystals in 2D heterostructures 199

You Zhou

Tuning Magnetic Symmetries in a Moiré Magnet..... 204

Liuyan Zhao

Coherent Exciton-Magnon-Photon interaction in van der Waals magnet CrSBr..... 209

Vinod Menon

Poster Session I.....212

Exotic Transport Phenomena in Layered Topological Materials..... 213

Jin Hu

Discovery and Synthesis of New Altermagnets for Quantum Geometric Properties..... 218

Sheng Ran

Anomalous transport in a Spin Textured Altermagnet 221

Linda Ye

Quantum Fluctuations in Narrow Band Systems – Thrust 1 224

Filip Ronning

Complex States, Emergent Phenomena, and Superconductivity in Intermetallic and Metal-like Compounds FWP: Near-room-temperature ferromagnetism in pressurized $SrCo_2P_2$ 229

Sergey Bud'ko, Paul Canfield, Yuji Furukawa, Adam Kaminski, Ruslan Prozorov, Aashish Sapkota, Tyler Slad, Makariy Tanatar, and Linlin Wang

Understanding and Tuning the Interplay Between Electronic Topology and Magnetism in Magnetic Topological Materials 233

Chetan Dhital and Madalynn Marshall (Kennesaw State University), Andrew Christianson, and Huibo Cao

Geometry and frustration-induced phenomena in nanomagnet arrays 236

Peter Schiffer

Unconventional superconductivity in strongly correlated triangular adatom lattices 240

Hanno H. Weitering and Ruixing Zhang

Crystal electric-field effect under magnetic field and uncovering field-induced magnetic phase transition in triangular rare-earth magnet $CsErSe_2$ 243

Minhyea Lee

Nuclear Magnetic Resonance Resolves Charge Order Structure in Kagome Metals 247

Xiaoling Wang, Brenden R. Ortiz

Induced Atomic Order in FeNi 252

Laura H. Lewis

Insights into the electronic properties and pairing symmetry of UTe_2 using a vector magnet STM 257

Vidya Madhavan

Superconductivity and magnetism in d- and f-electron quantum materials 260

M. Brian Maple

Correlated Topological Quantum Heterostructures 269

Ho Nyung Lee

Definitive Majorana Zero Modes in Optimized Hybrid Nanowires 274

Sergey Frolov

$Ti_3C_2T_x$ MXene Composites for Electrochemical Applications 277

Bhoj Raj Gautam, Daniel Autrey, Chandra Mani Adhikari, Shubo Han, Bishnu Prasad Bastakoti, and Binod Kumar Rai

Science of 100 tesla: The reverse quantum limit and its implications for unconventional quantum oscillations in YbB_{12} 281

Neil Harrison, Mun Chan, Arkady Shekhter, John Singleton, Priscila Rosa, Scott Crooker, and Marcelo Jaime

Prediction, Design, and Synthesis of New Magnetic Nitrides 286

Sage Bauers

Poster Session II 291

Controlled electronic coupling to graphene-based heterostructure materials: towards atomically precise two-probe STM transport..... 292

Marek Kolmer

Multidimensional Optical Probes of Quantum Materials..... 296

Albert Liu

Light-driven proximity control of designer moiré nanomaterials 300

Kyle Seyler

Ultrafast Spin Torque Dynamics in van der Waals Magnetic Heterostructures..... 303

Yunqiu Kelly Luo

Engineering Correlated Phases in Higher-Order Moiré Quantum Matter 307

Kenji Yasuda

Twisted oxide membrane interface by local atomic registry design 312

Chang-Beom Eom

Ultrafast Isospin Dynamics in Flatband Graphene 318

Chenhao Jin

Selective Area Epitaxial Growth of Superconducting MgB_2 Nanowires and MgB_2/graphene hybrid structures on SiC 322

Qi Li

Tunable Exciton and Spin Dynamics in 2D Materials: Role of Thickness, Defects, Synthesis Method and Substrates..... 327

Birol Ozturk

Probing Chirality-Dependent Magnetotransport in 2D $(MBA)_2PbI_4$ Hall Devices 332

Meenakshi Singh

Heteroepitaxial growth and surface investigation of Weyl semimetals Mn3Ga and Mn3Sn on hexagonal wurtzite GaN substrates..... 337

Arthur R. Smith

Abelian and Non-Abelian Quantum Entanglement in Landau Flatbands..... 342

Gabor Csathy

Generalizing Quantum Geometry to many-body wavefunctions 347

N. Peter Armitage

Understanding and Harvesting Topological Transport in Centrosymmetric Layered Ferromagnets and Their Heterostructures 349

Luis Balicas

Heterogeneous Integration of 2D-3D Materials for Energy Efficient Electronics..... 354

Nihar R. Pradhan, Anirudha V. Sumant, Jerzy Leszczynski, Dinesh Kumar Sengottuvelu, Mohammed Majdoub, Sasan Nouranian, and Ahmed Al-Ostaz

Influence of Dimensional Confinement at the Metal-Layered Crystal Interface 359

Andrew Stollenwerk, Paul Shand, and Pavel Lukashev

Electrical Switching and Antiferromagnetic Domain Imaging of $LaFeO_3$ Epitaxial Thin Films..... 364

Fengyuan Yang

Discovery of novel layered multiferroics 369

Nasim Alem

Program Title: Non-Equilibrium Magnetism: Materials and Phenomena 374

Frances Hellman, Peter Fischer, Sinéad Griffin, Sujoy Roy, Inna Vishik; and Josh Turner

Digital Synthesis: A pathway to novel states of condensed matter 380

A. Bhattacharya

Author Index 385

Participant List.....388

Agendas

2025 DOE-BES Experimental Condensed Matter Physics Principal Investigator Meeting

Meeting Chairs: Claudia Cantoni and Tim Mewes (DOE-BES)
Meeting Co-Chairs: Liuyan Zhao (University of Michigan) and Matthew Brahlek (Oak Ridge National Laboratory)

Tuesday, September 9, 2025		
7:30–8:15 AM	Breakfast	
8:15–8:40 AM	Welcome and Program Updates	Claudia Cantoni, ECMP Program Manager, DOE-BES Andrew Schwartz, Deputy Associate Director, DOE-BES
8:40–10:25 AM	**Session A1**	**Emergent Phenomena in Multilayer Graphene, Session Chair: Chenhao Jin**
8:40–9:10 AM	Long Ju	Chiral Superconductivity Found in Crystalline Graphene
9:10–9:25 AM	Andrea Young	Superconductivity and spin-canting in trilayer graphene
9:25–9:40 AM	David Goldhaber-Gordon	Fractional electronic states can be mysteriously robust
9:40–9:55 AM	Jun Zhu	Hetero-orbital two-component fractional quantum Hall effect
9:55–10:10 AM	Jeanie Lau	Dominant 1/3-filling Correlated Insulator States and Orbital Geometric Frustration in Twisted Bilayer Graphene
10:10–10:25 AM	Eva Andrei	Intercrystals – a New Class of Quasiperiodic Crystals
10:25–10:50 AM	Break	
10:50–12:20 PM	**Session B1**	**Novel Functional Devices and Measurements, Session Chair: Kelly Luo**
10:50–11:05 AM	Nai-Phuan Ong	Quantum-Point Contact and Shot Noise in Graphene
11:05–11:20 AM	Douglas Natelson	Quantum coherence of heavy fermion quasiparticles
11:20–11:35 AM	Gleb Finkelstein	Thermalization of Superconductor–Quantum Hall Interface
11:35–11:50 AM	Xiao-Xiao Zhang	Early Career: Detecting spin textures with nano-membrane vibrations
11:50–12:05 PM	Dan Ralph	Magnets Can Make Tilted Spin Currents Desired for Magnetic Memories
12:05–12:20 PM	James Analytis	Low-Field Regime of Magnon Transport in YIG Films
12:20–1:20 PM	**Lunch**	
12:50–1:20 PM	Lunch Talk: Philip Kim	Emergent Quasiparticles in Graphene Heterostructure
1:20–2:35 PM	**Session C1**	**Kagome Materials and Heavy Fermions, Session Chair: Badih Assaf**

1:20–1:50 PM	Lu Li	Quantum Oscillations in Kagome Mott insulators
1:50–2:05 PM	Michael McGuire	Discovery of New Kagome Metals Unveils Origins of Density Wave Instability
2:05–2:20 PM	Rob McQueeney	Chiral magnetic “particle” found in a kagome metal
2:20–2:35 PM	Xavier Roy	Nodal hybridization in CeSiI
2:35–3:00 PM	Break	
3:00–3:45 PM	**Session D1**	**Experiments Involving Machine Learning, Session Chair: Marek Kolmer**
3:00–3:15 PM	Judy Cha	Defect-mediated charge density wave transition
3:15–3:30 PM	Sage Bauers	Predicting and preparing new magnetic nitrides
3:30–3:45 PM	Tai Kong	Geometrically frustrated magnets with exotic Archimedean lattices
3:45–4:00 PM	Program Guidelines	Tim Mewes, ECMP Program Manager, DOE-BES
4:00–6:00 PM	Poster Session 1	
6:00–7:10 PM	**Dinner**	
6:30–7:10 PM	Dinner Talk: Harold Hwang	Ambient pressure superconductivity in thin film La3Ni2O7

Wednesday, September 10, 2025		
7:30–8:15 AM	Breakfast	
8:15–9:45 AM	**Session A2**	**Correlated Superconductors, Session Chair: Filip Ronning**
8:15–8:45 AM	Dillon Fong	Superconductivity in one unit-cell nickelate
8:45–9:00 AM	Charles Ahn	Unconventional superconductivity in nickelate thin films
9:00–9:15 AM	Danny Phelan	Polymorphism in Nickelate Superconductors
9:15–9:30 AM	Ian Fisher	Surprising new evidence for multicomponent superconducting state in an Fe-based superconductor
9:30–9:45 AM	Daniel Dessau	Cuprate strange metals as a quantum critical phase with linearly running power law exponent
9:45–10:15 AM	Break	
10:15–12:00 PM	**Session B2**	**Novel Magnetic Materials, Session Chair: Sheng Ran**
10:15–10:45 AM	Dmitry Smirnov	Spectroscopy of disorder in an incompressible magnetic state
10:45–11:00 AM	Ivan Schuller	Manipulate antiferromagnets with phase transitions and currents
11:00–11:15 AM	Xia Hong	Emergent Magnetism at the Metal-Insulator Transition in SrIrO3 Induced via Ferroelectric Polarization
11:15–11:30 AM	Haidong Zhou	Probing ice rule breaking in Dy2Ti2O7 thin film by proximitized transport and magnetic torque
11:30–11:45 AM	Art Ramirez	Single-Spin Relaxation in a Fire/Ice Magnet
11:45–12:00 PM	Matthew Brahlek	Early Career: Marrying Altermagnetism and Ferromagnetism in MnTe
12:00–1:00 PM	**Lunch**	
12:30–1:00 PM	Lunch Talk: T. Arul Mozhi	Convening the Condensed Matter & Materials Research Community since 1971
1:00–2:30 PM	**Session C2**	**Topological Phenomena and Responses, Session Chair: Peter Armitage**
1:00–1:30 PM	Jak Chakhalian	New quantum state discovered at a Weyl semimetal/spin ice pyrochlore interface with interacting topological electrons and magnetic monopoles
1:30–1:45 PM	Guang Bian	Realization of a 2D Weyl Semimetal in Epitaxial Bismuthene
1:45–2:00 PM	Qiang Li	Chiral magnetism in topological semimetals

2:00–2:15 PM	Ni Ni	Revealing the non-trivial topology and robust magnetism-induced gap opening in AAg4Sb2 (A=Sr, Eu)
2:15–2:30 PM	Mingzhong Wu	Quantum Oscillations of Nonlinear Electrical Transport
2:30–3:00 PM	Break	
3:00–3:45 PM	**Session D2**	**Novel Superconductors, Session Chair: Linda Ye**
3:00–3:15 PM	Daniel Rhodes	Anisotropic and Pressure-Dependent Superconductivity in Bilayer TdMoTe2
3:15–3:30 PM	Jifa Tian	Unconventional Superconductivity and Raman Anisotropy in 2M-WS2
3:30–3:45 PM	Badih Assaf	g-factor tunes the upper critical field in a van der Waals superconductor
3:45–5:45 PM	Poster Session 2	
5:45–7:15 PM	**Dinner**	
6:15–7:15 PM	Panel Discussion	**The Future of AI/ML in Condensed Matter Physics Experiments** **Panelists:** **Eun-Ah Kim**, Hans A. Bethe Professor, Cornell University **Rob Moore II**, Director of Interconnected Science Ecosystem and Distinguished Staff Scientist, Oak Ridge National Laboratory **Francesca M. Tavazza**, Data and AI-Driven Materials Science Group Leader, National Institute of Standards and Technology **David Alan Tennant**, Professor, University of Tennessee Knoxville and Director, Shull Wollan Center **Kevin Yaeger**, Director, AI-Accelerated Nanoscience, Center for Functional Nanomaterials, Brookhaven National Laboratory **Moderator:** **Ivan Schuller**, Distinguished Professor of Physics, University of California, San Diego

Thursday , September 11, 2025		
7:30–8:15 AM	Breakfast	
8:15–9:45 AM	**Session A3**	**Electromagnetic Responses in Condensed Matter, Session Chair: Albert Liu**
8:15–8:45 AM	Dmitri Basov	Good Plasmons in a Bad Metal
8:45–9:00 AM	Leonid Butov	Indirect excitons (IXs) in heterostructures
9:00–9:15 AM	Cui-Zu Chang	Interface-induced superconductivity in FeTe heterostructures
9:15–9:30 AM	James McIver	Early Career: Nonlinear transport from a Floquet-Weyl semimetal
9:30–9:45 AM	Dmytro Bozhko	Enabling hollow core fibers for Brillouin light scattering and control of magnetic excitations at cryogenic temperatures
9:45–10:15 AM	Break	
10:15–11:45 AM	**Session B3**	**Van der Waals Systems, Session Chair: Kyle Seyler**
10:15–10:30 AM	Ray Ashoori	Observation of a 1/3 Fractional Chern Insulator
10:30–10:45 AM	Claudia Ojeda-Aristizabal	Proximity effects of a molecular thin film on bilayer graphene revealed in the mesoscopic regime
10:45–11:00 AM	Feng Wang	Imaging quantum melting in a 2D Wigner solid
11:00–11:15 AM	You Zhou	Early Career: Optical magnetization and melting of Wigner crystals
11:15–11:30 AM	Liuyan Zhao	Magnetic Symmetries are Tuned in a Moiré Magnet
11:30–11:45 AM	Vinod Menon	Magnon mediated interaction between electronic excitations in a 2D magnet
11:45–11:55 AM	**Conclusion**	
11:55 AM	Adjourn	

Tuesday, September 9, 2025
4:00-6:00 PM

Poster Session 1

Presenter	Title
Jin Hu	Early Career: Anderson Localization in a Bulk Crystalline Material
Sheng Ran	Early Career: Synthesis of New Altermagnetic Candidate Materials
Linda Ye	Early Career: Anomalous transport in a Spin Textured Altermagnet
Filip Ronning	New insights into magnetic interactions of cerium-based metallic magnets
Paul Canfield	Near-room-temperature ferromagnetism in pressurized SrCo2P2
Chetan Dhital	Ferromagnetism and Large Anomalous Hall Effect in centrosymmetric magnet NdGaSi: Weyl Physics?
Peter Schiffer	Artificial Magnetic Tripods
Hanno Weitering	Unconventional superconductivity in triangular adatom lattices
Minhyea Lee	Field-induced transition uncovered from crystal electric field interaction in the triangular rareearth magnet
Xiaoling Wang	NMR Resolves Charge Order Structure in Kagome Metals
Laura Lewis	Accelerating Nature – induced atomic order in FeNi
Vidya Madhavan	Intertwined Orders in triplet superconductor UTe2
M. Brian Maple	U1-xThxTe2 : Three distinct Superconducting Phases
Johnpierre Paglione	Robust Spin-Triplet Superconductivity in UTe2
Ho Nyung Lee	Strain-induced nonsymmorphic symmetry creates a novel topological phase in a correlated oxide
Sergey Frolov	Robust Superconductivity in a High Spin-Orbit Quantum Wire
Bhoj Gautam	Improved Supercapacitance of Ti3C2Tx MXene with Polyacrylonitrile Nanoparticles Intercalation
Neil Harrison	Discovery of the Reverse Quantum Limit
Brad Ramshaw	High throughput search for topological superconductors
Eric Bauer	Recent Progress on the Superconductivity of UTe2 and CeCoIn5
Tyler Slade	Design and Discovery of New Quantum Materials in the Complex States FWP
Ulrich Welp	Origin of the Unusual Temperature Dependence of the Upper Critical Field of Kagome Superconductor CsV3Sb5: Multiple Bands or van Hove Singularities?
Brian Leonard	Synthesis and Characterization of doped 2M WS2 Crystals
Abhay Pasupathy	Two-dimensional Heavy Fermions and Beyond
Andrew Mannix	Tuning van der Waals Heterostructures with Strain and Chemistry.

Wednesday, September 10, 2025
3:45-5:45PM

Poster Session 2

Presenter	Title
Marek Kolmer	Early Career: Addressing high-energy interface states
Albert Liu	Early Career: Multidimensional Probes of Quantum Materials
Kyle Seyler	Early Career: A new approach to dynamically sculpt quantum materials
Yunqiu Kelly Luo	Early Career: Electrical detection and control of antiferromagnetic resonance in van der Waals devices
Kenji Yasuda	Fabrication of Higher-order moiré superlattice
Chang-Beom Eom	Twisted oxide membrane interface by local atomic registry design
Chenhao Jin	Surprising long-lived isospin modes in flatband graphene
Qi Li	Selective Area Epitaxy of Superconducting MgB2 Thin Films on Graphene-SiC
Birol Ozturk	Tunable Exciton and Spin Dynamics in 2D Materials for Quantum Sensing Applications
Meenakshi Singh	Probing Chirality Induced Spin Selectivity (CISS) in $(MBA)_2PbI_4$ via Hall Measurements
Art Smith	Heteroepitaxial growth and surface investigation of Weyl semimetals Mn3Ga and Mn3Sn on hexagonal wurtzite GaN substrates
Gabor Csathy	Complex anyonic order in topological flat bands: Abelian anyons with six quantized fluxes
Norman Peter Armitage	Generalizing Quantum Geometry to many-body wavefunctions
Luis Balicas	Local inversion symmetry breaking, Néel skyrmions, and ferrimagnetism in Fe3GaTe2
Nihar Pradhan	Heterogeneous Integration of 2D-3D Materials for Energy Efficient Electronics
Andrew Stollenwerk	Effects of Ni thin films on layered materials
Fengyuan Yang	Electrical Switching and Imaging of LaFeO3 Epitaxial Thin Films - A New Platform for Antiferromagnetic Spintronics and Insulating Altermagnetism
Nasim Alem	Discovery of novel layered multiferroics: Cu1-xMn1+ySiTe3
Frances Hellman	Thermodynamic Phase Transitions of Nematic Order in Magnetic Helices
Brenden Ortiz	Frontiers in kagome metals; development of the AM3X4 kagome magnets
Hu Miao	Chiral electronic orders and excitations
Yi-Ting Hsu	Detecting Topological Superconductors via Phase-space Berry Curvatures
Ruixing Zhang	Deciphering Chiral Superconductivity via Impurity Bound States
Benjamin Ueland	Magnetic Correlations in Flat-Band Metals
Anand Bhattacharya	Superconductivity at interfaces of KTaO3

Abstracts

Tuesday, September 9, 2025

Fractional Quantum Anomalous Hall Effect and Chiral Superconductivity in Rhombohedral Graphene

Long Ju, Massachusetts Institute of Technology

Keywords: Rhombohedral graphene, superconductivity, fractional quantum anomalous Hall, topological phase

Research Scope

We are currently focusing on understanding topological electron physics in rhombohedrally stacked multilayer graphene. Different from twisted graphene systems, we believe that crystalline graphene can host flat-band physics without introducing twisting or moiré superlattice effects. Our group established the crystalline rhombohedral form of graphene (with layer number >3) as a new playground for emergent quantum phenomena[1-3], by demonstrating integer and fractional quantum anomalous Hall effects (IQAHE and FQAHE), orbital multiferroicity, superconductivity, and correlated insulators. Especially, the observation of FQAHE in the pentalayer graphene/hBN moiré superlattice[1] was among the only two discoveries of this effect in condensed matter physics. The experiment was done in the absence of theoretical prediction and it challenges the conventional interpretation of how to obtain such states. It has triggered tremendous interest from the condensed matter physics community since its publication in Oct 2023.

We are now investigating both the FQAHE physics and unconventional superconductivity in rhombohedral graphene. The latter was not planned in the original proposal, but was observed when trying to understand the moiré effect on FQAHE. As we will explain in the next section, the superconductivity we observed in the absence of moiré effect happens to be likely a topological superconductor—expanding the range of topological phenomena in rhombohedral graphene system, which is the theme of this project.

Recent Progress

We have made breakthroughs in two directions in this project. The first breakthrough is about the Fractional Quantum Anomalous Hall Effect in rhombohedral graphene/hBN moiré superlattice, which was planned and proposed in our original proposal. The second breakthrough is about the discovery of Chiral Superconductivity in bare rhombohedral graphene without alignment with hBN, which was totally beyond the expectation and was not planned in our original proposal. To be more specific:

1. Fractional Quantum Anomalous Hall Effect (FQAHE)

Our group established the crystalline rhombohedral form of graphene (with layer number >3) as a new playground for emergent quantum phenomena, by demonstrating integer and fractional quantum anomalous Hall effects (IQAHE and FQAHE), orbital multiferroicity, superconductivity, and correlated insulators. Especially, the observation of FQAHE in the pentalayer graphene/hBN moiré superlattice was among the only two discoveries of this effect in condensed matter physics. The experiment was done in the absence of theory prediction and it challenges the conventional interpretation of how to obtain such states. It has triggered tremendous interest from the condensed matter physics community since its publication in Oct 2023, as can be seen from two Condensed Matter Journal Club reports, review by professional journals and news by public media.

In 2024, we further engineered the dilution fridge setup at MIT by fabricating and purchasing more electronic filters. These efforts helped reducing the electronic temperature in graphene to the level of ~30 mK. We also improved the sample quality by fabricating more uniform devices. Combining these efforts, in addition to the six FQAHE states we reported in early 2024, we were able to observe two more fractional states that show FQAHE. In addition, we observed large regions on the phase diagram of rhombohedral graphene/hBN moire superlattice devices that exhibit integer quantum anomalous Hall effect. These states reside at moiré filling factors very different from 1, and exhibit fundamentally different transport behavior from the Chern insulator state at moiré filling factor 1. We named these states as Extended Quantum Anomalous Hall (EQAH) states. The nature of these states are not entirely clear at this moment, but two candidates are plausible. The first candidate is the Anomalous Hall Crystal, which is a topological version of the Wigner Crystal state. This is a new topological phase of matter proposed by several theory groups including Ashvin Vishwanath, Senthil Todadri, and Ya-Hui Zhang. The second candidate is the anomalous version of the re-entrant quantum Hall state, similar to that in GaAs-based two-dimensional electron gas systems. More experiments are to be performed to differentiate between these possible scenarios.

The EQAH state is a new observation in this exciting FQAHE physics platform, and the results were published in early 2025 in Nature[4].

2. Chiral SuperConductivity (CSC)

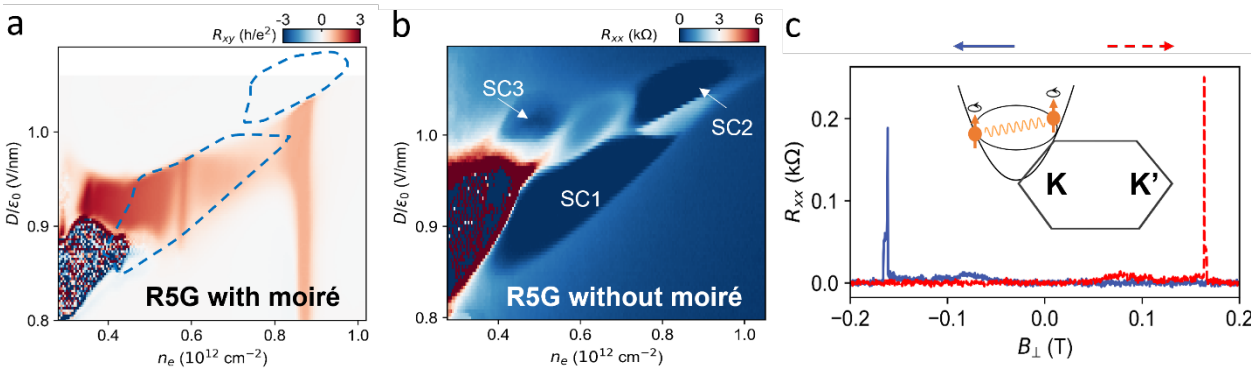


***Figure 1. Chiral superconductivity in rhombohedral pentalayer graphene. a&b**, Phase diagrams with and without moiré superlattice effect, exhibiting FQAHE and superconductivity respectively. **c.** Magnetic hysteresis in the SC1 state in resistance, due to valley polarization and orbital magnetism.*

Ju's group discovered a couple of new superconducting states in simple crystalline rhombohedral graphene, as part of graphite. These superconductivities exhibit magnetic hysteresis at both above and below the critical temperatures, as well as random time-dependent fluctuations in resistance. These observations suggest that the superconductor is simultaneously a magnet, which challenges the conventional impressions on these two phenomena. The observed superconductivity emerges from spin- and valley-polarized parent states, which endow angular momentum to the Cooper pairs and make it chiral superconductors. In addition, the high critical magnetic field suggests strongly coupled superconductivity. All together, these observations are unprecedented in any other superconductors, since the discovery by Kamerlingh Onnes in 1911. Many following theoretical works suggest one of the discovered superconductivity to be topological.

This discovery was made when trying to better understand the conditions for the fractional quantum anomalous Hall effect (FQAHE), which was discovered in rhombohedral graphene/hBN moiré superlattice devices by Ju's group in 2023. The observation of FQAHE in this material system was a total surprise to the community, and is still puzzling theorists to date on the microscopic mechanism. Some theory suggested a new form of topological matter, named as Anomalous Hall Crystal (AHC), which might exist in the absence of moiré effects. Ju's group made devices that have large twist angles between graphene and hBN to eliminate moiré effect. To their surprise, superconductivity instead of AHC was observed. While the team is still searching for AHC, given the observation of chiral superconductivity, a completely new and unexpected direction of exploring topological superconductivity is readily open for investigation in the chemically and structurally simple rhombohedral graphene.

The CSC state is a new observation in this exciting crystalline graphene platform, and the results were published in May 2025 in Nature[5].

Future Plans

We plan to continue investigating both the FQAHE and CSC physics in the rhombohedral graphene platform.

On the FQAHE end, we will search for even-denominator fractional states that might host non-abelian anyons as their excitations. We will investigate FQAHE in moiré superlattice devices composed of 4-7 layer of rhombohedral graphene, check the angle-dependence (between graphene and hBN), and explore the possibility of FQAHE under the strong-moiré condition by electrical gating.

On the CSC end, many theorists believe that this superconductivity is not only chiral, but topological. The prospect of it hosting Majorana edge modes at the edge and localized Majorana zero state at vortex making rhombohedral graphene a new frontier of topological superconductivity, which possess great potential for topological quantum computing. In the chiral superconductor state, Majorana modes might exist as localized modes in vortex cores or chiral modes on the edge. We will explore the superconducting transition temperature in 6-layer rhombohedral graphene and the effect of screening on chiral superconductivity. We will also explore new experimental techniques to determine if the chiral superconducting states are nodal (like p-wave) or nodeless (like p_x+-ip_y). If nodeless, it is one more step towards topological superconductivity.

References

Lu, Z., Han, T., Yao, Y., Reddy, A.P., Yang, J., Seo, J., Watanabe, K., Taniguchi, T., Fu, L. and Ju, L. Fractional Quantum Anomalous Hall Effect in Multilayer Graphene. *Nature* 626, 759–764 (2024). https://doi.org/10.1038/s41586-023-07010-7

Han, T., Lu, Z., Yao, Y., Yang, J., Seo, J., Yoon, C., Watanabe, K., Taniguchi, T., Fu, L., Zhang, F. and Ju, L. Large Quantum Anomalous Hall Effect in Spin-Orbit Proximitized Rhombohedral Graphene. *Science* 384,647-651(2024). DOI:10.1126/science.adk9749

Han, T., Lu, Z., Scuri, G., Sung, J., Wang, J., Han, T., Watanabe, K., Taniguchi, T., Fu, L., Park, H. and Ju, L. Orbital Multiferroicity in Pentalayer Rhombohedral Graphene. *Nature* 623, 41–47 (2023). https://doi.org/10.1038/s41586-023-06572-w

Lu, Z., Han, T., Yao, Y., Yang, J., Seo, J., Shi, L., Ye, S., Watanabe, K., Taniguchi, T. and Ju, L. Extended Quantum Anomalous Hall States in Graphene/hBN Moiré Superlattices. *Nature* 637, 1090–1095 (2025). https://doi.org/10.1038/s41586-024-08470-1

Han, T., Lu, Z., Hadjri, Z., Shi, L., Wu, Z., Xu, W., Yao, Y., Cotton, A.A., Sedeh, O.S., Weldeyesus, H., Yang, J., Seo, J., Ye, S., Zhou, M., Liu, H., Shi, G., Hua, Z., Watanabe, K., Taniguchi, T., Xiong, P., Zumbuhl, D.M., Fu, L. and Ju, L. Signatures of Chiral Superconductivity in Rhombohedral Graphene. *Nature* (2025). https://doi.org/10.1038/s41586-025-09169-7

Publications

*Han, T., Lu, Z., Hadjri, Z., Shi, L., Wu, Z., Xu, W., Yao, Y., Cotton, A.A., Sedeh, O.S., Weldeyesus, H., *Yang, J., *Seo, J., Ye, S., Zhou, M., Liu, H., Shi, G., Hua, Z., Watanabe, K.,

Taniguchi, T., Xiong, P., Zumbuhl, D.M., Fu, L. and Ju, L. Signatures of Chiral Superconductivity in Rhombohedral Graphene. *Nature* (2025). https://doi.org/10.1038/s41586-025-09169-7

Lu, Z., *Han, T., Yao, Y., *Yang, J., *Seo, J., Shi, L., Ye, S., Watanabe, K., Taniguchi, T. and Ju, L. Extended Quantum Anomalous Hall States in Graphene/hBN Moiré Superlattices. *Nature* 637, 1090–1095 (2025). https://doi.org/10.1038/s41586-024-08470-1

Superconductivity and spin-canting in trilayer graphene

Andrea Young, **University of California, Santa Barbara**

Keywords: graphene, superconductivity, magnetism

Research Scope

Graphene and transition metal dichalcogenide flat-band systems show similar phase diagrams, replete with magnetic and superconducting phases. An abiding question has been whether magnetic ordering competes with superconductivity or facilitates pairing. For example, recent studies of Bernal bilayer graphene in the presence of enhanced spin–orbit coupling show a substantial increase in the observed domain and critical temperature Tc of superconducting states [1]; however, the mechanism for this enhancement remains unknown. The correlation with spin orbit coupling strongly suggests that spin ordering is the relevant parameter, our research aims to directly probe this via local scanning SQUID-on-tip magnetometry.

Recent Progress

This reporting period, we showed that introducing spin–orbit coupling in rhombohedral trilayer graphene (RTG) by substrate proximity effect generates new superconducting pockets for both electron and hole doping, with maximal 300 mK, which is three times larger than in RTG encapsulated by hexagonal boron nitride. Using local magnetometry, we show that superconductivity straddles a transition between a spin-canted state with a finite in-plane magnetic moment and a state with complete spin–valley locking. This transition is reproduced in our Hartree–Fock calculations, in which this transition is driven by the competition between spin–orbit coupling and the carrier-density-tuned Hund's interaction. Our experiment suggests that the enhancement of superconductivity by spin–orbit coupling is driven by a quantitative change in the canting angle rather than a change in the ground state symmetry. These results align with a recently proposed mechanism for the enhancement of superconductivity [2], in which fluctuations in the spin-canting order contribute to the pairing interaction.

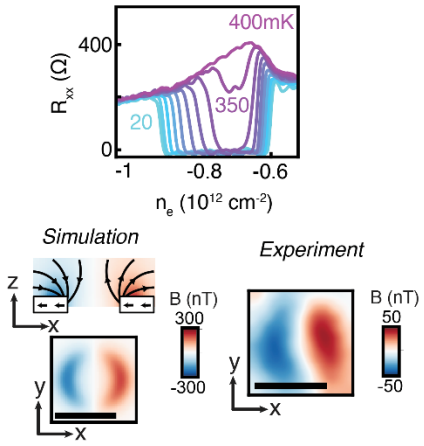


Figure 2: Superconductivity appears at comparatively high temperature in a WSe2/ABC trilayer graphene heterostructure. We used nanoSQUID on tip magnetometry to directly correlate the formation of in-plane magnetic order with superconductivity, as detailed in our paper [1].

Future Plans

In the immediate near term, we plan to use our ultra-low temperature SQUID on tip magnetometry to investigate the pairing symmetry in these spin-orbit enhanced superconductors directly. Magnetic signals from 2D superconductors in graphene have not been observed

previously, but are expected at low levels from several distinct mechanisms. For example, the Meissner effect, though strongly suppressed in a 2D superconductor, is potentially within our resolution; Pearl vortices may also provide finite signal due to the divergence of the penetrating field near the vortex core. Even more promising, theoretical modeling suggests that spontaneous chiral p-wave superconductivity as a candidate for the superconducting phase under some mechanisms, so that it is possible that the superconducting may produce a spontaneous ferromagnetic signal (easily distinguished from typical superconducting screening, which is diamagnetic). Resolving and distinguishing these effects is a key goal of work in the next reporting period.

References

1. Yiran Zhang, Gal Shavit, Huiyang Ma, Youngjoon Han, Chi Wang Siu, Ankan Mukherjee, Kenji Watanabe, Takashi Taniguchi, David Hsieh, Cyprian Lewandowski, Felix von Oppen, Yuval Oreg & Stevan Nadj-Perge. "Twist-programmable superconductivity in spin–orbit-coupled bilayer graphene." Nature 641, 625–631 (2025).
2. Zhiyu Dong, Étienne Lantagne-Hurtubise, Jason Alicea. "Superconductivity from spin-canting fluctuations in rhombohedral graphene." arXiv:2406.17036

Publications

1. Caitlin L. Patterson, Owen I. Sheekey, Trevor B. Arp, Ludwig F. W. Holleis, Jin Ming Koh, Youngjoon Choi, Tian Xie, Siyuan Xu, Yi Guo, Hari Stoyanov, Evgeny Redekop, Canxun Zhang, Grigory Babikyan, David Gong, Haoxin Zhou, Xiang Cheng, Takashi Taniguchi, Kenji Watanabe, Martin E. Huber, Chenhao Jin, Étienne Lantagne-Hurtubise, Jason Alicea & Andrea F. Young. "Superconductivity and spin canting in spin–orbit-coupled trilayer graphene." *Nature* **641**, 632–638 (2025).
2. Trevor Arp, Owen Sheekey, Haoxin Zhou, C. L. Tschirhart, Caitlin L. Patterson, H. M. Yoo, Ludwig Holleis, Evgeny Redekop, Grigory Babikyan, Tian Xie, Jiewen Xiao, Yaar Vituri, Tobias Holder, Takashi Taniguchi, Kenji Watanabe, Martin E. Huber, Erez Berg & Andrea F. Young. "Intervalley coherence and intrinsic spin–orbit coupling in rhombohedral trilayer graphene." *Nature Physics* **20**, 1413–1420 (2024).

Fractional electronic states can be mysteriously robust

David Goldhaber-Gordon, Marc Kastner, Aaron Sharpe,and Andrew Mannix, **Stanford Institute for Materials and Energy Sciences, SLAC National Accelerator Laboratory**

Keywords: 2-dimensional materials, topological materials, quantum many-body systems, electrical properties, magnetism

Research Scope

A new era in condensed matter physics has dawned with the remarkable discovery that stacking 2D Van der Waals layers one atop another can produce electronic states that the constituent layers did not even hint at. Such states include still-not-understood superconductors, entirely new types of magnets, strange metals, correlated insulators, and surely more yet to be discovered. But this powerful possibility has a flip side: the novel states are highly sensitive to newly-relevant tuning parameters such as interlayer twist angle – which determines the period of a moiré superlattice – and heterostrain. Besides discovering new states, we aim to identify the ingredients that favor those states, and the detailed nature of those states (e.g. the order parameter of a superconductor or a novel magnet in which spin, orbit, or both could be polarized.)

Accomplishing these goals will require the interplay of four main ingredients: (1) Measurement: Electronic transport has always been among the most powerful tools for discovering and elucidating many-body electronic phases in materials. In Van der Waals moirés, where traditional complementary tools to characterize order and excitations (e.g. neutron scattering) cannot hope for enough signal from tiny samples, microwave spectroscopy can combine with transport to map low-energy excitations, helping to diagnose the nature of those phases. (2) Synthesis and patterning: Developing a more sophisticated and powerful approach to VdW stack synthesis will enable setting parameters such as interlayer twist angle and strain precisely, uniformly, and reproducibly (identified as a key priority by the BES report on BRN for Synthesis Science). We will also develop non-moiré-based spatially-periodic patterns as a complementary way to tune and design electronic structure. (3) Characterization: Characterizing sample structure from the atomic scale through the moiré scale to the macro scale will provide tight feedback to guide synthesis. (4) Theory: Ab initio band structure and effective interacting model calculations from our collaborators can guide us in what types of structures we should anticipate new states emerging.

Recent Progress

When a Chern band is partially filled, a fractional Chern insulator (FCI) – the lattice analog of a fractional quantum Hall state – can arise. Though the full range of possible scenarios for producing such a state is not established, the most tractable models combine strong electronic interactions with the quantum geometry of the parent Chern band meeting specific criteria.

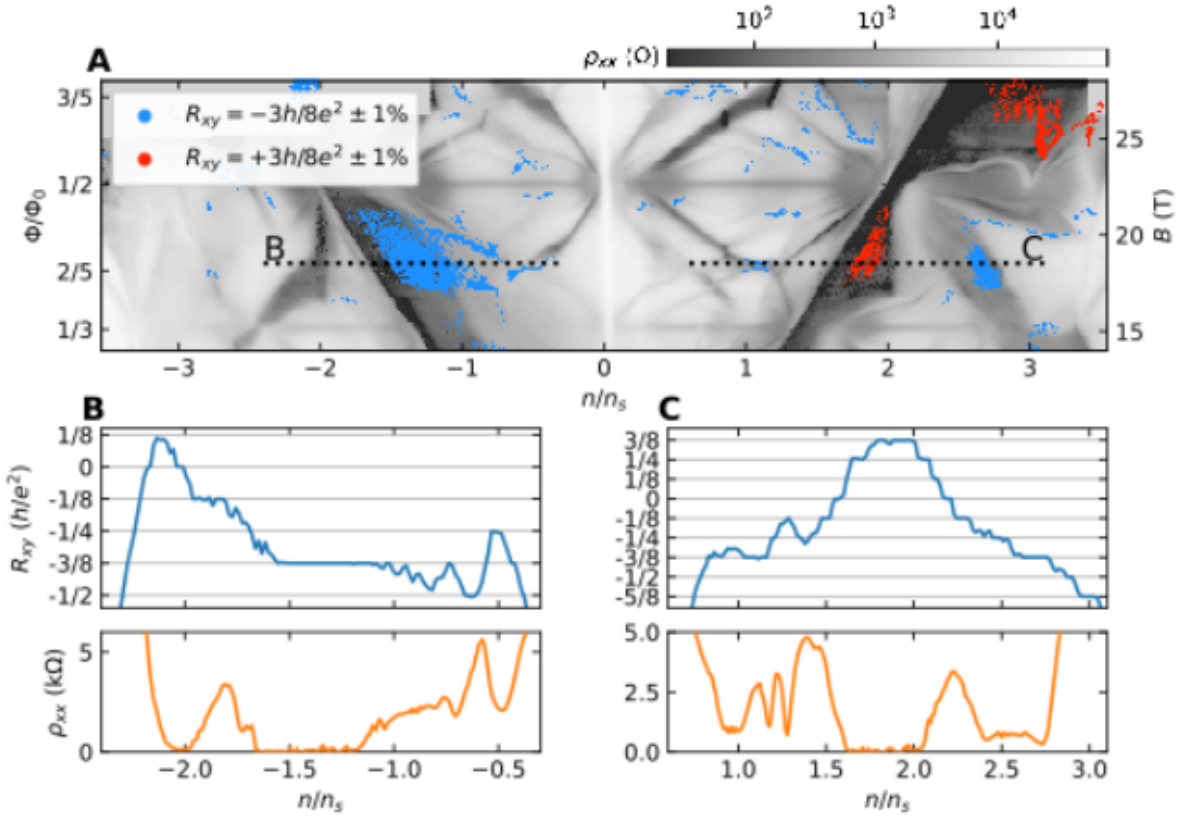
In twisted bilayer graphene, the importance of interactions can be tuned by varying the interlayer twist.

We have recently studied a sample with twist ~1.4°, large enough to suppress the zero-field correlated states. We find that applying a strong magnetic field restores the importance of electron-electron interactions: at nearly half a magnetic flux quantum per moiré unit cell, deep in the Hofstadter regime, odd-denominator FCIs appear in multiple Hofstadter subbands.

These fractional states persist over larger ranges of density, and are more robustly quantized, than nearby integer states, opposite to what is seen in other fractional quantum Hall or FCI systems.

For context, it's worth noting that only a few other examples of materials hosting FCIs have been experimentally reported: twisted $MoTe_2$ and graphene-based multilayers aligned with hexagonal boron nitride (hBN).

The graphene-based FCIs appear very sensitive to structural parameters; it is not known why particular configurations exhibit FCIs whereas others do not despite having flat bands with non-



Fractional Chern insulating Hall plateaus. (A) Longitudinal resistivity in gray-scale. Colored regions superimposed on the grey-scale plot mark where the Hall resistance for a neighboring contact pair is quantized to within 1% of −8/3 (blue) or +8/3 (red). (B, C) Hall resistance and longitudinal resistivity as a function of density at 18.5 T ($\Phi/\Phi_0 = 0.41$, black dashed lines in A). Figure from (1).

trivial quantum geometry. The electronic moiré miniband structure of TBG depends sensitively and predictably on twist angle. Near the magic angle of 1.1°, the large ~ 10nm moiré length scale enables tuning the density of charge carriers through entire minibands and the density of magnetic flux to on order one flux quantum $\Phi_0 = \mathrm{h/e}$ per moiré cell, where *e* is the elementary charge and *h* is Planck's constant. In this "Hofstadter's butterfly" regime the energy spectrum exhibits a fractal structure with field-induced topological subbands. Each gap in the fractal spectrum follows a "Streda line" in the space of flux and density, categorized by two numbers *(s,t)*. *s* is the intercept with the zero-flux axis, and *t* is both the slope of the line and the expected quantized value of the Hall conductance: $\sigma_{xy} = te^2/h$. FCIs are associated with Streda lines whose *t* is fractional, and whose *s* does not coincide with the charge neutrality point or a band edge.

Recently, fractional *t* states have been observed in high-quality magic-angle TBG. These occurred in Landau levels originating from charge neutrality ($s = 0$), just like conventional FQH. In TBG, FCIs with $\mathrm{s} \neq 0$, reflecting an underlying broken symmetry, have only been clearly demonstrated in samples in which the graphene lattice is aligned with that of hBN, a known source of symmetry breaking for electrons in graphene.

Since the early days of quantum Hall, in some samples integer quantum Hall states have extended over a broad density range, outcompeting fractional states that might be expected at those densities. This "re-entrant quantum Hall effect" has been explained as a consequence of a Wigner crystal coexisting with a filled Landau level, a scenario originally termed a partial Hall crystal. In our present work, in contrast with prior reports, the integer states are *less* robust and broad than the 8/3 fractional states.

One possible explanation for the surprising extended FCI region is the formation of a fractional partial Hall crystal.

Future Plans

What ingredients are needed to stabilize the observed FCIs remains an open question. The sample we studied is unusual in having substantial (0.2%) heterostrain between the two twisted layers of graphene, suggesting that this plays a role. We plan to make electrical measurements on strained samples nearer to magic angle, and unstrained samples that, like this one, are far from magic angle. In this sample strain was introduced unintentionally, and in almost all twisted moirés studied worldwide strain is uncontrolled and often inhomogeneous, so we are developing methods to impose controlled and spatially uniform strain. We are also refining techniques we have developed under BES support to spatially map twist angle and strain in such structures. We will also apply complementary techniques, including coupling to microwave resonators, to study electronic states in these samples.

References

1. Joe Finney, Aaron L. Sharpe, Linsey K. Rodenbach, Jian Kang, Xiaoyu Wang, Kenji Watanabe, Takashi Taniguchi, Marc A. Kastner, Oskar Vafek, David Goldhaber-Gordon, *Extended Fractional Chern Insulators Near Half Flux in Twisted Bilayer Graphene Above the Magic Angle*, arXiv:2503.12819 (2025).

Publications

1. M. P. Andersen, L. K. Rodenbach, I. T. Rosen, S. C. Lin, L. Pan, P. Zhang, L. Tai, K. L. Wang, M. A. Kastner, D. Goldhaber-Gordon, *Low-damage electron beam lithography for nanostructures on Bi_2Te_3-class topological insulator thin films*, J. Appl. Phys. **133**, 244301 (2023). Note: this was published near the end of FY23 but was inadvertently omitted from that year's report.

2. M. P. Andersen, E. Mikheev, I. T. Rosen, L. Tai, P. Zhang, K. L. Wang, M. A. Kastner, D. Goldhaber-Gordon, *Universal Conductance Fluctuations in a $MnBi_2Te_4$ Thin Film*, Nano Lett. **23**, 10802–10810 (2023).

3. M. Pendharkar, S. J. Tran, G. Zaborski, J. Finney, A. L. Sharpe, R. V. Kamat, S. S. Kalantre, M. Hocking, N. J. Bittner, K. Watanabe, T. Taniguchi, B. Pittenger, C. J. Newcomb, M. A. Kastner, A. J. Mannix, D. Goldhaber-Gordon, *Torsional force microscopy of van der Waals moirés and atomic lattices*, Proc. Natl. Acad. Sci. **121** (10), e2314083121 (2024).

4. M. Hocking, C. E. Henzinger, S. J. Tran, M. Pendharkar, N. J. Bittner, K. Watanabe, T. Taniguchi, D. Goldhaber-Gordon, A. J. Mannix, *Thermal relaxation of strain and twist in ferroelectric hexagonal boron nitride moiré interfaces*, J. Appl. Phys. **136**, 024303 (2024).

5. I. T. Rosen, C. J. Trimble, M. P. Andersen, E. Mikheev, Y. Li, Y. Liu, L. Tai, P. Zhang, K. L. Wang, Y. Cui, M. A. Kastner, J. R. Williams, D. Goldhaber-Gordon, *Fractional AC Josephson effect in a topological insulator proximitized by a self-formed superconductor*, Phys. Rev. B **110**, 06451 (2024).

6. S. J. Tran, J.-L. Uslu, M. Pendharkar, J. Finney, A. L. Sharpe, M. Hocking, N. J. Bittner, K. Watanabe, T. Taniguchi, M. A. Kastner, A. J. Mannix, D. Goldhaber-Gordon, *Quantitative determination of twist angle and strain in van der Waals moiré superlattices*, Applied Physics Letters **125** (11) 113106 (2024).

7. R. V. Kamat, A. L. Sharpe, M. Pendharkar, D. Goldhaber-Gordon, A. J. Mannix, M. Hocking, J. Hu, S. J. Tran, G. Zaborski, J. Finney, K. Watanabe, T. Taniguchi, M. A. Kastner, T. F. Heinz, *Deterministic fabrication of graphene hexagonal boron nitride moiré superlattices*, Proc. Natl. Acad. Sci. **121** (40), e2410993121 (2024).

8. Z. Zhang, M. Hocking, Z. Peng, M. Pendharkar, E. D. S. Courtney, J. Hu, M. A. Kastner, D. Goldhaber-Gordon, T. F. Heinz, A. J. Mannix. *Phase-Selective Synthesis of Rhombohedral WS_2 Multilayers by Confined-Space Hybrid Metal–Organic Chemical Vapor Deposition*, Nano Lett. 24, 12775–12782 (2024).

9. G. Chen, Y.-H. Zhang, A. Sharpe, Z. Zhang, S. Wang, L. Jiang, B. Lyu, H. Li, K. Watanabe, T. Taniguchi, Z. Shi, D. Goldhaber-Gordon, Y. Zhang, F. Wang, *Magnetic Field-Stabilized Wigner Crystal States in a Graphene Moiré Superlattice*, Nano Lett. **23**, 15, 7023–7028 (2023) Note: Collaborative publication. This was published in FY23 but was inadvertently omitted from that year's report.

10. Z. Zhang, L. Hoang, M. Hocking, Z. Peng, J. Hu, G. Zaborski, P. D. Reddy, J. Dollard, D. Goldhaber-Gordon, T. F. Heinz, E. Pop, A. J. Mannix. *Chemically Tailored Growth of 2D Semiconductors via Hybrid Metal–Organic Chemical Vapor Deposition*, ACS Nano **18**, 25414–25424 (2024). Note: Collaborative publication.

Hetero-orbital two-component fractional quantum Hall effect in bilayer graphene

Jun Zhu, **Department of Physics, Penn State University**

Keywords: fractional quantum Hall effect, 2D system, bilayer graphene

Research Scope

This project explores the emergent phenomena and their collective excitations in the E=0 Landau level octet of Bernal stacked bilayer graphene (BLG), where the interplay and competition among the anisotropy energies corresponding to the spin, valley isospin and orbital components of this multi-component system give rise to the formation of a plethora of many-body states, some of which are unique to this rich platform.

Recent Progress

In prior research, we have shown that the valley isospin in BLG behaves like an SU(2) pseudospin in controlling the formation of fractional quantum Hall states [1]. Supported by this project, we performed edge state scattering experiments to demonstrate that valley isospin remains a good quantum number for the edge states, the scattering of which follows a valley selection rule strictly. The equilibration of edge states in the presence of electron-hole inversed Landau levels, which is unique to BLG, are different from previous 2D systems (Guo et al, manuscript in prep). Spin and pseuspin degrees of freedom contribute additional correlations to enrich many-body phenomena. Electrons in a double layer 2D system conspire to form a two-component quantum

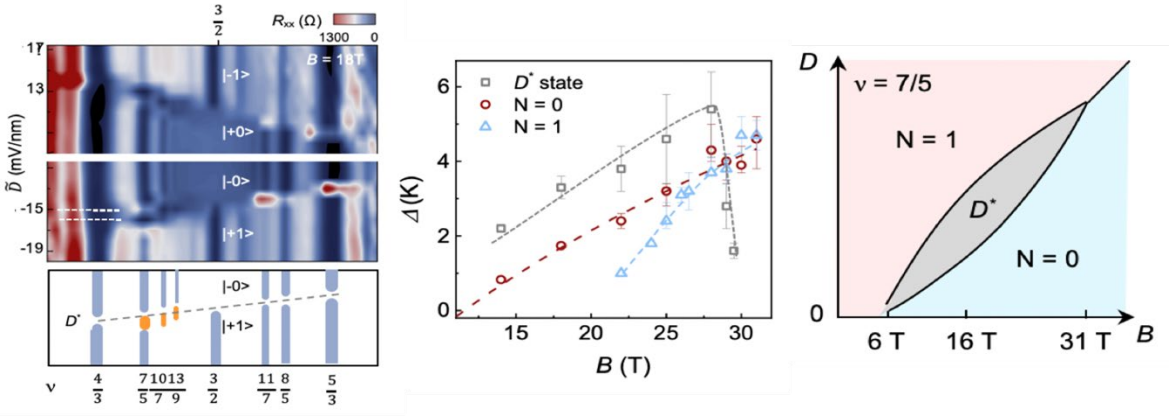


Figure 1: Hetero-orbital two-component fractional quantum Hall states in bilayer graphene. (a) Color map of R_{xx} (D, ν) showing D-field controlled crossing between the $|\pm 0\rangle$ and $|\mp 1\rangle$ Landau levels and the formation of two-component states at the coincidence points at filling factors 7/5, 10/7, 13/9, but not on the other side of 3/2. (b) Energy gaps of the three fractional quantum Hall states at 2/5. The two-component D^* state is the strongest state but disappears at 30 T. (c) The phase diagram of the 7/5 fractional quantum Hall state. From Ref. [2].

Hall ferromagnet described by the Halperin (111) wave function and exhibit fascinating properties of a superfluid. This system is a homo-orbital two-component state, meaning that both layers have the same orbital wave function and intra-layer interactions are SU(2) isotropic. Homo-orbital two-

component states also form in the fractional quantum Hall effect, where the electron spin or valley isospin in BLG is the active SU(2) degrees of freedom. For example, the 2/5 state forms a two-component spin singlet or isospin singlet described by the Halperin (332) wave function in the limit of vanishing spin or valley Zeeman energy. In this talk, I will highlight our recent discovery of a new type of two-component fractional quantum Hall states in BLG, in which the orbital index is part of the pseudospin and the underlying interactions are SU(2) anisotropic [2]. These hetero-orbital two-component states occur at the isospin transition of the $|\pm 0\rangle$ and $|\mp 1\rangle$ electron Landau levels and exhibit properties markedly different from previous homo-orbital two-component FQH states. In particular, we observe strikingly different behaviors for the parallel-flux and reverse-flux composite fermion states, and an anomalously strong two-component 2/5 state over a wide range of magnetic field before it abruptly disappears at a high field. Our findings, combined with detailed theoretical calculations by the Jain group, reveal the surprising robustness of the hetero-orbital FQH effects, significantly enriching our understanding of FQH physics in this novel regime. Other experiments supported by this project have elucidated the nature of the broken-symmetry ground states and charge excitations of the integer Landau levels in BLG (Guo et al, manuscript in prep) and discovered electric field driven topological phase transitions between Chern insulator states in the Hofstadter butterfly spectra of BLG aligned with h-BN (Huang et al, manuscript in prep).

Future Plans

One direction of future experiments will aim to further understand the spontaneously broken valley isospin symmetry at low magnetic field. A second direction will aim to fabricate quantum point contact and interferometer devices to probe the braiding statistics of fractionally charged and non-Abelian quasi-particles in the fractional quantum Hall effect. A third direction will further explore phase transitions between fractional Chern insulator states to illuminate the interplay between Moire and quantum Hall physics.

References

1. K. Huang, H. Fu, D.R. Hickey, N. Alem, X. Lin, K. Watanabe, T. Taniguchi, & J. Zhu, "Valley Isospin Controlled Fractional Quantum Hall States in Bilayer Graphene". *Physical Review X* 12 (3), 031019 (2022)

2. K. Huang, A.C. Balram, H. Fu, C. Guo, K. Watanabe, T. Taniguchi, J.K. Jain, & J. Zhu, "Hetero-Orbital Two-Component Fractional Quantum Hall States in Bilayer Graphene". *Physical Review X* 15 (3), 031023 (2025)

Publications

K. Huang, H. Fu, K. Watanabe, T. Taniguchi, & J. Zhu, "High-Temperature Quantum Valley Hall Effect with Quantized Resistance and a Topological Switch". *Science* 385, 657 (2024)

K. Huang, A.C. Balram, H. Fu, C. Guo, K. Watanabe, T. Taniguchi, J.K. Jain, & J. Zhu, "Hetero-Orbital Two-Component Fractional Quantum Hall States in Bilayer Graphene". *Physical Review X* 15 (3), 031023 (2025)

Symmetry Breaking in Two Dimensional Flat-band Systems for Spin, Charge and Cooper Pair Transport

Chun Ning (Jeanie) Lau

Marc Bockrath

Department of Physics, The Ohio State University, Columbus, OH 43210

Keywords: 2D and layered crystals, superconductivity, quantum Hall, moiré physics, transport

Research Scope

A flat-band electronic system host very slow-moving electrons, and its properties are determined predominantly by electron-electron interactions. This leads to a plethora of many-electron quantum states including superconductivity, magnetism, integer and fractional Chern insulators and charge ordered phases, which are important for quantum technologies. Predicting emergence of these phases in a given system constitutes one of the central challenges in materials science and condensed matter physics.

This program aims at addressing this challenge by exploring, understanding, and engineering these phases in flat band systems, via controlling and tuning the strength of electron-interactions. Material platforms include twisted bilayer graphene (tBLG), twisted few-layer graphene (tFLG), and Bernal-stacked multi-layer graphene.

Specifically, the program consists of three thrusts, investigating superconductivity and correlated insulating states at integer and fractional fillings of the electronic bands. These states' critical temperatures, critical fields, energy gaps, entropy, and spin and charge configurations will be examined via low temperature quantum transport measurements. Transport measurements will be performed while tuning a large number of experimental "knobs," including twist angle, dielectric constant, distance to nearby gates, charge density, perpendicular displacement field, bias, temperature, and in-plane and perpendicular magnetic fields.

Overall, we aim to uncover the qualitative and quantitative dependence of various correlated phases on the strength and range of interactions in addition to the hierarchy of competing symmetries and the ensuing ground states. Such knowledge will aid the distillation of general design principles and accurate prediction of emergent phases with relevance for quantum information sciences and novel nanoelectronics.

Recent Progress

Dominant 1/3-filling Correlated Insulator States and Orbital Geometric Frustration in tBLG

Geometric frustration is a phenomenon in a lattice system where not all interactions can be satisfied, the simplest example being antiferromagnetically coupled spins on a triangular lattice. Frustrated

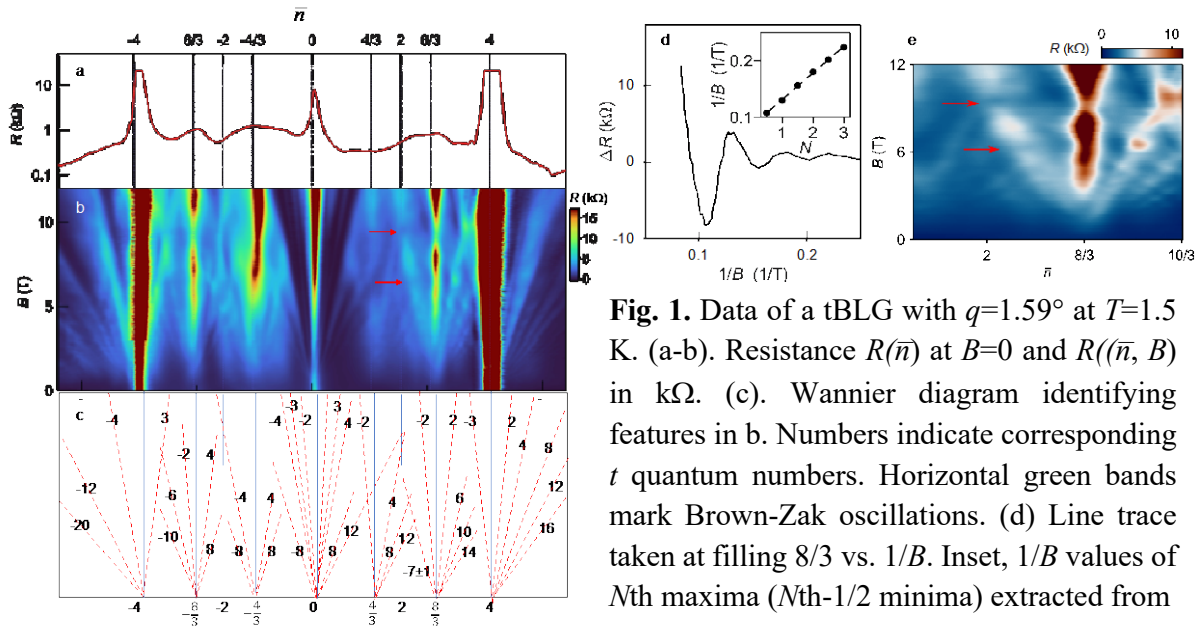


Fig. 1. Data of a tBLG with q=1.59° at T=1.5 K. (a-b). Resistance $R(\bar{n})$ at B=0 and $R((\bar{n}, B)$ in kΩ. (c). Wannier diagram identifying features in b. Numbers indicate corresponding t quantum numbers. Horizontal green bands mark Brown-Zak oscillations. (d) Line trace taken at filling 8/3 vs. 1/B. Inset, 1/B values of Nth maxima (Nth-1/2 minima) extracted from main panel. The slope of the fitted line yields the period in 1/B. (e) Zoom-in plot of region in (b) near $\bar{n}$=8/3, showing the density-independent minima in resistance in Brown-Zak bands.

systems are characterized by their many nearly degenerate ground states, leading to non-trivial phases such as spin ice and spin liquids. To date most studies are on geometric frustration of spins; much less explored is orbital geometric frustration. For electrons in tBLG at denominator-3 fractional filling, Coulomb interactions and the Wannier orbital shapes are predicted to strongly constrain spatial charge ordering, leading to geometrically frustrated ground states that produce a new class of correlated insulators. In this work, we report the observation of dominant denominator-3 fractional filling insulating states in large angle tBLG; these states persist in magnetic fields and display magnetic ordering signatures and tripled unit cell reconstruction (Fig. 3). These results are in agreement with a strong-coupling theory of symmetry-breaking of geometrically frustrated fractional states. This work was published by *Nature Physics*[2] (https://www.nature.com/articles/s41567-024-02546-5).

Half-integer Quantum Hall States in Thin Graphite

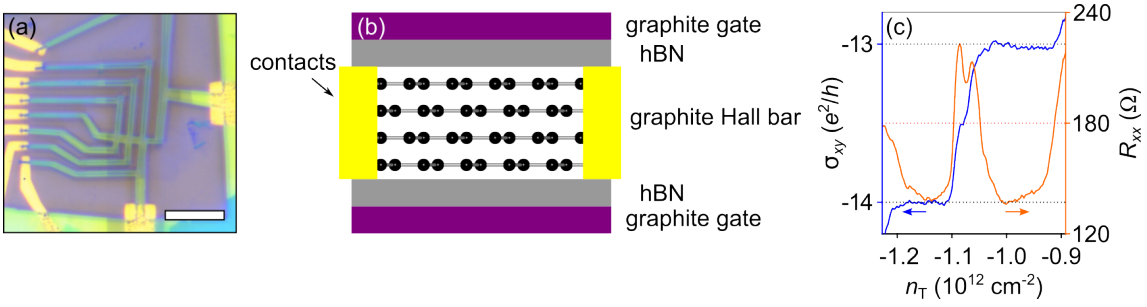


Fig. 2. (a) Optical image of completed device. Scale bar 10μm. (b) Device schematic showing the layer stacking. (c) Right axis: R_{xx} vs. density on the top layer, showing a dip at half-filling

Nonabelian fractionalized quasiparticles in half-integer QH states have been proposed as a platform for the realization of topologically protected fault-tolerant qubits. In our work, we observe half-integer QH states up to remarkably large Landau level filling factors larger than 30 in dual-gated ~3-10 nm-thick graphite devices (Fig. 5). We identify most as single-component states stabilized by fractional correlations in exterior bilayers. Multi-component (3,3,1) states with strong correlations between opposite-valley states on opposite sides of the graphite interior also appear. The facile integration of graphite with top and bottom surface gates makes thin film graphite an attractive platform to explore the physics of non-abelian fractionalized quasiparticles. This work was recently published by *Physical Review Letters* [3].

Tuning Superconductivity in situ and Evidence for Unconventional Superconducting Pairing Mechanism in tBLG

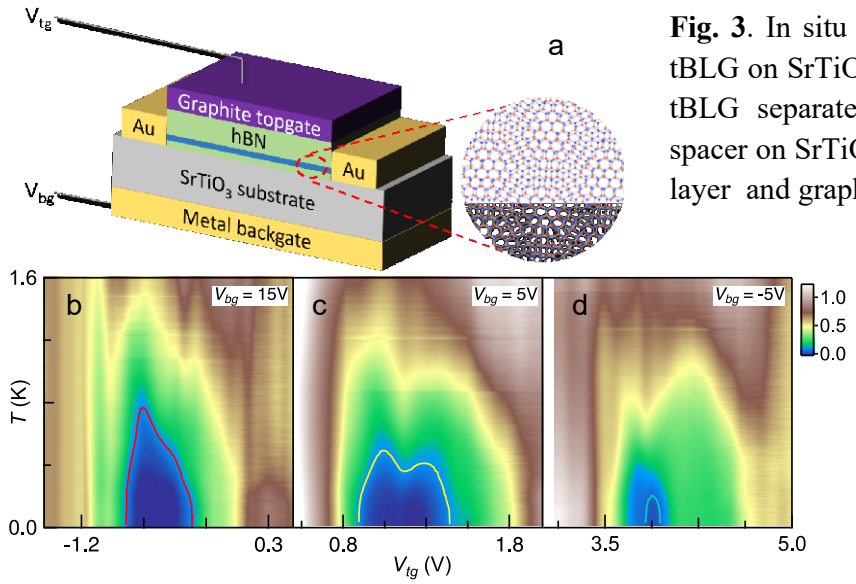


Fig. 3. In situ tuning superconductivity in tBLG on $SrTiO_3$. (a). Device schematics of tBLG separated by a thin (3 nm) hBN spacer on $SrTiO_3$, and a thick (30 nm) hBN layer and graphite serve as the top gate. (b-d). Data from a device with twist angle θ=1.05°, showing normalized resistance R_{xx}/R_N vs V_{tg} and T at V_{bg}=15, 5, and -5V, respectively. The solid lines outline the superconducting dome.

In conventional superconductors, the formation of Cooper pairs is mediated by phonons. For the superconducting phases in moiré materials such as that in tBLG, the pairing mechanism has been intensely debated. While theories indicate that electronic interactions can induce pair formation, prior experiments appear to suggest conventional phonon-mediated pairing. In this work, by performing transport studies on a substrate with an effective dielectric constant ε_r that is tunable in situ, we observe suppression of superconductivity with increasing ε_r, thus providing strong evidence that the pairing mechanism in superconducting tBLG is driven by electronic interactions (Fig. 6). The experimental results are in qualitative agreement with a theoretical model in which the pairing mechanism arises from Coulomb interactions that are screened by plasmons, electron-hole pairs, and longitudinal acoustic phonons. Our results highlight the unconventional nature of the superconductivity in tBLG, the important role played by electronic interactions in its formation, as well as their complex interplay with the correlated insulating states. This work is currently under review at *Nature Physics*, and a preprint is available at https://arxiv.org/abs/2412.01578.

Future Plans

Following the general direction outlined in the first section, our immediate plans for the next year include investigation of

- tuning superconductivity via dielectric screening in twisted bilayer and trilayer graphene
- correlated insulating states in graphene-based moiré systems at fractional fillings
- fractional quantum Hall states in Bernal-stacked few-layer graphene

List of 2-year Publications

1. "Evidence for Dirac flat band superconductivity enabled by quantum geometry," H. Tian, X. Gao, Y. Zhang, S. Che, T. Xu, P. Cheung, K. Watanabe, T. Taniguchi, M. Randeria, F. Zhang, C. N. Lau, and M. W. Bockrath, Nature 614, 440 (2023).
(https://www.nature.com/articles/s41586-022-05576-2)

2. "Dominant 1/3-filling correlated insulator states and orbital geometric frustration in twisted bilayer graphene," H. Tian, E. Codecido, D. Mao, K. Zhang, S. Che, K. Watanabe, T. Taniguchi, D. Smirnov, E.-A. Kim, M. Bockrath, and C. N. Lau, *Nature Physics* 20, 1407 (2024).
https://www.nature.com/articles/s41567-024-02546-5)

3. "Half-Integer Quantum Hall States in Two-Dimensional Graphite", N. Mazzucca, B. M. Kousa, K. Watanabe, T. Taniguchi, A. H. MacDonald, and M. W. Bockrath, Half-Integer Quantum Hall States in Two-Dimensional Graphite, *Phys. Rev. Lett.* **134,** 176302 (2025).

https://journals.aps.org/prl/abstract/10.1103/PhysRevLett.134.176302

4. "Double-edged Role of Interactions in Superconducting Twisted Bilayer Graphene," X. Gao, A. Jimeno-Pozo, P. A. Pantaleon, E. Codecido, D. L. Sharifi, Z. Zhang, Y. Liu, K. Watanabe, T. Taniguchi, M. W. Bockrath, F. Guinea, and C. N. Lau, , *Nature Physics*, under review (2024). A preprint is available at ttps://arxiv.org/abs/2412.01578.

5. "Quantum octets in high mobility pentagonal two-dimensional $PdSe_2$," Y. Zhang, H. Tian, H. Li, C. Yoon, R. A. Nelson, Z. Li, K. Watanabe, T. Taniguchi, D. Smirnov, R. K. Kawakami, J. E. Goldberger, F. Zhang, and C. N. Lau, *Nature Communications* 15, 761 (2024).

https://www.nature.com/articles/s41467-024-44972-2

Probing electronic and topological properties in 2D atomic crystals and their heterostuctures

Eva Y. Andrei, **Department of Physics and Astronomy, Rutgers, the State University of NJ**

Keywords: 2D and layered crystals, nanostructures, superconductivity, graphene, transport

Research Scope We study atomically thin crystals and their heterostructures using scanning tunneling microscopy and spectroscopy (STM, STS), planar tunneling, entropy and compressibility spectroscopy, transport and magneto-transport. In parallel we design and construct novel scanning probe instruments that enable characterization, manipulation and tuning of moiré heterostructures at low temperature and high magnetic fields.

Recent Progress

Quantum criticality and tunable Griffiths phase in superconducting twisted trilayer graphene. arXiv:2507.10687, 2025 ***Nature Physics – under review***

When dimensionality is reduced, enhanced quantum fluctuations can destroy long-range phase coherence, driving a superconductor–insulator transition (SIT), where disorder and electronic correlations give rise to novel many-body states. In this work we reported the first observation of a magnetic field–tuned SIT in mirror-symmetric twisted trilayer graphene (TTG). Remarkably, signatures of quantum criticality persist over an exceptionally broad range of magnetic fields and are well described by the formation of a quantum Griffiths phase, a regime in which rare spatially extended regions develop local order within a globally disordered phase. This leads to a quantum phase transition governed by an infinite-randomness fixed point and characterized by ultraslow relaxation dynamics. Near the quantum critical region, transport measurements reveal strongly nonlinear electrical behavior, including a current-BKTdriven reentrant transition from insulating to superconducting transport, providing direct evidence of local superconducting order. By tilting the magnetic field, we are able to collapse the broad Griffiths regime into a single quantum critical point (QCP), demonstrating a striking level of control over disorder-induced quantum dynamics. Our results further show that TTG strongly violates the Pauli limit with the in-plane critical field exceeds the Pauli limit by 300% - suggesting an unconventional pairing mechanism and triplet

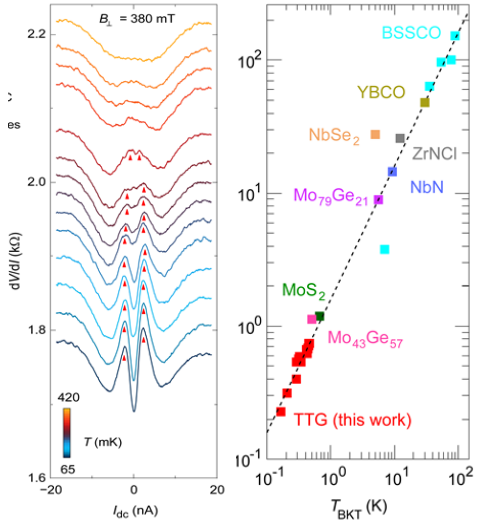


Figure 1. Left: Current driven SIT. Temperature dependence of the $\mathrm{d}V/\mathrm{d}I$ spectra at $B_\perp = 380$ mT. Right: Activation energy as a function of T_{BKT} for 2D superconductors shows that TTG has one of the lowest pinning barriers.

superconductivity. Moreover we showed that TTG has an ultralow vortex pinning barrier establishing it as one of the cleanest superconductor known.

- **Revealing Combinatorial Degeneracy, Local Moment Formation, and Heavy Fermion Mass Renormalization in Magic-Angle Graphene via Entropy and Compressibility Spectroscopy.** ***Nature - under review***

Heavy fermion behavior, where electron masses are strongly enhanced by interactions, gives rise to exotic quantum phenomena such as unconventional superconductivity and quantum criticality [1]. While traditionally associated with chemically complex, three-dimensional materials containing *f*-electron elements[2], such behavior was recently predicted in the flat bands of magic-angle twisted bilayer graphene (MATBG), a clean, carbon-based two-dimensional system [3-7]. However, experimental confirmation has remained elusive. By using high-resolution planar tunneling spectroscopy to obtain the temperature and filing dependence of the inverse compressibility and entropy of MATBG, we uncovered compelling evidence for topological heavy fermion behavior in MATBG. The entropy spectroscopy revealed plateau structures consistent with local moment formation and a striking pattern of combinatorial degeneracy. In parallel, compressibility data showed strong renormalization of the electronic mass, pointing to the interplay between localized and itinerant electrons. Our results provide the first experimental realization of a heavy fermion system with nontrivial topology, going beyond the conventional topologically trivial f-electron systems. Clear evidence of mass enhancement is observed, due to strong correlations, consistent with hybridization between localized and itinerant electrons in a Kondo lattice framework. The observed 4/8 combinatorial degeneracy transition in local moments presents a new type of entropic effect in Kondo systems, suggesting a novel route for moment screening and symmetry breaking in topological correlated systems.

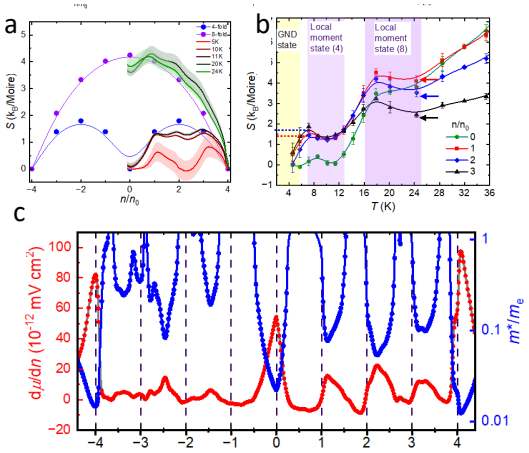


Figure 2. a) Filling and temperature dependence of electronic entropy. Blue and purple dots are calculated by counting all possible microstates with degeneracy of 4 and 8, respectively. b) Temperature dependence of entropy at non-zero integer fillings Two plateaus are observed near 10 K and 20 K. Arrows indicate the theoretical 8-microstate entropy for filling 1(red) 2 (blue) 3 (black). Dotted lines mark the 4-microstate entropy for filling 1,3(red) and 2 (blue). c) Inverse compressibility and effective as a function of measured at 4 K reveals the light to heavy mass transition near each integer filling.

- **Moiré Periodic and Quasiperiodic Crystals in Heterostructures of Twisted Bilayer Graphene and Hexagonal Boron Nitride**, ***Nature Materials 24, 1019–1026 (2025)***

Stacking two atomic crystals with a twist between their crystal axes produces moiré potentials that modify the electronic properties. In this work we discovered that double moiré potentials generated by

superposing three atomic crystals create a new class of tunable quasiperiodic structures that alter the symmetry and spatial distribution of the electronic wavefunctions in new and interesting ways. By using scanning tunneling microscopy and spectroscopy to study twisted bilayer graphene on hexagonal boron nitride (hBN), we unveiled a moiré phase diagram defined by the lattice constants of the two moiré lattices (graphene-on-graphene and graphene-on-hBN), comprising both commensurate periodic and incommensurate quasiperiodic crystals. Remarkably, the 1:1 commensurate crystal, which should theoretically exist at only one point on this phase diagram, is observed over a wide range, demonstrating an unexpected self-alignment mechanism. The incommensurate crystals include quasicrystals, which are quasiperiodic and feature a Bravais-forbidden dodecagonal symmetry, and previously unclassified structures, **intercrystals**, which are also quasiperiodic but lack forbidden symmetries. The intercrystals reveal intricate band structures with well defined flat bands that develop correlation induced gaps when tuned to the Fermi level. This rich variety of tunable double moiré structures offers a synthetic platform for exploring the unique electronic properties of quasiperiodic crystals, which are rarely found in nature.

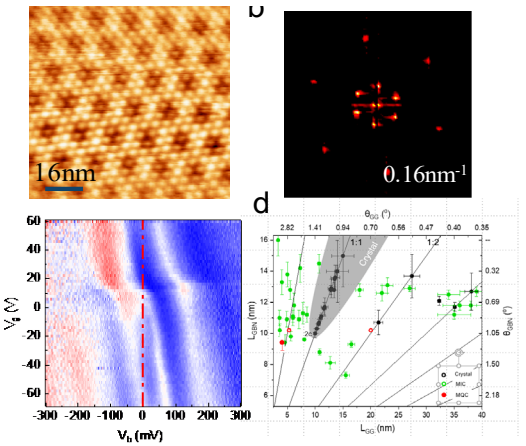


Figure 3. a,b) STM topography and FFT of a moiré intercrystal. c) STS of intercrystal showing flat band and its splitting when Fermi level is aligned with it. d) Phase diagram classifying the double moiré crystals (black), intercrystals (green) and quasicrystals (red) as a function of twist angles and lattice spacing.

- **Proximity Induced Charge Density Wave in a Graphene/TaS2 Heterostructure.** ***Nature Communications 15, 8056 (2024)***

- The proximity effect, whereby materials in contact appropriate each other's electronic-properties, is widely used to induce correlated states, such as superconductivity or magnetism, at heterostructure interfaces. Thus far however, demonstrating the existence of proximity induced charge-density-waves (PI-CDW) proved challenging. This is due to competing-effects, such as screening or co-tunneling into the parent-material, that obscured its presence. Here we report the observation of a PI-CDW in a graphene layer contacted by a 1T-TaS2 substrate. Using scanning-tunneling-microscopy (STM) and spectroscopy (STS) together with theoretical-modeling, we show that the coexistence of a CDW with a Mott-gap in 1T-TaS2 coupled with the Dirac-dispersion of electrons in graphene, makes it possible to unambiguously demonstrate the PI-CDW by ruling out alternative interpretations. Furthermore, we find that the PI-CDW is accompanied by a reduction of the Mott

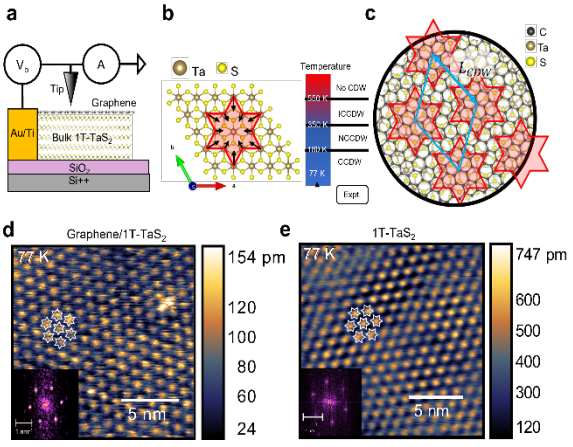
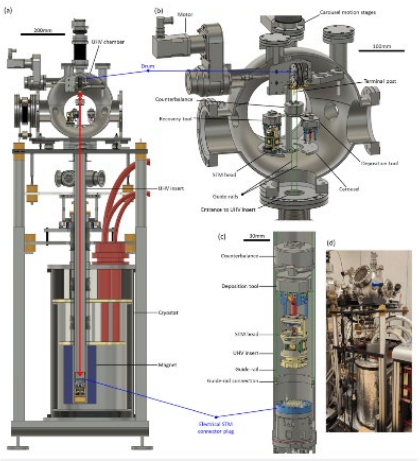


Figure 4. (a) Schematics of measurement setup. (b, left) Star-of-David (red) in TaS2. (b,right) CDW phases of TaS_2 as a function of temperature. (c) Schematics of graphene on TaS2. (d) STM topography and its 2D FFT(inset) showing proximity induced CDW in graphene. (e) STM topography and its 2D FFT(inset) of bulk TaS_2

gap in 1T-TaS2 and show that the mechanism underlying the PI-CDW is well-described by short-range exchange-interactions that are distinctly different from previously observed proximity effects.

- **Flexible internal transporter with gravity-assisted mechanism for vertical transfer of microscope head, *Rev. Sci. Instrum.* 96, 053701 (2025)**

We designed and constructed a flexible mechanism for vertically transferring scanning probe microscope (SPM) heads in ultra-high vacuum. The microscope head is transferred from a room temperature site down to an SPM pluggable connector at low temperatures within the bore of a superconducting magnet located in a top-loading cryostat. Insertion and extraction of the microscope head to and from the connector are accomplished with gravity-assisted tools. Contrasted with typical rigid designs, the low-profile mechanism described here has no external mounting structure, which reduces sensitivity to mechanical disturbances, decreases vacuum volume, and enables installation in standard laboratory spaces.



(a) Schematic of vacuum chamber and UHV insert assembly shown installed in a top-loading cryogen-free cryostat. (b) Vacuum chamber setup depicting winch-based pulley mechanism and the carousel holding the STM head and deposition and recovery tools. (c) Bottom of the UHV insert displaying the STM electrical connector plug located at LT. (d) Photograph of the assembly showing the vacuum chamber, UHV insert, and cryostat

- **Cryogen-free modular scanning tunneling microscope operating at 4-K in high magnetic field on a compact ultra-high vacuum platform. *Review of Scientific Instruments 95, 083702 (2024)***
- **Quick-connect scanning tunneling microscope head with nested piezoelectric coarse walkers. *Review of Scientific Instruments 95, 073703 (2024)***
- Completed the construction of a sorption pump based 300mK STM system, now undergoing final tests.

Future Plans

The symmetry of the superconducting wave function in graphene and twisted transition metal dichalcogenide heterostructures is one of the most intriguing outstanding questions in the field of twistronics. It is crucial for understanding the mechanism of superconductivity in moiré systems and for paving the way toward the design of high temperature superconductors. To address this question we will use a variety of twisted van der Waals materials including PtSe2, PdTe films, and other exfoliable TMDs proposed by our theory collaborators. The samples will be studied with several experimental setups. i) a home built 300mK STM which is in the final stages of testing. We will use superconducting tips to enhance sensitivity so as to enable us to observe Andreev bound states and the shape of the superconducting gap. ii) Planar tunneling geometry with a

superconducting top electrode acting as a tip. The advantage of the setup is insensitivity to vibrations making it possible to use an existing dilution refrigerator equipped with a large magnetic field. Dilution refrigerator transport setup with high magnetic field.

Publications

1. Quantum criticality and tunable Griffiths phase in superconducting twisted trilayer graphene, Phanibhusan S. Mahapatra, Haining Pan, Kenji Watanabe, Takashi Taniguchi, J. H. Pixley, Eva Y. Andrei, arXiv:2507.10687, 2025 **Nature Physics – under review**
2. Revealing Combinatorial Degeneracy, Local Moment Formation, and Heavy Fermion Mass Renormalization in Magic-Angle Graphene via Entropy and Compressibility Spectroscopy, Zhenyuan Zhang, Shuang Wu, Dumitru Călugăru, Haoyu Hu, Takashi Taniguchi, Kenji Wanatabe, Andrei B Bernevig, Eva Y Andrei, arXiv:2503.17875 (2025) **Nature – under review**)
3. Moiré periodic and quasiperiodic crystals in heterostructures of twisted bilayer graphene on hexagonal boron nitride, Lai, X.; Li, G.; Coe, A. M.; Pixley, J. H.; Watanabe, K.; Taniguchi, T.; Eva Y. Andrei, ***Nature Materials 24, 1019–1026 (2025)***.
4. Flexible internal transporter with gravity-assisted mechanism for vertical transfer of microscope head, Angela M. Coe, Guohong Li, Eva Y. Andrei, **Rev. Sci. Instrum** 95, 083702 (2025)
5. Twisted 2D materials –a new era in condensed matter physics, Eva Y. Andrei, **Europhysics News** 55/4 (2024) 11.
6. Proximity induced charge density wave in a graphene/1T-TaS2 heterostructure, Nikhil Tilak, Michael Altvater, Sheng-Hsiung Hung, Choong-Jae Won, Guohong Li, Taha Kaleem, Sang-Wook Cheong, Chung-Hou Chung, Horng-Tay Jeng, Eva Y. Andrei, **Nature Communications** | (2024)15:8056
7. Cryogen-free modular scanning tunneling microscope operating at 4-K in high magnetic field on a compact ultrahigh vacuum platform, Angela M. Coe, Guohong Li, Eva Y. Andrei, **Rev. Sci. Instrum**. 95, 083702 (2024)
8. Quick-connect scanning tunneling microscope head with nested piezoelectric coarse walkers, Angela M. Coe, Guohong Li, Eva Y. Andrei, **Rev. Sci. Instrum**. 95, 073703 (2024)

Publications with collaborators

9. Vacancy-Induced Tunable Kondo Effect in Twisted Bilayer Graphene, Yueqing Chang, Jinjing Yi, Ang-Kun Wu, Fabian B. Kugler, Eva Y. Andrei, David Vanderbilt, Gabriel Kotliar, J. H. Pixley, **Phys. Rev. Lett.** 133, 126503 (2024)
10. Kelvin Probe Force Microscopy Imaging of Plasticity in Hydrogenated Perovskite Nickelate Multilevel Neuromorphic Devices, Tamal Dey, Xinyuan Lai, Sukriti Manna, Karan Patel, Ranjan Kumar Patel, Ravindra Singh Bisht, Yue Zhou, Shaan Shah, Eva Y Andrei, Subramanian KRS Sankaranarayanan, Duygu Kuzum, Catherine Schuman, Shriram Ramanathan, **ACS Nano** 19, 6815 (2025)

Patents

1. DAMPING BASE FOR MODULAR SCANNING PROBE MICROSCOPE HEAD Patent No. 12,360,136 within United States on 7/15/2025, Inventors: Angela Coe, LI Guohong, Eva Y Andrei,
2. Low profile transfer mechanism for controlled environment. US Patent number 12098026 Publication date 2024/9/24 Inventors: Angela Coe, LI Guohong, Eva Y Andrei,

Quantum Point Contact and Shot Noise in Monolayer Graphene

Sangwoo Sim, Nicholas P. Quirk, Yue Tang, Sanfeng Wu, and N. P. Ong

Keywords: Quantum Hall Edge Modes, Graphene, Shot Noise, Point Contact

Research Scope

Quantum shot-noise is produced when chiral edge modes are funneled through a very small gap in the mountain-pass potential topography created at a quantum point contact (QPC). Although the shot noise spectrum is flat to very high frequencies f, it is usually measured at an RF frequency (1 MHz) high enough to evade the ubiquitous $1/f$ noise. The shot-noise power is reported as the power spectral density $S(\omega)$ where $\omega = 2\pi f$. Using a tank circuit, we measured $S(\omega)$ in Quantum Hall (QH) states in monolayer graphene at 300 mK. Theoretically, $S(\omega)$ is proportional to the current-current correlation function $\langle \Delta I \Delta I \rangle$ which yields potentially incisive information on the charge of the carriers e^* and their quantum statistics.

Recent Progress

Although shot noise has been applied to the 2D electron gas in GaAs heterostructures since 1996, no shot-noise results have been published in graphene (aside from ours, 2 other groups have made progress). The QH states in graphene are far richer than in GaAs. Moreover, one can tune *in situ* the chemical potential μ by the back-gate voltage V_b as well as the height of the mountain-pass QPC barrier by the split-gate voltage V_{sg}. Thirdly, the potential walls are much steeper than those in GaAs (where the 2D gas is buried 100 nm deep). To begin, we determined the transmission map at 300 mK by measuring the QH conductance produced by modes transmitted through the QPC (Fig. 1). We tune μ to bring the QH state with filling $\nu = 2$ into approximate alignment with the QPC potential barrier. In the $\nu = 2$ state, 2 chiral edge modes flow in the bulk of the film. By tuning the QPC barrier we control the number of modes transmitted (0, 1 or 2) (Fig. 1 right panel). We also vary the bias current I. The noise power $S(\omega)$ is measured vs. V_{sg} (lower panel). Generally, $S(\omega)$ peaks sharply when the QPC switches between mode transmission number.

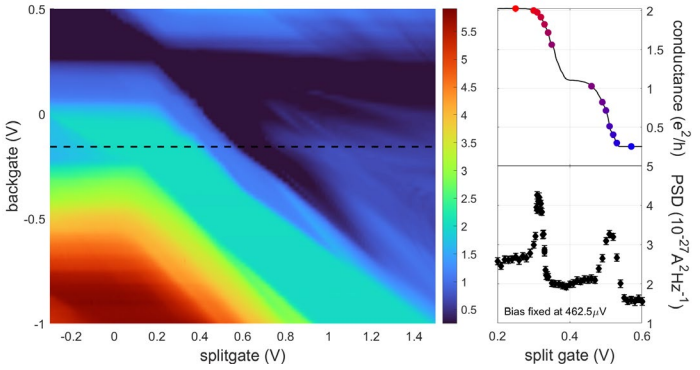


Figure 1 The transmission map of a QPC on monolayer graphene measured at 0.3 K and $B = 13$ T. The color scale is the QH conductance. The Hall conductance G shows step decreases vs. V_{sg} (upper right panel). The lower panel shows $S(\omega)$ vs. V_{sg}. Shot-noise power peaks when the transmitted mode numbers changes (0 to 1, 1 to 2).

With one mode the noise power $S(\omega)$ plotted versus bias current I follows the Landauer-Buttiker equation with $e^* = 1$ ("orthodox behavior"). However, when both modes are transmitted the profile of $S(\omega)$ is anomalous, displaying a "gap" profile very different from the orthodox behavior. This may arise from strong Coulomb repulsion between two modes forced into proximity at the QPC.

Future Plans

We plan to investigate how the anomalous noise spectrum density may be altered by widening the QPC width (now 25 nm). This will test if the Coulomb repulsion idea is valid. We also plan to improve our contact resistance and quality of the graphene film to extract finer features. Our overarching goal is to use quantum shot noise to measure the quantum statistics of carriers in "anyon collider" experiments.

Reference

Sangwoo Sim, Nicholas P. Quirk, Yue Tang, Sanfeng Wu, N. P. Ong, *in preparation*.

Publications

1) Tiancheng Song, Yanyu Jia, Guo Yu, Yue Tang, Pengjie Wang, Ratnadwip Singha, Xin Gui, Ayelet J. Uzan, Michael Onyszczak, Kenji Watanabe, Takashi Taniguchi, Robert J. Cava, Leslie M. Schoop, N. P. Ong, Sanfeng Wu, Unconventional Superconducting Quantum Criticality in Monolayer WTe2, Nature Physics 20, 269 – 274 (2024). DOI: 10.1038/s41567-023-02291-1

2) Stephan Kim, Shiming Lei, Leslie M. Schoop, R. J. Cava and N. P. Ong, "Edge supercurrent reveals competition between condensates in a Weyl superconductor" Nature Physics 20, 261—268 (2024). DOI: 10.1038/s41567-023-02316-9

3) Sanfeng Wu, Leslie M. Schoop, Inti Sodemann, Roderich Moessner, Robert J. Cava & N. P. Ong, Charge-neutral electronic excitations in quantum insulators, Nature 635, 301 (2024). doi.org/10.1038/s41586-024-08091-8

4) Yanyu Jia, Tiancheng Song, Ayelet J Uzan, Guo Yu, Yue Tang, Connor J. Pollak, Michael Onyszczak, Zhaoyi Joy Zheng, Kenji Watanabe, Takashi Taniguchi, Shiming Lei, Leslie M Schoop, N. P. Ong, Sanfeng Wu, Unconventional Superconductivity in Twisted MoTe2 nanojunctions, Sci. Adv. 11, eadq5712 (2025).

5) Tiancheng Song, Yanyu Jia, Guo Yu, Yue Tang, Pengjie Wang, Ratnadwip Singha, Xin Gui, Ayelet J. Uzan, Michael Onyszczak, Kenji Watanabe, Takashi Taniguchi, Robert J. Cava, Leslie M. Schoop, N. P. Ong, Sanfeng Wu, Unconventional Superconducting Quantum Criticality in Monolayer WTe2, Nature Physics 20, 269 – 274 (2024). DOI: 10.1038/s41567-023-02291-1

6) Tiancheng Song et al., Unconventional superconducting phase diagram of monolayerWTe2, Phys. Rev. Res. 7, 013224 (2025), DOI: 10.1103/PhysRevResearch.7.013224

7) Jiayi Hu, Ruidan Zhong, Peter Czajka, Tong Gao, R. J Cava, and N. P. Ong, Scaling behavior and giant field-enhancement of the thermal conductivity in the honeycomb antiferromagnet BaCo2(AsO4)2 . PHYSICAL REVIEW MATERIALS 9, L061401 (2025), DOI: 10.1103/6gbq-d7jk

Charge, Spin, and Thermal Transport in Nanostructured Quantum Materials: Quantum Coherence of Heavy Fermion Quasiparticles

Douglas Natelson, **Rice University**

Keywords: quasiparticles & collective excitations; fractionalization; quantum interference effects; heavy fermion systems; Mott insulators

Research Scope

This research program concentrates on nanostructure-based experiments that probe the emergent excitations in correlated quantum materials. The nanofabrication and nanoscale measurement techniques originally developed for semiconductor devices make possible measurements that can address the nontrivial charge, spin, and energy-carrying excitations in quantum materials. Current research this past year is examining three outstanding physics questions: (i) What is the nature of current-carrying excitations in "strange metals", systems that have temperature-dependent transport and thermodynamic properties that are anomalous compared to the predictions of Fermi Liquid theory? (ii) In Fermi Liquid (FL) phases that appear in strongly correlated materials like heavy fermion Kondo lattice compounds, do the emergent quasiparticles act as expected? (iii) In correlated insulators (specifically VO_2 and V_2O_3), what excitations transport angular momentum?

Regarding strange metals, we are embarking on a three-pronged campaign to better examine these systems. In $YbRh_2Si_2$ (with Prof. Silke Buehler-Paschen at TU Vienna), the system in which we have previously demonstrated a suppression of shot noise in sub-micron length nanowires[1], we have fabricated new devices from newly grown epitaxial films of improved quality, including sections of a film demonstrated by our collaborators to exhibit the characteristic Néel ordering transition at ~ 70 mK. In longer nanowires, we are performing careful studies of magnetotransport as a function of temperature and magnetic field down to dilution refrigerator conditions, to use the appearance (or lack thereof) of any mesoscopic corrections to classical conduction (e.g. weak antilocalization [WAL] and universal conductance fluctuations [UCF]) to set limits on the coherence of any possible current carrying quasiparticles, across the strange metal phase diagram of this material. We are also preparing short wires for noise measurements in a dilution refrigerator in Vienna; optimizing the device design for much lower temperatures than those previously explored requires much larger contact pads for appropriate thermal sinking of the electrons[2]. Second, we are collaborating with the group of Prof. Yonglong Xie and performing initial measurements on twisted bilayer graphene devices thought to exhibit strange metallicity in certain parts of their charge density/displacement field phase diagram. Third, we are working on magnetotransport and noise measurements in heavy fermion materials that are thought to host FLs, for comparison with strange metals. Starting with films from Cornell (Kyle Shen), we have been measuring magnetotransport and noise in wires made from $YbAl_3$, a mixed valence heavy fermion metal, as discussed below. With collaborators at LANL (Filip Ronning) and Cornell (Kyle Shen)

on measurements to be done with $CeCoIn_5$, another heavy fermion system with strange metal phenomenology as well as indications of "hidden" FL response[3].

In terms of spin transport and spin caloritronics, recent efforts in collaboration with UC San Diego (Ivan Schuller) have focused on VO_2, a candidate spin Peierls insulator, and V_2O_3, an antiferromagnet long viewed as a Mott insulator. In the longer run, the plan is to examine spin transport in $ErFeO_3$, a rare earth orthoferrite in which there are THz experiments that are interpreted to argue for spontaneous strong coupling (and a superradiant transition) between Er moments and the Fe magnons at low temperatures.

A longer-term project is to examine the thermal Hall effect in correlated materials such as insulating quantum magnets. Initial demonstration experiments will involve test materials like $SrTiO_3$, known to exhibit a phonon-based thermal Hall response A postdoc with experience in such measurements is joining the group this fall with partial DOE award support who can help jumpstart this effort.

Recent Progress

We have fabricated nanowires from films of $YbAl_3$, a mixed valence metal with a single-ion Kondo temperature of about 670 K. The system is believed to assume a heavy Fermi liquid ground state below a coherence temperature $T^* \approx 37$ K, based on the onset of resistivity scaling $\rho = \rho_0 + AT^2$ below T^*. This material is an opportunity to test for other signatures of the onset of coherent FL quasiparticles.

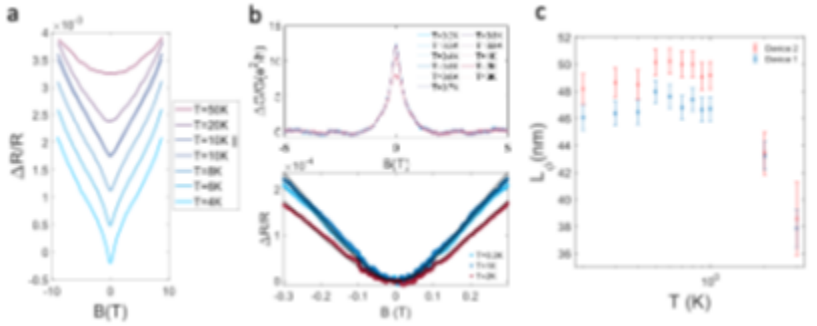


Figure 1. Measuring coherent quasiparticles in mesoscopic $YbAl_3$ heavy fermion wires. (a) Field-out-of-plane MR at different temperatures. (b) WAL and UCF in the magnetoconductance. (c) *T*-dependence of coherence lengths from WAL in two different wires.

In 30 μm long, 150 nm wide, 20 nm thick (15 nm $YbAl_3$, 5 nm $LuAl_3$) wires, below the coherence temperature we find a linear-in-*B* magnetoresistance (MR) background for *B* perpendicular to the plane of the nanowires. We observe the onset of a clear WAL magnetoresistance (negative magnetoconductance) that grows as *T* is further decreased. At larger fields we observe sample-specific conductance fluctuations that retrace as *B* is swept back and forth. These are consistent with universal conductance fluctuations (UCF). Both WAL and UCF are hallmarks of coherent quasiparticles, and to our knowledge this is the first observation of such mesoscopic quantum interference corrections to semiclassical conduction in a heavy fermion metal. Fitting the WAL MR to the expected quasi-2D functional form, we infer a coherence length $L_\phi \sim 50$ nm for the quasiparticles, with a saturation at low temperatures. Analysis of the magnetic field correlation scale for the UCF also finds $L_\phi \sim 50$ nm, adding consistency to this conclusion.

These experiments demonstrate that the mesoscopics "toolkit" can be applied to access coherence phenomena in correlated quantum conductors.

The plan had been to perform shot noise measurements in the $YbAl_3$ nanowires, but first it is necessary to assess the strength of electron-phonon scattering in this material, since rapid energy loss from the electrons to the lattice suppresses shot noise. We measured Johnson-Nyquist noise as a function of bias current in 30 μm long $YbAl_3$ wires and analyzed the data in terms of a simple 1D model[2] successfully used to characterize electron-phonon scattering in Au and $YbRh_2Si_2$. The inferred electron-phonon scattering coefficient Γ is large and strongly temperature dependent, growing as T is decreased. This is unusual and happens over the same temperature range in which the thermal expansion coefficient of $YbAl_3$ is known to be negative and strongly temperature dependent[4]. Strong electron-phonon interactions are expected based on the known thermoelectric properties of $YbAl_3$, but growth of Γ at low temperatures is surprising. In collaboration with theorists (Ruiwen Xie, Hongbin Zhang, TU Darmstadt), an analysis using density matrix renormalization group (DMRG) shows that this is a consequence of the evolving 4*f* electron hybridization even well below T^*. This work has been submitted for publication.

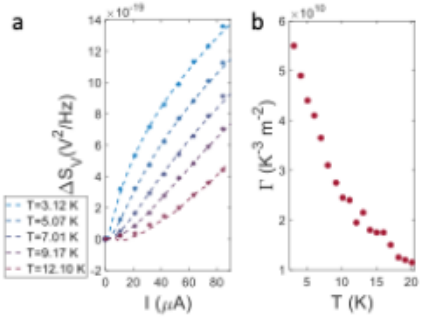


Figure 2. Noise and T-dependent electron-phonon coupling in $YbAl_3$. (a) Johnson-Nyquist noise vs bias current in a 250 nm wide $YbAl_3$ wire. (b) Inferred electron-phonon energy loss coefficient, which is large and surprisingly temperature-dependent.

Recent measurements in V_2O_3 films have revealed robust spin Seebeck effect (SSE) response at temperatures well below the ~ 150 K onset of the insulating antiferromagnetic phase. The SSE at fixed heater power grows with decreasing temperature, passing through a maximum at a temperature $T_{max}(B)$ of a few Kelvin, increasing with increasing in-plane B. This phenomenology is qualitatively similar to what has been seen in VO_2 and what has been observed in several other antiferromagetic systems. This T dependence has been attributed to strong phonon-magnon scattering, so that the SSE resembles the T-dependent phonon thermal conductivity. In contrast to the VO_2 case, there is a clear systematically decreasing SSE signal as V_2O_3 thickness increases, implying that the dominant SSE

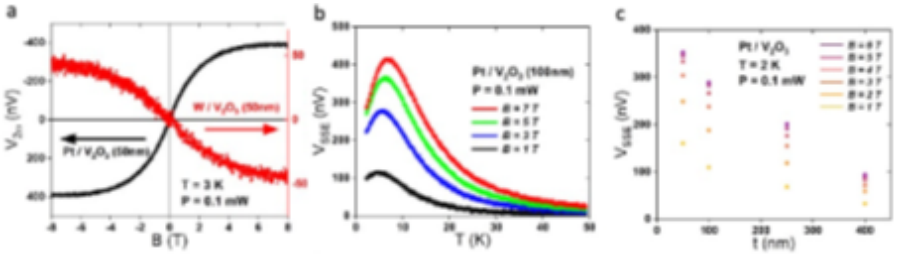


Figure 3. Spin Seebeck response in V_2O_3 films. (a) SSE saturates and high B fields and reflects the sign of the detector metal spin Hall angle. (b) SSE T dependence with B-dependent T_{max}. (c) Systematic thickness dependence of SSE, implying this is a bulk effect.

contribution in V_2O_3 comes from the bulk of the material. This trend can be explained in a model where the magnon-phonon thermal relaxation length is shorter than 50 nm, not surprising in a system like V_2O_3 known to have a strong coupling between spin and lattice degrees of freedom (clear from the structural transition coincident with antiferromagnetic ordering). This work has also been submitted for publication.

Future Plans

In the strange metal/heavy fermion/noise measurements, fresh $YbRh_2Si_2$ devices with optimized designs on the highest quality film will be sent to Prof. Paschen's group in Vienna for magnetotransport and noise measurements in their dilution refrigerator. The goal is to examine shot noise and possible quantum interference corrections to classical conduction while field tuning into and out of the strange metal regime. Future magnetotransport and noise measurements are planned for $CeCoIn_5$, Sr_2RuO_4, and overdoped cuprate nanowires as well, as a means of assessing other strongly correlated materials with connections to strange metallicity, for comparison. In addition, we will finish off a current study of the temperature and length-dependent suppression of shot noise in gold nanowires.

We will begin initial forays into thermal Hall effect measurements, starting with control experiments on materials with no expected thermal Hall signal. We will progress to phonon-based thermal Hall ($SrTiO_3$) and then to quantum magnets including systems believed to host topological magnons. Pending availability of $ErFeO_3$ crystals or films, we will also examine spin Seebeck response in that system.

References

1. Liyang Chen, Dale T. Lowder, Emine Bakali, Aaron M. Andrews, Werner Schrenk. Monkia Waas, Robert Svagera, Gaku Eguchi, Lukas Prochaska, Yiming Wang, Chandan Setty, Shouvik Sur, Qimiao Si, Silke Paschen, and Douglas Natelson, *Shot noise in a strange metal*, Science **382**, 907-911 (2023).
2. M.Henny, S. Oberholzer, C. Strunk, and C. Schönenberger, *1/3-shot-noise suppression in diffusive nanowires*, Phys. Rev. B **59**, 2871-2880 (1999).
3. L. Y. Shi, Z. Tagay, J. Liang, K. Duong, Y. Wu, F. Ronning, D. G. Schlom, K. M. Shen, and N. P. Armitage, *Low-energy electrodynamics and a hidden Fermi liquid in the heavy fermion compound $CeCoIn_5$*, Phys. Rev. B **111**, 1651113 (2025)
4. S. L. Bud'ko, J. C. Frederick. E. D. Mun, P. C. Canfield, and G. M. Schmiedeshoff, *Thermal expansion, heat capacity, and magnetostriction of RaI_3 (R=Tm, Yb, Lu) single crystals*, J. Phys. Cond. Matt. **20**, 025220 (2008)..

Publications

1. Liyang Chen, Dale T. Lowder, Emine Bakali, Aaron M. Andrews, Werner Schrenk. Monkia Waas, Robert Svagera, Gaku Eguchi, Lukas Prochaska, Yiming Wang, Chandan Setty, Shouvik Sur, Qimiao Si, Silke Paschen, and Douglas Natelson, *Shot noise in a strange metal*, Science **382**, 907-911 (2023).
2. Renjie Luo, Xuanhan Zhao, Tanner J. Legvold, Liyang Chen, Changjiang Liu, Deshun Hong, Anand Bhattacharya, and Douglas Natelson, *The challenges of measuring spin Seebeck noise*, Phys. Rev. B **109**, 104429 (2024).

3. Renjie Luo, Tanner J. Legvold, Liyang Chen, Henry Navarro, Ali C. Basaran, Deshun Hong, Changjiang Liu, Anand Bhattacharya, Ivan K. Schuller, and Douglas Natelson, *Low temperature spin Seebeck effect in non-magnetic vanadium dioxide*, Phys. Rev. B **110**, 024415 (2024).
4. Yiming Wang, Chandan Setty, Shouvik Sur, Liyang Chen, Silke Paschen, Douglas Natelson, and Qimiao Si, *Shot noise and universal Fano factor as characterization of strongly correlated metals*, Phys. Rev. Res. **6**, L042045 (2024).
5. Ken W. Ssennyimba, Shusen Liao, Yunxuan Zhu, Tanner J. Legvold, Dale T. Lowder, Karthik Pagadala, Alexandra Boltasseva, Vladimir M. Shalaev, and Douglas Natelson, *Plasmonic heating, thermoelectric response, and thermal emission in titanium nitride nanowires*, APL Mater. **13**, 081108 (2025).
6. Dale T. Lowder, Gage Eichmann, Yuxin Wan, Karthik Rao, Ruiwen Xie, Hongbin Zhang, Shouvik Chatterjee, Kyle Shen, Emilia Morosan, and Douglas Natelson, *Quasiparticle properties below coherence onset in YbA_3 nanostructures*, submitted (2025).
7. Renjie Luo, Tanner J. Legvold, Gage Eichmann, Henry Navarro, Ali C. Basaran, Erbin Qiu, Ivan K. Schuller, and Douglas Natelson, *Thickness-dependent spin Seebeck response in antiferromagnetic V_2O_3 thin films*, submitted (2025).

Symmetries, Interactions and Correlation Effects in Carbon Nanostructures

Gleb Finkelstein, *Duke University*

Keywords: superconductivity, topology-quantum Hall, spin and thermal transport.

Research Scope

The PI's group had performed some of the early studies of the superconducting proximity in quantum Hall (QH) samples. The highlights included: the first Josephson junction made in a QH regime, and creating a QH-based SQUID. More recently, we have observed for the first time the "chiral Andreev edge states" – proximitized QH edge states – and explored their properties. In the past two years, we explored the thermal and spin transport properties of the superconductor-QH hybrid structures.

Recent Progress

1. Spin properties of the chiral Andreev edge states. At the interface between a superconductor (**SC**) and a quantum Hall (**QH**) system, the QH edge states are expected to be proximitized, turning into the chiral Andreev edge states (**CAES**). These are dispersive states that combine both the electron and the hole amplitudes, which are the hybridized via Andreev reflections. An electron approaching the superconducting contact is converted to a linear combination of CAES, which interfere while propagating along the interface (Figure 1). We have directly detected this interference and extensively studied the CAES in several publications.

This year, we focused on understanding the spin properties of the CAES. By using local top gates, we can spin-filter electrons upstream and downstream from the superconducting contact, thereby gaining insights into the spin scattering processes at the interface (Figure 2). Analyzing the same-spin (up to up) and spin-flipped (up to down) channels, we find that they are dominated respectively by normal (electron to electron) and Andreev (electron to hole) reflections (Figure 3).

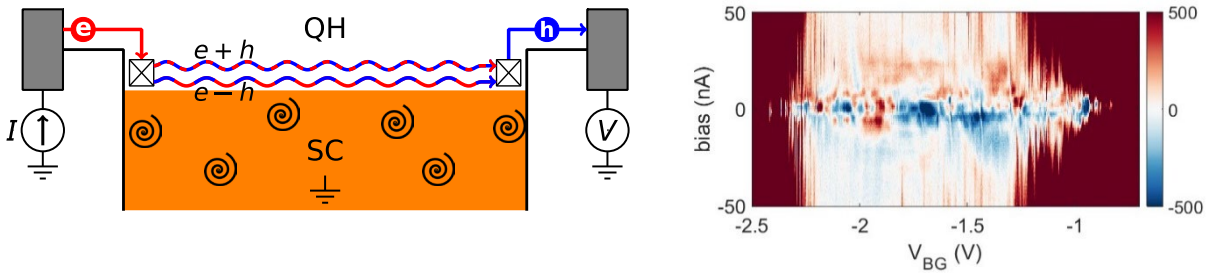


Figure 1. Schematic of the CAES propagation at the QH-SC interface and the detection scheme. Nonlocal downstream resistance dV/dI is measured. The pattern of resistance vs. gate show regions of positive and negative differential resistance, with roughly equal probability. Negative signal corresponds to Andreev conversion of an electron to a hole. The pattern of dV/dI is very random, but reproducible for a given realization, being determined by the positions of the vortices in the superconductor.

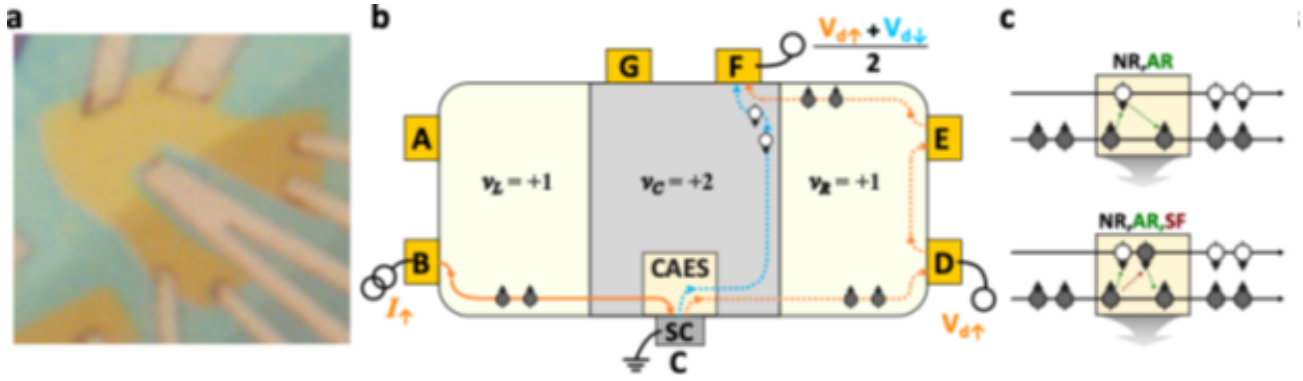


Figure 2. (a,b) Optical image and the schematic of the sample. This device can spin-filter the incoming and outgoing channels to/from the superconducting contact (at the center). The left and right regions are gated by a graphite bottom gate to the filling factors $\nu_L=\nu_R=1$, thus forming spin polarizers. The central region next to the superconductor is gated by the silicon back gate to $\nu_C=2$. In this measurement setup, we bias from contact B, ground the superconducting contact C, and measure the downstream resistances at contacts D and F. By biasing from contact B, only spin-up electrons are injected to the central region. Contact D collects only spin-up downstream current directly yielding the downstream resistance $R_{d\uparrow}$. Contact F collects both spin signals, from which the spin-down downstream resistance $R_{d\downarrow}$ can be extracted. (c) Schematic of the quasi-particle scattering between CAES when only spin-up electrons enter. The top inset includes only normal reflection (NR) and Andreev reflection (AR). This case only allows spin-up electrons and spin-down holes to emerge from the CAES. The bottom inset includes spin-flips (SF) in addition to NR and AR. With this added process, the outgoing quasi-particles can include spin down electrons and spin-up holes.

Our findings demonstrate a presence of spin-orbit coupling that induces spin flip of electrons undergoing Andreev reflections at the QH/SC interface. This spin-orbit interaction enables same-spin Andreev reflections even at the spin-polarized QH filling factor of $\nu=1$. Theoretically, coupling of the $\nu=1$ state to the superconductor has been proposed as a route to create chiral Majorana fermions.

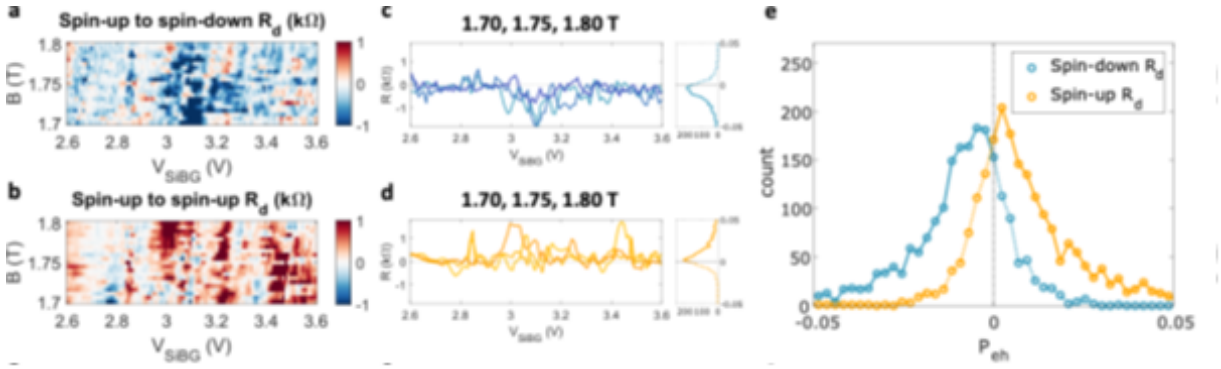


Figure 3. (a,b) Maps of spin-down and spin-up R_d as a function of the B field and Si gate voltage, which controls the density near the SC contact. (c,d) Horizontal cuts of the maps at a few selected fields. $R_{d\downarrow}$ in (a,c) is mostly negative, indicating Andreev reflections (e to h), and $R_{d\uparrow}$ in (b,d) is mostly positive, indicating normal reflections (e to e). However, opposite signs are occasionally observed, indicating that spin-down electrons and spin-up holes are present. (e) Histograms of the downstream resistances in maps (a,b), converted to the probability of an electron or a hole to be emitted from the SC contact. Clearly, same spin channel is dominated by normal reflections and spin-flipped channel is dominated by Andreev reflections, but the tails of the distributions directly prove the presence of the spin-flipping processes.

2. Thermal properties of the QH-superconductor interfaces. In the second major project, we examined the thermal properties of the interface between the superconducting electrodes and graphene in the QH regime. Originally, we were intended to measure the heat propagation via the CAES introduced on page 1. We have expected that both the SC and the QH bulk would provide negligible thermal conductivity, leaving CAES as the main route for heat flow. However, our measurement indicate that the thermal conductivity of the superconductor is relatively high and greatly exceeds that of the chiral Andreev edge states.

To measure the heat conductivity, we have used the thermal (Johnson-Nyquist) noise measurement to probe the local electron temperature at the SC-QH interface. The measurements were conducted via low-temperature amplifiers and superconducting resonators which we have recently set up in one of my group's dilution refrigerators. This type of setup was first used in the celebrated measurements of the fractional charge and the statistics of the QH anyons. Later, researchers used similar circuitry to measure thermal properties of QH samples, such as the quantized heat flow of the QH edge states.

We measured the Johnson-Nyquist noise signatures in the sample shown in Figure 3a. Here, graphene is separated into two regions by a common superconducting contact, forming two interfaces which can be measured separately by the corresponding amplifiers (A and B). We bias the bottom interface, delivering a known power P via Joule heating, and measure the resulting noise by amplifier B located downstream (Figure 4a, bottom right). By studying the dependence of the signal on V_G, B, and the filling factor ν, we can verify that the measured signal corresponds to the local temperature T_B of the bottom interface. The dependence indicate that the cooling of the interface proceeds primarily not via the CAES, but through the superconductor.

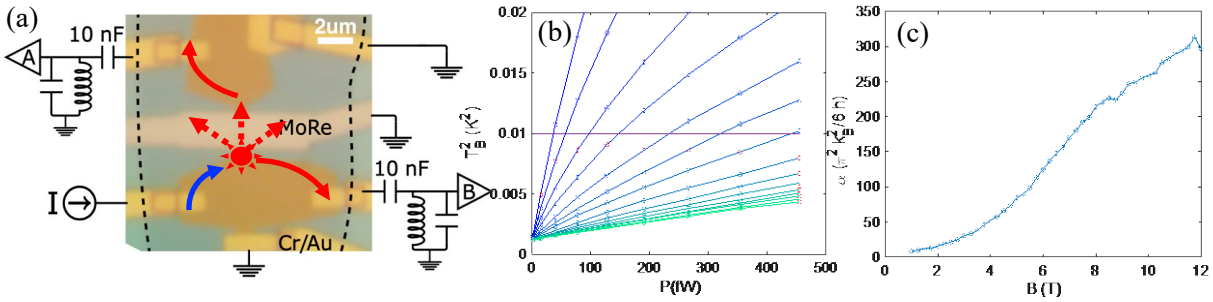


Figure 4. a) Image of the sample and schematics of the measurement. Graphene is separated into two regions by a grounded superconducting strip. Current is injected to the contact on the bottom left, which heats the bottom QH-superconductor interface. Two amplifiers and LC circuits are connected to the two graphene regions to measure the electronic temperatures of the two QH-superconductor interfaces. b) Temperature at the bottom QH-superconductor interface plotted vs. applied power, which reveals the Wiedemann-Franz behavior, $P = \alpha (T^2 – T_0^2)$. From top to bottom, different curves correspond to magnetic fields increasing from 1 to 12 T. e) Coefficient α measured in units corresponding to one quantum channel. The initial rise of α is exponential in B. Superconductor is found to conduct heat tens to hundred times more efficiently than a single QH edge channel.

Specifically, we have found that the temperature rise follows the Wiedemann-Franz (WF) law, $P = \alpha (T_B^2 - T_0^2)$, where T_0 is the base temperature (Figure 4b). This indicates that the SC strip dissipates heat like a normal metal, which is unexpected, because the number of the quasiparticles in the superconductor should be suppressed by $\exp(-\Delta/kT)$. [Note that the cooling power via phonons emission is negligible in the temperature range below 100 mK.] We argue that the measured electronic heat conductivity of the superconductor is due to the overlap of the normal states in the vortex cores. As the overlap increases with magnetic field, the coefficient α introduced just above grows from tens to hundreds in quantized units of $\pi^2 k_B^2/6h$ (Figure 4c).

Our results may be important for understanding the energy balance in a whole class of hybrid semiconductor-superconducting devices operating at high magnetic fields.

Future Plans

We plan to work on the following directions. 1) We aim to control the length of the interface between the superconductor and graphene using patterned gates. The point-like interfaces should reduce CAES losses and potentially enable coupling between the superconductor and the fractional quantum Hall states. We have reproduced the recently developed technique of the anodic oxidation of graphite for making patterned bottom gates and incorporated them in the test samples.

2) We are working on patterning the superconducting contacts on the smallest possible scale – making dot-shaped circular contacts down to 50 nm in diameter. The idea here is to make the dots small enough to suppress the vortex formation. Further, the CAES should form close trajectories around the dots resulting in energy quantization, which should allow us to directly measure the dispersion of the CAES. The dots are incorporated in the quantum point contacts (QPC), which should allow us to independently control their coupling to two sets of the QH edge states (Figure 5).

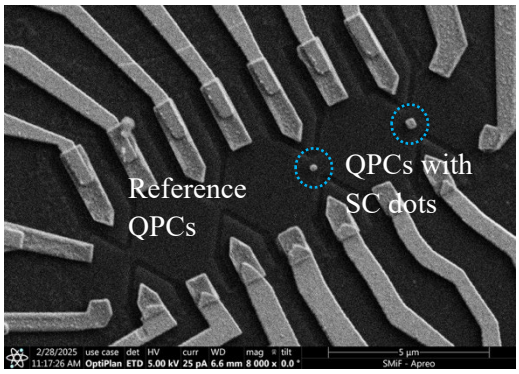


Figure 5. Image of the sample with two reference QPCs and two QPCs containing SC dots (circled).

3) We are making very narrow (50 nm) wire-shaped superconducting contacts to the QH samples. Similar to plan (2) above, the vortex formation in the wires should be suppressed. The geometry should potentially enable hybridization of the CAES which are propagating along the opposite sides of the wire. Several theoretical predictions exist for this regime, including the perfect Andreev cross-conversion of the incoming electrons to the outgoing holes.

Publications

1. L. Zhao, T.F.Q. Larson, Z. Iftikhar, J. Chiles, K. Watanabe, T. Taniguchi, F. Amet, G. Finkelstein, *Thermal Properties of the Superconductor--Quantum Hall Interface*, Phys. Rev. Lett. **134**, 066001 (2025). https://doi.org/10.1103/PhysRevLett.134.066001.

2. E.G. Arnault, J. Chiles, T.F.Q. Larson, C.-C. Chen, L. Zhao, K. Watanabe, T. Taniguchi, F. Amet, G. Finkelstein, *Multiplet Supercurrents in a Josephson Circuit*, Phys. Rev. Lett. **134**, 067001 (2025). https://doi.org/10.1103/PhysRevLett.134.067001.

3. A. Sharma, C.-C. Chen, J. McCourt, M. Kim, K. Watanabe, T. Taniguchi, L. Rokhinson, G. Finkelstein, I. Borzenets, *Fermi Velocity Dependent Critical Current in Ballistic Bilayer Graphene Josephson Junctions*, ACS Nanoscience Au **5**, 65–69 (2025). https://doi.org/10.1021/acsnanoscienceau.4c00080.

4. T.F.Q. Larson, L. Zhao, E.G. Arnault, M.T. Wei, A. Seredinski, H. Li, K. Watanabe, T. Taniguchi, F. Amet, G. Finkelstein, *Noise-induced stabilization of dynamical states with broken time-reversal symmetry*, Phys. Rev. B **112** 014502 (2025). https://doi.org/10.1103/mg84-y5vj.

5. L. Zhao, E.G. Arnault, T.F.Q. Larson, K. Watanabe, T. Taniguchi, F. Amet, G. Finkelstein, *Nonlocal transport measurements in hybrid quantum Hall–superconducting devices,* Phys. Rev. B **109**, 115416 (2024). https://doi.org/10.1103/PhysRevB.109.115416.

6. E.G. Arnault, A.H. Al-Tawhid, S. Salmani-Rezaie, D.A. Muller, D.P. Kumah, M.S. Bahramy, G. Finkelstein, K. Ahadi, *Anisotropic superconductivity at KTaO3(111) interfaces*, Science Advances **9**, eadf1414 (2023). https://doi.org/10.1126/sciadv.adf1414.

7. J. Chiles, E.G. Arnault, C.-C. Chen, T.F.Q. Larson, L. Zhao, K. Watanabe, T. Taniguchi, F. Amet, G. Finkelstein, *Nonreciprocal Supercurrents in a Field-Free Graphene Josephson Triode*, Nano Lett. **23**, 5257–5263 (2023). https://doi.org/10.1021/acs.nanolett.3c01276.

8. L. Zhao, Z. Iftikhar, T.F.Q. Larson, E.G. Arnault, K. Watanabe, T. Taniguchi, F. Amet, G. Finkelstein, *Loss and Decoherence at the Quantum Hall-Superconductor Interface*, Phys. Rev. Lett. **131**, 176604 (2023). https://doi.org/10.1103/PhysRevLett.131.176604.

Mechanical Resonant Sensing of Spin Texture Dynamics in a 2D Antiferromagnet

Xiao-Xiao Zhang, *University of Florida*

Keywords: Magnetism; 2D Material; Mechanical Resonator; Spin Dynamics

Research Scope

The recently discovered atomically-thin magnetic crystals provide a unique playground for understanding magnetization in 2D confinement and developing new approaches to manipulating magnetism for novel spintronic devices. In particular, antiferromagnets (AFMs) are promising for realizing high-speed information processing given their THz magnetic resonance frequency. However, they are also less sensitive to optical and electrical detection due to their net zero magnetization. In this talk, I will discuss our recent results on 2D AFM transition-metal trichalcogenides, where we couple the magnetic transitions into the mechanical degree of freedom. We observed the expected steady-state spin transitions based on magnetostriction effects and also saw signatures of additional transition points related to the magnetic domain dynamics.

Recent Progress

We recently made the first the mechanical detection of nanoscale spin texture formation in 2D AFM materials enabled by exchange magnetostriction[1]. The detection is enabled by exchange-induced magnetostriction during the formation of spin textures, where the rearrangement of neighboring spins leads to changes in magnetic exchange interactions. While AFM spin textures and domains are conventionally difficult to detect due to the vanishing magnetization and nanoscale sizes, we expect high-sensitivity magnetostriction measurements to provide access to detecting the formation and dynamics of spin textures.

To achieve ultrasensitive mechanical sensing of the spin texture, we fabricate 2D AFM material MnPS3 into resonant nanoelectromechanical systems (NEMS) operating in the radio frequency (RF) range. One of the best devices, a 25 nm-thick MnPS3 drumhead, shows a very high Q of ~56,000 at 4 K. Combined with the extracted Young's modulus of this material, we estimate a lattice parameter change resolution down to the attometer (10^{-18} m) level, which corresponds to $\delta a/a \sim 10^{-9}$(a: lattice constant) and membrane transverse displacement sensitivity of femtometer scale with such a high Q factor.

An out-of-plane magnetic field was applied while measuring the mechanical resonance. $MnPS_3$ is known to exhibit a spin-flop transition near 4T from prior magnetic measurements. We examined the magnetic field dependence of the resonance frequency in its linear operation regime with a perturbative small RF driving voltage (10 mV). Figure 1 shows the resonance frequency shift while sweeping the magnetic fields. Two sharp frequency drops were observed at ±4.6 T (H_1) and at ±7 T (H_2), which are direct indications of sudden tension reduction and mark the presence of two distinct magnetic transitions (Fig. 1 upper panel). In addition, the resonance Q factor shows orders of magnitude decreases at these two transitions, which indicates the much enhanced scattering and additional relaxation channels (Fig. 1 lower panel). While H_1 is close to the spin-flop field, the higher 7T transition has not been identified before. Based on analytical modeling of magnetostriction, a spin-flop transition would only lead to continuous changes and the sharp dips in resonance frequency is beyond the simple model considering only the spin-flop. They are eventually attributed to the collective in-plane magnetic domain emergence (at spin-flop field) and the domain realignment (at 7T), which is also supported by spin dynamics simulation provided by our theory collaborator Elton Santos (the University of Edinburgh, UK).

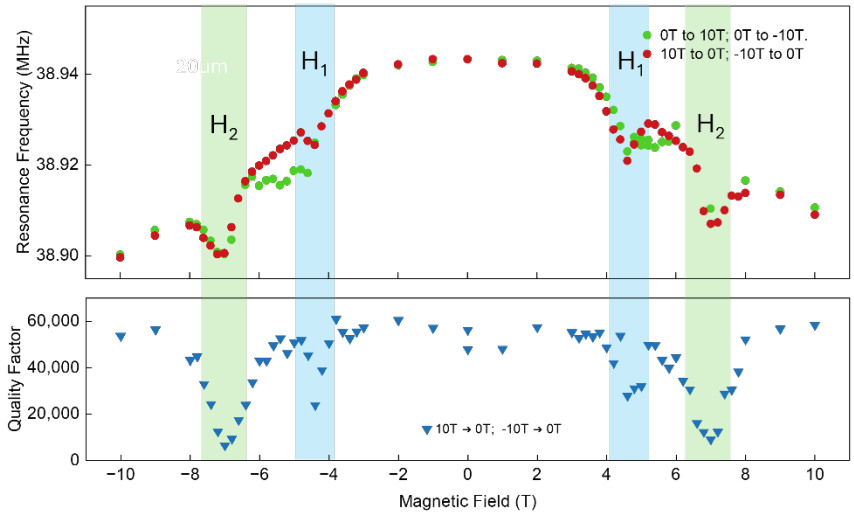


Figure 1. Upper panel: Resonance frequency shifts of $MnPS_3$ resonator as a function of magnetic field under different field sweeping directions. Lower panel: Corresponding Q factor changes as a function of the field. The tinted region corresponds to the two magnetic transitions H_1 (blue) and H_2 (green).

We also identify for the first time of the intriguing correlation between magnetic transitions and high order mechanical nonlinearity. Under a strong mechanical drive, the membrane displacement is no longer linear and higher order terms need to be included. The mechanical resonance will evolve from a Lorentzian-like peak to a asymmetric peak shape with bistable regions, with a frequency hysteresis gap depending on the frequency scan direction. We examined the frequency hysteresis as a function of the magnetic field. The two sharp transitions observed in the linear region can be clearly identified in the linear regime. From further fitting of the nonlinear coefficient, we find significant modulation of the higher order mechanical stiffness, which indicates a strong magnetic origin of nonlinearity. Such higher order nonlinearity are important in realizing energy transduction, quantum hybrid devices and constructing squeezed states. Our results open up new avenues to explore the rich physics with strong spin-lattice coupling and their dynamic feedback.

Future Plans

We will further explore the magnetic resonance responses under coupled multi-excitations, specifically under an AC magnetic field excitation. The impacts of the pure magnetic RF excitations in a mechanical resonator will be explored for the first time. Based on the strongly nonlinear magnetostriction effects near the spin-flop field, we expect a pure magnetic excitation can also cause macroscopic mechanical motion. The cross coupling between the magnetic and mechanical excitations will be further explored to understand the coupling strength and dynamics.

References

1. S M E. H. Yousuf, Y. Wang, S. Ramachandran, J. Koptur-Palenchar, C. Tarantini, L. Xiang, S. McGill, D. Smirnov, E. J. G. Santos, P. X. Feng, X.-X. Zhang, Mechanical Resonant Sensing of Spin Texture Dynamics in a 2D Antiferromagnet. Adv. Mater. 2025, **37**, 2420168.

Publications

Put the list of publications in the recent 2-years SUPPORTED BY BES here. **If more than 10 publications, list only the 10 most relevant.**

1. S M E. H. Yousuf, Y. Wang, S. Ramachandran, J. Koptur-Palenchar, C. Tarantini, L. Xiang, S. McGill, D. Smirnov, E. J. G. Santos, P. X. Feng, X.-X. Zhang, Mechanical Resonant Sensing of Spin Texture Dynamics in a 2D Antiferromagnet. Adv. Mater. 2025, 37, 2420168. https://doi.org/10.1002/adma.202420168

2. Yunong Wang; S M Enamul Hoque Yousuf; Xiao ‐ Xiao Zhang; Philip X. ‐ L. Feng, "Two ‐ dimensional FePS3 nanoelectromechanical resonators with local gate electrostatic tuning at room temperature ", J. Appl. Phys. 21 December 2024; 136 (23): 234303., https://doi.org/10.1063/5.0243387

3. Khanh Duy Nguyen, Woojoo Lee, Jianchen Dang, Tongyao Wu, Gabriele Berruto, Chenhui Yan, Chi Ian Ip, Haoran Lin, Qiang Gao, Seng Huat Lee, Binghai Yan, Chaoxing Liu, Zhiqiang Mao, Xiao-Xiao Zhang, Shuolong Yang, "Distinguishing surface and bulk electromagnetism via their dynamics in an intrinsic magnetic topological insulator ", Sci. Adv.10,eadn 5696 (2024). DOI:10.1126/sciadv.adn5696

4. Jianchen Dang, Tongyao Wu, Kenji Watanabe, Takashi Taniguchi, Hechang Lei, Xiao-Xiao Zhang, "Electrical switching of spin polarized light emitting diode based on a monolayer WSe2/hBN/CrI3 heterostructure" Nat Commun 15, 6799 (2024). https://doi.org/10.1038/s41467-024-51287-9

Broken Symmetries for Control of Electrically-Generated Spin Currents and Torques

Daniel C. Ralph, *Cornell University*

Keywords: spin current, spin torque, ferromagnet, magnetic resonance

Research Scope

This project is investigating how electrically-generated spin currents and the spin-transfer torques they exert can be modified and controlled. This research has both fundamental and applied objectives. From a fundamental perspective, the most efficient mechanisms for generating spin currents are the result of phenomena at the forefront of condensed matter physics – e.g., the interplay of charge, spin, and orbital degrees of freedom, and particularly spin-momentum coupling arising from the topology of electron bandstructures. The project seeks to provide deeper understanding of these phenomena by using measurements of spin currents and their orientation as an experimental probe. From an applied perspective, these fundamental physics issues are directly relevant to the development of magnetic memory and logic applications, because the torques that electrically-generated spin currents can exert on magnetic layers provide the most efficient known mechanism to reliably write information in magnetic samples. One focus of the proposed research is to understand what physics phenomena can be used to maximize the efficiency of a particular component of electrically-generated torque (out-of-plane anti-damping torque) that is forbidden in high symmetry materials but which has the potential to drive switching of nanoscale magnetic memories approximately a factor of 100 times more efficiently than conventional in-plane anti-damping torque produced by high-symmetry materials.

Recent Progress

As part of this project, the Ralph group has pursued several different materials systems and physical mechanisms for controlling the spin direction within electrically-generated spin currents. As background, we consider the sample geometry shown in Fig. 1. An electric field within a spin source layer can generate a vertically-flowing spin current (e.g., via spin-orbit interactions) that can be absorbed by an adjacent magnet to exert a spin-transfer torque. In materials with high symmetry, the direction of the spin within the spin current is constrained by symmetry to lie strictly in the sample plane and perpendicular to the current. This orientation is useful for some purposes, but for nanoscale magnetic memory applications it would be much more useful to have a vertically-flowing spin current with a strong component of spin pointing perpendicular to the

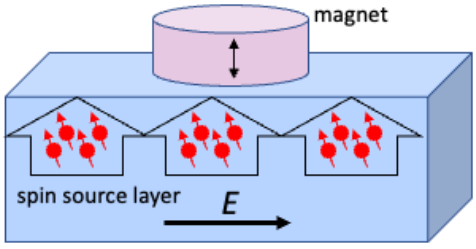


Fig. 1. Goal: Spin-source layers in which an electric field generates an upward-flowing spin current with a strong out-of-plane component of spin direction.

device plane. This can be achieved using a spin-source material with reduced symmetry, e.g., a material with either low intrinsic crystal symmetry or magnetic ordering that provides sufficient symmetry breaking. The project has made progress with both of these strategies, but in this abstract I will focus on the generation of unconventional spin currents with two types of magnetic spin source materials.

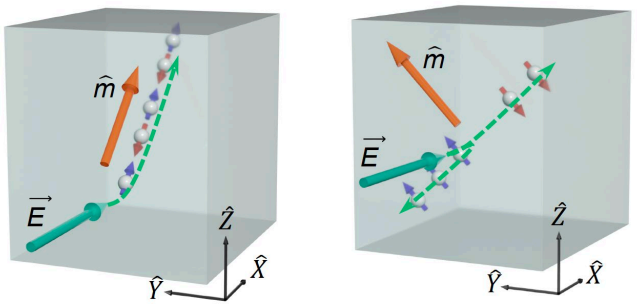


Fig. 2. Unconventional spin currents generated by the planar Hall effect (left) and the spin anomalous Hall effect (right).

Spin currents from canted ferromagnets. Theoretical predictions suggest that vertically-flowing spin currents with an out-of-plane component can be generated within a metallic ferromagnet by means of the spin anomalous Hall effect or the planar Hall spin current [1] (Fig. 2). The difficulty is that both of these mechanisms require that the magnetization of the spin-source layer be canted partially out of the sample plane (*i.e.*, neither fully in the sample plane or fully perpendicular to the plane): the out-of-plane anti-damping torque due to the spin anomalous Hall effect is predicted to be proportional to $m_y m_z$ and that due to the planar Hall spin-current mechanism is predicted to be proportional to $m_x m_z^2$. (Here $\hat{m}$ is the magnetic orientation and x is the direction of the in-plane applied charge current.) For a thin film, achieving a partly-canted magnetization that is stable at zero applied magnetic field is not possible using only the shape anisotropy and interface anisotropy; one must rely on strong magnetocrystalline anisotropy.

In collaboration with the research groups of Chang-Beom Eom, Darrell Schlom, and Lane Martin, we have provided the first verification of these predictions for a sample with zero applied magnetic field using $SrRuO_3$ as the spin-source material [2]. $SrRuO_3$ is orthorhombic ferromagnet with a Curie temperature slightly below 150 K for thin films, with a large magnetocrystalline anisotropy along the $[010]_o$ axis (effective anisotropy field ~ 12 T). Twin domain formation in $SrRuO_3$ thin films can be suppressed using vicinal $SrTiO_3$ substrates with an appropriate miscut angle; a controlled orientation of the orthorhombic film can be nucleated from the step edges on the substrate. In this way, we grow predominantly single-domain $SrRuO_3$ with a $(110)_o$ orientation in which the $[010]_o$ anisotropy axis is controllably canted away from the surface normal.

We have demonstrated using ST-FMR in (110) $SrRuO_3$/Permalloy samples that after the magnetization direction is set by field cooling $SrRuO_3$ can generate a significant out-of-plane anti-damping torque below its Curie temperature (Fig. 3). Measurements as a function of varying the angle of applied electric field relative to the tilted magnetization axis show that both the anomalous Hall spin current and the planar Hall spin current contribute. The maximum torque efficiency is at most about 0.018, about a factor of two below the threshold required for out-of-plane spin-orbit torque to surpass the efficiency of existing spin-transfer-torque magnetic memories (STT-MRAM). Part of the planned future research is to realize the same physics mechanisms in canted room-temperature magnets, seeking more efficient out-of-plane torques.

Spin current carried by magnons in multiferroic $BiFeO_3$. $BiFeO_3$ is an intriguing material because its ferroelectricity provides a source of broken symmetry that can be switched by an electric field, and the magnetoelectric coupling between its ferroelectricity and antiferromagnetism provide a potential strategy for using broken symmetries with the $BiFeO_3$ to control the flow of angular momentum. Together with the research groups of Ramesh Ramamoorthy, Darrell Schlom, and others, my group showed that a source of conventional spin-orbit torque (non-magnetic $SrIrO_3$) can generate a magnon spin current on one side of a $BiFeO_3$ thin film, and that these magnons can travel through the film to exert a torque on a magnetic layer on the other side with an efficiency comparable to the spin-orbit torque from a heavy metal [3]. What's more, if the ferroelectricity is initialized with an upward-pointing component as compared to a downward-pointing component, the efficiency of the magnon transport changes by 18%. We ascribe this difference to the coupling between spin cycloids and the ferroelectricity that makes the dynamics of chiral magnons sensitive to the ferroelectricity direction.

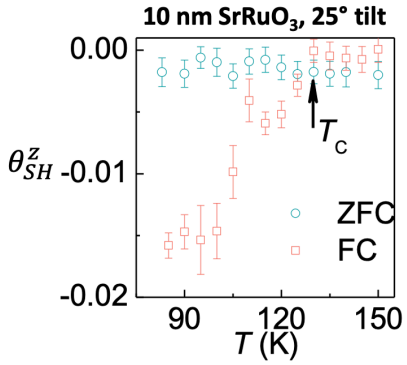


Fig. 3. Out-of-plane anti-damping torque efficiency as a function of temperature, showing that the efficiency turns on below the Curie temperature when a canted $SrRuO_3$ sample is field-cooled so that the net magnetization is canted, but not in a zero-field-cooled sample with randomly-oriented magnetization domains.

Our initial experiment on $BiFeO_3$ magnon torques revealed only a conventional torque (in-plane and perpendicular to the applied charge current) [3]. More recently, we have also shown that magnons in $BiFeO_3$ can exert an unconventional torque, with a component of spin parallel to the applied charge current [4]. We study $BiFeO_3$ grown epitaxially on orthorhombic $DyScO_3$ substrates with $(110)_o$ orientation, so that the ferroelectricity of $BiFeO_3$ has a two-variant domain structure with a well-controlled cycloid spin structure within each domain. We find the spin polarization transported through $BiFeO_3$ can be rotated by as much as 11° away from the conventional axis within the sample plane when the current is oriented appropriately relative to the ferroelectric polarizations. As a function of the angle of the applied current φ_E, this unconventional torque has a $\sin(2\varphi_E)$, dependence, consistent with a symmetry analysis of the cycloid pattern within the two-variant domain structure. As a control experiment, this unconventional torque is absent in samples with a disordered ferroelectric domain structure.

Future Plans

Future research plans within the project include promising extensions of the current work: to realize canted configurations of room-temperature metallic ferromagnets for the generation of out-of-plane spin-orbit torques (aiming initially for $L1_0$ FePt and $L1_0$ FePd), and to use spacer layers other than $BiFeO_3$ to reorient the spins within spin currents (our next targets are spacers made from $SrRuO_3$, WTe_2, IrO_2, and RuO_2). In addition, we plan a new research effort to

investigate torques due to the flow of orbital angular momentum as well as spin, and we will also begin a new experiment to perform sensitive optical measurements with Sagnac interferometry to study spin-current-driven interactions in superconductor/magnet heterostructures. If we are successful in identifying sources of spin current (or orbital current) capable of driving out-of-plane anti-damping torques with sufficient efficiency to be of interest for applications, we will also study the detailed dynamics for the switching of nanoscale magnets driven by these torques.

References

1. T. Taniguchi, J. Grollier, and M. D. Stiles, *Spin-Transfer Torques Generated by the Anomalous Hall Effect and Anisotropic Magnetoresistance*, Phys. Rev. Appl. **3**, 044001 (2015).

2. X. Huang, D. A. Pharis, H. Zhou, Z. Tian, T. M. J. Cham, K. Lee, Y. E. Li, C. Wang, Y. Liang, M. Olszewski, D. Yi, C.-B. Eom, D. G. Schlom, L. W. Martin, D.-F. Shao, and Daniel C. Ralph, *Control of out-of-plane anti-damping spin torque with a canted ferromagnetic spin source*, submitted.

3. X. Huang, X. Chen, Y. Li, J. Mangeri, H. Zhang, M. Ramesh, H. Taghinejad, P. Meisenheimer, L. Caretta, S. Susarla, R. Jain, C. Klewe, T. Wang, R. Chen, C.-H. Hsu, I. Harris, S. Husain, H. Pan, J. Yin, P. Shafer, Z. Qiu, D. R. Rodrigues, O. Heinonen, D. Vasudevan, J. Iniguez, D. G. Schlom, S. Salahuddin, L. W. Martin, J. G. Analytis, D. C. Ralph, R. Cheng, Z. Yao, and R. Ramesh, *Manipulating chiral-spin transport with ferroelectric polarization*, Nature Materials **23**, 898 (2024).

4. Y. Liang, X. Yan, X. Jiang, D. Jiang, H. Bai, H. Chen, D. A. Pharis, X. Huang, R. Jain, W. Jiang, D. Yi, T. Nan, and D. C. Ralph, *Observation of Unconventional Magnon Torque Using Multiferroic $BiFeO_3$*, submitted.

Publications

1. M. Patton, G. Gurung, D.-F. Shao, G. Noh, J. A. Mittelstaedt, M. Mazur, J.-W. Kim, P. J. Ryan, E. Y. Tsymbal, S.-Y. Choi, D. C. Ralph, M. S. Rzchowski, T. Nan, and C.-B. Eom, *Symmetry Control of Unconventional Spin-Orbit Torques in IrO_2*, Advanced Materials **35**, 2301608 (2023).

2. R. Jain, M. Stanley, A. Bose, A. R. Richardella, X. S. Zhang, T. Pillsbury, D. A. Muller, N. Samarth, and D. C. Ralph, *Thermally-generated spin current in the topological insulator Bi_2Se_3*, Science Advances **9**, eadi4540 (2023).

3. X. Huang, X. Chen, Y. Li, J. Mangeri, H. Zhang, M. Ramesh, H. Taghinejad, P. Meisenheimer, L. Caretta, S. Susarla, R. Jain, C. Klewe, T. Wang, R. Chen, C.-H. Hsu, I. Harris, S. Husain, H. Pan, J. Yin, P. Shafer, Z. Qiu, D. R. Rodrigues, O. Heinonen, D. Vasudevan, J. Iniguez, D. G. Schlom, S. Salahuddin, L. W. Martin, J. G. Analytis, D. C. Ralph, R. Cheng, Z. Yao, and R. Ramesh, *Manipulating chiral-spin transport with ferroelectric polarization*, Nature Materials **23**, 898 (2024).

4. M. Patton, D. A. Pharis, G. Gurung, X. Huang, G. Noh, E. Y. Tsymbal, S.-Y. Choi, D. C. Ralph, M. S. Rzchowski, and C.-B. Eom, *Crystallographic spin torque conductivity tensor of epitaxial IrO_2 thin films for oxide spintronics*, Advanced Materials **37**, 2414267 (2025).

5. R. Jain, *Spin Physics in Topological Insulators and Spin Split Antiferromagnets*, Ph.D. Dissertation, Cornell University (2025).

6. Y. Tang, P. Pal, M. Roddy, J. Schad, R. Li, J. Lee, F. Rana, T. Nan, C.-B. Eom, and D. C. Ralph, *Unusual dependence on the angle of magnetic field for the spin Hall magnetoresistance of monodomain epitaxial $BiFeO_3$ thin films*, submitted.

7. M. Patton, D. Go, D. A. Pharis, X. Huang, G. Gurung, E. Y. Tsymbal, D. C. Ralph, M. S. Rzchowski, Y. Mokrousov, and C.-B. Eom, *Symmetry-controlled orbital Hall effect in IrO_2*, submitted (arXiv:2410.02996).

8. X. Huang, Q. Song, G. Gurung, D. A. Pharis, T. M. J. Cham, Y. Chen, R. Jain, M. Olszewski, Y. Feng, A. El-Ghazaly, E. Y. Tsymbal, D. G. Schlom, and D. C. Ralph, *Turn-on of current-induced spin torque upon noncollinear antiferromagnetic ordering in delafossite $PdCrO_2$*, submitted.

9. X. Huang, D. A. Pharis, H. Zhou, Z. Tian, T. M. J. Cham, K. Lee, Y. E. Li, C. Wang, Y. Liang, M. Olszewski, D. Yi, C.-B. Eom, D. G. Schlom, L. W. Martin, D.-F. Shao, and Daniel C. Ralph, *Control of out-of-plane anti-damping spin torque with a canted ferromagnetic spin source*, submitted.

10. Y. Liang, X. Yan, X. Jiang, D. Jiang, H. Bai, H. Chen, D. A. Pharis, X. Huang, R. Jain, W. Jiang, D. Yi, T. Nan, and D. C. Ralph, *Observation of Unconventional Magnon Torque Using Multiferroic $BiFeO_3$*, submitted.

Low-Field Regime of Magnon Transport in PLD-Grown YIG Films

James Analytis

Keywords: Non-collinear spin order, spintronics, magnons, van der Waals magnets, thin films, spin transport

Research Scope

One area of the collaborative research of the Quantum Materials FWP is focused on the exploration and manipulation of emergent quantum phenomena in advanced magnetic materials. The intellectual thread is centered on understanding and controlling the collective behavior of spins, from frustrated antiferromagnets to topologically protected skyrmions. A central theme is the investigation of how spin textures can be controlled and utilized for next-generation spintronic and magnonic devices. This research pushes the boundaries of fundamental condensed matter physics, with a clear eye toward technological applications.

A key area of this research is the study of non-local and collective spin dynamics. This includes investigating how spin information can be transported over long distances and manipulated in ways not possible with conventional electronics. Our recent work on dipolar spin wave packet transport in van der Waals antiferromagnets [1] and the non-local switching of spin textures in frustrated antiferromagnets exemplifies this focus [2]. These studies aim to uncover the fundamental mechanisms of spin transport, which is crucial for developing low-dissipation, high-speed information processing technologies.

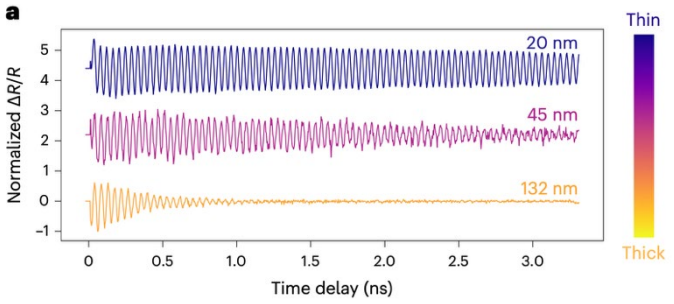


Figure 3: Recently we demonstrated that magnon propagation is mediated by long-range dipole–dipole interaction in the van der Waal magnet CrSBr. This coupling is an inevitable consequence of fundamental electrodynamics and, as such, will likely mediate the propagation of spin at long wavelengths in the entire class of van der Waals magnets currently under investigation. In this figure we show the thickness dependence of the transient reflectance which points directly to the non-local nature of magnetic-dipole interactions. The decay time is seen to decrease dramatically with increasing thickness. See Ref. [1]

Staying with van der Waals magnets, another significant thrust of this research is the exploration of topologically non-trivial spin textures, such as skyrmions [3]. Our investigations of how these quasiparticles can be ordered and controlled at room temperature in polar materials like (Fe0.5Co0.5)5GeTe2, could pave the way to high-density, robust magnetic data storage. This research is not only about discovering new materials but also about understanding the complex interplay between material structure, magnetic interactions, and topology.

We use advanced experimental techniques to probe and manipulate these delicate quantum states. From non-local transport measurements to advanced microscopy and spectroscopy, the group employs a multifaceted approach to gain a comprehensive understanding of the materials studied. This allows us to connect fundamental theoretical concepts to real-world material properties, paving the way for the design of new quantum materials with tailored functionalities.

Recent Progress

The work of the Quantum Materials FWP has achieved a series of key breakthroughs in the control and understanding of spin dynamics in a variety of material systems.

A major advancement has been in the understanding and utilization of magnon transport, see Figure 2 [4]. In the study of YIG films, the team has explored the low-field regime of magnon diffusion, revealing that even modest magnetic fields can significantly attenuate spin voltage. This work identified in-plane uniaxial magnetic anisotropy as a dominant factor in low-field magnon transport, a crucial insight for the development of field-free magnonic devices. This research provides a roadmap for optimizing magnon transport in thin-film devices, a key step toward practical applications.

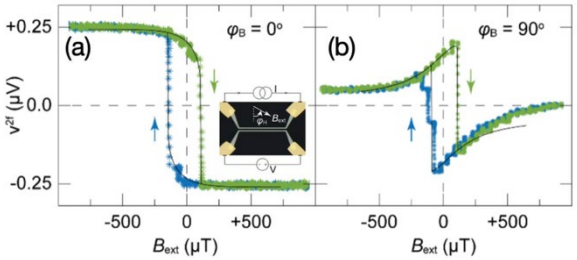


Figure 4: Field-Free Magnon Transport in YIG. (Inset) Nanofabricated devices of Pt contacts on YIG, with an injector and detector of spin current, carried by magnons in the YIG. (a), (b) The spin current signal (measured in the 2ω channel) in two different field orientations has significant anisotropy that can be observed in ultra-low magnetic fields. This anisotropy is not expected in cubic YIG. After Ref. [4].

Furthering the understanding of spin transport, the group has demonstrated dipolar spin wave packet transport in a van der Waals antiferromagnet [1]. This work identified long-range dipole-dipole interactions as the mechanism for magnon propagation in this class of materials, with example data shown in Figure 1. This is a significant finding because it provides a universal mechanism for spin transport in the rapidly expanding family of 2D magnets, offering a clear set of rules for optimizing materials for magnonic applications.

In the realm of spin texture manipulation, the team has made a remarkable discovery of long-range, non-local switching of spin textures in a frustrated antiferromagnet FexNbS2 [2]. We have shown that spin information can be transported and stored away from the region of current flow, a phenomenon amplified by strong magnetoelastic coupling. An example of a device we fabricated from single crystals using Focused Ion Beam is shown in Figure 2. This suggests a new way to store and transport spin information, with potential applications in low-power spintronic memory and logic devices.

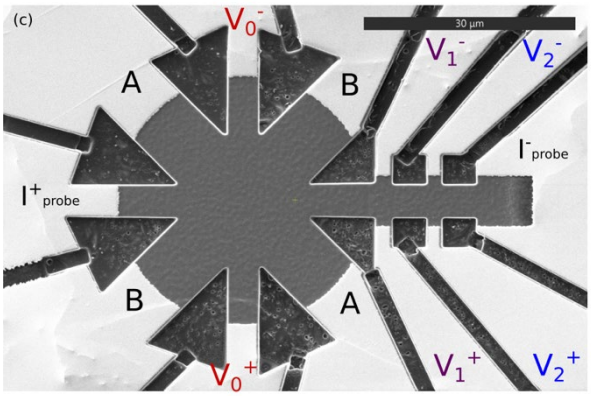


Figure 5: A switching device made from a bulk crystal using Focused Ion Beam. The two pulse bars are marked A and B. The AC probe current is applied along the path marked Iprobe. The local signal is measured using the contacts labeled V0, and the non-local signals are measured using the contacts labeled V1 and V2. From Ref. [2]

In the broader context of transition metal dichalcogenides, the team has discovered charge order in FexNbS2 which may underly some of the physics behind its low-power, lattice coupled switching [5]. This work provides a new platform for studying the interplay between charge, spin, and lattice degrees of freedom in these complex materials. The discovery of charge order in this system opens new avenues for exploring emergent phenomena and provides a new material system for testing theoretical models of correlated electron physics.

The group has also made significant progress in the study of topological spin textures [3]. We have demonstrated the ordering of room-temperature magnetic skyrmions in a polar van der Waals magnet. By using structural confinement, we have been able to engineer an ordered skyrmion crystal, demonstrating control over the order-disorder transition on a scale relevant for device applications. This is a critical step toward the realization of skyrmion-based memory and logic devices that can operate at room temperature.

The work of the QM FWP has advanced the understanding and control of spin phenomena in quantum materials. This has leveraged the powerful synergy between materials synthesis, advanced experimental techniques, and theoretical understanding, potentially laying a foundation for the development of next-generation quantum technologies.

Future Plans

Building directly on our recent breakthroughs, our future research will focus on designing and controlling complex quantum phenomena in engineered materials. We will leverage our established expertise in non-local spin dynamics and topological textures to explore the next frontier: non-equilibrium control of quantum phases and the creation of novel spin transport paradigms. This work will extend our foundational discoveries into new, uncharted territories of condensed matter physics.

A primary objective is to build upon our demonstration of long-range spin transport in van der Waals (vdW) magnets. Having identified the fundamental mechanisms of magnon propagation, we will now aim to realize and manipulate more exotic collective spin states, such as topological magnons and neutral gapless states. This involves designing and synthesizing vdW heterostructures that host these states, directly extending our work on dipolar spin waves and non-local switching into systems with designed topological properties; for example we have preliminary results on MnPS3 (thought to host topological magnons) and CoxTaS2 (scalar spin chirality). Our ability to control magnon transport at low fields provides a critical foundation for engineering these fragile, dissipationless spin-current-carrying states, which are essential for future low-power information technologies.

Finally, we will extend our paradigm of "quantum by design" to the grand challenge of topological superconductivity, a critical step towards fault-tolerant quantum computing. We will pursue this by engineering structurally chiral TMDs on non-Euclidean surfaces, aiming to induce topological superconductivity. Concurrently, we will investigate intrinsically topological superconductors such as intercalated 2H-TaS2, applying novel tuning knobs like uniaxial strain to control the superconducting order parameter and stabilize different topological phases. This leverages our core strengths in advanced material synthesis and spectroscopy to create and verify novel states of matter that have no counterpart in existing materials.

References

1. Yue Sun, Fanhao Meng, Changmin Lee, Aljoscha Soll, Hongrui Zhang, Ramamoorthy Ramesh, Jie Yao, Zdeněk Sofer, Joseph Orenstein, *Dipolar spin wave packet transport in a van der Waals antiferromagnet*, Nature Physics **20**, 794 (2024).
2. Shannon C. Haley, Eran Maniv, Tessa Cookmeyer, Susana Torres-Londono, Meera Aravinth, Joel Moore, James G. Analytis, *Long-range, Non-local Switching of Spin Textures in a Frustrated Antiferromagnet,* Nature Communications, 14:4691 (2023)
3. Peter Meisenheimer, Hongrui Zhang, David Raftrey, Xiang Chen, Ying-Ting Chan, Rui Chen, Reed Yalisove, Mary C. Scott, Jie Yao, Weida Wu, Peter Fischer, Robert J. Birgeneau, Ramamoorthy Ramesh, *Nature Communications*, 14:3744 (2023)
4. Hossein Taghinejad, Kohtaro Yamakawa, Xiaoxi Huang, Yuanqi Lyu, Luke Pritchard Cairns, Sajid Husain, Ramamoorthy Ramesh, James G. Analytis, *Low-Field Regime of Magnon Transport in PLD-Grown YIG Films,* Nano Lett. 25, 16, 6438–6444 (2025)
5. Shan Wu, Rourav Basak, Wenxin Li, Jong-Woo Kim, Philip J. Ryan, Donghui Lu, Makoto Hashimoto, Christie Nelson, Raul Acevedo-Esteves, Shannon C. Haley, James G. Analytis, Yu He, Alex Frano, Robert J. Birgeneau*, Discovery of Charge Order in the Transition Metal Dichalcogenide FexNbS2*, PHYSICAL REVIEW LETTERS 131, 186701 (2023)

Publications

1. X. Chen, W. Tian, Y. He, H. R. Zhang, T. L. Werner, S. Lapidus, J. P. C. Ruff, R. Ramesh and R. J.Birgeneau. "Thermal cycling induced alteration of the stacking order and spin-flip in the room temperature van der Waals magnet Fe5GeTe2," Physical Review Materials 7 (4) (2023). 10.1103/PhysRevMaterials.7.044411
2. P. Meisenheimer, H. R. Zhang, D. Raftrey, X. Chen, Y. T. Shao, Y. T. Chan, R. Yalisove, R. Chen, J. Yao, M. C. Scott, W. D. Wu, D. A. Muller, P. Fischer, R. J. Birgeneau and R. Ramesh. "Ordering of room-

temperature magnetic skyrmions in a polar van der Waals magnet," Nature Communications 14 (1) (2023). 10.1038/s41467-023-39442-0

3. C. Lee, Y. Sun, L. Ye, S. Rathi, K. Wang, Y.-M. Lu, J. Moore, J. G. Checkelsky and J. Orenstein, "Spin wavepackets in the Kagome ferromagnet Fe3Sn2: Propagation and precursors", Proceedings of the National Academy of Sciences 120 (21), e2220589120 (2023). 10.1073/pnas.2220589120
4. Y. Song, S. Wu, X. Chen, Y. He, H. Uchiyama, B. Z. Li, S. Z. Cao, J. Y. Guo, G. H. Cao and R. Birgeneau. "Phonon softening and slowing-down of charge density wave fluctuations in BaBi2As2," Physical Review B 107 (4) (2023). 10.1103/PhysRevB.107.L041113
5. V. Sunko, Y. Sun, M. Vranas, C. C. Homes, C. Lee, E. Donoway, Z. C. Wang, S. Balguri, M. B. Mahendru, A. Ruiz, B. Gunn, R. Basak, S. Blanco-Canosa, E. Schierle, E. Weschke, F. Tafti, A. Frano and J. Orenstein, "Spin-carrier coupling induced ferromagnetism and giant resistivity peak in EuCd2P2", Physical Review B 107 (14), 144404 (2023). 10.1103/PhysRevB.107.144404
6. S. Susarla, S. L. Hsu, F. Gómez-Ortiz, P. García-Fernández, B. H. Savitzky, S. Das, P. Behera, J. Junquera, P. Ercius, R. Ramesh and C. Ophus. "The emergence of three-dimensional chiral domain walls in polar vortices," Nature Communications 14 (1) (2023). 10.1038/s41467-023-40009-2
7. S. Wu, R. Basak, W. Li, J.-W. Kim, P. J. Ryan, D. Lu, M. Hashimoto, C. Nelson, R. Acevedo-Esteves, S. C. Haley, J. G. Analytis, Y. He, A. Frano and R. J. Birgeneau, "Discovery of Charge Order in the Transition Metal Dichalcogenide ${\mathrm{Fe}}_{x}{\mathrm{NbS}}_{2}$", Physical Review Letters 131 (18), 186701 (2023). 10.1103/PhysRevLett.131.186701
8. L. Chen, X. Teng, D. Hu, F. Ye, G. E. Granroth, M. Yi, J.-H. Chung, R. J. Birgeneau and P. Dai, "Thermal evolution of spin excitations in honeycomb Ising antiferromagnetic FePSe3", npj Quantum Materials 9 (1), 40 (2024). 10.1038/s41535-024-00651-5
9. Y. Sun, F. Meng, C. Lee, A. Soll, H. Zhang, R. Ramesh, J. Yao, Z. Sofer and J. Orenstein, "Dipolar spin wave packet transport in a van der Waals antiferromagnet", Nature Physics 20 (5), 794-800 (2024). 10.1038/s41567-024-02387-2
10. E. Donoway, T. V. Trevisan, A. Liebman-Peláez, R. P. Day, K. Yamakawa, Y. Sun, J. R. Soh, D. Prabhakaran, A. T. Boothroyd, R. M. Fernandes, J. G. Analytis, J. E. Moore, J. Orenstein and V. Sunko, "Multimodal Approach Reveals the Symmetry-Breaking Pathway to the Broken Helix in ${\mathrm{EuIn}}_{2}{\mathrm{As}}_{2}$", Physical Review X 14 (3), 031013 (2024). 10.1103/PhysRevX.14.031013

Magnetometry Studies of Quantum Correlated Topological Materials in Intense Magnetic Fields

Lu Li, *University of Michigan*

Keywords: magnetism, single crystals, topological materials, magnetometry, thermodynamics

Research Scope

This project investigates the fundamental nature of quantum correlated topological materials by advanced magnetometry such as torque magnetometry, torque resonance magnetometry, and gradient magnetometry in intense magnetic fields and extreme conditions. The proposal addresses how strong electronic interaction leads to novel topological quantum states. In particular, our proposal will address three questions: (a). Does strong electronic correlation help generate a topological material? (b). What are the ground states of quantum topological materials under intense magnetic fields? (c). How do we experimentally distinguish the novel topological nontrivial correlated state from the conventional electronic and magnetic states?

These questions test the *hypothesis* that, in quantum material, the strong electronic interaction creates unique topological quantum states that are not feasible in weakly interacting materials.

This proposal aims to use advanced magnetometry techniques to give conclusive evidence for the novel electronic and magnetic states in quantum correlated topological materials. Our research starts with magnetometry measurements in intense magnetic fields on quantum correlated topological material. With these efforts, we hope to carry out the following tasks: (1) Detecting quantum oscillations of the bulk and the surface states in quantum correlated topological materials; (2) Revealing the origin of magnetic oscillations in quantum correlated topological materials; (3) Searching for novel electronic and magnetic ground states in quantum correlated topological materials.

Recent Progress

(a). Unconventional magnetic oscillations in kagome Mott insulators. (*Proceedings of the National Academy of Sciences* 2025, Ref. [1])

In metals, electrons in a magnetic field undergo cyclotron motion, leading to oscillations in physical properties called quantum oscillations. This phenomenon has never been seen in a robust insulator because there are no mobile electrons. We report an exception to this rule. We study a Mott insulator on a kagome lattice which does not order magnetically down to milli-Kelvin temperatures despite antiferromagnetic interactions. We observe a plateau at magnetization equal to 1/9 Bohr magneton per magnetic ion, accompanied by oscillations in the magnetic torque, reminiscent of quantum oscillations in metals. The temperature dependence obeys Fermi distribution. These phenomena are consistent with a quantum spin liquid state whose excitations are fermionic spinons with a Dirac-like spectrum coupled to an emergent gauge field.

Fractionalization is a central theme of modern condensed matter physics, as exemplified by the fractional quantum Hall effect. Another example that has been long sought after is quantum spin liquid, where antiferromagnetic order has been suppressed by quantum fluctuations and the spin–charge separation of electrons can lead to charge-neutral spinons. Applying ultrasensitive magnetometry to a kagome-lattice Mott insulator with a 3-eV charge gap, we report quantum oscillations in the magnetic torque. The observation is strong evidence for fermionic spinons, and

an effective gauge field which allows the coupling of the applied magnetic field to charge-neutral particles. A phenomenological model of spinon band structure that includes Dirac nodes near the 1/9 magnetization plateau shows predictions consistent with the observed oscillation patterns.

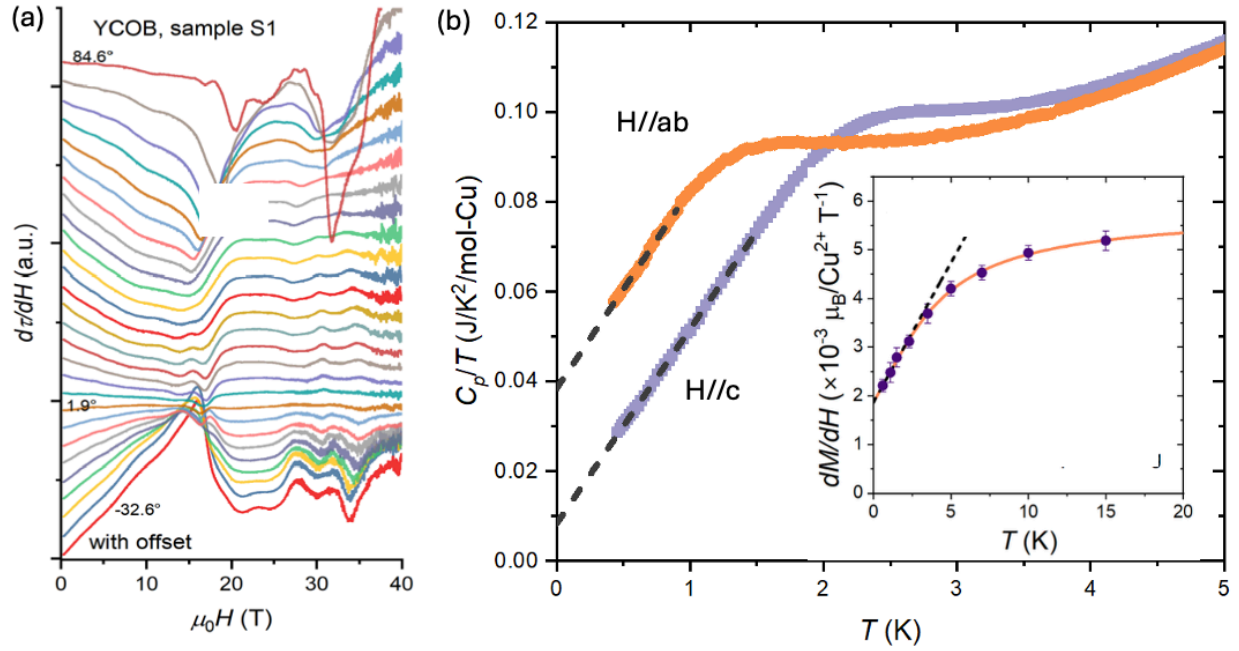


Figure 1. Examples of the magnetic oscillations shown in the magnetic torque in Mott insulator $YCu_3(OH)_6[Br_x(OH)1-_x]$ (YCOB). (b) The heat capacity and magnetic susceptibility exhibit unconventional temperature dependence at the 1/9 plateau state. Taken from Ref. [1, 2].

(b). Thermodynamic evidence of fermionic behavior in the vicinity of one-ninth plateau in a kagome antiferromagnet (*Physical Review X* 2025, Ref. [2])

The spin-1/2 kagome Heisenberg antiferromagnets are believed to host exotic quantum entangled states. Recently, the reports of 1/9 magnetization plateau and magnetic oscillations in a kagome antiferromagnet $YCu_3(OH)_6Br_2[Br_x(OH)_{1-x}]$ (YCOB) have made this material a promising candidate for experimentally realizing quantum spin liquid states. Here, we present measurements of the specific heat Cp in YCOB in high magnetic fields (up to 41.5 T) down to 0.46 K, and the 1/9 plateau feature has been confirmed. Moreover, the temperature dependence of Cp/T in the vicinity of 1/9 plateau region can be fitted by a linear in T term which indicates the presence of a Dirac spectrum, together with a constant term, which indicates a finite density of states contributed by other spinon Fermi surfaces. Surprisingly, the constant term is highly anisotropic in the direction of the magnetic field. Additionally, we observe a double-peak feature near 30 T above the 1/9 plateau which is another hallmark of fermionic excitations in the specific heat. This combination of gapless behavior and the double-peak structure strongly suggests that the 1/9 plateau in YCOB is nontrivial and hosts fermionic quasiparticles.

(c). Large oscillatory thermal Hall effect in kagome metals (*Nature Communications* 2024, Ref. [3])

The thermal Hall effect recently provided intriguing probes to the ground state of exotic quantum matters. These observations of transverse thermal Hall signals lead to the debate on the fermionic versus bosonic origins of these phenomena. The recent report of quantum oscillations

(QOs) in Kitaev spin liquid points to a possible resolution. The Landau level quantization would most likely capture only the fermionic thermal transport effect. However, the QOs in the thermal Hall effect are generally hard to detect. In this work, we report the observation of a large oscillatory thermal Hall effect of correlated Kagome metals. We detect a 180-degree phase change of the oscillation and demonstrate the phase flip as an essential feature for QOs in the thermal transport properties. More importantly, the QOs in the thermal Hall channel are more profound than those in the electrical Hall channel, which strongly violates the Wiedemann–Franz (WF) law for QOs. This result presents the oscillatory thermal Hall effect as a powerful probe to the correlated quantum materials.

(d). Quantum oscillations in the heat capacity of Kondo insulator YbB_{12} (*Physical Review Letters, under review,* Ref. [4])

We observe the magnetic quantum oscillation in the heat capacity of the Kondo insulator YbB_{12}. The frequency of these oscillations $F = 680$ T, aligns with findings from magnetoresistance and torque magnetometry experiments for $B > 35$ T in the Kondo insulating phase. Remarkably, the quantum oscillation amplitudes in the heat capacity are substantial, with $\Delta C/T = 0.5$ mJ/mol.K^2 at 0.8 K, accounting for 13% of the known linear heat capacity coefficient . Double-peak structures of quantum-oscillation amplitudes due to the distribution function of fermions were identified and used to determine the value of the effective mass from the heat capacity, which agrees well with that from torque magnetometry. These observations support charge-neutral fermions contributing to the quantum oscillations in YbB_{12}.

(e). Field tunable BKT and quantum phase transitions in spin-1/2 triangular lattice antiferromagnet (*Newton*, *accepted*, Ref. [5])

Quantum magnetism is one of the most active fields for exploring exotic phases and phase transitions. The recently synthesized Na2BaCo(PO4)2 (NBCP) is an ideal material incarnation of the spin-1/2 easy axis triangular lattice antiferromagnet (TLAF). Experimental evidence shows that NBCP hosts the spin supersolid state with a giant magnetocaloric effect. It was also proposed that the applied magnetic field B can drive the system through Berezinskii-Kosterlitz-Thouless (BKT) and other richer quantum phase transitions. However, the detection of these transitions is challenging because they onset at extremely low temperature T at around 60 mK, and the measurement of the magnetic susceptibility of these transitions requires high sensitivity. With the help of our newly developed gradient force magnetometer in a dilution refrigerator, we constructed the contour diagram of the magnetic susceptibility in the B-T phase diagram in T as cold as 30 mK. These results provide a more comprehensive and accurate understanding of the several field-tunable quantum phase transitions and BKT melting of the spin supersolidity, which are especially significant when their giant magnetocaloric effects highlight potential applications for sub-Kelvin refrigeration under concerns about global helium shortages.

Future Plans

(a). Resolving the quantum oscillations in magnetization using resonant torque differential magnetometry for pulsed magnetic fields up to 65 T and 100 T.

The quantum oscillation pattern in the ultrahigh magnetic field has only been observed in the conduction channels. For a different comparison, we would need to resolve the oscillations in magnetization (the dHvA effect) using sensitive torque differential magnetometry [8] under pulsed magnets. Quantum oscillations in magnetic susceptibility create small oscillatory forces.

Therefore, the magnetic force acting on a sample glued to a resonating cantilever will shift the resonating frequencies or broaden the resonance. We choose to use quartz tuning forks for the resonating cantilevers. Our preliminary experiment succeeded in ran 192 kHz tuning forks to detect the M-H hysteresis loop of underdoped YBa2Cu3O$_{6.56}$ (YBCO). A tuning fork is glued to the heavy block ("qPlus" mode named for Atomic Force Microscopy), and a small AC voltage is applied to drive it to resonance. As the impedance changes, the resonance is observed in the current of the device. The technical challenge still exists to resolve the quantum oscillations when the resonant frequency is too low and the frequency resolution in sliding FFT is about 10 Hz. And this resolution is still too large to determine quantum oscillations. To solve the problem, we have tested a range of quartz resonators with resonance frequencies in the 1.5-4 MHz range. In addition, we have built a current-voltage converter to detect excitation signals. Moreover, the tuning fork resonance is significantly damped by liquid Helium 3 when we tried to cool down samples to 0.4 K. This cold temperature is needed to resolve the dHvA effect for many materials. Therefore, we will build vacuum cells for tuning forks.

(b). Measuring the overall magnetization directly using the gradient magnetometry

While our torque magnetometry detects sensitive magnetic features, the magnetic torque method measures only the magnetic anisotropy. The overall magnetization is also a crucial piece of information at extreme conditions for quantum materials. We develop a sensitive gradient magnetometry [5]. As shown in Fig. 2, the setup consists of a cantilever with a metal pad. The sample is glued on the other metal pad. The external magnetic field B and a constant field gradient $\nabla B = 10\ \mathrm{T/m}$ were applied along the z-direction. In an external magnetic field, the sample exhibits intrinsic magnetization M, generating two torque signals. The dominant signal is the H-antisymmetric gradient torque $\tau_{\mathrm{gradient}} = L\,M\,\nabla B$, where L is the distance from the sample to anchor. With the controllable field gradient, we use the cantilever deflection to get the gradient torque and directly measure the intrinsic magnetization.

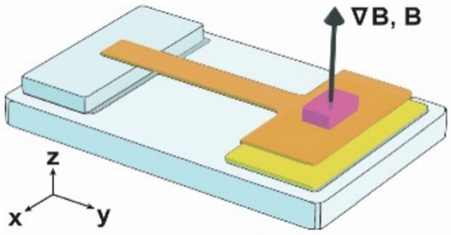


Figure 2. Sketch of apparatus of the gradient magnetometry setup using a cantilever and a metal plate capacitor for DC magnetization measurements.

References

1. G. Zheng, Y. Zhu, K.-W. Chen, B. Kang, D. Zhang, K. Jenkins, A. Chan, Z. Zeng, A. Xu, O. A. Valenzuela, J. Blawat, J. Singleton, P. A. Lee, and L. Li. *Unconventional Magnetic Oscillations in Kagome Mott Insulators*, Proceedings of the National Academy of Sciences **122**, e2421390122 (2025).

2. G. Zheng, D. Zhang, Y. Zhu, K.-W. Chen, A. Chan, K. Jenkins, B. Kang, Z. Zeng, A. Xu, D. Ratkovski, J. Blawat, A. F. Bangura, J. Singleton, P. A. Lee, S. Li, L. Li. *Thermodynamic evidence of fermionic behavior in the vicinity of one-ninth plateau in a kagome antiferromagnet,* Physical Review X **15**, 021076 (2025).

3. D. Zhang, K.-W. Chen, G. Zheng, F. Yu, M. Shi, Y. Zhu, A. Chan, K. Jenkins, J. Ying, Z. Xiang, X. Chen, and L. Li. *Large oscillatory thermal Hall effect in kagome metals,* Nature Communications **15**, 6224 (2024).

4. K.-W. Chen, Y. Zhu, D. Ratkovski, G. Zheng, D. Zhang, A. Chan, K. Jenkins, J. Blawat, T. Asaba, F. Iga, C. M. Varma, Y. Matsuda, J. Singleton, A. F. Bangura, L. Li. *Quantum oscillations in the heat capacity of Kondo insulator YbB12*, arXiv:2501.07471 (2025).

5. D. Zhang, Y. Zhu, G. Zheng, K.-W. Chen, Q. Huang, L. Zhou, Y. Liu, K. Jenkins, A. Chan, H. Zhou, L. Li. *Field tunable BKT and quantum phase transitions in spin-1/2 triangular lattice antiferromagnet*, *Newton*, *accepted*, arXiv:2411.04755 (2024).

Publications

1. G. Zheng, Y. Zhu, K.-W. Chen, B. Kang, D. Zhang, K. Jenkins, A. Chan, Z. Zeng, A. Xu, O. A. Valenzuela, J. Blawat, J. Singleton, P. A. Lee, and L. Li. *Unconventional Magnetic Oscillations in Kagome Mott Insulators*, Proceedings of the National Academy of Sciences **122**, e2421390122 (2025).

2. G. Zheng, D. Zhang, Y. Zhu, K.-W. Chen, A. Chan, K. Jenkins, B. Kang, Z. Zeng, A. Xu, D. Ratkovski, J. Blawat, A. F. Bangura, J. Singleton, P. A. Lee, S. Li, L. Li. *Thermodynamic evidence of fermionic behavior in the vicinity of one-ninth plateau in a kagome antiferromagnet,* Physical Review X **15**, 021076 (2025).

3. D. Zhang, K.-W. Chen, G. Zheng, F. Yu, M. Shi, Y. Zhu, A. Chan, K. Jenkins, J. Ying, Z. Xiang, X. Chen, and L. Li. *Large oscillatory thermal Hall effect in kagome metals,* Nature Communications **15**, 6224 (2024).

4. Y. Zhu, D. Zhang, G. Zheng, K.-W. Chen, H. Bhandari, K. Jenkins, A. Chan, N. J. Ghimire, L. Li*. Geometrical Nernst effect in the kagome magnet YMn6Sn4Ge2*, Physical Review B **110,** 195125 (2024).

5. S. Mozaffari, W. R. Meier, R. P. Madhogaria, N. Peshcherenko, S.-H. Kang, J. W. Villanova, H. W. S. Arachchige, G. Zheng, Y. Zhu, K.-W. Chen, K. Jenkins, D. Zhang, A. Chan, L. Li, M. Yoon, Y. Zhang, D. G. Mandrus. *Universal sublinear resistivity in vanadium kagome materials hosting charge density waves,* Physical Review B **110**, 035135 (2024).

6. G. Zheng, Y. Zhu, S. Mozaffari, N. Mao, K.-W. Chen, K. Jenkins, D. Zhang, A. Chan, H. W. S. Arachchige, R. P. Madhogaria, M. Cothrine, W. R. Meier, Y. Zhang, D. Mandrus, L. Li. *Quantum oscillations evidence for topological bands in kagome metal ScV6Sn6*, Journal of Physics: Condensed Matter **36,** 215501 (2024).

7. Y. Zhang, Z. Li, K.-W. Chen, L. Li, C. Uher. *Extremely large magnetoresistance and quantum oscillations in semimetal Ni3In2S2*, Materials Today Physics **40,** 101318 (2024).

8. X. Guo, W. Liu, J. Schwartz, S. H. Sung, D. Zhang, M. Shimizu, A. L. N. Kondusamy, L. Li, K. Sun, H. Deng, H. O. Jeschke, I. I. Mazin, R. Hovden, B. Lv, L. Zhao. *Extraordinary phase transition revealed in a van der Waals antiferromagnet,* Nature Communications **15,** 6472 (2024).

9. Z. Sun, G. Ye, C. Zhou, M. Huang, N. Huang, X. Xu, Q. Li, G. Zheng, Z. Ye, C. Nnokwe, L. Li, H. Deng, L. Yang, D. Mandrus, Z. Y. Meng, K. Sun, C. R. Du, R. He, and L. Zhao. *Dimensionality crossover to a two-dimensional vestigial nematic state from a three-dimensional antiferromagnet in a honeycomb van der Waals magnet,* Nature Physics **20,** 1764 (2024).

10. K.-W. Chen, G. Zheng, D. Zhang, A. Chan, Y. Zhu, K. Jenkins, F. Yu, M. Shi, J. Ying, Z. Xiang, X. Chen, Z. Wang, J. Singleton, L. Li. *Magnetic breakdown and spin-zero effect in quantum oscillations in kagome metal CsV3Sb5*, Communications Materials **4**, 96 (2023).

Correlated Quantum Materials

Michael A. McGuire[1], Andrew F. May[1], Brenden R. Ortiz[1], Jiaqiang Yan[1], David Mandrus[1,2]

[1] Oak Ridge National Laboratory, Oak Ridge, TN

[2] University of Tennessee, Knoxville, TN

Keywords: Magnetism, emergent phenomena, kagome materials, van der Waals layered materials

Research Scope

The overarching goal of this project is to advance our experimental understanding of quantum materials that exhibit collective phenomena and adopt ground states associated with electron correlations. Specifically, we aim to understand magnetism, excitations, and transport in van der Waals layered antiferromagnets, discover emergent physics and instabilities in kagome-based systems, and probe coupling of crystal chemistry and physical behaviors in topological and chiral crystals. To address these aims we identify, develop, and study model material systems. This leverages our core strengths in synthesis of high-quality crystals and investigation of physical properties using crystallographic, transport, and thermodynamic measurements. We pursue deeper understanding of the most interesting materials through collaborations involving theoretical, spectroscopic, and scattering techniques. Overall, our research addresses the ability to control and exploit quantum mechanical behaviors targeting novel functionality, a priority research direction identified in the BES report on Quantum Materials. More specifically, developments in 2D materials, antiferromagnets, and topological materials will impact microelectronics, spintronics, and quantum technologies, key research areas for energy and information applications.

Recent Progress

Discovery of New Kagome Metals Unveils Origins of Density Wave Instability. The kagome motif is a versatile platform for condensed matter physics, hosting rich interactions among magnetic, electronic, and structural degrees of freedom. The density-wave transitions in $A V_3Sb_5$ compounds and ScV_6Sn_6 are motivating examples. Recently we have been investigating families of compounds that combine rare-earth elements along with a kagome net of transition metals. This not only introduces 4f magnetism but also provides a way to probe structural dependencies and instabilities by tuning the size of the rare-earth ion. This work recently led to the discovery of $LnNb_6Sn_6$ (*Ln* = Ce−Nd, Sm, Gd−Tm, Lu, Y), a new family of kagome metals that displays both complex rare-earth magnetism and a density-wave transition that provides insight into isostructural ScV_6Sn_6 and the broader class AM_6X_6 materials [1].

The crystal structure of $LnNb_6Sn_6$ is shown in Figure 1. It contains Nb kagome nets and chains of *Ln* and Sn atoms that thread the kagome nets. The rare earth sites form a triangular lattice. While the lattice instability was the focus of our work, interesting electronic and magnetic aspects that may warrant further study were observed. Our collaborators observed van Hove singularities

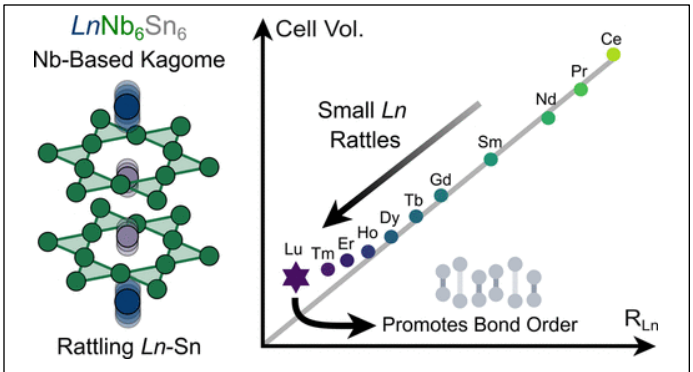


Figure 1. (left) The structure LnNb$_6$Sn$_6$, emphasizing the kagome net of Nb atoms (green) and the chains of *Ln* (blue) and Sn (gray) atoms. "Rattling" in these chains is the precursor to the density wave transition. (right) Contraints from the Nb-Sn framework result in oversized strucures for the smallest *Ln* atoms, promoting the rattling and the lattice instability. From Ref. 1.

and Dirac points near the Fermi level in both experiment and theory, and we observed antiferromagnetic transitions below about 3 K in several of the materials, with metamagnetic transition also observed for *Ln* = Gd, Tb, and Dy.

Returning to the lattice, the dependence of the unit cell volume on the ionic radius R of the *Ln* ion is shown in Figure 1, and shows anomalous behavior at small R. This is an indication of a lattice instability, and it motivated a detailed study of LuNb$_6$Sn$_6$. Evidence of a density-wave transition at 68 K was indeed observed and is summarized in Figure 2. Refinements of atomic displacement parameters in the room temperature phase showed rattling tendency in the Lu-Sn chains, and X-ray diffraction below the phase transition revealed the emergence of superlattice peaks described by wavevector (1/3, 1/3, 1/3). The distorted structure, like that observed in ScV$_6$Sn$_6$, can be visualized as a density-wave modulating the Sn-Sn and Lu-Sn distances along the chains that run through the kagome nets. Intricate diffuse scattering patterns were also observed, indicating further, more subtle complexity in the structure at low temperature.

Overall, our analysis of the structural data supports the "rattling mode" density-wave model and highlights the importance of steric interactions between the rare-earth filler element and the Nb−Sn kagome framework. Importantly, this was only made possible by the discovery and study

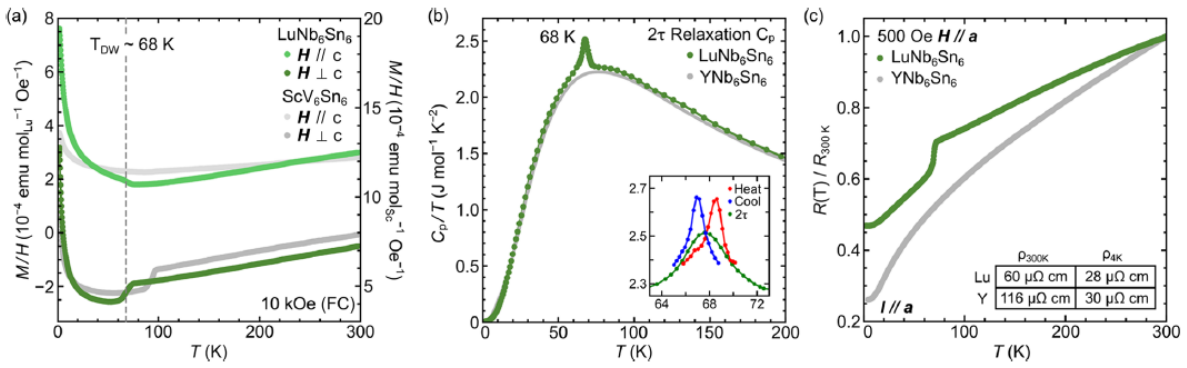


Figure 2. Evidence of the density-wave transition at 68 K in LuNb$_6$Sn$_6$ single crystals. (a) Magnetic susceptibility shows the absence of local moments and a sharp drop in the susceptibility at the transition. Similarities to the density wave compound ScV$_6$Sn$_6$ (data shown in gray) are clear. (b) Heat capacity measurements show a relatively sharp anomaly with first-order character. (c) Electrical resistance shows a sharp drop at the transition. In (b) and (c) analogous data from YNb$_6$Sn$_6$ (no density wave transition) are shown in gray. From Ref. 1.

of the new *Lu*Nb_6Sn_6 compounds, through which we have added to our understanding of the AM_6X_6 family as well as the physics and instabilities in kagome metals more broadly.

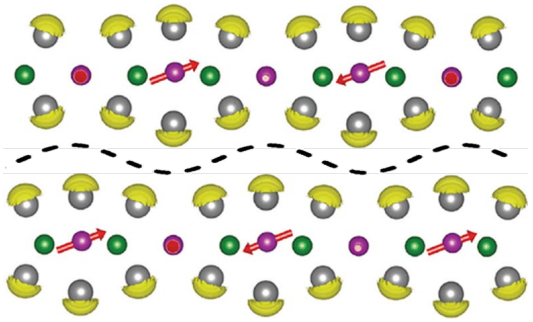


Figure 3. The van der Waals layered structure of $MnRhBi_3$. Mn (purple), Rh (green), and Bi (gray) atoms form a quasi-2D layered structure, with layers separated by a corrugated vdW gap (dashed line). Lone-pair electrons on Bi atoms (yellow) extend into this gap. Moments on Mn (red) order into a noncollinear structure at low temperature.

Lone Electron Pairs Add New Wrinkles to Van der Waals Layered Magnets. Cleavable metallic antiferromagnets may be of use for low-dissipation spintronic devices; however, few are currently known. Our interest in this area led us to consider $MnRhBi_3$ [2]. This compound adopts a layered crystal structure, shown in Figure 3. The structure consists of layers of composition MnRh capped above and below by Bi atoms. Thus, we expected this to be a good candidate for combining magnetism and metallicity in a layered and potentially cleavable crystal structure. To study this material, we grew crystals from a bismuth flux. The crystals adopted a ribbon-like morphology and showed good cleavability. The van der Waals (vdW) nature of the interlayer bonding and cleavability was studied through collaboration using density functional theory and mechanical exfoliation. A cleavage energy similar to those of vdW layered chalcogenides was found, and flakes as thin as 2 nm (three structural layers, or 1.5 unit cells) were produced. The resistivity showed metallic behavior, and evidence for antiferromagnetic ordering was seen in magnetization measurements.

These observations established $MnRhBi_3$ as a cleavable antiferromagnetic metal and motivated our detailed experimental study, which revealed interesting and complex properties and behaviors in this material. In particular, we observed a complex phase evolution at low temperatures. A series of four phase transitions were observed, illustrated in Figure 4. Heat capacity data (Fig. 4a) show four clear anomalies, and corresponding features are seen in the electrical resistivity as well (Fig. 4b). Neutron diffraction showed that at least two of the transitions involve the formation of antiferromagnetic order (Fig. 4c). A non-coplanar structure with Mn moments of about 2.5 μ_B was determined at 50 K (Fig. 3). Measurements of the lattice parameters showed anomalous thermal expansion through the range of phase transitions. This suggests $MnRhBi_3$ may have strong magnetoelastic coupling, an interesting avenue for further exploration.

Finally, we note that crystal chemistry of $MnRhBi_3$ is itself interesting, apart from the complex physical property behaviors that have been noted above. The vdW gap in this compound is between neighboring layers of Bi, instead of the usual case of ionic species like halogens or chalcogens in closed shell configurations. We found this particularly interesting because Bi is known to sometimes possess stereoactive lone pairs of non-bonding electrons, and the van der Waals gap provides an ideal empty space for these electrons to reside. To examine this possibility,

we collaborated with theory colleagues to show that indeed Bi atoms in $MnRhBi_3$ have stereoactive lone pairs that extend into the vdW gap. Thus, the material may be expected to have dangling lone pairs at its cleavage surface. This may provide exciting opportunities for future studies in the 2D limit and at interfaces, since the lone pairs may influence surface reconstruction and chemistry, as well as quantum mechanical proximity effects.

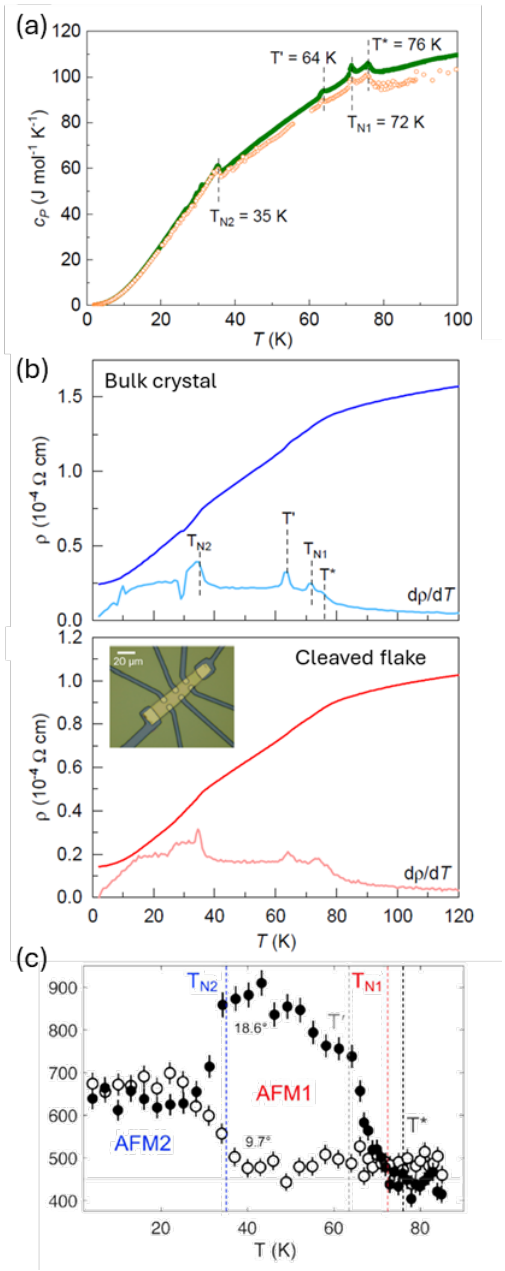


Figure 4. Phase transitions in $MnRhBi_3$. (a) Heat capacity and (b) resistivity show multiple phase transitions below room temperature. (c) Intensity of magnetic Bragg peaks reflect the evolution of the magnetic structure. From Ref. 2.

Future Plans

Over the next few years, we intend to continue to study and develop AM_yX_z systems combining lanthanide elements with kagome nets of transition metals, including development of new families and detailed studies of electronic structure and emergent states. We also expect to complete ongoing investigations of distorted kagome structures based on the ZrNiAl structure type. We will continue to design and discover new intergrowth or modular compounds with distinct structural or functional motifs in single crystals, including misfit compounds where incommensurability may give rise to moiré physics. Among modular materials, we will work to understand the unconventional Hall effect in $Eu_2CuZn_2P_3$ by studying its electronic structure and through the development of related quaternary phases. Finally, we intend to investigate the thermal Hall effect in quantum materials hosting chiral phonons and magnons or other charge neutral quasiparticles to probe their quantum properties.

References

1. B. R. Ortiz, W. R. Meier, G. Pokharel, J. Chamorro, F. Yang, S. Mozaffari, A. Thaler, S. J. Gomez Alvarado, H. Zhang, D. S. Parker, G. D. Samolyuk, J. A. M. Paddison, J. Yan, F. Ye, S. Sarker, S. D. Wilson, H. Miao, D. Mandrus, and M. A. McGuire, *Stability Frontiers in the AM_6X_6 Kagome Metals: The $LnNb_6Sn_6$ (Ln:Ce-Lu,Y) Family and Density-Wave Transition in $LuNb_6Sn_6$*, J. Am. Chem. Soc. **147**, 5279 (2025).

2. E. M. Clements, D. Ovchinnikov, P. R. Raghuvanshi, V. R. Cooper, S. Okamoto, A. D. Christianson, J. A. M. Paddison, B. R. Ortiz, S. Calder, A. F. May, X. Xu, J. Yan, and M. A.

McGuire, *$MnRhBi_3$: A Cleavable Antiferromagnetic Metal*, Chem. Mater. **36**, 11306 (2024).

Publications

This project published more than 60 papers in the last two years. Two are cited in References above and ten selected additional publications are listed here.

1. A. F. May, C. Tabata, S. Okamoto, B. R. Ortiz, A. D. Christianson, J. Yan, K. Kaneko, and M. A. McGuire *Physical Properties of intergrowth compound $Eu_2CuZn_2P_3$,* Phys. Rev. Mater. **9**, 024406 (2025).
2. A. F. May, G. Yumnam, R. P. Hermann, S. Calder, B. M. Lefler, S. J. May, Z. E. Brubaker, M. Brahlek, X. Xu, D. Ovchinnikov, and M. A. McGuire, *Cleavable quaternary oxychlorides with high magnetic ordering temperatures,* Phys. Rev. Mater. **9**, 034002 (2025).
3. H. Zhang, N. Peshcherenko, F. Yang, T. Z. Ward, P. Raghuvanshi, L. Lindsay, Claudia Felser, Yang Zhang, J.-Q. Yan, and H. Miao, *Measurement of phonon angular momentum*, Nat. Phys., 10.1038/s41567-025-02952-3 (2025).
4. A. F. May, E. M. Clements, X. Wang, H. Zhang, and B. R. Ortiz, *Crystal growth and evolution of magnetism in the EuCuP-EuCuAs solid solution*, Phys. Rev. Mater. **9**, 084410 (2024).
5. B. R. Ortiz, H. Zhang, K. Górnicka, D. S. Parker, G. D. Samolyuk, F. Yang, H. Miao, Q. Lu, R. G. Moore, A. F. May, and M. A. McGuire, *Intricate Magnetic Landscape in Antiferromagnetic Kagome Metal, $TbTi_3Bi_4$ and Interplay with $Ln_{2-x}Ti_{6+x}Bi_9$ (Ln: Tb···Lu) Shurikagome Metals*, Chem. Mater. **36**, 8002 (2024).
6. P. Park, B. R. Ortiz, M. Sprague, A. P. Sakhya, S. A. Chen, M. D. Frontzek, W. Tian, R. Sibille, D. G. Mazzone, C. Tabata, K. Kaneko, L. M. DeBeer-Schmitt, M. B. Stone, D. S. Parker, G. D. Samolyuk, H. Miao, M. Neupane, and A. D. Christianson, *Spin density wave and van Hove singularity in kagome metal $CeTi_3Bi_4$*, Nat. Commun. **16,** 1 (2024)
7. S. D. Wison and B. R. Ortiz, *AV_3Sb_5 kagome superconductors*, Nat. Rev. Mater. **9**, 420 (2024).
8. B. R. Ortiz, H. Miao, D. S. Parker, F. Yang, G. D. Samolyuk, E. M. Clements, A. Rajapitamahuni, T. Yilmaz, E. Elio Vescovo, J. Yan, A. F. May, M. A McGuire, *Evolution of Highly Anisotropic Magnetism in the Titanium-Based Kagome Metals $LnTi_3Bi_4$ (Ln: La^{3+}···Gd^{3+}, Eu^{2+}, Yb^{2+})*, Chem. Mater. **35**, 9756 (2023).
9. J. Yan, A. Kumar, M. Chi, M. Brahlek, T. Z. Ward, and M. A. McGuire, *Orbital degree of freedom in high entropy oxides*, Phys. Rev. Mater. **8,** 024404 (2024).
10. R. Baral, A. F. May, and S. Calder, *Short-range magnetic order and planar anisotropy in the topological ferrimagnet $Mn_3Si_2Te_6$*, Phys. Rev. B **112**, 024405 (2025).

Magnetic Interactions and Excitations in Quantum Materials (MIEQM)

L. Ke, R. J. McQueeney, A. Sapkota, T. J. Slade, B. G. Ueland, D. Vaknin

Ames National Laboratory and Iowa State University, Ames, Iowa 50011

Keywords: magnetism, topological materials, flat bands, rare-earths, neutron scattering

Research Scope

The mission of the MIEQM FWP is to understand phenomena when topological electronic bands on frustrated lattices are intertwined with magnetism. We are motivated by Goals to (1) discover quantum phases and phenomena in geometrically frustrated metals, (2) reveal topological signatures in flat-band magnets, and (3) establish how rare-earth magnetism can be utilized to tune topological materials. These goals are pursued by a team with experience in the synthesis and discovery of quantum materials, the characterization of their magnetic, structural, and transport properties, neutron-scattering investigations of magnetic order and fluctuations, and first-principles electronic-structure calculations.

We define three integrated research Thrusts. Thrust 1 focuses on understanding how flat electronic bands on kagome and pyrochlore lattices control the development of itinerant magnetism. Thrust 2 is motivated to understand the role of rare-earth magnetism in developing topological phases in kagome metals. Thrust 3 investigates the perturbation of topological and correlated phases of matter with magnetic impurities. Our research aligns with the DOE-BES strategy in quantum materials by addressing fundamental issues in magnetism, including the development of itinerant magnetism, magnetic frustration, chirality, and the role of defects. Success in achieving our Goals will result in the discovery of new and tunable flat-band and topological magnets and provide a deep understanding of the interplay between magnetism and the electronic bands.

Recent Progress

Magnetic interactions in kagome metals. In kagome metals, the frustrated lattice geometry results in uncommon electronic features, such as flat bands and Dirac points, that are the source of novel correlated and topological ground states. In collaboration with CATS EFRC, we are investigating the magnetic properties of RT_6Sn_6 kagome metals where ferromagnetic (FM) triangular rare-earth (R) layers interact with transition metal (T) kagome layers. In RMn_6Sn_6 compounds with FM kagome layers, we use inelastic neutron scattering (INS), magnetization measurements, and density-functional theory (DFT) to develop magnetic models that accurately predict the critical temperatures and fields of a variety of collinear (ferrimagnetic), non-collinear (canted or spiral) and non-coplanar (conical) magnetic phases across the RMn_6Sn_6 series [R1, P10]. These magnetic phases are associated with magnetotransport anomalies, including anomalous and topological Hall effects, the latter of which suggests the spontaneous development of scalar spin chirality (SSC) [R2]. The SSC phenomenon is under current investigation and described in future work.

Deeper analysis of INS data reveals flat-band and chiral magnetic excitations within the kagome layers of $TbMn_6Sn_6$ [P6]. Whereas flat-band magnon excitations are expected in a FM kagome layer, the observation of chiral excitations is unexpected. The chiral excitations are localized to a hexagonal plaquette in the kagome layer (see FIG. 1) and heavily damped, with steep dispersion extending from 30 – 150 meV. We hypothesize that these chiral quasiparticles originate from electronic carriers in the kagome layer and are the subject of future work.

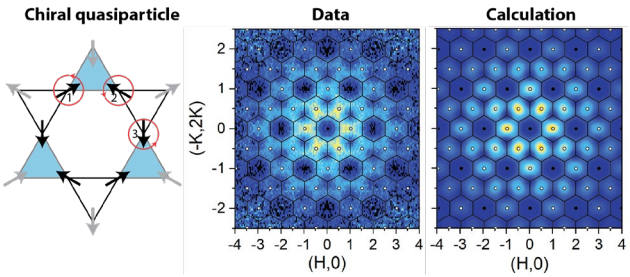


FIG. 1. Localized chiral quasiparticle (black arrows) identified by the momentum dependence of the neutron scattering data for $TbMn_6Sn_6$ over an energy range from 130-150 meV.

In the RV_6Sn_6 series, V kagome layers are non-magnetic and FM *R* layers adopt different magnetic anisotropies across the *R* series. TbV_6Sn_6 has strong Ising character with an isolated ground state doublet that is confirmed by INS measurements [P1]. Mean-field model calculations find TbV_6Sn_6 to be in proximity to a first-order spin reorientation and second-order quantum critical and tricritical points in an applied transverse field. The nature of the quantum phase transition is controlled by the field direction and, surprisingly, by the strength of the planar magnetic anisotropy. Pulsed transverse field magnetization measurements performed at the NHMFL find a quantum phase transition at 26 T, in accordance with predictions.

Magnetic interactions in topological insulators. Stoichiometric TIs in the $MnBi_2Te_4$ family have revealed a variety of topological optical and transport responses in applied field [R3]. Natural heterostructures consist of magnetic $MnBi_2Te_4$ blocks that are separated by Bi_2Te_3 TI blocks. We compared the spin excitations in $MnBi_2Te_4$ and $MnBi_4Te_7$ (FIG. 2), finding identical magnetic interactions within a $MnBi_2Te_4$ block. Much weaker interactions are found between magnetic blocks in $MnBi_4Te_7$, due to the Bi_2Te_3 spacer block, making $MnBi_4Te_7$ a candidate for quasi-2D ferromagnetism [P5].

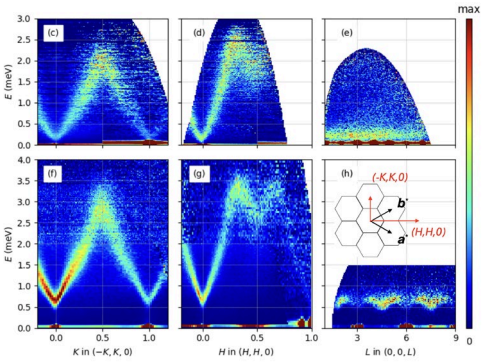


FIG. 2. INS data comparing the spin excitations in $MnBi_2Te_4$ (c)-(e) and $MnBi_4Te_7$ (f)-(h).

Future Plans

Magnetic chirality in kagome metals. RMn_6Sn_6 kagome metals have different sources of static and dynamical magnetic chirality, all of which can affect electronic transport. In zero-field spiral magnetic phases, the application of a magnetic field in the spiral plane leads to a conical magnetic phase that hosts the topological Hall effect (THE). The conical phase does not have a SSC $[\sum_{ijk} \mathbf{S}_i \cdot (\mathbf{S}_j \times \mathbf{S}_k)]$ that is often associated with the THE (in skyrmions, for example) leading to a hypothesis that magnon fluctuations drive this behavior [R2]. INS measurements of $ErMn_6Sn_6$ in an applied magnetic field are being used to test this hypothesis. Our magnetic models provide

accurate magnon polarization vectors which allow for the SSC to be enumerated by averaging over spin triangles on a discrete lattice. We find an inhomogeneous SSC which does not survive spatial and temporal averaging, bringing the fluctuation hypothesis into question.

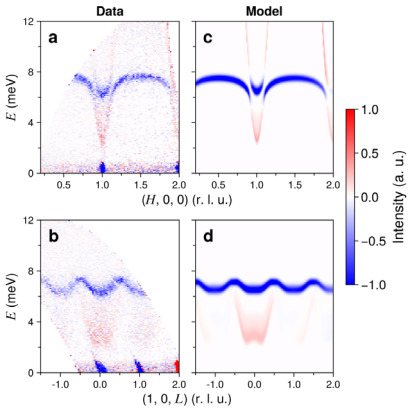


FIG. 3. Polarized INS data from $ErMn_6Sn_6$ measured on HYSPEC showing mixing of right (red) and left-handed (blue) chiral magnons.

Another source of dynamical chirality is the magnons themselves. Acoustic and optical magnon modes in ferrimagnets such as RMn_6Sn_6 possess right and left-handed chirality, respectively. In the ferrimagnetic phase of $ErMn_6Sn_6$, these modes hybridize, which we predict will produce a unique chirality switching mechanism. Magnon hybridization and mixing do not occur in $TbMn_6Sn_6$, a phenomenon associated with the different magnetic symmetries (planar and uniaxial, respectively) of these two materials. We have recently confirmed chiral magnon mixing in $ErMn_6Sn_6$ using polarized INS (FIG. 3), enabling an understanding of how magnetic symmetries drive chiral phenomena with application in spintronics, magnonics, and quantum information.

Finally, our discovery of novel chiral magnetic quasiparticles within the kagome layers of $TbMn_6Sn_6$ opens questions about the ubiquity of this phenomenon in other kagome metals. We have observed similar chiral quasiparticle excitations in $R166$ compounds (R = Y, Ho, Er) possessing different magnetic ground states (FIG. 4). Chiral excitations are robust in this series and we plan to investigate other kagome metal families in the future.

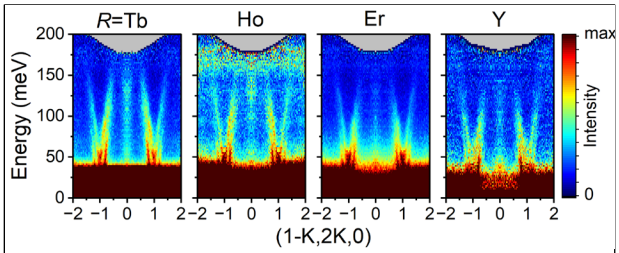


FIG. 4. Chiral magnetic mode in (1,0,0) zone (vertical streak) seen in RMn_6Sn_6 with R=Tb, Ho, Er, and Y.

Ising ferromagnetism in kagome metals. SULI student Olivia Medina performed mean-field calculations that predict a transverse-field FM quantum critical point in HoV_6Sn_6 at $\mu_0 H_c \sim 2$ T, agreeing with preliminary magnetization and neutron diffraction data (FIG. 5). The low critical field enables INS studies that find softening of the transverse fluctuations near the quantum critical point. We plan to investigate scaling behavior of the quantum fluctuations near H_c for comparison with heat capacity (LANL) and susceptibility data. Building on the mean-field predictions, we plan to experimentally investigate the quantum phase transitions in DyV_6Sn_6.

One open question is whether the interaction between R magnetism and kagome electronic bands can lead to novel topological phenomena. Exciting evidence of strong orbital magnetization in TbV_6Sn_6 in applied magnetic fields [R4] motivates the examination of their magnetic excitations. We recently discovered a splitting of spin-flip excitations in TbV_6Sn_6 using INS (FIG. 6) that provides evidence for subtle time-reversal symmetry breaking that occurs in parallel with FM Tb

ordering. This time-reversal symmetry breaking presumably occurs on the V sublattice and must also break translational symmetry (i.e it is antiferromagnetic). To understand this phenomenon, INS measurements in a magnetic field are planned and collaborations are providing complementary NMR (Ames), Raman (Florida A&M), dilatometry (LANL), and muSR measurements (PSI).

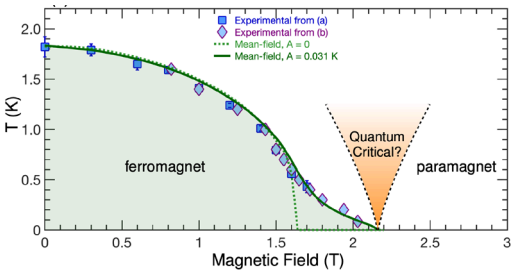


FIG. 5. Preliminary phase diagram for HoV_6Sn_6 from neutron diffraction in a transverse field.

Flat-band magnetism. We seek to discover the origins of magnetism occurring on frustrated lattices with flat bands near the Fermi energy. In collaboration with Rice University, we are studying the cubic Laves phase metal YCo_2 where Co ions form a pyrochlore sublattice. YCo_2 does not develop long-range magnetic order, but INS data find strong itinerant-like FM fluctuations. We are interpreting this data using ab initio calculations of the itinerant excitations within a flat-band picture. In the kagome metals, we plan to study YCr_6Ge_6 which is a Stoner enhanced paramagnet that may show similar fluctuations to YCo_2.

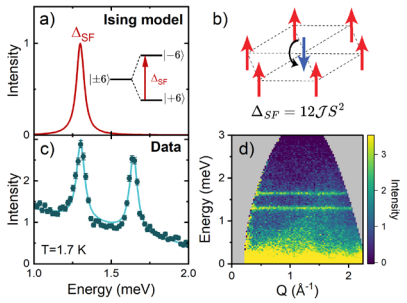


FIG. 6. Two spin-flip excitations are observed in TbV_6Sn_6 in the Ising FM ground state, in disagreement with Ising model predictions.

Finding signatures of flat-band magnetism would benefit from studies of chemically similar systems that host traditional narrow bands originating from atomically localized states, rather than flat bands that are enforced by destructive hopping pathways. RT_2Zn_{20} and RT_2Al_{20} families (T = Fe, Co), have an expanded pyrochlore lattice in which the T-T distance is nearly double that found in RCo_2. YFe_2Zn_{20} is an enhanced Pauli paramagnet, similar to YCo_2, yet the longer bond lengths suggest that its magnetic instability is driven by narrow electronic bands. These factors make RT_2Zn_{20} an attractive material for INS studies that may be directly compared to RCo_2.

Magnetic defects in topological insulators. Dilute and stoichiometric magnetic TIs are influenced by magnetic defects. We are analyzing INS data describing the spin dynamics in the presence of substantial (~20%) Mn-Sb anti-site defects in $MnSb_2Te_4$. These defect states form identical magnetic bonds to those found in our previous work in dilute TIs [eg. see R5, P7].

References

R1. Nil L, T. Victa Trevisan, and R. J. McQueeney, *High-field magnetic phase diagrams of the RMn_6Sn_6 kagome metals*, Phys. Rev. B **111**, 054410 (2025).

R2. N. J. Ghimire, R. L. Dally, L. Poudel, D. C. Jones, D. Michel, N. T. Magar, M. Bleuel, M. A. McGuire, J. S. Jiang, J. F. Mitchell, J. W. Lynn, I. I. Mazin, *Competing magnetic phases and fluctuation-driven scalar spin chirality in the kagome metal YMn_6Sn_6*, Sci. Adv. **6**, eabe2680 (2020).

R3. A. Y. Vyazovskaya, M. Bosnar, E. V. Chulkov, and M. M. Otrokov, *Intrinsic magnetic topological insulators of the $MnBi_2Te_4$ family,* Commun. Mater. **6**, 88 (2025).

R4. H. Li, S. Cheng, G. Pokharel, P. Eck, C. Bigi, F. Mazzola, G. Sangiovanni, S. D. Wilson, D. Di Sante, Z. Wang, I. Zeljkovic, *Spin Berry curvature-enhanced orbital Zeeman effect in a kagome metal*, Nat. Phys. **20**, 1103 (2024).

R5. F. Islam, Y. Lee, D. M. Pajerowski, J. Oh, W. Tian, L. Zhou, J. Yan, L. Ke, R. J. McQueeney, and D. Vaknin, *Role of Magnetic Defects in Tuning Ground States of Magnetic Topological Insulators*, Adv. Mater. **35**, 2209951 (2023).

Publications

P1. Tianxiong Han, R. D. McKenzie, Joanna Blawat, Tyler J. Slade, Y. Lee, D. M. Pajerowski, John Singleton, Bing Li, Paul C. Canfield, Liqin Ke, Ross McDonald, Rebecca Flint, R. J. McQueeney, *Proximity to quantum criticality in the Ising ferromagnet TbV_6Sn_6*, arXiv:2412.02010.

P2. Zhenhua Ning, Pinaki Das, Y. Lee, N. S. Sangeetha, D. L. Abernathy, D. C. Johnston, R. J. McQueeney, D. Vaknin, Liqin Ke, *Spin dynamics in itinerant antiferromagnet $SrCr_2As_2$*, Phys. Rev. B **111**, 134438 (2025).

P3. Liqin Ke, Y. Lee, Z. Ning, R. Flint, R. J. McQueeney, I. I. Mazin, I*mportance of Enforcing Hunds Rules in Density Functional Theory Calculations of Rare Earth Magnetocrystalline Anisotropy*, npj Comput. Mater. **11**, 168 (2025).

P4. Min-Chul Kang, Ping Lu, Farhan Islam, Jiaqiang Yan, David Vaknin, Robert J. McQueeney, Lin Zhou, *Atomic-Scale Characterization of Dilute Dopants in Topological Insulators via STEM EDS Using Registration and Cell Averaging Techniques*, Microscopy and Microanalysis **30**, 807 (2024).

P5. Bing Li, D. M. Pajerowski, J.-Q. Yan, R. J. McQueeney, *Role of non-magnetic spacers in the magnetic interactions of antiferromagnetic topological insulators $MnBi_4Te_7$ and $MnBi_2Te_4$*, Phys. Rev. B **111**, 064418 (2025).

P6. S. X. M. Riberolles, T. J. Slade, T. Han, B. Li, D. L. Abernathy, P. C. Canfield, B. G. Ueland, P. P. Orth, L. Ke, R. J. McQueeney, *Chiral and flat-band magnetic quasiparticles in ferromagnetic and metallic kagome layers*, Nat. Comm. **15**, 1592 (2024).

P7. F. Islam, D. Schlagel, Y. Lee, S. Pakhira, D. M. Pajerowski, D. C. Johnston, L. Ke, D. Vaknin, R. J. McQueeney, *Coexistence of Ferromagnetism and Antiferromagnetic Dimers in Topological Insulators*, Phys. Rev. B **110**, 014408 (2024).

P8. T. Han, S. Pakhira, N. S. Sangeetha, S. X. M. Riberolles, T. W. Heitmann, Y. Wu, D. C. Johnston, R. J. McQueeney, B. G. Ueland, *Europium c-axis ferromagnetism in $Eu(Co_{1-x}Ni_x)_{2-y}As_2$: A single-crystal neutron diffraction study*, Phys. Rev. B **109**, 174428 (2024).

P9. Z. Ning, B. Li, W. Tang, A. Banerjee, V. Fanelli, D. L. Abernathy, Y. Liu, B. G. Ueland, R. J. McQueeney, L. Ke, *Magnetic interactions and excitations in $SrMnSb_2$*, Phys. Rev. B, **109**, 214414 (2024).

P10. S.X.M. Riberolles, T. Han, T.J. Slade, J.M. Wilde, A. Sapkota, W. Tian, Q. Zhang, D. L. Abernathy, L.D. Sanjeewa, S.L. Bud'ko, P.C. Canfield, R.J. McQueeney, B.G. Ueland, *New insight into tuning magnetic phases of RMn_6Sn_6 kagome metals*, npj Quant. Mater. **9**, 42 (2024).

Two Dimensional Heavy Fermions in the van der Waals Metal CeSiI

Xavier Roy and Abhay Pasupathsy

Keywords: Magnetism, Kondo lattice physics, 2D and layered crystals, scanning tunneling microscopy, quasiparticle interference, nodal hybridization

Research Scope

Heavy-fermion compounds host emergent quasiparticles produced by Kondo hybridization between local *f* moments and itinerant electrons. Dimensionality is a key tuning knob for this physics: confining carriers to two-dimensional layers reshapes the Fermi surface, changes point group symmetries, and alters the balance between magnetic interactions and Kondo screening. van der Waals, exfoliable crystals make this limit experimentally accessible, avoiding the challenges of complex thin film synthesis. In our project, we focus on the antiferromagnetic van der Waals metal CeSiI, which realizes a Kondo lattice in a quasi-2D electronic structure (Fig. 1). Our recent study uses scanning tunneling microscopy and spectroscopy with quasiparticle interference to reveal a striking, symmetry-guided form of hybridization: the coupling between conduction and 4*f* states is highly anisotropic in momentum space, producing nodes where the hybridization vanishes. Consequently, quasiparticle masses vary by orders of magnitude around the Fermi surface, and unhybridized carriers persist alongside heavy electrons. This nodal hybridization framework unifies thermodynamic, transport, and spectroscopic observations in CeSiI and establishes it as a platform for understanding heavy fermions at the monolayer limit. It also clarifies how orbital symmetry and reduced dimensionality can produce directionally selective interactions, motivating routes to engineer correlations and competing orders through strain, gating, and heterostructure design. CeSiI and related materials therefore provide a clean, tunable system in which two-dimensionality and crystalline symmetries act together to control heavy-fermion coherence.

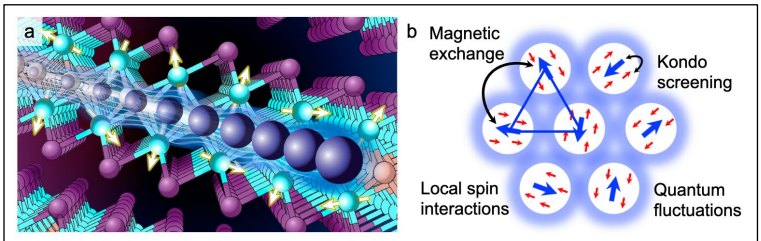


Fig. 1. (a) Formation of 2D heavy fermions in a vdW metal. (b) Competing interactions in 2D heavy fermion materials.

Recent Progress

We performed low-temperature imaging and tunneling spectroscopy on *in situ* cleaved CeSiI single crystals that were transferred using a nitrogen suitcase directly from a glove box to eliminate ambient exposure. Results for CeSiI were directly compared with isostructural LaSiI as a non-Kondo control. Tunneling spectra on CeSiI display a pronounced Fano-like line shape and a dip near the Fermi level, consistent with the emergence of a hybridization gap and a lattice of Kondo resonances. High-energy features attributable to crystal-field excitations are visible at approximately 40 and 100 meV, while the overall background density of states matches that of LaSiI, reflecting similar conduction bands.

Energy-resolved conductance maps reveal robust quasiparticle interference (QPI) from silicon-site defects (Fig. 2a-h); Fourier transforms of these maps show a hexagonal pattern of

scattering vectors inherited from the conduction-band Fermi surface. Crucially, an additional set of low-momentum peaks at a specific wavevector q_H appears in CeSiI at the Fermi level and vanishes outside the hybridization energy window (approximately 40 meV). Control measurements on LaSiI verify that the additional peaks q_H are not artifacts of band structure differences or charge order but are tied to Kondo physics. These peaks align with a symmetry-enforced nesting vector that links regions on the Γ-centered pockets. Together, these observations imply the presence of a residual Fermi surface in the heavy fermion state of CeSiI, where certain directions in reciprocal space do not participate in the heavy fermion hybridization leading to the formation of hybridization nodes.

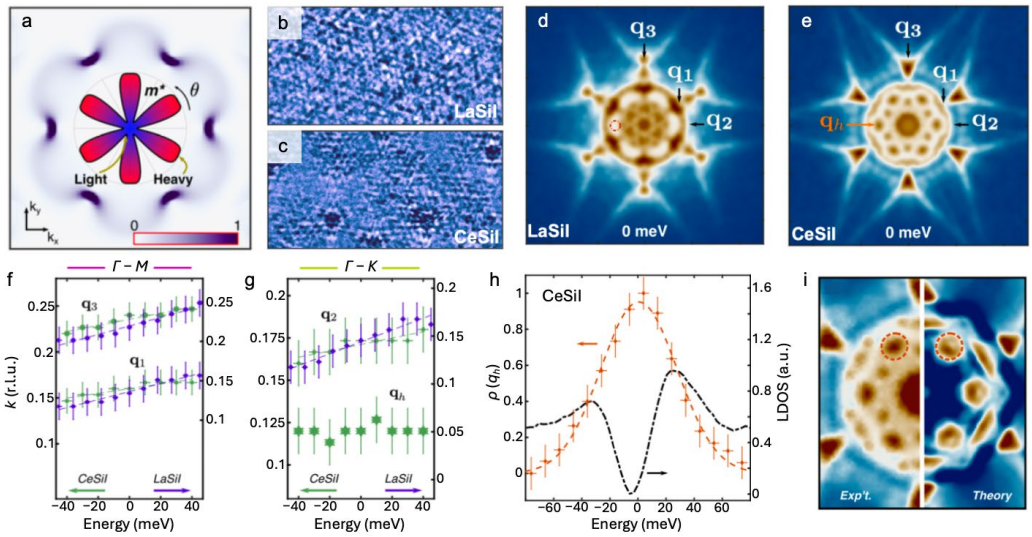


Fig. 2. (a) Tunneling spectral function for a two-band Kondo lattice model with nodal *c*/*f*-electron hybridization. Center inset: polar plot of calculated effective mass m^* showing the coexistence of heavy (red) and light (blue) quasiparticles. (b,c) Real space LDOS maps acquired on surfaces of LaSiI (b) and CeSiI (c) at an energy of 0 meV. (d,e) Fourier transformed LDOS corresponding to (b,c). An additional set of six peaks at ~ 0.12 r.l.u. along Γ−K (q_h) emerges at low energy in CeSiI (e) that are absent in LaSiI (d). (f,g) Dispersion of the QPI peaks as a function of energy along the Γ−M (f) and Γ−K (g) directions. Left axes: CeSiI; right axes: LaSiI. (h) Intensity of the hybridization spot at wave vector q_h in CeSiI as a function of energy (left axis) overlaid on the tunneling spectrum. The hybridization spot appears only at energies within the hybridization gap. (i) Simulated (right) and measured (left) Fermi surface QPI spectroscopy of CeSiI.

To understand the origin of this anisotropy, we carried out first-principles calculations with spin–orbit coupling as well as constructed a minimal three-band model in which a flat $4f$ resonance hybridizes with two dispersive conduction bands through a nodal form $v(k) = v_0 cos(3\theta_k)$. The resulting tunneling spectral function reproduces the coexistence of heavy, gapped antinodal states and light, ungapped nodal states. Full Green's-function QPI simulations match the measured redistribution of intensity (Fig. 4a,i): a reduction of scattering along $\Gamma - M$, the emergence of intense 'hot spots' at q_H along $\Gamma - K$, and persistence of features associated with the unhybridized conduction states. Because the nodal axes coincide with symmetry lines enforced by the near-C_6 symmetry of the Ce site, the position of the nodes is fixed by symmetry while the magnitude of the maximum hybridization gap is set by microscopic overlaps and related Kondo physics.

Experimentally, the momentum selectivity of hybridization has clear thermodynamic and transport consequences. The Kadowaki–Woods ratio in CeSiI is strongly reduced relative to canonical lanthanide heavy-fermion metals, consistent with transport being dominated by light

carriers on the nodal arcs while the specific heat remains sensitive to heavy antinodal carriers. Recent neutron data indicate that unhybridized parts of the Fermi surface can support incommensurate antiferromagnetism without destroying coherence in the heavy sector, rationalizing the weak impact of magnetic order on mass enhancement. Finally, the van der Waals structure allows mechanical exfoliation to bilayer flakes, where magnetotransport and Hall measurements reveal unexpected relaxation dynamics, suggesting that dimensional confinement tunes the balance between Kondo coupling and magnetic exchange. These combined spectroscopic, theoretical, and transport results identify CeSiI as a model platform in which two-dimensionality, orbital symmetry, and strong correlations come together to generate nodal hybridization and a momentum-dependent heavy mass. They also provide concrete design rules for engineering magnetism and Kondo physics in these and similar compounds.

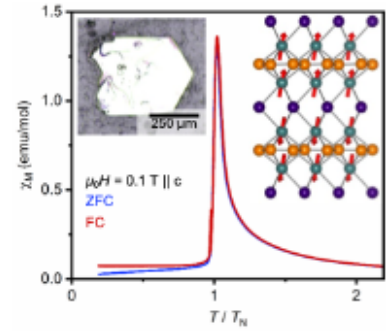


Fig. 3. Magnetic susceptibility of Ce_2Co_2I. Left inset: Image of a crystal. Right inset: altermagnetic structure determined by neutron diffraction.

Using these design rules we recently synthesized a new family of layered rare-earth compounds, with the chemical formula R_2M_2I (R = La, Ce, Pr, Nd; M = Co, Ni), structurally related to CeSiI. The $4f^1$ Ce compounds show signatures of combined $4f$ and $3d$ magnetism, with Ce coupled antiferromagnetically for M = Co or Ni. Uniquely among these materials, Ce_2Co_2I hosts an antiferromagnetic ground state with antiferromagnetic interactions between intermetallic [Ce_2Co_2] layers, as confirmed through neutron diffraction experiments (Fig. 3). Because the two antiferromagnetic subunits are linked only through a crystallographic screw-axis, this material falls into a subcategory of antiferromagnets termed altermagnets, which host non-relativistic spin splitting in their electronic band structure.

This new family of materials is amenable to STM studies using the same nitrogen transfer techniques developed for CeSiI. Figure 4a is an STM topograph of the surface of Ce_2Co_2I that shows atomic resolution. Strong quasiparticle interference is detected using spectroscopic imaging as shown in Figure 4b, and its Fourier transform in figure 4c. Interestingly, the quasiparticle interference breaks the C_3 symmetry expected from the top layer. We expect this to be related to

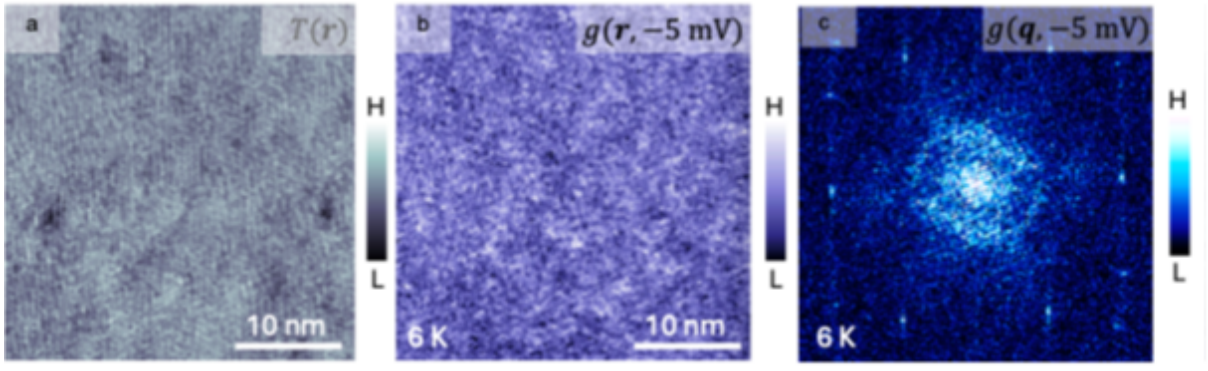


Fig. 4. (a) STM topographic image of Ce_2Co_2I (V = 100 mV, I = 100 pA) (b) Spectroscopic image at V = −5 meV showing strong quasiparticle scattering (c) Fourier transform of (b) showing clear breaking of C_3 symmetry

the altermagnetism present in the compound, and are performing theoretical modeling to understand this effect.

Future Plans

Building on these results, we will exploit device-compatible control knobs to tune the hybridization and coherence scales in CeSiI. First, we will pursue chemical substitution at the Ce, Si, and I sites to modify Kondo coupling, introduce carriers, or generate chemical pressure, providing access to the quantum-critical regime and to competing ordered states. Second, we will improve encapsulation, transfer, and contacting protocols for this extremely air-sensitive material to reliably reach the monolayer limit. One experiment we are preparing with these improved transfer techniques is THz spectroscopy. We will stack CeSiI on thin flakes of $NbOI_2$, a van der Waals THz emitter recently discovered by Roy and co-workers. We will measure the complex optical conductivity spectra to reveal the effective mass, scattering time, and potentially the degree of electron-electron correlation, offering spectroscopic insights into Kondo physics in CeSiI. Third, we will deploy electrostatic and ionic gating to modulate carrier density and Kondo coupling in situ, enabling systematic maps of the hybridization amplitude, Kondo temperature, and crossover scales as functions of electrostatic doping and temperature. Fourth, we will fabricate van der Waals heterostructures that couple CeSiI to metallic, magnetic, or polar layers to engineer interfacial charge transfer and symmetry breaking, creating targeted changes in the hybridization texture. Finally, we will apply uniaxial and biaxial strain using piezoelectric stacks and flexible substrates to manipulate crystal-field splittings and orbital overlaps, thereby steering the nodal geometry and the relative weight of heavy and light sectors.

Beyond the CeSiI heavy fermion family, we will continue to investigate the R_2M_2I family due to the unique coexistence of Kondo behavior and unique magnetic states. Low-temperature STM/S and QPI will be next be used to visualize the states in Pr_2Co_2I and Nd_2Co_2I, both of which feature ferro/ferrimagnetic ground states. How Kondo lattice behavior coexists with these new magnetic orders is an important unresolved question. We will continue to use ARPES to study the Fermi surfaces and the 4*f* occupied states, as well as the thermodynamic, transport, neutron and resonant x-ray scattering techniques that we have successfully used for CeSiI. We will continue our strong collaboration with *ab-inito* and analytical theorists to develop the physics of Kondo lattices in the two-dimensional limit.

Publications

Publications supported by the ECMP program:

1. V. A. Posey, S. Turkel, M. Rezaee, A. Devarakonda, A. K. Kundu, C. S. Ong, D. G. Chica, R. A. Vitalone, R. Jing, S. Xu, D. R. Needell, E. Meirzadeh, M. L. Feuer, A. Jindal, T. Valla, P. Thunström, T. Yilmaz, E. Vescovo, D. Graf, X.-Y. Zhu, A. Scheie, A. F. May, O. Eriksson, D. N. Basov, C. R. Dean, A. Rubio, P. Kim, M. E. Ziebel, A. J. Millis, A. N. Pasupathy, X Roy, "Two-dimensional heavy fermions in the van der Waals metal CeSiI", *Nature* **625**, 483-488 (2024).

2. K. Torres, J. Y. Park, M. E. Ziebel, C. E. Casaday, K. J. Anderton, D. Cui, B. Tang, T. Taniguchi, K. Watanabe, A. N. Pasupathy, X. Roy, P. Kim, "Glassy Relaxation Dynamics in the Two-Dimensional Heavy Fermion Antiferromagnet CeSiI", *Nano Lett.* **25**, 6848-6854 (2025).

3. S. Turkel, V. A. Posey, C. S. Ong, S. Gosh, X. Huang, A. K. Kundu, E. Vescovo, D. G. Chica, P. Thunström, O. Eriksson, W. Simeth, A. Scheie, A. Rubio, A. J. Millis, X. Roy, A. N. Pasupathy, "Nodal hybridization in a two-dimensional heavy fermion material", *Nature Physics* (2025), in press.

Defect-mediated charge density wave transition

Judy J. Cha (PI), and Eun-Ah Kim (co-PI), *Cornell University*

Keywords: charge density waves, stacking faults, layered crystals, machine learning, scanning transmission electron microscopy

Research Scope

The research scope is to understand charge density waves (CDWs) and their phase transitions in layered materials, with a particular focus on tantalum disulfide (TaS_2) and rare-earth tritellurides (RTe_3), using nanoscale samples for their potential applications in future microelectronics and quantum information science. The CDWs in TaS_2 and RTe_3 have been studied using bulk crystals and ensemble-average methods. However, the stability and phase transitions of the CDWs change in these systems when the materials are confined in thickness, impacting their feasibility for applications. Nevertheless, the nanoscale effects on the CDW phase transitions have not been studied systematically. Further, there is a lack of real-space microscopic knowledge of CDW phase transition pathways, such as nucleation and growth of CDW domains, which would get greatly affected by local disorders and heterogeneities, presence of interfaces, and nanoscale morphologies, all of which will be present in actual devices.

For the current project, we employ the real-space probe of *in situ* cryogenic scanning transmission electron microscopy (cryo STEM) to directly visualize the CDWs and their phase transitions. Four-dimensional (4D) STEM, a STEM image where each pixel in the image contains a full 2D electron diffraction pattern, are carried out *in situ* to visualize the CDW transition pathways in real space. To handle and automate analysis of the large 4D STEM data series, we apply unsupervised machine learning to our 4D STEM data series, starting with the Gaussian mixture model we previously used for analyzing x-ray diffraction data.

Recent Progress

CDW behaviors of three systems – TaS_2, RTe_3, and FeGe – have been studied using cryogenic 4D STEM and unsupervised machine learning analysis. In each system, we revealed how the microstructure influences the CDW phase transitions and stability. Real-space mapping of the CDW transition was key in revealing microscopic insights. Unsupervised machine learning analysis applied to large 4D STEM data sets was effective in understanding phase transition behaviors and guiding next experiments. Below, we describe the three CDW systems we studied. These works are summarized in 6 publications in the last two years, as listed under Publications.

A. Defects-mediated CDW phase transition in 1T-TaS_2
(Nature Communications 2024, PNAS 2024)

We showed that mechanical exfoliation can easily create dislocations and stacking faults in layered materials [1], and these extended defects influence the CDW stability and phase transition. We

performed *in-situ* cryogenic 4D STEM on 1T-TaS_2, which transitions from electrically conducting incommensurate CDW, to conducting nearly commensurate (NC) CDW, and finally to insulating commensurate (C) CDW with decreasing temperature. We observed that the phase transition between the NC and C CDW state starts at dislocations and the boundaries between NC CDW domains get pinned at these dislocations. Further, the phase transition from the C CDW state to the NC CDW state proceeds in ways that reflect the underlying networks of dislocations. Unsupervised machine learning that tracked the number of superlattice peaks associated with the CDW state as a function of space and temperature was critical in revealing the phase transition behavior (Fig. 1).

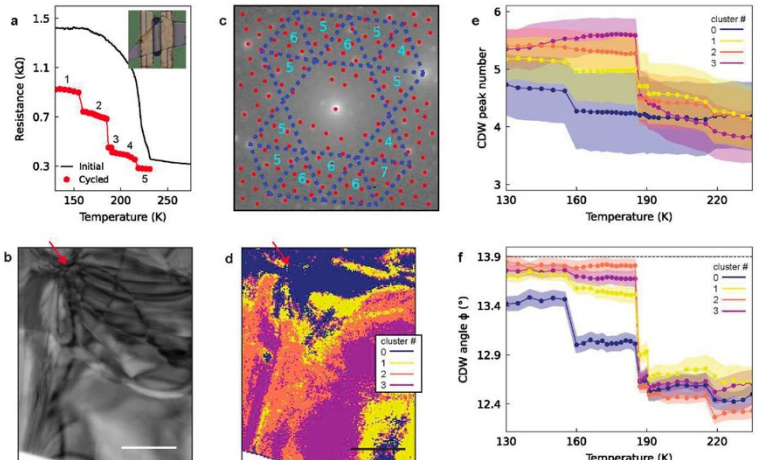


Fig. 1: Unsupervised machine learning (ML) on phase transition in 1T-TaS_2 from C- to NC-CDW state. A) *In-situ* cryogenic transport of flake in (B). (C) Electron diffraction pattern from 4D STEM and superlattice spots ML tracked. D) ML clustering results, showing heterogeneous phase transition. (E, F) Different phase transition behaviors from different regions of the flakes.

B. Ferro-axial CDW and CDW realignment in RTe_3

(Nature Physics 2025, in press)

The CDW observed in rare-earth tritellurides (RTe_3) is found to be ferro-axial from Raman studies [2]. Consequently, the ferro-axial CDW should break crystal symmetries that conventional CDWs will preserve. For RTe_3, all mirror symmetries should be broken for ferro-axial CDW while only some mirror symmetries are broken for conventional CDW.

Using large-angle convergent beam electron diffraction (LACBED) at cryogenic temperatures, we demonstrate the crystal symmetry breaking in $ErTe_3$ flakes at the onset of the CDW formation (Fig. 2). Our results support the ferro-axial nature of the CDW in RTe_3. The use of LACBED was important as the crystal symmetry breaking is too subtle to be captured by atomic-resolution imaging or conventional electron diffraction.

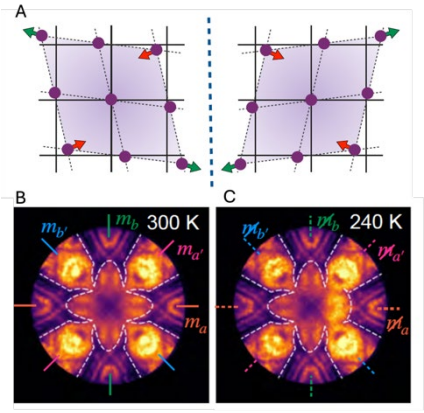


Fig. 2: Ferro-axial CDW in RTe_3. A) Atomic distortions in CDW state break all mirror symmetry. B) LACBED patterns indeed show all mirror symmetry breaking at 240 K.

C. Microscopic origin for CDW emergence in Kagome antiferromagnet FeGe

(Nature Communications 2025)

In Kagome lattice antiferromagnet FeGe, a CDW order is found deep within an antiferromagnetically ordered state, interacting with the magnetic order [3]. Surprisingly, post-growth annealing of FeGe at 560 °C suppresses the CDW order while annealing at 320 °C enhances the order. We used *in-situ* cryogenic 4D STEM and atomic-resolution STEM imaging to unveil the microscopic mechanism of the annealing process and its impact on the CDW order. We find that 560 °C annealing creates Ge vacancies uniformly distributed throughout the FeGe Kagome lattice, preventing the formation of Ge-Ge dimers necessary for the CDW order. Upon 320 °C anneal, the system segregates into stoichiometric FeGe regions that support long-range CDW order and regions with stacking faults that act as nucleation sites for the CDW.

D. Topological defects as emblems of pair density wave in rhombohedral graphene (arXiv: 2506.08087)

We explored how to detect a novel density wave state that intertwines charge density modulation with pairing: the pair density wave (PDW) state. Cryogenic 4D STEM could be powerful probe of PDW when the modulations in superconducting pair amplitude couples to charge density. A recent experiment on rhombohedral graphene has revealed superconductivity emerging from a quarter-metal state, providing the first experimental system where a pure PDW without uniform superconductivity is expected. This experiment presents a critical puzzle: unusual resistive switching behavior at zero magnetic field that cannot be explained by conventional superconductivity. We proposed that this behavior originates from topological defects with a remarkable dual identity unique to multi-component PDWs. These defects simultaneously function as fractional vortices carrying 1/3 flux quantum and as crystalline dislocations in the emergent PDW lattice. This dual nature allows charge disorder to source magnetic excitations---a striking manifestation of intertwined orders. Our theory establishes a framework for understanding pure PDW systems through their topological excitations, opening new research directions previously inaccessible in systems with coexisting uniform superconductivity.

Future Plans

Three projects are currently ongoing.

A. Melting point depression of CDW in 1T-$TiSe_2$ due to lateral confinement (Manuscript in preparation)

The first project is the observation of the melting point depression for CDW in 1T-$TiSe_2$ nanoflakes due to lateral confinement. While CDW behaviors of layered crystals were studied as a function of thickness for some materials (for example 1T-TaS_2), the effects of lateral confinement on the CDW phase transition and stability have not been investigated. Nevertheless, such information is critical as we aim to exploit these materials for microelectronic applications where the device size will be on the order of tens of nanometers. As the system size approaches the coherence length of the electronic state, large deviations are expected.

We observe a significant melting point depression of CDW as 1T-$TiSe_2$ flakes approach the coherence length scale of CDW. Cryogenic electron diffraction patterns were acquired down to 20 K as a function of $TiSe_2$ flakes (PI Cha's group) and a Ginzburg-Landau modeling was carried out to capture the size effects (Co-PI Kim's group). A manuscript is currently in preparation (Fig. 3).

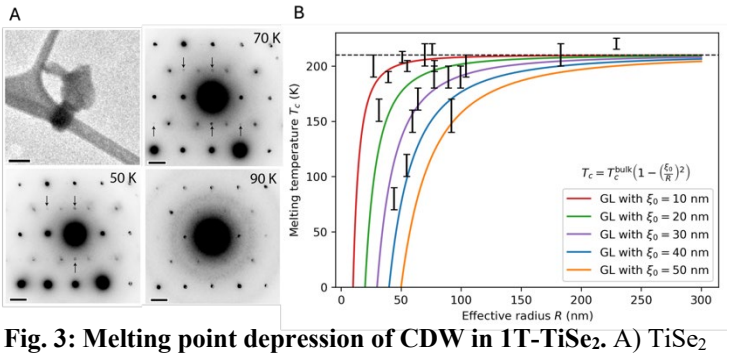


Fig. 3: Melting point depression of CDW in 1T-$TiSe_2$. A) $TiSe_2$ flake and electron diffraction at cryogenic temperatures. Disappearance of superlattice peaks (arrows) denote CDW melting. B) CDW melting as function of flake size and Ginzburg-Landau modeling to show confinement effects on CDW stability.

B. Effects of Moiré potentials on CDW stability

We hypothesize the presence of Moiré potentials will influence the stability of CDWs in layered materials, especially when the periodicity of Moiré potentials is on par with the coherence length of the system. To study this, we must deterministically create Moiré potentials in CDW materials. We apply stressor metal oxide films that are lithographically patterned on 2H and 3R MoS_2 flakes and induce hetero-strain on the top two layers of MoS_2. This creates Moiré patterns, determined by the patterns and thickness of the stressor film. We will apply this technique to CDW layered material and study the effects of Moiré potentials on CDW phase transition and stability.

C. Learning descriptors of material properties from curated database

Massive amounts of high-throughput *ab-initio* data and curated experimental data are becoming accessible to researchers. Much needed are data-centric approaches that accelerate discoveries from these data through synergetic interaction with expert human researchers' insights. As a first target we will leverage the database of over 9000 superconductors and train an interpretable machine learning model that can predict superconducting transition temperature. We will first develop featurization that turns chemical formula, elemental features of the elements in the material, and the structural information into input for the machine learning algorithm. If successful, this approach will generalize to other material properties of interest.

References

1. J. L. Hart, L. Bhatt, Y. Zhu, M-G. Han, S. Li, D. Hynek, J. A. Schneeloch, Y. Tao, D. Louca, P. Guo, Y. Zhu, F. Jornada, E. J. Reed, L. F. Kourkoutis, J. J. Cha, *Emergence of layer stacking disorder in c-axis confined $MoTe_2$*, Nature Communications **14**:4803 (2023)
2. Y. Wang, I. Petrides, G. McNamara, M. M. Hosen, S. Lei, Y.-C. Wu, J. L. Hart, H. Lv, J. Yan, D. Xiao, J. J. Cha, P. Narang, L. Schoop, K. Burch, *Axial Higgs mode detected by quantum pathway interference in RTe_3*, Nature **606**, 896-901 (2022)
3. Teng X, Chen L, Ye F, Rosenberg E, Liu Z, Yin JX, Jiang YX, Oh JS, Hasan MZ, Neubauer KJ, Gao B, Xie Y, Hashimoto M, Lu D, Jozwiak C, Bostwick A, Rotenberg E, Birgeneau RJ, Chu JH, Yi M, Dai P, *Discovery of charge density wave in a kagome lattice antiferromagnet,* Nature **609**:490-495 (2022)

Publications

1. O. Lesser, C. Huang, J. P. Sethna, E.-A. Kim, *Emblems of pair density waves: dual identity of topological defects and their transport signatures*, arXiv:2506.08087 (2025)
2. B. Singh, G. McNamara, K.-M. Kim, S. Siddique, S. D. Funni, W. Zhang, X. Luo, P. Sakrikar, E. M. Kenny, R. Singha, S. Alekseev, S. A. A. Ghorashi, T. Hicken, C. Baine, H. Luetkens, Y. Wang, V. Plisson, M. Geiwitz, C. A. Occhialini, R. Comin, M. J. Graf, L. Zhao, J. Cano, R. M. Fernandes, J. J. Cha, L. M. Schoop, K. S. Burch, *Uncovering the hidden ferroaxial density wave as the origin of the axial Higgs mode in RTe_3*, accepted in Nature Physics (2025), arXiv:2411.08322
3. M. Klemm, S. Siddique, Y.-C. Chang, S. Xu, Y. Xie, T. Legvold, M. T. Kiani, X. Teng, B. Gao, F. Ye, H. Cao, Y. Hao, W. Tian, H. Luetkens, M. Matsuda, D. Natelson, Z. Guguchia, C.-L. Huang, M. Yi, J. J. Cha, P. Dai, *Vacancy-induced suppression of charge density wave order and its impact on magnetic order in Kagome antiferromagnet FeGe*, Nature Communications **16**:3313 (2025)
4. S. Siddique, J. L. Hart, D. Niedzielski, R. Singha, M.-G. Han, S. D. Funni, M. Colletta, M. T. Kiani, N. Schnitzer, N. L. Williams, L. F. Kourkoutis, Y. Zhu, L. M. Schoop, T. Arias**,** J. J Cha, *Realignment and suppression of charge density wave in the rare-earth tritellurides RTe_3 (R=La, Gd, Er),* Phys. Rev. B **110**, 014111 (2024)
5. J. L. Hart, H. Pan, S. Siddique, N. Schnitzer, K. Mallayya, S. Xu, L. F. Kourkoutis, E.A. Kim, J. J. Cha, *Real-space visualization of a defect-mediated charge density wave transition*, Proc. Natl. Acad. Sci. **121**, e2402129121 (2024)
6. J. L. Hart, S. Siddique, N. Schnitzer, S. D. Funni, L. F. Kourkoutis, J. J. Cha, *In operando cryo-STEM of pulse-induced charge density wave switching in TaS_2*, Nature Communications **14**:8202 (2023)

Prediction, Design, and Synthesis of New Magnetic Nitrides

Sage Bauers | National Renewable Energy Laboratory

Keywords: ferromagnets, polycrystalline materials, materials discovery, metastability

Research Scope: Magnetic Materials Discovery
This program seeks to discover new magnetic materials toward lanthanide-free permanent magnet applications. Inspired by examples of sub-nitrides with high magnetic performance, we elected to focus on similar chemical spaces. The underlying hypothesis is that nitrogen's intermediate electronegativity enables strong magnetic exchange and structural distortions that enhance magnetocrystalline anisotropy energy without driving metals into highly oxidized states. Over the period of this program, we have integrated high-throughput prediction, computationally guided synthesis, and advanced characterization to identify and realize several new magnetic nitrides.

Recent Progress
Materials discovery efforts often begin with prediction of candidate phases using ionic substitution-based strategies (the underlying assumption being two metals with the same preferred oxidation state are likely to substitute).[1,2] Such approaches often fail for intermetallic or anion-lean systems where oxidation states are ambiguous. To map the stability of *metal-rich* ternary nitrides, we instead developed and employed a new strategy where substitutions are performed based on the *number of shared structural prototypes* between metals. This approach generated 1800 new candidate nitrides, and follow-on thermochemical calculations revealed many of the candidate structures to be stable. In total, 70 new ternary chemical systems with no previously known nitride phases were identified. Of these new predictions, 49 contain two non-alkaline metals plus nitrogen, making many of them promising candidates for magnetic behavior. **Fig 1** shows some of the predicted materials containing ferrous 3d elements, where each colored swatch represents a unique ternary chemical space and swatches with a border are spaces where stable nitrides are predicted but none are currently known.

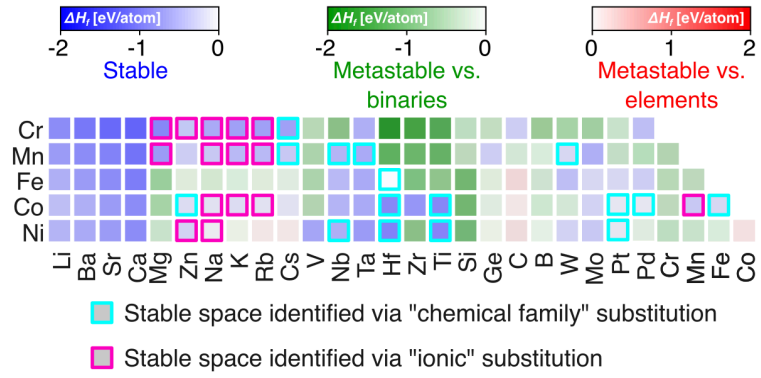


Fig 1: Snippet of a larger map of calculated ternary nitride stability. Chemical spaces with a cyan border were identified using our beyond-ionic substitution "chemical family" algorithm and are less likely to be anion rich than spaces identified using ionic substitution (magenta).

The row of Co-containing nitrides contains 5 compounds predicted to be stable using our updated prediction algorithm. From left to right these are: Co_3ZnN, Hf_4Co_2N, Ti_4Co_2N, Co_3PtN, Co_3PdN, and $CoFeN_2$. Previous ionic substitution efforts also identified new compositions, including $MnCoN_2$.[1] To demonstrate the efficacy of these predictions, several of the predicted nitrides were synthesized in the lab.

Antiperovskite Co_3PdN

Although Co_3PdN has been repeatedly flagged by computation[3,4]—including our novel beyond ionic algorithm—its synthesis and stability had never been experimentally verified. Using reactive sputtering, we achieved the first experimental realization of Co_3PdN[5] (**Fig 2a**), verifying its antiperovskite crystal structure through both laboratory and synchrotron x-ray scattering. Importantly, we established the compound's thermal stability to 600 K (persisting even to ~700 K under inert atmosphere), showing its practical viability in the use environment.

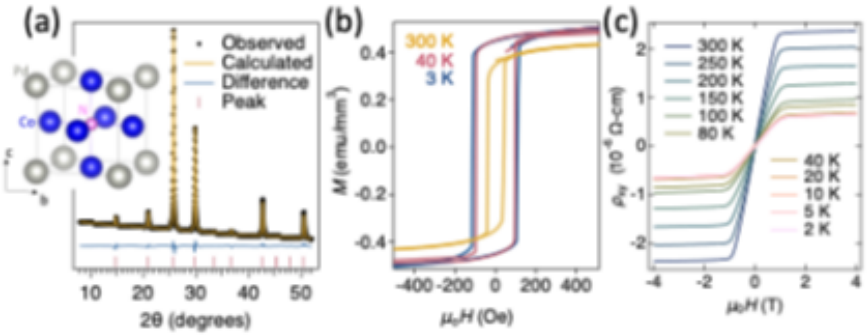


Fig 2: Characterization of Co_3PdN. (a) X-ray diffraction confirming antiperovskite structure. (b) Magnetic hysteresis loops from this ferromagnetic material. (c) Hall resistivity showing saturation of the anomalous signal.

Magnetometry demonstrated that Co_3PdN is a soft ferromagnet (**Fig 2b**) with a Curie temperature of $\mathbf{T_c = 560 \pm 5\ K}$, well above room temperature and squarely within the range needed for applications. The measured saturation magnetization (1.2 μ_B/Co) is close to—but slightly below—the theoretical expectation (1.7 μ_B/Co), reflecting subtle electronic effects. A narrow hysteresis loop with a coercive field of 100 Oe at low temperature highlights potential for **fast magnetic switching**, relevant to electronic and spintronic applications. A clear anomalous Hall effect (**Fig 2c**) further confirms Co_3PdN's ferromagnetism.

We also resolved conflicting reports on its electronic structure. Prior predictions suggested a gapped state, but we demonstrated that this arose from incomplete Brillouin-zone sampling. Our calculations and transport measurements confirm **metallic behavior with a sizable anomalous Hall effect**, reinforcing Co_3PdN as both a scientifically and technologically intriguing magnetic nitride.

Together, these results establish Co_3PdN as a **benchmark for predictive nitride discovery**, demonstrating the transition from theory to experiment while opening the door to a broader family of unexplored antiperovskites. A similar suite of experiments on other predicted antiperovskites, Co_3ZnN and Co_3PtN, including through epitaxial stabilization, showed that Co_3ZnN can be synthesized using very similar methods to Co_3PdN, but Co_3PtN cannot; an ongoing scientific question is why this is the case.

Disordered Rocksalt $MnCoN_2$

$MnCoN_2$ represents one of the few ternary nitrides composed exclusively of transition metals that were predicted by ionic substitution, making it a compelling discovery target. Although originally proposed in a zincblende-derived structure with tetrahedral coordination,[1] our follow-on calculations revealed a more stable rocksalt-derived polymorph with octahedral coordination (**Fig 3a, 3b**). We realized this phase experimentally as thin films synthesized by reactive sputtering within a narrow growth window just above ambient temperature, demonstrating that careful kinetic control can stabilize $MnCoN_2$ over competing binaries and amorphous products.[6]

Laboratory and synchrotron diffraction confirm that $MnCoN_2$ adopts a cation-disordered rocksalt structure (**Fig 3c**). X-ray absorption spectroscopy further verifies octahedral coordination of Mn^{3+} and Co^{3+}.

Importantly, $MnCoN_2$ cannot be described as a simple mixture of binary nitrides but instead represents a genuinely new ternary phase space.

Magnetometry (**Fig 3d**) reveals a canted antiferromagnetic ground state below ~10 K, with a Weiss temperature of –50 K indicating strong AFM correlations. This contrasts sharply with the high-T_N antiferromagnetism of MnN and the paramagnetism of CoN, clear evidence that the ternary chemistry drives emergent magnetic behavior not present in the binaries. At the last ECMP program meeting we showed with Monte Carlo + DFT calculations that similar behavior in $MnSnN_2$ arises from cation disorder.[7] A small net moment and coercivity at 2 K suggest weak canting or ferrimagnetic clusters within the disordered rocksalt lattice.

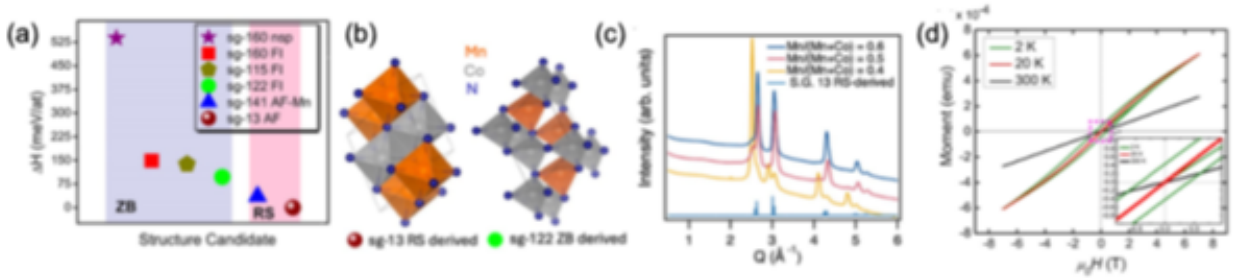


Fig 3: Discovery of $MnCoN_2$. (a) Calculated formation enthalpy of $MnCoN_2$ in various space groups and magnetic configurations. (b) Lowest-energy zincblende- and rocksalt-derived structures. (c) X-ray diffraction providing experimental confirmation of rocksalt $MnCoN_2$. (d) Small hysteresis at low temperature suggests canted antiferromagnetic order.

Altogether, $MnCoN_2$ expands the library of known ternary nitrides and establishes a blueprint for discovering other transition-metal–only compounds that may have structures that appear very similar to binary parent compounds when using global structure probes. It highlights how cation disorder, metastability, and multi-metal chemistries can combine to produce exotic magnetic ground states, offering fertile ground for both predictive design and future synthesis efforts.

η-nitride Hf_4Co_2N

An unexpected materials family identified by our substitution algorithm was compounds in the Fe_3W_3C prototype (space group 227), often associated with η-carbide superalloys. New Mn, Ni, Fe, and Co compositions were identified in subsets of this structure. To test the predictions, we elected to prepare Hf_4Co_2N, guiding our approach by also preparing Fe_4W_2N, which is known.

We found that direct growth of either phase was not possible because the requisite nitrogen chemical potential μ(N) is lower than can be supplied by a synthesis tool and an fcc phase forms at elevated deposition temperatures. However, we found that Fe_4W_2N can be prepared by post-annealing amorphous Fe-W-N thin films in a low μ(N) environment. Because of the very low μ(N) required for Hf_4Co_2N and strong competition from HfN (**Fig 4a**), even this approach was found intractable for Hf_4Co_2N. Instead, we designed a synthetic route consisting of depositing intermetallic Hf_2Co thin films, which have a very similar structure to Hf_4Co_2N, and then post-annealing in nitrogen-containing environments. This approach readily yields Hf_4Co_2N over HfN (**Fig 4b**), surprisingly even when μ(N) is high (NH_3 environment at 500 °C). We hypothesize that kinetic barriers to restructuring the Hf_2Co intermetallic lattice prevent conversion, enabling the stabilization of Hf_4Co_2N even at high μ(N).

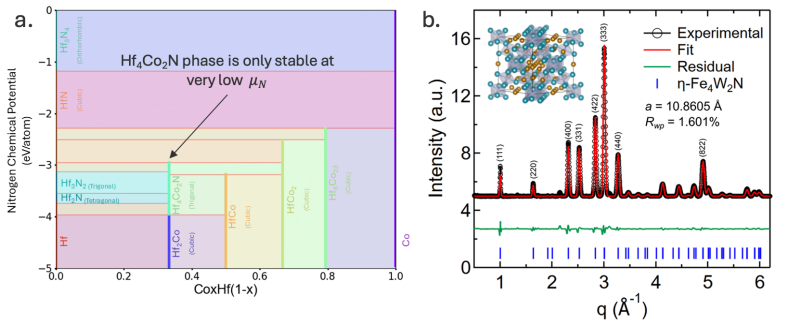


Fig 4: Synthesis of "η-nitride" Hf_4Co_2N. (a) Calculated phase diagram in mixed nitrogen chemical potential (y) and metal composition (x) axes, which was used to guide synthesis. (b) XRD of Hf_4Co_2N synthesized from Hf_4Co_2 intermetallic and nitrided in NH_3.

Future Plans

While we have demonstrated effective rational *discovery* of new magnetic compounds, there are currently no prescriptive *design* principles to navigate the structure-chemistry-bonding-property relationships of ferromagnets. For this reason, we lack a conceptual framework on how to navigate the bewilderingly high-dimensional "crystal chemistry" space for permanent magnet design.

However, we are now positioned to remedy this. Through our ECMP funding, we unveiled innovative new computational tools to extract real space bonding-magnetism relationships directly from spin-polarized electronic structure calculations,[8] and we have also refined our ability to selectively synthesize metastable magnetic sub-nitride powders[9] and thin films[5] with targeted structures and compositions. From this platform, our next stage will be to establish the first quantitative set of design principles to connect magnetic moment and magnetocrystalline anisotropy energies to the underlying bonding, structure, and stability of inorganic solids.

References

(1) Sun, W.; Bartel, C. J.; Arca, E.; Bauers, S. R.; Matthews, B.; Orvañanos, B.; Chen, B. R.; Toney, M. F.; Schelhas, L. T.; et al. *Nat. Mater. 2019 187* **2019**, *18* (7), 732–739.

(2) Hautier, G.; Fischer, C.; Ehrlacher, V.; Jain, A.; Ceder, G. *Inorg. Chem.* **2011**, *50* (2), 656–663.

(3) Singh, H. K.; Zhang, Z.; Opahle, I.; Ohmer, D.; Yao, Y.; Zhang, H. *Chem. Mater.* **2018**, *30* (20), 6983–6991.

(4) Ahmad Khandy, S.; Islam, I.; Kaur, K.; Laref, A.; Dhiman, S.; Rubab, S.; Gupta, D. C.; Khenata, R. *Results Phys.* **2020**, *17*, 103112.

(5) Dugu, S.; Mahatara, S.; Regier, C. E.; Leahy, I. A.; Zakutayev, A.; Neilson, J. R.; Lany, S.; Bauers, S. R. *Chem. Mater.* **2025**, *37* (5), 1906–1913.

(6) Dugu, S.; Smaha, R. W.; Quadir, S.; Treglia, A.; Martin, J.; O'Donnell, S.; Mahatara, S.; Teeter, G.; Lany, S.; Neilson, J. R.; Bauers, S. R. *Phys. Rev. Mater.* **2024**, *8* (10), 104411.

(7) Rom, C. L.; Smaha, R. W.; Melamed, C. L.; Schnepf, R. R.; Heinselman, K. N.; Mangum, J. S.; Lee, S.-J.; Lany, S.; Schelhas, L. T.; et al. *Chem. Mater.* **2023**, *35* (7), 2936–2946.

(8) Oliphant, E.; Mantena, V.; Brod, M.; Snyder, G. J.; Sun, W. *Mater. Horiz.* **2025**, *12* (9), 3073–3083.

(9) O'Donnell, S.; Mahatara, S.; Lany, S.; Bauers, S. R.; Smaha, R. W.; Neilson, J. R. *Inorg. Chem.* **2024**, *63* (34), 16075–16080.

Publication List (since last PI meeting)

Led by this FWP

(1) Oliphant, E.; Mantena, V.; Brod, M.; Snyder, G. J.; Sun, W. Why Does Silicon Have an Indirect Band Gap? *Mater. Horiz.* 2025, 12 (9), 3073–3083.

(2) Dugu, S.; Mahatara, S.; Regier, C. E.; Leahy, I. A.; Zakutayev, A.; Neilson, J. R.; Lany, S.; Bauers, S. R. Synthesis, Stability, and Magnetic Properties of Antiperovskite Co_3PdN. *Chem. Mater.* 2025, 37 (5), 1906–1913.

(3) O'Donnell, S.; Leahy, I. A.; Jana, S.; Gabilondo, E. A.; Halasyamani, P. S.; Maggard, P. A.; Smaha, R. W. Magnetic Properties and Large Second-Harmonic Generation Response of a Chiral Ternary Chalcogenide: Eu_2SiSe_4. *Chem. Mater.* 2025, 37 (14), 5036–5042.

(4) Bauers, S. R. Combinatorial investigation of the Mn-Ge-N chemical system containing ternary nitrides Mn_3GeN and $MnGeN_2$. Accepted at *MRS Commun.* for 2025 Distinguished Early Career Special Issue.

(5) Dugu, S.; Smaha, R. W.; Quadir, S.; Treglia, A.; Martin, J.; O'Donnell, S.; Mahatara, S.; Teeter, G.; Lany, S.; Neilson, J. R.; Bauers, S. R. Thin Film Synthesis, Structural Analysis, and Magnetic Properties of Novel Ternary Transition Metal Nitride $MnCoN_2$. *Phys. Rev. Mater.* 2024, 8 (10), 104411.

(6) O'Donnell, S.; Mahatara, S.; Lany, S.; Bauers, S. R.; Smaha, R. W.; Neilson, J. R. "Mn_3AlN" Is Really Mn_4N. *Inorg. Chem.* 2024, 63 (34), 16075–16080.

(7) Rom, C. L.; Smaha, R. W.; O'Donnell, S.; Dugu, S.; Bauers, S. R. Emerging Magnetic Materials for Electric Vehicle Drive Motors. *MRS Bull.* 2024, 49 (7), 738–750.

(8) Chen, J.; Powell-Palm, M. J.; Sun, W. The Geometry of High-Dimensional Phase Diagrams: III. Engineering Relative Stability in Four Dimensions. arXiv April 9, 2024.

(9) Regier, C. E.; O'Donnell, S.; Goyal, A.; Dzara, M. J.; Park, J. E.; Bell, R. T.; Kramer, M. J.; Paddison, J. A. M.; Shulda, S.; Ginley, D. S.; Yahne, D. R.; Lany, S.; Smaha, R. W.; Klein, R. A. Interlayer Ions Control Spin Canting in Low-Dimensional Manganese Trimers in 12R-$Ba_4MMn_3O_{12}$ (M = Ce, Pr) Layered Perovskites. *Inorg. Chem.* 2024, 63 (51), 24176–24186.

Acknowledging this FWP

(1) Lee, C.-W.; Smaha, R. W.; Brennecka, G. L.; Haegel, N. M.; Gorai, P.; Yazawa, K. From Prediction to Experimental Realization of Ferroelectric Wurtzite $Al_{1-x}Gd_xN$ Alloys. *APL Mater.* 2025, 13 (2), 021114.

(2) Brown, W. K.; Oyekunle, I. P.; Truong, E.; Chen, Y.; Ogbolu, B.; Schundelmier, B.; O'Donnell, S.; Smaha, R. W.; Hu, Y.-Y.; Wei, K.; McCandless, G. T.; Chan, J. Y. $Co_3Ga_2Ge_5$: Probing Site Mixing of the Ru_3Sn_7 Structure Type with Elements Difficult to Distinguish by Diffraction. *J. Alloys Compd.* 2025, 1010, 177828.

(3) Julien, B.; Leahy, I. A.; Smaha, R. W.; Mangum, J. S.; Perkins, C. L.; Bauers, S. R.; Zakutayev, A. Structural Stability, Elemental Ordering, and Transport Properties of Layered $ScTaN_2$. In revision at *Phys. Rev. Mater.* arXiv July 8, 2025.

(4) Smaha, R. W.; Mangum, J. S.; Yadav, N.; Rom, C. L.; Wieliczka, B. M.; Julien, B.; Treglia, A.; Perkins, C. L.; Gorai, P.; Bauers, S. R.; Zakutayev, A. $GdWN_3$ Is a Nitride Perovskite. *Appl. Phys. Lett.* 2024, 125 (11), 112902.

(5) Jana, S.; O'Donnell, S.; Leahy, I. A.; Koldemir, A.; Pöttgen, R.; Smaha, R. W.; Maggard, P. A. Synthesis, Crystal Structure, and Physical Properties of the Eu(II)-Based Selenide Semiconductor: $EuHfSe_3$. *J. Mater. Chem. C* 2024, 12 (31), 11769–11777.

Geometrically frustrated magnets with exotic Archimedean lattices

Tai Kong, *University of Arizona*

Keywords: magnetism, geometrically frustrated magnet, specific heat

Research Scope

Understanding magnetic behavior in different crystalline environments has been one of the main drives in condensed matter physics. It has been shown that frustrated magnetic systems offer unique access to exotic magnetic states [1]. Geometrical frustration, where a triangular motif is present in the magnetic sublattice, is an important factor that can help achieve magnetic frustration. This is because nearest-neighbor antiferromagnetic interaction cannot be simultaneously satisfied within a triangular unit. Triangular and Kagome lattices are intensively studied based on this idea behind geometrical frustration. Since a single triangular motif in a lattice is sufficient to introduce geometrical frustration, more lattice types can be considered geometrically frustrated, and thus lead to potential novel magnetic ground states [2]. **In this research program,** we aim to expand the material pool of geometrically frustrated magnets by identifying and characterization of compounds that host triangle-containing Archimedean lattices (ALs). Particularly, we focus on maple leaf (ML), ruby, Shastry-Sutherland (SS), trellis and star lattices.

Recent Progress

1. Survey of exotic ALs with triangular motif

An important task in this project is to identify possible material systems that can be described by exotic ALs. We conducted a thorough survey that combined both manual and automated searches. The manual search was done via a keyword search in existing literature. The automated search

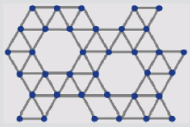
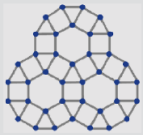
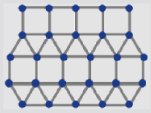
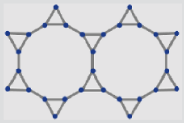
Maple-leaf (3^4,6)	Bounce/Ruby (3,4,6,4)	Shastry-Sutherland (3^2,4,3,4)	Trellis (3^3,4^2)	Star (3,12^2)
				
Na$_2$Mn$_3$O$_7$ (ICSD: 92858) **Zn**Mn$_3$O$_7$·3H$_2$O (ICSD: 202701) Bi$_4$Mn$_3$O$_{11.5}$ (ICSD: 424652) Pb$_3$Cu$_6$TeO$_6$(OH)$_7$Cl$_5$ (2 ICSD: 290104) Cu$_6$TeO$_4$(OH)$_9$Cl (ICSD: 241339) Cu$_6$IO$_3$(OH)$_{10}$Cl (ICSD: 241338) Cu$_2$ZnAsO$_4$(OH)$_3$ (ICSD: 0006608) Cu$_6$**Al**(SO$_4$)(OH)$_{12}$Cl$_3$·3H$_2$O (ICSD: 73424) **K**$_x$[Fe(O$_2$CCH$_2$)$_2$NCH$_2$PO$_3$]$_6$·nH$_2$O (CCDC: 279858)	CsBa**Cr**$_3$F$_{12}$ (ICSD: 67209) Y**Ni**$_2$**Al**$_3$ type (ICSD: 54425) Ba**Eu**$_6$(Si$_3$B$_6$O$_{24}$)(OH)$_2$ (ICSD: 194860)	**AlCu**$_2$**Re**$_2$ (ICSD: 57706) **Ti**$_2$**ReB**$_2$ (ICSD: 44554) Zr$_4$CuSb$_7$ (ICSD: 195056) Li$_2$Ca(MnN)$_2$ (ICSD: 411203) Ca$_5$Cd**Cu**$_2$ (ICSD: 423251) BaCa$_4$**Cu**$_2$N$_4$ (ICSD: 86066) **Co**[PH$_2$O$_2$]Cl[H$_2$O] (ICSD: 69561) **Er**AlGeO$_5$ (ICSD: 171495) Ba**Nd**$_2$**ZnS**$_5$ (ICSD: 93714) **Tm**B$_4$ (ICSD: 109209) **Yb**$_2$**Ru**$_3$Ga$_{10}$ (ICSD: 107022) **Ca**Co$_2$**Al**$_8$ (ICSD: 57533) **Eu**$_2$SiCl$_2$O$_3$ (ICSD: 400126) **Dy**$_2$**Be**$_2$**Si**O$_7$ (ICSD: 126614) H$_2$CoP$_3$O$_{10}$[NH$_3$]$_3$ (ICSD: 15552)	**LiV**$_2$O$_5$ (ICSD: 175737) **Ca**V$_2$O$_5$ (ICSD: 82689) Ce$_2$Te$_7$**Br**$_2$O$_{17}$ (ICSD: 250636) **CeTl**$_2$P$_2$S$_7$ (ICSD: 171219) **Eu**$_2$B$_4$Rh$_5$ (ICSD: 68540) **Gd**$_2$Ge(BO$_4$)$_2$ (ICSD: 168967) **Gd**$_2$B$_3$C$_2$ (ICSD: 67980) **Pr**Sn$_2$ (ICSD: 657389) **Sm**$_2$(CN$_2$)$_3$ (ICSD: 240312) CaFeO$_2$Cl (ICSD: 96556)	[Fe$_3$(μ_3-O)(μ-OAc)$_6$(H$_2$O)$_3$] [Fe$_3$(μ_3-O)(μ-OAc)$_{7.5}$]$_2$·7H$_2$O (CCDC: 643841) [(CH$_3$)$_2$(NH$_2$)]$_3$[Cu^{II}$_3$(μ_3-OH)(μ_3-SO$_4$)(μ_3-SO$_4$)$_3$]·0.24H$_2$O (CCDC: 1977730)

Table 1 Underlined elements exhibit the lattice type in the column. Bold atoms can be replaced by other elements within similar structural types. Numbers in the parenthesis after each compound is an example ICSD or Cambridge Crystallographic Data Centre (CCDC) number that can be used to find the corresponding crystal structure and structure type.

used crystallographic information from the Materials Project [3] and lattice match program, Systre. To avoid complications due to multiple magnetic elements, only compounds that contain one and only one common magnetic 3d transition metal elements (Ti-Cu) and magnetic rare-earth elements (Ce-Nd and Sm-Yb) were used for analysis. A total of 51,340 compounds were analyzed. The lattice identification results from Systre were then manually screened to ensure the final lattice type is correct. The combined search was completed during the last funding period. Results are presented in Table 1, and published in Ref [4].

We show that geometrical frustration can be studied in all exotic ALs. In Table 1, representative compounds are shown for each proposed lattice type. Listed compounds may be expanded to a family of compounds that crystallize in the same structure type. The underlined elements represent the magnetic element of interest and bold elements can be replaced by other elements. While some compounds in the table have been studied with consideration of their underlying lattice type, most of the listed compounds are yet to be studied with respect to their lattice type, which calls for more experimental investigations in the future.

2. Dimer ground state in $BaCe_2ZnS_5$

SS lattice is one of the exotic ALs. Previously, we were able to synthesize single crystalline $BaRE_2ZnS_5$ (RE = La-Pr) family of compounds for the first time. While $BaNd_2ZnS_5$ shows antiferromagnetic ordering, $BaCe_2ZnS_5$ show a broad dome in low temperature specific heat with no signature that can be associated with long-range magnetic ordering. During the past funding period, we worked with Oak Ridge National Lab (ORNL) to combine neutron scattering data and our in-house thermodynamic data for a better understanding of the magnetic ground state in $BaCe_2ZnS_5$. By considering a localized spin dimer model, we were able to reproduce experimental data nicely. The measured and simulated magnetic specific heat data is shown in Figure 1 and reported in Ref [5]. According to our model, intra-dimer exchange interaction shows strong XY-type anisotropy and the ground state of $BaCe_2ZnS_5$ is in an entangled state $(|\uparrow\uparrow\rangle - |\downarrow\downarrow\rangle)/\sqrt{2}$. This contrasts with the singlet dimer state that is obtained for Heisenberg interactions. By including a small interdimer

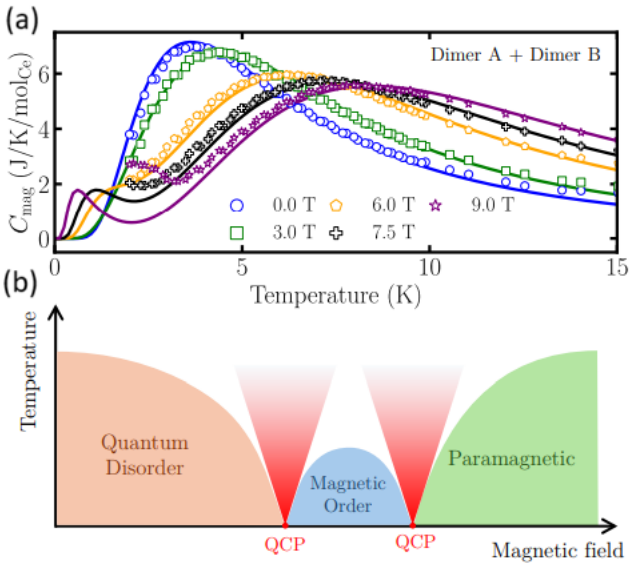


Figure 1 (a) temperature dependent specific heat of $BaCe_2ZnS_5$ measured at different applied magnetic field along [110]. Symbols are experimental data. Solid lines represent simulation considering two sets of orthogonal dimers. (b) proposed magnetic phase diagram illustrating potential quantum critical points.

interaction, we propose that there could be a field induced magnetically ordered phase and associated field driven quantum critical point. This work is currently under review.

Future Plans

Since the survey on exotic ALs was completed within the first year of this project, we will start synthesizing compounds that can potentially host lattice relevant phenomena and novel quantum magnetism states. In the next funding period, we will synthesize samples that crystalize in ruby, ML and SS lattices. For ruby lattice, we will focus on polycrystalline $CsBaCr_3F_{12}$. For ML lattice, we will focus on polycrystalline $Na_2Mn_3O_7$ and $ZnMn_3O_7$ where Mn-Mn bonding distance can be gradually tuned. For SS lattice, we will focus on the single crystal synthesis of the $Yb_2Ru_3Ga_{10}$ family and polycrystalline Ca_5CdCu_2 family. Compounds, if synthesized successfully, will be characterized to identify corresponding magnetic ground states.

With our existing single crystalline family of compounds, $BaRE_2ZnS_5$, we will continue working with ORNL to use neutron scattering to investigate the spin dynamics in $BaNd_2ZnS_5$ near the spin disordered region. Our recent neutron scattering experiment proposal on $BaPr_2ZnS_5$ has been approved and will be performed in November 2025. Detailed results will be analyzed in collaboration with ORNL.

References

[1] A. P. Ramirez, Annu. Rev. Mater. Sci. **24**, 453 (1994).

[2] D. J. J. Farnell, O. Götze, J. Schulenburg, R. Zinke, R. F. Bishop, and P. H. Y. Li, Phys. Rev. B **98**, 224402 (2018).

[3] A. Jain, S. P. Ong, G. Hautier, W. Chen, W. D. Richards, S. Dacek, S. Cholia, D. Gunter, D. Skinner, G. Ceder, and K. a. Persson, APL Mater. **1**, 11002 (2013).

[4] S. Guo, D. A. Krug, B. R. Billingsley, J. Wang, Z. Qiu, and T. Kong, Innovation **0**, 100981 (2025).

[5] Q. Ma, B. R. Billingsley, M. Marshall, D. A. Dahlbom, Y. Hao, D. M. Pajerowski, A. I. Kolesnikov, X. Bai, C. D. Batista, T. Kong, and H. Cao, ArXiv: 2412.17913 (2024).

Publications

1. S. Guo, D.A. Krug, B.R. Billingsley, J. Wang, Z. Qiu, T. Kong. The Innovation 6 (2025) 100981, DOI: 10.1016/j.xinn.2025.100981

2. Q. Ma, B.R. Billingsley, M. Marshall, D.A. Dahlbom, Y. Hao, D.M. Pajerowski, A.I. Kolesnikov, X. Bai, C.D. Batista, T. Kong, H. Cao. arXiv: 2412.17913

Wednesday, September 10, 2025

Unconventional Superconductivity in Magnetic Rare-Earth Doped Nickelate Thin Films

Charles H. Ahn, Yale University, New Haven, CT 06511

Department of Applied Physics, Department of Physics, Department of Mechanical Engineering and Materials Science, Yale University

Keywords: superconductivity, nickelate superconductor, thin film heterostructures, molecular beam epitaxy, x-ray scattering

Research Scope

This project develops and characterizes new quantum materials that exhibit unconventional superconductivity and other emergent behaviors, focusing on square-planar rare-earth nickelates. These materials have parallels to high-T_c cuprates but possess distinct orbital and magnetic characteristics. The overarching goal is to establish a robust experimental foundation for understanding the superconducting mechanism in $Nd_{1-x}Eu_xNiO_2$ (NENO) thin films, a recently discovered infinite-layer nickelate superconductor in which Eu substitution provides both charge doping and magnetic interactions that modify the electronic structure of the superconducting state (1). We use molecular beam epitaxy (MBE) to grow high-quality thin films, perform in-situ reduction using metallic Al, and employ advanced synchrotron and high field transport probes to study the resulting superconducting and magnetic phases.

The key electronic structure of NENO arises from the interplay of 3d orbitals of Ni and 4f orbitals of rare-earth ions, where dimensionality, electron correlation, and magnetism are intertwined. Our work explores how the NiO_2 planes, embedded within a rare-earth oxide framework, support superconductivity that may differ from both cuprates and conventional BCS superconductors. In particular, Eu doping introduces a novel pathway for tuning electronic interactions via simultaneous charge transfer and magnetic exchange coupling with the superconducting state.

Our approach combines molecular beam epitaxy (MBE), in-situ UHV-compatible solid-state reduction, synchrotron-based spectroscopy, and high-field transport. This multi-pronged strategy enables us to systematically explore the role of rare-earth chemistry in modulating orbital occupancy, magnetic correlations, and pairing mechanisms. Through targeted synthesis and advanced characterization, we aim to reveal the key ingredients required for stabilizing and enhancing superconductivity in layered nickelates. The insights gained here are expected to guide the design of quantum materials with tailored functionalities, including magnetically mediated superconductors and tunable correlated systems.

Recent Progress

We have demonstrated an all-in-situ UHV-compatible reduction method using metallic aluminum to reduce epitaxial $NdNiO_3$ films into infinite-layer $NdNiO_2$ structure, avoiding hydrogen-based CaH_2 reduction routes (2) and producing atomically smooth, highly crystalline films. Next, we introduced Eu dopants to achieve hole doping required for superconductivity and demonstrated superconducting $Nd_{1-x}Eu_xNiO_2$ (NENO) thin films (Figure 1). Here, the Eu dopant plays a dual role: it introduces holes via Eu^{2+}/Eu^{3+} valence mixing and contributes localized 4f magnetic moments. In-situ synchrotron-based CTR diffraction and dXANES measurements track lattice changes and Ni valence evolution, confirming controlled reduction from the perovskite to infinite-layer phase. The Eu valence is found to evolve from 3+ to mixed 2+/3+ upon reduction, as shown by Eu L3 edge dXANES (1). The divalent Eu^{2+} has a half-full 4f orbital with a large magnetic moment and is expected to introduce new physics to the system, as we will show.

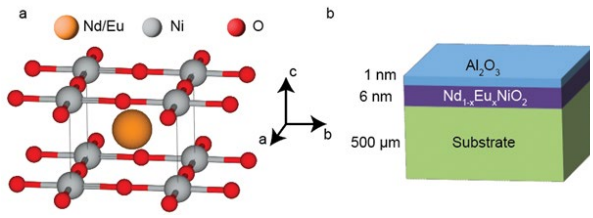


Figure 1. Thin film infinite-layer nickelates. (a) Schematic showing the atomic arrangement in Eu doped $NdNiO_2$. The rare-earth layer (Nd/Eu) is intercalated between the NiO_2 planes in an infinite layer structure (b) NENO thin film of 6-nm-thickness was grown on a 500-µm-thick LSAT substrate and capped with a 1nm thick Al_2O_3 layer.

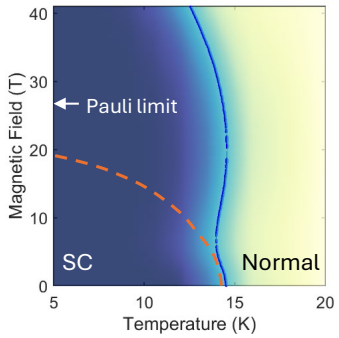


Figure 2. The temperature dependence of upper critical field (blue line) is pushed far above that of $Nd_{1-x}Sr_xNiO_2$ (orange) (3), exceeding the Pauli limit, with magnetic-field-enhanced superconducting state visible around 21 T.

NENO exhibits a superconducting transition with T_c up to 21 K and shows remarkable robustness in an applied magnetic field across a wide range of Eu doping concentrations (x = 0.2 - 0.35). High-field magnetotransport measurements reveal that the upper critical field H_{c2} far exceeds the Pauli paramagnetic limit $H_{c2,Pauli}=1.86T_c$ for weakly coupled superconductors (Figure 2), potentially suggesting unconventional pairing. Moreover, reentrant superconductivity behavior is observed around 20 T at low temperatures. This unusual field-induced enhancement is consistent with a Jaccarino-Peter (J-P) compensation mechanism, in which the internal exchange field from Eu^{2+} 4f magnetic moments counteracts the applied magnetic field. The superconducting phase boundary forms a dome-shaped region in the H–T plane, centered at the compensation field ~21 T.

To interpret this result, we developed a microscopic model based on Ginzburg-Landau theory augmented by density functional theory (DFT) calculations (Ismail-Beigi, Yale). These calculations reveal that magnetic moments at Eu sites induce an antiferromagnetic exchange field acting on the Ni $dx^2–y^2$ orbital. This orbital-selective field compensation effect suppresses the pair-breaking Zeeman term at the

compensation point, which enables superconductivity to reappear under strong magnetic fields. The calculated exchange field is estimated to be 21.3 T, closely matching the compensation field observed experimentally.

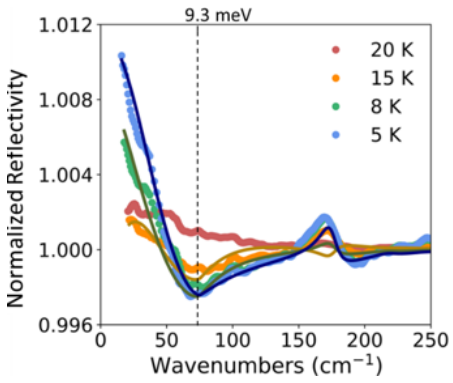


Figure 3. Temperature dependence of the normalized reflectivity of NENO/LSAT (colored circles). The fits were calculated with the same *d*-wave Mattis-Bardeen model as the dashed line. The gap was set to be constant at 75 cm^{-1}, while the contribution of uncondensed quasiparticles was allowed to increase with temperature.

To provide further insight into the unusually high H_{c2} in NENO, optical reflectivity measurements via FTIR spectroscopy were performed independently (Cavalleri, Max Planck). The measurements reveal a superconducting gap $2\Delta \approx 9.3$ meV (Figure 3), corresponding to a gap-to-T_c ratio of approximately 5.5. This strongly exceeds the BCS weak-coupling limit and contrasts with Sr-doped nickelates (NSNO), where the ratio is closer to 3.3 (4). By modeling the optical conductivity using the Mattis-Bardeen theory for a d-wave superconductor in the dirty limit, we can fit the reflectivity kink, an indication of the gap opening, and residual low-energy spectral weight, suggesting the presence of unpaired quasiparticles and possible nodal d-wave behavior. Together with the large H_{c2} values, this finding yields a self-consistent picture of strong-coupling superconductivity. These results establish NENO as an infinite-layer nickelate that simultaneously exhibits strong coupling and magnetically enhanced superconductivity, attributed to the effect of Eu in the rare-earth layer.

To further understand the underlying electronic and magnetic structure of NENO and its correlation with the observed intriguing macroscopic properties, we also performed X-ray absorption spectroscopy (XAS) measurements on NENO films at Brookhaven National Laboratory, beamline 6BM. At the Eu L3 edge, no linear dichroism was observed between in-plane and out-of-plane geometries, consistent with the isotropic charge distribution expected for the half-filled 4f^7 configuration of Eu^{2+} (L = 0). This result also shows that Eu^{2+} moments are (S = 7/2) magnetically isotropic, with no long-range order, characteristic of a paramagnetic state at room temperature. The Eu L3 near edge structure confirms the coexistence of Eu^{2+} and Eu^{3+} states. In contrast, Nd L edge spectra show a single valence state, consistent with single valence Nd^{3+}. At the Ni K edge, strong dichroism is observed between polarizations,

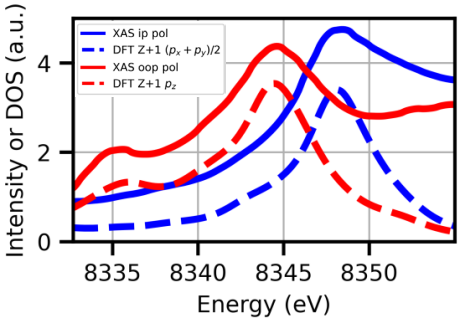


Figure 4. Ni K-edge XAS was performed on $Nd_{0.75}Eu_{0.25}NiO_2$ with out-of-plane (red) and in-plane (blue) polarization. For comparison, DFT calculations are shown as dashed curves, indicating Ni-p_z states as the origin of the pre-peak features in XAS data.

reflecting the quasi-2D nature of the electronic structure in the infinite-layer phase. The observed dichroism for a pre-edge peak can be attributed to Ni-p_z states crossing the Fermi level at the A point of the Brillouin-zone, an observation which is supported by DFT calculations (Figure 4). This result gives a new perspective to the origin of the A site pocket in infinite layer nickelates. By correlating these spectral signatures with superconducting gap evolution across doping, we can gain microscopic insight into the interplay of orbital selectivity, dimensionality, and pairing strength in NENO.

Future Plans

We will build on these findings through three coordinated research directions:

Electronic structure: We will use synchrotron-based ARPES on UHV-grown films to probe band structure and gap anisotropy. Band-selective polarization measurements will test the dominance of $d_{x^2-y^2}$ vs d_{z^2} or p_z orbitals. In situ MBE growth connected to beamline measurements at Brookhaven National Laboratory will allow momentum-resolved spectroscopy without air exposure.

Magnetism and pairing: We will use high-field transport studies to map $H_{c2}(T, x)$ anisotropy and characterize reentrant behavior. RIXS and dXANES will be employed to understand the magnetic excitation spectrum and Eu-Ni exchange interactions. The Eu doping dependence of electronic and magnetic structure using XAS will be analyzed across the superconducting dome (1).

Optical dynamics: Time-resolved THz spectroscopy will be used to explore nonequilibrium superconductivity and quasiparticle dynamics. Pump-probe studies will investigate transient enhancement of superconductivity and gap modulation across different doping levels. These experiments will assess the feasibility of optically controlling superconducting states via lattice or electronic excitation.

Together, this integrated effort aims to elucidate the interplay of charge, spin, and orbital degrees of freedom in nickelate superconductivity and guide future material design.

References

1. W. Wei, D. Vu, Z. Zhang, F. J. Walker, C. H. Ahn, Superconducting $Nd_{1-x}Eu_xNiO_2$ thin films using in situ synthesis, *Science Advances* **9**, eadh3327 (2023).

2. D. Li et al., Superconductivity in an infinite-layer nickelate, *Nature* **572**, 624 (2019).

3. Bai Yang Wang et al. ,Effects of rare-earth magnetism on the superconducting upper critical field in infinite-layer nickelates.Sci. Adv.9,eadf6655 (2023).

4. B. Cheng et al., Evidence for d-wave superconductivity of infinite-layer nickelates from low-energy electrodynamics, *Nature Materials* **23**, 775 (2024).

Publications

1. D. Vu, et. al, Unconventional superconductivity in $Nd_{1-x}Eu_xNiO_2$ thin films, submitted.

2. Z. Jin, et. al, Revealing the A-pocket mystery in infinite-layer nickelates from first principles calculations and X-ray absorption spectroscopy, in preparation.

3. W. Wei, D. Vu, Z. Zhang, F. J. Walker, C. H. Ahn, Superconducting Nd1-xEuxNiO2 thin films using in situ synthesis, Science Advances 9, eadh3327 (2023).

4. W. Wei, K. Shin, H. Hong, Y. Shin, A. S. Thind, Y. Yang, R. F. Klie, F. J. Walker, C. H. Ahn, Solid state reduction of nickelate thin films, Phys. Rev. Materials 7, 013802 (2023).

Emerging Materials

Daniel Phelan (Argonne), John F. Mitchell (Argonne), Ulrich Welp (Argonne); Nirmal Ghimire (Notre Dame)

Keywords: superconductivity, single crystals, transition metal compounds, transport, magnetism

Research Scope

The Emerging Materials FWP investigates topical problems that generally fall into a framework of developing an understanding of the myriad properties that are exhibited by quantum materials and that are related to degeneracy breaking in structural, magnetic, orbital, vibrational, or electronic degrees of freedom. We choose problems and materials that exemplify underlying microscopic physics, possess a potential for broad and far-reaching impact, and are of significant current interest to the materials physics community. We also leverage the impacts of defects, chemical substitutions, and chemical stoichiometry to solve our chosen research problems.

As an experimental FWP, we strategically target the making of materials to solve the scientific problems that we have identified. The group possesses expertise in synthesis of polycrystalline materials and growth of high-quality single crystals by a variety of methods. Our FWP also specializes in measuring magneto-transport, thermodynamic, dielectric, and magnetic properties in its labs at Argonne and Notre Dame. We also fabricate simple device structures to probe magneto-transport properties. We frequently utilize user facilities, such as synchrotron facilities (e.g., the APS), neutron facilities (HFIR, SNS), nanofabrication facilities (CNM), and high magnetic field facilities as primary principal investigators. We collaboratively work with many of the other BES-MSE supported programs at Argonne, both theoretical and experimental, to pursue shared research goals. Finally, we interact with many external collaborators in the US and worldwide, enabling them to perform specialized experiments that will give insight into our own research problems or to pursue their own science with material platforms grown by our FWP.

Generally, the research problems that we have investigated over the last two years can be classified into three categories. The first, which is expanded upon below, concerns the intertwined charge, spin, and transport properties of nickelates. We investigated competing structural morphologies in nickelates, investigated various forms of charge and spin order in nickelates and their impacts on magneto-transport characteristics and superconductivity. The second research problem focuses on degeneracy breaking and chirality in topological and superconducting systems; i.e., the emergence of anomalous magnetic and transport properties due to real or reciprocal space topology. Along this front, we investigated Kagome metals (1-3-5 and 1-6-6 systems), charge density waves (CDWs) and superconductivity in A15 intermetallic compounds (i.e., A_3B), and the emerging field of altermagnetism. Finally, we have worked on quantum magnets by investigating frustration of pentagonal Cairo-lattice systems ($Bi_2Fe_4O_9$) and magnetic phases and excitations in potential quantum spin-liquids ($Na_3SbCo_2O_6$, $Ba_3ZnRu_2O_9$, $Ba_3CoSb_2O_9$). For coherence, we focus our recent progress and future plans below only on the nickelate topic.

Recent Progress

The discovery and report of pressure-induced superconductivity in the bilayer Ruddlesden-Popper nickelate, $La_3Ni_2O_7$, in 2023 [1] significantly influenced the direction of our research in nickelates. Although we had been growing $n=\infty$, 3, 2, and 1 Ruddlesden-Popper phase $(La/Pr)_{n+1}Ni_nO_{3n+1}$ single crystals for the last dozen years, we had not previously investigated their pressure-dependent properties nor focused on the bilayer system – this quickly changed. X-ray measurements on our $La_3Ni_2O_7$ single crystals led us to the discovery of polymorph Ruddlesden-Popper structures [2]. As shown in Figure 1, we found that two types of crystals formed within a boule during high oxygen pressure floating-zone growth, both possessing an average stoichiometry of $La_3Ni_2O_7$. The first possessed the standard bilayer structure, which we deemed the "2222 phase" (panel a), and the second possessed a polymorph structure with alternating trilayer and single-layer structures which we named the "1313 phase" (panel b). This was confirmed by direct real-space imaging via scanning transmission electron microscopy (Klie Group at University of Illinois Chicago). Band structure calculations (Botana Group at Arizona State University) indicated that the band structure of the 1313 phase could be thought of as a superposition of the band-structures of the single-layer and trilayer systems. Our transport measurements, shown in Figure 2, indicated that both forms possessed CDW transitions similar to the trilayer phase, with the CDW transition temperature systematically increasing from the 2222, 1313, and 3333 phases. Remarkably, this was the first discovery of polymorphic layer stacking in bulk Ruddlesden-Popper single crystals of any phase, which suggested that similar polymorphism could occur in other Ruddlesden-Popper materials and potentially lead to novel properties. Subsequent reports have independently confirmed our findings [3], and some disparate nickelate layer-stacking schemes (e.g., 1212 [4]) have now been reported by other groups.

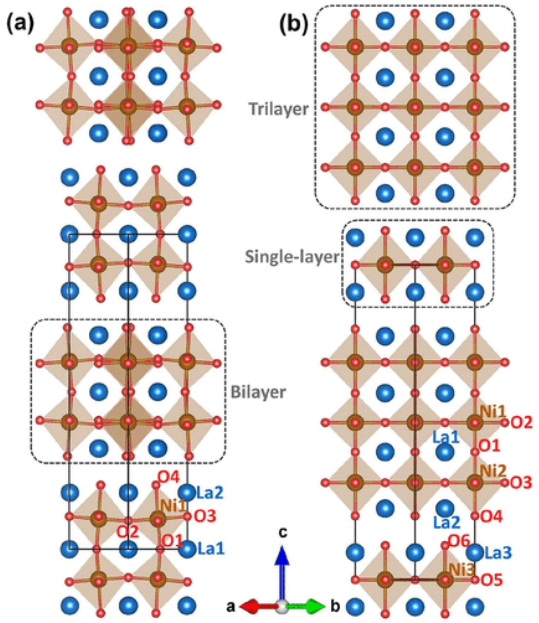


Figure 1: Two polymorph structures of $La_3Ni_2O_7$. (a) The 2222 structure consists of stacked bilayers. (b) The 1313 structure consists of alternating single and trilayers. After Ref. [2].

Pressure-induced superconductivity in $La_3Ni_2O_7$ led us to question whether it would also occur in the trilayer Ruddlesden-Popper phase and what the effect of different lanthanides on the A-site would be. We therefore investigated the pressure and temperature-dependent electrical transport and magnetic susceptibility of $Pr_4Ni_3O_{10}$ single crystals in collaboration with the Hemley Group at University of Illinois Chicago and the Canfield Group at Iowa State University. In this work [5], we discovered a low-volume (up to 10%), non-percolating volume fraction of

superconductivity in our crystals with T_c up to 31 K as shown in Figure 3. Significant variation in transport results was observed between different crystals and even between permuted contacts of a particular crystal as shown in Figure 4. Our results were thus indicative of a minority superconducting phase, though the origin of the inhomogeneity, particularly strain/stress, stoichiometry, or pressure media is a continuing topic of research in the community since there is disparity between our results and the volume fractions in single crystals reported subsequently by other groups. Inasmuch as $Pr_4Ni_3O_{10}$ possesses a superconducting phase, our results suggested a lack of significant inhibiting Pr-O hybridization, which is a known manifestation in cuprates that destroys superconductivity. Our results also suggested that a spin density wave on the Pr sites at low temperature in ambient pressure did not adversely affect the superconductivity under pressure.

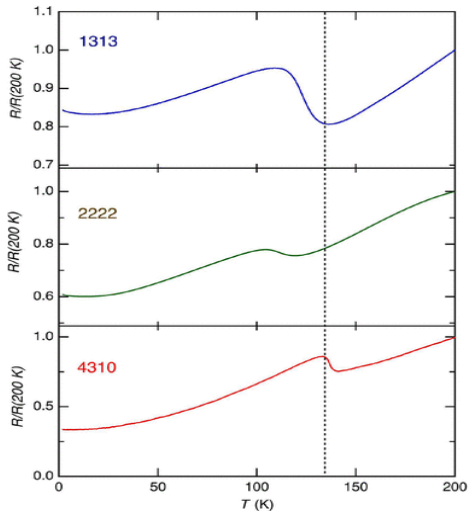


Figure 2: Comparison of CDW anomalies in electrical transport of 1313, 2222, and 3333. After Ref. [2]. structures.

Future Plans

We plan to continue pursuing research that investigates the interplay between superconductivity, structure, stoichiometry, and charge and spin density waves in nickelates. A particular avenue that we will pursue is the effect of synthesis conditions on resultant structural phases. For instance, using a unique high pO_2 quenching furnace that we designed, we will explore effects of oxygen pressure on the resultant crystal structure, stoichiometry, and transport and magnetic properties, focusing on metastable phases that require high oxygen pressure treatment and quenching. We plan to also continue measuring the fascinating interaction between spin and charge density waves in $Pr_4Ni_3O_{10}$. Some open questions that we hope to address are whether Pr 4f electrons participate in the CDW state in conjunction with Ni 3d electrons such that there are potentially two charge order parameters (Ni and Pr) as well as two spin order parameters (Ni and Pr). We plan to study the effect of pressure on these co-existing order parameters to see if there is any bifurcation which can lead to understanding of primary and secondary nature of order parameters at a Landau level of treatment proposed by collaborator Mike Norman. We have

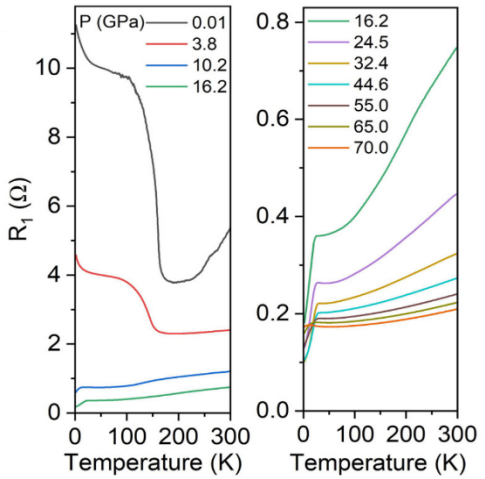


Figure 3: Pressure-dependence of resistance for a single crystal of $Pr_4Ni_3O_{10}$. After Ref. [5].

resonant X-ray scattering and magneto-transport measurements planned toward this goal. We continue to search for and study the evolution of CDWs in nickelates with different compositions and will employ the diffraction beamlines at the APS in this effort. For instance, we will investigate the CDW in the 327 system and seek to understand how the 2222 CDW compares to the 1313 and 3333 structures. We also intend to explore flux growth of nickelates with different lanthanides on the A-site which haven't been achieved by floating-zone growth so that we can understand the impact of chemical pressure on magnetic and transport properties. Finally, inspired by recent preliminary data on the non-linear electrical transport in La- and Pr-4-3-10 in the CDW phase, we will investigate the dynamical behavior of CDW domains in these materials under high drive in point contacts and nano-constrictions. We aim at supplementing these studies with direct imaging of the CDW state using dark field X-ray microscopy at the Advanced Photon Source.

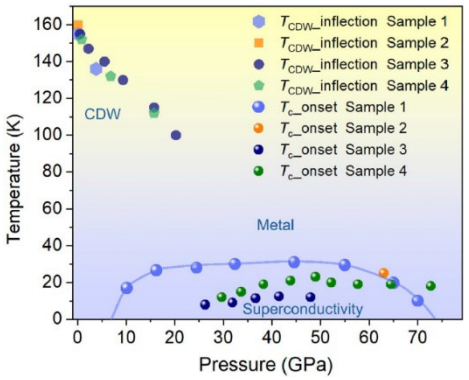


Figure 4: Compilation of CDW transition temperature and superconducting T_c for different crystals under pressure. After Ref. [5].

References

1. H. Sun, M. Huo, X. Hu, J. Li, Z. Liu, Y. Han, L. Tang, Z. Mao, P. Yang, B. Wang, J. Cheng, D.-X. Yao, G.-M. Zhang, and M. Wang, *Signatures of Superconductivity near 80 K in a nickelate under high pressure*, Nature **621**, 493 (2023).

2. X. Chen, J. Zhang, A. S. Thind, S. Sharma, H. LaBollita, G. Peterson, H. Zheng, D. Phelan, A. S. Botana, R. F. Klie, and J. F. Mitchell, *Polymorphism in the Ruddlesden-Popper Nickelate $La_3Ni_2O_7$: Discovery of a Hidden Phase with Distinctive Layer Stacking*, J. Am. Chem. Soc. **146**, 3640 (2024).

3. P. Puphal, P. Reiss, N. Enderlein, Y. -M. Wu, G Khaliullin, V. Sundaramurthy, T. Priessnitz, M. Knauft, A. Suthar, L. Richter, M. Isobe, P. A. van Aken, H. Takagi, B. Keimer, Y. E. Suyolcu, B. Wehinger, P. Hansmann, and M. Hepting, Unconventional crystal structure of the high-pressure superconductor La3Ni2O7, Phys. Rev. Lett. **133**, 146002 (2024).

4. F. Li, N. Guo, Q. Zheng, Y. Shen, S. Wang, Q. Cui, C. Liu, S. Wang, X. Tao, G. -M. Zhang, and J. Zhang, *Design and synthesis of three-dimensional hybrid Ruddlesden-Popper nickelate single crystals*, Phys. Rev. Materials **8**, 053401 (2024).

5. X. Chen, E. H. T. Poldi, S. Huyan, R. Chapai, H. Zheng, S. L. Bud'ko, U. Welp, P. C. Canfield, R. J. Hemley, J. F. Mitchell, and D. Phelan, *Low Fractional Volume Superconductivity in Single Crystals of $Pr_4Ni_3O_{10}$ Under Pressure*, Phys. Rev. B **111**, 094525 (2025).

Publications

1. X. Chen, J. Zhang, A. S. Thind, S. Sharma, H. LaBollita, G. Peterson, H. Zheng, D. Phelan, A. S. Botana, R. F. Klie, and J. F. Mitchell, *Polymorphism in the Ruddlesden-Popper Nickelate $La_3Ni_2O_7$: Discovery of a Hidden Phase with Distinctive Layer Stacking*, J. Am. Chem. Soc. **146**, 3640 (2024).

2. X. Chen, E. H. T. Poldi, S. Huyan, R. Chapai, H. Zheng, S. L. Bud'ko, U. Welp, P. C. Canfield, R. J. Hemley, J. F. Mitchell, and D. Phelan, *Low Fractional Volume Superconductivity in Single Crystals of $Pr_4Ni_3O_{10}$ Under Pressure*, Phys. Rev. B **111**, 094525 (2025).

3. A. M. Samarakoon, J. Strempfer, J. Zhang, F. Ye, Y,. Qiu, J. -W. Kim, H. Zheng, S. Rosenkranz, M. R. Norman, J. F. Mitchell, and D. Phelan, *Bootstrapped dimensional crossover of a spin density wave*, Phys. Rev. X **13**, 041018 (2023).

4. H. Bhandari, R. L. Dally, P. E. Siegfried, R. B. Regmi, K. C. Rule, S. Chi, J. W. Lynn, I. I. Mazin, and N. J. Ghimire, *Magnetism and Fermiology of Kagome Magnet $YMn_6Sn_4Ge_2$*, npj Quantum Matter **9**, 6 (2024).

5. Y. Li, D. Phelan, F. Ye, H. Zheng, E. Krivyakina, A. Samarakoon, P. G. LaBarre, J. Neu, T. Siegrist, and S. Rosenkranz, *Evolution of magnetic surfboards and spin glass behavior in $(Fe_{1-p}Ga_p)_2TiO_5$*, J. Phys.: Condens. Matter **35**, 475401 (2023).

6. R. Chapai, G. Peterson, M. P. Smylie, X. Chen, J. S. Jiang, D. E. Graf, J. F. Mitchell, and U. Welp, *Fermi surface topology and magneto-transport properties of superconducting $Pd_3Bi_2Se_2$*, Phys. Rev. B **110**, 075152 (2024).

7. M. P. Smylie, Z. Islam, A. Glatz, G. D. Gu, J. A. Schneeloch, R. D. Zhong, S. Rosenkranz, W. -K. Kwok, and U. Welp, *Multimodal synchrotron x-ray diffraction across the superconducting transition of $Sr_{0.1}Bi_2Se_3$*, Phys. Rev. B **110**, 024509 (2024).

8. A. Vasdev, G. Sheet, R. Chapai, T. Polakovic, V. Novosad, J. S. Jiang, D. Y. Chung, U. Welp, and J. F. Mitchell, Superconducting and normal state properties of $Ba_{0.6}K_{0.4}Fe_2As_2$, Phys. Rev. B **110**, 094518 (2024).

9. H. Bandari, P. H. Chang, R. B. Regmi, B. G. Markus, L. Forro, J. F. Mitchell, I. I. Mazin, and N. J. Ghimire, *Tunable topological transitions in the frustrated magnet HoAgGe*, Comm. Mater. **6**, 52 (2025).

10. A. E. Koshelev, R. Chapai, D. Y. Chung, J. F. Mitchell, and U. Welp, *Origin of anomalous magnetotransport in Kagome superconductors AV_3Sb_5 (A=K, Rb, Cs)*, Phys. Rev. B **110**, 024512 (2024).

Correlated Materials – Synthesis and Physical Properties

I. R. Fisher[1,2], A. Kapitulnik[1,2,3] and S. A. Kivelson[1,3]

1. Stanford Institute for Materials and Energy Sciences, SLAC National Accelerator Laboratory, 2575 Sand Hill Road, Menlo Park, California 94025
2. Department of Applied Physics, Stanford University, Stanford, California 94305
3. Department of Physics, Stanford University, Stanford, California 94305

Keywords: superconductivity; strain; elastocaloric effect; single crystals;

Research Scope

An enduring aim of our FWP has been to discover and understand the nature, causes and consequences of emergent behavior in quantum materials, especially in relation to the occurrence of superconductivity. Our collaborative work in this area involves theory, crystal growth, and detailed experimental investigations, often involving new techniques that we have pioneered. Current efforts focus on (a) the occurrence and properties of CDW order in several families of quasi-two-dimensional compounds, including rare earth tritellurides and Kagome metals, and including investigations of novel broken symmetries, including ferroaxial order; (b) the inter-relation of nematicity and superconductivity in Fe-based superconductors and related materials, and including investigation of self-organization at the mesoscale via DFXM; and (c) a more general investigation of the inter-relation of a variety of competing, coexisting and intertwined multi-component electronic orders (including in materials such as UTe_2, Sr_2RuO_4 etc., and in appropriate physical models). A pervasive recent emphasis has been the use of symmetry-breaking strain as a probe of, and tuning parameter for, a variety of emergent electronic phases, and the development of suitable experimental means to achieve these goals and to develop an appropriate theoretical framework to understand results and guide ongoing experimental investigations.

Recent Progress

(1) Elastocaloric evidence for a multicomponent superconductor in $Ba(Fe_{1-x}Co_x)_2As_2$: The iron-based superconductors exhibit rich phase diagrams with intertwined phases, including magnetism, nematicity and superconductivity. Here, we used the AC elastocaloric effect (ECE) to map out the phase diagram of $Ba(Fe_{1-x}Co_x)_2As_2$ near optimal doping. The ECE signature at Tc on the overdoped side, where superconductivity condenses without any nematic order, is quantitatively consistent with other thermodynamic probes that indicate a single-component superconducting state. In contrast, on the slightly underdoped side, where superconductivity condenses within the nematic phase, ECE reveals a second thermodynamic transition proximate to and below Tc. We rule out magnetism and re-entrant tetragonality as the origin of this transition, and find that our observations strongly suggest a phase transition into a multicomponent superconducting state. This implies the existence of a sub-dominant pairing instability that competes strongly with the dominant s ± instability. Our results motivate a re-examination of the pairing state and its interplay

with nematicity in this extensively studied iron-based superconductor. They also indicate two crucial and previously unappreciated roles of the nematic order in affecting superconductivity. First, the nematic phase appears to be a key determinant for the SC pairing symmetry, rendering the SC order parameter different in the orthorhombic phase compared to the tetragonal phase. This suggests a possible scenario where the nematic transition ends in a line of first order transitions below the SC dome. Second, Tc appears to be maximized when the nematic transition line meets the superconducting dome, which defines the optimal doping point in the phase diagram. Thus nematic order seems to play an important role in terms of both determining the pairing symmetry at optimal doping, and in shaping the overall phase diagram. See ref (5).

(2) Effect of disorder on the strain-tuned charge density wave multicriticality in Pd_xErTe_3: We explored, through a combination of x-ray diffraction and elastoresistivity measurements, the effect of disorder on the strain-tuned charge density wave and associated multicriticality in Pd_xErTe_3 (x = 0, 0.01, 0.02 and 0.026). We focused particularly on the behavior near the strain-tuned bicritical point that occurs in pristine $ErTe_3$ (x=0). Our study revealed that while Pd intercalation somewhat broadens the signatures of the CDW phase transitions, the line of first-order transitions at which the CDW reorients as a function of applied strain persists in the presence of disorder and still seemingly terminates at a critical point. The critical point occurs at a lower temperature and a lower strain compared to pristine $ErTe_3$. Similarly, the nematic elastoresistance of Pd_xErTe_3, though suppressed in magnitude and broadened relative to that of $ErTe_3$, has a markedly more symmetric response around the critical point. These observations point to disorder driving a reduction in the system's electronic orthorhombicity even while the material remains irrevocably orthorhombic due to the presence of a glide plane in the crystal structure. Disorder, it would appear, reinforces the emergence of a "pseudo-tetragonal" electronic response in this fundamentally orthorhombic material. See refs (1), (3) and (6).

(3) Spin-glass state in nickelate superconductors: Despite six years of intense scrutiny, the magnetic ground state of superconducting infinite-layer nickelates is still unsettled. Our new studies use the Zero-area magneto-optic Sagnac interferometer with nanoradian-sensitivity to measure the magneto-optical Kerr effect in $La_{0.8}Sr_{0.2}NiO_2$ and $Nd_{0.825}Sr_{0.175}NiO_2$ thin films. We then demonstrate that these films enter a spin-glass phase at temperatures up to 80 K - well above their superconducting critical temperatures. This high-temperature glassiness, which is absent in copper oxides, now brings up the issue of to what level superconductivity and magnetism are mutually exclusive in layered d-electron materials. Equally striking, the magnitude and onset of the Kerr rotation in $Nd_{0.825}Sr_{0.175}NiO_2$ differ by an order of magnitude when the same film is grown on STO versus LSAT substrates. The result reveals a substrate “knob” that selectively tunes time-reversal-odd order without perturbing pairing - an effect not anticipated in current theories. Our results (i) pin down the dominant magnetic coupling in infinite-layer nickelates, (ii) show that the ordered state is highly sensitive to growth conditions yet largely independent of the rare-earth ion, and (iii) impose stringent constraints on theories that still treat Ni spins as purely fluctuating and unfrustrated. See ref (7).

(4) Optical control of orbital magnetism in magic angle twisted bilayer graphene: Flat bands in graphene-based moire structures host a wide range of emerging strongly correlated and topological phenomena. Optically probing and controlling them can reveal important information such as symmetry and dynamics, but have so far been challenging due to the small energy gap compared to optical wavelengths. Here, we report near infrared optical control of orbital magnetism and associated anomalous Hall effects (AHE) in a magic angle twisted bilayer graphene (MATBG) on monolayer WSe_2 device. We show that the properties of the AHE, such as hysteresis and amplitude, can be controlled by light near integer Moire fillings, where spontaneous ferromagnetism exists. By modulating the light helicity, we observe periodic modulation of the transverse resistance in a wide range of fillings, indicating light induced orbital magnetization through a large inverse Faraday effect. At the transition between metallic and AHE regimes, we also reveal large and random switching of the Hall resistivity, which are attributed to optical control of percolating cluster of magnetic domains. Our results open the door to optical manipulation of correlation and topology in MATBG and related structures. See ref (9).

(5) Discovery of spontaneous mesoscopic strain waves in nematic domains using dark-field X-ray microscopy: Electronic nematic order is a correlated phase of matter in which low-energy electronic states spontaneously break a discrete rotational symmetry of a crystal lattice. Bilinear coupling between the electronic nematic and strains of the same symmetry yields a single pseudoproper ferroelastic phase transition at which both the nematic and lattice strain onset concurrently. To minimize elastic energy, the crystal forms structural twin domains, each with a distinct orientation of the nematic director (i.e. each with a specific sign of the induced shear strain). While the effects of externally induced strains on these domains are well established, the intrinsic behavior of spontaneous strain fields within individual domains has been hitherto unexplored, largely due to the lack of appropriate experimental tools. Here, we report the discovery of spontaneous mesoscopic strain waves within individual nematic domains of an underdoped iron-based superconductor, observed using dark-field X-ray microscopy (DFXM). This technique combines high spatial and reciprocal-space resolution with full-field, bulk-sensitive imaging, enabling direct visualization of subdomain strain modulations emerging concurrently with the onset of nematic order. The elastic compatibility relations that govern inhomogeneous strains in continuous solids provide a natural mechanism for the emergent strain waves that we observe. This work was performed in close collaboration with Z. Islam at the APS. See ref (10).

6) A Modified Interferrometer to Measure Anyonic Braiding Statistics: In the last few years, it has for the first time been possible to experimentally measure the braiding statistics of anyons in a fractional quantum Hall fluid. In addition to its fundamental interest, this has long been seen as a first step in enabling various visionary proposals to use braiding for fault-tolerant quantum information processing. So far, existing quantum Hall interferometers measure twice the braiding phase, $e^{i2\theta}$, of Abelian anyons, i.e. the phase accrued when one quasi-particle encircles another clockwise. In Ref. (8), we propose a modified Fabry-Pérot or Mach-Zehnder interferometer that can measure $e^{i\theta}$.

Future Plans

We will continue to explore the signatures and effects of subtle forms of broken symmetries in quantum materials, with a special focus on probing these states and their fluctuations via combinations of light, strain and magnetic fields using our uniquely appropriate set of experimental tools. By studying the evolution of the high-rank tensors that describe the response to mixed stimuli (including for example the magneto-elastocaloric effect; elasto-gyrotropy; non-linear elastoresistivity, and the elasto-photogalvanic effect), we will be able to extract detailed information about various types of subtle symmetry-breaking. Immediate plans for FY26 include:

(1) Determine whether the CDW state in 1T-$TiSe_2$ has a ferroaxial symmetry, and establish the extent to which ferroaxial fluctuations are present across the intercalation-tuned phase diagram in Cu_xTiSe_2, and any roles they might play in the emergent superconducting state. Primary experiments include non-linear elastoresistivity.

(2) Continue our investigations of $ErTe_3$ and closely related materials with the goals to (a) Determine the nature, causes and consequences of the putative ferroaxial order in the CDW phase; and (b) Determine the extent to which Einstein relations are violated and understand the origin of this effect. Primary experiments include (a) photogalvanic effect and elastoresistivity and (b) thermal diffusivity measurements. From a theoretical perspective, we will also carry out studies of a microscopically reasonable model of electron-phonon interactions in $ErTe_3$ in order to explore the origin of the CDW state, what determines its pattern of spontaneously broken symmetries, and the extent to which the proposed ferroaxial order is theoretically plausible.

(3) Continue our study of CsV_3Sb_5 with the goal of establishing the symmetry of the CDW state, and understanding in detail how this interacts with light to yield the observed training effects. Primary experiments include photogalvanic effect and thermal diffusivity.

(4) We have begun a preliminary study of several altermagents, drawing on our collective experience of combining strain and magnetic fields to study emergent properties and broken symmetries.

(5) We have also begun a study exploring how strain derivatives of transport and thermodynamic quantities, such as elastoresistance and elastocaloric effect measurements, can be used to directly reveal strain derivatives of fundamental electronic properties (including the effective mass and the Fermi surface area) in quantum materials via quantum oscillations.

(6) We will continue our collaborative work with Z. Islam at the APS using DFXM to probe local structural modulations in a variety of quantum materials.

(7) We will likely revisit ideas concerning the relationship between nematic quantum criticality and superconductivity, especially in the context of increasing (although still far from conclusive) evidence that one can zoom in on the quantum critical regime in $FeSe_{1-x}Ax$ where A is S or Te.

Publications (Sept 2023 – Sept 2025)

1) Steven A. Kivelson, Akshat Pandey, Anisha G. Singh, Aharon Kapitulnik, and Ian R. Fisher, "Emergent $\mathbb{Z}_2$ symmetry near a charge density wave multicritical point" Phys. Rev. B **108**, 205141 – Published 17 November 2023

2) Erik D. Kountz, Chaitanya R. Murthy, Dong Chen, Linda Ye, Mark P. Zic, Claudia Felser, Ian R. Fisher, Steven A. Kivelson, and Aharon Kapitulnik, "Thermal transport measurements through the charge density wave transition in CsV_3Sb_5" Phys. Rev. B **109**, L201120 (2024) – Published 17 May 2024

3) Anisha G. Singh, Maja D. Bachmann, Joshua J. Sanchez, Akshat Pandey, Aharon Kapitulnik, Jong-Woo Kim, Philip Ryan, Steven A. Kivelson and Ian R. Fisher, "Emergent tetragonality in a fundamentally orthorhombic material" Science Advances, Volume **10**, Issue 21 (2024) – Published 23 May 2024

4) Yi-Ming Wu, Chaitanya Murthy, and Steven A. Kivelson, "Possible sliding regimes in twisted bilayer WTe_2" in the physics of the cuprates, the Hubbard model, and other highly correlated electronic systems,," Phys. Rev. Lett. **133**, 246501 (2024) - published December 13, 2024.

5) Sayak Ghosh, Matthias S. Ikeda, Anzumaan R. Chakraborty, Thanapat Worasaran, Florian Theuss, Luciano B. Peralta, P. M. Lozano, Jong-Woo Kim, Philip J. Ryan, Linda Ye, Aharon Kapitulnik, Steven A. Kivelson, B. J. Ramshaw, Rafael M. Fernandes, Ian R. Fisher, "Elastocaloric evidence for a multicomponent superconductor stabilized within the nematic state in $Ba(Fe_{1-x}Co_x)_2As_2$" In press - accepted for publication in PNAS. arXiv:2402.17945

6) Anisha G. Singh, Matthew Krogstad, Maja D. Bachmann, Paul Thompson, Stephan Rosenkranz, Ray Osborn, Alan Fang, Aharon Kapitulnik, Jong Woo Kim, Philip J. Ryan, Steven A. Kivelson, Ian R. Fisher, "Effect of disorder on the strain-tuned charge density wave multicriticality in Pd_xErTe_3", In press - accepted for publication in PRB. arXiv:2412.20706 [cond-mat.str-el]

7) David R. Saykin, Martin Gonzalez, Jennifer Fowlie, Steven A. Kivelson, Harold Hwang, and Aharon Kapitulnik, "Spin-glass state in nickelate superconductors," In press – accepted for publication in npj Quantum Materials. arXiv:2506.03262 [cond-mat.str-el]

8) Steven A. Kivelson and Chaitanya Murthy, "A modified interferometer to measure anionic braiding statistics," In press -- accepted for publication in PRL. arXiv:2403.12139.

9) Eylon Persky, Minhao He, Jiaqi Cai, Takashi Taniguchi, Kenji Watanabe, Xiaodong Xu, Aharon Kapitulnik, "Optical control of orbital magnetism in magic angle twisted bilayer graphene," Under review - arXiv:2503.21750 [cond-mat.str-el]

10) Kaan Alp Yay, W. Joe Meese, Elliot Kisiel, Matthew J. Krogstad, Anisha G. Singh, Rafael M. Fernandes, Zahir Islam, Ian R. Fisher "Discovery of spontaneous mesoscopic strain waves in nematic domains using dark-field X-ray microscopy," Under review - arXiv:2507.23752 [cond-mat.str-el]

Cuprate strange metals as a quantum critical phase with linearly running power law exponent

*Dan Dessau***,** *University of Colorado Boulde***r**

Keywords: Electronic Structure, Superconductivity, Quasiparticles and Collective Excitations, Transport Phenomena, Topological Phases of Matter

Research Scope

The broader scope of research of our long-running DOE-ECMP program is electronic correlations, which take multiple guises in quantum materials. These can be broadly classified as: (a) The generation of flat (high mass) bands, which are especially important when they are at the Fermi energy as these give a high density of states at E_F that can make an electronic system susceptible to superconductivity, density waves, strange metal physics, etc. The direct detection of such flat bands with ARPES as well as strong connections to theoretical efforts to understand the generation of these flat bands forms an important component of our effort [pubs 2,3,4]. (b) Electronic scattering rates or band-broadenings and the associated ideas of non-Fermi liquid states, "unparticles", strange metals, non-Planckian dissipation, etc. Since the concept of quasiparticles (originating with Landau's Fermi Liquid theory) has formed the backbone for almost all of our understanding of quantum condensed matter physics, progress along these lines is especially critical. This is the main subject of this Extended Abstract [pub 1] as well as our other work in [refs 1,3].

Both the generation of flat bands (a, above) and electronic scattering rates/band broadenings (b, above) are described in quantum many-body language by the electronic self-energy, which contains all the details of the electronic interactions or correlations. The real part of the self-energy is responsible for the band renormalizations/flattening while the imaginary part is responsible for the band broadening. Both the real and imaginary parts are often directly accessible by ARPES and are also related via the Kramers-Kronig relations. One of the major goals of our program through the years has been developing ARPES into a truly quantitative probe of the self-energy, i.e. turning it into a "self-energy spectroscopy" [refs 1,3; pub 4].

The extended abstract discussed here focusses on the self-energies/scattering rates of the cuprate high temperature superconductors. Next year will mark the 40th anniversary of the discovery of these materials, with the mechanism of the superconductivity as well as many other aspects of the physics remaining unsolved. It is worthwhile to ask "Why has it been such a struggle to solve this problem?" The general consensus is that this is because the "normal" state out of which the superconductivity is borne is anything but "normal", being termed the "strange-metal" state that is prevalent in cuprates but also more recently observed in other correlated electronic materials. The key characteristic of

the strange metal is that it deviates from the Landau quasiparticle paradigm that has sharp quasiparticle excitations – without such quasiparticle excitations much of the machinery our community has developed to describe and understand the electronic structure and electronic interactions is no longer applicable.

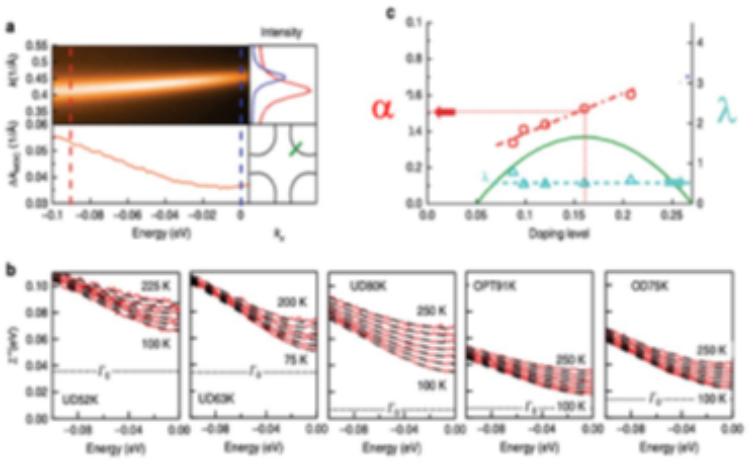


Fig 1. Our prior ARPES results from the strange metal state of $Bi_2Sr_2CaCu_2O_8$ cuprates that introduced the Power Law Liquid (PLL) scattering rate (Σ" = imaginary part of self-energy) phenomenology as an ansatz. The most important parameter is the power law exponent α which we found to linearly run as a function of doping (red circles in b). From ref [1].

One of our prior DOE-supported papers on the cuprates used ARPES to study the strange metal state ($T>T_c$) of the cuprates, focusing on the nodal states that have the largest velocity and thus dominate the transport. To explain the data we made an ansatz for the scattering rate (or Σ" = imaginary part of self-energy) where the key parameter is a power law exponent α – we term this the Power Law Liquid or PLL form. All other parameters are either constant (for example the coupling parameter λ) or largely irrelevant. The key finding is that the exponent α linearly runs with doping (Fig 1c). Recent experimental work from Amsterdam on a different class of cuprates that are more naturally overdoped fall on exactly the same trend lines that we predict from our ansatz [ref 2], strengthening the case that this ansatz is realistic and powerful.

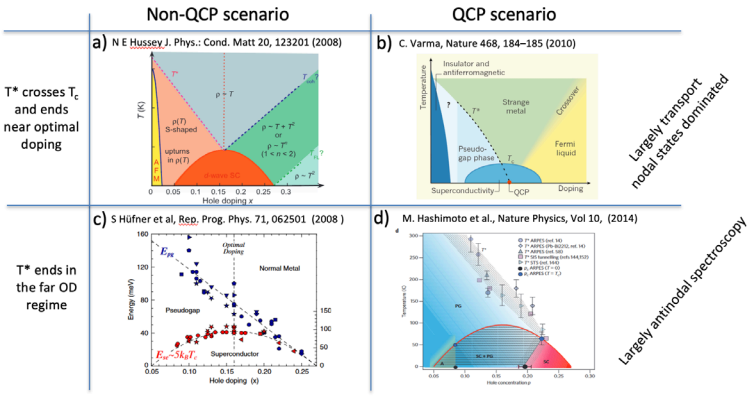


Fig 2. Four representative examples of the phase diagram of hole-doped cuprates showing confusion in the nature of the states above the superconducting dome and whether or not a quantum critical point (QCP) exists under the dome.

Recent Progress

Building upon the PLL ansatz of [ref 1] (Fig 1), we studied the electrical resistivity of a wide range of cuprate superconductors across the strange metal phase, bringing a clarification of the doping phase diagram of the cuprates.

As shown in Fig 2, there is strong confusion as to the nature of the states above the superconducting dome and whether or not a quantum critical point (QCP) exists under the dome. In this work we developed a new unbiased method to fit the electrical resistivity data to various models as well as to determine the bottom of the range of good fitting for each of the models. We applied this to the resistivity of a wide range of hole-doped cuprates, finding a few key universalities: (a) The PLL model $\rho_{PLL} \sim \rho_0 + AT^{2\alpha}$ originally derived for our ARPES data fits the resistivity data better than the typical model $\rho_{Quad} \sim \rho_0 + AT + BT^2$ (b) The fits to the PLL model show that the α parameter also runs linearly with hole doping, with almost exactly the same parameters as obtained from ARPES (Fig 3a). Here we must exclude some of the most underdoped transport samples that deviate strongly from the general trend line (grey shaded region) that we argue are affected by localization physics. The same fits also return the lower temperature scale at which the fits start to deviate from the PLL model, which we label T* and plot in Fig 3b.

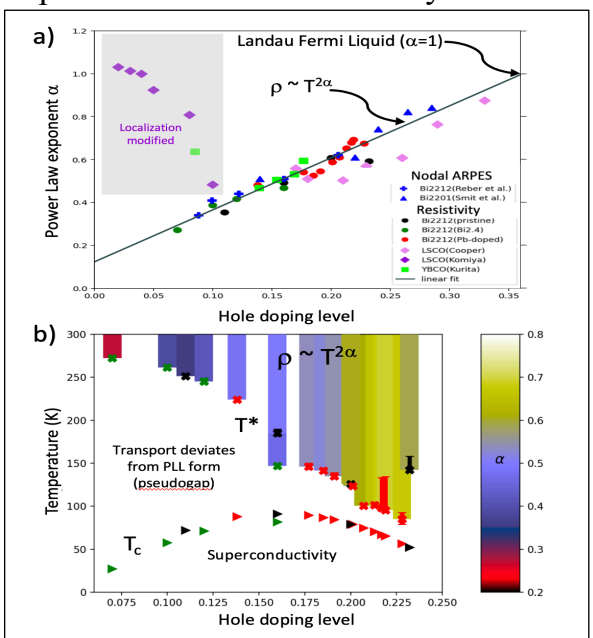


Fig 3 (a) The scattering rate of both nodal ARPES (blue) and transport experiments in the strange metal phase follow the identical power law scaling $T^{2\alpha}$. (b) The bottom of the strange metal meets the pseudogap phase, with no quantum critical point under the dome. From [pub 1].

The phase diagram of Fig 3b is quantitatively similar to the phase diagram of Fig 2c (after scaling energy to temperature) which was compiled largely from antinodal spectroscopies, but it is qualitatively different from the majority of other published phase diagrams which were dominated by transport studies, though our analysis includes both transport and spectroscopy. Our diagram is also inconsistent with the QCP-under-the-dome scenario that is a key feature of many phase diagrams, with expectations that the strange metal phase (and potentially superconducting phase as well) originates from the QCP and the proposed "fan" above it.

Both the ARPES and the new transport analysis show that the electronic coupling strengths are essentially constant across the entire doping range (for example the λ parameter in Fig 1c, with a related parameter extracted from transport), even though the scattering rates vary dramatically across doping – this non-intuitive result is due to the effect of the varying α term, which dominates the physics. We also note that the scattering rates can all be considered to be in the "Planckian" regime and that these states deviate strongly from the Landau Fermi Liquid regime – so much so that the quasiparticle residue formally goes to zero for all samples with $\alpha<0.5$ (all underdoped samples), i.e. the electronic states could be called "unparticles".

Future Plans

Seeing the great power of the self-energy analysis from ARPES for determining the intrinsic properties of the cuprates, it is imperative to extend this as much as possible. The analysis discussed here began with temperature-dependent and energy-dependent ARPES data from the nodal lines where the d-wave superconducting gap is zero, so it is actually only a small portion of what can be carried out. Our plans for the near future will be to:

a) Extend this type of analysis away from the nodes, where the transport is less sensitive (due to the reduced Fermi velocities of those states) but the ARPES is still very sensitive. These states also of course directly participate in (or drive) the superconductivity, with both the states themselves and the self-energies being strongly modified at low temperatures as the superconducting gap and pseudogap open. With prior DOE support we have already made major advances in our understanding of the evolution of the self-energies in this regime, including through the normal to pseudogap to SC states [ref 3], though this was only one doping and a limited k-space range.

b) Utilize the experimentally determined spectral function to calculate other properties of the cuprates. The resistivity/phase diagram shown above is one great example, but other properties such as thermodynamics, optics, magnetic susceptibility etc. can also be calculated and compared.

c) Apply a similar analysis to other correlated electron and "strange metal" systems. Our initial work on nickelates indicates that the PLL phenomenology from the cuprates works quite well there, albeit with different coupling strengths than the cuprates [pub 6]. It will be important to know general this phenomenology is.

d) Work to determine, or at least heavily constrain, the origin of the PLL phenomenology.

Outside of work on cuprates, strange metals, and related compounds, we will continue ARPES and spin-ARPES studies of other interesting superconductors, topological superconductors, magnetic topological and altermagnetic materials, etc.

References

1. T.J. Reber, J.A. Waugh, N.C. Plumb, S. Parham, Y. Cao, Z. Sun, Q. Wang, J.S. Wen, Z.J. Xu, G. Gu, Y. Yoshida, H. Eisaki, Y. Aiura, G.B. Arnold, D. S. Dessau, *A Unified Form of Low-Energy Nodal Electronic Interactions in Hole Doped Cuprate Superconductors,* Nature Communications **10**, 5737 (2019)
2. S. Smit, E. Mauri, L. Bawden, F. Heringa, F. Gerritsen, E. van Heumen, Y. K. Huang, T. Kondo, T. Takeuchi, N. E. Hussey, M. Allan, T. K. Kim, C. Cacho, A. Krikun, K. Schalm, H.T.C. Stoof & M. S. Golden, *Momentum-dependent scaling exponents of nodal self- energies measured in strange metal cuprates and modelled using semi-holography* Nature Communications 15, 4581 (2024)
3. Haoxiang Li, Xiaoqing Zhou, Stephen Parham, Theodore J. Reber, Helmuth Berger, Gerald Arnold, Daniel S. Desssau, *Coherent organization of electronic correlations as a mechanism to enhance and stabilize high temperature cuprate superconductivity*, Nature Communications **9**, 26 (2018) doi:10.1038/s41467-017-02422-2

Publications

1. Peipei Hao, Aksaj Bharatwaj, Keiichi Harada, Tomohiro Usui, K. Kawamura, Yuki Teramoto, Daiki Fujiwara, Takao Watanabe, and Daniel S. Dessau, *Cuprate strange metals as a quantum critical phase with linearly running power law exponent*. Preprint
2. R. Kurleto, C. -H. Wu, S. Acharya, D. M. Narayan, B. S. Berggren, P. Hao, A. Shackelford, H. R. Whitelock, Z. Sierzega, M. Hashimoto, D. Lu, C. Jozwiak, R. P. Cline, D. Pashov, J. Chen, M. van Schilfgaarde, F. M. Grosche, D. S. Dessau *Flat Bands at the Fermi Level in Unconventional Superconductor YFe_2Ge_2*. Preprint
3. Songyuan Geng, Xin Wang, Risi Guo, Chen Qiu, Fangjie Chen, Qun Wang, Kangjie Li, Peipei Hao, Pengxiao Bao, Hanpu Liang, Yang Huang, Yunbo Wu, Shengtao Cui, Zhe Sun, Timur K. Kim, Cephise Cacho, Daniel S. Dessau, Benjamin T. Zhou, Haoxiang Li, *Experimental realization of dice-lattice flat band at the Fermi level in layered electride YCl*. Preprint
4. Dimitar Pashov, Swagata Acharya, Stephan Lany, Daniel S Dessau, Mark van Schilfgaarde, *Multiple Slater determinants and strong spin-fluctuations as key ingredients of the electronic structure of electron- and hole-doped $Pb_{10-x}Cu_x(PO_4)_6O$ Crystals.* Crystals **15**(7), 621 (2025); https://doi.org/10.3390/cryst15070621
5. Dushyant M. Narayan, Peipei Hao, Rafał Kurleto, Bryan S. Berggren, A. Garrison Linn, Christopher Eckberg, Prathum Saraf, John Collini, Peter Zavalij, Makoto Hashimoto, Donghui Lu, Rafael M. Fernandes, Johnpierre Paglione, Daniel S. Dessau, *Potential Lifshitz Transition at Optimal Substitution in Nematic Pnictide $Ba_{1-x}Sr_xNi_2As_2$* Science Advances **Vol 9**, Issue 42 (2023) DOI: 10.1126/sciadv.adi4966
6. Haoxiang Li, Peipei Hao, Junjie Zhang, Kyle Gordon, A. Garrison Linn, Xinglong Chen, Hong Zheng, Xiaoqing Zhou, J.F. Mitchell, D. S. Dessau *Electronic structure and correlations in planar trilayer nickelate $Pr_4Ni_3O_8$* Sci Advances 9, eade4418 (2023)
7. A. Garrison Linn, Peipei Hao, Kyle N. Gordon, Dushyant Narayan, Bryan S. Berggren, Nathaniel Speiser, Sonka Reimers, Richard P. Campion, Vıt Novak, Sarnjeet S. Dhesi, Timur K. Kim, Cephise Cacho, Libor Smejkal, Tomas Jungwirth, Jonathan D. Denlinger, Peter Wadley, and Daniel S. Dessau, *Experimental electronic structure of the electrically switchable antiferromagnet CuMnAs*, NPJ Quantum Materials (2023)

Magneto-optical Study of Correlated Electron Materials in High Magnetic Fields

Dmitry Smirnov1; Co-PI: Zhigang Jiang[2]

[1] National High Magnetic Field Laboratory, Tallahassee, FL 32310

[2] Georgia Institute of Technology, Atlanta, GA 30332

Keywords: General: frustrated magnetism, Weyl fermions; **Physical Systems:** magnetic insulators, topological materials; **Techniques:** infrared and optical techniques

Research Scope

This program is aimed at studying electronic structure, low-energy excitations, and many-body effects in novel quantum materials via high-field magneto-optical spectroscopy. The current research is mostly focused on the spectroscopy of the exotic quantum states and excitations in quantum magnetic systems.

Recent Progress

Tilting Effect in Coupled Weyl Bands: A Case Study of Weyl Semimetal Niobium Phosphide
(Moon *et al.* Nano Lett. **25**, 2858 (2025))

Weyl semimetals are characterized by unique band structures in which the conduction and valence bands intersect at discrete points known as Weyl points (WPs). These points, possessing specific chirality, are of great interest in quantum material research and quantum information science. WPs always appear in pairs and are typically situated away from high-symmetry points in the Brillouin zone, giving rise to the commonly observed phenomenon of band tilting. The tilting effect is considered a solid-state realization of Lorentz violation, significantly influencing the transport and optical properties of Weyl semimetals. It leads to intriguing phenomena such as chiral photocurrents and the anisotropic chiral magnetic effect. Although band tilting has been confirmed via angle-resolved photoemission spectroscopy, most research has focused on large tilting angles (type-II tilting), which result in open Fermi surfaces and the co-existence of electrons and holes. By contrast, smaller tilting angles (type-I tilting) cause less pronounced Fermi surface reconstructions, making experimental identification much more challenging.

In our work, we demonstrate that magneto-infrared spectroscopy is an effective tool for probing the tilting effect in electronic band structures. This effect relaxes optical selection rules, allowing for transitions that would otherwise be forbidden in the non-tilt case, even for relatively small tilting angles. Using the well-established Weyl semimetal NbP, where type-I tilting is expected [1–3], we measure its magneto-reflectance spectra. The second derivative of the measured spectra is presented in Fig. 1(a). By comparing the experimental results with a four-band coupled WP model, we identify numerous LL transitions that cannot be explained by the non-tilt model. However, these transitions are well captured by the coupled tilted WP model, especially at

low energies as shown in Fig. 1(c), providing clear spectroscopic evidence of the tilting effect in this material.

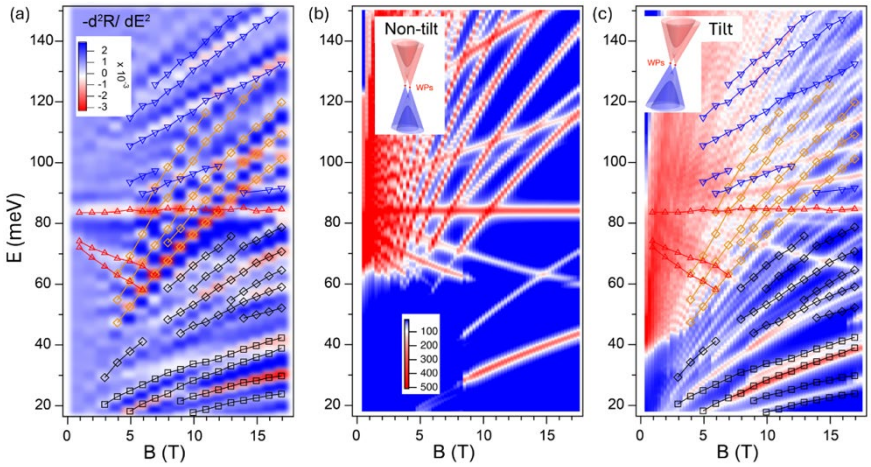


Figure 6: (a) False-color plot of the second derivative, $-\boldsymbol{d^2R/dE^2}$, of the normalized magneto-reflectance spectra, $\boldsymbol{R(B)/R(B = 0T)}$, of NbP, measured at 5 K. Symbols represent extracted transition energies, grouped into four sets and color-coded accordingly. (b,c) Calculated magneto-absorption spectra of NbP from a non-tilt model (b) and a tilt model (c). Symbols correspond to the transition energies plotted in (a).

Moreover, we observe unconventional interband transitions characterized by flat and negative magnetic field dispersions (i.e., red modes in Fig. 1(a)). These transitions highlight the critical role of Weyl band coupling, which leads to distinct magnetic field dispersions between the upper valence/conduction bands and the lower valence/conduction bands, resulting in these unconventional behaviors. In the absence of coupling between the Weyl bands, all interband and intraband LL transitions would exhibit positive magnetic field dispersions, which cannot account for the observed unconventional transitions. Overall, our experimental findings shed light on the universal behavior of the tilting effect in Weyl semimetals, offering valuable insights into their electronic and optical properties.

Sharp spectroscopic fingerprints of disorder in an incompressible magnetic state
(Kim *et al.* arXiv:2506.08112v1, 2025)

Disorder significantly impacts the electronic properties of metallic quantum materials by inducing electron localization and thus altering the local density of states and electric transport. In insulating quantum magnetic materials, the effects of disorder are less understood and can drastically impact fluctuating spin states like quantum spin liquids (QSLs). In the absence of transport tools, disorder is typically characterized using chemical methods or by semi-classical modeling of spin dynamics. This requires high magnetic fields that may not always be accessible. Here, we show that magnetization plateaus—incompressible states found in many quantum magnets—provide an exquisite platform to uncover otherwise undetectable amounts of disorder, regardless of the origin of the plateau.

To demonstrate this spectacular effect, we focus on the Heisenberg-Ising (or XXZ) triangular-lattice antiferromagnet $K_2Co(SeO_3)_2$ (KCSO). It features a robust up-up-down (UUD) phase associated with a 1/3 magnetization plateau that spans an extraordinarily wide field range, from 2 to 17 T [4] , and is flanked by compressible spin supersolid phases at low temperatures [4–6] . Here, we utilize far-infrared magneto-optical spectroscopy (FIRMS) and thermomagnetic measurements to investigate the behavior of KCSO near and within the 1/3 magnetization plateau. The FIRMS measurements in the UUD phase reveal: (i) two dominant modes that can be naturally attributed to single spin-flip excitations, and (ii) three satellite modes (Fig. 2a) that cannot be explained by clean system models. Through analytical and numerical modeling, we show that the satellite modes are unique spectroscopic fingerprints of disorder and identify their nature as dilute spin vacancies (Fig. 2b, when the disorder-induced bonding reduction $d_{zz} \rightarrow 100\%$). Remarkably, this model explains all details of the thermomagnetic response of our system, including the existence of multiple plateaus. Our findings provide a new approach to identifying disorder in quantum magnets.

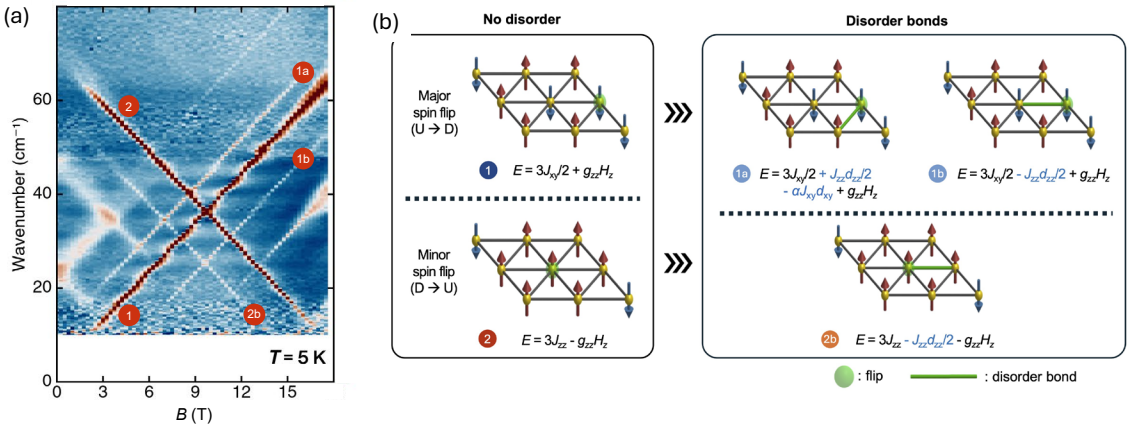


Figure 2: (a) Energy and magnetic field dependence of the normalized magneto-transmission spectra of KCSO measured in Faraday geometry at $T = 5$ K with the magnetic field direction z along the c-axis. (b) Schematic interpretation of magnetic excitations in the UUD phase of KCSO.

Future Plans

In the next three years, we plan to continue applying high-field optical magneto-spectroscopy to probe and understand emerging unconventional quantum phases and properties driven by magnetic interactions in quantum magnetic systems. Our goal is to establish strong connections between quantum magnetism and the optical responses of materials. The current efforts are focused on quasi-two-dimensional Co-based magnets, aiming at understanding of (i) competing magnetic interactions in candidate QSL material $Na_3Co_2SbO_6$, and (ii) chiral phonon interactions with magnetic fields in $Na_3Co_2SbO_6$ and $K_2Co(SeO_3)_2$.

References

[1] C.-C. Lee et al., Fermi surface interconnectivity and topology in Weyl fermion semimetals TaAs, TaP, NbAs, and NbP, Phys. Rev. B **92**, 235104 (2015).

[2] D. Grassano, O. Pulci, E. Cannuccia, and F. Bechstedt, Influence of anisotropy, tilt and pairing of Weyl nodes: the Weyl semimetals TaAs, TaP, NbAs and NbP, Eur. Phys. J. B **93**, 157 (2020).

[3] L. Zhang, Y. Jiang, D. Smirnov, and Z. Jiang, Landau quantization in tilted Weyl semimetals with broken symmetry, J. Appl. Phys. **129**, 105107 (2021).

[4] M. Zhu et al., Continuum Excitations in a Spin Supersolid on a Triangular Lattice, Phys. Rev. Lett. **133**, 186704 (2024).

[5] T. Chen et al., Phase Diagram and Spectroscopic Signatures of Supersolids in Quantum Ising Magnet K2Co(SeO3)2, arXiv:2402.15869 (2024).

[6] Y. Xu, J. Hasik, B. Ponsioen, and A. H. Nevidomskyy, Simulating spin dynamics of supersolid states in a quantum Ising magnet, Phys. Rev. B **111**, L060402 (2025).

Publications (2023-2025)

1. C. Kim et al., Sharp spectroscopic fingerprints of disorder in an incompressible magnetic state, arXiv:2506.08112 (2025).
2. S. Moon, Y. Jiang, J. Neu, T. Siegrist, M. Ozerov, Z. Jiang, and D. Smirnov, Magneto-optical Evidence of the Tilting Effect in Coupled Weyl Bands, Nano Lett. **25**, 2858 (2025).
3. B. S. Mou et al., Comparative Raman scattering study of crystal field excitations in Co-based quantum magnets, Phys. Rev. Mater. **8**, 084408 (2024).
4. L. Xiang et al., Disorder-Enriched Magnetic Excitations in a Heisenberg-Kitaev Quantum Magnet Na2Co2TeO6, Phys. Rev. Lett. 131, 076701 (2023).
5. Y. Jiang, M. Ermolaev, S. Moon, G. Kipshidze, G. Belenky, S. Svensson, M. Ozerov, D. Smirnov, Z. Jiang, and S. Suchalkin, g -factor engineering with InAsSb alloys toward zero band gap limit, Phys. Rev. B **108**, L121201 (2023).
6. K. Thirunavukkuarasu et al., Magnetoelastic interactions in SrCu2(BO3)2 studied by Raman scattering experiments and first principles calculations, Phys. Rev. B **107**, 064410 (2023).
7. Y. Jiang, T. Zhao, L. Zhang, Q. Chen, H. Zhou, M. Ozerov, D. Smirnov, and Z. Jiang, Revealing temperature evolution of the Dirac band in ZrTe5 via magnetoinfrared spectroscopy, Phys. Rev. B **108**, L041202 (2023).
8. X. Wang et al., Unveiling the spin evolution in van der Waals antiferromagnets via magneto-exciton effects, Nat. Commun. **15**, 8011 (2024).
9. C. Tang et al., Exciton-activated effective phonon magnetic moment in monolayer MoS2, Phys. Rev. B **109**, 155426 (2024).
10. W. Pan et al., Lithography-Defined Semiconductor Moirés with Anomalous In-Gap Quantum Hall States, Nano Lett. **25**, 10536 (2025).

Control of antiferromagnetic order using voltage, current and temperature

Ivan K. Schuller, *Department of Physics, University of California San Diego*

Keywords: proximity effect, antiferromagnet, heterostructure, phase transitions, spin-orbit torque

Research Scope

The research pursued under this project is dedicated to understanding and manipulating the properties of magnetic materials when restricted to the nanoscale in a variety of dimensions and when are in proximity to dissimilar materials. In this fashion, new properties can be engineered into materials which do not exist in nature. A particularly interesting class of magnetic materials are antiferromagnets (AFMs) which have compensated spin structure that turns on or order at the so-called Néel temperature (T_N) or blocking temperature (T_B). Antiferromagnets have received renewed attention recently because of their basic research properties and potential applications in fault-tolerant, high frequency spintronic applications. Moreover, it is worth noting that AFMs serve as magnetic anchors or pinning layers and thus are the basic constituents in Giant Magnetoresistance based devices.

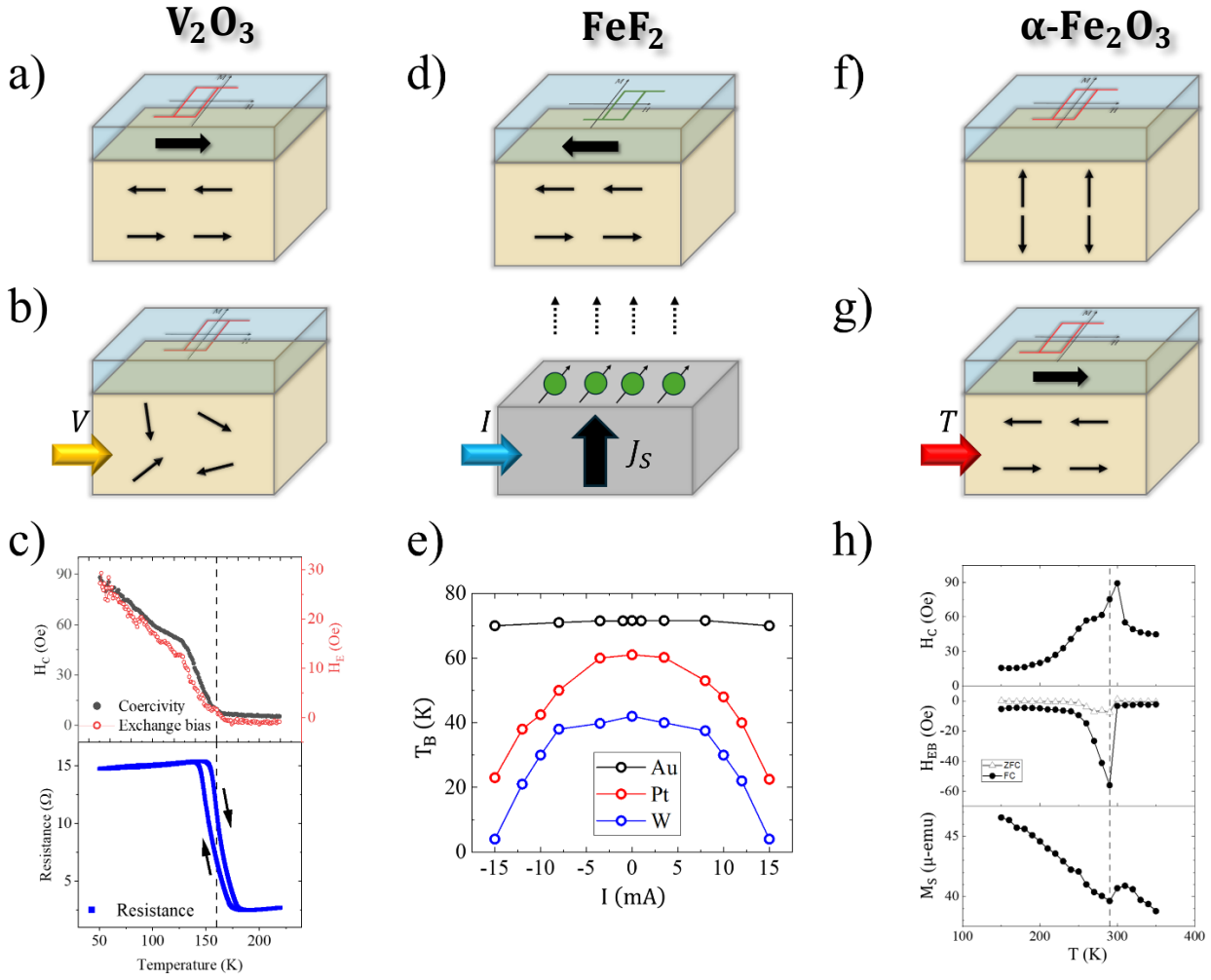
Detecting bulk antiferromagnetism at the atomic scale is practically impossible using laboratory-based techniques. However, at the nanoscale the surface of AFMs reflect their bulk magnetic configuration and can be detected using a variety of technique. In particular, an AFM in proximity to a ferromagnet (FM), under the proper conditions, shifts the FM hysteresis curve along the field axis by a quantity now known as the Exchange Bias (EB). We have developed (under DOE sponsorship) a thorough understanding of this phenomenon under all experimental conditions: field, temperature, interfacial roughness, crystallographic orientation, conductivity etc. So, EB is a very effective tool that can be used as a diagnostic of the surface spin structure of an AFM.

Manipulation of the AFM spins is a much more challenging task. The reason for this is that since the spin structure of the AFM is fully compensated, the application of a small magnetic field has little effect on the AFM order. This is a double-edged sword. While the fact that the spins are compensated, makes the AFM impervious to external disturbances, it also makes it very difficult to manipulate. So more creative ways of changing and affecting their order should be invented and used. In this project we aim to address precisely this issue.

Recent Progress

During the last two years of this DOE funded project, we have developed and investigated three different ways of manipulating the spin structure of an AFM device. The way we accomplished this is by incorporating the AFM thin film into a heterostructure and by applying 3 types of external stimuli: voltage, current or temperature. Particular classes of AFMs are affected differently by these 3 different types of stimuli. Extensive studies as a function of relevant

parameter have been pursued and published. Here we show just some iconic examples which illustrate the effects and ideas pursued recently.



Antiferromagnets controlled through voltage-triggered magnetic order (a-c), charge current generated spin current (d, e) and temperature-triggered spin reorientation (f-h).

V_2O_3 is a strongly correlated AFM which exhibits an insulator-metal transition (IMT) which coincides with a magnetic and structural transition that occurs at the same temperature. Below the T_{IMT} (Fig. a)) when the AFM V_2O_3 is subject to a voltage above a certain threshold the material undergoes the IMT and also an AFM-paramagnetic transition as shown in Fig. b). As a consequence, the EB and the coercivity (H_C) enhancement of the FM turn off at the same temperature as the IMT (see Fig. c)). So, this method for manipulating the AFM order could be applied to many other similar systems that exhibit IMT which coincides with an antiferromagnetic order. **[1]**

FeF_2 is an insulating AFM that exhibits large EB. We incorporated this AFM into a heterostructure with a nonmagnetic heavy (W or Pt) or normal (Au) metals. When a current is passed through the nonmagnetic (W, Pt) metal a spin torque develops at the interface which produces a pure spin current in the perpendicular direction (Fig. d)). This pure spin current is able to apply a torque on the AFM thereby shifting its blocking temperature (T_B) as shown in Fig. e). Very interestingly a large shift is observed as a function of current for Pt and W while the Au control experiment shows no shift. This implies that this effect is related to the large spin-orbit coupling present in W and Pt but not in the Au. These types of effects should be observable in whole classes of insulating AFMs. [**2]**

α-Fe_2O_3 is an AFM which exhibits a Morin transition (T_M), in which the spins undergo a rotation of their orientation from perpendicular to the surface (Fig. f)) at high temperature, to parallel to the surface at low temperature (Fig. g)). This change in orientation has a major effect on the properties of a FM in close proximity incorporated into a heterostructure. Below T_M, when the AFM spins are perpendicular to the FM spins, the EB is null and the H_C is small as in the FM. Interestingly, at the T_M a large negative EB develops which again disappears at low T, whereas the hysteresis curve shows a substantially enhanced H_C at the T_M (Fig. h)). **[3]**

Future Plans

One of the key issues which needs to be addressed experimentally is the role that thermal effects play in these types of nanostructured materials. In many cases the current densities and voltages that are applied are small in absolute values but are very large when normalized to the size of the devices. In general, control experiments or modelling are used to assure that thermal effects are minimized. However, it would be desirable to perform direct local thermal measurements to evaluate experimentally the role of thermal effects in magnetic devices. We are quite excited to report that we have developed such a thermal measurement apparatus that is able to measure local temperature in-situ, in-operando. This is done by measuring the IR emission or the thermo-reflectance, in-situ, at the submicron scale, as a function of time. The instrument is tested and functional awaiting application to AFM materials, among many others.

In the future we will expand on the recent accomplishments outlined above by developing novel detection mechanisms. Until now the detection of the AFM state was done essentially using magneto Kerr effect for the magnetization measurements. In order to make the detection more versatile in a device, it would be desirable to incorporate magneto-transport measurements. The new detection mechanisms for antiferromagnetism that we will explore in an integrated device will include: anomalous magnetoresistance, inverse spin Hall effect and longitudinal Spin Seebeck effect. All these method have been used in our laboratory in some form or another so we have confidence that some will be successful.

To add additional functionalities to some of the antiferromagnetism based devices mentioned above, we will explore new potential methods which already have been tested to some

level in our laboratory. A potentially interesting method to add new device functionalities is by adding local stress. We have shown earlier that large changes in the magnetic properties of FMs can be accomplished by incorporating them into a heterostructure with an oxide which undergoes a structural phase transition. Another method to change the local stress is to use local ion beam modification and /or implantation [4]. We have some experience of both methods in different contexts and so we are confident that they can be applied successfully to AFMs.

To explore potential optical methods to affect the AFM state we will incorporate them into a heterostructure with a photo sensitive material such as CdS. Application of light to the photosensitive material changes its properties and consequently it may change the properties of an adjacent material by the injection of nonequilibrium charge carriers. We have already implemented this idea in a CdS/V_2O_3 heterostructure and have shown that the transport properties can be modified in this fashion [5]. This implies that the AFM properties may also change when exposed to light and therefore this looks like a promising avenue for exploration.

References

1. R. El Hage, T. D. Wang, J. Li, A. C. Basaran, F. Torres, I. K. Schuller, *Antiferromagnetic V_2O_3 Based Exchange Coupling*, Phys. Rev. Materials **8**, 054407 (2024).

2. F. Ajejas, F. Torres, A. C. Basaran, P. Salev, I. K. Schuller, *Current-driven Switching of Néel vector of an antiferromagnetic insulator thin film*, Adv. Electron. Mater. **9**, 2300385 (2023).

3. T. D. Wang, A. C. Basaran, R. El Hage, J. Li, H. Navarro, F. Torres, O. Rodríguez de la Fuente, I. K. Schuller, *Coercivity enhancement in hematite/permalloy heterostructures across the Morin transition*, J. Magn. Magn. Mater. **597**, 172024 (2024).

4. N. Ghazikhanian, J. del Valle, P. Salev, R. El Hage, Y. Kalcheim, C. Adda, I. K. Schuller, *Resistive Switching Localization by Selective Focused Ion Beam Irradiation*, Appl. Phys. Lett. **123**, 123505 (2023).

5. H. Navarro, J. del Valle, Y. Kalcheim, N. M. Vargas, C. Adda, M. H. Lee, P. Lapa, A. Rivera-Calzada, I. A. Zaluzhnyy, E. Qiu, O. Shpyrko, M. Rozenberg, A. Frano, I. K. Schuller, *A Hybrid Optoelectronic Mott Insulator*, Appl. Phys. Lett. **118**, 141901 (2021).

Publications

1. A. J. Breindel, Y. Deng, C. M. Moir, Y. Fang, S. Ran, H. Laub, S. Shubin, Q. Zeng, L. Shu, C. T. Wolowiec, I. K. Schuller, P. F. S. Rosa, Z. Fisk, J. Singleton, and M. B. Maple, *Probing FeSi, a d-electron topological Kondo insulator candidate, with magnetic field, pressure, and microwaves*, Proc. Natl. Acad. Sci. U.S.A. **120**, e2216367120 (2023).
2. H. Navarro, A. C. Basaran, F. Ajejas, L. Fratino, S. Bag, T. D. Wang, E. Qiu, V. Rouco, I. Tenreiro, F. Torres, A. Rivera-Calzada, J. Santamaria, M. Rozenberg, and I. K. Schuller, *Light-Induced Decoupling of Electronic and Magnetic Properties in Manganites*, Phys. Rev. Appl. **19**, 044077 (2023).
3. F. Ajejas, F. Torres, A. C. Basaran, P. Salev, and I. K. Schuller, *Current-driven switching of Néel vector of an antiferromagnetic insulator thin film*, Adv. Electron. Mater. **9**, 2300385 (2023).
4. P. Salev, L. Fratino, D. Sasaki, S. Bag, Y. Takamura, M. Rozenberg, and I. K. Schuller, *Magnetoresistance anomaly during the electrical triggering of a metal-insulator transition*, Phys. Rev. B **108**, 174434 (2023).

5. P. Salev, I. Volvach, D. Sasaki, P. Lapa, Y. Takamura, V. Lomakin, and I. K. Schuller, *Voltage-controlled magnetic anisotropy enabled by resistive switching*, Phys. Rev. **B 107**, 054415 (2023).
6. A. C. Rodríguez, A. Reiber, I. K. Schuller, D. Muraca, and J. G. Ramírez, *Evidence of a glassy magnetic transition driven by structural disorder in $BiFeO_3$ nanoparticles*, J. Magn. Magn. Mater. **563**, 169917 (2022).
7. T. D. Wang, A. C. Basaran, R. El Hage, J. Li, H. Navarro, F. E. Torres, O. R. de la Fuente, and I. K. Schuller, *Coercivity enhancement in hematite/permalloy heterostructures across the Morin transition*, J. Magn. Magn. Mater. **597**, 172024 (2024).
8. R. Luo, T. J. Legvold, L. Chen, H. Navarro, A. C. Basaran, D. Hong, C. Liu, A. Bhattacharya, I. K. Schuller, and D. Natelson, *Low-temperature spin Seebeck effect in nonmagnetic vanadium dioxide*, Phys. Rev. **B 110**, 024415 (2024).
9. D. Carranza-Celis, C. T. Wolowiec, A. C. Basaran, P. Salev, I. K. Schuller, and J. G. Ramírez, *Low-temperature paramagnetic phase reentrance in praseodymium-doped manganites*, Phys. Rev. Materials **8**, 054401 (2024).
10. *Antiferromagnetic V_2O_3 based exchange coupling*. Ralph el Hage, Tianxing D. Wang, Junjie Li, Ali C. Basaran, Felipe Torres, and Ivan K. Schuller. Phys. Rev. Materials **8**, 054407 (2024)

Ferroelectric Polarization Control of Metal-Insulator Transition and Magnetism in Ultrathin $SrIrO_3$

Xia Hong, Department of Physics and Astronomy, University of Nebraska-Lincoln

Tula Paudel, Department of Physics, South Dakota School of Mines and Technology

Keywords: correlated oxide; ferroelectric field effect; metal-insulator transition; weak-antilocalization; anomalous Hall effect

Research Scope

The scope of the research is to achieve ferroelectric polarization control of magnetotransport properties and induce metal-insulator transition and magnetism in 5*d* iridate $SrIrO_3$ (SIO). $SrIrO_3$ is a correlated semi-metal with strong spin-orbit coupling (SOC), which competes with the electron itinerancy, crystal field splitting, and on-site Coulomb interaction in determining the electronic and magnetic states.[1,2] For epitaxial SIO thin films, the dimensionality, charge density, lattice distortion, and SOC can be individually manipulated or collectively controlled via quantum confinement, electric field effect doping, strain modulation, symmetry breaking, and interfacial orbital design. Leveraging the nonvolatile polarization of an interfacial ferroelectric layer, we aim to design emergent phenomena such as reversible quantum phase transitions and chiral spin textures (Fig. 1a) and identify interfacial coupling mechanisms mediated by charge, lattice, and polar symmetry. The ***objectives*** include: 1) achieving metal-insulator transition in $SrIrO_3$ via the ferroelectric field effect combined with the interfacial lattice coupling; 2) modulating quantum transport such as weak localization and weak antilocalization; and 3) assessing ferroelectric control of magnetism and topological spin textures in ultrathin $SrIrO_3$.

The results can shed light on the important energy and length scales and underlying mechanisms for driving the electronic and magnetic phase transitions, which can be further utilized to design more exotic topological states and superconductivity in correlated oxides.

Recent Progress

We fabricated epitaxial heterostructures composed of ferroelectric $PbZr_{0.2}Ti_{0.8}O_3$ (PZT) gates and 3-5 unit cell (uc) $SrIrO_3$ channels, where

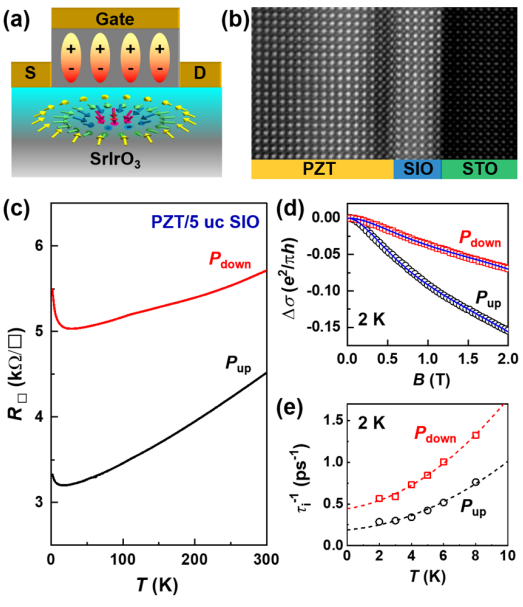


Fig. 1. (a) Sample schematic. **(b)** HRSTEM image of PZT/SIO deposited on $SrTiO_3$ (STO). **(c)** $R_{\square}(T)$, **(d)** $\Delta\sigma(B)$, and **(e)** $\tau_i^{-1}(T)$ for a 5 uc $SrIrO_3$ in the P_{up} and P_{down} states of PZT.

the interfacial PZT can not only induce charge density modulation in ultrathin $SrIrO_3$ but also enhance the Rashba SOC. In collaboration with Yimei Zhu group at Brookhaven National Lab, we performed high resolution transmission electron microscopy (HRTEM) studies on these samples, which reveal high crystallinity and atomically sharp interfaces (Fig. 1b). In 5 uc $SrIrO_3$, switching PZT polarization induces nonvolatile modulation of resistance (Fig. 1c) and magnetoconductance (Fig. 1d). Ultrathin $SrIrO_3$ is in the two-dimensional limit, which exhibit weak localization and weak antilocalization at low temperatures.[3] By fitting the magnetic field dependence of conductance change $\Delta\sigma(B)$ to the Maekawa-Fukuyama model (Fig. 1d), we deduced the inelastic scattering time and spin-orbit scattering time. The inelastic scattering rate (τ_i^{-1}) exhibits an unusual saturation at low temperatures (Fig. 1e), which suggests possible spin-flip scattering due to emergence of magnetic moments.

In bulk, the ground state of orthorhombic $SrIrO_3$ is paramagnetic.[2] Due to the strong SOC, $SrIrO_3$ thin films provide a promising platform for achieving electrical control of chiral spin textures such as the skyrmion state if $SrIrO_3$ can host a magnetic order. By switching PZT polarization, we induced reversible metal-insulator transition in 3-4 uc $SrIrO_3$ thin films (Fig. 2a). Close to the metal-insulator transition, $SrIrO_3$ exhibits anomalous Hall effect, signaling emergent magnetic order (Fig. 2b). It also shows topological Hall effect, which can be related to chiral spin textures. To understand the origins of magnetism and possible induced Dzyaloshinskii-Moriya interaction (DMI), we performed density functional theory modeling (DFT+LDA) of symmetric heterostructures of $PbTiO_3$ (PTO)/SIO/STO/SIO/PTO. Reversing the polarization of PTO shifts the Ir *d*-bands at the Fermi level and therefore alters the charge compensations at the interface. It further induces lattice distortion in the interfacial layers of $SrIrO_3$ (Fig. 2c), corroborating the polarization-dependent SOC and DMI. Our study presents a new venue to explore quantum phase transitions and design emergent spin phenomena.

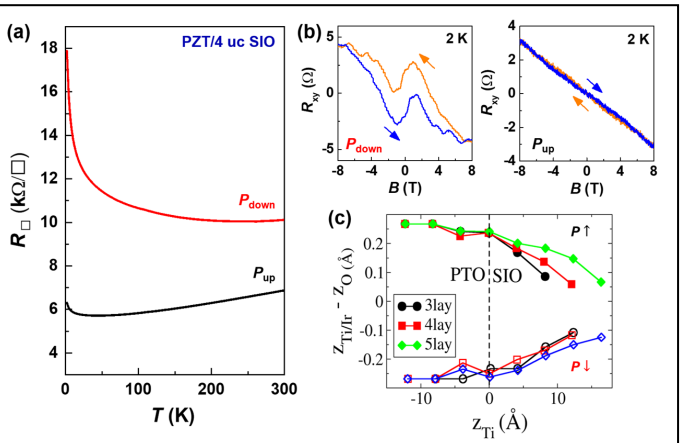


Fig. 2. (a) $R_\square(T)$, and **(b)** $R_{xy}(B)$ for a 4 uc $SrIrO_3$ in the P_{up} and P_{down} states of PZT. **(c)** DFT modeling of off-center displacement of interfacial B-site atoms in PTO/SIO heterostructures with 3, 4, 5 uc SIO.

Future Plans

Based on our current progress, we plan to carry out research in the following directions.

1) Carry out comprehensive magnetotransport studies of PZT/$SrIrO_3$ heterostructures, including weak (anti)localization, anomalous Hall effect, topological Hall effect, anisotropic magnetoresistance, and planar Hall effect, to evaluate the SOC,[3] magnetic transition, and magnetic anisotropy.[4]

2) Assess the magnetic/spin states in $SrIrO_3$ using techniques such as magnetometry, Lorentz TEM, and nitrogen-vacancy microscopy/spectroscopy.

3) Perform theoretical modelling of electronic and magnetic phases in $SrIrO_3$ controlled by SOC, electron correlation, and lattice distortion at the interface.

4) Apply the ferroelectric polarization control to other types of 5*d* Ruddlesden-Popper iridates (Sr_2IrO_4 and $Sr_3Ir_2O_7$) to understand the effects of doping control versus bandwidth control in inducing the electronic and magnetic phase transitions.

References

1. W. Witczak-Krempa, G. Chen, Y. B. Kim, and L. Balents, *Correlated Quantum Phenomena in the Strong Spin-Orbit Regime*, Annual Review of Condensed Matter Physics **5**, 57 (2014).

2. L. Zhang, B. Pang, Y. B. Chen, and Y. Chen, *Review of Spin–Orbit Coupled Semimetal $SrIrO_3$ in Thin Film Form*, Critical Reviews in Solid State and Materials Sciences **43**, 367 (2018).

3. L. Zhang, X. Jiang, X. Xu, and X. Hong, *Abrupt Enhancement of Spin–Orbit Scattering Time in Ultrathin Semimetallic SrIrO3 Close to the Metal–Insulator Transition*, APL Materials **8**, 051108 (2020).

4. Y. Zhang, Q. Wu, Y. Hao, and X. Hong, *Ferroelectric Control of Anisotropic Magnetoresistance in Ultrathin Sr_2IrO_4 Films toward 2D Metallic Limit*, Advanced Physics Research **4**, 2400208 (2025).

Probing ice-rule-breaking transition in $Dy_2Ti_2O_7$ thin film by proximitized transport and magnetic torque

Haidong Zhou (University of Tennessee), Jian Liu (University of Tennessee)

Keywords: magnetism, spintronics/magnonics, thin film heterostructures, antiferromagnets, magnetotransport,

Research Scope

The overarching goal of our project is to address the grand challenge of "metallizing quantum magnets", where emergent electronic phenomena are induced as quantum mechanical consequences of exotic spin states and excitations in insulating magnets. Our approach in this investigation focuses on (i) materials synthesis by both single crystal and epitaxial growth, and (ii) transport characterizations complemented by other necessary analysis. The specific directions include (i) synthesizing geometrically frustrated quantum magnets with strong quantum spin fluctuations and topological magnons, (ii) identifying the proximitized electronic response to these collective spin dynamics with various external controls; (iii) materials discovery of new quantum magnets in forms of crystals, films, and heterostructures.

Recent Progress

Anomalous proximitized transport in metal/quantum magnet heterostructure $Bi_2Ir_2O_7/Yb_2Ti_2O_7$ We completed the studies on the $Bi_2Ir_2O_7/Yb_2Ti_2O_7$ **(**BIO/YbTO) heterostructure, in which we show that the quantum fluctuations of a localized frustrated magnet induce strong proximitized charge transport of the conduction electrons in an epitaxial BIO ultrathin film deposited on a single crystal of YbTO. The proximity effects are evidenced by the scaling behavior of the BIO resistance in correspondence with the dynamic scaling of the dynamic spin correlation function of YbTO, which is a result of quantum fluctuations near a multiphase quantum critical point. The proximitized transport in BIO can be effectively tuned by a magnetic field through suppressing the quantum spin fluctuations (QSFs) as well as inducing transitions via magnetic anisotropy in YbTO. In this work, we establish a pathway for harnessing QSFs in magnetic insulators with electric transport, offering exciting prospects for potential applications in the realm of quantum spintronics. Our work was published in Physical Review Materials (PRM **8**, 114407 (2024)) and selected as the Editor's highlight.

Probing ice-rule-breaking transition in $Dy_2Ti_2O_7$ thin film by proximitized transport and magnetic torque We completed the proximitized transport study on the $Bi_2Ir_2O_7/Dy_2Ti_2O_7$ (BIO/DTO) heterostructure grown on (111)-oriented YSZ substrate. The motivation is to extend the approach of proximitized transport to thin films of insulating quantum magnets. This approach was recently established by our work [1] on BIO thin films grown on DTO single crystals, which together with $Ho_2Ti_2O_7$ are the bulk pyrochlore prototypes of spin ice physics with unique degenerate ground states and emergent monopole excitation [2, 3]. However,

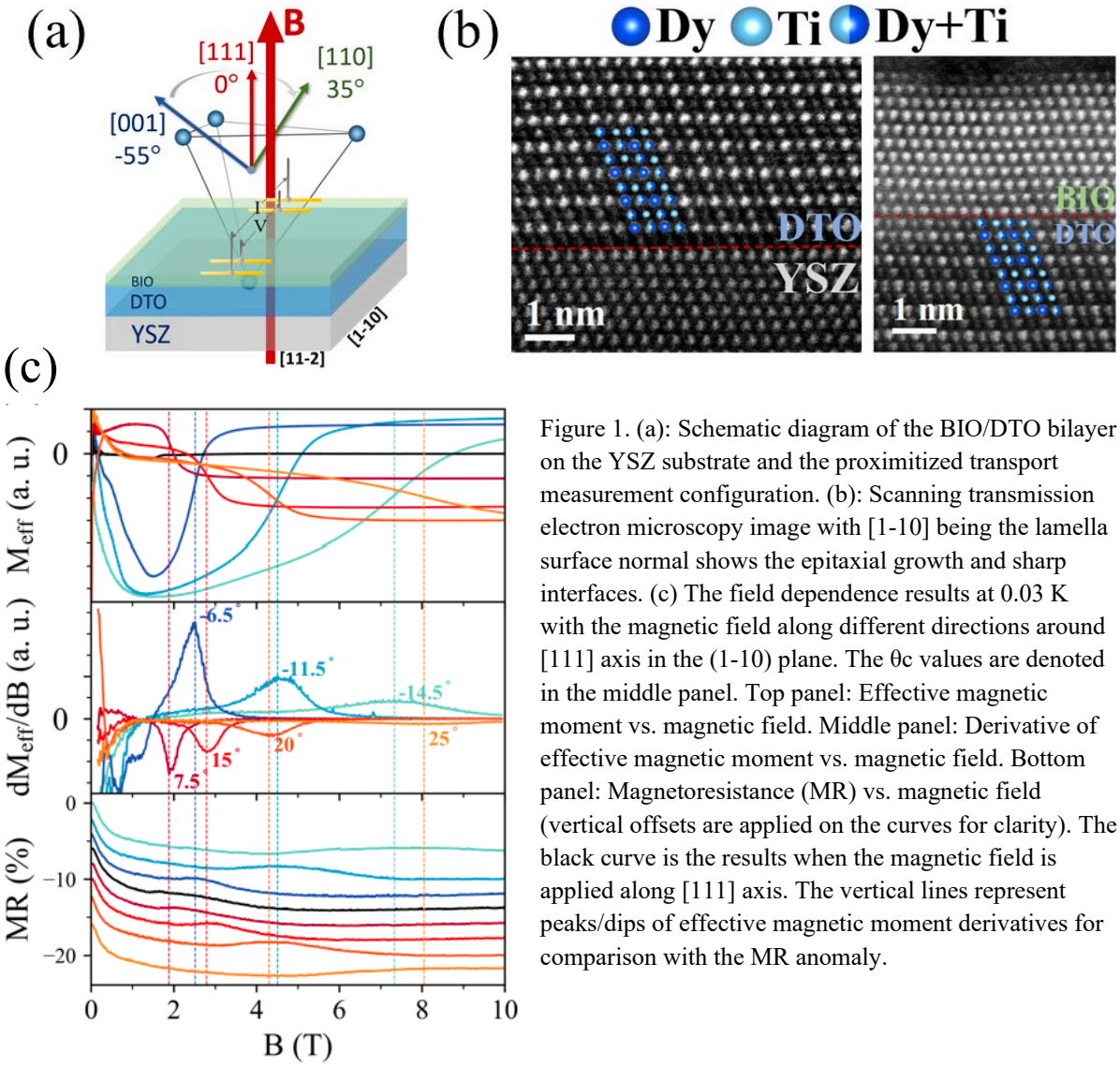


Figure 1. (a): Schematic diagram of the BIO/DTO bilayer on the YSZ substrate and the proximitized transport measurement configuration. (b): Scanning transmission electron microscopy image with [1-10] being the lamella surface normal shows the epitaxial growth and sharp interfaces. (c) The field dependence results at 0.03 K with the magnetic field along different directions around [111] axis in the (1-10) plane. The θc values are denoted in the middle panel. Top panel: Effective magnetic moment vs. magnetic field. Middle panel: Derivative of effective magnetic moment vs. magnetic field. Bottom panel: Magnetoresistance (MR) vs. magnetic field (vertical offsets are applied on the curves for clarity). The black curve is the results when the magnetic field is applied along [111] axis. The vertical lines represent peaks/dips of effective magnetic moment derivatives for comparison with the MR anomaly.

whether the spin ice state survives in the two-dimensional (2D) limit or generally in the thin film form remains a mystery. In addition to the presence of the substrate, the limited volume of thin film samples is the main challenge to study the intrinsic magnetic properties. Here, we synthesized 18nm-thick DTO thin film on YSZ substrate and capped it by a thin conductive BIO epilayer, and performed the proximitized magnetoresistance measurement, which clearly resolves the ice rule-breaking phase transition. The observation was confirmed by simultaneously measuring capacitive torque magnetometry on the DTO film. The results demonstrated that the spin ice state survives in the DTO thin film but with a modified effective nearest-neighbor interaction compared to the bulk crystal. Our study shows that proximitized transport is an effective probe to study the exotic magnetism in epitaxially engineered thin layers of insulating frustrated magnets. The manuscript of this work has been submitted for peer-review.

$Bi_2Ru_2O_7$ thin film We have performed a systematic study about the epitaxial synthesis of $Bi_2Ru_2O_7$ (BRO) thin films, which paves the way to extend the proximitized transport method by using BRO thin films. Our studies explored a wide range of temperature and oxygen partial pressure for the deposition. The results show that the epitaxial growth requires a minimal temperature about 500C and must be lower than a maximal temperature about 650C. Within this temperature window, epitaxial films can be stabilized in all pressures from 10^{-1} to 10^{-6} mbar. However, we found the cation stoichiometry varies significantly within such a wide pressure range and is still sensitive to temperature. A manuscript is under preparation to report these findings.

Local distortion driven magnetic phase switching in pyrochlore $Yb_2(Ti_{1-x}Sn_x)_2O_7$ We completed the studies of magnetic phase diagram of $Yb_2(Ti_{1-x}Sn_x)_2O_7$. While it is commonly accepted that the disorder induced by magnetic ion doping in quantum magnets usually generates a rugged free-energy landscape resulting in slow or glassy spin dynamics, the disorder/distortion effects associated with nonmagnetic ion sites doping are still illusive. Here, using AC susceptibility measurements, we show that the mixture of Sn/Ti on the nonmagnetic ion sites of pyrochlore $Yb_2(Ti_{1-x}Sn_x)_2O_7$ induces an antiferromagnetic ground state despite both parent compounds, $Yb_2Ti_2O_7$ and $Yb_2Sn_2O_7$, order ferromagnetically. Local structure studies through neutron total scattering reveals the local distortion in the nonmagnetic ion sites and its strong correlation with the magnetic phase switching. Our study demonstrates the local distortion as induced by the nonmagnetic ion site mixture could be a new path to achieve magnetic phase switching, which has been traditionally obtained by external stimuli such as temperature, magnetic field, pressure, strain, light, etc. Our results also help us to better understanding the disorder effects in $Yb_2Ti_2O_7$, and the related proximitized transport in the BIO/YbTO heterostructure. Our work was published in Physical Review B (PRB **109**, 144407 (2024)).

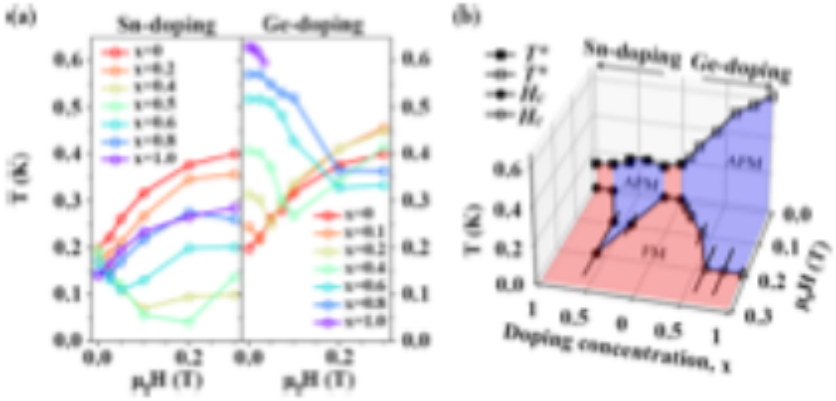


Figure 2 Magnetic phase diagram. (a) The field dependence of magnetic ordering temperature T^* for Yb2 $(Ti_{1-x}Sn_x)_2O_7$ and $Yb2(Ti_{1-x}Ge_x)_2O_7$ with different doping concentration. (b) Magnetic phase diagram as a function of the doping concentration x, temperature T, and external DC field. Red and blue regions represent the ferromagnetic and antiferromagnetic phases, respectively.

Universal dynamics of a pair condensate in $Na_2BaNi(PO_4)_2$ We completed the magnetic property studies of $Na_2BaNi(PO_4)_2$. Pair condensates appear in multiple branches of physics, always

introducing exotic phenomena [4, 5]. The pair condensate in quantum magnetism is the spin nematic, whose static (quadrupolar) order is difficult to access, favoring dynamical probes. While we search for suitable quantum magnets for heterostructure studies, we paid attention to $Na_2BaNi(PO_4)_2$, a triangular lattice antiferromagnet. We performed high-resolution neutron spectroscopy to obtain direct evidence for the presence of two spin-nematic phases induced in $Na_2BaNi(PO_4)_2$ by controlling the applied magnetic field. By combining precise experiments with quantitative theoretical and numerical analysis, we identify universal dynamics arising from the pair condensate. We show explicitly how the gapless Goldstone mode influences the dispersion and induces Cherenkov-like velocity-selective decay of the gapped single-quasiparticle band. These common spectral features shed new light on spin-nematic dynamics and underline the universal phenomenology shared by pair condensates across different physical systems. The manuscript of this work (arXiv:2503.13609v1) has been submitted for peer-review.

Future Plans

We will move forward on the directions we have embarked on and continue leveraging our capabilities of synthesizing and characterizing novel materials. In particular, our main focus will be (i) testing and extending the proximitized transport method to other non-magnetic metals grown on $Dy_2Ti_2O_7$ and $Yb_2Ti_2O_7$ in order to identifying the materials design principle; (ii) exploring proximitized transport behaviors in the transverse channel driven by topological properties of the insulating quantum magnets; (iii) synthesis of other frustrated magnets to explore the possibility of new heterostructures. We also plan establish micro-fabrication capability to make devices on our heterostructures, which is crucial for measuring Hall effect and other delicate transport properties at ultralow temperatures.

References

1. H. Zhang, C. K. Xing, K. Noordhoek, Z. Liu, T. Zhao, L. Horak, Q. Haung, L. Hao, J. Yang, S. Pandey, E. Dagotto, Z. Jiang, J. H. Chu, Y. Xin, E. S. Choi, H. D. Zhou, and J. Liu, *Anomalous magnetoresistance by breaking ice rule in $Bi_2Ir_2O_7/Dy_2Ti_2O_7$ heterostructure*, Nature Communications **14**, 1014(1-7) (2023).
2. J. S. Gardner, M. J. Gingras, and J. E. Greedan, *Magnetic pyrochlore oxides*, Reviews of Modern Physics **82**, 53 (2010).
3. M. J. Harris, S. Bramwell, D. McMorrow, T. Zeiske, and K. Godfrey, *Geometrical frustration in the ferromagnetic pyrochlore $Ho_2Ti_2O_7$*, Physical Review Letters **79**, 2554 (1997).
4. M. H. Anderson, J. R. Ensher, M. R. Matthews, C. E.Wieman, and E. A. Cornell, *Observation of Bose-Einstein Condensation in a Dilute Atomic Vapor*, Science **269**, 198–201 (1995),
5. W. Kohn and D. Sherrington, *Two Kinds of Bosons and Bose Condensates*, Rev. Mod. Phys. **42**, 1–11 (1970)

Publications

1. D. Gong, J. Yang, S. Zhang, S. Pandey, D. Cui, J. Ruff, L. Horak, E. Karapetrova, J. Kim, P. Ryan, L. Hao, Y. Zhang, and J. Liu, *Large asymmetric anomalous Nernst effect in the antiferromagnet $SrIr_{0.8}Sn_{0.2}O_3$*, Nature Communications **16**, 2888 (2025).

2. M. Xu, J. L. Gonzalex Jimenze, G. C. jose, A. Boonkird, C. Xing, C. Harrod, X. Li, H. D. Zhou, X. Ke, W.

Bi, M. Li, and W. Xie, *Spin flop and metamagnetic transition in monoclinic $Eu_4Bi_6Se_{13}$*, Chemistry of Materials **37**, 1935-1941 (2025).

3. H. Shiravi, W. Zheng, Y. He, S. Ran, D. A. Rhodes, L. Balicas, H. D. Zhou, and G. X. Ni, *Twist engineered phonon polaritons in α-V_2O_5*, Optics Letters **50**, 2986-2989 (2025).

4. C. Xing, S. Zhang, W. Yao, D. Cui, Q. Huang, J. Yang, S. Pandey, D. Dong, L. Horak, Y. Xin, E. S. Choi, Y. Zhang, H. D. Zhou, and J. Liu, *Anomalous proximitized transport in metal/quantum magnet heterostructure $Bi_2Ir_2O_7/Yb_2Ti_2O_7$*, Physical Review Materials **8**, 114407 (2024).

5. B. S. Mou, X. Zhang, L. Xiang, Y. Xu, R. Zhong, Rober J. Cava, H. D. Zhou, Z. Jiang, D. Smirnov, N. Drichko, and S. Winter, *Comparative Raman scatting study of crystal field excitations in Co-based quantum magnets*, Physical Review Materials **8**, 084408(1-11) (2024).

6. Y. Zhang, Z. Dun, Y. Cai, C. Xing, Q. Cui, N. Muniraju, Q. Zhang, Y. Li, J. Cheng and H. D. Zhou, *Local distortion driven magnetic phase switching pyrochlore $Yb_2(Ti_{1-x}Sn_x)_2O_7$*, Physical Review B **109**, 144407 (2024).

7. W. Yao, Q. Huang, T. Xie, A. Podlesnyak, A. Brassington, C. Xing, R. S. Dissanayaka Mudiyanselage, H. Wang, W. Xie, S. Zhang, M. Lee, V. S. Zapf, X. Bai, D. Alan Tennant, J. Liu, and H. D. Zhou, *Continuous spin excitations in the three dimensional frustrated magnet $K_2Ni_2(SO_4)_3$*, Physical Review Letters **131**, 146701(1-7) (2023).

8. N. Li, R. R. Neumann, S. K. Guang, Q, Huang, J. Liu, K. Xia, X. Y. Yue, Y. Sun, Y. Y. Wang, Q. J. Li, Y. Jiang, J. Fang, Z. Jiang, X. Zhao, A. Mook, J. Henk, I. Mertig, H. D. Zhou, and X. F. Sun, *Magnon-polaron driven thermal Hall effect in a Heisenberg-Kitaev antiferromagnet*, Physical Review B **108**, L140402 (2023).

9. D. Zhang, Y. Zhu, G. Zheng, K. Chen, Q. Huang, L. Zhou, Y. Liu, K. Jenkins, A. Chan, H. D. Zhou, and L. Li, *Field tunable BKT and quantum phase transitions in spin-1/2 triangular antiferromagnet*, arXiv2411.04755.

10. Q. Huang, H. Zhang, Y. Hao, W. Yao, D. Pajerowski, A. Aczel, E. S. Choi, K. Barros, B. Normand, H. D. Zhou, A. Lauchli, X. J. Bai, and S. S. Zhang, *Universal dynamics of a pair condense*, arXiv:2503.13609.

Single Spin Relaxation in a Fire/Ice Magnet

Arthur P. Ramirez, *University of California Santa Cruz*

Keywords: ferrimagnetism, Debye process, Orbach relaxation, high field switching

Research Scope

The research in our project seeks to understand relationships among different emergent degrees of freedom in strongly interacting quantum magnets, in particular the role of singlets for correlated phenomena. In the course of studying contributions to thermal conductivity in the rare-earth ortho-ferrites, we surveyed several adjacent ferrimagnets, including manganites and chromites, and some outside the orthorhombic structure type. A useful way of categorizing these ferrimagnets is the notion of fire and ice. Rare-earths ions typically possess small interaction strengths compared to 3*d* transition metals such as Cr, Fe, and Mn and thus are typically in a paramagnetic ("fire") state when the 3*d* ions are ordered ("ice"). We note that the rare-earths can be polarized by the exchange field of the 3*d* ions, but are not ordered by virtue of their mutual interactions and are, thus, in a paramagnetic phase. This is of importance for single-spin relaxation processes, as sought for next-generation information storage technologies, because uncorrelated spins can switch faster than clusters of correlated spins.

Recent Progress

In surveying various fire/ice systems, we found resonance phenomena in many of them, usually associated with domain wall relaxation around a spin-reorientation transition. Such effects are not uncommon in low-transition temperature ferromagnets, and are typically described by Debye-like relaxation with attempt frequencies in the MHz regime. A contrasting set of systems are the single-molecule magnets (SMMs) typically employing Ising-type ions such as Dy^{3+}.[1] Here the relaxation process is of a single Dy spin, separated from its Dy neighbors by residing at the center of a large organic molecule. While the observed single-spin relaxation effects in such systems demonstrate possible utility in storage devices, their incorporation of organic molecules presents challenges for device fabrication.

Our main result is the observation of a large resonance signal in ac-susceptibility measurements on the layered material $SmMn_2Ge_2$ ($ThCr_2Si_2$ structure) in the temperature range 30 – 50 K. This system possesses a unique (to our knowledge) phase diagram in which a re-entrant ferromagnetic phase appears below 100 K.[2] The peaks seen in the frequency dependence of the loss signal (χ'') occurs below 50 K, likely as a result of our limited excitation frequency range (0.1 – 1000 Hz). These resonances were analyzed using a modified Debye relaxation process model and demonstrate high-fidelity Arrhenius behavior. To our surprise, we found an attempt frequency in

the THz range, and an activation barrier that corresponds well with a low-lying Sm^{3+} crystal field level. Because the Mn spins are responsible for the ferromagnetism, and because domain wall processes typically exhibit attempt frequencies in the MHz regime, they are an unlikely origin for the resonance. Instead, both the energy barrier and the fact that the Sm^{3+} spins are non-interacting but polarized by the exchange field of the Mn subsystem, strongly suggest that the relaxation phenomenon is that of single Sm^{3+}spins.

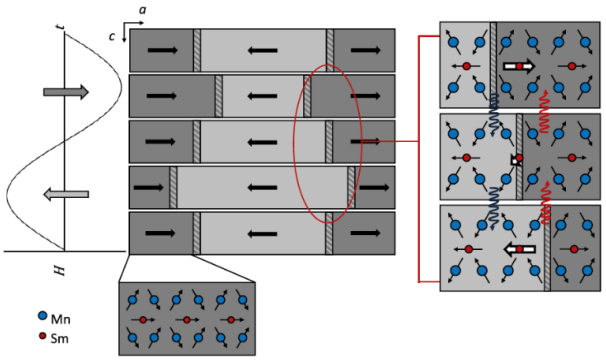


Fig. 1 Interpretation of the relaxation process in which domain wall motion flips the Sm spins. The layers in the left hand side of the diagram correspond to domain wall motion in successive time segments of the Mn ferromagnet. The right hand drawing shows how this domain wall motion can flip a Sm spin.

The physical picture for this effect is shown in Fig. 1. The Sm spins reside in layers sandwiched between Mn layers with twice the density as the Sm layer spins. The domain walls formed when the Mn system orders will, thus have a small fraction, estimated to be ~ 1%, of Sm spins in the wall's vicinity. Those outside the wall will be exchange-field polarized. When an oscillating magnetic field is applied, the domain walls move back and forth and thus modulate the exchange field at the oscillation frequency. It is thus possible that ~ 1% of the Sm spins are being switched at audio frequencies between magnetic fields the order of a few Tesla. We are not aware of the phenomenon of fast high-field switching, being discussed previously, but our results suggest a new way to perform spin resonance experiments. The special geometry presented by the $ThCr_2Si_2$ structure has likely variations achievable via atomic layer deposition, which may also provide routes for realizing similar effects at room temperature.

Future Plans

We are presently exploring relaxation effect in the rare-earth ortho-chromites and in particular, how the domain wall resonance changes through a spin-reorientation transition. This work is in addition to the proposed characterization of the order parameter in the eminuscent phase of geometrically frustrated magnets, which is ongoing.

References

1. J-L. Wu et al, *Switching the anisotropy barrier of a single-ion magnet by symmetry change from quasi-D5h to quasi-Oh*, Chemical Science, **4**, 3310 (2013).

2. H. Fujii et al., *Reentrant ferromagnetism observed in $SmMn_2Ge_2$*, Solid St. Comm., **53**, 715 (1985).

Publications

1. M. L. McLanahan, D. Lederman, and A. P. Ramirez, *Quantum spin relaxation with THz attempt frequency in the 1/3-fire, 2/3-ice ferrimagnet SmMn2Ge2*, Physical Review Materials, **9**, L051402 (2025).

Epitaxially-Imposed Control of Chiral Transport Phenomena

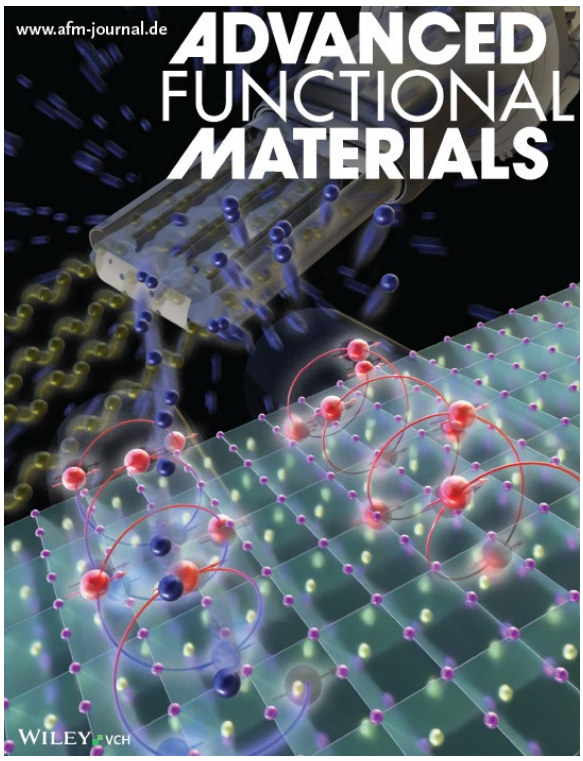
Matthew Brahlek, *Materials Science and Technology Division, Oak Ridge National Laboratory*

Keywords: Topology, Magnetism, Topological Superconductivity, Molecular Beam Epitaxy, Thin Film Heterostructures

Research Scope: This project aims to elucidate how interfaces and dimensionality govern novel transport phenomena by manipulating correlated electronic, magnetic, and lattice interactions within heterostructured quantum materials. Central to this effort is the development of new material paradigms via molecular beam epitaxy (MBE) that will enable the creation of high-quality, epitaxial systems that exhibit emergent properties, which centers on one-dimensional (1D) topological channels, emergent interfacial magnetism, and unconventional superconductivity. We pursue the three specific research directions: (1) creating and controlling 1D states through step-edge and defect engineering in topological insulators like Bi_2Se_3, with ongoing extension to magnetic systems such as $MnBi_2Te_4$, (2) understanding and integrating spin-polarized altermagnets (e.g., MnTe) with topological insulators and superconductors (e.g., Fe(Te,Se)), and (3) modifying correlated properties in high-conductivity metals such as $PdCoO_2$ via helium implantation to reversibly control magnetic states and study their interaction when interfaced with superconductors. These efforts are benchmarked by low-temperature transport, spectroscopy, scanning probe microscopy, and neutron/x-ray scattering, which enables us to directly link emergent phenomena with interfacial structure and designer properties.

Recent Progress: Our recent work has revealed critical insights into the fundamental physics of several epitaxial systems. Seeking to understand the physics of altermagnetism, we have undertaken work on MnTe, a leading altermagnetic candidate with high Néel temperature (~310 K). We found that substrate surface termination acts as a hair-pin trigger to program the crystalline phase during MBE growth [1]. Specifically, MnTe films grown on lattice-matched InP(111) exhibited a novel polymorph selection dictated by surface chemistry: indium termination stabilizes the ground-state altermagnetic NiAs structure, while phosphorus termination favors the ZnS phase. Modeling efforts revealed that these phases are nearly degenerate in energy, yet slighty different surface energies selectively favors a particular phase. Both polymorphs possess compelling functionalities—the NiAs phase supports altermagnetism, while ZnS is a metastable phase that exhibits a large band gap, is magnetic, and is non-centrosymmetric which together made it a potential new candidate for revealing new physics related to piezo- and ferroelectric and magnetic cross-coupling. Detailed characterization of the altermagnetic phase enabled us to show that small stoichiometric variation in MnTe significantly influences electronic and magnetic behavior [2]. This results not only provides clear insight into the fundamental properties this new phase of matter but also highlights new pathways to control altermagnetic properties for spintronic applications.

We have demonstrated how step-terminated structures can be used to assemble novel 1D states, offering new opportunities for engineering low-dimensional quantum phases [3,4]. This work lays the foundation for future studies on how highly anisotropic two-dimensional (2D) materials assemble at step edges, the associated defect formation, and the implications for new topological properties. These efforts have focused on Bi_2Se_3 but will extend to more complex magnetic topological systems such as $MnBi_2Te_4$. This study surprisingly revealed a solution to a long-standing problem for Bi_2Se_3 specifically and 2D materials in general, since the step-terminated Al_2O_3 substrates with high miscut angles (3°) effectively suppress antiphase twin defects by promoting twin-selective nucleation at atomic step edges. First-principles calculations support a significant energy barrier for twin formation at the steps edges, as well as novel 1D defect state arises due to the unique local bonding at the steps. Experiments, however, have revealed that the 2D layers exchange the disordered bonding environment for continuous, yet, strained layers. Together, these two motifs offer new physical systems to study new 1D states that arise in a topological system and underscore the critical role nucleation dynamics play in controlling defect landscapes in 2D materials, providing essential insights for advancing quantum and electronic device platforms.



The coexistence of ferromagnetism (right) and altermagnetism (left) in MnTe offers a novel pathway to exploit spin–momentum locking for next-generation spintronic information technologies. From Ref. 2

We have revealed a complex interplay of superconductivity and magnetism at heterointerfaces between topological insulators (Bi_2Te_3, Bi_4Te_3) and unconventional superconductors (Fe(Te,Se)) [5]. Open questions persist regarding the origin of superconductivity and its interaction with magnetic states arising from excess Fe or residual antiferromagnetism. Using neutron reflectometry, we have mapped the depth-resolved magnetic and chemical profiles across these interfaces, observing Meissner screening and vortex formation at low fields (~5–10 Oe) and emergent high-field magnetism (4.5 T), confirmed by low-energy muon spectroscopy. These results, combined with ongoing high-field (up to 30 T) transport measurements, will enable the first comprehensive model linking interfacial superconductivity, magnetism, and chemistry to the macroscopic transport behavior of this novel topological system.

Future Plans: Our ongoing research spans several interconnected efforts focused on emergent quantum states at interfaces and in low-dimensional materials. First, we are finalizing a study showing how step-terminated structures offer a solution to longstanding challenges in 2D materials synthesis by enabling the controlled formation of novel 1D states at step edges. This foundational work will be expanded in the coming year to explore how highly anisotropic 2D materials assemble at these step features, the resulting defects, and their implications for topological behavior—using scanning tunneling microscopy, electron microscopy, and transport measurements—with future extensions into complex magnetic topological systems like $MnBi_2Te_4$. Second, we will synthesis and probe MnTe, both the altermagnetic and non-centrosymmetric polymorphs, with the unconventional superconductors Fe(Te,Se) to understand how the novel spin-textures interplay with the superconductivity at the interfacial behavior. This will combine detailed spectroscopy, scanning probe microscopy and detail high-field transport measurements. Over the past year, we performed extensive neutron, muon, and high-field transport experiments to resolve how superconductivity and magnetism emerge at the Bi-Te/Fe(Te,Se) interfaces, and will continue integrating and modeling these results. Lastly, we are finalizing a study on $PdCoO_2$ that clarifies the mechanisms and length scales of emergent magnetism in this highly conductive metal. With this understanding, we will pursue nanoscale magnetic patterning and explore the integration of these tunable magnetic elements with superconductors for future quantum device architectures.

References

1. A. H. Chen, P. R. Raghuvanshi, J. Cook, M. Chilcote, J. Lapano, A. R. Mazza, Q. Lu, S. Kim, Y.-C. Wu, T. Z. Ward, B. Lawrie, G. Bian, J. Burns, J. D. Poplawsky, M.-G. Han, Y. Zhu, L. Lindsay, H. Miao, R. G. Moore, G. Eres, V. R. Cooper, and M. Brahlek, *Programmable phase selection between altermagnetic and non-centrosymmetric polymorphs of MnTe on InP via molecular beam epitaxy*, arXiv: 2507.18592 (2025).
2. M. Chilcote, A. R. Mazza, Q. Lu, I. Gray, Q. Tian, Q. Deng, D. Moseley, A.-H. Chen, J. Lapano, J. S. Gardner, G. Eres, T. Z. Ward, E. Feng, H. Cao, V. Lauter, M. A. McGuire, R. Hermann, D. Parker, M.-G. Han, A. Kayani, G. Rimal, L. Wu, T. R. Charlton, R. G Moore, and M. Brahlek, *Stoichiometry-induced ferromagnetism in altermagnetic candidate MnTe*, Adv. Funct. Mater. **1**, 202405829 (2024).
3. A. R. Mazza, J. Shi, G. A. Vazquez-Lizardi, A. H. Chen, K. Kisslinger, D. Mallick, S. Kim, Q. Lu, T. Z. Ward, V. Starchenko, N. Cucciniello, R. G. Moore, G. Eres, Y. Cao, D. Mukherjee, C. Nelson, D. R. Hickey, F. Xue, and M. Brahlek, *Nucleation and Antiphase Twin Control in Bi_2Se_3 via Step-Terminated AlO Substrates*, arXiv:2505.18103 (2025).
4. W. Ko, S.-H. Kang, J. Lapano, H. Chang, J. Teeter, H. Jeon, Q. Lu, A. H. Chen, M. Brahlek, M. Yoon, R. G. Moore, and A.-P. Li, *Interplay between Topological States and Rashba States as Manifested on Surface Steps at Room Temperature,* ACS Nano 18, 18405 (2024).
5. A.-H. Chen, Q. Lu, E. Hershkovitz, M. L. Crespillo, A. R. Mazza, T. Smith, T. Z. Ward, G. Eres, S. Gandhi, M. M. Mahfuz, V. Starchenko, K. Hattar, J. S. Lee, H. Kim, R. G. Moore, and M. Brahlek, *Interfacially Enhanced Superconductivity in Fe(Te,Se)/Bi_4Te_3 Heterostructures*, Adv. Mater. **36**, 2401809 (2024).

Publications

1. M. Chilcote, A. R. Mazza, Q. Lu, I. Gray, Q. Tian, Q. Deng, D. Moseley, A.-H. Chen, J. Lapano, J. S. Gardner, G. Eres, T. Z. Ward, E. Feng, H. Cao, V. Lauter, M. A. McGuire, R. Hermann, D. Parker, M.-G. Han, A. Kayani, G. Rimal, L. Wu, T. R. Charlton, R. G Moore, and M. Brahlek, *Stoichiometry-induced Ferromagnetism in Altermagnetic Candidate MnTe*, Adv. Funct. Mater. **1**, 202405829 (2024).

2. Q. Lu, P. V. Reddy, H. Jeon, A. R. Mazza, M. Brahlek, W. Wu, S. A. Yang, J. Cook, C. Conner, X. Zhang, A. Chakraborty, Y.-T. Yao, H.-J. Tien, C.-H. Tseng, P.-Y. Yang, S.-W. Lien, H. Lin, T.-C. Chiang, G. Vignale, A.-P. Li, T.-R. Chang, R. G. Moore, and G. Bian, *Realization of a Two-dimensional Weyl Semimetal and Topological Fermi Strings*, Nat. Commun. **15**, 6001 (2024).
3. D. J. P. de Sousa, S. Lee, Q. Lu, R. G. Moore, M. Brahlek, J. Wang, G. Bian, and T. Low, *Ferroelectric Semimetals with α-Bi/SnSe van der Waals Heterostructures and its Topological Currents*, Phys. Rev. Lett. **113**, 146605 (2024).
4. I. Gray, Q. Deng, Q. Tian, M. Chilcote, J. S. Dodge, M. Brahlek, and L. Wu, *Time-resolved Magneto-optical Kerr Effect in the Altermagnet Candidate MnTe*, Appl. Phys. Lett. **125**, 212404 (2024).
5. H. T. Yi, X. Yao, D. Jain, Y.-T. Chan, A.-H. Chen, M. Brahlek, K. Kisslinger, K. Du, M.-G. Han, Y. Zhu, W. Wu, S.-W. Cheong, and S. Oh, *Universal Superconductivity in FeTe and All-iron-based Ferromagnetic Superconductor Heterostructures*, Adv. Funct. Mater. 2418259 (2025).
6. A. R. Mazza, J. Yan, S. Middey, J. S. Gardner, A.-H. Chen, M. Brahlek, and T. Z. Ward, Embracing disorder in quantum materials design, Appl. Phys. Lett. **124**, 230501 (2024).
7. A.-H. Chen, Q. Lu, E. Hershkovitz, M. L. Crespillo, A. R. Mazza, T. Smith, T. Z. Ward, G. Eres, S. Gandhi, M. M. Mahfuz, V. Starchenko, K. Hattar, J. S. Lee, H. Kim, R. G. Moore, and M. Brahlek, *Interfacially Enhanced Superconductivity in Fe(Te,Se)/Bi_4Te_3 Heterostructures*, Adv. Mater. **36**, 2401809 (2024).
8. J. Yan, A. Kumar, M. Chi, M. Brahlek, T. Z. Ward, and M. A. McGuire, *Orbital degree of Freedom in High Entropy Oxides*, Phys. Rev. Mater. **8**, 024404 (2024).
9. D. Jain, H. T. Yi, A. R. Mazza, K. Kisslinger, M.-G. Han, M. Brahlek, and S. Oh, *Buffer-layer-controlled Nickeline vs. Zinc-blende/wurtzite-type MnTe Growths on c-plane Al_2O_3 Substrates*, Phys. Rev. Mater. **8**, 014203 (2024).
10. W. Ko, S.-H. Kang, J. Lapano, H. Chang, J. Teeter, H. Jeon, Q. Lu, A. H. Chen, M. Brahlek, M. Yoon, R. G. Moore, and A.-P. Li, *Interplay between Topological States and Rashba States as Manifested on Surface Steps at Room Temperature*, ACS Nano **18**, 18405-18411 (2024).

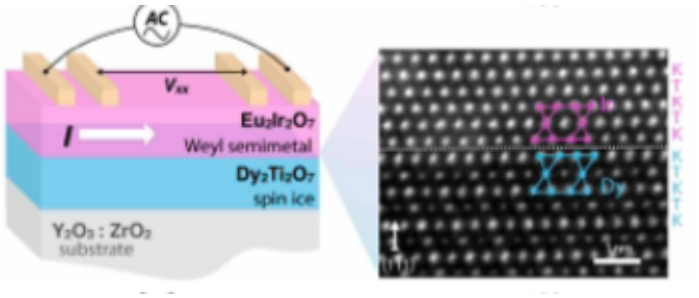
Weyl fermions meet magnetic monopoles: a quantum encounter

Jak Chakhalian Rutgers University

Keywords: Magnetic Weyl semimetals, spin ice, correlated electron interfaces, pyrochlores

Research Scope

Quantum materials with pyrochlore structures exhibit multiple interesting magnetic and topological phases; however, realizing their interfaces has been severely limited by issues in thin-film synthesis. In my talk, I will introduce a new materials growth strategy that combines ultra-high supersaturation and IR-laser–driven thermal gradients to convert amorphous ionic networks into atomically sharp, chemically ideal heterointerfaces. Based on this approach, I will discuss the implementation of a novel heterointerface between the classic spin-ice material $Dy_2Ti_2O_7$ and the antiferromagnetic Weyl semimetal $Eu_2Ir_2O_7$. The resulting artificial quantum structure under applied high magnetic fields exhibits a sixfold anisotropic transport response linked to a Kondo-coupled interface, where field-tuned spin-ice magnetic texture scatters relativistic carriers of the Weyl Fermi-arc states. Upon application of a higher magnetic field, the structure undergoes another transformation into an exotic, two-fold symmetry-broken many-body state akin to a quantum electronic nematic state.



These results demonstrate a strong coupling between relativistic Weyl fermions and the emergent magnetic states, including magnetic monopoles, and offer a general approach for engineering correlated topological interfacial states in frustrated oxide heterostructures [1].

Recent Progress

We have developed a new way to grow magnetic pyrochlore heterointerfaces based on the hybrid near-continuous UV laser-based deposition, followed by planar wave IR laser heating which converts covalent amorphous layer into stoichiometry perfect and atomically sharp interface. For the first time we have synthesized a novel hetero junction between spin ice $Dy_2Ti_2O_7$ and Weyl semimetal $Eu_2Ir_2O_7$ [2].

Based on the technology we have also grown a series of [111] oriented ultra-thin films of $Eu_2Ir_2O_7$ and $Y_2Ir_2O_7$.

In the ultra-thin limit, our RIXS measurements revealed the presence of a new chiral spin liquid states [3].

Upon increasing the film thickness beyond 20 nm, by combining state-of-the-art thin-film synthesis, RIXS, spin wave analysis, and dynamical spin susceptibility calculations, we have revealed the presence of spectrally sharp, gapped magnetic excitations in $Y_2Ir_2O_7$ that surprisingly persist far above the Néel transition temperature, signaling the presence of a quasi-universal regime connected to fluctuations on frustrated lattices. This finding implies the existence of a highly unusual cooperative paramagnetic phase above the ordering temperature and explains the puzzling high-temperature magnetic behavior observed across the family of metallic pyrochlore crystals [4].

Future Plans

1. Preliminary results with Thz based MOKE shows large Faraday rotation angle in $Eu_2Ir_2O_7$ due to the Weyl topological states. Since the pyrochlore iridates belong to the novel class of *altermagnets* they may show mesoscopic domain and domain walls structures.
2. Preliminary ultra-fast pump probe measurements on $Eu_2Ir_2O_7$ films show very rich and unusual dynamics below the magnetic transition temperature, signaling for the presence of novel Mott-Hubbard excitons.

References

Publications

1. Wu, T.-C. *et al.* Electronic anisotropy and rotational symmetry breaking at a Weyl semimetal/spin ice interface. *SCIENCE ADVANCES* **11**, (2025).
2. Kareev, M. *et al.* Epitaxial stabilization of a pyrochlore interface between weyl semimetal and spin ice. *NANO LETTERS* **25**, 966–972 (2025).
3. Liu, X. *et al.* Chiral spin-liquid-like state in pyrochlore iridate thin films. *NATURE COMMUNICATIONS* **15**, (2024).
4. Terilli, M. *et al.* Spectrally sharp magnetic excitations above the critical temperature in a frustrated Weyl semimetal. *NATURE COMMUNICATIONS* **16**, (2025).
5. Paudel, J. R. *et al.* Depth-resolved profile of the interfacial ferromagnetism in CaMnO3/CaRuO3 superlattices. *NANO LETTERS* **24**, 15195–15201 (2024).

Synthesis and Characterization of 2D Weyl Semimetals in Epitaxial Bismuthene

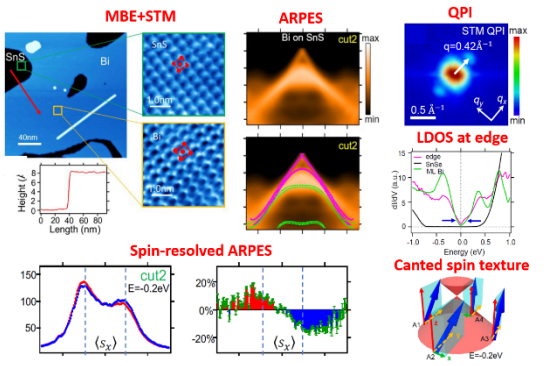
Guang Bian, *University of Missouri, Columbia*

Keywords:

Weyl semimetals, molecular beam epitaxy, heterostructures, spin-valley locking, bismuthene

Research Scope

2D Weyl semimetal is a topological matter with topologically protected boundary states-Fermi string edge states. It is a solid-state realization of Weyl fermion states in 2D space with exotic topological features such as chiral anomaly and charge fractionalization [1]. It also provides an ideal platform for exploring spin-valley locking, topological quantum criticality, and nonlinear electromagnetic properties of 2D Weyl fermion states. In this project, we explore the synthesis and characterization of 2D Weyl semimetals in epitaxial atomic layers.



Experimental realization of 2D Weyl fermion states in epitaxial bismuthene (Bi monolayer in black phosphorus phase) [1]

Recent Progress

We have successfully synthesized a 2D Weyl semimetal in bismuthene monolayer on SnSe substrate [1]. Our spin- and angle-resolved photoemission spectroscopy (spin-ARPES) experiments clearly demonstrated the linear band dispersion and spin texture of 2D Weyl fermion states. The scanning tunneling microscopy (STM) and quasiparticle interference (QPI) measurements showed enhanced local density of states (LDOS) at Fermi level near the edge of samples, suggesting the existence of Fermi arc edge states, a new type of topologically protected boundary modes.

Future Plans

We will search for 2D Weyl semimetals in different epitaxial atomic layers, build 2D Weyl semimetal/superconductor heterostructures, and perform transport measurements. To achieve our research goal, we are constructing an MBE-ARPES-STM-Transport 4-in-1 vacuum system. The equipment will be tested and operated in 2025 winter.

References

1. Q. Lu, P. V. S. Reddy, H. Jeon, A. R. Mazza, M. Brahlek, W. Wu, S. A. Yang, J. Cook, C. Conner, X. Zhang, A. Chakraborty, H.-J. Tien, C.-H. Tseng, P.-Y. Yang, S.-W. Lie, H. Lin, T.-C. Chiang, G. Vignale, A.-P. Li, T.-R. Chang, R. G. Moore, and G. Bian, Realization of a two-dimensional Weyl semimetal and topological Fermi strings, Nature Communications 15, 6001 (2024).

Publications

1. Q. Lu, P. V. S. Reddy, H. Jeon, A. R. Mazza, M. Brahlek, W. Wu, S. A. Yang, J. Cook, C. Conner, X. Zhang, A. Chakraborty, H.-J. Tien, C.-H. Tseng, P.-Y. Yang, S.-W. Lie, H. Lin, T.-C. Chiang, G. Vignale, A.-P. Li, T.-R. Chang, R. G. Moore, and G. Bian, *Realization of a two-dimensional Weyl semimetal and topological Fermi strings*, Nature Communications **15**, 6001 (2024).

2. D. J. P. de Sousa, S. Lee, Q. Lu, R. G. Moore, M. Brahlek, J.-P. Wang, G. Bian, and T. Low, *Ferroelectric Semimetals with α-Bi/SnSe van der Waals heterostructures and its Topological Currents*, Physical Review Letters **133**, 146605 (2024).

3. J. Cook, P.-Y. Yang, T. Volz, C. Connor, R. Satterfield, J. Berglund, Q. Lu, T.-R. Chang, and G. Bian, *Engineering a High Spin Chern-Number Insulator in Epitaxial Sb Monolayer*, Materials Today Physics **51**, 101664 (2025).

4. M. Le Ster, P. Krukowski, M. Rogala, P. Dabrowski, I. Lutsyk, K. Toczek, K. Podlaski, T. O. Mentes, A. Locatelli, G. Bian, T.-C. Chiang, S. A. Brown, and P. J. Kowalczyk, *Evidence of directional structural superlubricity and heavy-tailed flights in a van der Waals heterostructure*, Small **21**, 2408349 (2025).

5. A. Ghobadi, C. J. Mathai, J. Cook, G. Bian, S. Attar, M. Al-Hashimi, S. Gangopadhyay, and S. Guha, *Reducing the Barrier Height in Organic Transistors*, Advanced Electronic Materials **11**, 2400503 (2025).

Investigating the Interplay of Quantum Geometry, Magnetism, and Superconductivity in Topological Materials

Ni Ni

University of California, Los Angeles

Keywords: topological crystalline insulator, fermiology, quantum oscillation, magnetic topological insulator, incommensurate noncollinear magnetic structure

Program Scope

The overarching goal of this proposal is to addressing the grand challenge of basic energy science by discovering new intrinsic magnetic/superconducting topological materials, and characterizing them through thermodynamic, transport, X-ray, and neutron measurements. The focus of our proposed research program is to investigate the role of the geometric properties of electron wavefunctions in emergent quantum phenomena in condensed matter systems, including Berry curvature and quantum metric. Of particular interest in this research is to probe the interplay of band topology, structure, electronic and spin degrees of freedom in these materials through chemical doping, external pressure and uniaxial strains. The proposed research will accelerate the discovery of these materials and advance our understanding of the interplay of the topology and magnetism, potentially enabling us to manipulate the emergent phenomena arising from the interplay.

Recent Progress

During the funding period from 09/01/2023 to 08/15/2025, we have 12 papers published or under review. In this session, I will report the related progress.

1) We discovered a new topological crystalline insulator $SrAg_4Sb_2$[1]. Compared to time-reversal symmetry-protected Z2 topological insulators and Dirac/Weyl semimetals, there are significantly fewer candidates for topological crystalline insulators. $SrAg_4Sb_2$ is predicted to exhibit topological crystalline insulator behavior when considering spin-orbit coupling. In this study, we systematically investigate single crystals of $SrAg_4Sb_2$ using electrical transport and magnetic torque measurements, along with first-principles calculations. Our transport data reveals its compensated semimetal nature with a magnetoresistance up to around 700% at 2 K and 9 T. Analysis of de Haas-van Alphen oscillations uncovers a Fermi surface consisting of three distinct Fermi pockets with light effective masses.

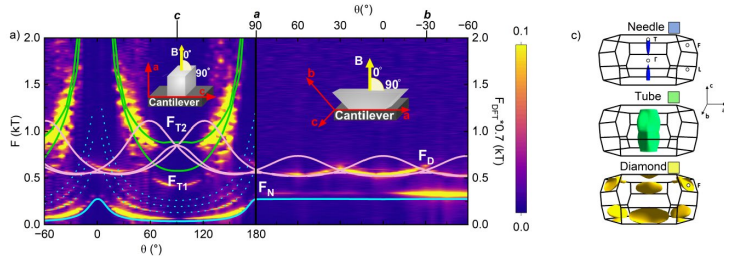


Figure 1. The angular-dependent quantum oscillation contour plot and Fermi surfaces of SrAg4Sb2 [1].

Comparison between the three-dimensional fermiology obtained from our oscillation data and the first-principles calculations demonstrates excellent agreement. This confirms the accuracy of the calculations, which indicate a band inversion centered at the Gamma point and identify the existence of nontrivial tube and needle hole Fermi pockets at Gamma, alongside one trivial diamond electron pocket at the T point in the Brillouin zone. Furthermore, symmetry and topology analysis results in two potential sets of topological invariants, suggesting the emergence of two-dimensional gapless Dirac surface states either on the ab planes or on both the ab planes and mirror planes, protected by crystal symmetries. Therefore, $SrAg_4Sb_2$ emerges as a promising candidate topological crystalline insulator. This work has been published on Physical Review Materials and selected as Editors' selection.

2) Magnetic topological insulators provide a platform for emergent phenomena arising from the interplay between magnetism and band topology. Here we report the single crystal growth, crystal structure, magnetic and transport properties, as well as the neutron scattering studies of topological insulator series $(Ge_{1-\delta-x}Mn_x)_2Bi_2Te_5$ ($x \leq 0.47$, $0.11 \leq \delta \leq 0.20$)[2]. Upon doping up to x = 0.47, the lattice parameter c decreases by 0.8%, while the lattice parameter a remains nearly unchanged. Significant Ge vacancies and Ge/Bi site mixing are revealed via elemental analysis as well as refinements of the neutron and X-ray diffraction data, resulting in holes dominating the charge transport. At x = 0.47, below 10.8 K, a bilayer A-type antiferromagnetic ordered state emerges, featuring an ordered moment of 3.0(3) μB /Mn at 5 K, with the c axis as the easy axis. Magnetization data unveil a much stronger interlayer antiferromagnetic exchange interaction and a much smaller uniaxial anisotropy compared to MnBi2Te4. We attribute the former to the shorter superexchange path and the latter to the smaller ligand-field splitting in $(Ge_{1-\delta-x}Mn_x)_2Bi_2Te_5$. Our study demonstrates that this series of materials holds promise for the investigation of the Layer Hall effect and quantum metric nonlinear Hall effect. The work has published in Physical Review Materials and selected as Editors' selection.

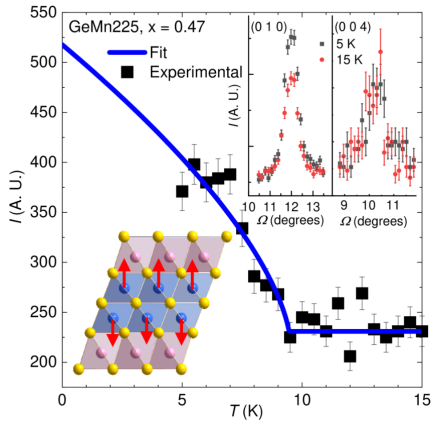


Figure 2. The neutron scattering data and magnetic structure of GeMn225 [2].

3) We have uncovered the three dimensional fermiology of the triangular antiferromagnet $EuAg_4Sb_2$[3]. This compound was of particular interest as it is the magnetic sister compound to the Topological Crystalline Insulator candidate $SrAg_4Sb_2$, which we discovered in 2024[1]. In this study we present the temperature-field phase diagram when an external magnetic field is applied along the *c* and *a* axis as well as systematically investigate the three-dimensional fermiology, utilizing quantum oscillation measurements, angle-resolved photoemission spectroscopy, and first-principles calculations. The complex magnetic phase diagram of EuAg4Sb2 highlights many transitions through nontrivial AFM states. Shubnikov-de Haas and de Haas-van Alphen

oscillations were observed in the polarized ferromagnetic state of EuAg4Sb2, revealing three pairs of distinct spin-split frequency branches with small effective masses. A comparison of the angle-dependent oscillation data with first-principles calculations in the ferromagnetic state and angle-resolved photoemission spectra shows good agreement, identifying tubular hole pockets and hourglass-shaped hole pockets at the Brillouin zone center, as well as diamond-shaped electron pockets at the zone boundary. As the temperature increases, the frequency branches of the tiny hourglass pockets evolve into a more cylindrical shape, while the larger pockets remain unchanged. This highlights that variations in exchange splitting, driven by changes in the magnetic moment, primarily impact the small Fermi pockets without significantly altering the overall band structure. This is consistent with first principles calculations, which show minimal changes near the Fermi level across ferromagnetic and simple antiferromagnetic states or under varying on-site Coulomb repulsion. This work has been published on Physical Review B and selected as Editors' selection.

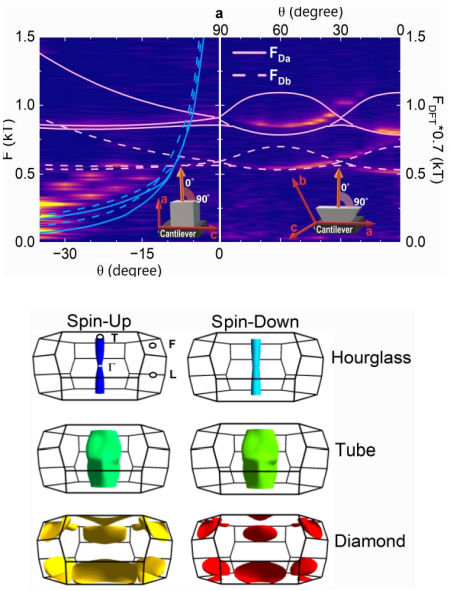


Figure 3. The angular-dependent quantum oscillation contour plot and Fermi surfaces of EuAg4Sb2 [3].

4) Electronic commensuration arising from a spin moiré superlattice (SMS) was proposed for EuAg4Sb2, being realized as double-q spin modulation when the system is subject to applied magnetic fields. To investigate the tunability of this SMS, we first reveal an incommensurate noncollinear cycloidal magnetic ground state, through the utilization of single crystal neutron diffraction measurements. We then applied an in-plane magnetic field at various tilt angles and resolved the complex temperature-field phase diagrams at each angle using magnetic and transport measurements. The resultant temperature-field phase diagrams uncover multiple spin-reoriented pdhases, suggesting the critical role of in-plane field components in driving magnetic transitions. Despite substantial spin reorientation of the double-q phase, we observe a persistent gap opening, evidenced by strong suppression in both Hall and longitudinal conductivities. Model calculations attribute this robustness to the stability of SMS under tilting fields. Our results establish EuAg4Sb2 as a tunable platform for exploring spin-texture-driven superzone gap opening in electronic states.

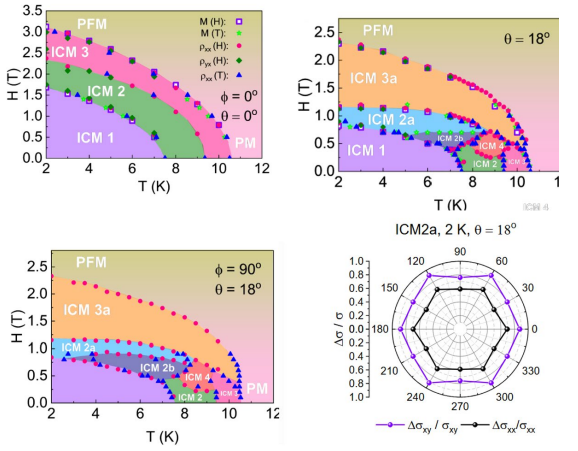


Figure 4. The temperature-field phase diagrams of and polar plot of the change of Hall conductivity and longitudinal conductivity of EuAg4Sb2 [4].

This work is in press at Nano Letters [4].

5) We have reviewed the recent progress of crystal growth, magnetism and chemical disorder in MnBi2nTe3n+1 intrinsic magnetic topological insulators. The search for magnetic topological materials has been at the forefront of condensed matter research for their potential to host exotic states such as axion insulators, magnetic Weyl semimetals, Chern insulators, etc. To date, the MnBi2nTe3n+1 family is the only group of materials showcasing van der Waals-layered structures, intrinsic magnetism and non-trivial band topology without trivial bands at the Fermi level. In this review, we provide a comprehensive review of the research progress in this intrinsic magnetic topological insulator family, with a focus on single-crystal growth, characterization of chemical disorder, manipulation of magnetism through chemical substitution and external pressure, and important questions that remain to be conclusively answered. The review paper was published on National Science Review [5].

Future Plans

We will explore various tuning on the SMS in EuAg4Sb2, including pressure and strain effect, doping effect. We will further investigate the potential SMS state in EuAg4As2, where large magnetoresistance was also observed. We will investigate new magnetic topological or superconducting materials we have grown.

References

1. J Green, Eve Emmanouilidou, Harry W. T. Morgan, William T. Laderer, Chaowei Hu, Jonathan Loera, Anastassia N. Alexandrova, Ni Ni, Fermiology and transport properties of the proposed topological crystalline insulator SrAg4Sb2, Phys. Rev. Materials, 8, 054205, Editors' suggestion (2024)
2. Tiema Qian, Chaowei Hu, Jazmine C. Green, Erxi Feng, Huibo Cao, Ni Ni, Single crystal growth, chemical defects, magnetic and transport properties of antiferromagnetic topological insulators $(Ge1-\delta-xMn_x)_2Bi_2Te_5$, Phys. Rev. Materials 8, 084203 Editors' suggestion (2024)
3. J. Green et al., Mapping the three-dimensional fermiology of the triangular lattice magnet $EuAg_4Sb_2$, Phys. Rev. B 111, 085139, Editors' suggestion (2025).
4. J. Green, A. Arora, M. Marshall, W. Shan, P. Udvarhelyi, Z. Morgan, P. Narang, H. Cao, and N. Ni, Robust Superzone Gap Opening in Incommensurate Antiferromagnetic Semimetal $EuAg_4Sb_2$ under In-Plane Magnetic Field, in press, Nano letts. (2025)
5. Chaowei Hu, Tiema Qian, Ni Ni, Recent progress in $MnBi_2nTe_3n_{+1}$ intrinsic magnetic topological insulators: crystal growth, magnetism and chemical disorder, *National Science Review, 11, nwad282, (2024)*

Publications

1. J Green, Eve Emmanouilidou, Harry W. T. Morgan, William T. Laderer, Chaowei Hu, Jonathan Loera, Anastassia N. Alexandrova, Ni Ni, Fermiology and transport properties of the proposed topological crystalline insulator SrAg4Sb2, Phys. Rev. Materials, 8, 054205, Editors' suggestion (2024)
2. Tiema Qian, Chaowei Hu, Jazmine C. Green, Erxi Feng, Huibo Cao, Ni Ni, Single crystal growth, chemical defects, magnetic and transport properties of antiferromagnetic topological insulators $(Ge1-\delta-xMn_x)_2Bi_2Te_5$, Phys. Rev. Materials 8, 084203 Editors' suggestion (2024)
3. J. Green et al., Mapping the three-dimensional fermiology of the triangular lattice magnet $EuAg_4Sb_2$, Phys.

Rev. B 111, 085139, Editors' suggestion (2025).
4. J. Green, A. Arora, M. Marshall, W. Shan, P. Udvarhelyi, Z. Morgan, P. Narang, H. Cao, and N. Ni, Robust Superzone Gap Opening in Incommensurate Antiferromagnetic Semimetal $EuAg_4Sb_2$ under In-Plane Magnetic Field, in press, Nano letts. (2025)
5. Chaowei Hu, Tiema Qian, Ni Ni, Recent progress in $MnBi_2nTe_3n_{+1}$ intrinsic magnetic topological insulators: crystal growth, magnetism and chemical disorder, *National Science Review, 11, nwad282, (2024)*
6. Anyuan Gao, Naoto Nagaosa, Ni Ni, Suayng Xu, Quantum Geometry Phenomena in Condensed Matter Systems, arxiv: arXiv:2508.00469v1, submitted, Review of Modern Physics (2025)
7. Jian Tang, et. al., Dual quantum spin Hall insulator by density-tuned correlations in TaIrTe4, Nature, 628, 515 (2024)
8. Anyaun Gao, et. al., An antiferromagnetic diode effect in even-layered MnBi2Te4, Nature Electronics, 7, 751, (2024)
9. Jian-Xiang Qiu, Barun Ghosh, Jan Schütte-Engel, Tiema Qian, Michael Smith, Yueh-Ting Yao, Junyeong Ahn, Yu-Fei Liu, Anyuan Gao, Christian Tzschaschel, Houchen Li, Ioannis Petrides, Damien Bérubé, Thao Dinh, Tianye Huang, Olivia Liebman, Emily M. Been, Joanna M. Blawat, Kenji Watanabe, Takashi Taniguchi, Kin Chung Fong, Hsin Lin, Peter P. Orth, Prineha Narang, Claudia Felser, Tay-Rong Chang, Ross McDonald, Robert J. McQueeney, Arun Bansil, Ivar Martin, Ni Ni, Qiong Ma, David J. E. Marsh, Ashvin Vishwanath, Su-Yang Xu, Observation of the Axion quasiparticle in 2D MnBi2Te4, Nature, 641, 62 (2025)
10. Xinshu Zhang, Tyler Carbin, Kai Du, Bingqing Li, Kefeng Wang, Casey Li, Tiema Qian, Ni Ni, Sang-Wook Cheong, Anshul Kogar, Directionally asymmetric nonlinear optics in planar chiral MnTiO3, arxiv: 2410.18086 (2025), under review PRL

Harnessing Topological Surface States in Dirac Semimetal α-Sn Thin Films

Mingzhong Wu, *Department of Physics and Department of Electrical and Computer Engineering, Northeastern University*

Keywords: Topological Dirac semimetal, topological surface states, quantum oscillations,

Research Scope

This project will take advantage of topological surface states in Dirac semimetal α-Sn thin films to explore new fundamental physics and develop novel materials and devices. In particular, we will study: (1) New strategies for growth of high-quality α-Sn thin films, (2) quantum oscillations of second-order electric transport, (3) single-element topological superconductors, and (4) manipulation of magnetization via topological surface states in α-Sn. The basic work under Topic (1) will lay the groundwork for the specific experiments under Topics (2)-(4). Topic (2) targets new fundamental physics - quantization of second-order electric transport. We discovered this effect very recently, and we will fully explore it in this new program. Under Topic (3), we will develop a Sn-based single-element topological superconductor that will offer a unique platform for the realization of Majorana zero modes for topological quantum computing. Topic (4) serves as a model example to establish the high potential of α-Sn in spintronics applications. Topics (2)-(4) will all leverage the topological surface states in α-Sn thin films.

Recent Progress

We recently completed our study on quantum oscillations of nonlinear electrical transport. When a material is exposed to a magnetic field, its electrical resistance varies periodically with field strength—a phenomenon known as quantum oscillations. These oscillations are powerful tools for probing key aspects of the Fermi surface in solids through electrical transport measurements. Until now, however, such studies have focused on linear electrical transport. We recently observed experimental evidence for quantum oscillations in nonlinear electrical transport, revealing entirely new insights into the Fermi surface—specifically its geometry and spin orientations—that conventional linear-transport quantum-oscillation measurements cannot access. Using α-Sn, a topological Dirac semimetal known to exhibit both linear and nonlinear electrical transport, it is shown that nonlinear-transport quantum oscillations are uniquely sensitive to the shape and spin texture of the Fermi contour. Moreover, these oscillations exhibit distinct dependencies on magnetic field strength and temperature compared to their linear-transport counterparts. These differences establish nonlinear-transport quantum oscillations as a transformative tool for investigating Fermi surface physics in solid-state systems, extending beyond the reach of conventional linear-transport quantum-oscillation studies. By opening a new frontier in electrical transport research, this work lays the foundation for discovering exotic states

of matter—mirroring the role of conventional quantum oscillations in the discoveries of high-temperature superconductors and topological insulators.

Figure 1 presents the main results. The first row shows quantum oscillations of the first-harmonic resistance $R_{1\omega}$ (i.e., linear transport) for currents applied along three distinct directions, as indicated by the diagrams at the top. The second row presents the quantum oscillations of the second-harmonic resistance $R_{2\omega}$ (i.e., nonlinear transport) for the same current configurations. All data are normalized to their non-oscillating backgrounds.

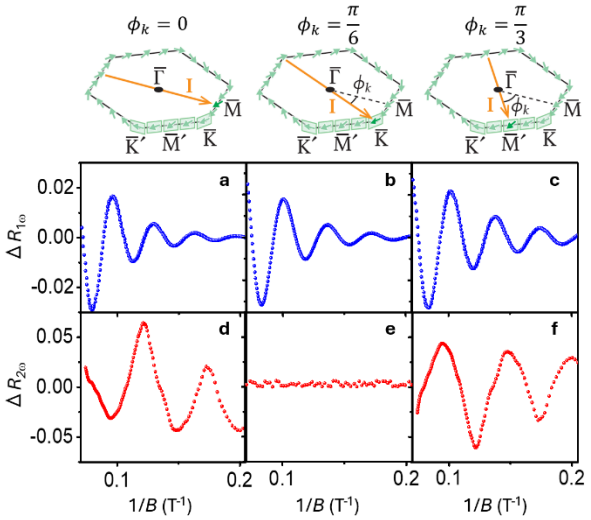


Fig. 1. Quantum oscillations of electrical transport in α-Sn for currents applied along different directions in the momentum space. a-c, oscillations of normalized first-harmonic resistance. d-f, oscillations of normalized second-harmonic resistance. The top diagrams indicate the directions of the currents relative to the $\bar{\Gamma}\bar{M}$ line in the reciprocal space. The green arrows indicate spin orientations at the Fermi contour. The data were measured with a magnetic field (B) applied perpendicular to the α-Sn film.

Two major results are evident in Fig. 3. First, as the current direction transitions from $\bar{\Gamma}\bar{M}$ to $\bar{\Gamma}\bar{K}$ and then to $\bar{\Gamma}\bar{M}'$, the quantum oscillations (e.g., oscillation amplitude $|\Delta R_{1\omega}|$ and oscillation frequency f) of the linear electrical transport remain almost unchanged, while those of the nonlinear transport vary significantly—from strong oscillations in Fig. 1**d** to no oscillations in Fig. 1**e**, and back to strong oscillations in Fig. 1**f**. This indicates that linear-transport oscillations are insensitive to the hexagonal geometry of the Fermi contour, while nonlinear-transport oscillations are highly sensitive. In other words, measurements of quantum oscillations of $R_{2\omega}$ can distinguish whether the current points from the $\bar{\Gamma}$ point to the middle point of a hexagonal side or to a vertex of the contour. However, measurements of quantum oscillations of $R_{1\omega}$ cannot.

Second, the oscillations of $R_{2\omega}$ are out of phase for currents along the $\bar{\Gamma}\bar{M}$ and $\bar{\Gamma}\bar{M}'$ directions, as shown in Figs. 1**d** and 1**f**. This is because the sign of $R_{2\omega}$ depends on the orientation of the out-of-plane spin component ($s_\perp$) of the topological surface states (TSS) at the Fermi level. If one denotes ϕ_k as the angle of the current relative to the $\bar{\Gamma}\bar{M}$ direction as shown in the top diagrams, $s_\perp$ can be expressed as[1]

$$s_\perp = \frac{\cos(3\phi_k)}{\sqrt{[\cos(3\phi_k)]^2 + \left(\frac{\hbar v_F}{\xi k_F^2}\right)^2}}, \quad (1)$$

where v_F is the Fermi velocity and ξ characterizes the strength of the hexagonal warping. According to Eq. (1), one has $s_\perp(\phi_k = 0) = -s_\perp(\phi_k = \frac{\pi}{6})$, which means that $s_\perp$ has opposite signs at the $\bar{M}$ and $\bar{M}'$ points of the Fermi contour, as shown schematically in the top diagrams.

This analysis demonstrates that nonlinear-transport oscillations provide access to the spin texture along the Fermi contour—information unattainable through linear-transport oscillation studies.

Future Plans

We plan to focus on single-element topological superconductors in the next reporting period. Specifically, we will grow a bi-layered heterostructure that consists of a thin film of topological Dirac semimetal α-Sn and a thin film of superconducting metal β-Sn. We will experimentally confirm the topological nature of the α-Sn layer and the superconducting behavior of the β-Sn layer. Afte that, we seek to confirm topological superconductivity in such Sn-based bilayers.

References

1. Y. Zhang, V. Kalappattil, C. Liu, M. Mehraeen, S.-L. Zhang, J. Ding, U. Erugu, Z. Chen, J. Tian, K. Liu, J. Tang, and M. Wu, *Large magnetoelectric resistance in the topological Dirac semimetal α Sn*, Science Advances **8**, eabo0052 (2022).

Publications

No publications in this reporting period.

Impact of Electric Field and Crystal Structure on Anisotropic Superconductivity in Few-Layer T′ Structured TMDs

Daniel Rhodes, University of Wisconsin Madison, Co-PI: Xiaofeng Qian, Texas A&M University

Keywords: superconductivity, 2D and layered crystals, ferroelectrics, transition metal dich alcogenide compounds, magnetotransport

Research Scope

Two years ago we demonstrated coupling between ferroelectricity and superconductivity (SC) in bilayer T_d-$MoTe_2$ [1]. Since then, we have focused on understanding the mechanisms that drive the coupling between FE and SC in this, and similar, material systems. This has led us to two experimental approaches: (**i.**) investigating the evolution of superconductivity throughout the ferroelectric (FE) hysteresis loop via electric-field and angle dependent magnetotransport measurements and (**ii.**) investigating the consequences of modifying the crystal structure – either through hydrostatic pressure or through preserving the inversion symmetry in similarly structured materials (the 2*M* structure), where FE behavior is forbidden. Leveraging our theory effort, we have connected our experimental observations to changes in the electronic band structure, as well as verified new electronic phenomena. In **i.**, we have shown that despite the dramatic changes in the superconducting critical temperatures and upper critical fields, the anisotropy of the superconducting state remains locked to the mirror plane, following a type II tilted Ising enhanced property. This behavior is confirmed through rigorous angular-dependent in-plane magnetic field magnetotransport measurements and further verified via calculations of the spin texture for the electron and hole pockets near the Fermi level. In **ii.**, we have applied hydrostatic pressures up to 2.5 GPa and observed multiple superconducting domes that all coexist with ferroelectricity. Surprisingly, within this regime of pressure we observe no substantial change to the Curie temperature or the coercive fields for ferroelectric switching. In addition, we have explored the consequences of preserving centrosymmetry in a similar material, 2*M*-WSe_2. In this material, we verify verified the topological nature of the bulk crystal via comparison between theoretical calculations and transport measurements of the Fermiology. In the few-layer limit, we verify verified that 2*M*-WSe_2 preserves its centrosymmetry and, within our experimental limitations, does not exhibit ferroelectric switching nor superconductivity, unlike few-layer WTe_2 and $MoTe_2$.

Recent Progress

Bilayer T_d-$MoTe_2$ exhibits a noncentrosymmetric, orthorhombic crystal structure with Mo chains along the b axis and a mirror-plane symmetry in the a-c plane, as shown in Fig. 1a. This symmetry gives rise to strong spin-orbit coupling (SOC) with twofold in-plane rotational symmetry. To understand the electronic structure of bilayer T_d-$MoTe_2$ we performed systematic density functional theory (DFT) calculations and found two spin-split electron-like and two spin-

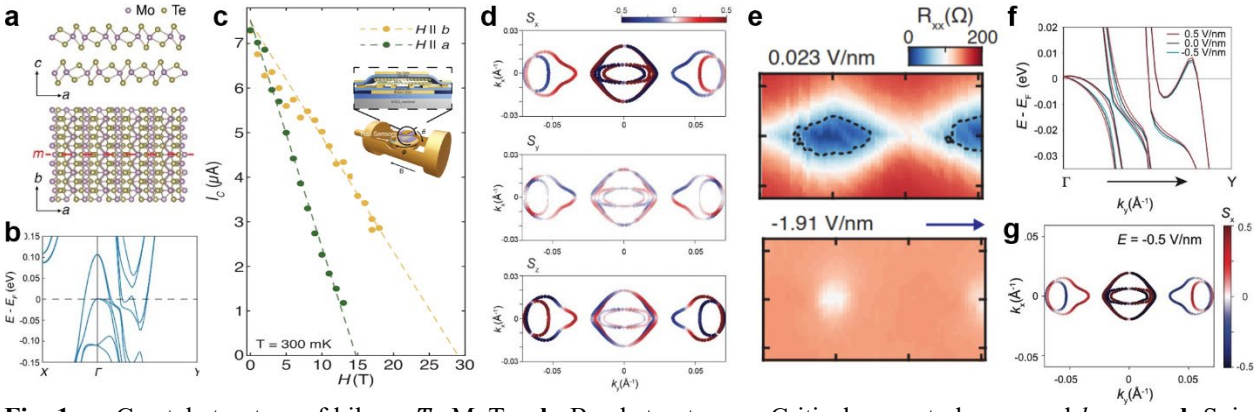


Fig. 1: a, Crystal structure of bilayer T_d-$MoTe_2$. **b,** Band structure. **c,** Critical current along *a* and *b* axes. **d,** Spin textures for different components. **e,** Angle-dependent magnetoresistance along different regions of the ferroelectric hysteresis loop. **f,g,** Band structure and spin texture S_x with applied out-of-plane electric field.

split hole-like bands crossing the Fermi level, with hole pockets centered at Γ and electron pockets at Γ-±Y (Fig. 1b). The broken inversion symmetry and large SOC lead to distinct spin textures with anisotropic upper critical fields of ~15 and 27 T along the *a* and *b* axes, respectively (Fig. 1c). The system is a nearly compensated semimetal, with calculated carrier densities of ~2.2×10^{13} cm^{-2}, in agreement with values from Hall measurements [1]. The anisotropic spin texture has been verified by DFT: the Γ-centered hole pockets show weak SOC strength with nontrivial oscillating in- and out-of-plane spin texture similar to monolayer $MoTe_2$ [2], while the electron pockets exhibit strong out-of-plane polarization. Our experimental observations of the SOC (up to 16.4 meV) agree with the spin texture and spin splitting from first-principles calculations, indicating that tilted Ising spin-orbit coupling is the dominant underlying mechanism.

Furthermore, the rotational symmetry that results from the anisotropic spin texture can persist under large out-of-plane displacement fields of up to -1.9 V/nm and polarization switching along the ferroelectric transition pathway (Fig. 1e). To understand how such anisotropy can survive under these conditions, we conducted first-principles calculations with varying out-of-plane electric fields from −0.5 to 0.5 V/nm. Our results show only small band energy shifts (~2 meV) with no appreciable modification in spin splitting (Fig. 1f), Fermi pocket size, or spin texture symmetry (Fig. 1g), suggesting the out-of-plane electric field is strongly screened by the carriers in bilayer $MoTe_2$ and thus any additional contribution to Rashba spin-orbit coupling is minimized.

To investigate the impact of interlayer coupling on the ferroelectricity and superconductivity we applied hydrostatic pressure (Fig. 2a) to bilayer T_d-$MoTe_2$ from 0.3 to 2.4 GPa. Starting at 0.3 GPa, we observe a single dome-like behavior of superconductivity with respect to change in carrier density (Δn) similar to ambient pressures, but with T_c increased from 2.5 to 5.0 K (Fig. 2b) [1]. Shown in Fig. 2c, increasing pressure to 1.3 GPa, we observe a monotonic shift of the superconducting dome towards higher hole carrier concentrations and a monotonic decrease in superconducting critical temperature (T_c). Further pushing to 2.4 GPa (Fig. 2d) shows a split in the superconducting dome into two separate domes. DFT calculations with pressure predict an initial increase in the density of states, in agreement with the enhanced T_c we observe at 0.3 GPa. However, more work is necessary to understand the behavior at higher pressure.

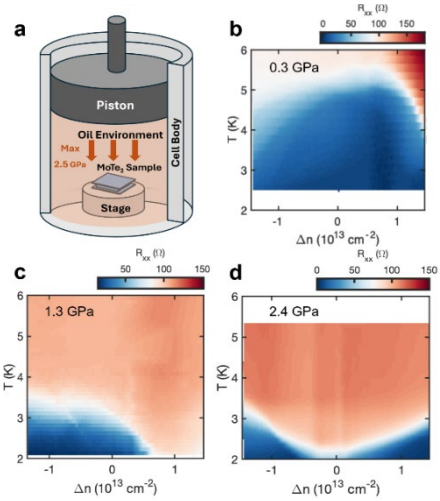


Fig. 2: a, Hydrostatic pressure setup for bilayer T_d-$MoTe_2$.**b-d,** Temperature vs change in carrier density maps for 0.3 (b), 1.3 (c), and 2.4 GPa (d).

Transition metal dichalcogenides (TMDs) with heavy chalcogens (e.g., Te) often crystallize in orthorhombic (Td) or monoclinic (T′) phases, exhibiting semimetallic behavior along with emergent phenomena like quantum spin Hall states, and superconductivity. While the T_d and T' phases of S- and Se-based TMDs are metastable, they can

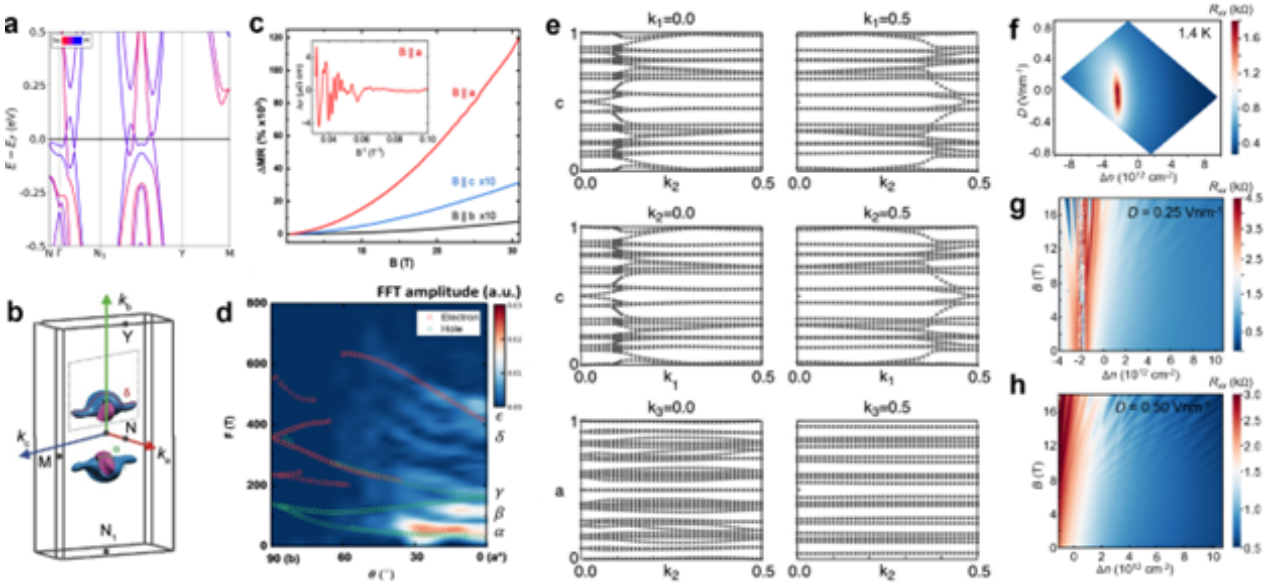


Fig. 3: **a,** Band structure of 2*M*-WSe_2. **b,** Calculated hole (magenta) and electron (blue) Fermi surfaces. **c,** Magnetotransport measurement. **d,** SdH frequencies with varying magnetic field orientation. **e,** Calculated Wannier charge center indicating 2*M*-WSe_2 holds a weak Z_2 topological invariant (0;110). **f,** Displacement field vs carrier density map of bilayer 2*M*-WSe_2. **g, h,** Landau fan diagrams for bilayer 2*M*-WSe_2 at D = 0.25 and 0.50 Vnm^{-1}.

be stabilized in a 2*M* structure, which shares the monolayer building block of T_d /*T*′ but adopts a centrosymmetric C2/m stacking with a 113.2° interlayer translation [3]. We performed first-principles calculations for bulk 2*M*-WSe_2 which reveals a semimetallic band structure and Fermi surface with nearly compensated electron and hole concentrations at the Fermi level (Fig. 3a and 3b), consistent with magnetotransport measurements (Fig. 3c). In addition, we calculated the Shubnikov-de Haas (SdH) oscillation frequencies as a function of magnetic field orientation (Fig. 3d). Comparison between theory and experiment shows good agreement: the lower-frequency α, β, and γ pockets are hole-like, while the higher-frequency electron-like feature corresponds closely to the ϵ pocket. Owing to its anisotropic ellipsoidal shape, we assign this electron pocket to the δ pocket. However, our calculations do not reproduce the 2D Fermi surface features of the ϵ pocket with quantitative accuracy. Overall, our analysis indicates that α and β frequencies arise from hole pockets, whereas the δ frequency originates from an electron pocket. We further calculated the topology of bulk 2*M*-WSe_2 using the Wannier charge center method (Fig. 3e), yielding a Z_2 invariant of (0;110) and indicating a weak topological phase consistent with literature [4, 5]. These results are corroborated by surface state calculations using semi-infinite Green's function, which show overlapping valence and conduction bands with band crossings near the Fermi level, suggesting the coexistence of semimetallicity and weak topological order. In summary, the nontrivial topology, semimetallicity, and SdH oscillations of bulk 2*M*-WSe_2 are consistent with the nontrivial Berry's phase and angular-dependent SdH frequencies observed in experiment.

With observations of topological states in the bulk in mind, we investigated bilayer 2*M*-WSe_2. Surprisingly, we observed increased quantum lifetime as layer number was decreased and a gap opening (Fig. 3f) at a displacement field of $D = 0$ Vnm^{-1}. This enabled us to observe well-resolved Landau fan diagrams and investigate the electronic band structure of bilayer 2*M*-WSe_2. The multiple fans suggest multiple hole and electron pockets near the Fermi level, each with a two-fold degeneracy. As *D* increases, we see the Landau fan diagrams split, indicating a significant renormalization of the electronic band structure with applied electric field. The evolution of these fans and their origins are part of an ongoing study as part of our future plans.

Future Plans

In the final year of our project, we plan to: **(1)** Continue to measure the impact of changes to the interlayer coupling via the application of pressure. These efforts will include diamond anvil approaches (in collaboration with Prof. Sheng Ran, WUSTL), enabling studies of up to 60 GPa. Our preliminary results up to 2.5 GPa have already shown significant changes to the superconductivity. Increased pressure may quench the polarization and will also have a significant impact on the lattice constants, changing the Fermi surface nesting and possibly the pairing mechanism of superconductivity in bilayer T_d-$MoTe_2$. We will also use these same devices for electric field-dependent low frequency Raman spectra, probing the shear modes in bilayer T_d-$MoTe_2$ related to the ferroelectric switching. Recent reports have also suggested that charged density waves (CDWs) exist in these materials. CDWs act as a super-potential, inducing band folding, and leading to correlated states at the Fermi level. Whether these CDWs exist and are related to the emergence and gate-tunability of bilayer T_d-$MoTe_2$ warrants exploration. Concomitant to the experimental efforts for (1), the evolution of the band structure under applied pressure, the phonon density of states and resulting vibrational modes, and the potential existence of CDWs will be theoretically calculated via DFT using either Quantum Espresso or VASP. **(2)** We will measure the polarization directly throughout the ferroelectric hysteresis loop using two approaches, using a graphene layer as a dual-gate and chemical potential monitoring layer and using a capacitive approach, combined with theoretical analysis of the electronic screening, to derive the polarization from the capacitance. This will allow us to accurately ascertain the value of polarization, when the polarization switches, and connect the changes in the electronic environment of bilayer T_d-$MoTe_2$ to the anomalous changes in the carrier density observed in ferroelectric hysteresis loop. **(3)** We will investigate the impact of Fermi surface nesting on the superconducting state via measurements of the band structure of few-layer T_d-$MoTe_2$. We will pursue nanoscale angle resolved photoemission spectroscopy in collaboration with Prof. Ming Yi (Rice University) and Dr. Aaron Bostwick (SLAC) and collaborate with Dr. Nathan Guisinger (ANL) for scanning tunneling spectroscopy and quasiparticle interference measurements. The connection between features of the band structure and superconductivity will be elucidated through local measurements of vortices via low-temperature STM integrated with applied magnetic field (Guisinger) and through NV spectroscopy in collaboration with Prof. Brian Zhou (BU).

References

[1] A. Jindal, A. Saha, Z. Li, T. Taniguchi, K. Watanabe, J. C. Hone, T. Birol, R. M. Fernandes, C. R. Dean, A. N. Pasupathy, and D. Rhodes, *Coupled ferroelectricity and superconductivity in bilayer T_d-$MoTe_2$*, Nature **613**, 48 (2023).

[2] D. A. Rhodes, A. Jindal, N. F. Q. Yuan, Y. Jung, A.Antony, H. Wang, B. Kim, Y. C. Chiu, T. Taniguchi, K. Watanabe, K. Barmak, L. Balicas, C. R. Dean, X. Qian, L. Fu, A. N. Pasupathy, and J. Hone. *Enhanced Superconductivity in Monolayer T_d-$MoTe_2$*, Nano Lett. **21**, 2505 (2021).

[3] Y. He, A. Strasser, N. Hagopian, B. Bierman, H. Ma, C. Fox, Z. Li, N. Pederson, T. Taniguchi, K. Watanabe, J. Xiao, Y. Wang, P. M. Voyles, X. Qian, and D. A. Rhodes, *Evidence for Topological States and a Lifshitz Transition in Metastable 2M-WSe_2*, Advanced Functional Materials **35**, 2420356 (2025).
[4] Y. Fang, J. Pan, J. He, R. Luo, D. Wang, X. Che, K. Bu, W. Zhao, P. Liu, G. Mu, H. Zhang, T. Lin, and F. Huang, *Structure Re-determination and Superconductivity Observation of Bulk 1T MoS_2*, Angew. Chem. **130**, 1246 (2018).

[5] L. Xu, Y. Li, Y. Fang, H. Zheng, W. Shi, C. Chen, D. Pei, D. Lu, M. Hashimoto, M. Wang, L. Yang, X. Feng, H. Zhang, F. Huang, Q. Xue, K. He, Z. Liu, and Y. Chen, *Topology Hierarchy of Transition Metal Dichalcogenides Built from Quantum Spin Hall Layers*, Adv. Mater. **35**, 2300227 (2023).

Publications

1. Z. Li, A. Jindal, A. Strasser, Y. He, W. Zheng, D. Graf, T. Taniguchi, K. Watanabe, L. Balicas, C. R. Dean, X. Qian, A. N. Pasupathy, and D. A. Rhodes, *Twofold Anisotropic Superconductivity in Bilayer T_d-$MoTe_2$*, Physical Review Letters **133**, 216002 (2024).

2. Y. He, A. Strasser, N. Hagopian, B. Bierman, H. Ma, C. Fox, Z. Li, N. Pederson, T. Taniguchi, K. Watanabe, J. Xiao, Y. Wang, P. M. Voyles, X. Qian, and D. A. Rhodes, *Evidence for Topological States and a Lifshitz Transition in Metastable 2M-WSe_2*, Advanced Functional Materials **35**, 2420356 (2025).

Growth, Anisotropy and Unconventional Superconductivity of 2M-WS_2

Jifa Tian and Brian M. Leonard, *University of Wyoming*

Keywords: topological superconductivity, intercalation, single crystal, Raman spectroscopy, quantum transport

Research Scope

Discovering and controlling nontrivial quantum phases in two-dimensional (2D) transition-metal dichalcogenide (TMD) layers is one of the central goals in current condensed-matter physics community. Among their polymorphs, the metastable monoclinic 2M phase, recently realized in compounds such as 2M-WS_2[1-5] and WSe_2[6], has attracted particular interest. Notably, 2M-WS_2 has been synthesized and shown to host topological surface states coexisting with robust bulk s-wave superconductivity, positioning it as a candidate 2D topological superconductor. This project aims to tackle a key question: how can we manipulate unconventional superconductivity in 2D topological materials? The goal of this project is to develop methods to grow high-quality intrinsic and doped 2M-WX_2 (X = S, Se) and systematically tune their band topology and superconductivity down to the monolayer limit, advancing pathways toward topological quantum computing.

Recent Progress

1) New methods to grow intrinsic 2M-WS_2 bulk crystals [1]. Since the growth of large, high-quality crystals of the intercalated or 2M phase WS_2 using our previously developed method[4] is quite difficult, we have been developing new methods to intercalate large 2H-WS_2 crystals at low temperatures or room temperature followed by thermal annealing to facilitate the phase transition from 2H to 2M. This method avoids the long (days to weeks) crystal growth phase with potassium or sodium present which allows us to convert the large crystals in hours resulting in large (centimeter-scale) 2M WS_2 bulk crystals. The 2M-WS_2 crystals showed high crystallinity through differential scanning calorimetry,

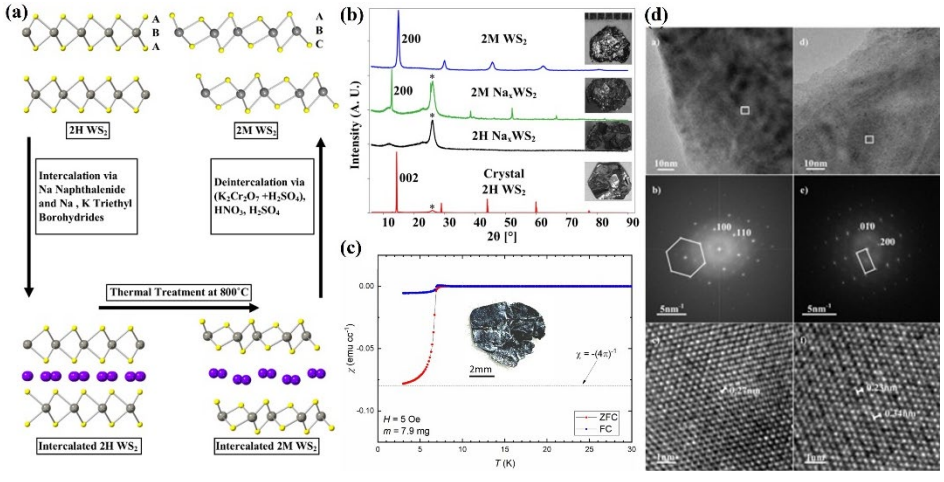


Figure 1. (a) Reaction scheme for the process to convert 2H to 2M-WS_2 via intercalation and thermal treatment. (b) XRD with optical images of 2H WS_2 bulk crystals. Na intercalated WS_2 followed by thermal treatment at 800 °C and deintercalation to yield 2M-WS_2. (c) Magnetic susceptibility measurements for a 2M-WS_2 crystal. (d) TEM, SAED, and HRTEM of 2H WS_2 (left) and 2M WS_2 (right).

and robust superconductivity consistent with previous literature reports. This method was also found to be general to potassium and sodium intercalation.

2) Anisotropic Raman Scattering and Lattice Orientation Identification of 2M-WS_2 [2]. Anisotropic materials with low symmetries hold significant promises for next-generation electronic and quantum devices. 2M-WS_2, which is a candidate for topological superconductivity, has garnered considerable interest. However, a comprehensive understanding of how its anisotropic features contribute to unconventional superconductivity, along with a simple, reliable method to identify its crystal orientation, remains elusive. In this work, we employed experimental and theoretical approaches to systematically investigate the anisotropic Raman modes of 2M-WS_2 thin layers using 532 and 638 nm excitation lasers. Employing first-principles calculations, we identify all observed Raman peaks of 2M-WS_2 corresponding to six A_g and three B_g modes. Angle-dependent polarized Raman spectroscopy reveals distinct symmetries in these modes, demonstrating the material's pronounced anisotropy. Furthermore, by coupling these findings with high-resolution transmission electron microscopy, we directly correlate the angle-dependent Raman spectra to the crystal orientation. This combination of experimental and theoretical methods allows us to demonstrate that polarized Raman spectroscopy can reliably determine the twist angle of 2M-WS_2/2M-WS_2 junctions. Our findings provide insights into the electron–phonon coupling and anisotropic properties of 2M-WS_2, paving the way for the use of anisotropic materials in advanced electronic and quantum devices.

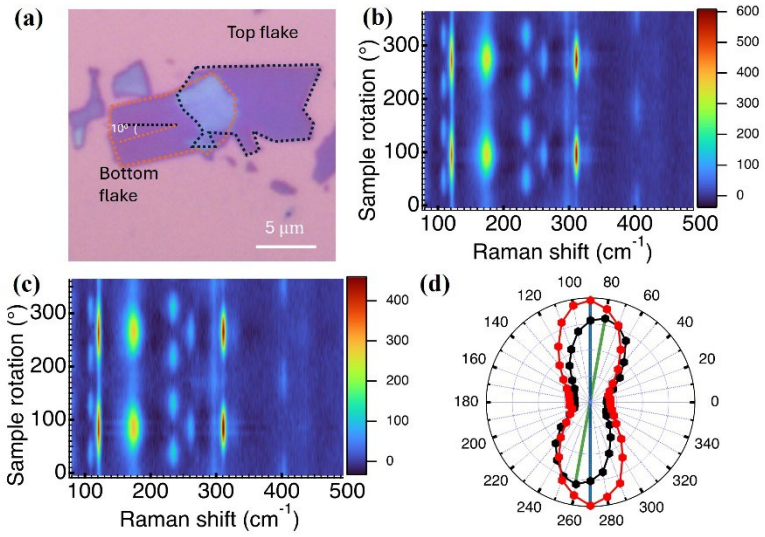


Figure 2. (a) Optical image of a 2M-WS_2/2M-WS_2 junction. (b) The false-color plot of polarized Raman intensities under parallel configuration for the top flake (b) and bottom flake (c), using the 638 nm excitation laser. (d) The polar plot of the A_g Raman mode at 178 cm^{-1} for both the bottom flake (black) and the top flake (red). The twist angle, approximately 10°.

3) Cross-over from conventional to unconventional superconductivity in 2M-WS2 thin layers [3]. Understanding how the numbers of layers affect the unconventional superconductivity in 2M-WS_2 is an important task. To achieve this goal, we fabricated more than 50 Hall-bar devices with 2M- WS_2 layers ranging from 3 to 50 nm. We demonstrated the first

transport evidence of thickness-induced crossover from conventional to unconventional superconductivity in 2M-WS_2. As the sample thickness reduced, we saw a significant shift in key superconducting metrics, including critical temperature, critical current, and carrier density. We further observed that while thick 2M-WS_2 samples show conventional (s-wave) superconductivity, with an in-plane upper critical field constrained by the Pauli limit, samples under 20 nm exhibit a pronounced in-plane critical field enhancement with values a few times higher than the Pauli limit, indicating the existence of unconventional superconductivity. Most importantly, the enhancement of the upper critical field is inversely correlated with 2D carrier density. This marks a distinct crossover to spin-orbit-parity coupled superconductivity. Our findings underscore the crucial role of dimensionality in accessing topological states in 2D topological superconductors, offering pivotal insights into the engineering of topological superconductivity.

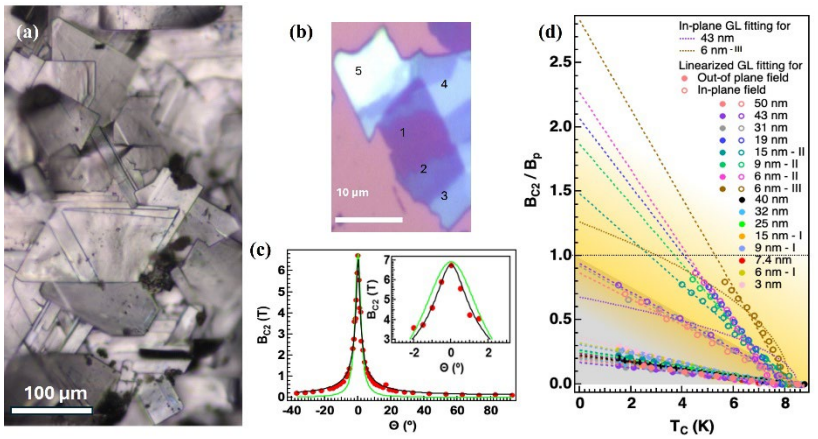


Figure 3. (a) Optical image of a centimeter-size 2M-WS_2 bulk crystal; (b) Optical image a 2M-WS_2 with different thicknesses; (2) 2D anisotropic superconductivity; (d) The calculated B_{C2}/B_P as a function of

Future Plans

We will continue to optimize the grow methods to obtain high quality Nb, Ta and Re doped (with controlled doping concentration) bulk crystals of 2M-WS_2. Then, we will fabricate the hall bar device on the doped 2M-WS_2 thin layers and study how doping concentration affects the topological and unconventional superconductivity of 2M-WS_2.

We will perform transport measurements on the fabricated twisted 2M-WS_2 bilayers to explore how superconductivity varies with the twist angle. These measurements are expected to provide insights into angle-dependent quantum phenomena and potentially reveal novel quantum states unique to twisted bilayers.

References

1. Y. Fang, J. Pan, D. Zhang, D. Wang, H. T. Hirose, T. Terashima, S. Uji, Y. Yuan, W. Li, Z. Tian, J. Xue, Y. Ma, W. Zhao, Q. Xue, G. Mu, H. Zhang, and F. Huang, *Discovery of Superconductivity in 2M WS_2 with Possible Topological Surface States*, Advcanced Materials **0**, 1901942 (2019).
2. Y. W. Li, H. J. Zheng, Y. Q. Fang, D. Q. Zhang, Y. J. Chen, C. Chen, A. J. Liang, W. J. Shi, D. Pei, L. X. Xu, S. Liu, J. Pan, D. H. Lu, M. Hashimoto, A. Barinov, S. W. Jung, C. Cacho, M. X. Wang, Y. He, L. Fu, H. J. Zhang, F. Q. Huang, L. X. Yang, Z. K. Liu, and Y. L. Chen, *Observation of topological*

superconductivity in a stoichiometric transition metal dichalcogenide 2M-WS_2, Nature Communications **12**, 2874 (2021).
3. S. Cho, S. Huh, Y. Fang, C. Hua, H. Bai, Z. Jiang, Z. Liu, J. Liu, Z. Chen, Y. Fukushima, A. Harasawa, K. Kawaguchi, S. Shin, T. Kondo, Y. Lu, G. Mu, F. Huang, and D. Shen, *Direct Observation of the Topological Surface State in the Topological Superconductor 2M-WS_2*, Nano Letters **22**, 8827 (2022).
4. P. Samarawickrama, R. Dulal, Z. Fu, U. Erugu, W. Wang, J. Ackerman, B. Leonard, J. Tang, T. Chien, and J. Tian, *Two-Dimensional 2M-WS_2 Nanolayers for Superconductivity*, ACS Omega **6**, 2966 (2021).
5. Y. Yuan, J. Pan, X. Wang, Y. Fang, C. Song, L. Wang, K. He, X. Ma, H. Zhang, F. Huang, W. Li, and Q.-K. Xue, *Evidence of anisotropic Majorana bound states in 2M-WS_2*, Nature Physics **15**, 1046 (2019).
6. Y. Q. Fang, D. Wang, W. Zhao, and F. Q. Huang, *Large magnetoresistance in the monoclinic 2M WSe_2*, Europhysics Letters **131**, 10005 (2020).

Publications

1. A K M Manjur Hossain, Joseph McBride, Masoumeh Mahmoudi Gahrouei, Sabin Gautam, Piumi Indrachapa Samarawickrama, Jefferson Allen Carter, John F Ackerman, Laura Rita de Sousa Oliveira, Jinke Tang, Jifa Tian and Brian M Leonard, *Intercalation-Induced Topotactic Phase Transformation of Tungsten Disulfide Crystals*, Chemistry of Materials **37**, 129 (2025).
2. Sabin Gautam, Sougata Mardanya, Joseph McBride, A K M Manjur Hossain, Qian Yang, Wenyong Wang, John Ackerman, Brian M. Leonard, Sugata Chowdhury and Jifa Tian, *Anisotropic Raman Scattering and Lattice Orientation Identification of 2M-WS2*, Nano Letters **25**, 1076 (2025).
3. Piumi I. Samarawickrama, Joseph McBride, Sabin Gautam, ZhuangEn Fu, Kenji Watanabe, Takashi Taniguchi, Wenyong Wang, Jinke Tang, John Ackerman, Brian M. Leonard and Jifa Tian, *"Crossover from Conventional to Unconventional Superconductivity in 2M-WS2*, Nano Letters **24**, 16184 (2024).
4. Sabin Gautam, Joseph McBride, William R. Scougale, Piumi I. Samarawickrama, Danilo de Camargo Branco, Peilin Yang, ZhuangEn Fu, Wenyong Wang, Jinke Tang, Gary J. Cheng, John Ackerman, TeYu Chien, Brian M. Leonard and Jifa Tian *Controllable superconducting to semiconducting phase transition in topological superconductor 2M-WS_2*, 2D Materials, **11**, 015018 (2024).
5. ZhuangEn Fu, Piumi I. Samarawickrama, Yanglin Zhu, Zhiqiang Mao, Wenyong Wang, Kenji Watanabe, Takashi Taniguchi, Jinke Tang, John Ackerman and Jifa Tian, *Non-volatile memristive effect in few-layer CrI_3 driven by electrostatic gating*, Nano Letters, **23**, 11866 (2023).

g-Factor–Enhanced Upper Critical Field in Superconducting $PdTe_2$ due to Quantum Confinement

Badih A. Assaf, Yi-Ting Hsu, Xiaolong Liu, Xinyu Liu

Department of Physics and Astronomy, University of Notre Dame

Keywords: Two-dimensional systems, Transition metal dichalcogenides, unconventional superconductors

Research Scope

The scope of the project is to tailor inversion symmetry breaking (ISB) in three-dimensional and van-der-Waals superconducting chalcogenides to pinpoint signatures of Berry curvature that arise when this symmetry is broken. Non-centrosymmetric superconductors can host mixed even/odd pairing. They serve as interesting platforms to understand the fundamental experimental consequences of non-s-wave pairing.

Our specific objective is to evidence the tuning of ISB in thin films of superconductors $NbSe_2$, $PdTe_2$ and (Ge,In)Te. In a second stage, we aim to experimentally and theoretically investigate nanoscale tunneling as well macroscopic transport behaviors that emerge when ISB is broken, potentially linking them to Berry curvature.

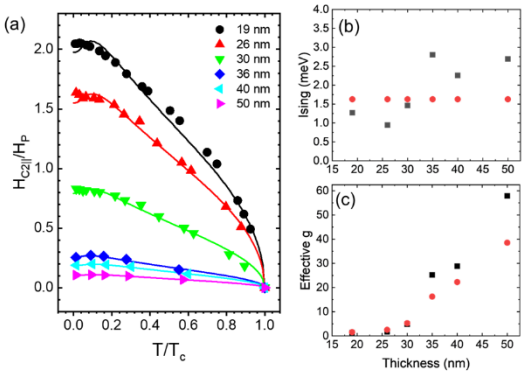


FIG 1. (a) Temperature dependences of the upper critical of $PdTe_2$ thin films of different thickness. (b) Thickness dependences of the Ising spin-orbit coupling and (c) the effective g-factor.

Recent Progress

The most common signature of ISB in superconductor thin films is the enhancement of their in-plane upper critical field beyond the Pauli limit [1]. This limit is determined by balancing the superconducting condensation energy with the magnetization energy. It is determined by the size of the superconducting gap, proportional to the critical temperature T_c and by the charge carrier g-factor [2]. In the weak coupling limit and for s-wave superconductors the Pauli limit is almost equal to $1.85T_c$.

In superconducting thin films of $NbSe_2$ and $PdTe_2$, below a critical thickness, we consistently observe an-plane upper critical field that exceeds $1.85T_c$ [3]. While $NbSe_2$ is known to break inversion symmetry for specific thicknesses, $PdTe_2$ is an established centrosymmetric superconductor. However, based on previous studies of its bulk band structure, others have identified quasi-linearly dispersing bands, with low effective masses and an effective g-factor exceeding 20. Interband interactions due to strong spin-orbit coupling are responsible for this behavior.

Here, we relate the changing upper critical field versus thickness in $PdTe_2$, to an enhanced g-factor in bulk, and its reduction under quantum confinement as $PdTe_2$ is thinned down below 40nm. Our measurements are carried out on thin films grown by physical vapor deposition. The temperature dependence of the in-plane H_{c2} is studied and fit by a model that includes Ising, spin Zeeman and orbital interactions (Fig. 1(a-c)). The model yields a g-factor changing by an order of magnitude as films are thinned down from 50nm to 19nm (Fig. 1(c)). This result is backed up by an analysis of the band structure of $PdTe_2$ under quantum confinement using a k.p model.

To our knowledge, the deviation of the g-factor from 2 is sometimes overlooked when studying the superconductivity of transition metal chalcogenides. While $PdTe_2$ hosts a unique band structure where spin-orbit interactions cause a thickness dependent g, other chalcogenide superconductors could host enhanced or depressed g-factors due correlations or due to quantum geometric factors in the presence of a Moiré potential [3,4]. It is thus important to account for this aspect of their band structure when claiming unconventional superconductivity to explain the violation of the Pauli limit.

Beyond centrosymmetric $PdTe_2$, we have also successfully grown wafer-scale superconducting bilayers of $MoTe_2/PdTe_2$ which we intend to study in the future.

Future Plans

- Search for a Berry curvature induced Nernst effect in broken ISB systems: ultra-thin $PdTe_2/MoTe_2$ bilayers and $NbSe_2$ thin films.
- Study the phase diagram of (Sn,Ge,In)Te in search for a chemically tunable non-centrosymmetric superconductor.
- Search for tunneling signature of broken inversion symmetry in $NbSe_2$

References

1. Kota Yoshimura, Tzu-Chi Hsieh, Huiyang Ma, Dmitry V. Chichinadze, Shan Zou, Michael Stuckert, David Graf, Robert Nowell, Muhsin Abdul Karim, Daichi Kozawa, Ryo Kitaura, Xiaolong Liu, Xinyu Liu, Dafei Jin, Cyprian Lewandowski, Yi-Ting Hsu, Badih A. Assaf. "g-Factor Enhanced Upper Critical Field in Superconducting $PdTe_2$ due to Quantum Confinement." arxiv2508.07547
2. S. Larentis, H. C. Movva, B. Fallahazad, K. Kim, A. Behroozi, T. Taniguchi, K. Watanabe, S. K. Banerjee, and E. Tutuc, "Large effective mass and interaction-enhanced Zeeman splitting of K-valley electrons in $MoSe_2$ Physical Review B 97, 201407 (2018)
3. Minxuan Wang, Xiaoyu Wang, and Oskar Vafek, Phase diagram of twisted bilayer MoTe2 in a magnetic field with an account for the electron-electron interaction, Phys. Rev. B 110, L201107 (2024)

Publications

1. Kota Yoshimura, Tzu-Chi Hsieh, Huiyang Ma, Dmitry V. Chichinadze, Shan Zou, Michael Stuckert, David Graf, Robert Nowell, Muhsin Abdul Karim, Daichi Kozawa, Ryo Kitaura, Xiaolong Liu, Xinyu Liu, Dafei Jin, Cyprian Lewandowski, Yi-Ting Hsu, Badih A. Assaf. "g-Factor Enhanced Upper Critical Field in Superconducting $PdTe_2$ due to Quantum Confinement." arxiv2508.07547

2. Seul-Ki Bac, Florian le Mardelé, Jiashu Wang, Mykhaylo Ozerov, Kota Yoshimura, Ivan Mohelský, Xingdan Sun, Benjamin Piot, Stefan Wimmer, Andreas Ney, Tatyana Orlova, Maksym Zhukovskyi, Günther Bauer, Gunther Springholz, Xinyu Liu, Milan Orlita, Kyungwha Park, Yi-Ting Hsu, Badih A Assaf, “Probing Berry curvature in magnetic topological insulators through resonant infrared magnetic circular dichroism.” Physical Review Letters 134, 016601 (2025).
3. Hyeok-Jun Yang and Yi-Ting Hsu, "Optical absorption signatures of superconductors driven by Van Hove singularities", Physical Review B, 111, 054514, (2025)
4. N. Sharma, J. McKenzie, M. Toole, B. R. Ortiz, A. Capa Salinas, S. D. Wilson, and Xiaolong Liu, "Deriving Material Properties from Feedback Error Signals in Scanning Tunneling Microscopy", Nanoletters, 25, 3309, (2025)
5. Yunxiang Liao and Yi-Ting Hsu, "Detecting topological superconductivity via Berry curvature effects in spectral functions", Phys. Rev. B, 111, 064508, (2024).
6. J. McKenzie, N. Sharma, and Xiaolong Liu, "Fabrication of pristine 2D heterostructures for scanning probe microscopy,", APL Materials, 12, 070602, (2024).

Thursday, September 11, 2025

Good Plasmons in a Bad Metal

D.N. Basov, *Columbia University*

Keywords: Quasiparticles, collective excitations, correlated systems, spectroscopy, nano-imaging

Research Scope

Strongly correlated materials may exhibit unusually high resistivity increasing linearly in temperature, breaking through the Mott-Ioffe-Regel bound, above which coherent quasiparticles are destroyed. The fate of collective charge excitations, or plasmons, in these systems is a subject of debate. Several studies suggest plasmons are overdamped while others detect unrenormalized plasmons. The PI has carried out direct optical imaging of ultra-low-loss and renormalized hyperbolic plasmon polaritons (HPPs) in the correlated van der Waals metal $MoOCl_2$. HPPs are plasmon-photon modes that waveguide through highly anisotropic media, and are found to be remarkably long-lived in $MoOCl_2$. Many-body theory supported by photoemission results acquired at the Advanced Light Source, Lawrence Berkeley National Laboratory reveals that $MoOCl_2$ experiences an orbital-selective Peierls distortion. Moreover, $MoOCl_2$ hosts rich correlated physics: the Fermi surface is reconstructed and made partly incoherent by electronic interactions. These effects together enable long-lived, strongly-correlated HPPs, making $MoOCl_2$ an ideal platform for plasmonics with interacting electrons. Ref.[1].

Recent Progress

Hyperbolic plasmon polaritons (HPPs) are deeply subdiffractional propagating modes occurring in anisotropic crystals. HPPs offer unique access to the electronic phenomena in the host material and hold promise for single-digit nanometer lithography. In order to investigate subdiffractional HPPs, the PI utilized a scattering-type scanning near-field optical microscope (s-SNOM) and a tunable continuous-wave near-infrared lasers. Fig.1a shows a schematic of the experiment, where a metallic s-SNOM tip is illuminated by incident laser light with wavevector k_0. The tip launches waveguiding HPPs with wavevector k in a metallic $MoOCl_2$ slab that transmit through the sample edge and interfere with tip-scattered light, creating standing wave fringes in real-space scans. Fig. 1 shows a room-temperature s-SNOM image of a representative $MoOCl_2$ microcrystal. Subdiffractional interference fringes attributed to HPPs can be seen propagating unidirectionally along the a-axis across the entire span of the crystals, highlighting their ultra-low damping. An example line profile with HPP oscillations is shown in brown. A remarkable result seen in Fig.1 is that highly confined plasmonic wave packets travel through the bulk of a metallic system with a relatively low loss.

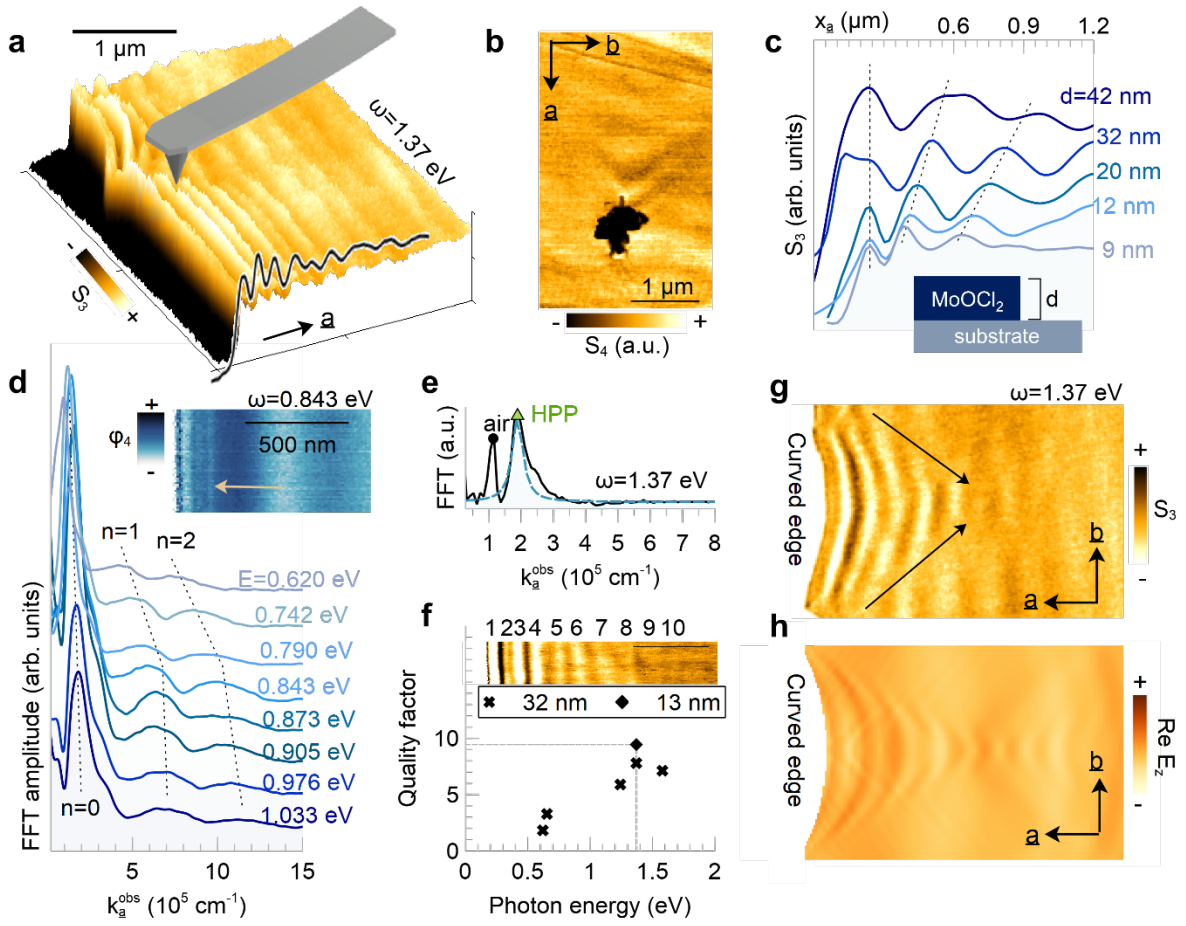


Fig.1 Near-infrared nano-imaging of hyperbolic plasmon polaritons. a, room-temperature near-field amplitude image of a 32 nm $MoOCl_2$ microcrystal showing ultra-low-loss propagation of hyperbolic plasmon polaritons (HPPs) along the a-axis. Black line is an averaged line profile. **b**, defect-launched hyperbolic wavefronts. **c**, near-field amplitude line profiles from $MoOCl_2$ samples with thicknesses between d=9 nm and 42 nm. HPP fringes show clear thickness dependence. **d**, fast Fourier transform (FFT) amplitude spectra of complex near-field line profiles with probe energies ω=0.620-1.033 eV. Three dispersive peaks are observed corresponding to the fundamental (n=0) and higher-order (n=1,2) HPP modes. Top inset is a near-field phase image displaying ultra-confined higher-order modes in real-space. **e**, FFT spectrum at ω=1.37 eV showing HPP and air mode peaks. Complex momenta are extracted from Lorentzian fits (dashed blue line). **f**, HPP quality factors reach ~10 at 1.37 eV and have strong energy dependence. Top inset, real-space image of highest-quality sample showing ten fringes. Scale bar is 1 μm. **g**, experimental and, **h**, simulated planar focusing of HPPs at a curved edge.

The PI demonstrated that HPPs are enabled by strong anisotropy of the dielectric function of $MoOCl_2$. The PI investigated the anisotropic dielectric function of $MoOCl_2$ by means of Fourier transform infrared (FTIR) spectroscopy. Nano-optical experiments in combination with FTIR data uncovered that the plasmonic response of $MoOCl_2$ is strongly renormalized by interactions in the electronic system of this compound. To gain insight into microscopic mechanisms behind the

renormalization, we performed ARPES experiments at ALS in collaboration with Eli Rotenberg. The theoretical analysis and modeling in collaboration with Andrew Millis, Swagata Acharya and Mark van Schilfgaarde revealed that the unconventional electrodynamics of $MoOCl_2$ originates in part from an orbital-selective Peierls distortion [1].

Future Plans

Current research in focused on the following directions. 1) The PI plans to perform nano-imaging experiments for a new generation of $MoOCl_2$ crystals synthesized in the laboratory of Prof. Xavier Roy at Columbia; 2) The PI embarked on nano-THz imaging/spectroscopy of $MoOCl_2$ in order to fully unravel the interdependence between transport and plasmonic characteristics; 3) Detailed nano-THz experiments are enabled by a new nano-imaging modality that is being implemented by the PI: nano-optical space-time metrology [2]; 4) The PI is working on hybrid van der Waals structures introduced by the PI in [3] in which near-infrared emitters (eg. $MoTe_2$) are coupled to hyperbolic modes of $MoOCl_2$ to utilize theoretically predicted Purcell enhancement; 5) Previously, the PI demonstrated that a slab of a hyperbolic crystal acts as a subdiffractional imaging device (Fig.6a in Ref.[4]); new experiments are aimed at exploring opportunities for subdiffractional imaging in the context of single-digit nanometer lithography applications based on the common visible range lasers.

References

[1] Francesco L. Ruta, Yinming Shao, Swagata Acharya, Anqi Mu, Na Hyun Jo, Sae Hee Ryu, Daria Balatsky, Yifan Su, Dimitar Pashov, Brian S. Y. Kim, Mikhail I. Katsnelson, James G. Analytis, Eli Rotenberg, Andrew J. Millis, Mark van Schilfgaarde, D. N. Basov, *"Good plasmons in a bad metal,"* Science **387**, 786 (2025).

[2] Suheng Xu, Yutao Li, Rocco A. Vitalone, Ran Jing, Aaron J. Sternbach, Shuai Zhang, Julian Ingham, Milan Delor, James W. McIver, Matthew Yankowitz, Raquel Queiroz, Andrew J. Millis, Michael M. Fogler, Cory R. Dean, Abhay N. Pasupathy, James Hone, Mengkun Liu, D. N. Basov, *"Electronic interactions in Dirac fluids visualized by nano-terahertz spacetime interference of electron-photon quasiparticles"* Science Advances **10**, eado5553 (2024).

[3] S. L. Moore, H. Y. Lee, N. Rivera, Y. Karube, M. Ziffer, E. Yanev, T. P. Darlington, A. J. Sternbach, M. A. Holbrook, J. Pack, X. Xu, C. R. Dean, J. S. Owen, P. J. Schuck, M. Delor, X.Y. Zhu, J. Hone, D. N. Basov "Van der Waals waveguide quantum electrodynamics probed by infrared nano- photoluminescence" Nature Photonics 2025 https://doi.org/10.1038/s41566-025-01694-1 (in press).

[4] D.N. Basov A. Asenjo-Garcia, P.J. Schuck, X.-Y. Zhu, A. Rubio, A. Cavalleri, M. Delor, M.M. Fogler, Mengkun Liu "*Polaritonic Quantum Matter*" Nanophotonics 2025. https://doi.org/10.1515/nanoph-2025-0001 (in press).

Publications

Francesco L. Ruta, Yinming Shao, Swagata Acharya, Anqi Mu, Na Hyun Jo, Sae Hee Ryu, Daria Balatsky, Yifan Su, Dimitar Pashov, Brian S. Y. Kim, Mikhail I. Katsnelson, James G. Analytis, Eli Rotenberg, Andrew J. Millis, Mark van Schilfgaarde, D. N. Basov, *"Good plasmons in a bad metal,"* Science **387**, 786 (2025)

Shuai Zhang, Jordan Fonseca, Daniel Bennett, Zhiyuan Sun, Junhe Zhang, Ran Jing, Suheng Xu, Leo He, S. L. Moore, S. E. Rossi, Dmitry Ovchinnikov, David Cobden, Pablo Jarillo-Herrero, M. M. Fogler, Philip Kim, Efthimios Kaxiras,

Xiaodong Xu, D. N. Basov, *"Plasmonic Polarization Sensing of Electrostatic Superlattice Potentials*," Physical Review X **15**, 011019 (2025).

S. L. Moore, H. Y. Lee, N. Rivera, Y. Karube, M. Ziffer, E. Yanev, T. P. Darlington, A. J. Sternbach, M. A. Holbrook, J. Pack, X. Xu, C. R. Dean, J. S. Owen, P. J. Schuck, M. Delor, X.Y. Zhu, J. Hone, D. N. Basov "Van der Waals waveguide quantum electrodynamics probed by infrared nano- photoluminescence" Nature Photonics 2025 https://doi.org/10.1038/s41566-025-01694-1 (in press).

M. Yannai, M. Haller, R. Ruimy, A. Gorlach, N. Rivera, D. Basov, and I. Kaminer, *"Opportunities in nanoscale probing of laser-driven phase transitions,"* Nature Physics **20**, 1383 (2024).

R.A. Vitalone, B.S. Jessen, R. Jing, D. Rizzo, S. Xu, V. Hsieh, M. Cothrine, D.G. Mandrus, L. Wehmeier, G. Lawrence Carr, V. Bisogni, C.R. Dean, J.C. Hone, M. Liu, M.I. Weinstein, M.M. Fogler, and D.N. Basov, *"Charge Transfer Plasmonics in Bespoke Graphene/α-$RuCl_3$ Cavities,"* ACS Nano **18**, 29648 (2024)

Suheng Xu, Yutao Li, Rocco A. Vitalone, Ran Jing, Aaron J. Sternbach, Shuai Zhang, Julian Ingham, Milan Delor, James W. McIver, Matthew Yankowitz, Raquel Queiroz, Andrew J. Millis, Michael M. Fogler, Cory R. Dean, Abhay N. Pasupathy, James Hone, Mengkun Liu, D. N. Basov, *"Electronic interactions in Dirac fluids visualized by nano-terahertz spacetime interference of electron-photon quasiparticles"* Science Advances **10**, eado5553 (2024).

Dmitri N. Basov and Michael M. Fogler, *"The unreasonable effectiveness of mathematics" in evading polaritonic losses,"* Nature Materials **23**, 445 (2024)

Indirect excitons in heterostructures

Leonid Butov, *University of California San Diego*

Keywords: excitons, polarons, heterostructures, semiconductors, optical spectroscopy

Program Scope

A spatially indirect exciton (IX), also known as an interlayer exciton, is a bound pair of an electron and a hole confined in separated layers in a heterostructure (HS).

- Due to the separation of electron and hole layers, IX have long lifetimes, orders of magnitude longer than direct excitons (DXs). Long IX lifetimes allow them to thermalize below the temperature of quantum degeneracy. This gives an opportunity to create quantum excitonic systems.

- The long IX lifetimes also allow them to travel over long distances, orders of magnitude longer than for DXs. This gives an opportunity to study transport phenomena in quantum excitonic systems.

- The built-in IX electric dipoles *ed* give an opportunity to effectively control IXs by voltage and, in particular, create tailored potential landscapes for IXs by voltage patterns (*d* is close to the distance between the centers of electron and hole layers).

IXs give an opportunity to study quantum systems of bosons in semiconductor materials. We explore IXs in GaAs HS, which form the low-disorder platform for IXs, and in van der Waals HS composed of atomically thin layers of transition-metal dichalcogenides (TMD), which were theoretically predicted to enable the realization of quantum IX phenomena at high temperatures.

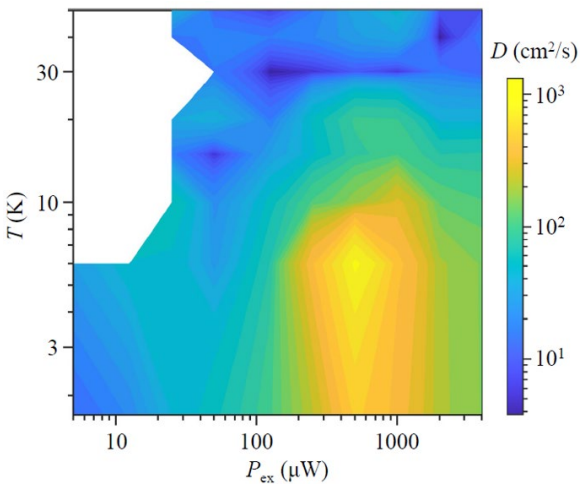


Fig. 1. Temperature and excitation power dependence of IX diffusivity. From [1].

In this contribution, we present (1) finding of long-range ballistic transport of IXs, (2) finding of long-distance decay-less IX mediated spin transport, (3) finding of excitonic Bose polarons, and (4) finding of the Mott transition in excitonic Bose polarons.

Recent Progress

1. Efficient transport of IXs in van der Waals HS [1].

Exciton transport is fundamental for understanding transport phenomena in bosonic systems and for embracing excitation energy transfer in materials.

Long IX lifetimes allow them to form quantum bosonic states and travel long distances. We measured IX transport in a $MoSe_2/WSe_2$ van der Waals HS by time-resolved photoluminescence imaging. These measurements probe the kinetics of IX cloud expansion and reveal the transport characteristics. We found IX transport with anomalously high diffusivity, orders of magnitude higher than for regular diffusive exciton transport in van der Waals heterostructures (Fig. 1). This efficient IX transport significantly deviates from diffusive transport and agrees with long-range ballistic transport, consistent with theoretically predicted superfluid [1].

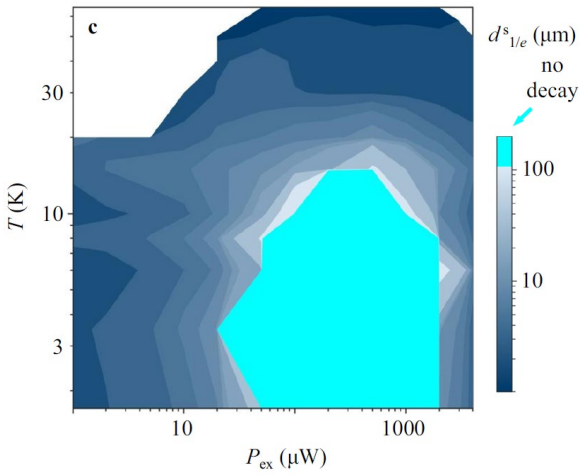


Fig. 2. The 1/*e* decay distance $d^s_{1/e}$ of IX mediated spin transport vs. temperature and excitation power. The data with diverging $d^s_{1/e}$ are presented by cyan color. From [2].

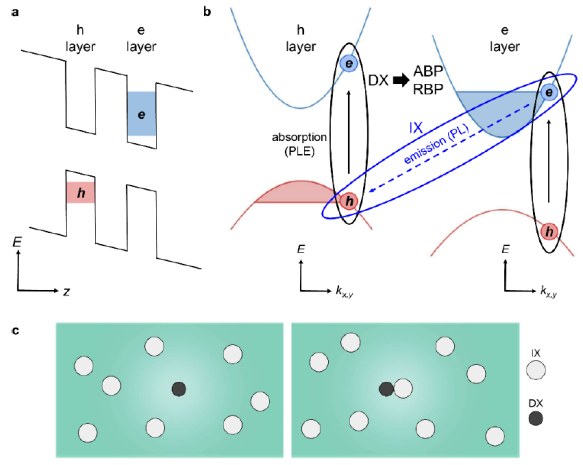


Fig. 3. (a) Electrons (e) and holes (h) are confined in separated HS layers. (b) Absorption (PLE) and emission (PL) in HS. IXs and DXs are shown by the ovals. (c) Free DXs (left) and DX-IX bound states (right) interact with surrounding IXs and form repulsive and attractive Bose polarons. From [4].

2. Long-distance decay-less IX mediated spin transport in van der Waals HS [2]. In addition to its fundamental interest, the long-distance spin transport is essential for spintronic devices. However, the spin relaxation caused by scattering of the particles carrying the spin limits spin transport. We explored IXs as spin carries. We observed in a $MoSe_2/WSe_2$ HS the IX-mediated long-distance spin transport: the spin-polarized IXs travel over the entire sample, ~10 μm away from the excitation spot, with no spin density decay. This transport is characterized by the 1/*e* decay distances reaching 100 μm (Fig. 2). The emergence of long-distance spin transport [2] is observed at the densities and temperatures where the IX transport decay distances and, in turn, scattering times are strongly enhanced [3]. The suppression of IX scattering suppresses the spin relaxation and enables long-distance spin transport. This mechanism of protection against spin relaxation makes IXs a platform for the realization of long-distance decay-less spin transport [2].

3. Excitonic Bose Polarons in Electron-Hole Bilayers [4]. Bose polarons are mobile particles of one kind dressed by excitations of the surrounding degenerate Bose gas of particles of another kind. These many-body objects have been realized in ultracold atomic gases and become a subject of intensive studies. Excitons in electron-hole (e-h)

bilayers offer new opportunities for exploring polarons in strongly interacting bosonic systems. We found that Bose polarons are formed by spatially direct excitons (DXs) immersed in degenerate Bose gases of IXs (Fig. 3). We detected both attractive and repulsive Bose polarons by measuring photoluminescence excitation (PLE) spectra. We controlled the density of IX Bose gas by optical excitation and observed an enhancement of the energy splitting between attractive and repulsive Bose polarons with increasing IX density, in agreement with our theoretical calculations [4].

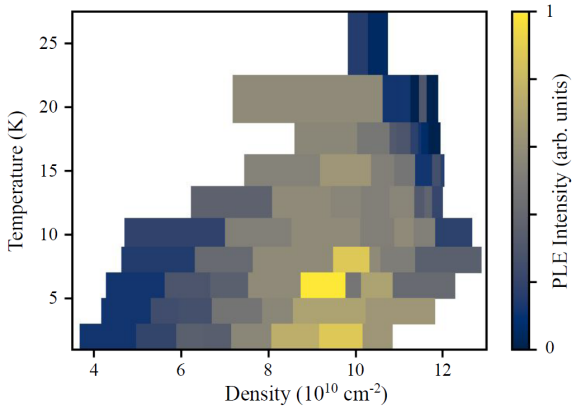


Fig. 4. The intensity of attractive Bose polaron peak in PLE spectra vs. density and temperature. At high e-h densities, the polaron state vanishes due to the Mott transition. From [5].

4. Mott transition in excitonic Bose polarons [5]. For a neutral system of positive and negative charges, such as atoms in a crystal, increasing the density causes the Mott transition from bound electrons to free electrons. The density of optically generated e-h systems can be controlled in situ by the power of optical excitation that enables the Mott transition from excitons, the bound pairs of electrons and holes, to free electrons and holes with increasing density. These Mott transitions occur in systems of pairs of the same kind, such as atoms or excitons. However, a different type of the Mott transition can occur for Bose polarons. A Bose polaron is a mobile particle of one kind surrounded by a Bose gas of particles of another kind. For the Mott transition in polarons, the polaron states vanish with increasing density of the surrounding gas. We found this type of the Mott transition (Fig. 4) and measured the Mott transition parameter in excitonic Bose polarons [5].

Future Plans

GaAs HS form the lowest-disorder platform for studying IXs. We plan to study quantum transport of IXs in quantum point contacts in GaAs HS and search for the new transport quantization, predicted theoretically.

IXs in van der Waals HS based on single-atomic-layers of TMD are characterized by high binding energies, significantly higher than in GaAs HS. Due to this property, theoretical predictions indicate that TMD HS can bring the IX quantum phenomena studied in GaAs HS at low temperatures, such as condensation and superfluidity, to high temperatures. Furthermore, IXs in moiré superlattices provide the experimental realization of the 2D Bose-Hubbard model. We plan to study Bose-Hubbard model physics with IXs in moiré potentials in TMD HS and search for IX high-temperature superfluidity, predicted theoretically.

References and Publications

1. Zhiwen Zhou, W.J. Brunner, E.A. Szwed, H. Henstridge, L.H. Fowler-Gerace, L.V. Butov, *Efficient transport of indirect excitons in a van der Waals heterostructure*, arXiv:2507.04556 (2025).

2. Zhiwen Zhou, E.A. Szwed, D.J. Choksy, L.H. Fowler-Gerace, L.V. Butov, *Long-distance decay-less spin transport in indirect excitons in a van der Waals heterostructure*, Nat. Commun. **15**, 9454 (2024).

3. L.H. Fowler-Gerace, Zhiwen Zhou, E.A. Szwed, D.J. Choksy, L.V. Butov, *Transport and localization of indirect excitons in a van der Waals heterostructure*, Nat. Photon. **18**, 823 (2024).

4. Erik A. Szwed, Brian Vermilyea, Darius J. Choksy, Zhiwen Zhou, Michael M. Fogler, Leonid V. Butov, Dmitry K. Efimkin, Kirk W. Baldwin, Loren Pfeiffer, *Excitonic Bose Polarons in Electron-Hole Bilayers*, Nano Lett. **24**, 13219 (2024).

5. E.A. Szwed, B. Vermilyea, D.J. Choksy, Zhiwen Zhou, M.M. Fogler, L.V. Butov, K.W. Baldwin, L.N. Pfeiffer, *Mott transition in excitonic Bose polarons*, arXiv:2504.07227 (2025).

6. D.J. Choksy, E.A. Szwed, L.V. Butov, K.W. Baldwin, L.N. Pfeiffer, *Fermi edge singularity in neutral electron-hole system*, Nat. Phys. **19**, 1275 (2023).

Exploring Topological Interfacial Superconductivity in Quantum Anomalous Hall/Iron Chalcogenide Heterostructures

Cui-Zu Chang

Department of Physics, The Pennsylvania State University, University Park, PA 16802

Keywords: molecular beam epitaxy, bilayer heterostructure, topological insulator, quantum anomalous Hall insulator, interfacial superconductivity

Research Scope

The current program focuses on investigating the interfacial superconductivity in molecular beam epitaxy (MBE)-grown $(Bi,Sb)_2Te_3$/FeTe and Cr-doped $(Bi,Sb)_2Te_3$/FeTe [i.e., quantum anomalous Hall (QAH)/FeTe] heterostructures. These systems will then be used to explore topological interfacial superconductivity and Majorana physics, with the ultimate goal of advancing topological quantum computation.

Recent Progress

Over the past two years, with the support from the DOE grant (DE-SC0023113, 09/01/2022 ~ 08/31/2025), Chang has published 8 high-profile papers and has 4 manuscripts under review (see Publications). Published papers include 1 in *Science*, 1 in *Review of Modern Physics*, 2 in *Nature Communications*, 1 in *Physical Review Letters*, 1 in *Advanced Materials*, and 2 in *Nano Letters*. The accomplishments with primary DOE support include the realization of the interface-induced superconductivity in magnetic TI films (*Science* 2024, #1 in Publications), the Dirac-fermion-assisted interfacial superconductivity in $(Bi,Sb)_2Te_3$/FeTe heterostructures (*Nature Communications* 2023, #2 in Publications), and the coexistence of superconductivity and antiferromagnetism in $MnBi_2Te_4$ films (*Nano Letters* 2024, #3 in Publications). In the following, I will focus on these three works with primary DOE support and describe their intellectual merits and scientific impacts.

1. Interface-induced superconductivity in magnetic TI films (*Science* 2024)

To date, QAH/superconductor hybrid structures have been fabricated by sputtering a thick *s*-wave superconductor (e.g., ~100 nm Nb) layer on magnetic TI films [1]. These superconducting films are usually polycrystalline, which weakens their proximity effect across the QAH/superconductor interface. QAH/superconductor heterostructures with atomically sharp interfaces are highly desirable for the exploration of chiral topological superconductivity (TSC) and chiral Majorana physics [2]. In this work, we employed MBE to synthesize heterostructures formed by two magnetic materials, a ferromagnetic TI Cr-doped $(Bi, Sb)_2Te_3$ with the QAH state and an AFM FeTe (Figs. 1a and 1b). We observed an emergent and, at first sight, unexpected phenomenon, interface-induced superconductivity. We showed evidence that this interface-induced superconductivity is robust, and the Cr-doped $(Bi, Sb)_2Te_3$/FeTe heterostructures possess the requisite properties of the much sought-after chiral TSC.

By performing reflective magnetic circular dichroism (RMCD), scanning transmission electron

microscopy (STEM), low-energy muon spin relaxation (LE-μSR), magnetic force microscopy (MFM), scanning tunneling microscopy and spectroscopy (STM/S), electrical transport, and angle-resolved photoemission spectroscopy (ARPES) measurements, we demonstrated the trifecta occurrence of superconductivity, ferromagnetism, and topological order in the Cr-doped $(Bi,Sb)_2Te_3$ layer (Figs. 1c to 1e). We found the upper critical magnetic field $\mu_0 H_{c2}$ of the emergent superconductivity to be very high (>40 T), which may be responsible for the robust superconductivity in Cr-doped $(Bi,Sb)_2Te_3$/FeTe heterostructures. The QAH/FeTe heterostructures will serve as the model material system for investigating chiral TSC and chiral Majorana physics.

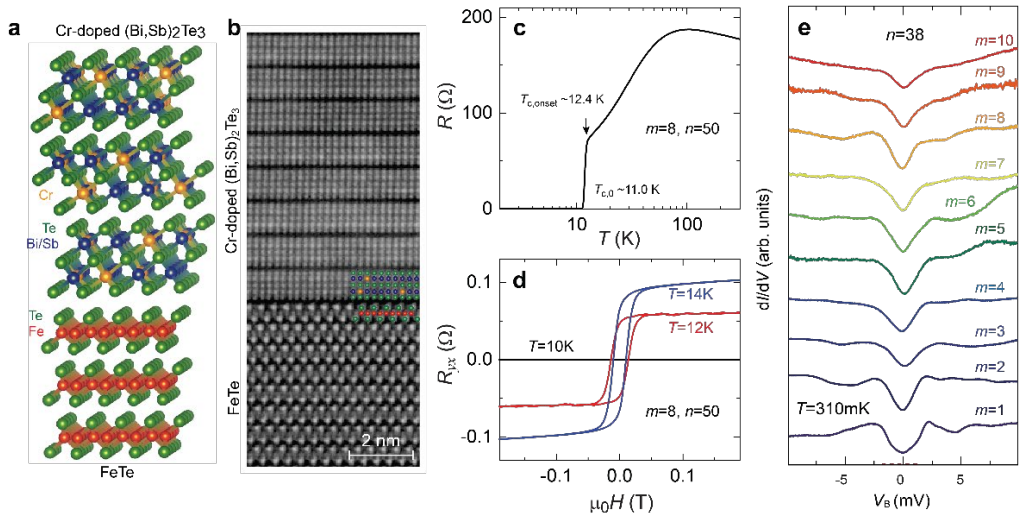


Fig. 1| Interface-induced superconductivity in Cr-doped $(Bi, Sb)_2Te_3$/FeTe heterostructures. a, Schematic lattice structure of the Cr-doped $(Bi, Sb)_2Te_3$/FeTe heterostructure. **b**, Cross-sectional STEM image of the (8,50) heterostructures grown on heat-treated $SrTiO_3(100)$ substrate. **c**, T dependence of the sheet longitudinal resistance R of the (8,50) heterostructure. **d**, $\mu_0 H$ dependence of the Hall resistance R_{yx} at T=10 K (black), T=12 K (red), and T=14 K (blue). **e**, m dependence of the dI/dV spectra on the surface of the (m,38) heterostructure (setpoint: V_B=+10 mV, I_t=300 pA, T=310 mK) (**Chang**, from #1 in Publications).

2. Dirac-fermion-assisted interfacial superconductivity in TI/FeTe heterostructures (*Nature Communications* 2023)

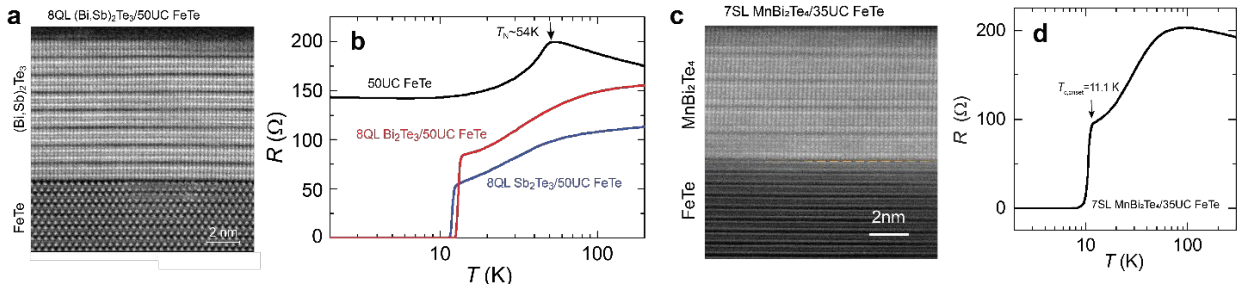


Fig. 2| Interface-induced superconductivity in $(Bi, Sb)_2Te_3$/FeTe and $MnBi_2Te_4$/FeTe heterostructures. a, Cross-sectional STEM image of the 8 QL $(Bi,Sb)_2Te_3$/50 unit cell (UC) FeTe heterostructure on $SrTiO_3(100)$. **b**, T-dependent R of 50 UC FeTe (black), 8 QL Bi_2Te_3/50 UC FeTe (red), and 8 QL Sb_2Te_3/50 UC FeTe (blue) heterostructures (**Chang**, from Ref. [38]). **c**, Cross-sectional STEM image of the 7 septuple layer (SL) $MnBi_2Te_4$/35 UC FeTe heterostructure on $SrTiO_3$ (100). **d**, T-dependent R of the 7 SL $MnBi_2Te_4$/35 UC FeTe heterostructure (**Chang**, from #2 and #3 in Publications).

Interface-induced superconductivity has been observed in both Bi_2Te_3/FeTe and Sb_2Te_3/FeTe heterostructures [3,4], where Bi_2Te_3 and Sb_2Te_3 are well-established 3D topological insulators (Ref. [5]). In this work, we used MBE to synthesize $(Bi,Sb)_2Te_3$/FeTe heterostructures with an atomically sharp interface (Fig. 2a), in which the chemical potential of $(Bi,Sb)_2Te_3$ can be tuned by varying the Bi/Sb ratio. By performing *in situ* ARPES and *ex situ* electrical transport measurements, we found that the superconducting transition temperature T_c and the upper critical magnetic field $\mu_0 H_{c2}$ are suppressed when the chemical potential approaches the Dirac point (Fig. 2b). This observation suggests a direct link between the interface-induced superconductivity and the Dirac electrons in the TI layer. We provided a scenario to understand the chemical potential dependence of interface-induced superconductivity as the complex competition between bicollinear AFM order in the FeTe layer and the Ruderman-Kittel-Kasuya-Yosida (RKKY) interaction mediated by surface Dirac electrons of the TI layer. Our experimental results strongly support the Dirac-fermion-assisted interfacial superconductivity in $(Bi,Sb)_2Te_3$/FeTe heterostructures. The $(Bi,Sb)_2Te_3$/FeTe heterostructures with atomically sharp interfaces provide a promising platform for investigating Majorana physics and the moiré-modulated Cooper-pair density.

3. Coexistence of superconductivity and antiferromagnetism in $MnBi_2Te_4$ films (*Nano Letters* 2024)

Motivated by observing interface-induced superconductivity in Cr-doped $(Bi,Sb)_2Te_3$/FeTe heterostructures, we employed MBE to grow heterostructures by stacking AFM $MnBi_2Te_4$ and AFM FeTe films (Fig. 2c). By performing *in situ* STM/S and *ex situ* electrical transport and LE-μSR measurements, we discovered interface-induced superconductivity in $MnBi_2Te_4$/FeTe heterostructures (Fig. 2d). We demonstrated the coexistence of superconductivity and antiferromagnetism in the $MnBi_2Te_4$ layer. Moreover, we found that the upper critical magnetic field $\mu_0 H_{c2}$ of the emergent superconductivity is exceptionally high (>39.5 T) and nearly isotropic at T=1.5 K, closely resembling the behavior observed in Cr-doped (Bi, $Sb)_2Te_3$/FeTe heterostructures.

Future Plans

Based on our recent progress, we will pursue the following projects:

1. Explore the superconducting mechanism of FeTe films and heterostructures.
2. Explore Majorana physics and moiré-modulated Cooper-pair density in $(Bi,Sb)_2Te_3$/FeTe and Cr-doped $(Bi,Sb)_2Te_3$/FeTe heterostructures..
3. Explore selective area growth of Cr-doped $(Bi,Sb)_2Te_3$ and FeTe materials and demonstrate chiral TSC and Majorana physics in in situ-fabricated QAH/FeTe Josephson junction, superconducting quantum interference device (SQUID), and interferometer devices.

References

1. Kayyalha, M., Xiao, D., Zhang, R. X., Shin, J., Jiang, J., Wang, F., Zhao, Y. F., Xiao, R., Zhang, L., Fijalkowski, K. M., Mandal, P., Winnerlein, M., Gould, C., Li, Q., Molenkamp, L. W., Chan, M. H. W., Samarth, N. & Chang, C. Z. Absence of evidence for chiral Majorana modes in quantum anomalous Hall-superconductor devices. *Science* **367**, 64-67 (2020).

2. Qi, X. L., Hughes, T. L. & Zhang, S. C. Chiral Topological Superconductor from the Quantum Hall State. *Phys. Rev. B* **82**, 184516 (2010).

3. He, Q. L., Liu, H. C., He, M. Q., Lai, Y. H., He, H. T., Wang, G., Law, K. T., Lortz, R., Wang, J. N. & Sou, I. K. Two-dimensional superconductivity at the interface of a Bi_2Te_3/FeTe heterostructure. *Nat. Commun.* **5**, 4247 (2014).

4. Liang, J., Zhang, Y. J., Yao, X., Li, H., Li, Z. X., Wang, J. N., Chen, Y. Z. & Sou, I. K. Studies on the origin of the interfacial superconductivity of $Sb_2Te_3/Fe_{1+y}Te$ heterostructures. *Proc. Natl. Acad. Sci.* **117**, 221-227 (2020).

5. Zhang, H. J., Liu, C. X., Qi, X. L., Dai, X., Fang, Z. & Zhang, S. C. Topological Insulators in Bi_2Se_3, Bi_2Te_3 and Sb_2Te_3 with a Single Dirac Cone on the Surface. *Nat. Phys.* **5**, 438-442 (2009).

Publications

1. Yi, H., Zhao, Y.-F., Chan, Y.-T., Cai, J., Mei, R., Wu, X., Yan, Z.-J., Zhou, L.-J., Zhang, R., Wang, Z., Paolini, S., Xiao, R., Wang, K., Richardella, A. R., Singleton, J., Winter, L. E., Prokscha, T., Salman, Z., Suter, A., Balakrishnan, P. P., Grutter, A. J., Chan, M. H. W., Samarth, N., Xu, X., Wu, W., Liu, C.-X. & Chang, C.-Z. Interface-Induced Superconductivity in Magnetic Topological Insulators. *Science* **383**, 634-639 (2024).

2. Yi, H., Hu, L.-H., Zhao, Y.-F., Zhou, L.-J., Yan, Z.-J., Zhang, R., Yuan, W., Wang, Z., Wang, K., Hickey, D. R., Richardella, A. R., Singleton, J., Winter, L. E., Wu, X., Chan, M. H. W., Samarth, N., Liu, C.-X. & Chang, C.-Z. Dirac-fermion-assisted interfacial superconductivity in epitaxial topological-insulator/iron-chalcogenide heterostructures. *Nat. Commun.* **14**, 7119 (2023).

3. Yuan, W., Yan, Z. J., Yi, H. M., Wang, Z. H., Paolini, S., Zhao, Y. F., Zhou, L. J., Wang, A. G., Wang, K., Prokscha, T., Salman, Z., Suter, A., Balakrishnan, P. P., Grutter, A. J., Winter, L. E., Singleton, J., Chan, M. H. W. & Chang, C. Z. Coexistence of Superconductivity and Antiferromagnetism in Topological Magnet $MnBi_2Te_4$ Films. *Nano Lett.* **24**, 7962-7971 (2024).

4. Chang, C.-Z., Liu, C.-X. & MacDonald, A. H. Colloquium: Quantum anomalous Hall effect. *Rev. Mod. Phys.* **95**, 011002 (2023).

5. Zhao, Y. F., Zhang, R. X., Sun, Z. T., Zhou, L. J., Zhuo, D. Y., Yan, Z. J., Yi, H. M., Wang, K., Chan, M. H. W., Liu, C. X., Law, K. T. & Chang, C. Z. 3D Quantum Anomalous Hall Effect in Magnetic Topological Insulator Trilayers of Hundred-Nanometer Thickness. *Adv. Mater.* **36**, 202310249 (2024).

6. Tay, H., Zhao, Y. F., Zhou, L. J., Zhang, R. X., Yan, Z. J., Zhuo, D. Y., Chan, M. H. W. & Chang, C. Z. Environmental Doping-Induced Degradation of the Quantum Anomalous Hall Insulators. *Nano Lett.* **23**, 1093-1099 (2023).

7. Zhou, L.-J., Mei, R., Zhao, Y.-F., Zhang, R., Zhuo, D., Yan, Z.-J., Yuan, W., Kayyalha, M., Chan, M. H. W., Liu, C.-X. & Chang, C.-Z. Confinement-Induced Chiral Edge Channel Interaction in Quantum Anomalous Hall Insulators. *Phys. Rev. Lett.* **130**, 086201 (2023).

8. Zhuo, D., Yan, Z. J., Sun, Z. T., Zhou, L. J., Zhao, Y. F., Zhang, R., Mei, R., Yi, H., Wang, K., Chan, M. H. W., Liu, C. X., Law, K. T. & Chang, C. Z. Axion insulator state in hundred-nanometer-thick magnetic topological insulator sandwich heterostructures. *Nat. Commun.* **14**, 7596 (2023).

9. Yan, Z.-J., Chan, Y.-T., Yuan, W., Wang, A. G., Yi, H., Wang, Z., Zhou, L., Rong, H., Zhuo, D., Wang, K., Singleton, J., Winter, L. E., Wu, W. & Chang, C.-Z. Meissner Effect and Nonreciprocal Charge Transport in Superconducting 1T-$CrTe_2$/FeTe Heterostructures. *arXiv:2412.09354* (2024).

10. Balakrishnan, P. P., Yi, H., Yan, Z.-J., Yuan, W., Suter, A., Jensen, C. J., Manuel, P., Orlandi, F., Hanashima, T., Kinane, C. J., Caruana, A. J., Maranville, B. B., Salman, Z., Prokscha, T., Chang, C.-Z. & Grutter, A. J. Complex Magnetic Ordering in Candidate Topological Superconductors1. *arXiv:2503.11502* (2025).

Ultrafast Control of Topological Transport in Quantum Materials

James McIver, *Columbia University in the City of New York*

Keywords: light-matter phenomena, topology, 2D and layered crystals, transition metal compounds, ultrafast optoelectronics

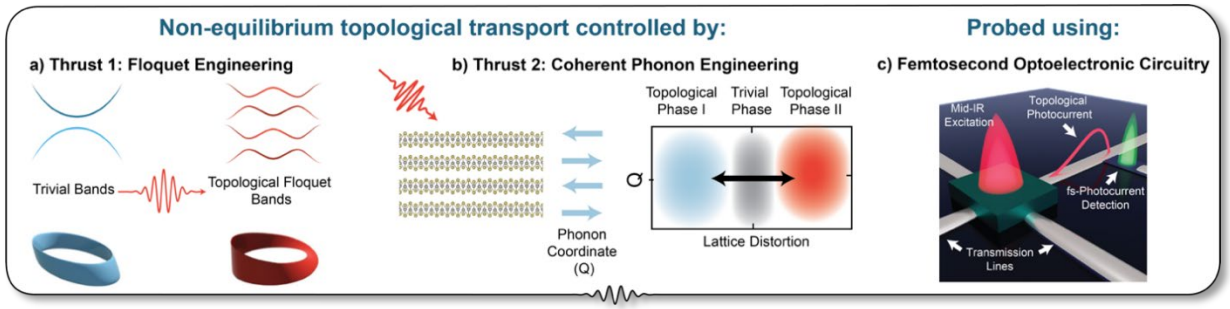


Figure 1. Pathways to controlling topological transport in quantum materials: (a) The creation of photon-dressed Floquet states and (b) the optical generation of coherent phonons can manipulate electronic topology. c) Femtosecond optoelectronic circuitry captures ultrafast topological transport responses on their characteristic timescales.

Research Scope

This program advances the optical control of topological transport through two complementary mechanistic approaches. The first thrust develops protocols for creating coherent light-matter hybrid states via Floquet-Bloch band engineering in Dirac/Weyl semimetals. Key achievements include the demonstration of a magnetic Floquet-Weyl semimetal state through circularly polarized light-induced time-reversal symmetry breaking (completed), complemented by microstructured cavity approaches [1,2] that extend light-matter hybridization beyond mid-infrared frequencies. Current efforts focus on Thrust 1-2's development of bi-chromatic drives with tunable polarizations to access diverse symmetry-broken Floquet states, while Thrust 1-3 will probe magnetic-field-induced topological axial transport in these engineered systems.

The second thrust pursues topological control through excitation of coherent phonons and cavity plasmons. Thrust 2-1 (underway) has already uncovered direct evidence of phonon-Berry curvature coupling through nonlinear Hall measurements. Building on this, Thrust 2-2 aims to dynamically steer semimetals across topological phases using symmetry-matched polarizations or cavity plasmon modes, while Thrust 2-3 (underway) explores pathways to persistent, switchable topological metastability. Together these approaches establish multiple routes for non-equilibrium control of quantum materials' topological properties.

Recent Progress

Thrust 1-1: Through controlled illumination with circularly polarized 10 μm light, we demonstrated the ability to dynamically reconfigure the topological phase of bulk T_d-$MoTe_2$ [3]. Ultrafast transport measurements reveal the emergence of a novel nonequilibrium state, a Floquet

magnetic Weyl semimetal characterized by broken time-reversal and inversion symmetries (Fig. 2). The signature of this Floquet-engineered states is the nonperturbative scaling of a putatively second-order injection currents, and the presence of a light-induced Hall effect whose strength is equivalent to a 30 Tesla magnetic field. We interpret the formation of this large effective magnetic field as light-induced Berry curvature engineered in the photon-dressed system. Our results establishing a new paradigm for controlling three-dimensional quantum materials with ultrafast pulses.

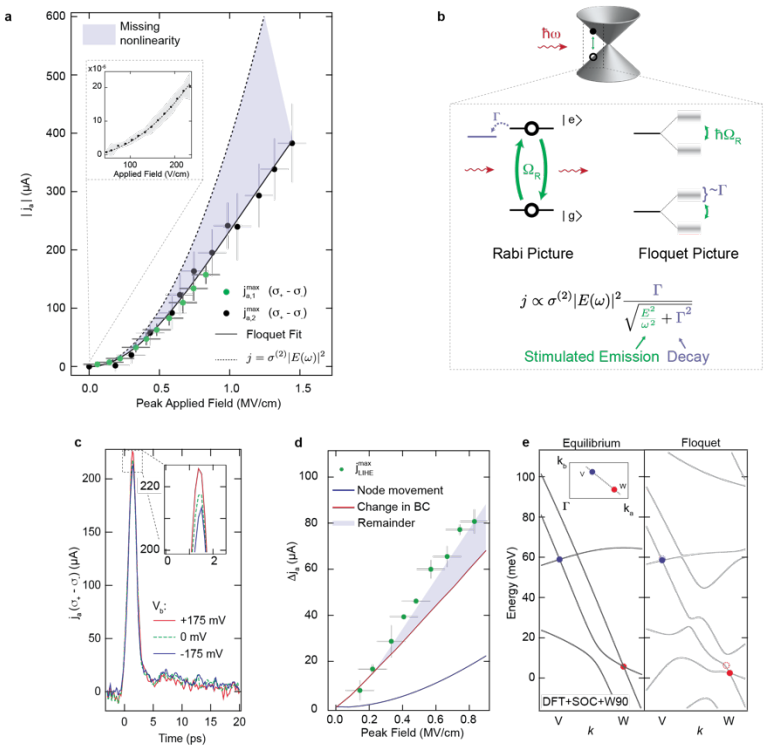


Fig. 1 **a**: Nonperturbative injection currents excited within the photon-dressed bandstructure scales in-line with Floquet theory. **b.** The source of the nonperturbative scaling is the result of stimulated emission from the photon-dressed bands. **c,d** A light-induced Hall effect is present at the peak of the ultrafast photocurrent signal. A majority of the Hall signal can be accounted for when examining the light-induced Berry curvature in the photon-dressed states. **e** The photon-dressed bandstructure along the cut connecting the two Weyl nodes, showing node displacement and ultrastrong light-matter coupling.

Building on our initial demonstration of Floquet-Bloch state formation under mid-infrared illumination, recent theoretical advances by Zhou et al. proposed that microstructured optical cavities (like those developed within our group) could dramatically enhance light-matter interactions [1,2], potentially extending Floquet control beyond the mid-infrared regime.

To experimentally test this concept, we adapted our near-field optoelectronic platform to incorporate the Weyl semimetal T_d-WTe_2 within microstructured cavities to enhance the light-matter interaction. When driven with 515 nm femtosecond pulses, the system exhibited clear signatures of topological shift currents. Most strikingly, the THz emission displayed characteristic nonperturbative scaling with excitation field strength (Fig. 2), mirroring the behavior we previously observed in the mid-infrared regime and providing compelling evidence for the formation of visible-frequency Floquet-Bloch states. These findings, published in Optical Materials Express [4], represent a significant expansion of the Floquet engineering toolkit and suggest that a much broader range of quantum phenomena may be amenable to optical control than previously realized.

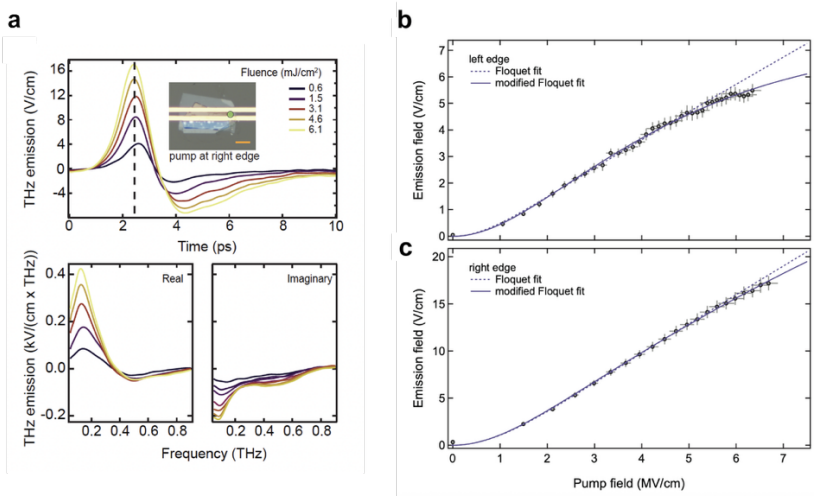


Fig. 2 **a**: Evidence for THz emission from Floquet-Bloch states in T_d-WTe_2. The time-resolved THz emission possesses signal symmetries consistent with shift currents. **b** Nonperturbative scaling of the peak of the time-resolved emission bears emission fingerprints of shift currents excited within photon-dressed states.

Thrust 2-1 and 2-2: Under the aegis of our progress in cavity-based Floquet engineering, we recognized an opportunity to explore phonon-mediated topological control by precisely matching cavity resonance frequencies to the interlayer shear phonon mode (~200 GHz) through careful thickness engineering of WTe_2 flakes. We fabricated specialized plasmonic cavities and probed their response using the same shift current mechanism demonstrated in our earlier work. While these experiments did not reveal the anticipated enhancement of the phase-transition-relevant phonon mode, they yielded an important secondary discovery: a clear Purcell enhancement of the cavity mode itself. This unexpected finding prompted us to systematically investigate the phenomenon across multiple cavity geometries with varying dimensions and resonance characteristics. The comprehensive results of this study, demonstrating robust Purcell enhancement of photocurrents currents in 2D plasmonic cavities, have been compiled in a manuscript titled "Purcell Enhancement of Photogalvanic Currents in WTe_2 Plasmonic Cavities," which has been submitted to Nature Communications.

Thrust 2-3: Our investigation of photoinduced phase transitions in Td-$MoTe_2$ has revealed a remarkable degree of optical control over its topological state. By employing single-pulsed near-infrared excitation and monitoring the nonlinear Hall effect at fixed bias, we have established a direct experimental probe of optically induced changes of the material's topological phase. The presence of this nonlinear transport signature serves as a definitive marker of the type-II Weyl phase, while its absence indicates transition to a trivial phase. Key findings demonstrate that individual optical pulses can reversibly switch the material between topological and non-topological phases (Fig. 3). Systematic variation of pulse power and sample temperature will allow us to reconstruct the free energy landscape under nonequilibrium driving conditions. Notably, when maintained at the structural phase transition temperature without illumination, the system spontaneously samples all three characteristic states of the nonlinear Hall response (positive, negative, and zero), reflecting thermal exploration of competing topological phases (Fig. 3). Current efforts focus on reproducing these measurements across two additional device configurations to ensure statistical robustness. The ability to optically toggle between distinct

topological orders on ultrafast timescales, while simultaneously mapping the underlying energy landscape, opens new possibilities for dynamic control of quantum phases in solid-state systems.

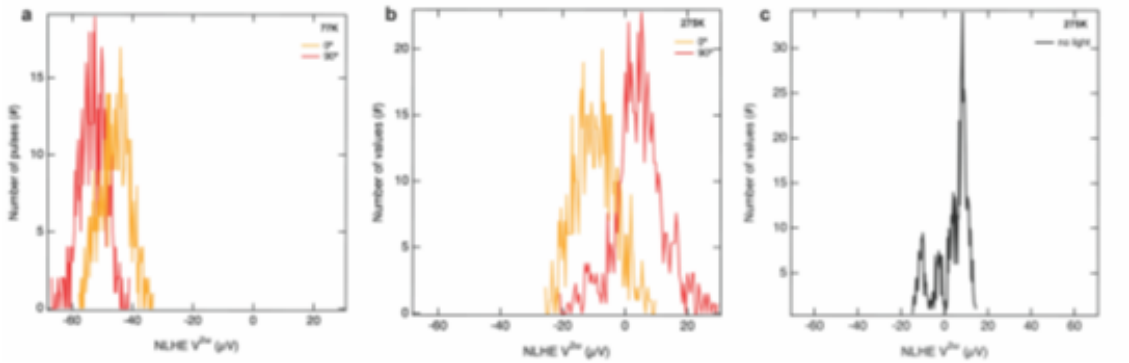


Fig. 3: Single-shot resolved changes in the nonlinear Hall effect. **a** Low- temperature polarization dependent changes in the nonlinear Hall effect indicate that there are light-induced changes in the value of the effect, but they do not induce a full destruction of the effect. **b** The high-temperature distribution of the changes in the nonlinear Hall effect shows that single pulses can flip, destroy, or revive the value of this observable. **c** Under no illumination, at the transition temperature, the flake explores all possible topological phases thermally, evidenced by a trimodal distribution of nonlinear Hall effect values over time.

Future Plans

Our plans are to primarily finish the development and measurements constituting Thrust 1. The top priority is to finalize the development of symmetry-tailored multi-frequency pump pulses to generate novel, symmetry-broken Floquet states reached by breaking spatial symmetries in addition to temporal symmetries. This is urgently needed because this is a qualitatively unique capability that enables the imposition of symmetries on materials which are outside of their crystal family, opening new avenues for photon-dressed control over material topology. Additionally, in the next funding period, we will finish data collection and interpretation for both Thrusts 2-1 and 2-3, for which we are completing experimental results currently.

References

1. Zhou, L., *et al.* Cavity Floquet engineering. *Nat Commun* **15**, 7782 (2024).
2. Kipp, G.*, Bretscher, H. M.*, *et al.* Cavity electrodynamics of van der Waals heterostructures. arXiv: 2403.19745v1 (2024).
3. Day, M. W., *et al.* Nonperturbative Nonlinear Transport in a Floquet-Weyl Semimetal. arXiv:2409.04531 (2024).
4. Li, X., *et al.* On-chip terahertz emission from Floquet-Bloch states [Invited]. Opt. Mater. Express **15**, 1765-1776 (2025).

Publications

1. "Nonperturbative Nonlinear Transport in a Floquet-Weyl Semimetal," Matthew W. Day, Kateryna Kusyak, Felix Sturm, Jose I. Aranzadi, Hope M. Bretscher, Michael Fechner, Toru Matsuyama, Marios Michael, Benedikt Schulte, Xinyu Li, Jesse Hagelstein, Dorothee Herrmann, Gunda Kipp, Alex. M. Potts, Jonathan M. DeStefano, Chaowei Hu, Yunfei Huang, Takashi Taniguchi, Kenji Watanabe, Guido Meier, Dongbin Shin, Angel Rubio, Jiun-Haw Chu,

Dante M. Kennes, Michael A. Sentef, James W. McIver; arXiv: 2409.04531 (2024). *Under review in Nature Materials.*

2. “Cavity electrodynamics of van der Waals heterostructures,” Gunda Kipp, Hope M Bretscher, Benedikt Schulte, Dorothee Herrmann, Kateryna Kusyak, Matthew W Day, Sivasruthi Kesavan, Toru Matsuyama, Xinyu Li, Sara Maria Langner, Jesse Hagelstein, Felix Sturm, Alexander M Potts, Christian J Eckhardt, Yunfei Huang, Kenji Watanabe, Takashi Taniguchi, Angel Rubio, Dante M Kennes, Michael A Sentef, Emmanuel Baudin, Guido Meier, Marios H Michael, James W McIver; arXiv:2403.19745 (2024); *Accepted to Nature Physics.*

3. “On-chip terahertz emission from Floquet-Bloch states,” Xinyu Li, Jesse Hagelstein, Felix Sturm, Kateryna Kusyak, Juan I. Aranzadi, Gunda Kipp, Yunfei Huang, Benedikt F. Schulte, Alex M. Potts, Victoria Quirós-Cordero, Chiara Trovatello, Zhi Hao Peng, Chaowei Hu , Jonathan M. DeStefano , Takashi Taniguchi, Kenji Watanabe, Michael A. Sentef, Dongbin Shin, P. James Schuck, Xiaodong Xu, Jiun-Haw Chu, Hope M. Bretscher, Matthew W. Day, James W. McIver. Under review in Optical Materials Express (2024). On-chip terahertz emission from Floquet-Bloch states [Invited]. Opt. Mater. Express 15, 1765-1776 (2025).

4. “Purcell enhancement of photogalvanic currents in WTe2 plasmonic cavities,” Xinyu Li, Jesse Hagelstein, Gunda Kipp, Felix Sturm, Kateryna Kusyak, Yunfei Huang, Benedikt F. Schulte, Alexander M. Potts, Victoria Quirós-Cordero, Chiara Trovatello, Zhi Hao Peng, Chaowei Hu, Jonathan M. DeStefano, Michael Fechner, Takashi Taniguchi, Kenji Watanabe, P. James Schuck, Xiaodong Xu, Jiun-Haw Chu, Angel Rubio, Marios H. Michael, Matthew W. Day, Hope M. Bretscher, James W. McIver; manuscript attached. Under review in Nat. Comms. (2025)

Enabling hollow core fibers for Brillouin light scattering and control of magnetic excitations at cryogenic temperatures

Dmytro Bozhko, University of Colorado Colorado Springs (Principal Investigator);
Zbigniew Celinski, University of Colorado Colorado Springs (Co-Investigator);
Valentine Novosad, Argonne National Laboratory (Co-Investigator)

Keywords: spintronics/magnonics, single crystals/nanostructures, antiferromagnets, Brillouin light scattering, microwave spectroscopy

Research Scope

The project aims to realize a comprehensive study of anti-ferro-magnons' BEC (at microwave frequencies ranging from GHz to THz) and related phenomena in a range of antiferromagnetic (AFM) materials in a wide range of temperatures from ambient to the quantum limit. To realize this ambitious project, both growth and measurement techniques need to be developed. In this abstract, we present the most recent results of the growth and characterization of thin-film fluoride and synthetic multilayer AFMs. Optical characterization of these materials at ultra-low temperatures is impossible without the development of a low-noise, vibration-free method of light delivery to and from the cryogenic environment. The ultra-low-noise fiber technology presented here enables over three orders of magnitude enhancement over the existing fiber-based waveguides for Brillouin Light Scattering (BLS) applications. Additionally, we developed a range of cryogenic methods to precisely control magnon-photon coupling to enable coherent manipulation and interfacing with superconducting circuits.

Recent Progress

Recently, we achieved particular advancements in the growth and characterization of thin films of $KMnF_3$ – the perspective fluoride AFM with perovskite structure grown on MgO, which very well matches the lattice constants of these AFMs (see Fig. 1a). The magnetometry of $KMnF_3$ films grown on an MgO (001) substrate is challenging due to the difference in thicknesses (250 nm

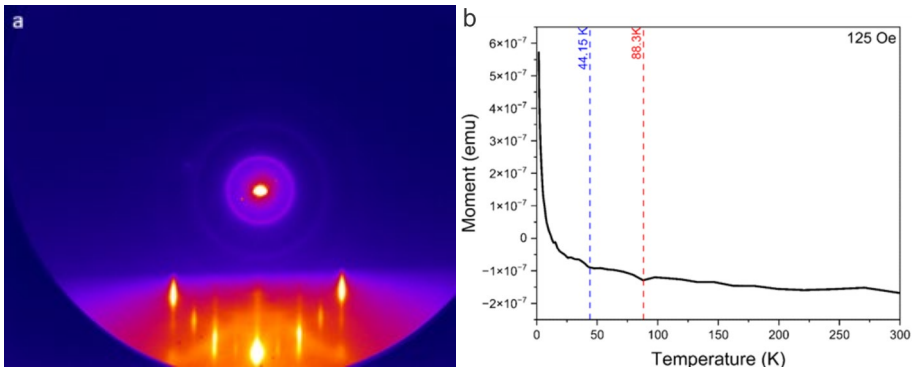


Figure 1. (a) RHEED image of $KMnF_3$ film grown on the MgO (001) substrate taken along [110] direction (electron energy up to 15 keV). (b) Magnetic moment vs. temperature of $KMnF_3$ films measured at 125 Oe.

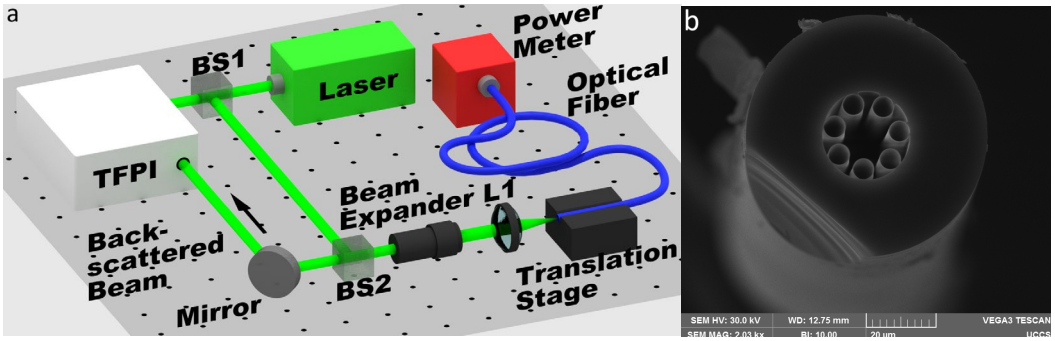


Figure 2. (a) Experimental setup for BLS spectroscopy of optical fibers. (b) Anti-resonant hollow core fiber cross-section imaged using SEM.

vs. 500000 nm) and a relatively weak moment of the antiferromagnetic film. Nevertheless, anomalies can be observed in the measurements of the magnetic moment as a function of temperature. Figure 1b depicts measurements of the magnetic moment vs temperature of the $KMnF_3$ film in 125 Oe field. A characteristic dip in data can be associated with the transition to the antiferromagnetic state at 88 K. This is the identical temperature at which the transition is observed in bulk material, indicating a stochiometric film. More clean and sensitive measurements could be enabled by BLS, which for decades has remained the primary spectroscopic probe of magnon and phonon dispersion [1], as well as their collective dynamics [2]. The quality and reliability of BLS measurements depend significantly on the performance of the optical components used in the setup. Typical BLS experiments [1,2] are being performed using free-space optics, but in some applications (e.g., in cryogenics), it could be much more convenient, or even necessary, to use optical fibers. However, conventional silica fibers introduce substantial spontaneous Brillouin background due to phonon scattering in the core and cladding, increasing background noise in the GHz frequency range and thus limiting the signal-to-noise ratio or even making measurements impossible. Recently, anti-resonant hollow core fibers (AR-HCFs) [3] have gained attention as a promising solution for low-noise photonic applications [4].

Here, we compare the performance of AR-HCFs to conventional fused silica fibers in the context of spontaneous BLS spectroscopy at GHz frequencies. The optical setup used for our study of the BLS in optical fibers is shown in Fig. 2a. The experimental arrangement allows convenient coupling of the light to different fibers with different numerical apertures and simultaneous control of the power and quality of the transmitted beam, which are necessary for the proper spectra normalization for different fibers. Figure 2b shows the SEM image of the AR-HCF. The frequency distribution of the photon count from the inelastically scattered light reflected from different optical fibers is shown in Fig. 3. In the case of the solid-core PM fiber (blue curve), it is possible to identify three peaks which correspond to specific phononic modes, namely longitudinal acoustic (LA 32.6GHz) and two transverse acoustic (TA, 19.8GHz and 18.3GHz) modes. The pronounced feature of the collected spectrum is the broadband optical noise, spanning over the whole range of

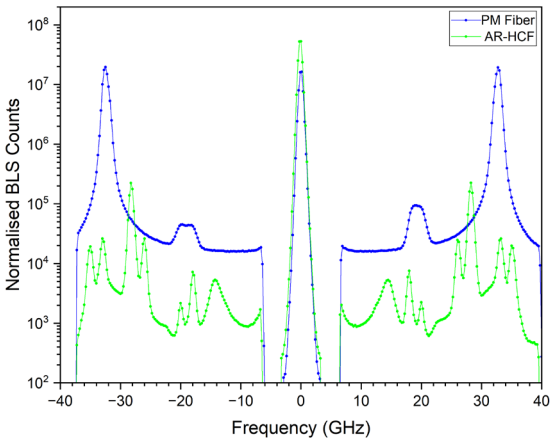


Figure 3. Normalized spontaneous Brillouin spectra of the PM fiber (Thorlabs PM-S405-XP) (blue) and the AR-HCF (green). The peak at zero frequency shift corresponds to the reference laser line.

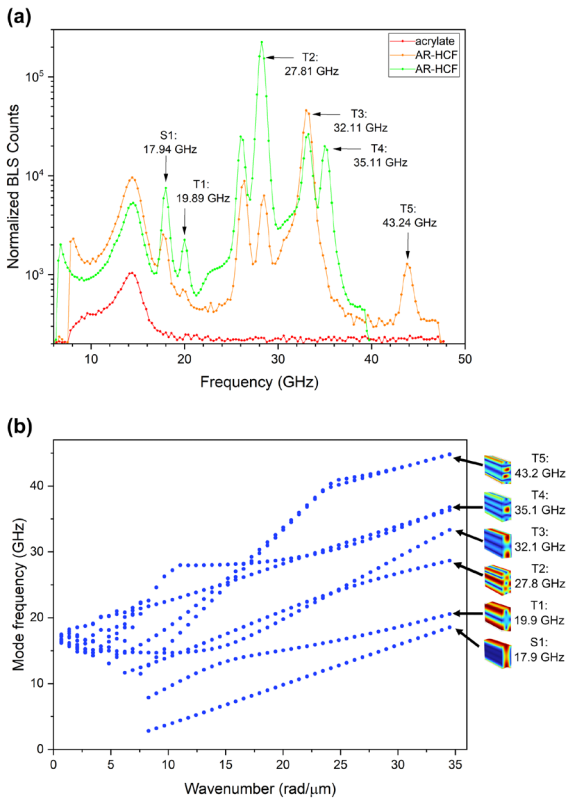


Figure 4. (a) Normalized BLS spectra of the AR-HCF recorded for different alignments (orange and green traces). The red trace corresponds to a spectrum collected from a piece of a pure acrylate coating separated from the fiber. (b) Numerically simulated dispersion of acoustic modes in a rectangular silica slab. The largest wavenumber in the simulation corresponds to the probed wavevector in the BLS experiments.

measured frequencies. The most plausible explanation of the origins of this noise is a glassy and strained structure of the fiber, resulting in a broad manifold of indistinguishable phononic modes. The Brillouin spectrum collected from the AR-HCF is shown in Fig. 3 as a green curve. The spectrum contains substantially more peaks than the solid core fiber. However, except for just one peak at 27.81GHz, the intensity of spectral features is consistently below that of the solid core fiber (up to 3 orders of magnitude, for example, at 32.6GHz), making AR-HCF a good choice for low-noise BLS experiments requiring fibers. However, the Brillouin spectrum of AR-HCF still contains plenty of well-defined peaks. We were able to identify their nature by performing a set of additional measurements and finite-element simulations.

In Fig. 4a, the BLS anti-Stokes part of the spectrum from the AR-HCF is shown for two different alignments and compared with that from a sample of bulk acrylate taken from the outer coating of the fiber. Comparing those spectra, we can conclude that below 17 GHz, the only contributor to the BLS signal is the coating with a broad peak centered at about 14 GHz. In our setup, variations in the probing beam alignment have caused differences in coupling to several of these modes, making the relative peak intensities vary. As evidenced by Fig. 4a, the frequencies at which modes occur are repeatable for different alignments, since they are determined by the boundary conditions and elastic properties of the material itself. These frequencies do not match exactly the dispersion for bulk TA and LA modes in fused silica, but it can be reasonably argued

that they originate from thickness modes within the thin capillary structures surrounding the hollow core. To reveal the role of confinement on the dispersion relations for the observed acoustic modes in the fused silica substructure, we performed a finite-element simulation of the system using COMSOL Multiphysics. The eigenfrequency study was performed using a simplified geometry of a quasi-infinite slab of 200 nm thickness with periodic boundary conditions over the other two dimensions. The results shown in Fig. 4b match perfectly the experimentally measured positions of the peaks.

Our findings establish AR-HCFs as highly suitable candidates for low-noise photonic applications. In particular, integration of AR-HCFs into light scattering experimental setups could open new avenues in fiber-based sensing, precision metrology, quantum communications, and the study of quasiparticle dynamics under extreme conditions, particularly in environments where free-space optics are impractical, such as cryogenic or integrated setups. Furthermore, tailoring the capillary wall geometry and material composition may enable engineered phonon responses, offering a path toward customizable acoustic backgrounds for light-matter interaction studies.

Future Plans

Upgrades to the 300 mK cryostat will be installed and tested, including home-built superconducting coils, precision temperature control of the sample stage, and an optical fiber scanning confocal Brillouin microscope. The nanostructures fabricated at Argonne National Lab this Summer will be tested both above and below T_N, and the attempts to achieve BEC using both rapid cooling and electromagnetic pumping will be performed. Also, we plan to continue fabrication, characterization, and nanofabrication of synthetic AFMs (Fe/Cu/Fe, Fe/Cr/Fe) structures.

References

1. R. E. Dunagin, A. A. Serga, and D. A. Bozhko, *Brillouin light scattering spectroscopy of magnon–phonon thermal spectra of an in-plane magnetized YIG film in two-dimensional wavevector space*, J. Appl. Phys. **137**, 083901 (2025)

2. P. Frey, D. A. Bozhko, V. S. L'vov, B. Hillebrands, and A. A. Serga, *Double accumulation and anisotropic transport of magnetoelastic bosons in yttrium iron garnet films*, Phys. Rev. B **104**, 014420 (2021)

3. R. Mears, K. Harrington, W. J. Wadsworth, J. M. Stone, and T. A. Birks, *Multi-core anti-resonant hollow core optical fiber,* Optics Letters **49**, 6761 (2024)

4. A. Iyer, W. Xu, J. E. Antonio-Lopez, R. A. Correa, and W. H. Renninger, *Ultra-low Brillouin scattering in anti-resonant hollow-core fibers*, APL Photonics **5**, 096109 (2020)

Publications

1. R. E. Dunagin, R. Mears, D. Bueno-Baques, V. S. Tyberkevych, Y. Li, W. J. Wadsworth, Z. Celinski, V. Novosad, and D. A. Bozhko, *Low Spontaneous Brillouin Scattering in Anti-Resonant Hollow-Core Fibers in GHz Frequency Range*, ArXiv: 2506.00287 (2025)

2. A. Joseph, J. M. P. Nair, M. A. Smith, R. Holland, L. J. McLellan, I. Boventer, T. Wolz, D. A. Bozhko, B. Flebus, M. P. Weides, and R. Macedo, *The role of excitation vector fields and all-polarisation state control of cavity magnonics*, npj Spintronics **2**, 59 (2024)

3. R. O. Serha, A. A. Voronov, D. Schmoll, R. Verba, K. O. Levchenko, S. Koraltan, K. Davídková, B. Budinska, Q. Wang, O. V. Dobrovolskiy, M. Urbánek, M. Lindner, T. Reimann, C. Dubs, C. Gonzalez-Ballestero, C. Abert, D. Suess, D. A. Bozhko, S. Knauer, and A. V. Chumak, *Magnetic anisotropy and GGG substrate stray field in YIG films down to millikelvin temperatures*, npj Spintronics **2**, 29 (2024)

Penetration-Capacitance Measurements and Noise Spectroscopies of Rhombohedral Multilayer and Twisted Bilayer Graphene

Raymond Ashoori, MIT

Keywords: Graphene, quantum anomalous Hall effects, compressibility measurements, noise measurements, pulsed transport measurementsResearch Scope

Two-dimensional moiré and multilayer graphene systems provide an extraordinary platform for studying correlated and topological electronic phases. Rhombohedral-stacked multilayer graphene (RSG) exhibits a wide array of emergent states, including fractional and integer quantum anomalous Hall effects[1], correlated insulators, and unconventional superconductivity[2]. Capacitance and penetration field measurements are uniquely sensitive to these phases, as they probe thermodynamic compressibility rather than transport (and bulk transport vs edge transport in quantum Hall regimes). Using this approach, we have studied features that transport cannot access such as negative compressibility, bulk conductivity, and the ability to directly measure energy gaps. Figure 1 shows the schematic of our capacitance bridge setup, which enables independent tuning of carrier density and displacement field. Our work involves a close collaboration with samples from Long Ju's group at MIT.

Flat-band conditions in RSG allow for electronic interactions to dominate over kinetic energy, leading to the stabilization of highly non-trivial correlated states. These include Wigner crystals, charge density waves, and Hall crystals. The ability to manipulate carrier density and displacement field in RSG provides a widely tunable environment for exploring these phases systematically. Our approach combines traditional capacitance techniques with novel pulsed and high-frequency probes, thereby offering both equilibrium and dynamic perspectives. This dual approach allows us to build a comprehensive understanding of correlated electronic matter and its phase transitions in these emerging two-dimensional materials.

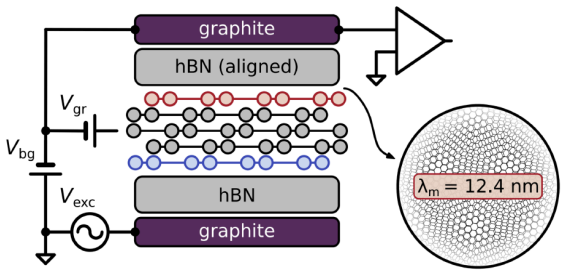


Figure 1: Schematic of the bridge sample-arm in the penetration capacitance measurement setup with pentalayer rhombohedrally stacked graphene (RSG). An ac excitation V_{exc} is applied to the bottom gate, and the penetrating signal is measured on the top gate. A moiré superlattice forms at the interface between the top layer of graphene and the aligned hBN. Pictured here is the setup that we used to take the data shown. This setup allows full and independent control of the electron density and the displacement field. Note that we can also measure direct capacitance of the sample by instead attaching the input of the amplifier to the RSG and connecting the battery V_{gr} to the sample using a very high resistance resistor to avoid shunting the capacitance signal to ground.

Recent Progress

Transport measurements on pentalayer RSG reveal the existence of a valley-polarized multiferroic state near charge neutrality.[3] As shown in Figure 2, capacitance uncovers incompressible states and negative compressibility not visible in transport, suggesting valley-ordered multiferroicity. These measurements show thermodynamic signatures of transitions that transport measurements miss, especially in regimes of high resistance. Boundaries that appear featureless in transport data correspond to sharp transitions in capacitance, hinting at isospin or Fermi surface reconstructions.

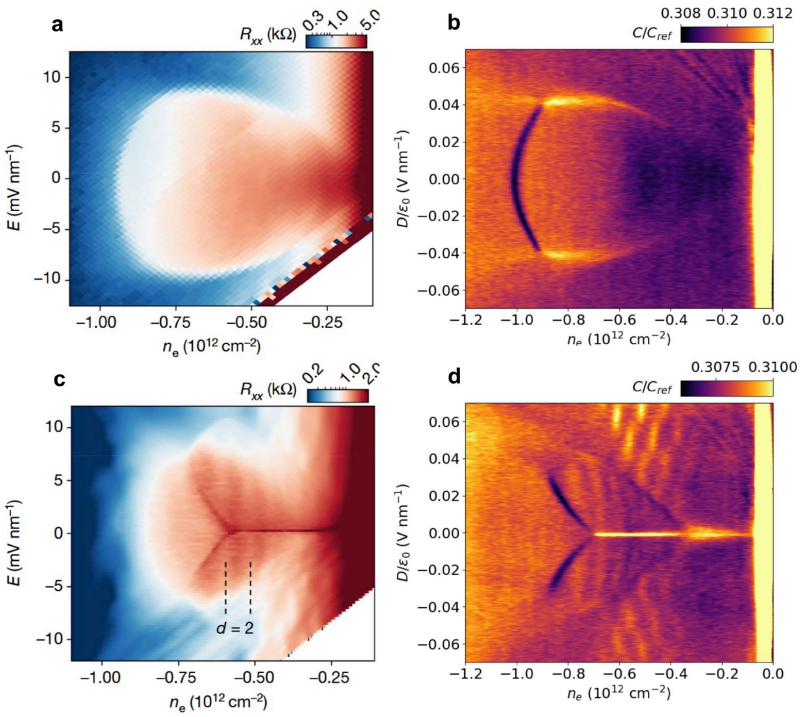


Figure 2: a) 300 mK transport (transport work is from Long Ju's group[3]) and b) capacitance measurements of the valley-polarized multiferroic bubble in pentalayer RSG near zero displacement field. The capacitance data shows a ring of incompressibility and negative compressibility surrounding the bubble that is not apparent in transport. c) Transport[9] and d) capacitance of the same region, now at a field of 2T. The three resistive lines inside the bubble seen in the transport data look strikingly different in capacitance; one appears incompressible, while the other two exhibit negative compressibility.

Additionally, in moiré RSG/hBN systems we identify clear signatures of generalized charge density waves (CDWs) at fractional fillings ($\nu = 1/3, 2/3$) as well as incommensurate Wigner crystal states away from commensurate fillings. Figure 3 highlights how capacitance distinguishes between CDW and Wigner solid phases with negative compressibility, where transport merely shows a band of high resistance. This demonstrates that capacitance can directly detect the compressibility signatures of crystalline order[4]. By combining capacitance with transport, we obtain a much more complete picture of correlated electronic phases, identifying both localized and delocalized electronic behaviors.

Our experiments also reveal negative compressibility in regimes associated with strong interactions, consistent with overscreening effects. Such behavior suggests that electrons can lower their energy by increasing local density, a hallmark of correlated crystalline phases. The sharp phase boundaries can show transitions between valley-polarized, multiferroic, and crystalline

states can be tuned with external fields. These findings set the stage for the next generation of experiments involving pulsed and high-frequency probes.

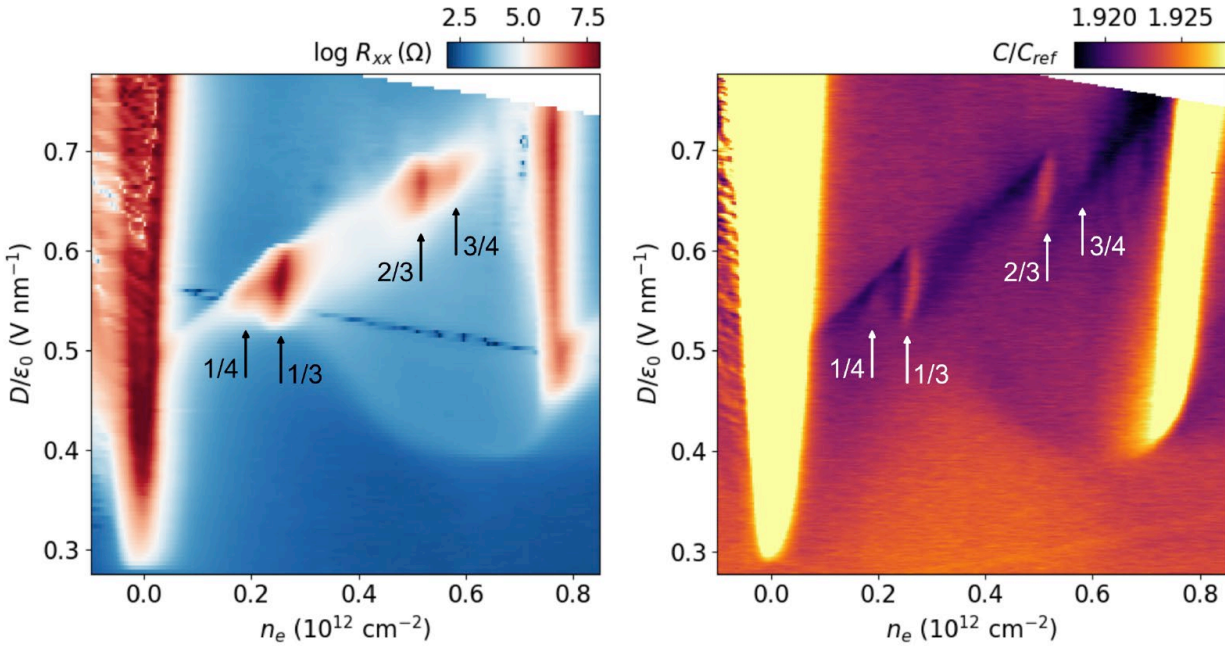


Figure 3: Comparison of charge density waves and the potential Wigner crystal in moiré pentalayer RSG between filling factors ν = 0 and 1. While both states have a high resistance in transport, the WC displays negative compressibility in the capacitance data.

Future Plans

We are extending our methods with pulsed and high-frequency measurements to probe dynamic behaviors of correlated states. Noise spectroscopy will search for narrowband noise from sliding Wigner crystals and CDWs at frequencies up to the GHz range. This will address the question of whether crystalline electronic phases in 2D systems exhibit coherent sliding dynamics analogous to those observed in one-dimensional charge density wave systems. By developing cryogenic broadband amplifiers with wide frequency response, we aim to directly measure these long-predicted yet unobserved signals.

Pulsed I–V techniques will mitigate Joule heating and enable measurement of intrinsic non-linear transport, including the search for Shapiro-like steps under RF drive. These steps, if observed, would provide definitive evidence of coherent sliding states. Pulsed methods also allow us to resolve the onset of conduction before heating suppresses correlation effects, offering a clear window into the intrinsic non-linearities of these systems. This capability will help us disentangle whether non-linear transport arises from disorder pinning, collective sliding, or other mechanisms.

Future directions include disentangling compressibility and polarizability with dual-excitation capacitance methods, which will allow us to separate the roles of density and displacement field

in driving transitions. We also plan to probe unconventional superconductivity in RSG, where strongly coupled superconductors may display negative compressibility, enabling them to be distinguished thermodynamically from surrounding metallic states. Ultimately, our goal is to map complete phase diagrams that include crystalline, superconducting, and topological states, thereby providing a comprehensive framework for correlated flat-band states in RSG.

References

1. Lu Z, Han T, Yao Y, Reddy AP, Yang J, Seo J, Watanabe K, Taniguchi T, Fu L, Ju L (2024) Fractional quantum anomalous Hall effect in multilayer graphene. *Nature*, 626(8000):759–764. https://doi.org/10.1038/s41586-023-07010-7

2. Han T, Lu Z, Yao Y, Shi L, Yang J, Seo J, Ye S, Wu Z, Zhou M, Liu H, Shi G, Hua Z, Watanabe K, Taniguchi T, Xiong P, Fu L, Ju L (2024) Signatures of Chiral Superconductivity in Rhombohedral Graphene. https://doi.org/10.48550/arXiv.2408.15233

3. Han T, Lu Z, Scuri G, Sung J, Wang J, Han T, Watanabe K, Taniguchi T, Fu L, Park H, Ju L (2023) Orbital multiferroicity in pentalayer rhombohedral graphene. *Nature*, 623(7985):41–47. https://doi.org/10.1038/s41586-023-06572-w

4. Aronson SH, Han T, Lu Z, Yao Y, Butler JP, Watanabe K, Taniguchi T, Ju L, Ashoori RC (2025) Displacement Field-Controlled Fractional Chern Insulators and Charge Density Waves in a Graphene/hBN Moir\’e Superlattice. *Physical Review X*, 15(3):031026. https://doi.org/10.1103/75gl-jzl6

Publications

This is a new award, so there are not yet publications with support from it.

Topology and molecular arrangement in low-dimensional magnetic materials

Claudia Ojeda-Aristizabal, *Department of Physics and Astronomy, California State University Long Beach*

Keywords: magnetism, topological phases of matter, 2-dimensional system, electronic transport, ARPES.

Research Scope

Our current research aims to understand and control properties derived from topologically protected phases, molecular arrangement and Moiré patterns in low dimensional materials that present a long-range magnetic order. Research efforts are organized into two thrusts. The first thrust focuses on two-dimensional Dirac semimetals such as $PtTe_2$ and $PdTe_2$ that when substituted with a magnetic element like Cr, become high transition temperature ferromagnets (T*c* up to 220 K). These materials have the important property of keeping the air-stability of their transition metal dichalcogenide (and topological) parent crystals. This effort intents to bring light on the intriguing interplay between magnetism and Dirac fermion physics in two dimensional materials but also, should provide details on the electronic structure of exfoliatable, metallic, air-stable ferromagnets. Our results characterizing the parent type-II Dirac semimetals PtTe2 and PdTe2 through photoemission experiments set a strong ground to understand the Cr alloys. Additionally, this thrust has developed efforts to measure through specialized transport methods, quantum materials that are highly insulating, and that present magnetically ordered ground states as well as more thrilling states such as spin liquids, which is the case of α-$RuCl_3$. Our transport results are cited in an invited review currently in preparation.

A second thrust of our research is centered on molecular solids made of C_{60} or metal-Phthalocyanines (MPc). MPc are versatile planar molecules that can host almost any transition metal from the periodic table, some of which transform these molecules into magnetic building blocks. C_{60} and MPc can form thin films on two-dimensional materials where molecular arrangements and Moiré patterns may have a profound impact on their electronic structure. Such patterns may result from a periodical variation of the orientation of the molecules on the substrate or simply from the non-commensurability of the molecular thin film unit cell with the one of the substrate. Specialized 4D Scanning Transmission Electron Microscopy (4D-STEM) has provided us information about the molecular arrangement of CuPc on graphene/h-BN. We have performed electronic transport studies in the quantum coherent regime of a similar heterostructure of CuPc/bilayer-graphene/h-BN, finding a restoration of weak localization in bilayer-graphene/h-BN by the presence of the Cu-phthalocyanine (CuPc) molecules. Additionally, we have performed ARPES measurements on a thin film of K_xC_{60} on hexagonal layered Bi_2Se_3, demonstrating the existence of a quantum phase transition induced by intercalation doping.

Recent Progress

Three-dimensional dispersion in the type-II Dirac semimetals $PtTe_2$ and $PdTe_2$ revealed through Angle Resolved Photoemission Spectroscopy (ARPES)

$PtTe_2$ and $PdTe_2$ are among the transition metal dichalcogenides that were first predicted to recreate type-II Dirac fermions, exotic particles prohibited in free space [1]. These materials are layered and air-stable, which makes them suitable for different technological applications. Most importantly, they have the particularity of not only hosting type-II Dirac particles at the bulk but also topologically protected chiral states at the surface. In this work, we provide a careful characterization of the electronic structure of $PtTe_2$ and $PdTe_2$ through Angle Resolved Photoemission Spectroscopy ARPES and Density Functional Theory DFT calculations, stressing the important role played by the different symmetries associated to their crystallographic space group, discernible in our data. We offer an alternative interpretation for one of the Dirac-like dispersions in these materials. Using circularly polarized light, we report a different behavior of such dispersion in PdTe2 compared to PtTe2, that we relate to a symmetry analysis of the dipole matrix element. Such analysis reveals a link between the observed circular dichroism and the different momentum-dependent terms in the dispersion of these two compounds, despite their close similarity in crystal structure. Additionally, our data show a clear difference in the circular dichroic signal for the type-II Dirac cones characteristic of these materials, compared to their topologically protected surface states. Our paper provides a useful reference for the ARPES characterization of other transition metal dichalcogenides with topological properties and illustrates the use of circular dichroism as a guide to identify the topological character and attributes of two otherwise equivalent band dispersions.

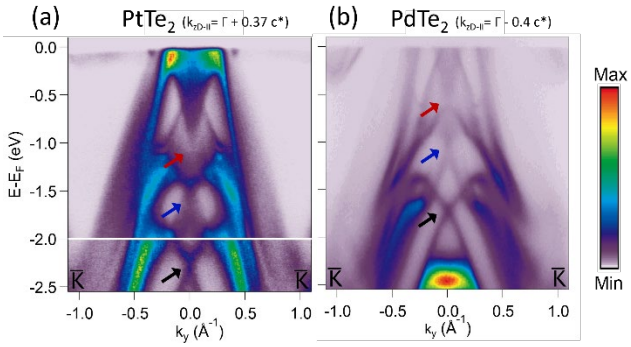


Figure 1: High resolution ARPES band structure of $PtTe_2$ (a) and $PdTe_2$ (b) along the K-Γ-K direction showing the type-II Dirac cone (red arrow), surface state cone (black arrow) and 3D-like Dirac dispersion for which we offer a new interpretation (blue arrow).

Restauration of weak localization in bilayer graphene by a molecular thin film

By using mesoscopic transport, we have found that CuPc molecules have the remarkable effect of restoring weak localization effects in bilayer graphene. Weak localization is a quantum correction to the conductance in metals and doped semiconductors, outcome of the interference of the charge carriers' electronic wave functions. In graphene, this interference process is highly influenced by the π Berry phase of its carriers, that leads to a destructive interference when the carriers follow time-reversed trajectories, leading to a suppression of backscattering and a positive correction to the conductivity, known as weak antilocalization. In the case of bilayer graphene, the Berry phase is 2π, leading instead to a constructive interference for time-reversed trajectories, and a negative

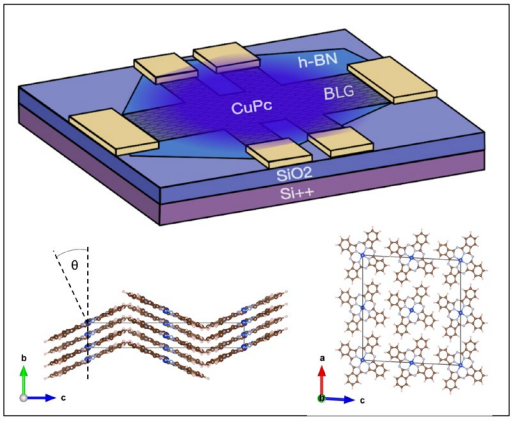


Figure 2: Top: Schematics of the CuPc/BLG/h-BN device. Bottom: Crystal structure of CuPc. The angle θ defines the different existing polymorphs.

correction to the conductivity, known as weak localization. The presence of weak localization (weak antilocalization) in bilayer (monolayer) graphene is linked to the geometrical phase of its carriers, that is related to their chirality [2,3].

In bilayer graphene, there is a special type of scattering mechanism that tends to destroy weak localization, called trigonal warping [3,4]. At low energies, trigonal warping is consequence of a skew interlayer hopping between carbon atoms that manifest itself as a threefold deformation of the Fermi surface. Trigonal warping has the effect of destroying the manifestation of the chirality of the carriers in localization effects in bilayer graphene. We have found, by comparing magnetoresistance measurements in our samples to the known theory of weak localization in bilayer graphene, that the presence of the CuPc molecules has tendency to revivify weak localization, and therefore the manifestation of the chiral character of the carriers in the localization properties of bilayer graphene. We have characterized the arrangement of the CuPc molecules in our transport sample using a control sample compatible with a sophisticated tunneling microscopy technique, 4D-STEM, that provides a high-resolution imaging while minimizing the radiation damage to the molecules.

Our work puts in evidence the potential of mesoscopic transport revealing important effects in van der Waals heterostructures. In particular, in the case of a molecular thin film on bilayer graphene, restoring the quantum interference effect of weak localization and imposing an important charge transfer while preserving the mobility of the original bilayer graphene / h-BN device.

Topological properties and Lifshitz transition in the $Cr_xPt_{1-x}Te_2$ family of ferromagnets

Having fully characterized the type-II Dirac semimetals PtTe2 and PdTe2, we have studied different magnetic alloys of PtTe2 using ARPES and a symmetry analysis of the Dirac Hamiltonian. To a first approximation, one would think that the introduction of a magnetic element such as Cr breaks time reversal symmetry, pulling apart the individual Weyl modes in momentum space [5].Our preliminary ARPES measurements show that instead of an antagonist role, Cr benefits the experimental reach of the type-II Dirac cone characteristic of the parent crystal, by introducing electron doping and bringing the type-II cone closer to the Fermi level. We have found that while the magnetic element substitution breaks space-time inversion symmetry and mirror symmetries, it preserves their combination. This creates a splitting of the type-II cone of the PtTe2 into two Weyl cones, without the creation of an energy gap. The 3-dimensional Dirac cone is therefore resilient to the presence of magnetism. On the other hand, the breaking of time-reversal summetry has a detrimental effect on the topologically protected surface states also characteristic

of PtTe2, creating an energy gap. Our ARPES measurements have confirmed that the type-II Dirac dispersion comes closer to the Fermi level as we increase the Cr substitution, which is very interesting, as it opens the possibility of having in the same material a ferromagnetic order at relatively high temperatures (220K for $Cr_{0.45}Pt_{0.55}Te_2$) and access to Dirac fermions.

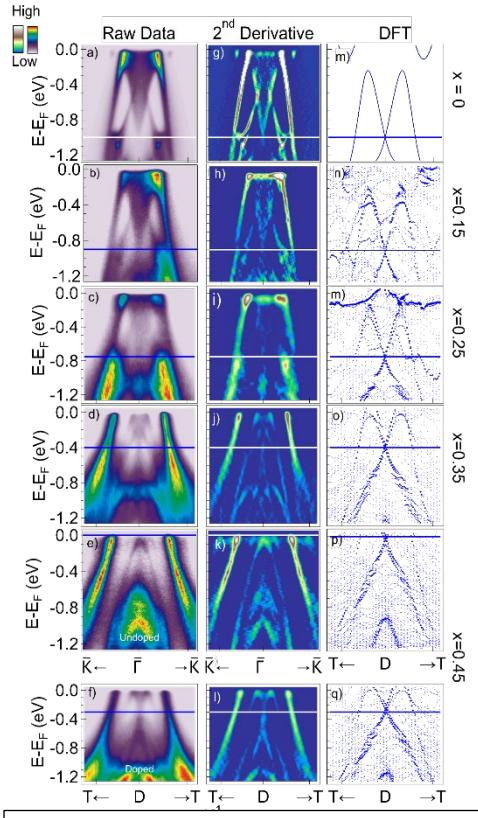


Figure 3: ARPES measurements of $PtTe_2$ and the different Cr alloys $Cr_xPt_{1-x}Te_2$ (x=0, 0.15, 0.25, 0.35 and 0.45) compared to DFT calculations. The horizontal line shows the location of the type-II cone.

Future Plans

Proximity effects in graphene by a ferromagnetic phthalocyanine

With the experience gained in the study of CuPc/bilayer-graphene/h-BN heterostrcutures, we plan to explore ferromagnetic phthalocyanines such as MnPc and FePc. A new dilution refrigerator will allow us to reach lower temperatures and explore possible proximity effects on graphene, visible in weak localization experiments and universal conductance fluctuations.

Effect of Ir on the CrxPt1-xTe2 family of ferromagnets

After having studied the $Cr_xPt_{1-x}Te_2$ family of materials, the following interesting question to address is what happens when both Cr and Ir are substituted into the Pt site of $PtTe_2$. It is known that $IrTe_2$ can host superconductivity when a structural phase transition is suppressed. This structural transition is accompanied by a jump in resistance, and it is associated to a charge density wave (CDW) anomaly. Superconductivity competes therefore with CDW in this compound [6]. It has been shown that suppression of the CDW phase can be achieved with Pt substitution [7], leading to a superconducting transition at 3K [8, 9]. Now, the additional substitution of Cr into the Pt site, will likely help with the tuning of the type-II Dirac point to the Fermi level, as we have observed for the $Cr_xPt_{1-x}Te_2$ family of materials. Most importantly, despite breaking time-reversal symmetry, the presence of Cr might allow the superconducting state to prevail. It has been shown by Cho, Lu, Moore et al. that in a doped Weyl semimetal where time-reversal symmetry is broken, one can have upon slight doping, a finite-momentum displacement of the Weyl nodes, that in combination with the non-trivial winding numbers of these nodes, can potentially lead to even- and also odd-parity superconductivity [10]. Our ARPES measurements on the $Cr_xPt_{1-x-y}Ir_yTe_2$ family of materials will probe the resilience of both the three-dimensional Dirac cone as well as the topologically protected surface state to the presence of Ir and Cr.

References

[1] H. Huang, S. Zhou, and W. Duan, Type-II Dirac fermions in the PtSe2 class of transition metal dichalcogenides, Phys. Rev. B 94, 121117 (2016).
[2] F. V. Tikhonenko, A. A. Kozikov, A. K. Savchenko, and R. V. Gorbachev, Transition between electron localization and antilocalization in graphene, Phys. Rev. Lett. 103, 226801 (2009).
[3] R. V. Gorbachev, F. V. Tikhonenko, A. S. Mayorov, D. W. Horsell, and A. K. Savchenko, Weak localization in bilayer graphene, Phys. Rev. Lett. 98, 176805 (2007).
[4] K. Kechedzhi, V. I. Fal'ko, E. McCann, and B. L. Altshuler, Influence of trigonal warping on interference effects in bilayer graphene, Phys. Rev. Lett. 98, 176806 (2007).
[5] J. Cano, B. Bradlyn, Z. Wang, M. Hirschberger, N. P. Ong, and B. A. Bernevig, Chiral anomaly factory "Creating Weyl fermions with a magnetic field" Phys. Rev. B 95, 161306 (2017).
[6] S. Pyon, K. Kudo, M. Nohara,"Superconductivity Induced by Bond Breaking in the Triangular Lattice of IrTe2", Journal of the Physical Society of Japan, 81, 053701 (2012)
[7] J. Jiang, S. Lee, F. Fei, F. Song, E. Vescovo; K. Kaznatcheev; F. J. Walker; C. H. Ahn, "A comprehensive ARPES study on the type-II Dirac semimetal candidate Ir1−xPtxTe2" APL Mater. **8**, 061106 (2020)
[8] B.-B. Fu, C.-J. Yi, Z.-J. Wang, M. Yang, B.-Q. Lv, X. Gao, M. Li, Y.-B. Huang, H.-M. Weng, Y.-G. Shi, T. Qian and H. Ding « Realization of low-energy type-II Dirac fermions in (Ir1-xPtx)Te2 superconductors" Chinese *Phys. B* **28** 037103 (2019).
[9] F. C. Fei, X. Y. Bo, P. D. Wang, J. H. Ying, J. Li, K. Chen, Q. Dai, B. Chen, Z. Sun, M. H. Zhang, F. M. Qu, Y. Zhang, Q. H. Wang, X. F. Wang, L. Cao, H. J. Bu, F. Q. Song, X. G. Wan, B. G. Wang, "Band Structure Perfection and Superconductivity in Type-II Dirac Semimetal Ir1−xPtxTe" Adv. Mater. 30, 1801556 (2018).
[10] G. Y. Cho, J. H. Bardarson, Y.-M. Lu, and Joel E. Moore "Superconductivity of doped Weyl semimetals: Finite-momentum pairing and electronic analog of the 3He-A phase" Phys. Rev. B **86**, 214514 (2012).

Publications

1. Patrick Barfield, Vinh Tran, Vikram Nagarajan, Maya Martinez, Amirari Diego, Derek Bergner, Alessandra Lanzara, James G. Analytis and Claudia Ojeda-Aristizabal "Electronic transport mechanisms in a thin crystal of the Kitaev candidate α-RuCl3 probed through guarded high impedance measurements" **Appl. Phys. Lett. 122, 243102 (2023)**
2. Ping Ai, Luca Moreschini, Ryo Mori, Drew W. Latzke, Jonathan D. Denlinger, Alex Zettl, Claudia Ojeda-Aristizabal and Alessandra Lanzara "Linearly dispersive bands at the onset of correlations in KxC60 films" **Phys. Rev. Research 5, L022042 (Letter) (2023)**
3. Ivan Pelayo, Derek Bergner, Archibald J. Williams, Jiayuwen Qi, Penghao Zhu, Mahfuzun Nabi, Warren L. B. Huey, Luca Moreschini, Ziling Deng, Tyler Hadsell, Jonathan Denlinger, Alessandra Lanzara, Yuan-Ming Lu, Wolfgang Windl, Joshua Goldberger and Claudia Ojeda-Aristizabal "Three-dimensional dispersion in the type-II Dirac semimetals PtTe2 and PdTe2 revealed through circular dichroism in angle-resolved photoemission spectroscopy"
   Phys. Rev. B 110, 195429 (2024)
4. Anise Mansour, Deanna Diaz, Movindu Kawshan Dissanayake, Erin Henkhaus, Jungyoun Cho, Vinh Tran, Francisco Ramirez, Eric Corona-Oceguera, Joshua Luna, Kenta Kodama, Yueyun Chen, Ho Chan, Jacob Weber, Blake Koford, Patrick Barfield, Maya Martinez, Kenji Watanabe, Takashi Taniguchi, B. C. Regan, Matthew Mecklenburg, Thomas Gredig and Claudia Ojeda-Aristizabal "Modification of the scattering mechanisms in bilayer graphene in proximity to a molecular thin film probed in the mesoscopic regime"
   ArXiv 2504.20990 (2025) Submitted to Physical Review Materials.
5. Claudia Ojeda-Aristizabal, Xiaohu Zheng, Changsong Xu, Zohar Nussinov, Yukitoshi Motome, Arnab Banerjee, Adam W. Tsen, Michael Knap,

Rui-Rui Du, Gajadhar Joshi, Andy Mounce, Youngwook Kim,17 Benjamin M. Hunt, Dmitry Shcherbakov, Boyi Zhou, Ran Jing, Mengkun Liu, Hui Zhao, Bolin Liao, Martin Claassen, Onur Erten and Erik A. Henriksen, "Lessons from α-RuCl3 for pursuing physics of quantum spin liquid in atomically thin materials"
Invited Review to be submitted to Journal of Physics: Condensed Matter. In preparation (2025)

6. Stability of a Type-II Dirac cone in the Van der Waals Ferromagnet CrxPt1−xTe2, Derek Bergner, Ivan Pelayo, Tyler Hadsell, Penghao Zhu, Archibald Williams, Jiayuwen Qi, Mahfuzun Nabi, Warren L. Huey, Luca Moreschini, Ziling Deng, Jonathan Denlinger, Alessandra Lanzara, Yuan-Ming Lu, Wolfgang Windl, Joshua Goldberger and Claudia Ojeda-Aristizabal **In preparation (2025)**
7. Master thesis dissertations by Derek Bergner (2023), Patrick Barfield (2023), Mahfuzun Nabi (2024), Deanna Diaz (2024), Ivan Pelayo (2024), Anise Mansour (2024), Tyler Hadsell (2025).

Van der Waals Heterostructures: Novel Materials and Emerging Phenomena

Feng Wang, Michael Crommie, Alessandra Lanzara, Steven Louie, Zi Q. Qiu, Archana Raja, Mike Zaletel

Materials Science Division, LBNL

Keywords: 2D and layered crystals, Wigner crystal, moiré physics, 2D exciton and light-matter phenomena, nanofabrication and 2D assembly

Research Scope

This program aims to exploit extraordinary new scientific opportunities enabled by designing van der Waals (vdW) heterostructures that allow creation of novel functional materials with unprecedented flexibility and control. The key innovation here is that van der Waal bonded materials with different dimensionality and wide-ranging properties can be integrated together to form a new class of materials – vdW-bonded heterostructures (vdW heterostructures) - in which each constituent can be engineered separately. In this program, we will design and create novel vdW heterostructures with in-situ twist angle and strain control. We will elucidate new electronic quantum phases, including anisotropic Wigner crystals, 1D Luttinger liquid arrays, non-conventional superconductors, and generalized Wigner crystals, in a variety of vdW heterostructures. We will gain microscopic understanding of emerging magnetic phenomena in 2D materials. We will further characterize and control excited states in 2D vdW heterostructures, including visualizing individual moiré excitons and probing dynamic transport of exciton, energy, and spin.

Recent Progress:

We have made important progress in exploring a variety of novel quantum phenomena that can arise in van der Waals heterostructures. Here we highlight three studies. (1) Observation of Wigner molecular crystals. (2) Imaging tunable Luttinger liquid systems in vdW heterostructures. (3) Imaging quantum melting of 2D Wigner solids.

Wigner molecular crystals from multi-electron moiré artificial atoms

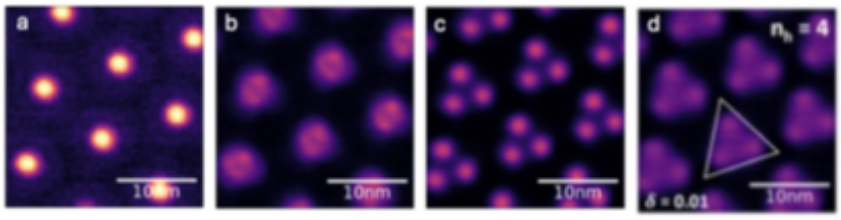


Fig. 1: STM images demonstrating the emergence of Wigner molecular crystals when multiple holes are present in a twisted WS2 moiré superlattice. (a) One hole per moiré unit cell. (b) Two holes per moiré unit cell. (c) Three holes per moiré unit cell. (d) Four holes per moiré unit cell.

Semiconductor moiré superlattices provide a versatile platform to engineer quantum electron solids composed of artificial atoms on moiré sites. Previous studies have focused on the simplest correlated quantum solid—the Fermi-Hubbard model—where intra-atom

interactions are simplified to a single onsite repulsion energy U. These studies have revealed novel quantum phases ranging from Mott insulators to quantum anomalous Hall insulators at the filling of one electron per moiré unit cell. In a collaborative work between ***Wang***, ***Crommie*** and ***Zettl***, we developed a non-invasive STM imaging technique to image Wigner molecular crystals for the first time [1]. **Figure 1a-d** show STM images of carrier distribution when one, two, three, and four holes are present in one moiré unit cell in twisted bilayer WS2. Charge distribution characteristic of Wigner molecules can be observed when there are multiple holes per moiré unit cell: Three-hole Wigner molecules, for example, exhibit a striking trimer pattern. The array of Wigner molecules in a moiré superlattice comprises a new crystalline phase of electrons: the Wigner molecular crystal. These Wigner molecular crystals are highly tunable through mechanical strain, moiré period, and carrier charge type. Such Wigner molecular crystals could exhibit strongly correlated quantum phenomena distinctly different from other known electronic phases.

Imaging tunable Luttinger liquid systems in van der Waals heterostructures

One-dimensional interacting electrons are often described as a Luttinger liquid having properties that are intrinsically different from those of Fermi liquids in higher dimensions. The behaviors of Luttinger liquids are predicted to change strongly with varying intra- and inter-1D-chain electronic interactions, but their experimental characterization can be challenging. In a collaborative research led by ***Wang***, ***Crommie, Zaletel,*** and ***Louie***, we demonstrate that layer-stacking domain walls (DWs) in van der Waals heterostructures provide a broadly tunable Luttinger liquid system that includes both isolated and coupled arrays[2]. We were able to image the evolution of the DW Luttinger liquids as a function of electron density using the non-invasive STM technique. In isolated DWs, we observe tunable 1D Wigner crystal at low electron densities (**Fig. 2a**) wehre

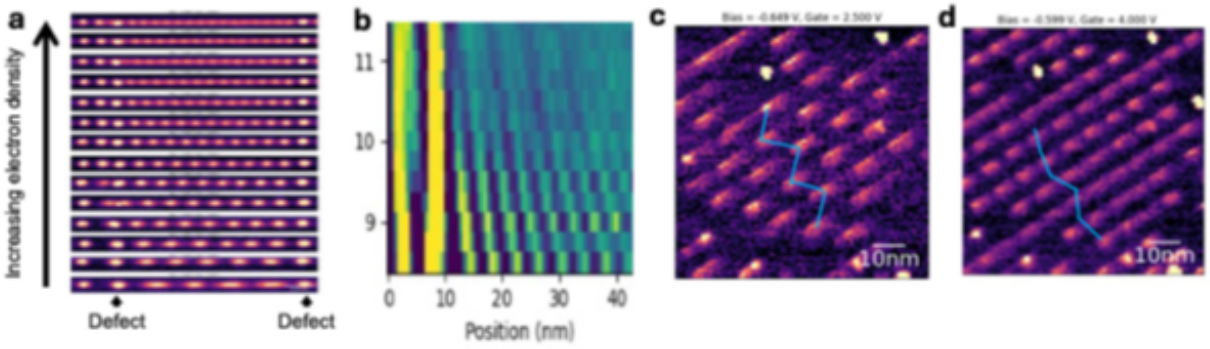


Fig. 2: (a) STM images of 1D Wigner crystal in an isolated domain at low electron densities (b) At increased electron densities, the 1D Wigner crystal dimerizes due to magneto-elastic coupling between strongly interacting 1D electrons. (3) 1D Wigner crystals in adjacent domain walls are phased locked with each other at low electron desnity, giving rise to a 2D electron lattice. (d) 1D Wigner crystals in different chains have random phases at increased electron densities, corresponding to an electronic smectic liquid crystal phase. states (d), and the Mott insulator state (e), respectively.

electrons are added one by one. At intermediate electron density, we reveal an unusual, dimerized Wigner crystal driven by the magneto-elastic coupling (**Fig. 2b**). At even higher densities, the electrons form a weakly interacting Luttinger liquid.

For periodic arrays of DWs the interplay between intra- and inter-chain interactions gives rise to new quantum phases. At low electron densities inter-chain interactions are dominant and induce a 2D electron crystal composed of phased-locked 1D Wigner crystal in a staggered configuration (**Fig. 2c**). Increased electron density causes intra-chain fluctuation potentials dominate, leading to an electronic smectic liquid crystal phase where electrons are algebraically ordered along the chain direction but disordered between chains. (**Fig. 2d**). This study establishes layer-stacking DWs in 2D heterostructures as an exciting new platform to realize tunable Luttinger liquid systems.

Imaging quantum melting of 2D Wigner solids

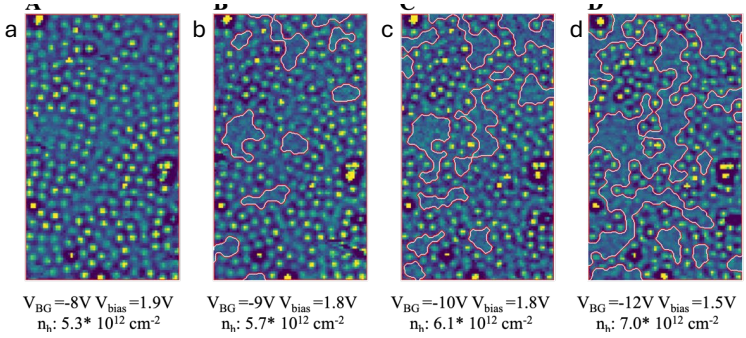


Fig. 3: (a) A disordered Wigner solid at low hole densities in bilayer $MoSe_2$. (b) A solid-liquid mixture phase starts to emerge above a critical hole density. The red lines outline the liquid region. (c) and (d): The liquid regions expand and form a percolation network with further increased hole densities.

The two-dimensional electron gas (2DEG) at very high densities is well-described by a weakly interacting Fermi liquid theory, whereas in the low-density limit electrons solidify into a Wigner crystal where Coulomb energy dominates over kinetic energy. At intermediate densities, however, the competition between Coulomb energy and kinetic energy is more pronounced and drives the emergence of exotic strongly correlated phases. Understanding the quantum melting behavior of a 2D Wigner solid remains an outstanding challenge after decades of research. In a collaboration between ***Wang***, ***Crommie***, and ***Louie***, we use non-invasive STM imaging technique to visualize for the first time a Wigner solid of holes, including its densification and quantum melting, in bilayer $MoSe_2$ at zero magnetic field [3]. At low hole density, we observe a disordered Wigner solid that exhibits a local triangular lattice but no long-range crystalline order owing to point defects that pin the Wigner solid and induce nanocrystalline domains (**Fig. 3a**). The Wigner solid exhibits an unusual densification behavior as the hole density is increased: instead of a continuous contraction of the lattice constant as expected for a perfect Wigner crystal, the holes appear to evolve via a quantum superposition state. Above a critical hole density, the Wigner solid starts to melt and enters a mixed phase with coexisting solid and liquid regions (**Fig. 3b**). The liquid regions continue to expand and form a percolation pattern with further increase of charge density (**Fig. 3c and 3d**).

Future Plans

We propose to push the frontiers of vdW heterostructure research with unique and collaborative efforts of our team members. Specifically, we will design and create a new class of artificial quantum materials that are enabled by integrating vdW materials with widely varying properties into vdW heterostructures. Using these artificial quantum materials, we will advance vdW heterostructure research in three closely connected directions.

(1) Design and control novel correlated electronic quantum phases in vdW heterostructures: Many fascinating correlated electronic quantum phases, ranging from correlated insulators and superconductors to Wigner crystals and Luttinger liquids, have been observed in van der Waals heterostructures. However, the explored materials represent only a small phase space within the vast synthetic quantum system enabled by van der Waals heterostructures. In addition, microscopic understanding of the emerging correlated phases is still lacking. Here we will explore completely new electronic quantum phases, such as anisotropic Wigner crystals and 1D Luttinger liquid arrays. We will also gain fundamental understanding of existing moiré physics by combining ab initio theory, in-situ twist angle control, and advanced experimental characterizations.

(2) Microscopic understanding of emerging magnetic phenomena in 2D materials: Beyond novel electronic quantum phases in vdW heterostructures, we will also gain fundamental understanding of emerging magnetic phenomena in 2D materials, including fractional Chern insulators and altermagnets.

(3) Understanding and control of non-equilibrium excited states and quantum transport in vdW heterostructures. In addition to novel quantum phases in the ground state, vdW heterostructures can also host fascinating non-equilibrium phenomena that are distinct from those in conventional materials. We will discover and control non-equilibrium excited states and quantum exciton, energy, and spin transport in 2D vdW heterostructures, ranging from probing invidual moiré excitons to focusing hydrodynamic energy waves in vdW materials.

References

(1) Li, H.; Xiang, Z.; Reddy, A. P.; Devakul, T.; Sailus, R.; Banerjee, R.; Taniguchi, T.; Watanabe, K.; Tongay, S.; Zettl, A.; Fu, L.; Crommie, M. F.; Wang, F. Wigner molecular crystals from multielectron moiré artificial atoms. *Science* **2024**, *385* (6704), 86-91. DOI: 10.1126/science.adk1348

(2) Li, H. Y.; Xiang, Z. Y.; Wang, T. L.; Naik, M. H.; Kim, W.; Nie, J. H.; Li, S. Y.; Ge, Z. H.; He, Z. H.; Ou, Y. B.; Banerjee, R.; Taniguchi, T.; Watanabe, K.; Tongay, S.; Zettl, A.; Louie, S. G.; Zaletel, M. P.; Crommie, M. F.; Wang, F. Imaging tunable Luttinger liquid systems in van der Waals heterostructures. *Nature* **2024**, *631* (8022) 765-770, Article. DOI: 10.1038/s41586-024-07596-6

(3) Xiang, Z.; Li, H.; Xiao, J.; Naik, M. H.; Ge, Z.; He, Z.; Chen, S.; Nie, J.; Li, S.; Jiang, Y.; Sailus, R.; Banerjee, R.; Taniguchi, T.; Watanabe, K.; Tongay, S.; Louie, S. G.; Crommie, M. F.; Wang, F. Quantum Melting of a Disordered Wigner Solid. *arXiv:1306.4972. Science* **2025**, *388* (6748), 736-740, DOI: 10.1126/science.ado7136

Publications:

1. H. Li, Z. Xiang, A. P. Reddy, T. Devakul, R. Sailus, R. Banerjee, T. Taniguchi, K. Watanabe, S. Tongay, A. Zettl, L. Fu, M. F. Crommie and F. Wang, *"Wigner molecular crystals from multielectron moiré artificial atoms"*, Science 385 (6704), 86-91 (2024). doi:10.1126/science.adk1348
2. H. Li, Z. Xiang, M. H. Naik, W. Kim, Z. Li, R. Sailus, R. Banerjee, T. Taniguchi, K. Watanabe, S. Tongay, A. Zettl, F. H. da Jornada, S. G. Louie, M. F. Crommie and F. Wang, *"Imaging moiré excited states with photocurrent tunnelling microscopy"*, Nature Materials 23 (5), 633-638 (2024). 10.1038/s41563-023-01753-4
3. H. Li, Z. Xiang, E. Regan, W. Zhao, R. Sailus, R. Banerjee, T. Taniguchi, K. Watanabe, S. Tongay, A. Zettl, M. F. Crommie and F. Wang, *"Mapping charge excitations in generalized Wigner crystals"*, Nature Nanotechnology 19 (5), 618-623 (2024). 10.1038/s41565-023-01594-x
4. H. Li, Z. Xiang, T. Wang, M. H. Naik, W. Kim, J. Nie, S. Li, Z. Ge, Z. He, Y. Ou, R. Banerjee, T. Taniguchi, K. Watanabe, S. Tongay, A. Zettl, S. G. Louie, M. P. Zaletel, M. F. Crommie and F. Wang, *"Imaging tunable Luttinger liquid systems in van der Waals heterostructures"*, Nature 631 (8022), 765-770 (2024). 10.1038/s41586-024-07596-6
5. C. Zhang, T. Zhu, S. Kahn, T. Soejima, K. Watanabe, T. Taniguchi, A. Zettl, F. Wang, M. P. Zaletel and M. F. Crommie, *"Manipulation of chiral interface states in a moiré quantum anomalous Hall insulator"*, Nature Physics 20 (6), 951-956 (2024). 10.1038/s41567-024-02444-w
6. E. C. Regan, Z. Lu, D. Wang, Y. Zhang, T. Devakul, J. H. Nie, Z. Zhang, W. Zhao, K. Watanabe, T. Taniguchi, S. Tongay, A. Zettl, L. Fu and F. Wang, "Spin transport of a doped Mott insulator in moiré heterostructures", Nature Communications 15 (1), 10252 (2024). 10.1038/s41467-024-54633-z
7. Q. Feng, C. B. Uzundal, R. Guo, C. Sanborn, R. Qi, J. Xie, J. Zhang, J. Wu and F. Wang, *"Femtojoule optical nonlinearity for deep learning with incoherent illumination"*, Science Advances 11 (5), eads4224. 10.1126/sciadv.ads4224
8. Xiang, Z.; Li, H.; Xiao, J.; Naik, M. H.; Ge, Z.; He, Z.; Chen, S.; Nie, J.; Li, S.; Jiang, Y.; Sailus, R.; Banerjee, R.; Taniguchi, T.; Watanabe, K.; Tongay, S.; Louie, S. G.; Crommie, M. F.; Wang, F. Quantum Melting of a Disordered Wigner Solid. *arXiv:1306.4972. Science* 2025, *388* (6748), 736-740, DOI: 10.1126/science.ado7136
9. J. Xie, Z. Zhang, H. Zhang, V. Nagarajan, W. Zhao, H.-L. Kim, C. Sanborn, R. Qi, S. Chen, S. Kahn, K. Watanabe, T. Taniguchi, A. Zettl, M. F. Crommie, J. Analytis and F. Wang, *"Low Resistance Contact to P-Type Monolayer WSe2"*, Nano Letters 24 (20), 5937-5943 (2024). 10.1021/acs.nanolett.3c04195
10. Z. He, S. P. Poudel, S. Stolz, T. Wang, A. Rossi, F. Wang, S.-K. Mo, A. Weber-Bargioni, Z. Q. Qiu, S. Barraza-Lopez, T. Zhu and M. F. Crommie, *"Synthesis and Polymorph Manipulation of FeSe2 Monolayers"*, Nano Letters 24 (28), 8535-8541 (2024). 10.1021/acs.nanolett.4c01286

Optical sensing and melting of Wigner crystals in 2D heterostructures

You Zhou, *University of Maryland*

Keywords: Electronic structure, Optical & microwave phenomena/Optoelectronics, Phase transitions/Quantum phase transitions, 2-dimentional system/Transition metal dichalcogenides, Strongly correlated systems

Research Scope

This project focuses on the study and control of collective electronic and excitonic phases that emerge in 2D heterostructures due to the interplay between quantum fluctuations and strong correlation effects. In the past year, we have made significant progress in demonstrating (1) quantum anomalous Hall effect in twisted WSe_2 [1], (2) quantum confinement of excitons by twisted hBN interface [2], and (3) optical sensing and control of Wigner crystals (WC) in WSe_2 [3]. Here, we primarily focus on the third part regarding recent progress regarding the WCs.

Wigner crystals (WCs) are prototypical correlated electron states that provide a platform to explore how the interplay between electron correlations and quantum fluctuations drives quantum phase transitions. Despite their significance, studies of zero-(magnetic)-field WCs have remained limited, with notable recent advances primarily in $MoSe_2$ [4-6]. Here, we not only introduce a new material system for investigating WCs but also reveal fundamentally new approaches to control their quantum phase transitions through optical excitation.

Recent Progress

Over the past year, we have successfully investigated the formation and melting of Wigner crystals (WC) in monolayer WSe_2 at zero magnetic field. Remarkably, we also demonstrate the control of the spins in WCs and the melting of WCs via optical excitation. Our study provides crucial insights into the fundamental physics of strongly correlated electronic states in 2D materials, representing a significant advancement in the optical detection and manipulation of these elusive phases.

We fabricate a device consisting of a monolayer WSe_2 encapsulated inside hBN with graphite serving as the gate electrode. We then vary the gate voltage to induce both electrons and holes, and investigate the possible formation of WCs by detecting the Umklapp scattering of excitons. In particular, the WC induces a periodic potential for excitons that folds high-momentum dark excitons into the light cone and produces an additional bright exciton resonance. This Umklapp process produces distinct spectral features that can be directly observed in the reflectance contrast spectra and in their voltage and energy derivatives. **Figure 1** shows the voltage derivative of the reflectance contrast, where a clear secondary resonance is observed at higher energies above the RP peak. This feature exhibits a pronounced blueshift with increasing doping density and

becomes indiscernible at carrier densities above $n_c > 10^{12}$ cm^{-2} where the WC melts via the quantum phase transition.

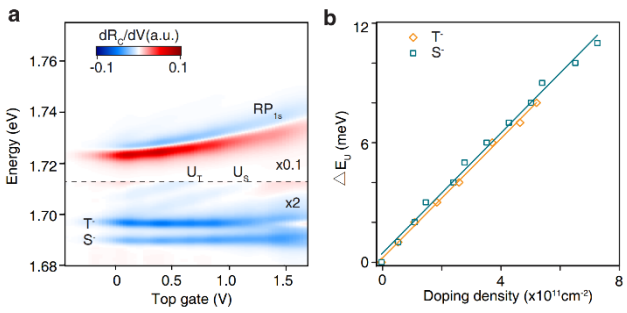


Figure 1. Umklapp of excitons and polarons in WSe_2. a, The voltage derivative of the reflectance contrast (dR_C/dV) in the low-density electron-doped regime. S^- and T^- donate singlet and triplet, respectively. The weak, higher energy resonance above the repulsive polaron RP_{1s} is due to Umklapp scattering of the excitons off the WC. **b**, Energy splitting ΔE_U between attractive polaron and Umklapp peak determined as a function of doping density.

Remarkably, in addition to the Umklapp resonance of RP, we observe for the first time the Umklapp replicas of attractive polarons. Specifically, two higher-energy resonances appear above the T^- and S^- states, which we denote as U_T and U_S, respectively. These Umklapp features shift almost linearly with density, albeit with a smaller slope compared to U_{RP}. In the limit of weak exciton–electron interactions, ΔE_U is set by the exciton kinetic energy $\hbar^2 {k_W}^2/(2m_X)$ where $\hbar$ is reduced Planck constant and m_X is the exciton mass. This allows us to directly measure the mass of repulsive and attractive polarons, which we find to be one-third larger than the exciton mass, for the first time.

Optical spin polarization of WC

The ground state of WC can host magnetic ordering, which would have a profound impact on the interactions between WC and excitons. However, the expected magnetic ordering temperatures of WC are extremely low, making it difficult to directly probe exciton–WC interactions in a spin-ordered phase without applying an external magnetic field.

Here, we demonstrate the optical control of WC spin polarization and explore how excitons interact with spin-ordered electron arrays (**Fig. 2a**). To do this, we excite the system using circularly polarized light and measure the reflectance spectra under different polarization configurations. We find that such circular pumping can induce strong spin polarization in electron-doped WSe_2, possibly due to distinct scattering dynamics between inter-valley and intra-valley processes, although the exact mechanism remains under investigation.

As shown in **Fig. 2b**, under co-circular polarization, the reflectance is dominated by the triplet feature, while under cross-circular polarization, the singlet feature becomes dominant (**Fig. 2c**). This behavior indicates that electrons become strongly spin-polarized in the -K valley when excitons are continuously pumped into the K valley under co-polarization and -K valley under cross-polarization. Remarkably, the Umklapp feature also displays strong spin selectivity: with

electrons polarized in the -K valley, excitons in the K valley can scatter only via inter-valley processes, resulting in a single Umklapp peak U_T under co-polarization.

Interestingly, this valley- and spin-dependent scattering behavior differs markedly between the AP and RP branches. **Figure 2d** presents line cuts of the dR_C/dV spectra, comparing spin-polarized and unpolarized WCs at a fixed doping level. While the AP branches exhibit distinct changes in scattering under spin-polarized conditions (stronger T^-/U_T under co-polarization and stronger S^-/U_S under cross-polarization), the Umklapp scattering of the RP branch remains largely unaffected.

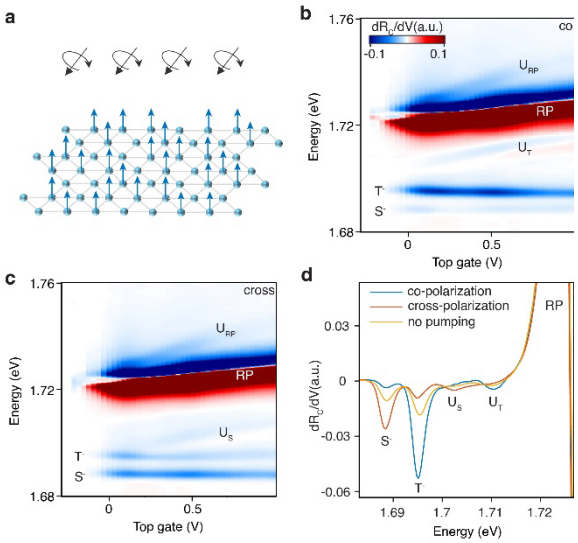


Figure 2. Optical control of WC spin. a, A schematic of optical control of WC spin polarization via circular pumping. **b, c,** The voltage derivative of the reflectance contrast (dR_C/dV) under **b,** co-circular and **c,** cross-circular polarization configuration. **d**, Representative line cuts of the dR_C/dV spectra, comparing spin-polarized (blue and orange lines) and unpolarized (yellow line) WCs at a fixed doping level.

Optical melting of WC

Finally, we demonstrate the optical melting of the Wigner crystal by tuning the exciton density. To achieve this, we excite the system using a pulsed supercontinuum laser with a pulse duration of approximately 100 ps and a repetition rate of 40 MHz. The laser energy is spectrally filtered to lie below the free-carrier bandgap of WSe_2, while still covering the exciton resonance. This approach allows us to selectively excite excitons without generating a significant number of free carriers, while simultaneously measuring their reflectance spectrum.

Figure 3a and 3b show the dR_C/dV maps of monolayer WSe_2 under increasing laser pump powers. As shown, the Umklapp resonance of RP state becomes significantly weaker under a pump power of 1000 nW. A complete disappearance of the U_{RP} resonance is observed when the pump power is increased over 4000 nW, indicating the melting of the Wigner crystal.

The melting of the Wigner crystal observed under optical pumping cannot be attributed solely to laser-induced heating or carrier injection. Instead, our results suggest that excitons themselves can destabilize the Wigner crystal by screening the Coulomb potential and weakening electron correlations. To quantify this effect, we convert the optical pump power into an estimated exciton density and examine how the critical electron density for Wigner crystallization, n^*, evolves as a function of exciton density (**Fig. 3c**). We estimate that bright exciton densities near the optical pump threshold reach $\sim 10^9$ cm^{-2}—far below the Wigner crystallization threshold, indicating they alone cannot melt the Wigner crystal.

However, strong spin–orbit coupling in monolayer WSe_2 leads to a high population ($\sim 10^{12}$ cm^{-2}) of long-lived, spin-forbidden dark excitons, whose density is comparable to critical densities of WC. These dark excitons effectively screen electron–electron interactions,

significantly weakening correlations and triggering Wigner crystal melting, even at low temperatures and without thermal effects—offering a new, optically driven pathway for quantum phase transitions.

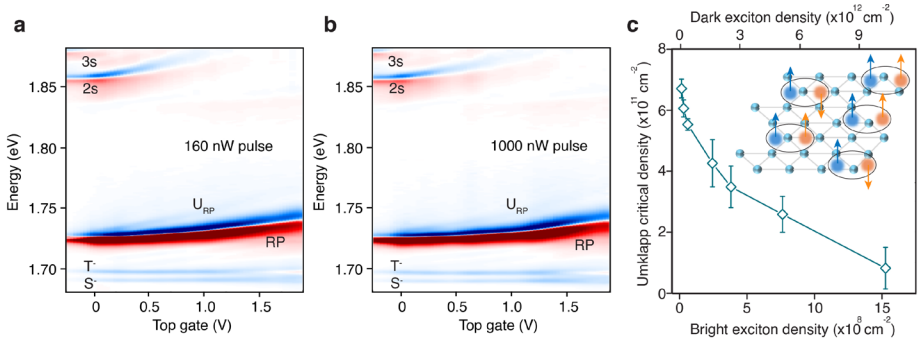


Figure 3. Optical melting of WC. a-b, The voltage derivative of the reflectance contrast (dR_C/dV) of monolayer WSe_2 in the low-density electron-doped regime under pulsed pumping of 160 nW (**a**) and 1000 nW (**b**). **c**, The critical electron density for Wigner crystallization as a function of estimated injected exciton density under pulsed pumping.

Future Plans

The optical probing and manipulation of zero-field Wigner crystals open exciting avenues for developing novel optoelectronic and quantum devices that leverage valleytronics and spintronics in spontaneously formed electron lattices. Currently, we are coupling Wigner crystals in bilayer structures composed of materials with distinct carrier types and effective masses, such as $MoSe_2$ and WSe_2, to study the formation of novel collective WC lattices, exciton condenstes, and supersolids.

References

1. B. Gao, M. Ghafariasl, M. J. Mehrabad, T.-S. Huang, L. Zhang, D. Session, P. Upadhyay, R. Ma, G. Alshalan, D. Suarez-Forero, S. Sarkar, S. Park, J. Houk, K. Watanabe, T. Taniguchi, M. Xie, Y. Zhou, and M. Hafezi, *Probing quantum anomalous Hall states in twisted bilayer WSe_2 via attractive polaron spectroscopy*, arXiv:2504.11530 (2025).
2. L. Gu, L. Zhang, S. Felsenfeld, B. Gao, R. Ma, S. Park, H. Jang, K. Watanabe, T. Taniguchi, and Y. Zhou, *Quantum confining excitons with electrostatic moiré superlattices*, Physical Review Letters **135**, 026901 (2025).
3. L. Zhang, L. Gu, R. Ni, S. Park, H. Jang, K. Watanabe, T. Taniguchi, I. Esterlis, A. Imamoglu, R. Schmidt, and Y. Zhou, *Optical sensing and melting of Wigner crystals*, in preparation (2025).
4. T. Smoleński, P. E. Dolgirev, C. Kuhlenkamp, A. Popert, Y. Shimazaki, P. Back, X. Lu, M. Kroner, K. Watanabe, T. Taniguchi, I. Esterlis, E. Demler, and A. Imamoğlu, *Signatures of Wigner crystal of electrons in a monolayer semiconductor*, Nature **595**, 53–57 (2021).
5. Y. Zhou, J. Sung, E. Brutschea, I. Esterlis, Y. Wang, G. Scuri, R. J. Gelly, H. Heo, T. Taniguchi, K. Watanabe, G. Zaránd, M. D. Lukin, P. Kim, E. Demler, and H. Park, *Bilayer Wigner crystals in a transition metal dichalcogenide heterostructure*, Nature **595**, 48–52 (2021).
6. Z. Xiang, H. Li, J. Xiao, M. H. Naik, Z. Ge, Z. He, S. Chen, J. Nie, S. Li, Y. Jiang, R. Sailus, R. Banerjee, T. Taniguchi, K. Watanabe, S. Tongay, S. G. Louie, M. F. Crommie, and F. Wang, *Imaging quantum melting in a disordered 2D Wigner solid*, Science **388**, 736–740 (2025).

Publications

1. B. Gao, M. Ghafariasl, M. J. Mehrabad, T.-S. Huang, L. Zhang, D. Session, P. Upadhyay, R. Ma, G. Alshalan, D. Suarez-Forero, S. Sarkar, S. Park, J. Houk, K. Watanabe, T. Taniguchi, M. Xie, Y. Zhou, and M. Hafezi, *Probing quantum anomalous Hall states in twisted bilayer WSe_2 via attractive polaron spectroscopy*, arXiv:2504.11530 (2025).
2. F. de Abajo, et al., *Roadmap for photonics with 2D materials*, arXiv:2504.04558 (2025).
3. L. Gu, L. Zhang, S. Felsenfeld, B. Gao, R. Ma, S. Park, H. Jang, K. Watanabe, T. Taniguchi, and Y. Zhou, *Quantum confining excitons with electrostatic moiré superlattices*, Physical Review Letters **135**, 026901 (2025).
4. L. Gu and Y. Zhou, *Nonlinear optics in 2D materials: from classical to quantum*, Applied Physics Reviews **12**, 011335 (2025).
5. S. Sarkar, M. J. Mehrabad, D. G. Suárez-Forero, L. Gu, C. Flower, L. Xu, K. Watanabe, T. Taniguchi, S. Park, J. Houk, Y. Zhou, and M. Hafezi, *Sub-wavelength optical lattice in 2D materials*, Science Advances **11**, eadv2023 (2025).
6. J. Sung, J. Wang, I. Esterlis, P. A. Volkov, G. Scuri, Y. Zhou, E. Brutschea, T. Taniguchi, K. Watanabe, Y. Yang, M. Morales, S. Zhang, A. J. Millis, M. D. Lukin, P. Kim, E. Demler, and H. Park, *Observation of an electronic microemulsion phase emerging from a quantum crystal-to-liquid transition*, Nature Physics **21**, 437–443 (2025).
7. D. G. Suárez-Forero, R. Ni, S. Sarkar, M. J. Mehrabad, E. Mechtel, V. Simonyan, A. Grankin, K. Watanabe, T. Taniguchi, S. Park, H. Jang, M. Hafezi, and Y. Zhou, *Chiral flat-band optical cavity with atomically thin mirrors*, Science Advances **10**, eadr5904 (2024).
8. L. Zhang, L. Gu, R. Ni, M. Xie, S. Park, H. Jang, R. Ma, T. Taniguchi, K. Watanabe, and Y. Zhou, *Electrical control and transport of tightly bound interlayer excitons in a $MoSe_2$/hBN/$MoSe_2$ heterostructure*, Physical Review Letters **132**, 216903 (2024).
9. L. Gu, L. Zhang, R. Ni, M. Xie, D. S. Wild, S. Park, H. Jang, T. Taniguchi, K. Watanabe, M. Hafezi, and Y. Zhou, *Giant optical nonlinearity of Fermi polarons in atomically thin semiconductors*, Nature Photonics **18**, 816–822 (2024).
10. Gao, D. G. Suarez-Forero, S. Sarkar, T. S. Huang, D. Session, M. J. Mehrabad, R. Ni, M. Xie, J. Vannucci, S. Mittal, K. Watanabe, T. Taniguchi, A. Imamoglu, Y. Zhou, and M. Hafezi, *Excitonic Mott insulator in a Bose-Fermi-Hubbard system of moiré WS_2/WSe_2 heterobilayer*, Nature Communications **15**, 2305 (2024).

Tuning Magnetic Symmetries in a Moiré Magnet

Liuyan Zhao, *University of Michigan, Ann Arbor*

Keywords: moiré superlattice, two-dimensional magnetism, phase transition, symmetry breaking, Raman and magnetic circular dichroism optical spectroscopy

Research Scope

Moiré magnetic superlattices, formed by vertically stacking two lattice- or angular-mismatched two-dimensional (2D) magnetic crystals, have been theoretically predicted to realize novel magnetic phases and furthermore topological electronic phases. Recently, there have been exciting experimental progress made in moiré magnets including twisted CrI_3 and twisted CrSBr, including the work from the PI's group [1,2]. Yet, despite these experimental advances, tuning symmetry breaking and therefore designing desired moiré magnetic phases remain limited, because twisted 2D magnets, such as rhombohedral (R)-stacked twisted CrI_3, largely inherit the magnetic properties and symmetries from their constituent layers.

This current work aims to approach the identified challenge above by studying hexagonal (H)-stacked twisted double bilayer (tDB) CrI_3. Due to the presence of ligand I atoms, individual layer CrI_3 only possess three-fold rotational (C_3) symmetry, rather than six-fold one (C_6) that the Cr lattice seemingly has. As a result, stacking CrI_3 around 0 degree (R-stack) is fundamentally different from doing that around 180 degrees (H-stack), and the atomic registry for I at the interface of two CrI_3 layers is clearly different between R- and H-stacked twisted CrI_3. These further lead to distinct mechanical, electronic, and magnetic properties between these two types of twisted CrI_3.

In this current work, we fabricated H-stacked tDB CrI_3 at a range of twist angles from 180° to 190°, and then, used a suite of experimental techniques, in combination of first-principles and continuum model theory, to understand their structural and magnetic properties (Figure 1) [3].

Structurally, we used selected area electron diffraction (SAED) to show the presence of sharp, well-defined moiré superlattice peaks surviving up to the high orders, proving a much higher moiré crystalline quality than the R-stacked counterpart. Our first-principles calculations identify the sole low energy stacking site (i.e., monoclinic) in H-stacked tDB CrI_3 to be the origin for this improvement in moiré superlattice quality, which contrasts with two low energy stacking sites (i.e., rhombohedral and monoclinic) in the R-stacked case.

Magnetically, we used a combination of scanning magnetic circular dichroism (MCD) microscopy and scanning NV magnetometry to show a homogeneous magnetic ground state with nearly zero net magnetization in H-stacked tDB CrI_3 of twist angle between 181° and 185° while exhibiting features that make them different from two decoupled CrI_3. We then focused on magnetic symmetry analysis with linearly polarized and circularly-polarized micro-Raman spectroscopy. From the linear basis Raman spectra, we observed broken rotational and mirror symmetries; and

from the circular basis Raman spectra, we detected broken time-reversal symmetry, below the magnetic phase transition. All these broken symmetries in the magnetic phase were detected over a twist angle range of 181° – 185° but no longer observed for angles greater than 185°.

To understand the cause of these surprising broken symmetries in H-stacked tDB CrI_3, we used continuum model to build a magnetic phase diagram as parameters of twist angle and magnetic anisotropy for the interfacial layers, while the other parameters are fed in with first-principles and experimental values. For a low twist angle with reduced magnetic anisotropy, we identify a moiré magnetic phase that exhibits all the broken symmetries and has nearly zero total magnetization. We reason the reduction in magnetic anisotropy from the interfacial I ligand cage distortion.

In summary, this current work shows H-stacked tDB CrI_3 as a promising platform for moiré magnetism that are substantially distinct from their composing 2D magnets.

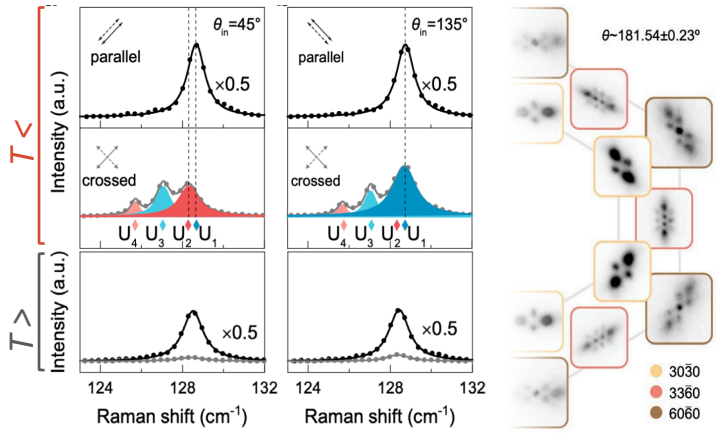


Figure 1. In hexagonal-stacked twisted double bilayer (H-tDB) CrI_3 whose twist angle is 180°+, the moiré superlattice quality is exceptionally high (right, electron diffraction patterns present up to multiple orders), and consequently, the moiré magnetic phase feature a whole series of broken symmetry that are absent in both natural bilayer/four-layer CrI_3 and rhombohedral (R)-stacked tDB CrI_3 at 0°+ (left, Raman spectroscopy in circular Raman spectroscopy).

Recent Progress

The PI's group is working on two more projects on the topic of optical spectroscopy studies of moiré and 2D magnetism.

1. <u>Moiré magnons in H-tDB CrI_3</u>.

Spin waves, or magnons, are collective excitations of ordered magnetic phases, and have characteristic momentum-dependent energy dispersion, namely, magnon band structure. Similar as the moiré electronic potential folding the electronic bands to modify the electronic band dispersion, the moiré magnetic exchange coupling is expected to create folded magnon bands and renormalize magnon band dispersion. However, moiré magnons have not been experimentally realized in any studied moiré magnets, primarily due to the incoherence of the moiré superlattices and the weakness of the moiré exchange coupling.

In H-tDB CrI_3, we have shown the high moiré crystalline quality and provided evidence of strong impact of moiré exchange coupling in the magnetic ground state. Building upon this,

we reason that H-tDB CrI_3 is a promising platform to realize and investigate moiré magnon. Using circularly polarized Raman spectroscopy, we have seen multiple additional magnon modes in 181° H-tDB CrI_3, both at 0T and 3T, as compared to Raman spectra of bilayer and four-layer CrI_3. Magnetic field dependence of these modes further confirms their magnon nature via their Zeeman shift and reveal differences between these magnon modes.

Same magnon spectra have been taken in H-tDB CrI_3 over a twist angle range of 180° – 190°. Ongoing analysis and calculations are made to understand these extra magnon modes and investigate their relationship with the moiré superlattices.

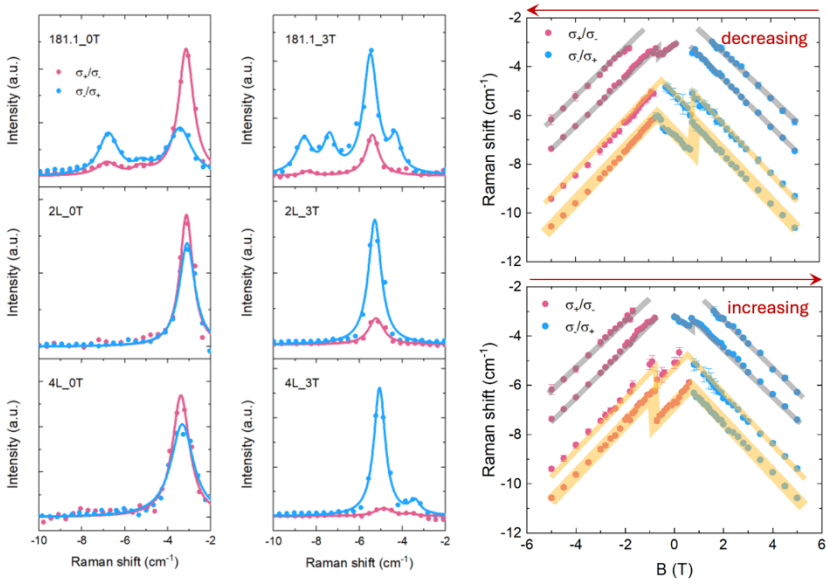


Figure 2. Raman spectroscopy for the magnon modes taken in 181.1° tDB CrI_3, bilayer (2L), and four-layer (4L) CrI_3, respectively, at both 0T (left) and 3T (middle), reveal additional magnon modes in 181.1° tDB CrI_3. Additionally, the magnetic field dependence of the magnon modes in 181.1° tDB CrI_3, for increasing and decreasing fields (right) confirms their magnon nature and show the differences and similarities between the four identified magnon modes.

2. <u>Tuning magnetic toroidicity and electric polarity in bilayer CrSBr</u>.

In this project, we are interested in understanding the magnetic state of bilayer CrSBr under magnetic fields. Without any magnetic field, bilayer CrSB realizes a layered antiferromagnetic (AFM) order where the spins algin ferromagnetically (FM) along the b-axis within layers, and antiferromagnetically between adjacent layers. Interestingly, this layered AFM order exhibits a magnetic toroidal moment that is a pseudovector along the a-axis. With the magnetic field applied along the c-axis, the spins in both layers cant towards the field direction, reducing the AFM order and equivalently the magnetic toroidicity but introducing an electric polarization along the b-axis according to the Katsura–Nagaosa–Balatsky mechanism.

We set up to measure the magnetic field dependent rotation anisotropy (RA) second harmonic generation (SHG) for bilayer CrSBr. We manage to extract the SHG susceptibility tensor elements, and furthermore, group them into two sets – one scales with the magnetic toroidal order parameter (equivalent, AFM order parameter), and the other is proportional to

the electric polarization order parameter (Figure 3). While the toroidal order parameter shows a monotonic decrease, the electric polarization order parameter maximizes at the field where the spins in the two layers are 90° rotated from each other. Their field dependencies are nicely explained by a simple model assuming the out-of-plane magnetization scales linearly with the applied out-of-plane magnetic field [4].

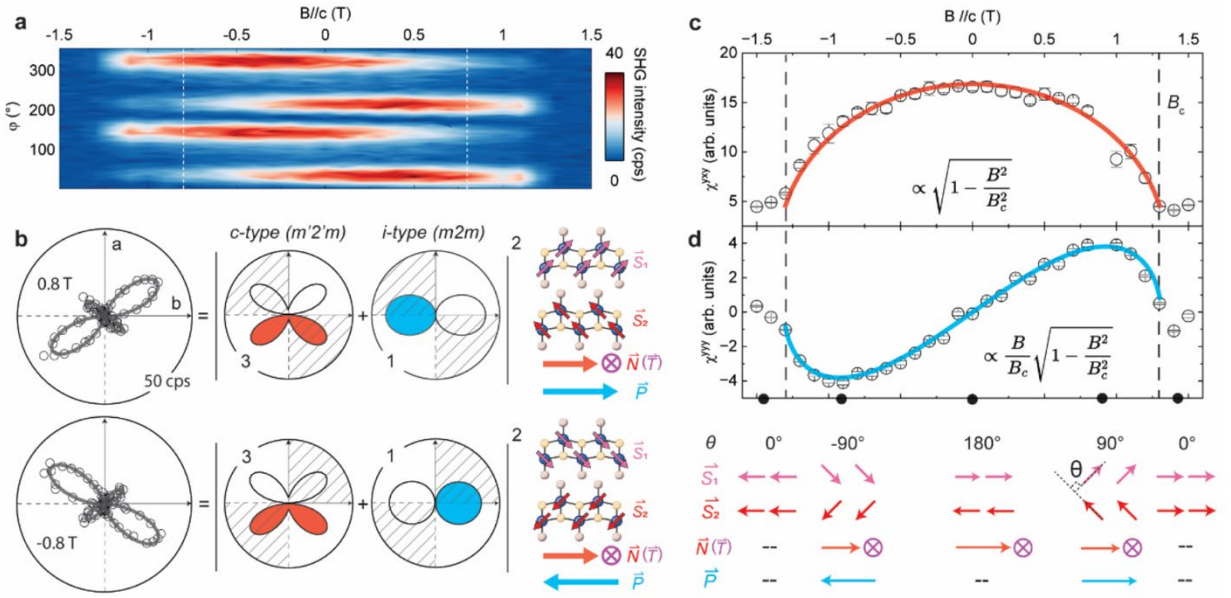


Figure 3. a. Magnetic field dependence of RA SHG for bilayer CrSBr taken at 80K. b. Decomposition of RA SHG into two contributions, one for the magnetic toroidal order (equivalently, AFM order) and the other for the electric polarization. c. magnetic field dependence of the two identified contributions (top), and cartoon diagram for the spin state, together with the toroidal moment and electric polarization for selected magnetic fields.

Future Plans

In the coming year, we plan to (1) resolve the origin of the extra magnons observed in H-tDB CrI_3; (2) study 90° twisted CrSBr bilayers. We have preliminary results showing that 90° twisted CrSBr bilayer is multiferroic. We plan to investigate it and its collective excitations.

References

1. H. Xie, X. Luo, G. Ye, Z. Ye, H. Ge, S. H. Sung, E. Rennich, S. Yan, Y. Fu, S. Tian, H. Lei, R. Hovden, K. Sun, R. He, L. Zhao "Twist engineering of the two-dimensional magnetism in double bilayer chromium triiodide homostructures" **Nature Physics** 18, 30 (2022)
2. H. Xie, X. Luo, Z. Ye, Z. Sun, G. Ye, S.-H. Sung, H. Ge, S. Yan, Y. Fu, S. Tian, H. Lei, K. Sun, R. Hovden, R. He, L. Zhao "Evidence of Noncollinear Spin Texture in Magnetic Moiré Superlattices" **Nature Physics**, 19, 1150 (2023)
3. Z. Sun, G. Ye, X. Wan, N. Mao, C. Nnokwe, S. Li, n. Agarwal, S. Sarkar, Z. Zhai, B. Lv, R. Hovden, C. R. Du, Y. Zhang, K. Sun, R. He, L. Zhao "Tunable symmetry breaking in a hexagonal-stacked moiré magnet" under revision at **Nature Physics** (2025)
4. Chuangtang Wang, Xiaoyu Guo, Zixin Zhai, Sang-Wook Cheong, Bing Lv, Liuyan Zhao "Tuning Magnetic Toroidicity and Electric Polarity in a Bilayer Antiferromagnet" under consideration at **Nature** (2025)

Publications

1. F. Chen, K. Das, B. Yang, C. Wang, S. Zhong, D. Golovanova, H. Ren, T. Wang, X. Luo, Y. Sun, L. Zhao, G.-X. Miao, B. Yan, A. W. Tsen "Direct observation of distinct bulk and edge nonequilibrium spin accumulation in ultrathin $MoTe_2$" **Nature Communications** 16, 6132 (2025)
2. F. J. G. de Abajo, D. N. Basov, F. H. L. Koppens, L. Orsini, M. Ceccanti, S. Castilla, L. Cavicchi, M. Polini, P. A. D. Gonçalves, A. T. Costa, N. M. R. Peres, N. A. Mortensen, S. Bharadwaj, Z. Jacob, P. J. Schuck, A. N. Pasupathy, M. Delor, M. K. Liu, A. Mugarza, P. Merino, M. G. Cuxart, E. Chávez-Angel, M. Svec, L. H. G. Tizei, F. Dirnberger, H. Deng, C. Schneider, V. Menon, T. Deilmann, A. Chernikov, K. S. Thygesen, Y. Abate, M. Terrones, V. K. Sangwan, M. C. Hersam, L. Yu, X. Chen, T. F. Heinz, P. Murthy, M. Kroner, T. Smolenski, D. Thureja, T. Chervy, A. Genco, C. Trovatello, G. Cerullo, S. Dal Conte, D. Timmer, A. De Sio, C. Lienau, N. Shang, H. Hong, K. Liu, Z. Sun, L. A. Rozema, P. Walther, A. Alù, M. Cotrufo, R. Queiroz, X.-Y. Zhu, J. D. Cox, E. J. C. Dias, Á. R. Echarri, F. Iyikanat, A. Marini, P. Herrmann, N. Tornow, S. Klimmer, J. Wilhelm, G. Soavi, Z. Sun, S. Wu, Y. Xiong, O. Matsyshyn, R. Krishna Kumar, J. C. W. Song, T. Bucher, A. Gorlach, S. Tsesses, I. Kaminer, J. Schwab, F. Mangold, H. Giessen, M. S. Sánchez, D. K. Efetov, T. Low, G. Gómez-Santos, T. Stauber, G. Álvarez-Pérez, J. Duan, L. Martín-Moreno, A. Paarmann, J. D. Caldwell, A. Y. Nikitin, P. Alonso-González, N. S. Mueller, V. Volkov, D. Jariwala, T. Shegai, J. van de Groep , A. Boltasseva, I. V. Bondarev, V. M. Shalaev, J. Simon, C. Fruhling, G. Shen, D. Novko, S. Tan, B. Wang, H. Petek, V. Mkhitaryan, R. Yu, A. Manjavacas, J. E. Ortega, X. Cheng, R. Tian, D. Mao, D. Van Thourhout, X. Gan, Q. Dai, A. Sternbach, Y. Zhou, M. Hafezi, D. Litvinov, M. Grzeszczyk, K. S. Novoselov, M. Koperski, S. Papadopoulos, L. Novotny, L. Viti, M. S. Vitiello, N. D. Cottam, B. T. Dewes, O. Makarovsky, A. Patanè, Y. Song, M. Cai, J. Chen, D. Naveh, H. Jang, S. Park, F. Xia, P. K. Jenke, J. Bajo, B. Braun, K. S. Burch, L. Zhao, X. Xu "Roadmap for Photonics with 2D Materials" **ACS Photonics** doi: 10.1021/acsphotonics.5c00353 (2025)
3. S. Li, Z. Sun, N. J. McLaughlin, A. Sharmin, N. Agarwal, M. Huang, S. H. Sung, H. Lu, S. Yan, H. Lei, R. Hovden, H. Wang, H. Chen, L. Zhao, C. R. Du "Observation of stacking engineered magnetic phase transitions within moiré supercells of twisted van der Waals magnets" **Nature Communications** 15, 5712 (2024)
4. Z. Sun, G. Ye, X. Wan, N. Mao, C. Nnokwe, S. Li, n. Agarwal, S. Sarkar, Z. Zhai, B. Lv, R. Hovden, C. R. Du, Y. Zhang, K. Sun, R. He, L. Zhao "Tunable symmetry breaking in a hexagonal-stacked moiré magnet" under revision at **Nature Physics** (2025)
5. Chuangtang Wang, Xiaoyu Guo, Zixin Zhai, Sang-Wook Cheong, Bing Lv, Liuyan Zhao "Tuning Magnetic Toroidicity and Electric Polarity in a Bilayer Antiferromagnet" under consideration at **Nature** (2025)
6. Q. Li, X. Wan, S. Li, A. Afrey, W. Alpers, Y. Yang, I. Wladyszewska, C. W. Beach, W. Liu, S. Cundiff, L. Zhao, B. Lv, C. R. Du, K. Sun, H. Deng "Twist-engineering of anisotropic excitonic and optical properties of a two-dimensional magnetic semiconductor" submitted (2025)

Coherent Exciton-Magnon-Photon interaction in van der Waals magnet CrSBr

Vinod Menon, *City College of New York*

Keywords: Excitons, Magnons, 2D magnets, Polaritons

Research Scope

van der Waals (vdW) magnetic semiconductors that host excitons that show a strong correlation to underlying magnetic order present a unique opportunity to realize strong interaction between magnons, excitons and photons. Furthermore, these systems facilitate the optical control of electronic and spin degrees of freedom. Under this project, we are investigating the vdW magnetic semiconductor CrSBr which is a layered antiferromagnet below 132K hosting magnons in the GHz frequency range and excitons in the near infrared.[1] In addition, owing to the large dielectric constant, the excitons in CrSBr are dressed by photons creating self-hybridized polariton states.[2] This aspect allows the control of magneto-optical response by tuning the photon fraction of the polariton states as well as the signature of coherent magnon oscillations imprinted on them. More recently, we investigated the role of magnons on nonlinear exciton-exciton interaction in CrSBr.[3] Unusually large nonlinear exciton and polariton interaction was observed when the exciton-magnon coupling was strongest.

Ongoing work includes the investigation of polariton condensation in CrSBr cavities under optical excitation and microwave spectroscopy of magnons in CrSBr.

Recent Progress

Magnon mediated exciton-exciton interaction: (*Nature Materials* 2025)

Recently we demonstrated the role of magnons in the interaction between excitons in CrSBr as shown schematically in Fig. 1a. The work started with our discovery of a higher energy exciton (X_H) at 1.7 eV compared to the more commonly studied 1.3 eV lower energy exciton (X_L). This exciton was found to have stronger correlation to magnetic order owing to its more Wannier-like character. Resonant nonlinear experiments were carried out to establish the nonlinear exciton-exciton interaction. At zero magnetic field, both the X_L and X_H did not show much nonlinearity indicative of the small Bohr radius of the excitons. However, upon application of finite magnetic field, it was found that the higher energy exciton (X_H) shows significant energy shift under optical excitation upon application of intermediate magnetic field as shown in Fig. 1b. This indicates that the canted spins where the magnon oscillation amplitude is largest shows the higher nonlinear interaction. Transient pump-probe measurements also showed the larger magnon oscillation amplitude at these intermediate magnetic fields indicating the stronger exciton-magnon coupling. These results show the role of magnons in the exciton-exciton interaction.

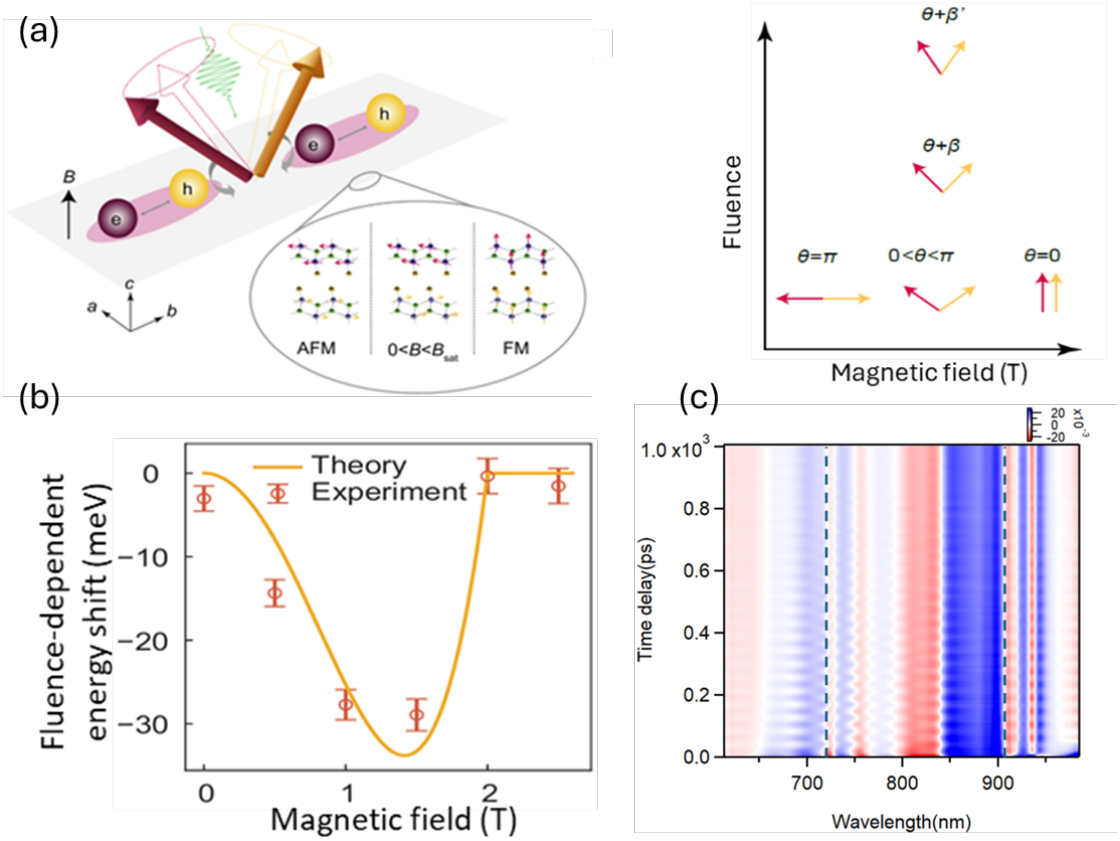


Fig. 1. a) Schematic of exciton–exciton interactions in CrSBr mediated by magnons under a perpendicular magnetic field along with cartoon showing the mechanism of fluence dependence on interlayer spin angle modification. (b) Fluence-dependent energy shift vs. magnetic field showing large shifts for intermediate B fields where the canting angle is largest. (c) Magnon dynamics investigated via polaritons. The dashed lines indicate the energies of the bare excitons.

As a follow up to this work, we are currently investigating the nonlinearity of magnons and their dynamics as well as the integration of the CrSBr films into high quality factor cavities with the goal to realize polariton condensation. Shown in Fig. 1c is the magnon dynamics probed via excitons and polaritons in CrSBr. The polariton states show higher signal to noise ratio for the magnon oscillations observed in transient spectroscopy.

Future Plans

(i) Integration of CrSBr into high Q cavities to study nonlinear effects in the weak pump limit.

(ii) Microwave spectroscopy of magnons in CrSBr embedded in microwave resonators.

References

1. Bae, Y. J.; Wang, J.; Scheie, A.; Xu, J.; Chica, D. G.; Diederich, G. M.; Cenker, J.; Ziebel, M. E.; Bai, Y.; Ren, H.; Dean, C. R.; Delor, M.; Xu, X.; Roy, X.; Kent, A. D.; Zhu, X. *Exciton-Coupled Coherent Magnons in a 2D Semiconductor,* Nature **609**, 282 (2022), DOI: 10.1038/s41586-022-05024-1
2. Dirnberger, F.; Quan, J.; Bushati, R.; Diederich, G.; Florian, M.; Klein, J.; Sofer, Z.; Xu, X.; Kamra, A.; Alù, A.; Menon, V. M. *Magneto-Optics in a van der Waals Magnet Tuned by Self-Hybridized Polaritons,* Nature **620**, 533 (2023). DOI: 10.1038/s41586-023-06275-2
3. Datta, B., Adak, P.C., Yu, S., Dharmapalan, A.V., Hall, S.H., Vakulenko, A., Komisserenko, F., Kurganov, E., Quang, J., Wang, W., Mosina, K., Sofer, Z., Pashov, D., Schilfgaarde M., Acharya, S., Kamra, A., Sfeir, M., Alu, A., Khanikaev, A., Menon, V.M., *Magnon-mediated exciton–exciton interaction in a van der Waals antiferromagnet,* Nat. Mater. **24**, 1027 (2025). DOI: 10.1038/s41563-025-02183-0

Publications (Year 1)

1. Datta, B., Adak, P.C., Yu, S., Dharmapalan, A.V., Hall, S.H., Vakulenko, A., Komisserenko, F., Kurganov, E., Quang, J., Wang, W., Mosina, K., Sofer, Z., Pashov, D., Schilfgaarde M., Acharya, S., Kamra, A., Sfeir, M., Alu, A., Khanikaev, A., Menon, V.M., *Magnon-mediated exciton–exciton interaction in a van der Waals antiferromagnet,* Nat. Mater. **24**, 102 (2025)

Poster Session I

Exotic Transport Phenomena in Layered Topological Materials

Jin Hu, *University of Arkansas*

Keywords: Topological material; Transport; Localization

Research Scope

Recent breakthroughs in topological quantum materials have transformed our understanding of quantum states of matter. These emergent systems hold enormous potential for identifying, engineering, and controlling a wide range of physical properties, enabling the foundation for next-generation technologies. Electronic correlations drive remarkable phenomena such as high-temperature superconductivity, heavy fermion behavior, and metal-to-insulator transitions. Extending topological quantum physics into the regime of strongly interacting electronic systems is therefore expected to produce entirely new quantum states and exotic physical responses. This project aims to realize this vision by developing novel material platforms and exploring their unconventional electronic states and properties.

Recent Progress

Over the past two years we have made significant progress in discovering exotic electronic transport and understanding the mechanisms in three topological materials and related systems: (1) Field-induced insulator-to-metal transition in GdPS and tuning [1,2]; (2) Large magnetoresistance (MR) arising from coupled degrees of freedom in off-stoichiometric topological materials *Ln*SbTe (*Ln* = Pr, Nd) [3-5]; and (3) Possible Anderson localization in doped Weyl semimetal WTe_2.

(1) Field-induced insulator-to-metal transition in GdPS and tuning

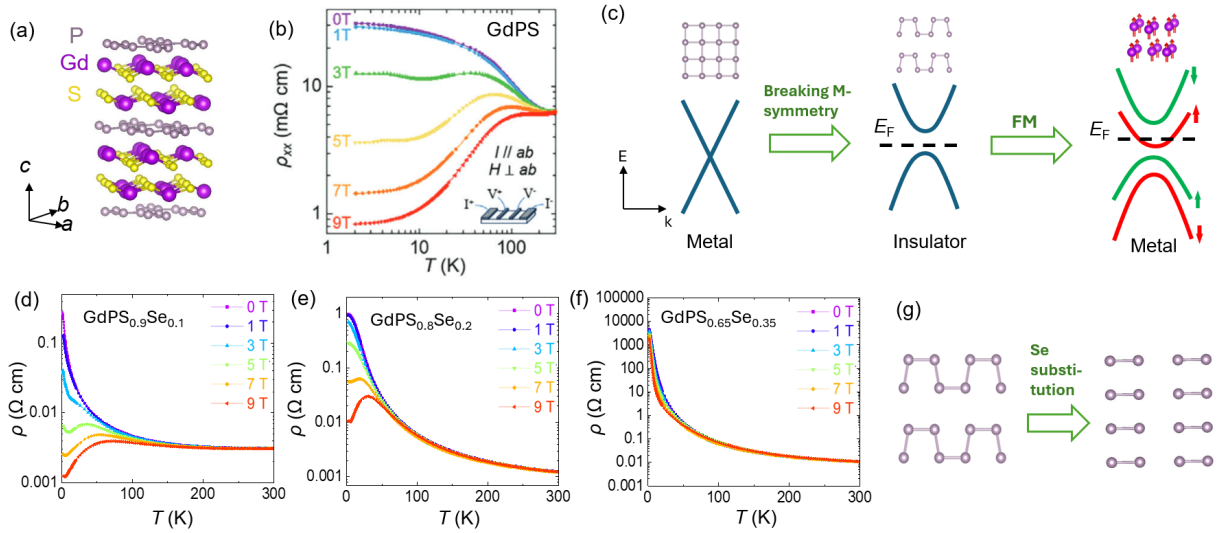


Figure 1 (a) Crystal structure of GdPS. (b) Resistivity measured under various magnetic fields, showing non-metallic behavior at zero field and metallic behavior above 7 T. (c) Multiple metal-insulator-metal transitions in GdPS. (d-f):

Temperature-dependent resistivity under various magnetic fields for substituted GdP($S_{1-x}Se_x$) [2]. (g) Se substitution effect on structure.

GdPS is a layered compound consisting of phosphorus planes sandwiched by Gd-S bilayers (Fig. 1a). Our earlier work [1] established the first observation of a field-induced insulator-to-metal transition, accompanied by a gigantic, isotropic negative magnetoresistance (MR) (Fig. 1b). In GdPS, distortion of the P-layer breaks the mirror symmetry protecting the Dirac nodal-line point, leading to a gapped insulating/semiconducting ground state (Fig. 1c). Applying a magnetic field generates strong on-site *d–f* exchange interactions in Gd, shifting the spin-split Gd *d*-band toward the Fermi level and eventually closes the bandgap (Fig. 1c). This drives a field-induced metallic state and produces gigantic negative MR (Fig. 1b). Notably, such phenomenon is isotropic with respect to field orientation, due to vanishing spin-orbit coupling of the half-filled Gd^{3+} *f*-orbitals.

The combination of isotropic and giant MR is rarely observed and holds promise for technology applications such as omnidirectional sensing. We further investigated the effect of Se substitution in GdPS [2]. As shown in Figs. 1d-f, replacing S with Se enhances the insulating behavior and progressively suppresses the field-induced metallic transition, which disappears entirely at 35% Se substitution. Our structural analysis (Fig. 1g) reveals that those observations are because that Se increases lattice distortion, enlarging the bandgap beyond what can be closed by *d–f* exchange splitting. Thus, lattice symmetry engineering via Se substitution provides a powerful approach to tuning transport and magnetic-field responses in this material system.

(2) Large MR arising from coupled degrees of freedom in off-stoichiometric topological materials *Ln*SbTe (*Ln* = Pr, Nd)

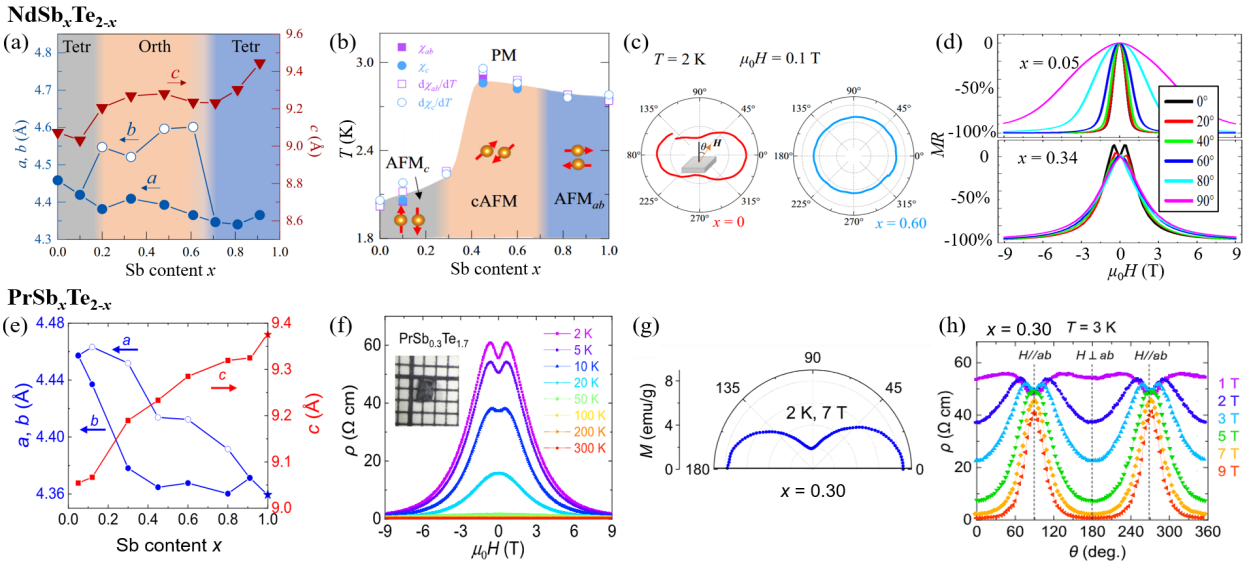


Figure 2 (a-d): Properties of NdSb$_x$Te$_{2-x}$ [3-4]. (a) Evolution of lattice with composition. (b) Evolution of magnetism. (c) Angular dependent magnetization for the x = 0 and 0.6 samples. (d) Normalized MR for the x = 0.05 and 0.34 samples. (e-h): Properties of PrSb$_x$Te$_{2-x}$ [5]. (e) Evolution of lattice with composition. (f) Magnetotransport for x = 0.30. (g) Angular dependent magnetization for the x = 0.30 sample. (h) Angular dependent MR for the x = 0.30 sample.

*Ln*SbTe compounds share structural similarities with GdPS, with Sb layers sandwiched between *Ln*-Te bilayers. Unlike the scenario in GdPS, the Sb-layers retain mirror symmetry, preserving Dirac nodal-line states and giving rise to a topological semimetal state. We successfully synthesized single crystals of $NdSb_xTe_{2-x}$ and $PrSb_xTe_{2-x}$ and characterized their structural, electronic, magnetic, and transport properties.

$NdSb_xTe_{2-x}$ displays composition dependent crystal structure, showing tetragonal phase (space group *P*4/*nmm*) for low- ($x < 0.2$) and high-Sb ($x > 0.7$) samples, and orthorhombic (space group *Pmmn*) phase in the intermediate composition range (Figs. 2a). Despite maintaining an antiferromagnetic (AFM) ground state across all compositions, magnetic moment orientation varies: out-of-plane (AFM_c) for low-Sb and in-plane (AFM_{ab}) for high-Sb contents, while a canted state (cAFM) for intermediate composition range (Fig. 2b). This leads to composition-dependent magnetic anisotropy (Fig. 2c) [1]. Magnetotransport studies [2] reveal correspondingly strong composition-dependent MR, approaching nearly -100% for $x = 0.05$ and 0.34 samples. The angular dependence of MR (Fig. 2d) agrees well with magnetic anisotropy, underscoring the strong coupling between magnetism and transport. Similarly, $PrSb_xTe_{2-x}$ [3] also exhibits a tetragonal-orthorhombic-tetragonal structure evolution (Fig. 2e) with large negative MR up to -50% for the $x = 0.05$ sample and -97% for the $x = 0.30$ samples. The agreement between MR and magnetism is reflected by their similar anisotropies (Figs. 2g & 2h).

Our studies [4,5] reveal that the large negative MR in these off-stoichiometric *Ln*SbTe compounds shares a similar mechanism with GdPS. While stoichiometric *Ln*SbTe remains gapless due to preserved symmetry, off-stoichiometric structure distortions induce charge density wave (CDW) that gaps or partially gaps the electronic states. The type and strength of the CDW depend sensitively on composition, leading to variable bandgaps. Therefore, with appropriate bandgap in certain compositions, field-induced electronic structure engineering can effectively reduce the bandgap, enhancing conductivity and thereby giving rise to large negative MR.

(3) Possible Anderson localization in doped Weyl semimetal WTe_2

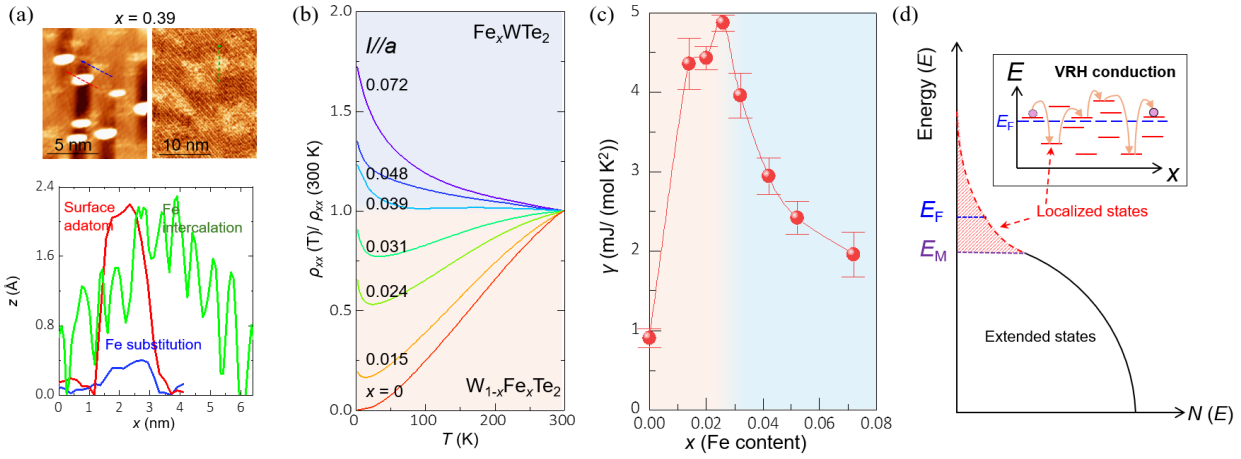


Figure 3 (a) STM observation for the x = 0.39 sample, showing coexistence of substitution and intercalation. (b) Temperature-dependent normalized resistivity of doped WTe_2, revealing a crossover from metallic to localized behavior. (c) Doping dependent Sommerfeld coefficient. (d) Schematic of doping-induced localization.

Another exciting discovery is the possible 3D Anderson localization in Weyl semimetal WTe_2. While Anderson localization has been widely studied in 2D system, examples in 3D crystalline systems are rare. Though Fe-doping, we observed transport signatures consistent with 3D Anderson localization in a Weyl semimetal. We found two doping regimes of Fe-doping in WTe_2: substitutional doping at low-Fe content (< 3%) and coexistence with intercalation for high-Fe levels (> 3%, Fig. 3a). As shown in Fig. 3b, for low Fe content, the system remains metallic at high temperatures and exhibits a low-temperature Kondo effect, characteristic of dilute magnetic doping. In contrast, high Fe content completely suppresses metallicity, with resistivity increasing continuously upon cooling across the entire temperature range. Heat capacity measurements further reveal gradual increase of Sommerfeld coefficient in the low-Fe Kondo region but gradual reduction in the high-Fe region (Fig. 3c). Combined with ARPES measurements, these results indicate that the suppression of metallicity with high-Fe content cannot be caused by significant reconstruction of electronic structure such as gap opening. rule out electronic band reconstruction (e.g., gap opening) as the cause of suppressed metallicity. Instead, the doping-driven metal-to-nonmetal crossover around ~3% Fe, together with variable-range hopping behavior in resistivity, strongly supports the presence of Anderson localization in three dimensions (Fig. 3d). This provides a rare platform to investigate Anderson localization in topological materials.

Future Plans

We will continue to explore novel material systems and uncover exotic transport phenomena arising from coupled degrees of freedom, particularly in the presence of strong electronic interactions. For *Ln*PS, we will extend studies to other rare-earth compounds such as SmPS and NdPS, where different *f*-electron configurations are expected to produce diverse phenomena. For *Ln*SbTe, we will focus on the effect of chalcogen substitution to further tune lattice symmetry, magnetism, and transport. For doped WTe_2, we will deepen our investigation of Anderson localization and its impact on topological fermions, and explore other dopants to reveal additional emergent phenomena.

References

[1] G. Acharya, B. Neupane, C.-H. Hsu, X.P. Yang, D. Graf, E.S. Choi, K. Pandey, M.R.U. Nabi, S.K. Chhetri, R. Basnet, S. Rahman, J. Wang, Z. Hu, B. Da, H.O.H. Churchill, G. Chang, M.Z. Hasan, Y. Wang, J. Hu, *Insulator-to-Metal Transition and Isotropic Gigantic Magnetoresistance in Layered Magnetic Semiconductors*, Advanced Materials, **36**, 2410655 (2024)

[2] G. Acharya, R. Basnet, S. K. Chhetri, D. Upreti, J. Sakon, J. Hu, *Chalcogen Doping Effect on the Metal-to-Insulator Transition in GdPS*, under review by *Physical Review B*

[3] S. K. Chhetri, R. Basnet, J. Wang, K. Pandey, G. Acharya, M. R. U. Nabi, D. Upreti, J. Sakon, M. Mortazavi, J. Hu, *Evolution of magnetism in magnetic topological semimetal* $NdSb_xTe_{2-x+\delta}$, Physical Review B, **109**, 184429 (2024)

[4] S. K. Chhetri, R. Basnet, K. Pandey, G. Acharya, S. Rahman, M.R.U. Nabi, D. Upreti, H. O.H. Churchill, J. Hu, *Evolution of Magnetoresistance in magnetic topological semimetal $NdSb_xTe_{2-x}$*, under review by Physical Review B

[5] G. Acharya, K. Pandey, M. M. Sharma, J. Wang, S.K. Chhetri, M. M. Sharma, D. Upreti, R. Basnet, J. Sakon, J. Hu, *Large Negative Magnetoresistance in off-Stochiometric Topological Semimetal $PrSb_xTe_{2-x}$*, Physical Review B, **111**, 024421 (2025)

Publications

1. G. Acharya, K. Pandey, M. M. Sharma, J. Wang, S.K. Chhetri, M. M. Sharma, D. Upreti, R. Basnet, J. Sakon, J. Hu, *Large Negative Magnetoresistance in off-Stochiometric Topological Semimetal $PrSb_xTe_{2-x}$*, Physical Review B, **111**, 024421 (2025)
2. G. Acharya, K. Pandey, M. M. Sharma, J. Wang, S.K. Chhetri, M. M. Sharma, D. Upreti, R. Basnet, J. Sakon, J. Hu, *Large Negative Magnetoresistance in off-Stochiometric Topological Semimetal $PrSb_xTe_{2-x}$*, Physical Review B, **111**, 024421 (2025)
3. S.K. Chhetri, G. Acharya, D. Graf, R. Basnet, S. Rahman, M. M. Sharma, D. Upreti, M.R.U. Nabi, S. Kryvyi, J. Sakon, M. Mortazavi, B. Da, H. Churchill, J. Hu, *Large Negative Magnetoresistance in Antiferromagnetic Gd_2Se_3*, Physical Review B, 111, 014431 (2025)
4. G. Acharya, B. Neupane, C.-H. Hsu, X.P. Yang, D. Graf, E.S. Choi, K. Pandey, M.R.U. Nabi, S.K. Chhetri, R. Basnet, S. Rahman, J. Wang, Z. Hu, B. Da, H.O.H. Churchill, G. Chang, M.Z. Hasan, Y. Wang, J. Hu, *Insulator-to-Metal Transition and Isotropic Gigantic Magnetoresistance in Layered Magnetic Semiconductors*, Advanced Materials, **36**, 2410655 (2024)
5. R. Basnet, J. Hu, *Understanding and Tuning Magnetism in van der Waals-type Metal Thiophosphates*, Nanoscale, **16**, 15851 (2024)
6. D. Baral, R. Basnet, W. R. Scougale, R. Q. Rivlis, D. Upreti, Y. Dahnovsky, J. Hu, T. Chien, *Possible Coexistence of Magnetism and the Paramagnetic singularity in Lightly Fe doped WTe_2*, Physical Review B, **109**, 245419 (2024)
7. S. K. Chhetri, R. Basnet, J. Wang, K. Pandey, G. Acharya, M. R. U. Nabi, D. Upreti, J. Sakon, M. Mortazavi, J. Hu, *Evolution of magnetism in magnetic topological semimetal $NdSb_xTe_{2-x+\delta}$*, Physical Review B, **109**, 184429 (2024)
8. R. Basnet, D. Upreti, T. Patel, S. K. Chhetri, G. Acharya, M. R. U. Nabi, J. Sakon, M. Mortazavi, J. Hu, *Field-induced spin polarization in the lightly Cr-substituted layered antiferromagnet $NiPS_3$*, Physical Review B **109**, 184405 (2024)
9. R. Basnet, T. Patel, J. Wang, D. Upreti, S. K. Chhetri, G. Acharya, M. R. U. Nabi, J. Sakon, J. Hu, *Understanding and tuning magnetism in layered Ising-type antiferromagnet FePSe3 for potential 2D magnet*, Advanced Electronic Materials, **10**, 2300738 (2024)
10. S. Acharya, K. Pandey, R. Basnet, G. Acharya, M. R. U. Nabi, J. Wang, J. Hu, *Single Crystal Growth and Characterization of Topological Semimetal ZrSnTe*, Journal of Alloys and Compounds, **968**, 171903 (2023)

Discovery and Synthesis of New Altermagnets for Quantum Geometric Properties

Sheng Ran, *Washington University*

Keywords: altermagnet, anomalous Hall, nonlinear Hall, single crystal

Research Scope

Altermagnets represent a newly discovered class of magnetic materials that challenge the traditional dichotomy between ferromagnets and antiferromagnets. Combining zero net magnetization with spin-split electronic bands arising from unconventional magnetic symmetries, altermagnets provide a promising platform for novel spintronic functionalities without relying on spin–orbit coupling. Despite their potential, the quantum geometric properties of altermagnets—particularly Berry curvature and quantum metric—remain largely unexplored. This project aims to discover and synthesize new altermagnets and to systematically investigate how their unique magnetic symmetries give rise to enhanced quantum geometric responses and associated transport phenomena.

The project is guided by the hypothesis that symmetry-protected band crossings in altermagnets, which are spin-degenerate in the absence of spin–orbit coupling, become weakly gapped when spin–orbit interaction is introduced. These avoided crossings lead to sharply concentrated Berry curvature and quantum metric features—key ingredients for anomalous and nonlinear transport. We will synthesize high-quality single crystals of altermagnetic candidates with diverse magnetic symmetries and characterize their electronic and magnetic properties. Anomalous Hall, elasto-Hall, and nonlinear transport measurements will be used to probe Berry curvature and quantum metric effects. The project will not only provide critical insights into an emerging area of condensed matter physics but also disseminate well-characterized crystals to the broader community, enabling advances in spintronics, low-dissipation electronics, and quantum information science.

Recent Progress

We have synthesized single crystals of two promising new candidates for altermagnetism: UCr_2Si_2C and NiS. Previous neutron diffraction studies indicate that UCr_2Si_2C is an antiferromagnet with a Néel temperature above room temperature [1], and its magnetic structure is consistent with the requirements for altermagnetism. NiS, meanwhile, crystallizes in the same structure as the prototype altermagnets MnTe and CrSb, and prior neutron diffraction results suggest that it, too, could host altermagnetism [2]. However, to date, no investigations have been carried out on single crystals of either UCr_2Si_2C or NiS. In this work, we

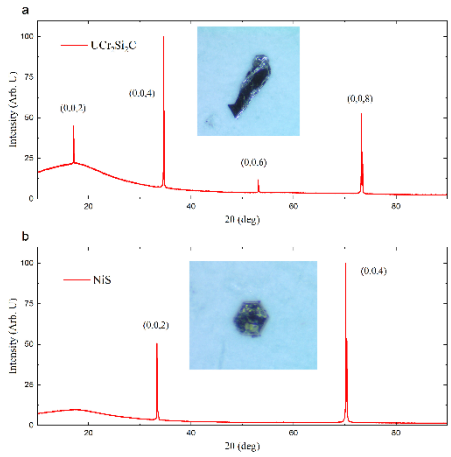


Fig. 1 Xray diffraction pattern on the single crystals of NiS and UCr_2Si_2C that we synthesized.

successfully synthesized NiS single crystals using chemical vapor transport, while UCr_2Si_2C crystals were obtained via arc melting, with single crystals forming on the surface of the arced sample. X-ray diffraction from single crystals oriented along the c-axis is shown in Fig. 1.

Future Plans

We will synthesize high-quality single crystals of the potential candidates for altermagnets, including NiS family and $CuMP_2X_6$ van der Waals materials (M = Cr, Mo, W; X = S, Se). A variety of synthesis techniques will be employed, including the high-temperature molten flux method and chemical vapor transport. To confirm the crystal structure, we will perform X-ray diffraction. The bulk single crystals will be further characterized using electric transport, magnetic, and specific heat measurements. These measurements will be conducted using a Quantum Design PPMS, covering a temperature range of 2–400 K and magnetic fields up to 9 T, as well as a Bluefors dilution refrigerator for lower temperatures.

We will perform DFT calculations to gain an initial understanding of the magnetic and electronic structures of the target materials through collaboration. To experimentally determine the magnetic structure, we will conduct neutron diffraction measurements. To probe the electronic band structure, we will perform ARPES measurements on bulk single crystals through collaboration. The neutron diffraction and ARPES results will be directly compared with DFT predictions to achieve a comprehensive understanding of the material systems. If a target material is confirmed to be an altermagnet, we will further investigate magnetic properties of the material using tuning knobs, including chemical doping and hydrostatic pressure, to provide rich information about control and manipulate altermagnetism.

Once an altermagnet is fully confirmed, we will continue to measure anomalous transport to probe the effect of the Berry curvature. Certain altermagnets are expected to exhibit anomalous transport properties under ambient conditions, depending on their specific magnetic and crystallographic symmetries [3]. For such materials, we will measure the anomalous Hall effect, as well as the anomalous thermal Hall effect and the anomalous Nernst effect. These measurements will be carried out using the electric and thermal transport options of the Quantum Design PPMS system. To distinguish between intrinsic contributions from Berry curvature and extrinsic contributions from scattering mechanisms, we will perform scaling analyses.

In altermagnets that do not exhibit AHE under ambient condition, applying uniaxial strain can break the rotational symmetry, and lead to a finite anomalous Hall conductivity, a phenomenon often referred to as elasto-conductivity [4]. To probe this effect, we will employ a commercial strain cell from Razorbill Instruments to apply precise, controlled strain. The samples will be glued to the strain cell using black Stycast epoxy. The Hall effect measurements will primarily be conducted in our Bluefors dilution refrigerator, using a specially designed insert compatible with the strain cell. Coaxial wires will be used to apply voltage to the strain cell and measure capacitance

at a frequency of a few hundred Hz, which is optimal for minimizing noise and ensuring accurate measurements.

We will also use nonlinear transport as a probe for the quantum metric part of the quantum geometry. It has been theoretically shown that both the quantum metric and the Berry curvature contribute to the nonlinear transport in altermagnets, and their respective contributions can be distinguished by measuring both longitudinal and transverse component and performing scaling analysis [5]. Nonlinear transport in altermagnets is expected to emerge at the third order, providing a distinct and definitive signature of altermagnetism. However, this also indicates that the signal will be small. We will fabricate micron-scale Hall bars from bulk materials using a focused ion beam. The small dimensions will significantly enhance current density, amplifying nonlinear responses that would otherwise be difficult to detect. The nonlinear transport $J \sim E^n$ will lead to higher order harmonic voltage, which can be easily measured with lock-in technique. To get linear and nonlinear responses, we will measure electrical conductivity at fundamental, second-order, and third-order harmonics. By simultaneously measuring longitudinal and transverse responses, we will perform scaling analysis to systematically separate and quantify the quantum metric and Berry curvature contributions. We will collaborate to theoretically calculate the 3rd order transport response and compare with our experimental data to fully understand the quantum geometry of these materials.

References

1. Pierric Lemoine, Anne Vernière, Mathieu Pasturel, Gérard Venturini, and Bernard Malaman, *Unexpected Magnetic Ordering on the Cr Substructure in UCr2Si2C and Structural Relationships in Quaternary U-Cr-Si-C Compounds*, Inorganic Chemistry **57**, 2546-2557 (2018).

2. J. T. Sparks and T. Komoto, *Metal-to-Semiconductor transition in Hexagonal NiS*, Reviews of Modern Physics **40**, 752 (1968)

3. Libor Šmejkal, Allan H. MacDonald, Jairo Sinova, Satoru Nakatsuji, and Tomas Jungwirth, *Anomalous Hall antiferromagnets*, Nature Reviews Materials **7**, 483 (2022)

4. Keigo Takahashi, Charles R. W. Steward, Masao Ogata, Rafael M. Fernandes, and Jorg Schmalian, *Elasto-Hall conductivity and the anomalous Hall effect in altermagnets*, arXiv: 2502.03517 (2025)

5. Yuan Fang, Jennifer Cano, and Sayed Ali Akbar Ghorashi, *Quantum geometry induced nonlinear transport in altermagnets*, Phys. Rev. Lett. **133**, 106701 (2024).

Publications

No publications have resulted yet, as the project only began in August 2025.

Anomalous transport in a Spin Textured Altermagnet

Linda Ye, *California Institute of Technology*

Keywords: Altermagnetism, antiferromagnetism, anomalous transport, spin texture, Berry curvature

Research Scope

Altermagnetism [1] is a recently discovered form of magnetic order, characterized by large spin splittings in momentum space—an effect conventionally associated only with ferromagnets. This embedded spin texture opens exciting opportunities, both as a platform for diverse spintronic functionalities and as a potential modular building block for unconventional superconductivity. The development of altermagnetic materials is therefore of fundamental significance while also holding strong prospects for technological applications. Although substantial spin splitting has been firmly established through both theoretical predictions and experimental observations in several altermagnetic systems, a central challenge remains: realizing emergent electronic responses that transcend the spin splitting itself. Such responses are often suppressed, or outright forbidden, by the symmetries intrinsic to altermagnetic states. A case in point is the collinear g-wave altermagnetic order with out-of-plane magnetic moments (Fig. 1a), observed in prototypical compounds such as CrSb [2] and $CoNb_4Se_8$ [3], where symmetry constraints strictly prohibit a finite anomalous Hall effect. In this work, we demonstrate that the superposition of a non-collinear spin texture onto the g-wave collinear altermagnetic background can unlock a large anomalous Hall response (Fig. 1b). This approach highlights a new pathway to deliberately "break" the delicate balance between symmetry and magnetic order, thereby engineering emergent electronic functionalities in altermagnetic materials.

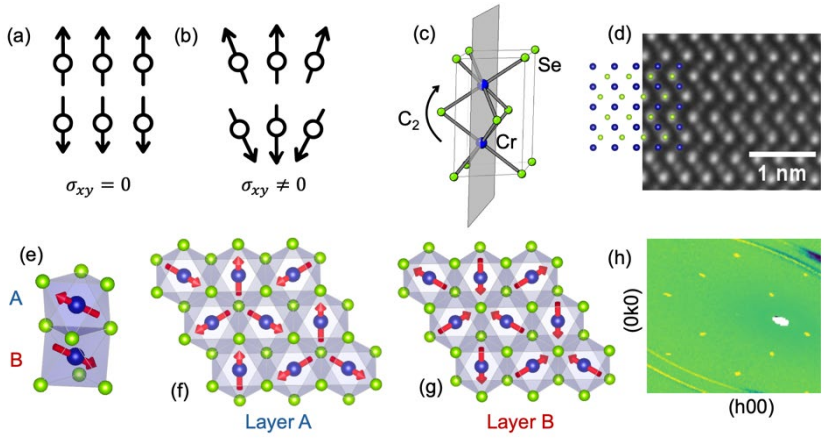


Fig. 1 (a,b) Schematic of a collinear g-wave altermagnet with out of plane moments (a) and a g-wave altermagnet with out of plane moments superimposed with a non-coplanar spin texture. The former forbids an anomalous Hall effect while the latter allows it. (c) Schematic of the magnetic sites in a crystallographic unit cell of CrSe. The two inequivalent sites are connected by C2 rotation symmetry. (d) Cross section of transmission electron microscopy of our CrSe crystals overlaid with the anticipated crystal structure. (e-g) Magnetic structure of CrSe. (h) In-plane superlattice peaks in neutron scattering characteristic of the spin structure shown in (e-g).

Recent Progress

In this context, we introduce CrSe [4] as a new altermagnetic material that uniquely combines a g-wave altermagnetic order with a non-coplanar spin texture. The crystallographic unit cell of CrSe is depicted in Fig. 1(c), highlighting two inequivalent magnetic sites related by a C_2 symmetry operation. A transmission electron microscopy (TEM) image of our high-quality single crystals, obtained in collaboration with Dr. Yu-Tsun Shao at the University of Southern California, is shown in Fig. 1(d). The TEM image reveals the vertically stacked Cr atoms (blue) alongside the zig-zag stacked Se atoms (green), which modulate the local environment of the Cr sites and play a key role in stabilizing the altermagnetic order in the system. Figures 1(e–g) provide a detailed illustration of the magnetic structure: panel (e) shows the antiferromagnetic arrangement of spins between adjacent layers, which forms the basis of the g-wave altermagnetic order, while panels (f) and (g) present top views of the non-collinear spin components residing on the A and B layers, respectively. This spin state has been experimentally confirmed through neutron scattering measurements carried out in collaboration with Dr. Huibo Cao at Oak Ridge National Laboratory, where the in-plane superlattice peaks associated with the non-collinear spin component are clearly resolved, as displayed in Fig. 1(g).

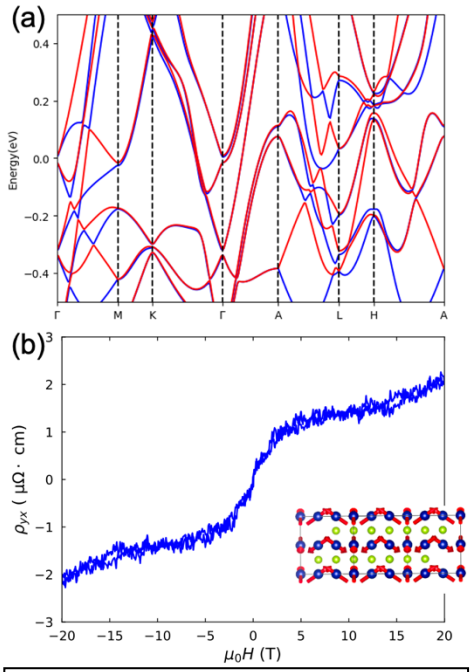


Fig. 2 (a) DFT band structure of CrSe without spin-orbit coupling. A g-wave pattern of spin splitting can be identified. (b) Anomalous Hall effect in CrSe and the magnetic structure extracted from neutron scattering at ORNL are shown as inset.

We note that the magnetic order in CrSe is fully consistent with a g-wave altermagnetic state (Fig. 1e), and the corresponding momentum-dependent spin splitting is clearly resolved in the electronic band structure (Fig. 2a). Along the Γ–M direction, this spin splitting reaches values as large as 0.5 eV, underscoring the robustness of the underlying altermagnetic order. Importantly, when this collinear g-wave order is superimposed with the non-collinear spin texture identified in CrSe, it enables a finite anomalous Hall conductivity that would otherwise be strictly forbidden in a pure collinear g-wave antiferromagnet with out-of-plane moments. Experimentally, we observe a sizable anomalous Hall effect of approximately 100 $\Omega^{-1}cm^{-1}$ at 2 K (Fig. 2b). This magnitude is on par with that of canonical ferromagnetic metals known to host strong Berry curvature sources. Furthermore, the combination of longitudinal and Hall conductivities places CrSe squarely in the intrinsic regime of the universal anomalous Hall effect diagram [5], strongly suggesting that the observed Hall response originates from Berry curvature hot spots induced by the non-coplanar spin structure.

Our findings demonstrate that symmetry modification through spin textures provides a powerful and broadly applicable strategy for engineering emergent electronic phenomena in altermagnets.

By deliberately tailoring the interplay between magnetic order and symmetry, it becomes possible to realize responses that are otherwise forbidden in purely collinear states. This approach not only deepens the fundamental understanding of how to engineer emergent transport properties from altermagnets, but also lays the groundwork for exploiting altermagnets in practical contexts with symmetry-tunable electronic properties.

Future Plans

We are currently pursuing theoretical symmetry analysis, effective modeling, and density functional theory calculations of the Berry curvature to further solidify the connection between the observed spin texture and the measured anomalous Hall effect. These efforts aim to provide a microscopic understanding of how non-collinear components in CrSe interplay with the altermagnetic spin splitting to generate Berry curvature hot spots and drive emergent transport responses. Looking forward, an especially exciting direction will be to extend this concept of spin-structure modification to *d*-wave altermagnets with simpler spin splitting in the momentum space. In parallel, we will continue the experimental search for new altermagnetic candidates stabilized by non-symmorphic symmetries with CrSe being one successful example for designing new spin splitting patterns and electronic responses.

References

1. A. B. Author, C. D. Author, and E. F. Co-Author, Title of the Publication, Journal Volume, page (year). L. Šmejkal, J. Sinova, and T. Jungwirth, *Emerging Research Landscape of Altermagnetism*, **Phys. Rev. X**, **12**, 040501 (2022).
2. S. Reimers, L. Odenbreit, L. Šmejkal, *et al.*, *Direct observation of altermagnetic band splitting in CrSb thin films*, **Nat. Commun.**, **15**, 2116 (2024).
3. **R. B. Regmi, H. Bhandari, B. Thapa, Y. Hao, et al.,** *Altermagnetism in the layered intercalated transition metal dichalcogenide* $CoNb_4Se_8$. **Nat. Commun. 16**, 4399 (2025).
4. **L. M. Corliss, N. Elliott, J. M. Hastings, and R. L. Sass,** *Magnetic Structure of Chromium Selenide,* **Phys. Rev. 122**, 1402 (1961).
5. **S. Onoda, N. Sugimoto, and N. Nagaosa,** *Quantum transport theory of anomalous electric, thermoelectric, and thermal Hall effects in ferromagnets,* **Phys. Rev. B 77**, 165103 (2008).

Publications

Work in progress

Quantum Fluctuations in Narrow Band Systems – Thrust 1

Filip Ronning, Eric Bauer, Michihiro Hirata, Priscila Rosa, Allen Scheie, and Sean Thomas

(Los Alamos National Lab)

Keywords: Magnetism, Topology, f-electron materials, Single crystals, Non-Fermi liquid behavior and charge dynamics

Research Scope

Coherence and topologically protected modes in quantum matter arise from highly entangled spin, charge, lattice, and orbital degrees of freedom. Narrow band systems, whose renormalized electronic bandwidth is comparable to other relevant energy scales in the material, inherently have strong interactions and a proliferation of quantum fluctuations. 4*f*- and especially 5*f*-materials possess strong Coulomb repulsion, large spin-orbit coupling, and multiple competing energy scales, which generate coherent narrow bands and topologically non-trivial states of matter. This complexity provides a rich environment for discovering new states of matter, as well as providing ideal representatives that enable the understanding of quantum matter that arises across the periodic table more generally. In thrust 1 we address how quantum fluctuations renormalize excitations in topologically trivial and non-trivial matter and will develop conceptual frameworks for understanding and controlling the consequences of quantum fluctuations in classes of electronically correlated systems. Currently, we are focusing on the role of magnetic frustration in renormalizing the electronic structure and generating instabilities towards new states of matter.

Recent Progress

f-based materials contain localized magnetic moments due to the strong Coulomb interaction and weak hybridization with neighboring atoms. The finite hybridization, however, leads to a quantum entanglement of the local moments with the conduction electron sea at low temperatures through the Kondo effect. As the temperature is lowered, incoherent scattering evolves to a lattice coherent state at T^* (also often labeled T_{coh} or T_K), in which an emergent narrow *f*-band electronic structure is heavily renormalized from the non-interacting state found at high temperatures. Understanding the resulting narrow band renormalized electronic structure is key to unlocking the power of quantum materials. By comparing spectroscopic results with dynamical mean field theory calculations, we determine whether the electron self-energy $\Sigma(\boldsymbol{k},\omega)$ is momentum independent or not, reflecting the range of the interactions responsible for the electronic renormalization. Following previous work on cubic $CePd_3$, we recently performed optical spectroscopy on CeRhSn and $CeIr_3B_2$ whose reduced dimensionality and increased magnetic fluctuations lead to stronger quantum fluctuations [1]. Even in these systems we found good agreement with theory validating a local interaction picture, despite the proximity to magnetic instabilities in these compounds.

On the magnetically ordered side of the phase diagram we have performed careful investigation into the low energy magnetic excitations of $CeIn_3$ using inelastic neutron scattering and heat capacity measurements. $CeIn_3$ is a prototypical Kondo-lattice antiferromagnet (T_N = 10 K) at ambient pressure and transforms to a superconductor at the antiferromagnetic quantum critical pressure of 2.6 GPa. As we previously proposed, our inelastic neutron scattering measurements on $CeIn_3$ have validated a powerful approach to determine all necessary parameters of a minimal (3-band) Kondo lattice model from first principles calculations that is material specific and expected to capture the quantum critical, non-Fermi liquid, and unconventional superconductivity that occurs in cerium and ytterbium-based systems [2]. Additionally, by analyzing the derivation of the low energy spin model, we identified the conditions necessary to produce an anisotropic exchange interaction in cerium and ytterbium compounds. Notably, it is essential to have strong charge fluctuations to the 2-electron $4f^2$ or 2-hole $4f^{12}$ configurations with magnetic bonds that lack inversion symmetry to generate anisotropic exchange interactions. This result has a broad impact on understanding magnetic anisotropy in rare-earth magnets.

Another striking consequence of our inelastic neutron scattering work was the realization that the magnon dispersion has a high spin wave velocity (due to the RKKY interaction) [2]. As shown in **Fig. 2**, our measured spin wave velocity (v = 600 m/s) predicts a T^3 term of the heat capacity (α $1/v^3$) that is two orders of magnitude lower than the measured T^3 contribution [3]. This implies that there is either a missing excitation (beyond phonons, electrons, or transverse magnons) or more likely, that the spin, lattice, and/or charge degrees of freedom are highly entangled in $CeIn_3$. We further examined five other cerium-based systems for which inelastic neutron scattering had been measured and found a similar discrepancy [3]. This poses a fundamental conundrum that forms the basis for a significant effort of our planned work.

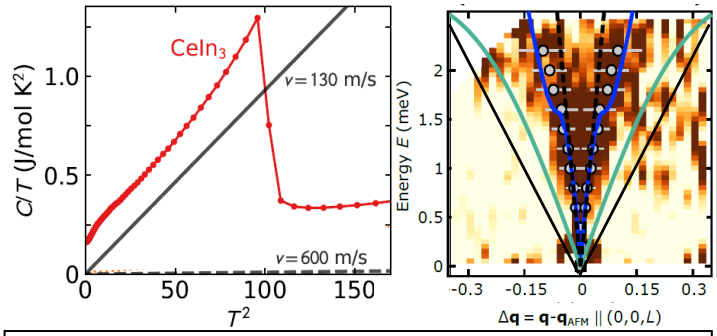


Fig. 1: Heat capacity of $CeIn_3$ (left) compared to inelastic neutron scattering measurements of the transverse magnons (right). Solid black lines give the magnon contribution as expected from the T^3 term of C, while the dashed lines are the magnon contribution from a fit to the spin wave dispersion as measured by neutrons.

We have continued our materials discovery effort, with a focus on the intersection between strong correlations and enhanced quantum fluctuations through magnetic frustration and/or reduced dimensionality [4]. This led to the discoveries of $CeLiBi_2$, KU_2Te_6, $UPd_{0.65}Bi_2$, UV_6Sn_6, and UNb_6Sn_6, and the investigation of $CeLi_3Bi_2$ and β-UTe_3 enabled by our synthesis of sizable single crystals. The uranium-based Kagome materials provide a platform to investigate the interplay between Kondo physics of the uranium lattice with a flat band density of states generated by the Kagome lattice of the transition metal that introduces frustration as a tuning parameter. Finally,

following up on the colossal negative magneto resistance we found in $Eu_5In_2Sb_6$, we demonstrated using transport, thermodynamic, and spectroscopic measurements that this behavior, common to many Eu-based compounds, is consistent with magnetic polaron formation. Additionally, we showed that the magnetic structure of $Eu_5In_2Sb_6$ permits a finite Ising ferromagnetic component, which is consistent with the possibility that $Eu_5In_2Sb_6$ hosts an axionic insulator state.

Future Plans

Our prior work on cubic $CeIn_3$ validated a protocol for deriving a materials-specific low energy spin Hamiltonian from first principles. It also illustrated a discrepancy between the magnetic excitations observed by inelastic neutron scattering and the low temperature density of states inferred from heat capacity (see **Fig. 1**). To determine the origin of this behavior we will investigate a set of compounds in a similar fashion to determine how this discrepancy correlates with other material properties. We have begun inelastic neutron scattering measurements on the tetragonal antiferromagnet $CePd_2Si_2$, which shows many similarities to $CeIn_3$. We will also perform measurements in magnetic fields up to 9 T, which is expected to gap the magnon spectrum, and thereby can confirm whether the excess heat capacity is in any way related to transverse spin excitations. As we hypothesize that the excess heat capacity arises from longitudinal spin fluctuations associated with the Kondo effect, we will also perform measurements on more localized magnets, for which we anticipate better agreement between heat capacity and inelastic neutron scattering if our hypothesis is correct.

Our prior work on cubic $CePd_3$, CeRhSn, and $CeIr_3B_2$ show that the electronic renormalization of cerium-based compounds can be well described by single-site DMFT calculations with a momentum independent self-energy indicative of the dominance of local interactions in the renormalization. Extending these studies, we will explore whether the more extended wave functions of 5*f*-orbitals cause a breakdown of the dominance of the local interactions. The breakdown of single parameter scaling of the Kondo scale measured by heat capacity, magnetic susceptibility, and inelastic neutron scattering in the mixed valent regime for uranium-based compounds in fact suggests this to be a likely possibility. To test this hypothesis, we will perform ARPES, optical spectroscopy, RIXS, and inelastic neutron scattering on UAl_3, a cubic mixed valent compound with energy scales similar to $CePd_3$ and $YbAl_3$. Similar work will be performed on β-UTe_3 (see below).

Reduced dimensional systems, and in particular quasi-1D systems, have enhanced quantum fluctuations and provide an ideal platform to compare experiment and theory. Additionally, as demonstrated in 2D transition metal dichalcogenides and few layer graphene, 2D systems can be highly tunable via exfoliation and gating and a source for discovering new states of matter such as superconductivity and fractional Chern insulators. We have recently synthesized the 2D van der Waals bonded *f*-electron systems Ce_2Te_5 and β-UTe_3. β-UTe_3 orders ferromagnetically with a

Sommerfeld coefficient of the heat capacity of 130 mJ/molK^2, revealing the presence of strong electronic correlations. Excitingly, we have already been able to exfoliate β-UTe_3 to a thickness of a single bilayer (½ unit cell) [5]. Remarkably, in this limit our Kerr rotation measurements have demonstrated that the bulk ferromagnetic transition is enhanced from 15 K to 35 K (see **Fig. 2**). A small anomaly is seen in the bulk at 35 K with the opposite Kerr rotation further suggesting anomalous behavior at the surface of the crystal. A large enhancement of the ordering temperature in the 2D limit is highly unusual, though not unheard of as in the case of superconductivity of FeSe on $SrTiO_3$. We will understand this behavior through the full suite of transport, thermodynamic, and spectroscopic probes available to us. To enable NQR/NMR measurements on air sensitive samples such as this, we will develop printed circuit boards with RF coils that will enable easier encapsulation.

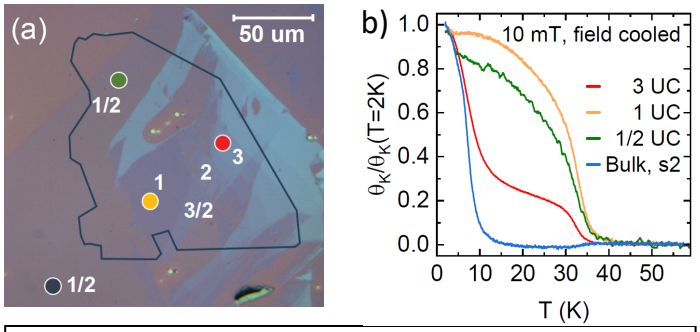


Fig. 2: (a) Optical image of exfoliated β-UTe_3 before placing h-BN capping layer (indicated by gray outline). Numbers indicate the number of unit cells (each unit cell contains two bilayer units of UTe_3). (b) Normalized Kerr rotation versus temperature for different thicknesses.

References

1. T.U. Boehm, N. Sirica, B.G. Jang, Y. Liu, E.D. Bauer, Y. Huang, C.C. Homes, J.-X. Zhu, and F. Ronning, *"Anisotropic hybridization in CeRhSn"* Physical Review B, **110**, L121107 (Sep. 2024).

2. W. Simeth, Z. Wang, E.A. Ghioldi, D.M Fobes, A. Podlesnyak, N.H. Sung, E.D. Bauer, J. Lass, S. Flury, J. Vonka, D.G. Mazzone, C. Niedermayer, Y. Nomura, R. Arita, C.D. Batista, F. Ronning, and M. Janoschek, *"A microscopic Kondo lattice model for the heavy fermion antiferromagnet $CeIn_3$"* Nature Communication **14**, 8239 (Dec. 2023).

3. A.O. Scheie, Yu Liu, E.A. Ghioldi, S. Fender, P.F.S. Rosa, E.D. Bauer, Jian-Xin Zhu, and F. Ronning, "*Excess heat capacity in magnetically ordered Ce heavy fermion metals*," Physical Review B **110**, 085123 (Aug. 2024).

4. P.F.S. Rosa and F. Ronning "*A quantum collaboration for flat bands*," Nature Physics **20**, 539 (Jan. 2024).

5. S.M. Thomas, A.E. Llacsahuanga, W. Simeth, C.S. Kengle, F. Orlandi, D. Khalyavin, P. Manuel, F. Ronning, E.D. Bauer, J.D. Thompson, Jian-Xin Zhu, A.O. Scheie, Y.P. Chen, P.F.S. Rosa, "*Enhanced two-dimensional ferromagnetism in van der Waals β-UTe_3 monolayers*," arXiv:2506.15667.

Publications (From 30 publications supported by this thrust over the past 2 years)

1. Z.W. Riedel, W. Simeth, C.S. Kengle, S.M. Thomas, J.D. Thompson, A.O. Scheie, F. Ronning, C. Lane, Jian-Xin Zhu, P.F.S. Rosa, and E.D. Bauer, *Magnetic order and physical properties of the Kagome metal UNb_6Sn_6*, Phys. Rev. Materials **9**, 084401 (Aug. 2025).

2. S.M. Thomas, C.S. Kengle, W. Simeth, C-y Lim, Z. Riedel, K. Allen, A. Schmidt, M. Ruf, S. Gim, J.D. Thompson, F. Ronning, A.O. Scheie, C. Lane, J. Denlinger, S. Blanco-Canosa, J. Zhu, E.D. Bauer, and P.F.S. Rosa, *Unusual 5f magnetism in new kagome material UV_6Sn_6*, npj Quantum Materials **10**, 66 (Jul. 2025).

3. S. Mishra, C.S. Kengle, J.D. Thompson, A.O. Scheie, S.M. Thomas, F. Ronning, and P.F.S. Rosa, *Evidence for incommensurate antiferromagnetism in nonsymmorphic $UPd_{0.65}Bi_2$*, Physical Review Materials, **9**, 014409 (Jan. 2025).

4. E.D. Bauer, K.E. Avers, T. Asaba, S. Seo, Y. Liu, A. Weiland, M.A. Continentino, J.M. Lawrence, S.M. Thomas, P.F.S. Rosa, A.P. Dioguardi, J.D. Thompson, and F. Ronning, *Quantum Critical Scaling in Quasi-One-Dimensional $YbFe_5P_3$*, Physical Review B, **110**, 205141 (Nov. 2024).

5. P.F.S. Rosa and F. Ronning, *A quantum collaboration for flat bands*, Nature Physics **20**, 539 (Jan. 2024).

6. W. Simeth, Z. Wang, E.A. Ghioldi, D.M Fobes, A. Podlesnyak, N.H. Sung, E.D. Bauer, J. Lass, S. Flury, J. Vonka, D.G. Mazzone, C. Niedermayer, Y. Nomura, R. Arita, C.D. Batista, F. Ronning, and M. Janoschek, *A microscopic Kondo lattice model for the heavy fermion antiferromagnet $CeIn_3$,* Nature Communication **14**, 8239 (Dec. 2023).

7. A.O. Scheie, Yu Liu, E.A. Ghioldi, S. Fender, P.F.S. Rosa, E.D. Bauer, Jian-Xin Zhu, and F. Ronning, *Excess heat capacity in magnetically ordered Ce heavy fermion metals*, Physical Review B **110**, 085123 (Aug. 2024).

8. M.C. Rahn, M.N. Wilson, T.J. Hicken, F.L. Pratt, C. Wang, F. Orlandi, D.D. Khalyavin, P. Manuel, L.S.I. Veiga, A. Bombardi, S. Francoual, P. Bereciartua, A.S. Sukhanov, J.D. Thompson, S.M. Thomas, P.F.S. Rosa, T. Lancaster, F. Ronning, and M. Janoschek, *Magnetism in the axion-insulator candidate $Eu_5In_2Sb_6$*, Physical Review B, **109**, 174404 (May 2024).

9. S.M. Thomas, S. Seo, T. Asaba, F. Ronning, P.F.S. Rosa, E.D. Bauer, and J.D. Thompson, *Probing quantum criticality in ferromagnetic $CeRh_6Ge_4$*, Physical Review B, **109**, L121105 (Mar. 2024).

10. H. Wang, T. B. Park, J. Kim, H. Jang, E. D. Bauer, J. D. Thompson and T. Park, *Evidence for Charge Delocalization Crossover in the Quantum Critical Superconductor $CeRhIn_5$*, Nature Communication, **14**, 7341 (Nov. 2023).

Complex States, Emergent Phenomena, and Superconductivity in Intermetallic and Metal-like Compounds FWP: Near-room-temperature ferromagnetism in pressurized $SrCo_2P_2$

Complex States PIs: *Sergey Bud'ko, Paul Canfield (PI), Yuji Furukawa, Adam Kaminski, Ruslan Prozorov, Aashish Sapkota, Tyler Slade, Makariy Tanatar, Linlin Wang*

Keywords: Phase transitions, Electrical Properties, Magnetism, Structural Properties, Materials Modeling

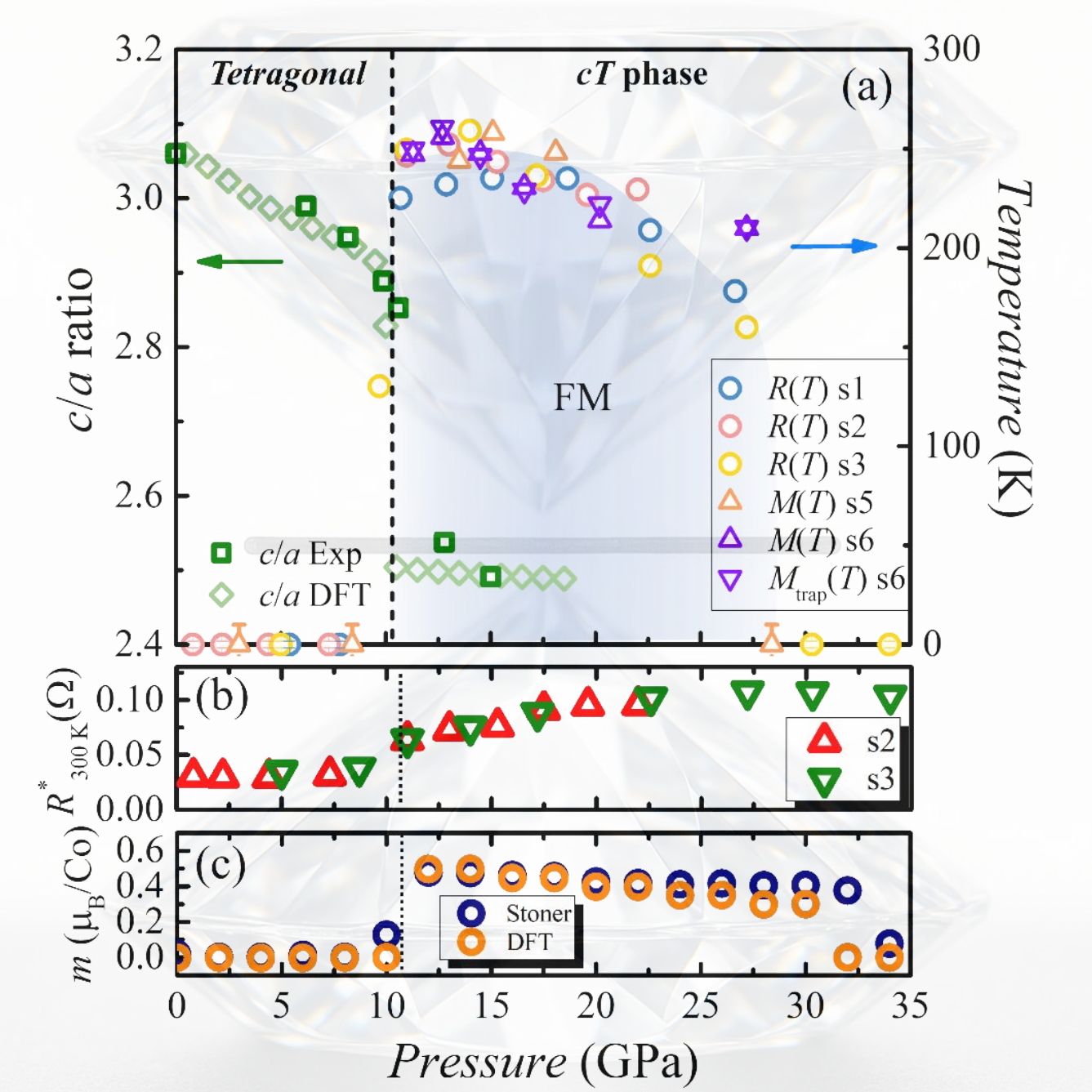
Research Scope

The question to be addressed by the Complex States, Emergent Phenomena, and Superconductivity in Intermetallic and Metal-like Compounds FWP is: how can we develop, discover, understand, and ultimately control and predictably modify new and extreme examples of complex states, emergent phenomena, and superconductivity? Over the next review period, we will study materials manifesting specifically clear or compelling examples of superconductivity, strongly correlated electrons, novel electronic topology, quantum criticality, and exotic, bulk magnetism because of their potential to lead to revolutionary steps forward in our understanding of their complex, and potentially energy-relevant, properties. For example, the FWP proposes to design and utilize novel synthetic routes to enable the discovery of new magnetic and superconducting systems that will be tuned by substitution and pressure through quantum critical points and study superconductivity in the fullness of its diverse manifestations, ranging from FeAs-based systems to the spin-triplet system UTe_2, to the unconventional superconductor $Rh_{17}S_{15}$, to pressure-stabilized superconductivity. This work will be leveraged via highly collaborative interactions between the scientists within this FWP, as well as through extensive collaborations with other Ames Laboratory FWPs, other DOE laboratories, and other universities and labs throughout the world. Experiment and theory will be implemented synergistically. The experimental work will consist of new materials development and crystal growth, combined with detailed and advanced measurements of microscopic, thermodynamic, transport, and spectroscopic properties, as well as electronic structure, at extremes of pressure, temperature, magnetic field and resolution. The theoretical work focuses on understanding and modeling transport, thermodynamic and spectroscopic properties using world-leading and advanced phenomenological approaches to superconductors and electronic band structure. For this ECMP PI meeting we will present recent work on controlling the collapsed tetragonal phase transition with the aim of discovering new moment bearing compounds focusing on the $Sr(Ni_{1-x}Co_x)_2P_2$ doping series as well as $SrCo_2P_2$ under applied pressures. [1,2]

Recent Progress

The Complex States FWP has made recent progress in the discovery and characterization of $Rh_{17}S_{15}$ (synthetic Miassite) [3], finding unusual superconducting gap symmetries; it has found a new type of spin-textured, surface band splitting in RBi and RSb compounds;[4] it has developed new materials search and synthesis strategies based on immiscible pairs of elements (referred to as the antagonistic pairs approach) and developed multiple innovations and improvement to the solution growth of single crystals using frit-disc crucible sets (Canfield Crucible Sets or CCS);[5]

and it has discovered new, magnetic states in proximity to collapsed tetragonal phase transitions induced either by substitution or application of hydrostatic pressure. It is the last topic that will be highlighted for this ECMP meeting.



Pressure and temperature dependence of electronic, magnetic and structural properties on $SrCo_2P_2$ from both experiments and theoretical calculations. [2]

Future Plans

We propose to continue our efforts directed toward the development and understanding of model systems of complex states, emergent phenomena, topologically protected states, fragile magnetic systems and SC combined with agile and flexible responses to, and leadership in, a rapidly changing materials landscape. We will accomplish this by creating, testing, and ultimately understanding systems that exhibit compelling physical properties and ground states. We will examine outstanding issues in superconductivity, across a breadth of systems; understand magnetism across the spectrum from local moments to fragile and tunable systems and examine the role of magnetic frustration. We will examine quantum phase transitions and tunable systems, that allow deeper understanding of competing behaviors. And, as always, we will continue to explore new materials design, discovery, and growth of systems that may be model systems for revealing focused, basic questions about complex behaviors. We will create new materials and model systems to allow for the study of emergent states in proximity to suppressed, fragile magnetism; we will examine how new spin textured states can be discovered and controlled in rare earth and transition metal based systems; we will use controlled substitution and defect creation to discover and understand new examples of exotic superconducting, magnetic and topological states and we create and utilize new synthetic routes and algorithms to discover new, low dimensional (often magnetic) systems.

References

1. J. Schmidt, G. Gorgen-Lesseux, R. A. Ribeiro, S. L. Bud'ko, and P. C. Canfield, Effects of Co Substitution on the Structural and Magnetic Properties of Sr(Ni1−xCox)2P2, Phys. Rev. B **108**, 174415 (2023).

2. S. Huyan, J. Schmidt, A. Valadkhani, H. Wang, Z. Li, A. Sapkota, J. L. Petri, T. J. Slade, R. A. Ribeiro, W. Bi, W. Xie, I. I. Mazin, R. Valenti, S. L. Bud'ko, and P. C. Canfield, Near-room-temperature ferromagnetic ordering in the pressure-induced collapsed-tetragonal phase in SrCo2P2, Phys. Rev. B **112**, L041102 (2025).

3. H. Kim, M. A. Tanatar, M. Kończykowski, R. Grasset, U. S. Kaluarachchi, S. Teknowijoyo, K. Cho, A. Sapkota, J. M. Wilde, M. J. Krogstad, S. L. Bud'ko, P. M. R. Brydon, P. C. Canfield, R. Prozorov, *Nodal Superconductivity in Miassite Rh17S15*, Commun. Mater. **5**, 17 (2024).

4. B. Schrunk, Y. Kushnirenko, B. Kuthanazhi, J. Ahn, L.-L. Wang, E. O'Leary, K. Lee, A. Eaton, A. Fedorov, R. Lou, V. Voroshnin, O. J. Clark, J. Sanchez-Barriga, S. L. Bud'ko, R.-J. Slager, P. C. Canfield, and A. Kaminski, "Emergence of Fermi arcs due to magnetic splitting in an antiferromagnet," Nature, **603**, 610 (2022).

5. P. C. Canfield and T. J. Slade, Use of Frit-Disc Crucible Sets to Make Solution Growth More Quantitative and Versatile, Z. Für Anorg. Allg. Chem. **651**, (2025).

Publications

1. P. C. Canfield and T. J. Slade, Use of Frit-Disc Crucible Sets to Make Solution Growth More Quantitative and Versatile, Z. Für Anorg. Allg. Chem. 651, (2025).

2. T. J. Slade, N. Furukawa, M. Dygert, S. Mohamed, A. Das, W. Xia, C.-Z. Wang, S. L. Bud'ko, and P. C. Canfield, La4Co4X (X=Pb, Bi, Sb): A demonstration of antagonistic pairs as a route to quasi-low-dimensional ternary compounds, Phys. Rev. Mater. **8**, 064401 (2024).

3. H. Kim, M. A. Tanatar, M. Kończykowski, R. Grasset, U. S. Kaluarachchi, S. Teknowijoyo, K. Cho, A. Sapkota, J. M. Wilde, M. J. Krogstad, S. L. Bud'ko, P. M. R. Brydon, P. C. Canfield, R. Prozorov, *Nodal Superconductivity in Miassite Rh17S15*, Commun. Mater. **5**, 17 (2024).

4. N. K. Nepal, P. C. Canfield, and L.-L. Wang, HTESP (High-throughput electronic structure package): A package for high-throughput ab initio calculations, Comput. Mater. Sci. 244, 113247 (2024).

5. Y. Kushnirenko, L.-L. Wang, Z. Li, B. Kuthanazhi, B. Schrunk, E. O'Leary, A. Eaton, P. C. Canfield, and A. Kaminski, Long-range magnetic order induced surface state in GdBi and DyBi, Phys. Rev. B 110, 115151 (2024).

6. S. Huyan et al., *Strong Enhancement of Magnetic Ordering Temperature and Structural/Valence Transitions in EuPd3S4 under High Pressure*, Proc. Natl. Acad. Sci. United States Am. **120**, e2310779120 (2023).

7. S. Huyan, J. Schmidt, A. Valadkhani, H. Wang, Z. Li, A. Sapkota, J. L. Petri, T. J. Slade, R. A. Ribeiro, W. Bi, W. Xie, I. I. Mazin, R. Valenti, S. L. Bud'ko, and P. C. Canfield, Near-room-temperature ferromagnetic ordering in the pressure-induced collapsed-tetragonal phase in SrCo2P2, Phys. Rev. B **112**, L041102 (2025).

8. M. Xu, J. Schmidt, M. A. Tanatar, R. Prozorov, S. L. Bud'ko, and P. C. Canfield, Superconductivity and Magnetic and Transport Properties of Single-Crystalline CaK(Fe1−xCrx)4As4, Phys. Rev. B 107, 134511 (2023).

9. Q.-P. Ding, J. Schmidt, J. A. Moreno, S. L. Bud'ko, P. C. Canfield, and Y. Furukawa, Role of Nematic Fluctuations on Superconductivity in FeSe0.47Te0.53 Revealed by Nuclear Magnetic Resonance under Pressure, Phys. Rev. Lett. **134**, 226002 (2025).

10. Evan O'Leary, Zhuoqi Li, Lin-Lin Wang, Benjamin Schrunk, Andrew Eaton, Paul C. Canfield, and Adam Kaminski, "Topography of Fermi arcs in t-PtBi2 using high-resolution angle-resolved photoemission spectroscopy" Phys. Rev. B - DOI: https://doi.org/10.1103/n5pz-j2sl

Understanding and Tuning the Interplay Between Electronic Topology and Magnetism in Magnetic Topological Materials

Chetan Dhital and Madalynn Marshall (Kennesaw State University), Andrew Christianson, and Huibo Cao (Oak Ridge National Laboratory)

Keywords: Magnetic topological materials, Weyl fermions, Berry curvature, rare-earth intermetallics, anomalous Hall effect

Research Scope

This project investigates the interplay between local-moment magnetism and topological electronic structure in rare-earth intermetallics through an integrated experimental–computational approach. By combining Hall transport, neutron scattering, heat capacity, and thermal transport measurements with density functional theory (DFT), we aim to determine how magnetic ordering, magnetic anisotropy, and lattice tuning can generate and control Weyl points in correlated metals. Broken time-reversal symmetry from ferromagnetic or noncollinear magnetic states and/or broken inversion symmetry can create Berry curvature hot spots that strongly influence transport phenomena such as the anomalous Hall effect (AHE). Through systematic chemical substitution, chemical and uniaxial pressure, and broad exploration of rare-earth compounds, we seek to establish design principles for manipulating Weyl node positions, Berry curvature distributions, and quasiparticle dynamics via magnetic and structural control.

Recent Progress

Our initial focus has been on NdGaSi, where field- and temperature-dependent Hall transport measurements reveal a robust anomalous Hall effect below the ferromagnetic transition temperature. The magnitude of the AHE scales with magnetization, consistent with an intrinsic origin linked to the Berry curvature from the Weyl nodes. Single-crystal neutron diffraction has confirmed a collinear ferromagnetic ground state with moments aligned along the crystallographic *c*-axis, thereby breaking time-reversal symmetry in a centrosymmetric lattice—an essential condition for Weyl physics. Complementary DFT calculations using the experimental magnetic configuration identify multiple Weyl nodes near the Fermi level, with the calculated Berry curvature distribution reproducing the sign, magnitude, and temperature evolution of the observed AHE. Thermodynamic measurements further support this picture: heat capacity data reveal a low-temperature Schottky anomaly and a gapped magnon spectrum with a gap of 6.7 K, while the recovered magnetic entropy approaches Rln10 by 60 K, consistent with the full crystal-field-split J = 9/2 multiplet of Nd^{3+}. Together, these results demonstrate a coherent link between magnetic order, Berry curvature, and topological transport in NdGaSi.

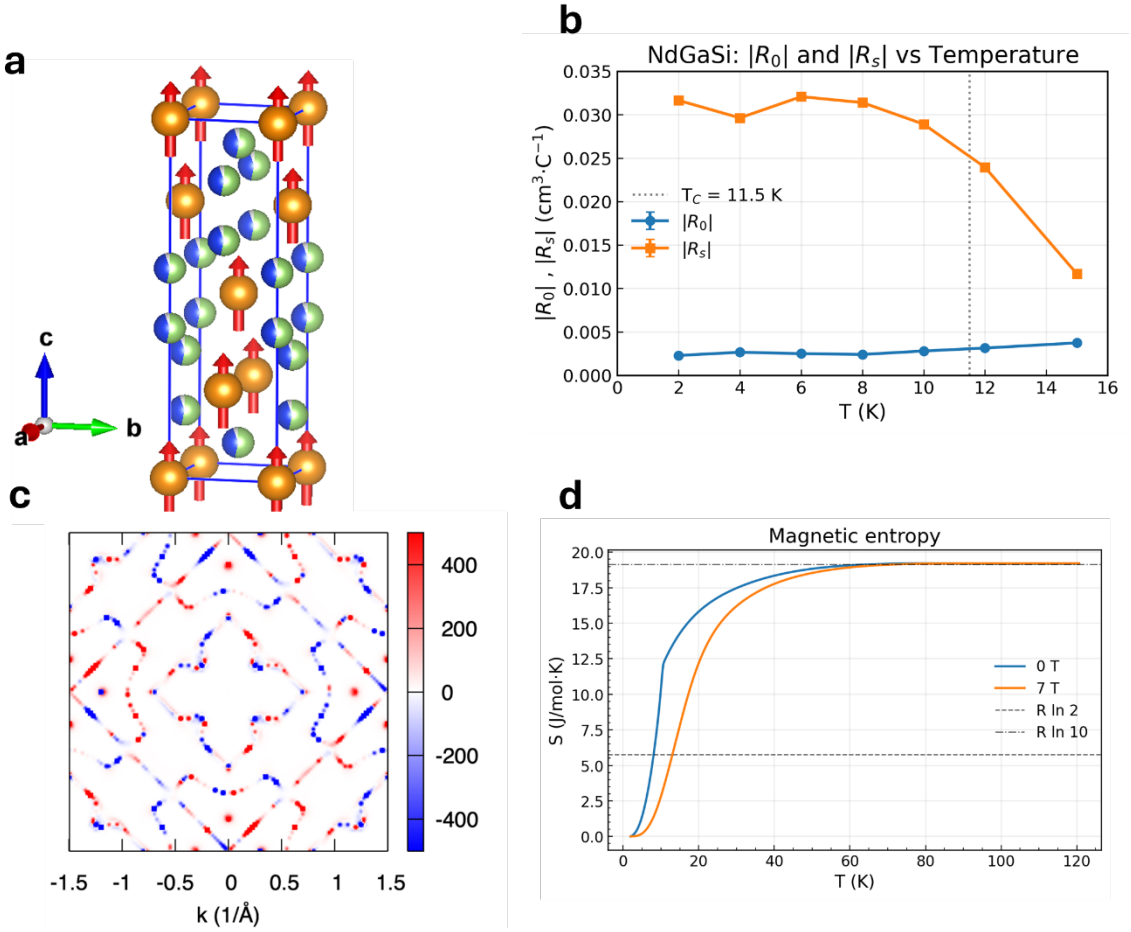


Figure 1: Structural, transport, and thermodynamic properties of NdGaSi. (a) Crystal and magnetic structure, highlighting Nd (orange), Ga (blue), and Si (green) atoms with ferromagnetic ordering along the *c*-axis. (b) Temperature dependence of $|R_0|$ and $|R_s|$, showing a sharp suppression of $|R_s|$ above T_C =11.5 K. (c) Calculated Berry curvature Ωz(k) in the Brillouin zone, revealing hot spots near Weyl nodes. (d) Magnetic entropy $S(T)$ from heat capacity at 0 T and 7 T, approaching $R\ln 10$ at high T, consistent with the full Nd^{3+} multiplet.

Future Plans

Building on these findings, we plan to expand our studies to a broader family of rare-earth intermetallics, including DyAgGe, ErAgGe, PrGaSi, NdGaGe, and PrGaGe, to examine how 4*f* configuration, exchange interactions, and spin–orbit coupling influence Weyl physics. Chemical pressure tuning will be pursued through synthesis of $RAgGe_{1-x}Si_x$ and $RGaSi_{1-x}Ge_x$ (R = rare earth), allowing lattice constants to be varied without carrier doping and providing controlled pathways to modify exchange interactions, crystal fields, and Weyl node positions. Field–temperature phase diagrams will be constructed by combining magnetization, Hall effect, and neutron scattering measurements to identify Berry curvature–enhanced regimes and detect field-induced magnetic transitions. Low-temperature thermal conductivity experiments will probe phonon, magnon, and potential Weyl fermion contributions, as well as magnon–phonon coupling. Finally, uniaxial strain will be applied in situ during transport to directly tune magnetic anisotropy and lattice symmetry, enabling exploration of strain-driven topological phase transitions.

Overall, this project seeks to establish rare-earth intermetallics as a tunable platform for magnetically induced topological states, providing fundamental insight and strategies for designing correlated Weyl metals and controlling Berry curvature–driven transport in quantum materials.

Publications

Publications from this project are currently in progress. Manuscripts under preparation focus on the large anomalous Hall effect and Berry curvature origin in NdGaSi, the magnetic structure and anisotropy of rare-earth intermetallics probed via neutron scattering, and the tunability of topological transport properties through chemical substitution and lattice control. These studies will collectively establish the experimental–theoretical framework for engineering Weyl physics in correlated rare-earth materials.

Geometry and frustration-induced phenomena in nanomagnet arrays

Principal Investigator: *Peter Schiffer*, *Princeton University*

Keywords: Magnetism, Nanostructures, Spin models, Topology

Research Scope

This program studies lithographically fabricated "artificial spin ice" arrays of nanometer-scale single-domain ferromagnetic islands. The physics of artificial spin ice offers intersects with a range of important topics, including the effects of frustration and topology. Since the arrays are created lithographically, we can easily vary the array characteristics, including the geometry of the lattice, the nature of the moments, and the level and type of lattice disorder. We can probe the local properties of the arrays by imaging individual moments, and we can also probe thousands of moments simultaneously, allowing us to gain insight into the collective properties of the system and observe novel phenomena that are not accessible in other systems.

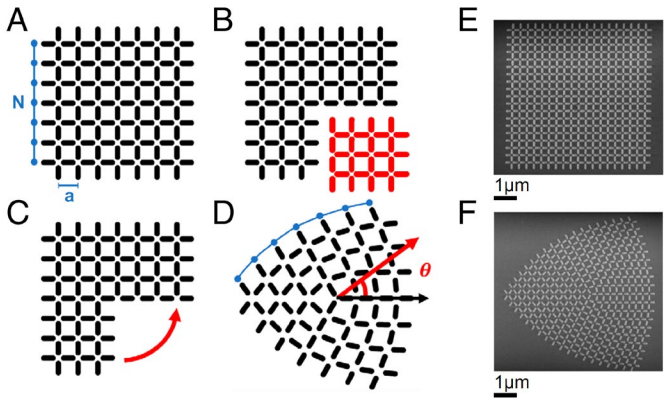
This research program focuses on the properties of these systems, probing the collective behavior of different geometries, and exploring arrays of more complex nanomagnet shapes. Specific thrusts include examinations of new lattice geometries, low-frequency dynamics of the moments, finite size effects in smaller arrays, and magnetic moments that are not simple dipoles. The research program uses permalloy as the ferromagnetic material, taking advantage of its well-understood magnetic properties and low magnetocrystalline anisotropy.

Recent Progress

While experimental progress has been slightly impacted by the move from Yale to Princeton in late 2023, and the need to reconstruct the laboratory at Princeton, there have been a number of recent accomplishments. This includes some simulations based on earlier studies of topological strings in Sante Fe ice [1] and a final paper on mobile excitations studied through noise measurements in tetris ice [2]. Other areas of recent activity include the following studies:

Topologically-induced fractional charges in a finite size artificial spin ice array: We have designed and studied a finite nanomagnet array based on the well-studied square ice structure, but with the intentional insertion of a topological defect known as a disclination. This system demonstrates how topological defects in the structure of a collective system influence the magnetic ensemble's global behavior [4].

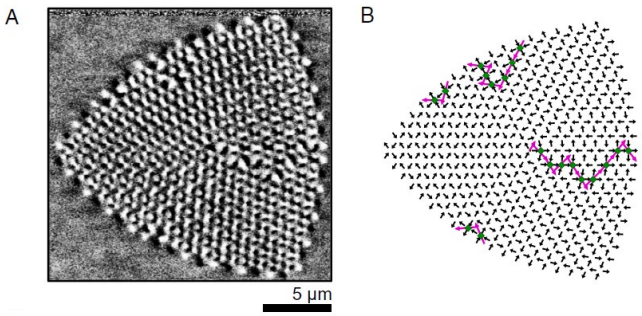
Within square ice, the moments have a well-ordered ground state, and excitations above the ground state can be characterized as effective magnetic charges. By introducing a disclination into a square ice array, we force the trapping of a fractional charge with effects on the collective behavior of the entire array. While the concept of a fractional charge is more commonly associated with exotic quantum materials, our research reveals a parallel occurrence in the classical nanomagnet



The cut-and-glue procedure used to form a disclination array. (A) A square ice array with size N = 7. (B and C) Illustration of the removal of a quadrant of the square ice array and the reconnection of the remainingislands. (D) The resulting disclination array. (E and F). Scanning electron microscope images of square ice and disclination arrays with N = 19. Reproduced from [4].

ensemble of artificial spin ice. The induced charge is truly fractional: it has ground state values of ±1, whereas magnetic charges in square ice without such a defect are constrained to values of ±2 or ±4.

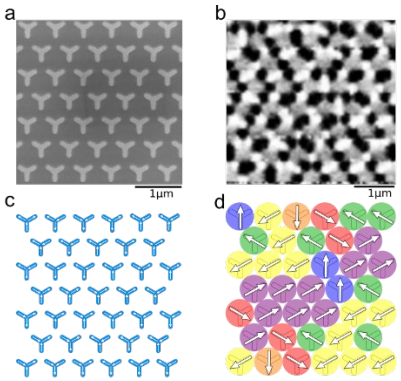
Furthermore, according to Gauss' theorem, the existence of a fractional charge within the bulk necessitates a corresponding net flux at the boundary, equivalent in magnitude to the charge. Previous theoretical work on artificial spin ice has established that, at the lowest energy state, this flux must be carried by a singular entity known as a "Faraday Line." In square ice with no defects, Faraday lines cannot terminate or originate within the system's bulk. Rather, they must form loops or enter and exit from the boundaries. However, the trapping of the fractional charge ±1 compels the existence of a Faraday line ending in it, fundamentally altering the expected behavior within the system.



Example disclination array configuration and vertex types. A) Magnetic force microscopy (MFM) image and B) moment map of a disclination array. The lines show the flow of magnetic flux through the sample, notably the line coming from the central topological defect. Reproduced from [4].

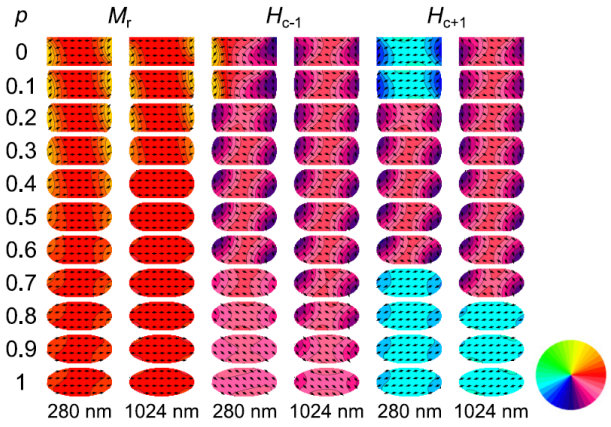
Our results demonstrate how a topological defect affects the global physics of the ensemble. A related and equally compelling issue we address is the direct visualization, within a geometrically intuitive system, of the so-called bulk-to-edge correspondence. We show that trapping of a fractional charge in the bulk implies a line of excited vertices extending all the way to the system's edges. Furthermore, by engineering the geometry of the array, we can tune the energy landscape through which the flux lines travel, demonstrating an interesting nexus of geometrical and topological effects.

Collective behavior of magnetic tripods: Previous studies of artificial spin ice have focused on stadium-shaped islands or nanowires whose magnetization can be described by Ising-like binary moments. A few studies have looked at effective XY and quadrupolar moments by altering the island shape – but always staying within paradigms of types of moments that have been studied in atomic magnetic systems. In our group's recent work, we created a new object, a magnetic tripod, that has three-fold symmetry with six possible magnetic states [3]. We explore its collective behavior by realizing interacting triangular arrays of these objects which individually map well onto theoretical models for Potts or clock states. To our knowledge there has been no prior experimental realization of a 6-state object of this nature, and certainly no realization of interacting arrays of such objects. After thermalizing these arrays, which we have named "magnetic tripod ice", we demonstrate collective ferromagnetic behavior that has qualitative differences with the well-studied kagome ice system of similar geometry. We thus demonstrate the importance of the tripod moment as an emergent variable and we are now exploring a range of new lattices in which we anticipate finding new physical phenomena associated with these unusual structures.



Magnetic tripod ice. (a) Scanning electron microscopy image of triangular lattice of interacting tripods as an example of magnetic tripod ice (b) Magnetic force microscopy (MFM) image of the same sample. (c) Map of the moments of the individual legs from the MFM image. (d) Map of the tripod moments from the MFM image. Reproduced from [3]

Micromagnetic study of nanomagnet shape in artificial spin ice: Artificial spin ice studies often treat the nanomagnets as simple Ising moments, when their finite size actually leads to internal magnetic textures. These textures can affect the physics of interacting arrays, and we investigated how varying the shape of elongated nanomagnets, from rectangular to elliptical geometries, influences the magnetic reversal process in artificial spin ice square arrays. While previous studies have emphasized the effects of island size and lattice geometry, how the end geometry of nanomagnets impacts both internal magnetic textures and inter-island coupling has not been well-explored. Using micromagnetic simulations [5], we address this gap, providing new insights into fundamental magnetic phenomena and highlighting opportunities to tailor magnetic behavior through island shape.



Magnetization maps of nanomagnets in square ice with length 180 nm and varying pointiness ranging from elliptical to rectangular and lattice spacings of 280, 400 and 1024 nm. The magnetization map at remanence and at the simulation step in the hysteresis loop prior to and after the coercivity inflection point. Arrows within the maps indicate the local direction of the magnetization. Color coding of the moment direction is based on the color wheel to the bottom right. Reproduced from [5].

Future Plans

The research program has a number of ongoing activities such as ongoing studies of the physics of other lattices of magnetic tripods in which we expect to encounter new behavior. We also are looking at the low frequency dynamics of artificial spin ice through AC susceptibility measurements that were delayed because of the move to Princeton. Finally, we expect to continue investigations of novel finite systems, especially in the context of topological effects of the sort seen with disclinations and the Santa Fe lattice.

References and Publications

[1]. Xiaoyu Zhang, Grant Fitez, Shayaan Subzwari, Nicholas S. Bingham, Ioan-Augustin Chioar, Hilal Saglam, Justin Ramberger, Chris Leighton, Cristiano Nisoli, and Peter Schiffer, *Topological Kinetic Crossover in a Nanomagnet Array*, Science, **380**, 526-531 (2023).

[2]. Mateusz Goryca, Xiaoyu Zhang, Justin Ramberger, Justin D. Watts, Cristiano Nisoli, Chris Leighton, Peter Schiffer, and Scott A. Crooker, *Deconstructing magnetization noise: Degeneracies, phases, and mobile fractionalized excitations in tetris artificial spin ice*, Proceedings of the National Academy of Sciences **120**, e2310777120 – 1-6. (2023).

[3]. Xiaoyu Zhang, Ioan-Augustin Chioar, Grant Fitez, Anthony Hurben, Michael Saccone, Nicholas S. Bingham, Justin Ramberger, Chris Leighton, Cristiano Nisoli, Peter Schiffer, *Artificial tripod ice*, Physical Review Letters **131**, 126701 – 1-7 (2023).

[4]. Anthony Hurben, Yinchen Hao, Ioan-Augustin Chioar, Liu Yang, Nanny Strandqvist, Michael Saccone, Nicholas S. Bingham, Justin Ramberger, Chris Leighton, Cristiano Nisoli, and Peter Schiffer, *Fractional magnetic charges and channeling of Faraday lines by disclinations in artificial spin ice*, Proceedings of the National Academy of Sciences **122**, e2415101122 – 1-7 (2025).

[5]. N. Strandqvist, G. Fitez, O. Heinonen, and P. Schiffer, *Nanomagnet shape effects on magnetic reversal in artificial spin ice*, Physical Review B **111**, 184420 – 1-7 (2025).

Unconventional superconductivity in strongly correlated triangular adatom lattices

Hanno H. Weitering and Ruixing Zhang

Keywords: Superconductivity, strong correlated electron systems, topology, molecular beam epitaxy, scanning tunneling microscopy.

Research Scope

This new BES/ECMP project seeks to explore chiral superconductivity in artificially structured semiconductor platforms and develop novel machine learning protocols to extract the pairing symmetry from quasi-particle interference patterns. Semiconductor templates represent ideal model systems for elucidating the role of electron correlations and magnetic frustration in establishing unconventional superconductivity and may pave the way for integrating topological superconducting architectures with 21st century silicon technology.

Recent Progress

We recently demonstrated that a $(\sqrt{3} \times \sqrt{3})$R30° Sn adatom layer on a heavily-doped p-type Si(111) substrate (Fig. 1) is superconducting with a critical temperature T_C as high as 9 K.This result is truly remarkable: It only takes 1/3 monolayer of Sn to create a 2D superconductor on bulk Si with T_c rivaling that of Nb and exceeding those of all other elements in the Periodic Table. In this lattice, there is one half-filled dangling-bond orbital per site (Fig. 1a) and, accordingly, the undoped system is a single-band antiferromagnetic Mott insulator with a Hubbard U of about 0.6 eV and band width of 0.5 eV. Hole doping metallizes the Mott surface state which allows the system to become superconducting. Because of the strong correlations and triangular lattice symmetry, a chiral *d*-wave scenario seems likely. Experimental evidence in support of chiral *d*-wave pairing includes the observation of (*i*) a hard gap in the tunneling spectrum, (*ii*) time-reversal symmetry breaking in quasi-particle interference (QPI) imaging, (*iii*) in-gap bound states at each defect, and (*iv*) existence of edge states at domain boundaries. However, these criteria represent a necessary but insufficient condition for demonstrating chiral superconductivity.

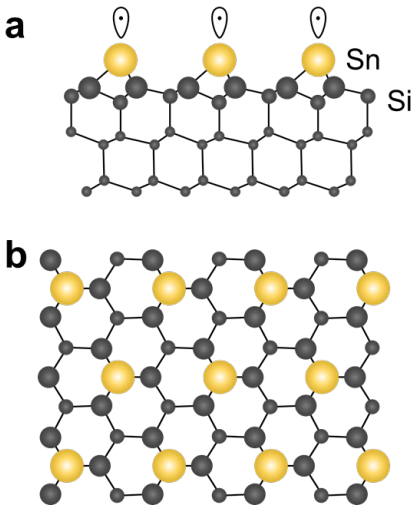


Fig. 1. (a) Side and (b) top view of the Sn/Si(111) interface. The Sn atoms (yellow) adsorb right above the second-layer Si atoms (small gray spheres). The Sn-Sn adatom spacing is 6.65 Å. The dangling bonds are half-filled, producing a single-band Mott insulator.

Very recently, we identified a microscopic fingerprint of chiral Cooper pairing from high-quality real-space QPI data centered at atomic-scale point defects in the Sn layer. Remarkably, the

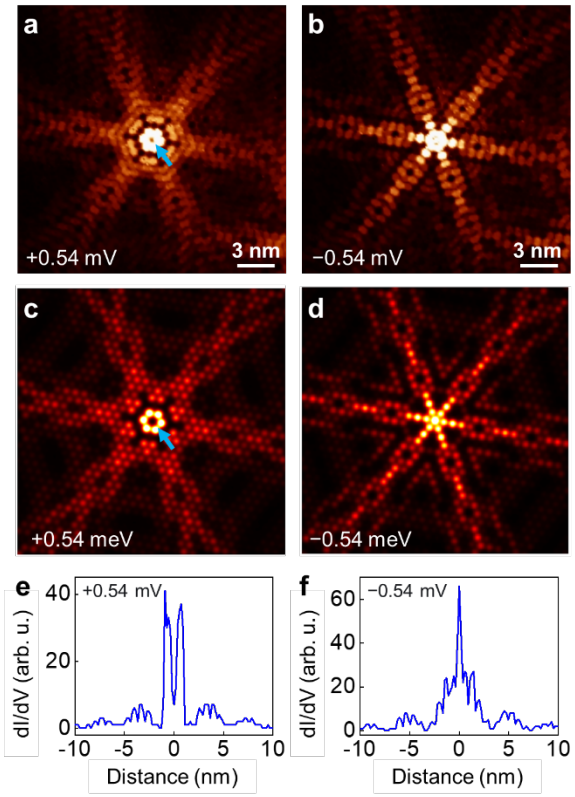


Fig. 2 (a) and (b) Experimental *dI/dV* maps of a substitutional Si defect, Data were collected at 400 mK. (c) and (d) Theoretical LDOS maps. Notice the pronounced dark spot at the center of panels (a) and (c), indicated by blue arrows, which is a key signature of a chiral superconducting order parameter. (e) and (f) *dI/dV* line scans along the atom rows from (a) and (b), showing the strong node or antinode at the defect site, respectively.

scattering potential at these defects is extremely simple, well described by a delta function, while electrons tunnel directly into the active layer. The observed anisotropic interference patterns are almost perfectly reproduced theoretically without parameter fine-tuning. Specifically, we detected symmetry-locked nodal and antinodal points in the Bogoliubov quasiparticle wavefunction, tightly bound to atomic point defects in the tin lattice (Fig. 2). These nodal features, along with their surrounding texture, form a distinct real-space pattern exhibiting a clear and exclusive hallmark of chiral superconductivity.

The definitive identification of chiral superconductivity presented here is made possible by the structural simplicity of the Sn/Si(111) system, which permits unambiguous detection of atomic-scale point defects that preserve the underlying C_6 symmetry and facilitates modeling of the corresponding scattering potentials. In contrast, more complex or disordered defect configurations tend to obliterate the characteristic chiral LDOS signature due to symmetry breaking and the increased complexity of the scattering potential.

Future Plans

1. Electronic phase diagram. Our investigations of Sn triangular adatom system suggest the presence of a superconducting dome on the hole-doped side, which possibly emerges from antiferromagnetic spin correlations. The maximum T_c reached so far is 9 K, but the doping range was very limited. We will expand our doping range and explore the electron-doped side of the phase diagram as well. We aim to establish the pairing symmetry in different parts of the phase diagram and investigate the nature of the normal state. Extended Hubbard models indicate that the chiral *d*-wave order parameter is favored close to half filling, while triplet $p_x \pm ip_y$ pairing would be preferred with increased hole-doping; *f*-wave pairing should be observed with electron doping. The possibility of accessing these exotic pairing symmetries within this model system would be most fascinating and a powerful test of modern theories of superconductivity.

2. Pairing symmetry. We will study real-space and momentum-space interference patterns of Bogoliubov quasi-particles with STM. Bogoliubov quasi-particles live inside the superconducting

gap, scatter off lattice defects, and carry information about the pairing symmetry. Experimental QPI images are usually compared to theoretical *T*-matrix simulations for various order parameters. Such comparisons are rarely conclusive because the patterns often look similar. We will develop a convolutional neural network (CNN) decoder to efficiently and accurately decrypt the pairing symmetry from the QPI images. Conventional CNNs typically function as black boxes with limited interpretability. To address this challenge, we plan to integrate advanced deep-learning techniques into our network design. With this update, the decoder will generate interpretable maps that highlight the key differentiating features in the QPI spectra, elucidating the basis of its classification decisions. This interpretability not only provides clarity in understanding the network's decision process but also offers insights into the underlying physics of the Sn/Si system.

3. Other materials platforms. We will expand these investigations to related model systems such as Pb and Sn on Ge(111) and SiC(0001) as well as Kagome adatom lattices. The use of Pb is expected to enhance spin-orbit coupling, which in conjunction with Zeeman splitting could produce Majorana states at the edges of the defect lattices and superconducting domains. Not all systems may become superconducting but understanding these differences will also be an important part of the investigations.

References

1. F. Ming, X. Wu, C. Chen, K. D. Wang, P. Mai, T. A. Maier, J. Strockoz, J. W. F. Venderbos, C. Gonzalez, J. Ortega, S. Johnston, and H. H. Weitering, Evidence for chiral superconductivity on a silicon surface. Nature Physics 19, 500–506 (2023).
2. G. Li, P. Höpfner, J. Schäfer, C. Blumenstein, S. Meyer, A. Bostwick, E. Rotenberg, R. Claessen, and W. Hanke, Magnetic order in a frustrated two-dimensional atom lattice at a semiconductor surface. Nat. Commun. 4, 1620 (2013).
3. F. Ming, S. Johnston, D. Mulugeta, T. S. Smith, P. Vilmercati, G. Lee, T. A. Maier, P. Snijders, and H. H. Weitering, Realization of a hole-doped Mott insulator on a triangular silicon lattice. Phys. Rev. Lett. 119, 266802 (2017).
4. R. Nandkishore, L. S. Levitov and A. V. Chubukov, Chiral superconductivity from repulsive interactions in doped graphene, Nature Phys. 8, 158 (2012).
5. Xuefeng Wu, Xuan Hao, Zhuo Chen, Yuchang Cai, Minghao Wu, Congrun Chen, Kedong Wang, Fangfei Ming, Steven Johnston, Rui-Xing Zhang, Hanno H. Weitering, Microscopic Fingerprint of Chiral Superconductivity, https://doi.org/10.48550/arXiv.2507.18693
6. S. Wolf, D. Di Sante, T. Schwemmer, R. Thomale, and S. Rachel, Triplet Superconductivity from Nonlocal Coulomb Repulsion in an Atomic Sn Layer Deposited onto a Si(111) Substrate. Phys. Rev. Lett. 128, 167002 (2022).

Crystal electric-field effect under magnetic field and uncovering field-induced magnetic phase transition in triangular rare-earth magnet $CsErSe_2$

Minhyea Lee, *University of Colorado Boulder*

Keywords: Magnetism, Rare-earth compounds, Crystal electric field, Optical spectroscopy

Research Scope

Unconventional magnetic phases in condensed matter systems lie at the forefront of advances in spintronics and quantum information processing. Applications in these fields are firmly rooted in utilizing novel functional materials; hence, they require a complete understanding of the properties of magnetic states that are characterized by ordering, spin excitations, or exotic ground states, as well as of the nature of the interaction between spin and lattice degrees of freedom. This project aims to capture the interactions between spin and lattice by examining the rare-earth insulating magnetics system, where the strong spin-orbit coupling dictates fundamental magnetic properties like anisotropy and crystal electric field (CEF) effect, but also creates a diverse energy hierarchy that can lead to magnetic frustration. We leverage intense magnetic fields and inherent magnetic anisotropies to investigate how the CEF level splitting under a magnetic field manifests the multi-faceted natures of the coupling between spin and lattice degrees of freedom within a single-ion description. Furthermore, we explore the possibilities to utilize the lattice degrees of freedom as a direct probe for magnetic degrees of freedom, via thermal conductivity and the CEF-level-hybridization with phonons. This, in turn, offers novel insights and clues for pinning down highly sought-after entangled and unconventional magnetic states.

Recent Progress

We use the RE-based insulating triangular delafossites, $AREX_2$ (A = alkali ions of Cs, Na, K, RE = rare-earth ions, X = chalcogen of O, S, Se) as a model system to explore the scope described above. RE-based delafossites have been shown to host a range of novel quantum phenomena due to the interplay and competition between spin-orbit coupling, crystal electric fields, and exchange interactions of spins in the presence of geometric frustration inherent to the triangular lattice [**1,2,3**]. In particular, the crystal electric field (CEF) interactions of *RE* ions play a crucial role in determining the system's magnetic ground state and anisotropy. The localized 4f electrons bring down the typical CEF energy range to 10^{-1}-10^{1} meV, much smaller than their *3d* counterparts, which can be easily manipulated with a moderate magnetic field via Zeeman splitting. With Kramer's ions, each CEF level is doubly degenerate and becomes split into two states under a magnetic field. At sufficiently low temperatures, where the energy of the first excited state lies beyond thermal excitation, the dynamics of spin degrees of freedom are restricted to the lowest such doublet and invoked to justify using an effective pseudospin-1/2 model. My group's research efforts have been centered on various aspects of these insulating RE magnets with a range of experimental probes, including cantilever-based magnetometry [**2**], thermal transport [**3**], and AC magnetic susceptibility and magnetooptical spectroscopy [**4**].

For the last two-year period, we have focused on $CeErSe_2$ and its magnetic field dependence of the CEF level splitting. Since the Er^{3+} ion has the total angular momentum $J = 15/2$, when the Er ion is placed in the octahedral environment, i.e., surrounded by six anion Se^{2-} (D_{3d} site symmetry) [**Fig. 1(a)**], its 16 eigenstates rearrange into eight doublets at zero field (ZF). Each doublet splits under a magnetic field. Interestingly, due to the narrow energy spacing among adjacent levels, the CEF levels of $CeSeEr_2$ inevitably exhibit multiple crossings as a function of field, as shown in **Fig. 1(b)**. In addition to the intricate myriad of the level crossings, it unequivocally illustrates the magnetic anisotropies with distinct spectra for B || ab and B || c.

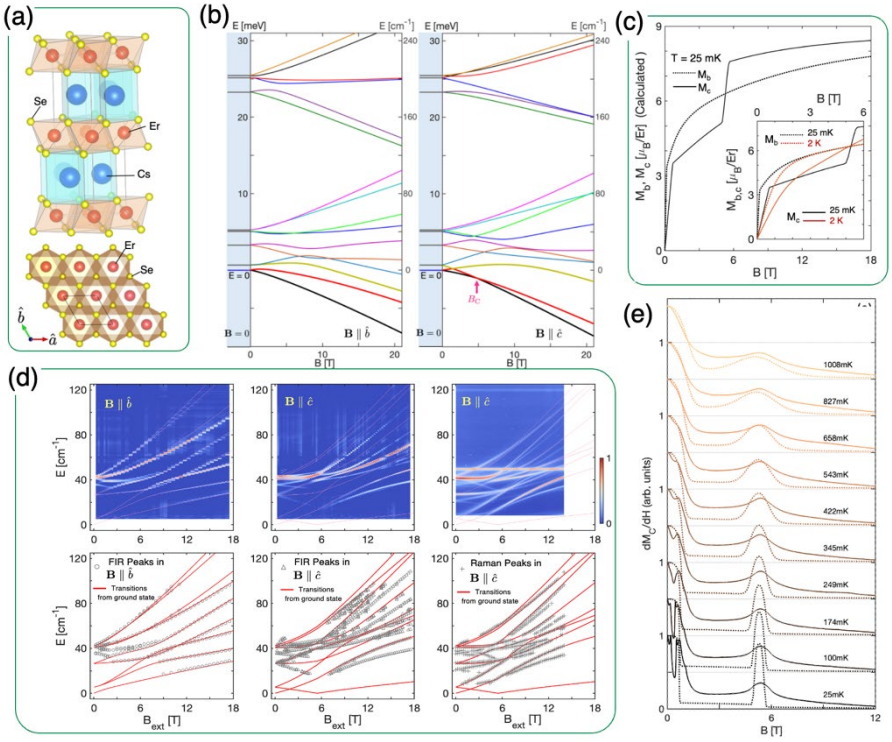


Figure 7 The CEF physics of CeErSe2 : (a) Crystal structure of $CsErSe_2$ (upper) and the triangular lattice on the ab plane consisting of edge-sharing ErSe6 octahedra(lower) **(b)** The calculated CEF splitting's depending on the field directions of B || b (left) and B || c (right). The CEF parameters **(c)** The magnetization of $CeErSe_2$ based on the CEF parameter at T = 25 mK and 2 K (inset) **(d)** A direct measurements of the CEF splitting under magnetic field using the magneto-optical spectroscopies are plotted in color maps (upper panels) and peak position read off from the data (lower panels). FIR results in B || b (left-most) and in B || c (middle) and Raman in B || c (right-most) are shown. **(e)** AC magnetic susceptibility as a function of applied field to track out the level crossing of the ground state, marked by the pronounced peaks at $B = B_C = 5.4$ T (dotted and solid lines for data and calculation, respectively, which exhibits a strong temperature dependence thanks to the Boltzmann factor.

Our recent progress on this project involves *directly* measuring the CEF splitting using magneto-optical spectroscopy, as shown in **Fig. 1(c)**, and obtaining the CEF parameters from the spectroscopy results with high fidelity, which enables us to create **Fig. 1(b)**. These single-ion properties play a crucial role as a guide reveling unusual magnetic properties; (i) the quadratic Zeeman splitting [2] which is essential to understanding the low temperature magnetic susceptibility, (ii) the g-factor for the $CsErSe_2$ in B || c is found to have strong B dependence due to non-monotonic field dependences of the low energies levels in **Fig. 1(b)**, (iii) the pseudospin-1/2 approximation should be treated with extreme care due to the level crossings. (iv) Most importantly, we uncovered the ground state crossing at $B_C = 5.4$ T as marked with the pink arrow on the right panel of **Fig. 1(b).** Due to the change of the wave function across B_C, the calculated magnetization displays a step-like increase in M_C as shown in **Fig. 1(d)**, exhibiting the first-order transition. We emphasize that this feature originates solely from the CEF physics, as the spin

exchange energy scale is much smaller. To experimentally verify the magnetic behavior near B_C, we measured the ac magnetic susceptibility at low temperatures as a function of applied magnetic field, and we displayed it in **Fig. 1(e)** with solid lines at various temperatures in comparison with calculations in dotted lines. The sharp features at BC quickly smear out with increasing temperature due to the changes in population of the levels subject to the Boltzmann factor.

Our work unambiguously demonstrates the essential role of single-ion physics in driving collective magnetic phenomena under intense magnetic fields, as well as rich physics involving the low-energy excitations, offering a new route to the emergence of magnetic frustration. We will outline the future directions devised based on this work [**4**].

Future Plans

Our progress offers critical perspectives not only for advancing the understanding of magnetism unique to rare-earth triangular systems, but also for generating new approaches to spin–lattice interactions starting from the viewpoint of the single magnetic ion. Moreover, the insights gained here can be extended to other rare-earth magnetic compounds, enabling informed and effective predictions involving the field evolution of the CEF levels as demonstrated in this work. Here we list our plans, which we have already been working on or plan to implement in the very near future.

(1) Determining the accurate magnetic anisotropy of a single ion is an indispensable step toward understanding any magnetic phenomena in rare-earth magnets. We find that the magneto-optical spectroscopy is a superb experimental method to obtain the CEF parameters with unprecedented precision. Similar magneto-optical spectroscopy on a couple of other RE compounds is underway.

(2) The CEF parameters determined with sufficient precision lead to uncovering the field-induced transition like the one in Fig. 1(b). Although we used the Weiss mean field approximation, this can be treated with more sophisticated spin models, for example, including diagonal terms in the XXZ model, which was found to be cancelled out in the mean field theory. Although this transition in $CsErSe_2$ has manifested as a straightforward first-order like transition because of a discontinuous transition of the wave of $CsErSe_2$ function with very little contribution from the spin Hamiltonian, however, this can turn into a very large degeneracy when the involving RE ions exhibit strong interaction with each other, potentially leading to strong quantum fluctuation, a prerequisite for a quantum spin liquid state.

(3) Most importantly, the well-characterized CEF levels are also used to investigate the hybridization between the phonon energy spectrum and the CEF levels, of which hybridized quasiparticles are responsible for the physical properties such as specific heats and other thermodynamic quantities and thermal conductivities [3,5]. We are actively investigating the heat transport carried out by these hybridized quasiparticles.

(4) Finally, we have extended our study to rare-earth-based magnets containing non-Kramers ions (i.e., ions with integer total spin). This effort is motivated by preliminary measurements on $CsTbSe_2$, where the zero-field ground state is a singlet, yet level crossings play a crucial role in

producing the unusual field-dependent magnetization. Building on this, we have recently initiated investigations of additional rare-earth insulating magnets to test these ideas further.

References

1. M. M. Bordelon, E. Kenny, C. Liu, T. Hogan, L. Posthuma, M. Kavand, Y. Lyu, M. Sherwin, N. P. Butch, C. Brown, M. J. Graf, L. Balents, and S. D. Wilson. *Field-tunable quantum disordered ground state in the triangular lattice antiferromagnet $NaYbO_2$.* Nature Physics **15**, 1058 (2019)

2. C. A. Pocs, P. E. Siegfried, J. Xing, A. Sefat, M. Hermele, B. Normand, and M. Lee. *Systematic extraction of crystal electric field effects and quantum magnetic model parameters in triangular rare-earth magnets*. Physical Review Research **3**, 043202 (2021)

3. C. A. Pocs, I. A. Leahy, J. Xing, E. S. Choi, A. Sefat, M. Hermele, and M. Lee. *Heat conduction in magnetic insulators via hybridization of acoustic phonons and spin-flip excitation*. Physical Review Research **7**, L022007 (2025).

4. H. G. Whitelock, A. O. Scheie, M. McMaster, L. Xing, E. S. Choi, D. Rehn, M. Ozerov, D. Smirnov, I. A. Leahy, J. Xing, A. S. Sefat, and Minhyea Lee. *Crystal electric field effects under magnetic field and uncovering field-induced magnetic phase transition in a triangular rare-earth magnet CsErSe2*. to be submitted (2025)

5. A. O. Scheie, S. J. Li, S. D. Wilson, and D. Rehn. *Explaining the extra crystal-field mode in $ACeX_2$ (A = K, Rb, Na; X= O, S, Se, Te)*. Physical Review B **112**, 014415 (2025).

Publications

1. C. A. Pocs, I. A. Leahy, J. Xing, E. S. Choi, A. Sefat, M. Hermele, and M. Lee. *Heat conduction in magnetic insulators via hybridization of acoustic phonons and spin-flip excitation*. Physical Review Research **7**, L022007 (2025).
2. I. A. Leahy, A. C. Treglia, G. Cao, B. Skinner, and M. Lee. *Refining the two-band model for highly compensated semimetals using thermoelectric coefficients.* Physical Review B **112,** 035135 (2025).
3. P. E. Siegfried, M. Maus, A. C. Bornstein, D. Wulferding, J. Kim, R. E. Baumbach, E. D. Bauer, F. Ronning, and M. Lee. *Evolution of magnetic bubble domains in the uniaxial ferromagnet $CeRu_2Ga_2B$ inferred from the Hall effect and ac magnetic susceptibility*. arXiv:2508.xxxxx (2025).
4. K. Feng, C. Bush, O. Oladehin, M. Lee, and R. Baumbach. *Ferromagnetic order in the metallic triangular lattice compound $SmAuAl_4Ge_2$.* Physical Review B **109**, 014436 (2024).

Nuclear Magnetic Resonance Resolves Charge Order Structure in Kagome Metals

Xiaoling Wang, California State University, East Bay

Brenden R. Ortiz, Oak Ridge National Laboratory

Keywords: Charge Density Wave, Kagome Metals, Microstructure, Knight Shift, Electric Field Gradient

Research Scope

We apply orientation-resolved nuclear magnetic resonance (NMR) and high-field, multi-frequency electron magnetic resonance (EMR) to investigate how charge order and magnetism develop across kagome metals of AV_3Sb_5 (A = K, Rb, Cs), ScV_6Sn_6, and rare-earth $LnTi_3Bi_4$. (This abstract focuses on NMR results, with EMR efforts noted for scope.) Our work addresses three objectives. First, in AV_3Sb_5 we constrain the site-specific charge density wave (CDW) microstructure and characterize a low-temperature first-order instability in the CDW state using ^{51}V NMR. Second, in ScV_6Sn_6 we distinguish competing c-axis charge-order modulations and establish ^{119}Sn and ^{45}Sc NMR observables to track their evolution across the transition. Third, we extend high-field, angle-resolved EMR to $LnTi_3Bi_4$ to quantify local anisotropy and magnetic correlations. Collectively, these efforts define the current scope of the project: an integrated magnetic-resonance approach that provides isotope- and site-specific observables of charge order and magnetism in kagome metals, and develops methods transferable to related quantum materials.

Recent Progress

Angle-resolved ^{51}V (I = 7/2) NMR tracks changes in the Knight-shift tensor across T_{CDW} in RbV_3Sb_5 and CsV_3Sb_5. In CsV_3Sb_5, the central transition splits into four components whose field-linear separation indicates a Knight-shift origin, consistent with four inequivalent V environments in the CDW state (Fig.2a). The pairwise sums of component intensities evolve together while the total intensity is conserved (Fig. 2b-d); the redistribution from V2 to V2′ on cooling is consistent with the growth of a period-4 registry. These observations, combined with the Knight-shift anisotropy shown in Fig. 1, are compatible with an interlayer-modulated 3q CDW with 2×2×4 domains that could involve mixing of trihexagonal (TrH) and Star-of-David (SoD) layers in CsV_3Sb_5. By contrast, RbV_3Sb_5

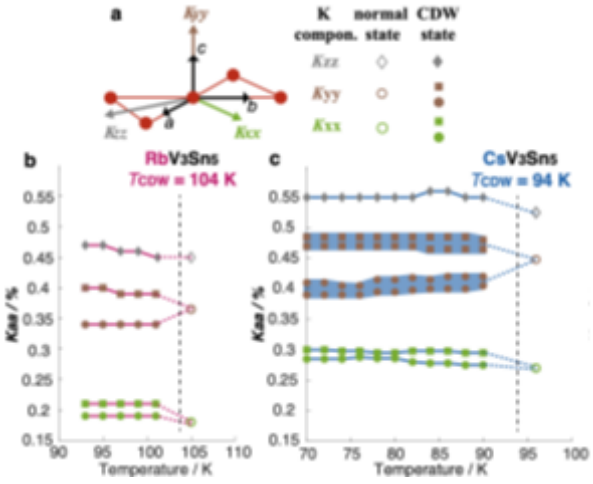


Figure.1 ^{51}V Knight-shift tensor through the CDW transition in RbV_3Sb_5 and CsV_3Sb_5. (a) Definition of principal components with respect to crystal axes. (b)&(c) Temperature dependence of tensor components in RbV_3Sb_5 across T_{CDW} = 104 K and for CsV_3Sb_5 across T_{CDW} = 94 K.

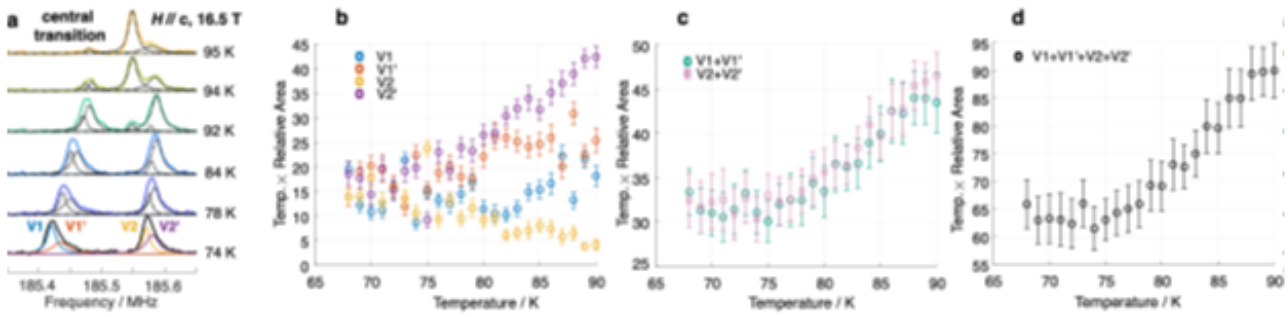


Figure.2 Temperature evolution of ^{51}V central transition (CT) and component intensities in CsV_3Sb_5 (H_0 // c). (a) Stacked CT spectra measured at 16.5 T for selected temperatures. (b) Boltzmann-corrected integration areas I(T)T for the four fitted components (V1,V1′,V2,V2′). (c) Pairwise sums I(T)T for V1+V1′ and V2+V2′. (d) Total I(T)T.

remains consistent with uniform TrH 2×2×2 stacking within our resolution. Together, Figs. 1 and 2 provide site-resolved constraints on the AV_3Sb_5 CDW microstructure targeted in this project.

Building on the interlayer-modulated 3q CDW microstructure in CsV_3Sb_5 (Figs. 1-2), we probe the ^{51}V quadrupolar satellites with H_0 // c across the intermediate-temperature regime near $T_{CO} \approx 65$ K (Fig. 3). On cooling through T_{CO}, two well-resolved electric field gradient (EFG) manifolds appear and coexist over a finite interval; their relative spectral weights shift from the high-T manifold to the low-T manifold while the sum of integrated satellite intensity is conserved within experimental uncertainty (Fig. 3b-d). The sustained coexistence of two EFG environments without critical broadening, together with the nearly temperature-independent ν_Q within each manifold, provides bulk evidence consistent with a first-order charge order transition near T_{CO}. Although the ~65 K transition is often discussed as distinct from the primary CDW at 94 K, our measurements do not resolve that relationship; rather, they delineate this window by providing

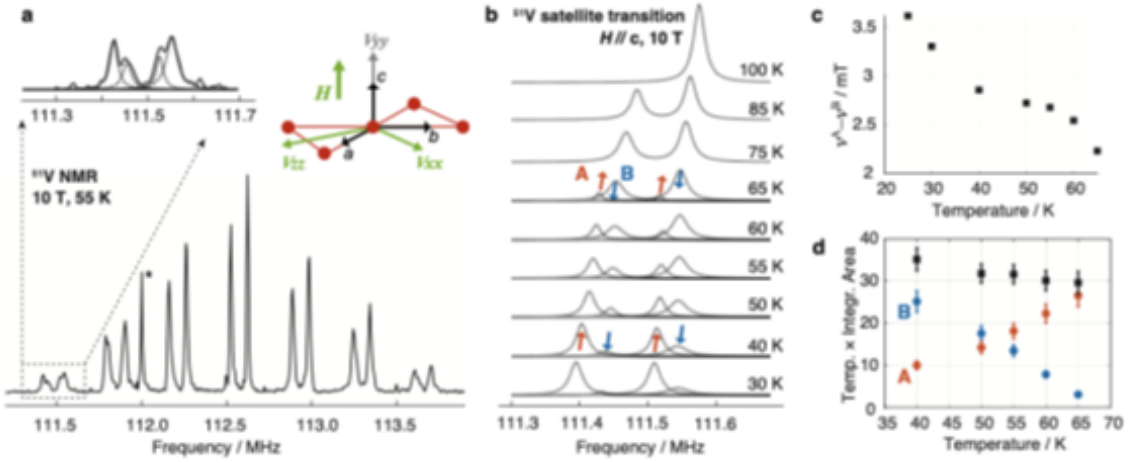


Figure.3 Evolution of ^{51}V satellite transition (ST) in CsV_3Sb_5 across the intermediate transition (H_0 // c). (a) Static spectrum acquired at 55 K and 10 T. (b) Temperature series of the ST manifolds showing the emergence of two sets of EFG on cooling. (c) Temperature dependence of the inter-manifold splitting. (d) Relative spectral weights of the two EFG manifolds.

bulk evidence for first-order behavior, whereas prior optical, Raman, and STM studies reported anomalies or stripe-like order without demonstrating a bulk thermodynamic phase transition.

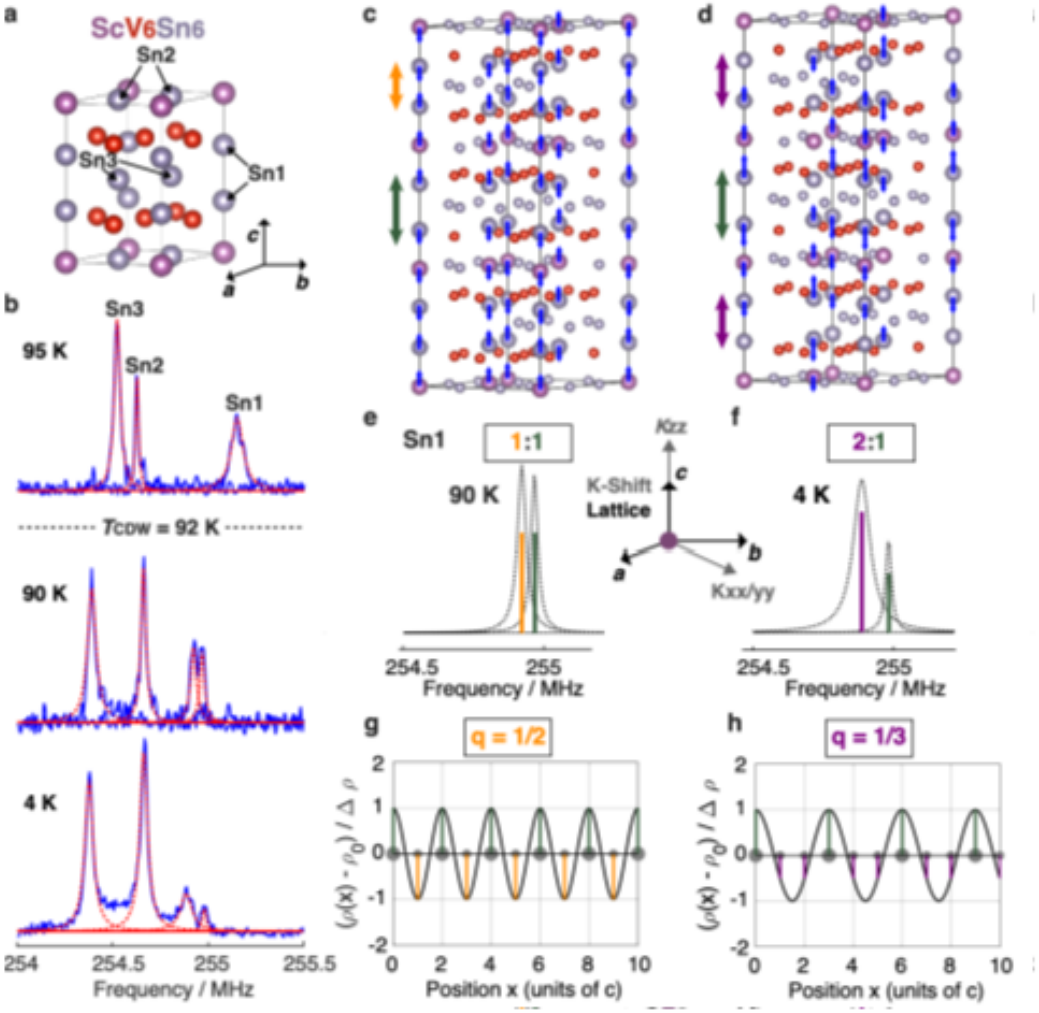


Figure.4 (a) Crystal structure of ScV_6Sn_6. (b) ^{119}Sn NMR spectra above and below T_{CDW} = 92 K. (c)(d) Illustrations of the proposed lattice distortion patterns (Ref). (e)(f) ^{119}Sn NMR resonances and multiplicities at 90 K and 4 K of Sn1-Sc-Sn1 sites. (g)(h) Charge density modulation $\rho(x) = \rho_0 + \Delta\rho\ cos\ (q \cdot x + \phi)$ with propagating wave vectors $q = 1/2$ and $q = 1/3$ along c-axis. Grey dots of different sizes depict atoms with varying charge density. Colored bars mark positive and negative CDW amplitude the atomic positions of Sn1 sites.

Extending our site-resolved approach beyond AV_3Sb_5, we examine ScV_6Sn_6, a phonon-driven CDW with competing c-axis stacking modes, in contrast to the VHS-centered electronic instabilities emphasized for AV_3Sb_5. In Fig. 4, ^{119}Sn (I = 1/2) NMR of the Sn1-Sc-Sn1 chains resolves two Sn1 sites at both 90 K and 4 K, with intensities evolving from 1:1 at 90 K to 2:1 at 4 K (Fig. 4b-h). These observations are consistent with chain distortions where a $q_c = 1/2$

dimerization would alternate short and long Sn1-Sc-Sn1 bonds in equal numbers (two sites, 1:1; Fig. 4e), whereas a $q_c = 1/3$ trimer would render 'up'/'down' equivalent and 'stationary' distinct (two sites, 2:1; Fig. 4f), consistent with rattling-chain and frustrated-stacking models. A complementary charge-modulation framework likewise yields equal weights for $q_c = 1/2$ and a 2:1 ratio for $q_c = 1/3$, providing an internal cross-check based solely on Knight-shift sensitivity to local charge density (Fig. 4g-h). Thus, NMR supplies bulk, site-resolved constraints, capturing the distinct Sn1-chain environments and their temperature evolution that diffraction averages over, while remaining consistent with scattering-based proposals for competing CDW stackings in ScV_6Sn_6.

Future Plans

Building on the site-resolved results above, we will advance three tightly focused thrusts. (i) AV_3Sb_5: *Which broken symmetries are bulk at low temperature and how do they couple to superconductivity?* We will combine angle-resolved ^{51}V NMR with $^{121/123}Sb$ Nuclear Quadrupole Resonance (NQR), using field and angle control and strain bias to distinguish domain selection from intrinsic symmetry breaking – addressing specific open questions highlighted by recent surveys of AV_3Sb_5 phenomenology. (ii) ScV_6Sn_6: *What is the microscopic origin and timescale of the competition between the q = 1/2 and q = 1/3 c-axis orders?* In collaboration with ORNL, we will integrate ^{119}Sn Mössbauer spectroscopy (isomer shift and quadrupole splitting) with our ^{119}Sn and ^{45}Sc NMR to quantify Sn1 site populations and hyperfine fields across T_{CDW}, discriminate static from slowly fluctuating distortions via Mössbauer linewidths, and correlate these with element-specific phonon signatures from nuclear resonant inelastic scattering on Sn (and Tm in isostructural $LnNb_6Sn_6$ reference compounds) to test the rattling-chain and soft-phonon mechanism that couples to the out-of-plane CDW. (iii) Rare-earth kagome magnets ($LnTi_3Bi_4$): *What crystal-field anisotropy and exchange scales govern the kagome-derived magnetism?* We will carry out multi-frequency, high-field EMR with angle control to resolve magnetic resonances, extract magnetic interactions as a function of temperature and external magnetic field, constraining single-ion anisotropy and exchange and providing benchmarks for microscopic spin Hamiltonians; this work leverages established high-field EMR infrastructure and collaborations.

References

1. B. R. Ortiz, S. M. L. Teicher, Y. Hu, J. L. Zuo, P. M. Sarte, E. C. Schueller, A. M. M. Abeykoon, M. J. Krogstad, S. Rosenkranz, R. Osborn, R. Seshadri, L. Balents, J. He, and S. D. Wilson, *CsV_3Sb_5: A $\mathbb{Z}_2$ Topological Kagome Metal with a Superconducting Ground State*, Physical Review Letters **125**, 247002 (2020).
2. H. W. S. Arachchige, W. R. Meier, M. Marshall, T. Matsuoka, R. Xue, M. A. McGuire, R. P. Hermann, H. Cao, and D. Mandrus, *Charge Density Wave in Kagome Lattice Intermetallic ScV_6Sn_6*, Physical Review Letters **129**, 216402 (2022).
3. H. Zhao, H. Li, B. R. Ortiz, S. M. L. Teicher, T. Park, M. Ye, Z. Wang, L. Balents, S. D. Wilson, and I. Zeljkovic, *Cascade of correlated electron states in the kagome superconductor CsV_3Sb_5*, Nature **599**, 216-221 (2021).

4. N. Ratcliff, L. Hallett, B. R. Ortiz, S. D. Wilson, and J. W. Harter, *Coherent phonon spectroscopy and interlayer modulation of charge density wave order in the kagome metal CsV_3Sb_5*, Physical Review Materials **5**, L111801 (2021).
5. S. Wu, B. R. Ortiz, H. Tan, S. D. Wilson, B. Yan, T. Birol, and G. Blumberg, *Charge density wave order in the kagome metal AV_3Sb_5 (A=Cs, Rb, K)*, Physical Review B **105**, 155106 (2022).

Publications

1. A manuscript detailing the $A V_3Sb_5$ results has been prepared and is in final stages of submission.
2. T. Orlando, H. Bui, J. Cabigting, N. Ibbetson, J. van Tol, T. Dubroca, X. Wang, and F. Mentink-Vigier, *Impact of non-polar solvents in dynamic nuclear polarization at high magnetic fields*, Journal of Magnetic Resonance **375**, 107885 (2025).*
3. D. M. Halat, H. Liu, K. Kim, G. C. B. Alexander, X. Wang, A. Venkatesh, A. R. Altenhof, H. E. Mason, S. H. Lapidus, J. S. Yoon, I. Hung, Z. Gan, J. Cabana, D. J. Siegel, J. A. Reimer, and B. Key, *Mg-Ion Conduction in Antiperovskite Solid Electrolytes Revealed by ^{25}Mg Ultrahigh Field NMR and First-Principles Calculations*, Journal of the American Chemical Society **147**, 27949–27961 (2025).*

(*Portions of these works were supported by this award and contributed to student training relevant to the project goals.)

Induced Atomic Order in FeNi

Laura H. Lewis[1], George Hadjipanayis,[1,2], Chaoying Ni,[3] and Julie B. Staunton[4],

[1]College of Engineering, Northeastern University, Boston MA

[2]Department of Physics and Astronomy, [3]Department of Materials Science and Engineering, University of Delaware, Newark DE

[4]Department of Physics, University of Warwick, Coventry, UK

Keywords: magnetism, magnets, critical materials, phase transitions, atomic order, transition metal compounds

Research Scope

In support of secure critical mineral and materials supply chains, there is great interest in developing strong permanent magnets that contain minimal or no constrained elements for technological applications underlying the DOE mission. In particular, atomically ordered FeNi, known by its meteoritic mineralogic name tetrataenite, shows promise as a robust, rare-earth-free permanent. However, it is extraordinarily challenging to create and validate atomic order in this alloy: extremely slow kinetics and unfavorable thermodynamic driving forces restrict tetrataenite's formation to meteorites that have been cooled over hundreds of millions of years. Here, processing-induced atomic order in FeNi is examined and quantified using experimental and computational approaches. Outcomes furnish atomic-scale insight into the extent and mechanisms of the resultant atomic order, strengthening the proposition that tetrataenite can indeed play an important role in a comprehensive critical materials strategy.

Recent Progress

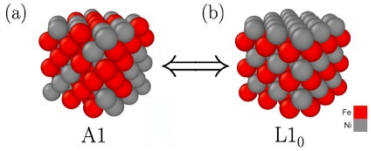


Figure 1. a) atomically disordered cubic (A1) structure; b) atomically ordered tetragonal $L1_0$ structure.

Equiatomic FeNi is known to undergo a first-order phase transition from the disordered fcc phase to form an atomically ordered $L1_0$-structured (AuCu-I type) phase upon cooling through an equilibrium transformation temperature of 320 K. The formation of the $L1_0$ superstructure is accompanied by strongly enhanced magnetocrystalline anisotropy, with an easy axis of spontaneous magnetization oriented along the tetragonal *c*-axis, Figure 1.[1] In this study, FeNi-based specimens were solidified from the melt and subjected to severe mechanical deformation ($\epsilon \sim 85–95\%$) by cold-rolling. The resultant deformed strips were thermally treated for 6 weeks under either conventional, field-free conditions or combined stress and mild magnetic fields.[2] Recent investigation of these stress-/magnetic-field-annealed samples employing simultaneous conversion X-ray and backscattered γ-ray ^{57}Fe Mössbauer spectroscopy confirmed production of up to 22 vol% locally atomically ordered FeNi with the remainder identified as the cubic FeNi alloy. In contrast, all precursor samples consist only of the cubic FeNi alloy.[3] However, details of the location and degree of atomic order of these

induced $L1_0$ regions is not available from Mössbauer spectroscopy. Continuing such inquiries, time-of-flight neutron diffraction and high-resolution transmission electron microscopy have successfully quantified the size, extent and locations of regions of the induced atomic order in these specimens.[4] Complementing these investigations, exploration of the mobility of both Fe and Ni atoms in ferromagnetic Fe_xNi_{1-x} alloys ($0.4 \leq x \leq 0.6$) within the framework of *ab initio* electronic structure calculations has successfully quantified energetic barriers to lattice vacancy migration, as well as offered a phenomenological explanation of the long-standing issue of highly sluggish diffusion of Ni in ferrous alloys.[5]

Time-of-flight neutron diffraction data conducted on isotopically pure $Fe^{62}Ni$ show clear and broad $L1_0$-type superlattice Bragg reflections at low q but not at higher q/d-spacings, consistent with the existence of short-range, but not long-range, $L1_0$-type atomic order, Figure 2. Data are consistent with the existence of discrete regions of short-range $L1_0$-type atomic order with an estimated coherency length of ~ 40 nm, residing within a crystalline fcc FeNi matrix. The neutron diffraction results are augmented and deepened by assessment of complementary TEM data, Figure 3. At low magnification, a quasi-uniform microstructure of elongated FeNi crystallites is noted. At higher magnification, high-angle annular dark-field imaging and accompanying selected area electron diffraction (SAED) confirm the existence of a large number of very small $L1_0$- ordered regions concentrated largely at the boundaries of the elongated crystallites. These crystallites are located within deformed lattice planes arranged along the crystallite peripheries parallel to the direction of elongation. Fourier-transformed data permits visualization and quantification of the extent and locality of the $L1_0$-type regions. The atomic layering signature of the $L1_0$ regions reveals that atomic order develops more extensively within a given layer than between the layers; the atomic stacking extends approximately 5 nm along the *c*-axis direction, creating a magnetic easy axis that is in the plane of the specimens but perpendicular to the direction of rolling. The |q|-discriminated images permit quantification of the $L1_0$ regions at approximately 19 %, in very good agreement with the value reported in the earlier Mössbauer spectroscopy study conducted on this specimen.

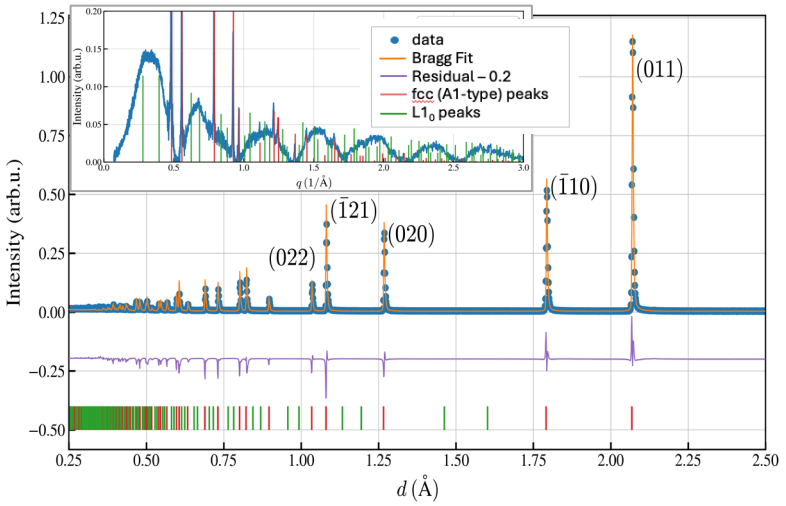


Figure 2: Neutron diffraction data from $Fe^{62}Ni$ field-stress-annealed sample, with main fcc peaks identified by their Miller indice plane designations. The data fit is shown in orange with the residual in purple below. The nominal Bragg peak positions for the A1 (fcc) and $L1_0$ phases are shown in green and red, respectively.

Ab initio electronic structure calculations were conducted using the nudged elastic band (NEB) method to accurately quantify energetic barriers to lattice vacancy migration. Both the atomically disordered (A1) fcc phase, as well as the atomically ordered, tetragonal $L1_0$ phase were investigated. Across an ensemble of NEB calculations performed on supercell configurations spanning a range of compositions and containing disordered, partially ordered, and fully ordered structures, it is found that Fe atoms are consistently significantly more mobile than Ni atoms, Figure 4. These findings may be interpreted in terms of the ferromagnetic alloy's underlying spin-polarized electronic structure. Specifically, coupling between the magnitude of the local electronic spin polarization and the size of local lattice distortions around vacancies causes Fe atoms to relax significantly into lattice vacancies, while Ni atoms remain much more rigidly fixed to their original lattice positions. The relaxation of Fe bond length relative to Ni bond length is proposed to underlie the significant difference in diffusional energy barrier heights. This effect plays a key role in determining the reduced mobility of Ni atoms compared to that of Fe atoms, providing an explanation of the longstanding experimental observation that Ni exhibits remarkably slow atomic diffusion in Fe-Ni alloys.

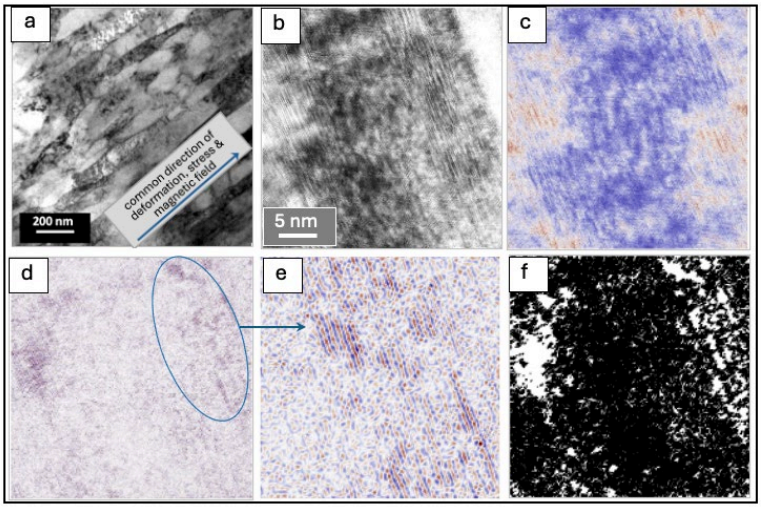


Figure 3: TEM micrographs and analyses of the field-stress-annealed FeNi specimen. (a) Crystallites are elongated along the rolling direction, which is also the direction of applied stress and magnetic field. (b) High-magnification image that incorporates a region of an elongated crystallite (center portion of the image) sandwiched between two adjacent regions of lattice slippage. (c) Color-enhanced image constructed from the real part of a Fourier transformation of the image in (b) that allowed disambiguation of the $L1_0$ regions (red) from fcc regions (blue). (d) $|q|$-filtered image, showing the locus of $L1_0$ local order, with a selected region enlarged in (e) highlighting $L1_0$ atomic layering and orientation. (f) $|q|$-discriminated image that allows visualization of the scale, distribution and arrangement of $L1_0$-crystallized regions (white contrast) within the fcc matrix (black contrast).

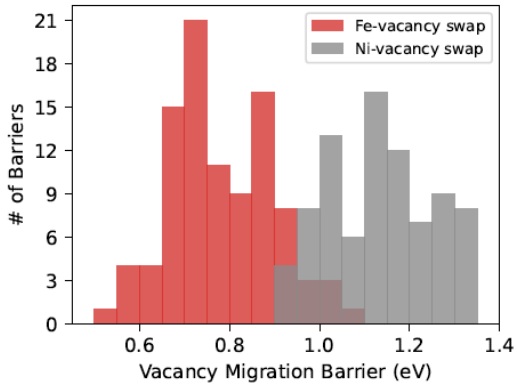


Figure 4. Histograms of lattice vacancy migration barriers across the ensemble of considered Fe-Ni alloy supercell configurations in this study. Results are compared for swaps where Fe atoms are switched with vacancies (red) versus swaps where Ni atoms are switched into vacancies (grey). Across the ensemble of 188 considered barriers, it can be seen that barriers for Fe-vacancy swaps are significantly lower than for Ni-vacancy swaps, suggesting Fe atoms are significantly more mobile in these alloys.

Future Plans

Overall, these results provide fundamental information concerning factors that impact the rate of formation and the arrangement of tetrataenite crystallites in nominally equiatomic FeNi alloys. For example, as the first-order A1-$L1_0$ equilibrium phase transformation in FeNi is reported to occur at the fairly low temperature of 320 °C, it is expected that slight compositional modifications that raise this transition temperature, even by a modest amount, will exponentially increase the rate of transformation by increasing the thermodynamic driving force for phase formation. To that end, To that end, preliminary calculations predict that minor additions to FeNi (less than 15 at%) of Ru, Pd, Pt as well as Al and P can increase the order-disorder temperature and thereby drastically increase the propensity for atomic order. Continuing, the application of a magnetic field during thermal treatment has been determined to be key to realizing the $L1_0$ phase in FeNi.[3] However, as was discussed recently in paper examining the transition of the ferromagnetic $L1_0$ analog, MnAl, very large magnetic fields are found to be not only ineffective in promoting atomic order, they may actually oppose it. Future efforts will seek to determine origins of these effects and how combined magnetic and strain energies alter the Fe-Ni thermodynamic landscape.

References

1. S. S. A. Razee, J. B. Staunton, B. Ginatempo, F. J. Pinski, and E. Bruno, *Ab Initio Theoretical Description of the Interrelation between Magnetocrystalline Anisotropy and Atomic Short-Range Order*, Phys. Rev. Lett. **82**, 5369 (1999).

2. N. Maât, I. McDonald, R. Barua, B. Lejeune, X. Zhang, G. M. Stephen, A. Fisher, D. Heiman, I. V. Soldatov, R. Schäfer, and L. H. Lewis, *Creating, Probing and Confirming Tetragonality in Bulk FeNi Alloys*, Acta Materialia **196** 776 (2020).

3. Lewis, Laura H., and Plamen S. Stamenov. "*Accelerating nature: induced atomic order in equiatomic FeNi*." Advanced Science **11**, 2302696 (2024).

4. *in preparation*: "Towards New Magnets: Induced Atomic Order in FeNi", Laura H. Lewis, Chaoya Han, Plamen Stamenov, Paul F. Henry, Jack O'Brien, Chaoying Ni, George Hadjipanayis, Sean Langridge.

5. *in preparation*: "Lattice vacancy migration barriers in Fe-Ni alloys, and why Ni atoms diffuse slowly: An ab initio study", Adam M. Fisher, Christopher D. Woodgate, Xiaoyu Zhang, George Hadjipanayis, Laura H. Lewis and Julie B. Staunton.

Publications

1. Zhang, Xiaoyu, Brian T. Lejeune, George A. Marchant, Henri Baldino, Maria Aguiar, Julie B. Staunton, and Laura H. Lewis. "*Driving rapid atomic order in MnAl via low-magnitude magnetic field annealing*." Acta Materialia **288**, 120868 (2025).

2. Han, Chaoya, A. M. Gabay, Christopher Chan, L. H. Lewis, G. C. Hadjipanayis, and Chaoying Ni. "*Structural evolution and magnetic hardness of (Sm, Zr)(Fe,Co,Ti)$_{12}$ alloy particles via reduction-diffusion*." Journal of Alloys and Compounds **1017**, 179003 (2025).

3. Woodgate, Christopher D., Laura H. Lewis, and Julie B. Staunton. "*Integrated ab initio modelling of atomic ordering and magnetic anisotropy for design of FeNi-based magnets*." npj Computational Materials **10**, 272 (2024).

4. Patrick, Christopher E., Yixuan Huang, Laura H. Lewis, and Julie B. Staunton. "*Theory of defect-induced crystal field perturbations in rare-earth magnets*." Physical Review Letters **132**, 056703 (2024).

5. Lewis, Laura H., and Plamen S. Stamenov. "*Accelerating nature: induced atomic order in equiatomic FeNi*." *Advanced Science* **11**, 2302696 (2024).

6. C. D. Woodgate, D. Hedlund, L. H. Lewis, J. B. Staunton, *Interplay Between Magnetism and Short-Range Order in Ni-Based High-Entropy Alloys: CrCoNi, CrFeCoNi, and CrMnFeCoNi*, Physical Review Materials **7**, 053801 (2023).

7. Woodgate, Christopher D., Christopher E. Patrick, Laura H. Lewis, and Julie B. Staunton. "*Revisiting Néel 60 years on: The magnetic anisotropy of $L1_0$ FeNi (tetrataenite)*." Journal of Applied Physics **134**, no. 16 (2023).

8. C. Han, B.T. Lejeune, X. Zhang, C. Ni, L.H. Lewis, *$L1_0$ Ordering in MnAl and FeNi Influenced by Magnetic Field and Strain,* Microscopy and Microanalysis **29** (Suppl 1), 1346 (2023).

9. O'Brien, Jack, Hasan Ahmadian Baghbaderani, Frederico O. Keller, Nora Dempsey, Laura H. Lewis, and Plamen Stamenov. "*Hardware, methodology and applications of 2+ D backscatter Mössbauer spectroscopy with simultaneous x-ray and γ-ray detection*." Measurement Science and Technology **35**, 025503 (2023):.

10. A. M. Gabay, C.-Y. Han, C.-Y. Ni, G. C. Hadjipanayis, *Re-investigation of High-Temperature Phase Equilibria in Fe-rich Sm–Fe–Ti Alloys*, Journal of Alloys and Compounds **947**, 169520 (2023).

Insights into the electronic properties and pairing symmetry of UTe_2 using a vector magnet STM

Vidya Madhavan, *University of Illinois, Urbana-Champaign*

Keywords: Superconductivity, scanning tunneling microscopy, topology, single crystals,

Research Scope

Over the past few decades there is has been an intense search for topological superconductors (TSs). Some of the interest in realizing and exploring these materials stems from the possibility of realizing exotic particles such as Majorana fermions. But even beyond this, there are many experimental and theoretical unknowns about these new phases. Our goal is to investigate TSs with low temperature scanning tunneling microscopy (STM) and spectroscopy (STS). We are deploying a variety of tuning knobs such magnetic fields and temperature to obtain answers to fundamental questions on the nature of superconductivity and the low energy excitations of these systems.

Our overarching goals are to investigate new classes of unconventional superconductors which break time-reversal or additional crystalline symmetries and find new paths to realizing topological superconductivity. We will experimentally determine the answers to questions about the order parameter and the topological nature of superconductivity in UTe_2; the presence of a parent pair density wave state on the surface of UTe_2; and the nature of the superconducting phase in the parent and doped Kagome compounds.

Recent Progress

In the ongoing search for new phases of matter, the recently discovered heavy fermion superconductor UTe_2, which combines triplet-superconductivity and non-trivial topology with strong correlations, is a unique and extremely promising system. It exhibits a very rich phase diagram at low temperatures in both magnetic field and pressure arising from competing electronic and magnetic interactions.

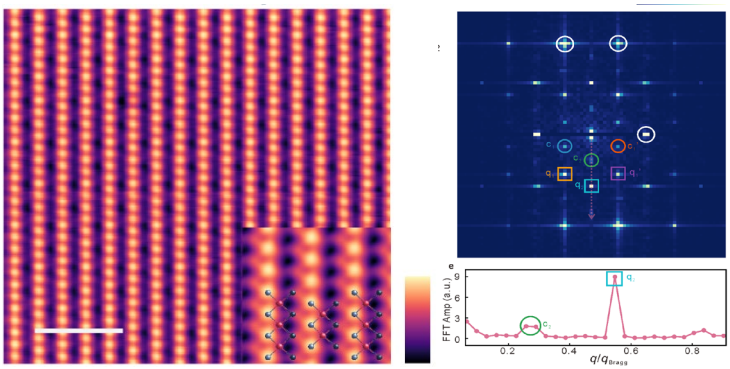
In our previous work we used scanning tunneling microscopy and spectroscopy at 300 mK to uncover the existence of an unusual incommensurate charge density wave order (CDW) which is suppressed by an external magnetic field and vanishes at the upper critical field H_{c2} of the superconducting order. A CDW which is suppressed with magnetic field in a manner similar to superconductivity has never been observed before and implies that the CDW and superconducting order parameters in UTe_2 are not merely coexisting but are in fact strongly intertwined. There are very few explanations for a CDW that is sensitive to magnetic fields and disappears at H_{c2}. To explain our data, we constructed a Ginzburg-Landau theory for a uniform triplet superconductor coexisting with ***triplet*** pair density wave (PDW) state. While many papers have been written about singlet PDW states, triplet PDWs have not been considered before by theory or observed in experiments. This theory shows that the PDW gives rise to daughter CDWs which would be

sensitive to magnetic field due to their origin in a triplet PDW state and naturally explains our data.

Over the last year we have carried out extensive studies on UTe_2 using quasiparticle interference and by studying the response of the system to a vector magnetic field. Our latest results are described below.

1) While the (0-11) facet of $UTe_2$is the most heavily studied, the fermiology of this surface that gives rise to exotic phenomena such as a triplet PDW is still lacking and continues to be an area of active interest. We employed spectroscopic imaging to reveal the Fermi surface of UTe_2 through quasiparticle interference. We find scattering originating from the uranium-derived bands that play a major role in the formation of the CDW and the PDW phases. Additionally, we detect the spectral fingerprints of the CDW gap through tunneling spectroscopy that matches with the onset temperature of the CDW. Suppressing the CDW with a magnetic field, highlights the presence of small, circular Fermi pockets that disperse strongly near the Fermi energy. A paper based on this work is ready for submission.

2) By studying clean areas of UTe_2 we identified a second CDW phase on at 300mK, which also consists of three ordering vectors and displays hexagonal modulation in real space. For clarity we designate the previously known phase q_i and the newly discovered phase c_i. The magnitude of the c_1 wave vector is approximately one-half that of the q_i. This relationship is energy-independent in a wide energy range. Detailed temperature-dependent measurements show that c_1 intensity almost vanishes near 2.5 K, close to our sample's Tc=2.1K, implicating a strong coupling between 1Q-M and the superconducting order parameter. Notably, the q_i orders remain robust at 4 K but are almost suppressed at 4.8K. The two CDW orders are further disentangled under vector magnetic field at different temperatures. We find that c_1 is suppressed after applying fields nearly along the crystallographic a, b, and c axes at 300 mK and simultaneously generates additional peaks that are absent at 4.2 K, implying that this extra peak is a field-induced descendant of q_i. In contrast, the q_i order is robust against the largest accessible fields at 300 mK, but is completely suppressed at 4 K. The critical field required to extinguish q_i is highly anisotropic, smallest for H||a, intermediate for H||c, and largest for H||b—in quantitative accord with the established anisotropy of Hc2 in UTe_2. These observations demonstrate that q_i stability depends on both temperature and crystal orientation, whereas c_1 is intimately tied to superconductivity and exhibits a distinctive field-induced evolution. These studies have allowed us to further refine our theories on the PDW order in this system. Our data suggest that the c_1 order is associated with the PDW while the q_i order is an intertwined CDW. A paper based on this work is currently in preparation.



3) Ultra-clean single crystals of UTe_2grown recently by a molten-salt–flux technique show an elevated Tc≈2.1 K together with an almost vanishing residual DOS in specific heat. Utilizing a scanning-tunnelling microscope with vector field, we investigate ultra-clean crystals at 300 mK. We find that even in the higher Tc samples, the superconducting gap displays a substantial zero bias DOS. When a magnetic field of 0.8 T is applied nearly along the b axis (close to the surface normal), an asymmetric out-of plane vortex appears whose right flank exhibits a locally deepened gap and sharpened coherence peaks. A field of comparable magnitude along the c axis generates a symmetric in-plane vortex; the global gap remains essentially unchanged on either side of the core. In contrast, a field of 0.8T along the a axis, shows no vortices within a region where at least one vortex would be expected from vortex-density considerations. Instead, it induces a spatially uniform enhancement of superconductivity over a wide area, which saturates near 0.8 T. Defining the gap height as the energy difference between the coherence peak and the gap minimum, we find that spatial average gap height increases steadily with field and is roughly twice its zero-field value at 0.8 T. These observations provide clues to the superconducting pairing symmetry in UTe_2. A paper based on this work is currently in preparation.

Future Plans

We plan to publish our findings on UTe_2 in four distinct papers, one focused on the PDW state and the other three on the order parameter and topology. In addition, we will continue working on the doping dependence of the superconducting phase in the Kagome compound RbV_3Sb_5 and study the response of the CDW and superconductivity to in plane magnetic fields.

Publications

1. Nina Bielinski, e.al., Revealing the Hidden Dirac Gap in a Topological Antiferromagnet Using Floquet-Bloch Manipulation Nat. Phys. 21, 458-463 (2025).
2. Anuva Aishwarya, Julian May-Mann, Sheng Ran, Shanta R. Saha, Johnpierre Paglione, Nicholas P. Butch, Eduardo Fradkin, Vidya Madhavan, Melting of the Charge Density Wave by Generation of Pairs of Topological Defects in UTe_2, Nat. Phys. 20, 964-969 (2024).
3. Caitlin S. Kengle, Dipanjan Chaudhuri, Xuefei Guo, Thomas A. Johnson, Simon Bettler, Wolfgang Simeth, Matthew J. Krogstad, Zahir Islam, Sheng Ran, Shanta R. Saha, Johnpierre Paglione, Nicholas P. Butch, Eduardo Fradkin, Vidya Madhavan, Peter Abbamonte, Absence of a Bulk Signature of a Charge Density Wave in Hard X-Ray Measurements of UTe_2, Phys. Rev. B 110, 145101 (2024) (Editors' Suggestion).
4. Aishwarya, A., May-Mann, J., Raghavan, A. et al. Magnetic-field-sensitive charge density waves in the superconductor UTe_2, Nature 618, 928–933 (2023).

Superconductivity and magnetism in d- and f-electron quantum materials

PI: *M. Brian Maple*
Department of Physics, University of California, San Diego, La Jolla, California 92093
Email: mbmaple@ucsd.edu

Keywords: magnetism, superconductivity, single crystals, semiconductors, magnetotransport

Research Scope

The general theme of this research program is the investigation of emergent phenomena in correlated electron and topological quantum materials. Emergent phenomena of interest include unconventional spin-singlet and spin-triplet superconductivity (SC), high temperature SC, charge and spin ordered phases, "hidden order", topological Kondo insulator (TKI) behavior, heavy fermion behavior, non-Fermi liquid behavior, etc. A combination of materials synthesis and physical properties measurements are employed to characterize these phenomena, map out complex phase diagrams in which they reside, determine how different phases are related to one another, probe the underlying physics, and, when possible, test relevant theoretical models. We are also interested in studying quantum matter under extreme conditions of pressure, P (megabar range), magnetic field, B (65 T), and temperature, T (mK region). In the following, we briefly describe progress in studies of the physical properties of several correlated electron materials currently underway in our lab: (1) The heavy fermion f-electron compound UTe_2 which is widely believed to exhibit spin-triplet SC [1,2], (2) the nickelate compound $La_3Ni_2O_7$ in which application of pressure suppresses a charge density wave and induces SC with a SCing critical temperature (T_c) ≈ 80 K at a critical pressure (P_c) ≈ 14 GPa [3], and (3) the d-electron narrow gap semiconductor FeSi which is a candidate for a TKI [4]. We also describe progress in the development of a nitrogen vacancy (NV) microscope for magnetization measurements at ambient and high pressure [5].

Recent Progress

Experiments probing the unconventional superconductivity of UTe_2 single crystals

Experiments on UTe_2 have yielded evidence for unconventional SC that is widely suspected to involve spin-triplet pairing of electrons [1]. During the past five years, we have worked with collaborators on several experiments designed to probe the unconventional SC of UTe_2 single crystals prepared in our lab. Inelastic neutron scattering (INS) experiments [P1] on UTe_2 revealed the surprising presence of antiferromagnetic (AFM) fluctuations coupled to SC. X-ray diffraction (XRD) and resonant inelastic x-ray scattering (RIXS) measurements under pressure to 30 GPa at room temperature (RT) [P5] uncovered a structural transition from body-centered orthorhombic to body-centered tetragonal at ~5-7 GPa, with a large volume collapse of nearly 11% and an increase in nearest U-U distance by about 4%. The RIXS spectra at the U $L_{\alpha 1}$ edge reveals a U valence of +3.74 at 1.8 GPa and RT, which shifts towards 4+ with increasing P, passes through a peak at 2.8 GPa, and then decreases towards 3+, settling down to a nearly constant value above 15 GPa. The selection rule in the orientation dependence of the Josephson coupling between In, an s-wave SCor, and UTe_2 in Josephson junction experiments [P7] suggests that UTe_2 has an odd-parity pairing state of B_{1u} symmetry in near zero magnetic fields, and thereby exhibits spin-triplet SC.

High-Magnetic Field Phases in $U_{1-x}Th_xTe_2$

Recent experiments by Moir *et al*. [P9] have explored the effect of Th substitution for U on the remarkable high field SCing phases observed in UTe_2 [1]. These effects may, in turn, provide clues to the origin and nature of SC in UTe_2. Thorium substituents are expected to perturb UTe_2 in several ways – increase

disorder, and, in turn, scattering of electrons, increase the electron concentration, and interrupt the U-dimers that some researchers believe are involved in the SC.

At temperatures much lower than its T_c of 2.1 K, UTe_2 has a unique phase diagram of magnetic field H vs. φ and θ, angles H is tilted from the b-axis toward the a- and c-axes, respectively (see Fig. 1(a)). The phase diagram contains three distinct superconducting phases: SC_1 in which φ and θ extend from 0 to 90° and $H \leq$ ~15 T; SC_2 for φ ≤ ~7°, θ ≤ ~4° and ~15 T ≤ $H \leq H_m$ = ~35 T, the onset of the magnetic field polarized (FP) phase; and SC_{FP} which resides entirely within the FP phase in a pocket of SC extending from θ ≈ 20° to 40° and $H \approx$ 40 T to above 60 T. We studied the evolution of the H vs θ phase diagram for Th concentrations 0.005 ≤ x ≤ 0.047 in the $U_{1-x}Th_xTe_2$ system at ~0.6 K in a series of experiments on $U_{1-x}Th_xTe_2$ single crystals in high magnetic fields to 60 T at the Pulsed Field Facility at LANL. Within this range of x values, SC_1 extends over 0 ≤ θ ≤ 90° and $H \leq$ ~10 T for x = 0.047, while SC_2 is suppressed. The SC_{FP} and FP phases are unaffected to x = 0.02 but are completely suppressed in the region x = 0.025 to 0.047 where the residual resistance ratio RRR ~3 indicates a significant amount of disorder. These results complement recent studies on non-SCing disordered UTe_2 single crystals in which the SC_1 and SC_2 phases are absent, but the FP and so-called "orphan" SC_{FP} phases are retained [2]. These results suggest that the SC_1 and SC_2 phases are distinct SCing phases with different types of pairing symmetry and/or mechanisms. The SC_{FP} phase that emerges from the FP phase in a SCing pocket for 20° ≤ θ ≤ 40° in fields above 40 T could be produced by electron pairing interactions associated with the FP phase or be restored from the SC_1 phase by the interplay of the FP phase and the magnetic field H such as the exchange field compensation effect. These experiments will provide information that may yield insight into the origin of the high field SCing phases in UTe_2.

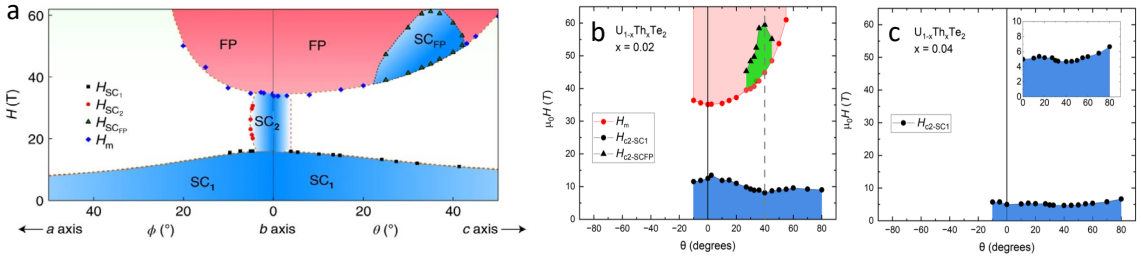


Fig. 1. (a) High field phase diagram ref. [1], (b) At x = 0.02, SC_2 is suppressed and there is a minimum in the upper critical field H_{c2}-SC_1 at the same angle as the maximum in H_{c2}-SC_{FP}; (c) At x = 0.04, the field polarized (FP) phase and SC_{FP} are completely suppressed (inset: Fig. 1 (c) data zoomed in).

Pressure-induced suppression of charge density wave order and emergence of superconductivity in $La_{3-x}Ln_xNi_2O_7$ compounds

The bilayer Ruddlesden-Popper nickelate $La_3Ni_2O_7$ is a newly discovered SCor under high pressure, with an onset of SC at $P_c \approx$ 14 GPa and a T_c of about 80 K [3]. Enormous effort has been expended to study its SCing mechanism and whether chemical substitution and oxygen annealing could reduce P_c. To study how substitution of *Ln* ions with magnetic moments for La changes the properties of $La_3Ni_2O_7$, we prepared powdered samples of $La_2PrNi_2O_7$, $La_{2.7}Eu_{0.3}Ni_2O_7$, $La_{2.7}Gd0.3Ni_2O_7$, $La_{2.7}Tb_{0.3}Ni_2O_7$, and $La_{2.7}Dy_{0.3}Ni_2O_7$

and made electrical transport and magnetization measurements on the samples before and after high-pressure high-temperature oxygen annealing. Density-wave transitions were found in these heavy lanthanide (Ln) doped samples whether they were annealed or not, and apparent AFM transitions below 5 K were revealed in $La_{2.7}Tb_{0.3}Ni_2O_7$ (see Fig. 2) and $La_{2.7}Dy_{0.3}Ni_2O_7$ which vanished after oxygen annealing. This distinguishes Tb and Dy from those lanthanide substituents (e.g., Pr, Nd, Sm) that do not order magnetically or modify SC in the $La_3Ni_2O_7$ host. Despite the fact that our experimental results indicate that local magnetic moments and itinerant electrons are separately responsible for magnetism and electrical conductivity at ambient pressure, the coexistence of density wave and magnetic order in Tb and Dy substituted nickelates could still provide an interesting platform to test whether the magnetic ordering can perturb the SC in the nickelates, since a possible superexchange interaction between Tb (Dy) ions via O or Ni sites of $La_3Ni_2O_7$ could affect nickelate SC.

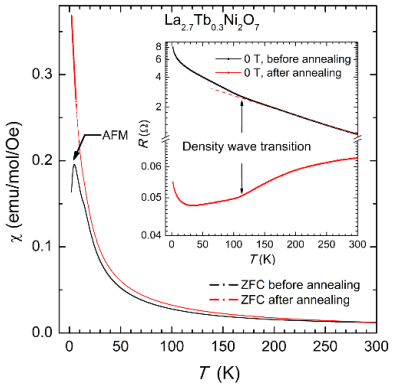


Fig. 2. $La_{2.7}Tb_{0.3}Ni_2O_7$ showing AFM and density wave transitions. High-P – high-T annealing in O_2 metallizes the sample and destroys the magnetic order.

Influence of various fluxes on morphology and electrical resistivity of FeSi

Recent studies of the *d*-electron narrow gap semiconductor FeSi revealed the presence of a conducting surface state [4] and evidence for a ferro-magnetic surface state [P4], suggesting that FeSi could be a candidate for a topological Kondo insulator. Previous electrical resistivity measure-ments have shown strong sample dependence, empha-sizing the need to explore synthesis conditions to ensure reproducibility and consis-tency in producing high-quality FeSi single crystals. Motivated by this issue, we synthesized and characterized FeSi single crystals using various molten metal fluxes, including Sn, Te, and Ga [P10]. The types of flux significantly influenced the crystalline morphology (see Fig. 3), yielding crystals shaped like needles, triangular prisms, and polyhedra for Sn, Te, and Ga, respectively. Electrical resistivity measurements revealed two distinct Arrhenius-like regions below 200 K for Sn- and Te-flux-grown FeSi crystals, but only one for Ga-flux-grown FeSi crystals. Additionally, measurements of the residual resistivity ratio (RRR) between 2 and 300 K yield values of 4×10^3, 2×10^4, and ~10 for Sn-, Te-, and Ga-flux samples, respectively. Moreover, measurements of the temperature-dependent electrical resistivity reveal distinct features at lower temperatures – a peak at around 20 K for Sn-flux, a plateau around 5 K for Te-flux, and a peak near 30 K for Ga-flux.

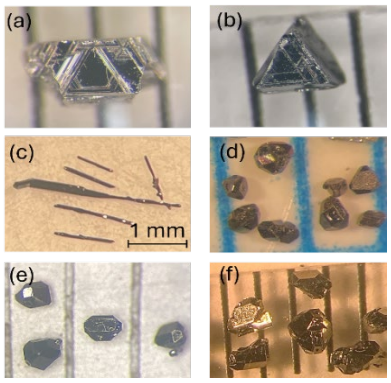


Fig. 3. Microscope images of FeSi single crystals grown using three different fluxes: (a,b) Te flux, (c,d) Sn flux, and (e,f) Ga flux. Panels (a,c,e) show crystals grown with Fe and Si as starting materials, while panels (b,d,f) display crystals grown with FeSi polycrystal as the starting material. For reference, the distance between adjacent lines in panels (a, b, d-f) is 1 mm.

Development of a nitrogen vacancy microscope for magnetization measurements at ambient and high pressures

Nitrogen vacancy optically detected magnetic resonance (NV ODMR) spectroscopy is a robust technique that is sensitive to lattice strain, magnetic fields, and electric fields at extreme conditions of high pressure and low temperature – making it ideally suited to study hydrostatic pressure induced phase transitions in correlated electron materials [5]. Recent NV ODMR research has mostly been used to study materials that are mechanically easy to integrate with NV's, primarily to reduce NV to sample distances to increase resolution [5]. An advantage of high-pressure NV ODMR is using pressure to reduce the sample to NV distance and increase detection sensitivity, while also allowing ODMR spectroscopy to investigate pressure-induced phase transitions. Additionally, recent advances in ion implantation of <111> oriented diamonds have raised the upper pressure limit for NV ODMR in DACs [5]. Progress for our own custom NV widefield microscope for ODMR spectroscopy has moved forward. Stress testing at temperatures as low as 2 K and magnetic fields as high as 75 G in a standard Quantum Design Dynacool Physical Property Measurement System (PPMS) have been completed. Current experiments are on-going with initial focus on imaging the ferromagnetic heavy fermion compound $URu_{2-x}Re_xSi_2$ (x = 0.3) and the unconventional superconductor $Y_{1-x}Pr_xBa_2Cu_3O_7$ (x = 0.3) at ambient pressure. Our collaboration with Dr. Andy Mounce at Sandia National Laboratory has also progressed, with ion implantation of <111> diamond anvils with 300 μm and 500 μm culet sizes expected to ready by September for future NV high pressure measurements in our custom NV widefield PPMS probe.

Future Plans

- Electrical resistivity measurements at high pressure on UTe_2 and $U_{1-x}Th_xTe_2$ single crystals to determine the *T* vs *P* phase diagrams and search for other emergent phases.
- Continue studies of UTe_2-based single crystals; e.g., INS with Prof. Dai's group, Josephson junction coupling with Prof. Liu's group, PDO measurement at high fields at LANL PFF.
- Conduct low temperature neutron diffraction experiments on Tb- and Dy- substituted $La_3Ni_2O_7$ nickelates to determine their magnetic structures; synthesize post-Dy Ln-substituted $La_3Ni_2O_7$ samples to search for magnetic order and density wave transitions.
- Attempt molten salt flux methods to grow $La_{3-x}Ln_xNi_2O_7$ single crystals for more advanced characterization methods (anisotropy of physical properties, ARPES, etc.) at ambient pressure.
- Collaborate with groups at the University of British Columbia and Stanford University on MOKE and ARPES measurements on FeSi single crystals to study surface magnetism and surface/bulk electronic structures.
- Perform magnetization measurements with NV microscope to study SCing and magnetically ordered phases at ambient and high pressure on pure and chemically-substituted UTe_2, $La_3Ni_2O_7$, URu_2Si_2, $YBa_2Cu_3O_7$ compounds

References

1. Sheng Ran, I-Lin Liu, Yun Suk Eo, Daniel J. Campbell, Paul M. Neves, Wesley T. Fuhrman, Shanta R. Saha, Christopher Eckberg, Hyunsoo Kim, David Graf, Fedor Balakirev, John Singleton, Johnpierre Paglione and Nicholas P. Butch, "Extreme magnetic field-boosted superconductivity," *Nat. Phys.* **15**, 1250 (2019).
2. Corey E. Frank, Sylvia K. Lewin, Gicela Saucedo Salas, Peter Czajka, Ian M. Hayes, Hyeok Yoon, Tristin Metz, Johnpierre Paglione, John Singleton, and Nicholas P. Butch, "Orphan high field superconductivity in non-superconducting uranium ditelluride," *Nat. Commun.* **15**, 3378 (2024).
3. Hualei Sun, Mengwu Huo, Xunwu Hu, Jingyuan Li, Zengjia Liu, Yifeng Han, Lingyun Tang, Zhongquan Mao, Pengtao Yang, Bosen Wang, Jinguang Cheng, Dao-Xin Yao, Guang-Ming Zhang, and Meng Wang, "Signatures of superconductivity near 80 K in a nickelate under high pressure," *Nature* **621**, 493 (2023).
4. Yuankan Fang, Sheng Ran, Weiwei Xie, Shen Wang, Ying Shirley Meng, and M. Brian Maple, "Evidence for a conducting surface ground state in high-quality single crystalline FeSi," *Proceedings of the National Academy of Sciences* **115**, 8558 (2018).

5. P. Bhattacharyya, W. Chen, X. Huang, S. Chatterjee, B. Huang, B. Kobrin, Y. Lyu, T. J. Smart, M. Block, E. Wang, Z. Wang, W. Wu, S. Hsieh, H. Ma, S. Mandyam, B. Chen, E. Davis, Z. M. Geballe, C. Zu, V. Struzhkin, R. Jeanloz, J. E. Moore, T. Cui, G. Galli, B. I. Halperin, C. R. Laumann, and N. Y. Yao, "Imaging the Meissner effect in hydride superconductors using quantum sensors," *Nature* **627**, 73 (2024).

Publications with DOE support

1. Chunruo Duan, R. E. Baumbach, Andrey Podlesnyak, Yuhang Deng, Camilla Moir, Alexander J. Breindel, M. Brian Maple, E. M. Nica, Qimiao Si, and Pengcheng Dai, "Resonance from antiferromagnetic spin fluctuations for superconductivity in UTe_2," *Nature* **600**, 636 (2021).
2. Alejandro Ruiz, Brandon Gunn, Yi Lu, Kalyan Sasmal, Camilla M. Moir, Rourav Basak, Hai Huang, Jun-Sik Lee, Fanny Rodolakis, Timothy J. Boyle, Morgan Walker, Yu He, Santiago Blanco-Canosa, Eduardo H. da Silva Neto, M. Brian Maple, and Alex Frano, "Stabilization of three-dimensional charge order through interplanar orbital hybridization in $Pr_xY_{1-x}Ba_2Cu_3O_{6+d}$," *Nature Communications* **13**, 6197 (2022).
3. Alexander Breindel, Yuhang Deng, Camilla M. Moir, Yuankan Fang, Sheng Ran, Hongbo Lou, Shubin Li, Qiaoshi Zeng, Lei Shu, Christian T. Wolowiec, Ivan K. Schuller, Priscila F. S. Rosa, Zachary Fisk, John Singleton, and M. Brian Maple, "Probing FeSi, a *d*-electron topological Kondo insulator candidate with magnetic field, pressure, and microwaves," *Proceedings of the National Academy of Sciences* **120**, e2216367120 (2023).
4. Yuhang Deng, Yifei Yan, Haozhe Wang, Eric Lee-Wong, Camilla M. Moir, Yuankan Fang, Weiwei Xie, and M. Brian Maple, "Possible surface magnetism in the topological Kondo insulator candidate FeSi," *Physical Review B* **108**, 115158 (2023).
5. Yuhang Deng, Eric Lee-Wong, Camilla M. Moir, Ravhi S. Kumar, Nathan Swedan, Changyong Park, Dmitry Yu Popov, Yuming Xiao, Paul Chow, Ryan E. Baumbach, Russell J. Hemley, Peter S. Riseborough and M. Brian Maple, "Structural transition and uranium valence change in UTe_2 at high pressure revealed by x-ray diffraction and spectroscopy," *Physical Review B* **110**, 075140 (2024).
6. Yuhang Deng, Farhad Taraporevala, Haozhe Wang, Eric Lee-Wong, Camilla M. Moir, Jinhyuk Lim, Shubham Sinha, Weiwei Xie, James Hamlin, Yogesh Vohra, and M. Brian Maple, "Pressure-induced metallization and loss of surface magnetism in FeSi," *Physical Review B* **110**, L121403 (2024).
7. Zixuan Li, Camilla M. Moir, Nathan J. McKee, Eric Lee-Wong, Ryan E. Baumbach, M. Brian Maple, and Ying Liu, "Observation of odd-parity superconductivity in UTe_2," *Proceedings of the National Academy of Sciences* (2025).
8. Yuhang Deng, Naveen Pouse, Zhekai Yang, Christian T. Wolowiec, Dom L. Kunwar, Sheng Ran, Kevin Huang, Kalyan Sasmal, Carmen C. Almasan, and M. Brian Maple, "Study of the anisotropic hidden order and antiferromagnetic phases of $URu_{2-x}Os_xSi_2$ by thermal expansion and magnetoresistance measurements," *Physical Review Materials* **9**, 075001 (2025).
9. Camilla M. Moir, John Singleton, Joanna M. Blawat, Eric Lee-Wong, Yuhang Deng, Keke Feng, Tyler Wannamaker, Ryan E. Baumbach, and M. Brian Maple, "High-Magnetic Field Phases in $U_{1-x}Th_xTe_2$," submitted to *Proceedings of the National Academy of Sciences* (2025).
10. Keke Feng, Caleb Robinson, Tyler Woods Wannamaker, Gabriel Mercado, Eric-Lee-Wong, Yuhang Deng, Weiwei Xie, and M. Brian Maple, "Tailoring FeSi Single Crystals: Influence of Sn, Te, and Ga Flux on Morphology and Electrical Resistance," submitted to *Physical Review Materials* (2025).

Project Title: Topological Superconductivity in Strong Spin-Orbit Materials

Principal Investigator: *Johnpierre Paglione*, *University of Maryland*

Keywords: topological superconductivity, topological materials

Research Scope

This program aims to elucidate the fundamental nature of superconductivity in topological materials with strong spin-orbit coupling using a joint experimental and theoretical effort to focus on understanding the topological superconductivity found in materials lacking inversion symmetry and hosting odd-parity pairing states. Our focus lies on three specific systems of interest: the noncentrosymmetric cubic half-Heusler family of compounds, the multiple superconducting phases of spin-triplet superconductor UTe_2, and novel 5d-based materials exhibiting indications of topological superconductivity. This program is designed to explore these materials using an established in-house synthesis and characterization program and an extensive collaboration network in order to elucidate the potential of these materials to form the next generation platform for quantum technologies. We utilize an extensive set of experimental facilities for the study of normal state topology using transport, magnetic and thermodynamic properties measurements, and of multi-component, multi-phase superconductivity using spectroscopic, phase-sensitive probes of tunneling and Josephson spectroscopy. We also explore ground state tuning using chemical manipulation, applied pressure and high magnetic fields to map the relevant phase spaces of these systems. With collaborators, current research focuses on exploring tunneling phenomena, ultrasound signatures and high-pressure techniques to achieve our goals. Together, our studies of these systems have strong potential for leading the development, understanding and potential of a new generation of topological superconductors.

Recent Progress

Our discovery of superconductivity in nearly–ferromagnetic UTe_2 in 2018 is one of our surprising but grand accomplishments in the last few years. This superconductor is a strong candidate for spin-triplet pairing, based on an extremely large, anisotropic upper critical field H_{c2}; temperature-independent nuclear magnetic resonance (NMR) Knight shift; and power law behavior of electronic specific heat and nuclear spin-lattice relaxation rate in the superconducting state. In addition, UTe_2 closely resembles ferromagnetic superconductors,

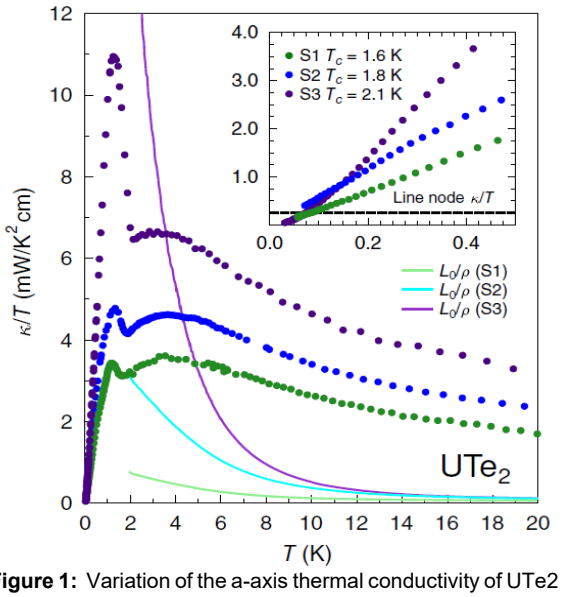


Figure 1: Variation of the a-axis thermal conductivity of UTe2 with disorder. The measured thermal conductivity of three samples of UTe2 with varying RRRs and superconducting transition temperatures are presented as a function of the temperature. The overall shape of the curves is similar for all three samples, but with noticeably stronger peaks below Tc in the higher RRR samples. The inset shows the very low-temperature portion of the data.[Hayes, PRX (2025)].

but in this case having a paramagnetic normal state that harbors spin fluctuations that drive the superconductivity. Our discovery launched an intense race with several groups worldwide now investigating various aspects of this material, producing upwards of *nearly 200 papers to date*. Our work has focused on elucidating both the superconducting state, and the normal state from which this exotic superconductivity arises. In addition to several papers where collaborators have been the main drivers of the experimental results using our supplied samples, the projects below reflect experiments where a significant component was performed by the PI's team:

a) Thermal conductivity studies of superconducting state: Our primary work in the last reporting period has been to elucidate the superconducting order parameter symmetry (or symmetries, considering the presence of multiple superconducting states), and one of the key experiments has been our comprehensive study of the influence of disorder on the thermal transport in the superconducting state of UTe2. Through detailed measurements of the magnetic field dependence of the thermal conductivity in the zero-temperature limit, we obtained clear evidence for the presence of point nodes in the superconducting gap for all samples with transition temperatures ranging from 1.6~K to 2.1~K obtained by different synthesis methods, including a refined self-flux method. This robustness implies the presence of symmetry-imposed nodes throughout the range studied, further confirmed via disorder-dependent calculations of the thermal transport achieved in close collaboration with Peter Hirschfeld at U Florida. This work is currently in press and will appear soon: *I. Hayes et al., "Robust nodal behavior in the thermal conductivity of superconducting UTe2" Physical Review X – to appear (2025).* b) High pressure studies of magnetic tuning and non-Fermi liquid behavior: Following our previous work on electrical resistivity anisotropy [Eo et al, PRB 2022], which found that the ab-plane resistivity is consistent with typical incoherent-to-coherent crossover phenomena, whereas a qualitatively different behavior in the c-axis transport exhibits a pronounced local maximum around 12 K, we have probed the pressure dependence of the c-axis transport in this recently reported study. We found the tuning of a magnetic energy scale in UTe2, previously identified with a peak in the c-axis electrical transport temperature dependence, using applied hydrostatic pressures and a-axis-oriented magnetic fields as complementary (and opposing) tuning parameters: the characteristic peak in c-axis resistivity decreases in temperature with applied pressure before vanishing near the critical pressure of 15 kbar, while the application of field shifts the peak to a higher temperature and broadens it under all studied pressures. At the critical pressure, the transport behavior deviates from Fermi liquid behavior, exhibiting a nearly linear temperature dependence of resistivity with an enhanced pre-factor. Our results shed light on the microscopic origin of the c-axis resistivity peak and provide a clear picture of magnetic energy scale evolution relevant to quantum criticality in UTe2. This work was recently published: *H. Kim et al., "Tuning a magnetic energy scale with pressure in UTe2", Nature Comm. Mat. (2025).*

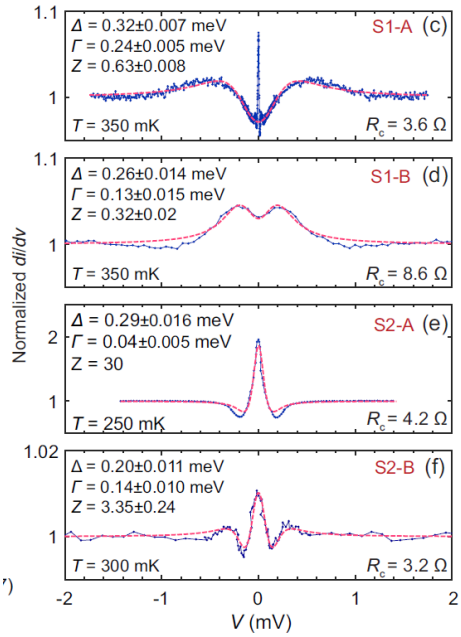


Figure 2: Normalized differential conductance spectra (blue) and fits (magenta) of UTe2 junctions at 300 mK. Fits are performed using a p-wave BTK model, yielding fit parameter values for gap energy Δ, scattering rate Γ, impedance Z, and temperature T as noted. [Yoon, npj Quantum Materials (2024)].

c) Spectroscopic studies of gap structure: We have been pursuing point contact Andreev reflection (PCAR) spectroscopy to probe superconductivity in UTe_2, and have had some success in fabricating and measuring point contact spectra of single-crystal based devices. We measured conductance through point-contact junctions formed by metallic contacts on different crystalline facets down to 250 mK and up to 18 T. Fitting a range of qualitatively varying spectra with a Blonder-Tinkham-Klapwijk (BTK) model for p-wave pairing together with collaborator P. Brydon (Otago University), we extracted gap amplitude and interface barrier strength for each junction. We find good agreement with the data for a dominant p-wave gap function with amplitude 0.26 ± 0.06 meV. Our work provides spectroscopic evidence for a gap structure consistent with the proposed spin-triplet pairing in the superconducting state of UTe2, and is consistent with recent work with STM collaborators. The PCAR work was recently published: *H. Yoon et al., "Probing p-wave superconductivity in UTe2 via point-contact junctions" npj Quantum Materials (2024).*

d) Ultrasound studies at ambient and high pressures: Working closely with the group of B. Ramshaw (Cornell), including several on-site visits by UMD students to help develop the experiments, we have made great progress in using ultrasound to probe the superconducting state in UTe2. Recent work published with the Ramshaw group have found results in studying the behavior of elastic moduli through Tc more consistent with a single-component order parameter in both single- and double-Tc samples. The strictest interpretation of this result is that it rules out all multi-component order parameters that have a bilinear coupling to strain. However, there is no dispute about the fact that the superconducting transition splits into two well-defined thermodynamic transitions under applied pressures, so we have pursued an ultrasound experiment to probe the symmetry of the distinct superconducting transitions under pressure that will establish the exact order parameter symmetries of the superconducting states of UTe_2, both at low and high fields. In preparation, the PI has recently sent a graduate student to Cornell for repeated visits, bringing our pressure apparatus to set up sound velocity and attenuation experiments under pressure. Preliminary measurements are extremely successful, and work is under way to analyze the velocity and attenuation data as a function of pressure. Previous work studying ambient pressure response is now published in these works: *F. Theuss et al., "Single-Component Superconductivity in UTe2 at Ambient Pressure", Nature Physics (2024).*

Future Plans

The main effort is focused on elucidating the superconductivity of UTe2, including continued work on thermodynamic and spectroscopic measurements aimed at identifying the exact pairing symmetry of this superconductor as well as the opportunities to observe, isolate and manipulate Majorana fermions to establish a platform for future quantum technologies. We are also working very closely with the groups of V. Madhavan (UIUC) and J.C.S. Davis (Oxford/Cornell) on STM studies of a newly discovered charge ordered phase in UTe2 that may have implications for both normal and superconducting states of this material. Ongoing experiments are probing the sample dependence and correlation with experiments our group at Maryland are conducting on the normal state properties. Continued work on the RPtBi series is aimed in the same direction, with projects focused on further elucidating this exotic superconducting phase and its implications. We continue to probe further substitution series including both magnetic ion and heavy fermion mixing of the j=3/2 superconducting state, and are collaborating with the group of C. Felser (Max Planck).

Publications

1. A. Carlton-Jones, A. Suarez, Y.-S. Eo, I. M. Hayes, S. R. Saha, J. Paglione, N.P. Butch, S.M. Anlage, "*Revealing isotropic abundant low-energy excitations in UTe2 through complex microwave surface impedance*", Phys. Rev. B 112, 014519 (2025).
2. G. Gu, S. Wang, J.P. Carroll, K. Zhussupbekov, C. Broyles, S. Ran, N.P. Butch, S. Saha, J. Paglione, X. Liu, J.C.S Davis, D.-H. Lee, "*Pair wave function symmetry in UTe2 from zero-energy surface state visualization*", Science 388, 938 (2025).
3. I.M. Hayes, T.E. Metz, C.E. Frank, S.R. Saha, N.P. Butch, V. Mishra, P. J. Hirschfeld, J. Paglione, "Robust Nodal Behavior in the Thermal Conductivity of Superconducting UTe2", Phys. Rev. X 15, 021029 (2025).
4. H. Kim, I.L. Liu, W.C. Lin, Y.S. Eo, S. Ran, N.P. Butch, J. Paglione, "*Tuning a magnetic energy scale with pressure and field in UTe2*," Nature Comm. Mat. 6, 6 (2025).
5. T. Chen, H. Siddiquee, Q. Xu, Z. Rehfuss, S. Gao, C. Lygouras, J. Drouin, V. Morano, K.E. Avers, C.J. Schmitt, A. Podlesnyak, J. Paglione, S. Ran, Y. Song, C. Broholm, "Quasi-2D Antiferromagnetic Spin Fluctuations in the Spin-Triplet Superconductor Candidate CeRh2As2", Phys. Rev. Lett. 133, 266505 (2024)
6. S.K. Lewin, J.J. Yu, C.E. Frank, D. Graf, P. Chen, S. Ran, Y.S. Eo, J. Paglione, S. Raghu, N.P. Butch, "Field-angle evolution of the superconducting and magnetic phases of UTe2 around the b axis" Phys. Rev. B 110, 184520 (2024)
7. H. Yoon, Y. S. Eo, J. Park, J.A. Horn, R.G. Dorman, S.R. Saha, I.M. Hayes, I. Takeuchi, P.M.R. Brydon, J. Paglione, "Probing p-wave superconductivity in UTe2 via point-contact junctions" npj Quantum Materials 9, 91 (2024)
8. F. Theuss, A. Sheragai, G. Grissonnanche, I.M. Hayes, S.R. Saha, Y.S. Eo, A. Suarez, T. Shishidou, N.P. Butch, J. Paglione, B.J. Ramshaw, "Single-Component Superconductivity in UTe2 at Ambient Pressure", Nature Physics 20, 1124 (2024).
9. C.E. Frank, S.K. Lewin, G. S. Salas, P. Czajka, I.M. Hayes, H. Yoon, T. Metz, J. Paglione, N.P. Butch, "Orphan high field superconductivity in non-superconducting uranium ditelluride" Nature Comm. 15, 3378 (2024).
10. A. Aishwarya, J. May-Mann, S. Ran, S.R. Saha, J. Paglione, N.P. Butch, E. Fradkin, V. Madhavan, "Melting of the charge density wave by generation of pairs of topological defects in UTe2", Nature Physics 20, 964 (2024)

Correlated Topological Quantum Heterostructures

Ho Nyung Lee (PI), Matt Brahlek, Gyula Eres, Hu Miao, and T. Zac Ward; *Oak Ridge National Laboratory, Oak Ridge, TN 37831*

Keywords: Thin film heterostructure, transition metal compounds, pulsed laser deposition, molecular beam epitaxy

Research Scope

A material's combination of correlation and topology is predicted to realize novel quantum states of matter. Despite various attempts to realize correlated topological materials with intertwined charge, spin, and orbital degrees of freedom, only a handful of materials have been experimentally identified. Furthermore, while intriguing topological quantum phenomena are realized, such as, the quantum anomalous Hall effect, for instance, their reproduction remains limited and challenging, and the origin of such remarkable properties is still under debate. Thus, the overarching goal of this project is to understand and discover correlated and topological states of matter by exploiting the interplay between symmetry, correlation, and topology in oxide- and chalcogenide-based quantum heterostructures. To achieve this goal, we focus on three specific aims: (1) Create and control topological phases in correlated perovskite oxide thin films and 2D membranes by interrogating the role of oxygen octahedral symmetry and strain; (2) Understand complex magnetism in kagome metals and altermagnets as well as their heterostructures; and (3) Unveil how to control topological wavefunctions in magnetic topological insulators and their heterostructures by manipulating magnetic orders and disorder. Underpinning this work combines expertise and experimental capabilities based on precision synthesis by pulsed-laser deposition (PLD) and molecular-beam epitaxy (MBE) with advanced characterization tools. The latter include spin- and angle-resolved photoemission spectroscopy, inelastic x-ray scattering, neutron reflectometry, optical spectroscopy, and milli-Kelvin quantum transport. The fundamental knowledge obtained in this proposed work will provide useful information to advance next-generation information and energy technologies, thereby supporting the DOE missions to achieve the vision of a secure and sustainable energy future.

Recent Progress

The research in this project is focused on the discovery of new correlated and topological materials and their emergent phenomena arising from well-controlled, functionally cross-coupled interfaces. Special emphasis was on understanding and controlling the interplay between correlation and spin-orbit coupling in 4*d* correlated oxide heterostructures grown by PLD and their physical property control by deliberately manipulating the degree of epitaxial strain. This project has also developed a novel synthesis route for growing high-quality delafossite thin films on triangular substrates mediated by an interfacial sacrificial layer. This rational design of the interfacial layer allowed tailoring of magnetism and transport properties. The interface between magnetic materials and topological insulators in thin films grown by MBE was also studied to understand the formation of exotic phases of matter that enable functionality through manipulation of strong spin polarized transport. The use of wide range of characterization methods,

including microstructural imaging, local spectroscopy, neutron scattering, optical and soft x-ray spectroscopy, in combination with theory plays a key role in performing this research. A few research accomplishments achieved over the last two years are highlighted as follows:

Strain-induced nonsymmorphic symmetry creates a novel topological phase in a 4d correlated oxide

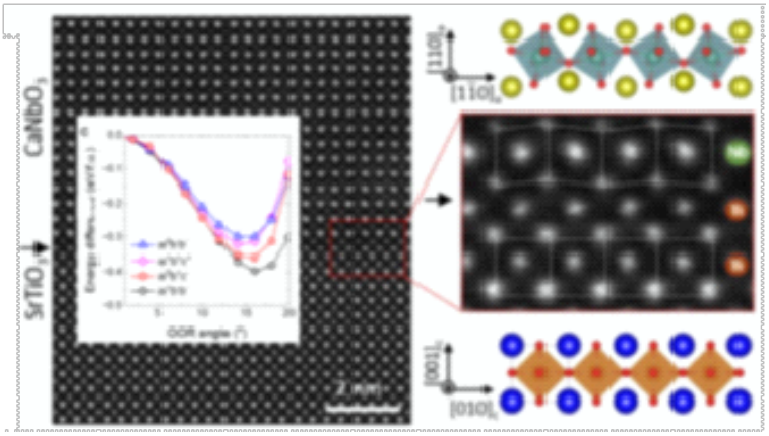


Fig.1. Precision synthesis of quantum heterostructures. An example of cross-sectional scanning transmission electron microscopy images that reveal a clear oxygen octahedral rotation (ORR) in a $CaNbO_3$ film grown on a cubic $SrTiO_3$ substrate. The ORR controlled by epitaxial strain can induce a nonsymmorphic symmetry that yields Dirac band crossing. The inset shows a

The collective rotations of oxygen octahedra play an important role in determining the physical properties of functional perovskite oxides. The epitaxial strain can serve as an effective means to modify the oxygen octahedral symmetry (OOS), i.e., oxygen octahedral rotation or tilt (OOR/OOT). However, the strain-OOS coupling that may alter the details of the OOS, thereby the physical properties, has not been fully understood. In a recent study [1], we demonstrated that epitaxial strain can not only induce a structural phase transition but also precisely tune the degree of OOR. The correlated metal $CaNbO_3$, which is orthorhombic, is studied by growing as epitaxial thin films. By imposing epitaxial strain, it is found that the film undergoes a structural phase transition from orthorhombic to tetragonal upon fully straining (i.e., from $a^+b^-b^-$ to $a^0a^0c^-$). In unstrained films, the octahedral rotation along the *c*-axis is as large as 15.7° that can be tuned to 6.6° by strain. This finding offers a rationa design approach to manipulating OOR/OOT via strain engineering in complex oxide heterostructures. Such an OOR is also found to induce a Dirac state, yielding a correlated topological quantum material.

Light-matter interactions reveal an unprecedented spontaneous chirality flipping

The asymmetric distribution of chiral objects with opposite chirality is of great fundamental interest ranging from molecular biology to particle physics. In quantum materials, chiral states can build on inversion-symmetry-breaking lattice structures or emerge from spontaneous magnetic ordering induced by competing interactions. Although the handedness of a chiral state can be changed through external fields, a spontaneous chirality flipping has yet to be discovered. We discovered experimental evidence of chirality flipping via changing temperature in a topological magnet $EuAl_4$, which features orthogonal spin density waves (SDW) and charge density waves (CDW) [2]. Using circular dichroism of Bragg peaks in the resonant magnetic x-ray scattering, we find that the chirality of the helical SDW flips through a first-order phase transition with modified SDW wavelength. Intriguingly, we observe that the CDW couples strongly with the SDW and displays a rare commensurate-to-incommensurate transition at the chirality flipping temperature. Combining with first-principles calculations and angle-resolved photoemission spectroscopy, our results support a Fermi surface origin of the helical SDW with intertwined spin, charge, and lattice degrees of freedom in $EuAl_4$. Our results reveal an unprecedented spontaneous chirality flipping and lay the groundwork for a new functional manipulation of chirality through momentum-dependent spin-charge-lattice interactions. This work ultimately highlights $EuAl_4$ as a new platform for emergent chiral interactions and open a new avenue for chiral microelectronic applications.

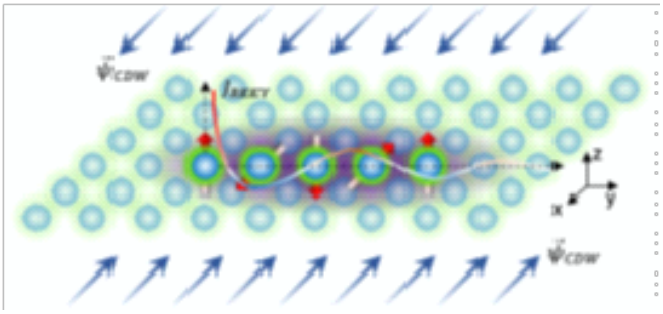


Fig. 2. A schematic of orthogonal spin-charge ordered topological magnet $EuAl_4$. The Ruderman-Kittel-Kasuya-Yosida interaction-driven chiral SDW intertwines with the CDW

Angular momentum of chiral phonons is experimentally probed

In condensed matter, angular momentum is intimately related to the emergence of topological quantum states, including chiral superconductivity, quantum spin liquids and various chiral quasiparticles. Recently, it has been predicted that microscopic lattice excitations, known as phonons, can carry finite angular momentum (AM), leading to specific physical properties of materials. However, phonon angular momentum has not yet been observed directly. In this work, we showed that due to AM conservation, applying a time-reversal symmetry breaking thermal gradient along the chiral axis of single crystal Te results in a macroscopic

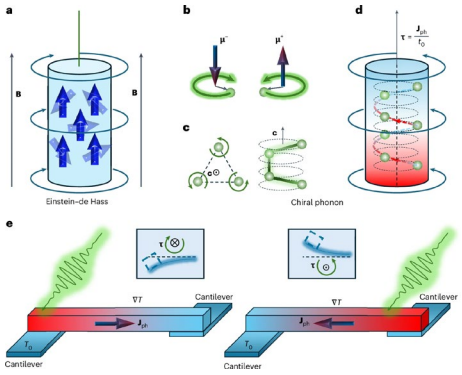


Fig. 3. Heat flowing through a crystal with a chiral structure (a-d) is carried by lattice vibrations (phonons) that also carry angular momentum. To conserve angular momentum, the crystal itself rotates. This rotation is measured by sensitive cantilevers (e), confirming the phonons indeed have non-zero angular momentum [3].

mechanical torque that can be observed using a cantilever-based device [3]. We probe this torque using a cantilever-based device and establish that it changes sign by flipping the chirality or thermal gradient. This behavior disappears in polycrystalline samples that lack a preferred chirality. Our results uncover phonon-AM and pave the way for phonon-AM enabled quantum states for microelectronic applications.

Future Plans

This project will advance our understanding on (1) correlated topological phenomena, (2) altermagnetism in oxide thin films, and (3) emergent phenomena in freestanding and twisted oxide membranes. For correlated topological phenomena, we will unveil the electronic structure transition from Dirac nodal line semimetal to Dirac semimetal in correlated $CaNbO_3$ thin films. Quantum transport properties will be studied at extremely low temperature and high-magnetic fields to understanding the details of the electronic and transport properties. We will also focus on 1H and 1T stacked transition metal dichalcogenides. The 1H layer hosts superconductivity whereas the 1T layer features charge ordered Mott insulator. For altermagnetism in oxide thin films, we will establish the epitaxy of high-quality thin films by PLD to enable the studies of altermagnetism in oxide materials, including RuO_2, ReO_2, and $LaVO_3$. The basic properties will be also characterized by magneto-transport measurements, and the electronic structure will be characterized by spin-ARPES. The magnetic structure will be studied using resonant x-ray scattering. For emergent phenomena in freestanding and twisted oxide membranes, we will establish the synthesis conditions using sacrificial layer lift-off to study emergent physical properties in artificial heterostructures by fabricating freestanding oxide membranes. The focus will be on dielectrics and ferroelectrics as well as correlated oxides for strain control, interfacial coupling, and twisting.

References

1. Y. Park, S.-H. Kang, J. Song, S. W. Hwang, S. Lin, J. M. Ok, F. Yang, H. Kim, A. R. Lupini, M. Yoon, S. Yoon, H. Zhou, and H. N. Lee, Strain Programming of Oxygen Octahedral Symmetry in Perovskite Oxide Thin Films, *Adv. Mater. Interfaces*, **12**, 2400697 (2025). DOI: 10.1002/admi.202400697
2. H. Miao, J. Bouaziz, G. Fabbris, W. R. Meier, F. Z. Yang, H. X. Li, C. Nelson, E. Vescovo, S. Zhang, A. D. Christianson, H. N. Lee, Y. Zhang, C. D. Batista, S. Blügel, Spontaneous chirality flipping in an orthogonal spin-charge ordered topological magnet, *Phys. Rev. X* **14**, 011053 (2024).
3. H. Zhang, N. Peshcherenko, F. Yang, T. Z. Ward, P. Raghuvanshi, L. Lindsay, C. Felser, Y. Zhang, J.-Q. Yan, and H. Miao, Measurement of phonon angular momentum, *Nat. Phys.* (2025). https://doi.org/10.1038/s41567-025-02952-3

Publications

1. H. Miao, T. T. Zhang, H. X. Li, G. Fabbris, A. H. Said, R. Tartaglia, T. Yilmaz, E. Vescovo, J. X. Yin, S. Murakami, L. X. Feng, K. Jiang, X. L. Wu, A. F. Wang, S. Okamoto, Y. L. Wang, and H. N. Lee, Signature of spin-phonon coupling driven charge density wave in a kagome magnet**,** *Nat. Commun*. **14,** 6183 (2023).
2. H. Miao, J. Bouaziz, G. Fabbris, W. R. Meier, F. Z. Yang, H. X. Li, C. Nelson, E. Vescovo, S. Zhang, A. D. Christianson, H. N. Lee, Y. Zhang, C. D. Batista, S. Blügel, Spontaneous chirality flipping in an orthogonal spin-charge ordered topological magnet, *Phys. Rev. X* **14**, 011053 (2024).
3. A.R. Mazza, J.-Q. Yan, S. Middey, J.S. Gardner, A.-H. Chen, M. Brahlek, T. Z. Ward, Embracing disorder in quantum materials design, *Appl. Phys. Lett*. **124**, 230501 (2024).
4. H. Jeon, H. Seo, J. Seo, Y. H. Kim, E. S. Choi, Y. Jo, H. N. Lee, J. M. Ok, J. S. Kim, Large anomalous Hall conductivity induced by spin chirality fluctuation in an ultraclean frustrated antiferromagnet $PdCrO_2$, *Commun. Phys.* **7**, 162 (2024).
5. A. Herklotz, R. Roth, Z.X. Chong, L. Luo, J.M. Park, M. Brahlek, J. Wang, K. Dorr, T.Z. Ward, Polarization rotation in a ferroelectric $BaTiO_3$ film through low-energy He-implantation, *APL Mater.* **13**, 031105 (2025).
6. Y. Park, S.-H. Kang, J. Song, S. W. Hwang, S. Lin, J. M. Ok, F. Yang, H. Kim, A. R. Lupini, M. Yoon, S. Yoon, H. Zhou, H. N. Lee, Strain programming of oxygen octahedral symmetry in perovskite oxide thin films, *Adv. Mater. Interfaces*, **12**, 2400697 (2025).
7. Y.-C. Wu, G. Halasz, J. Damron, Z. Gai, H. Zhao, Y. Sun, K. Dahmen, C. Sohn, E. Carlson, C. Hua, S. Lin, J. Song, H. N. Lee, and B. Lawrie, Nanoscale magnetic ordering dynamics in a high Curie temperature ferromagnet, *Nano Lett.* **25**, 1473 (2025).
8. H. Zhang, N. Peshcherenko, F. Yang, T. Z. Ward, P. Raghuvanshi, L. Lindsay, C. Felser, Y. Zhang, J.-Q. Yan, and H. Miao, Measurement of phonon angular momentum, *Nat. Phys.* (2025). https://doi.org/10.1038/s41567-025-02952-3
9. F. Z. Yang, H. D. Zhang, S. Mandal, F. Y. Meng, G. Fabbris, A. H. Said, P. Mercado Lozano, A. Rajapitamahuni, E. Vescovo, C. Nelson, S. Lin, Y. Park, E. M. Clements, T. Z. Ward, H. N. Lee, H. C. Lei, C. X. Liu, and H. Miao, Signature of magnetoelectric coupling driven finite momentum pairing in 3D ising superconductor, *Nat. Commun*. **16**, 6626 (2025).
10. S. Okamoto, N. Mohanta, H. N. Lee, A. Moreo, and E. Dagotto, Novel phenomena in transition-metal oxide thin films and heterostructures with strong correlations and spin-orbit coupling, *Phys. Rev. Mater.* **9**, 050301 (2025).

Definitive Majorana Zero Modes in Optimized Hybrid Nanowires

Sergey Frolov, *University of Pittsburgh*

Keywords: topological superconductivity, transport, nanostructures, quantum wells

Research Scope

The goals of this project are to establish Majorana Zero Modes in superconductor-semiconductor hybrid nanowire devices, as well as to search for induced triplet superconductivity.

The first objective is to develop and optimize improved nanowires. They come with two shells: a large bandgap semiconductor inner shell and a metallic superconductor outer shell. The inner shell is ZnTe and is from another family of materials (group II-VI rather than III-V), however its lattice constant is close to InAs, and this facilitates defect-free combinations. For the superconductor shell, we focus on beta-Sn (tin).

With optimized nanowires, we shall perform three-terminal transport experiments. Looking at the two ends of a nanowire and observing correlated signals is thus the most robust and straightforward way to separate topological and trivial states. In the three-terminal device setup, we can correlate zero-bias resonances across the two ends of the nanowire, inferring proof of their non-local nature that more uniquely identifies Majorana modes. At the same time, we shall pursue the observation of all other predicted Majorana signatures (Majorana oscillations, topological phase diagram) simultaneously on both ends of the same nanowire to exclude alternative explanations more reliably.

The interplay of magnetism, spin-orbit coupling and superconducting correlations is a fertile ground for exploration of exotic superconductivity more broadly. Beyond and besides topological effects, we are interested in exploring the triplet and odd-triplet superconducting phases that may arise when integrating semiconductor and superconducting materials. We shall focus on hybrid interfaces where symmetry is broken by adding an interlayer of a chiral material.

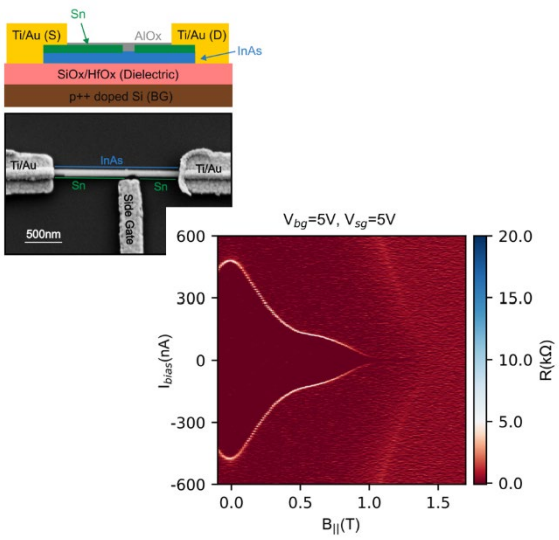
Recent Progress

1. Optimized Nanowires.

During the first reporting period of this renewal of the project, we focused on binary combinations of nanowires, specifically on InAs-Sn and InAs-ZnTe core-shell nanowires. These experiments have laid ground and informed the development of two-shell InAs-ZnTe-Sn nanowires.

1.a. InAs-Sn nanowire growth. With our materials science collaborators Palmstrom and Hocevar, we demonstrated the growth and performed transport measurements on novel InAs-Sn nanowires.

We previously studied Sn shells on InSb nanowires, where Sn-shells grew in a mixture of alpha- and beta- phases. Only the beta phase is superconducting thus for our project it is desired to grow pure beta-Sn shells. However, InSb is lattice-matched to alpha-Sn which promotes the growth of alpha grains. By switching to InAs, we achieved purely beta-Sn shells that exhibit an epitxial relationship to the InAs core.



Sn-InAs nanowire Josephson junction sustains high supercurrents (500 nA) to large magnetic fields (>1T)

1.b. Transport experiments on InAs-Sn nanowires. Using improved InAs-Sn nanowires, we have obtained a set of outstanding superconductor properties. These results are under review at Nano Letters. In particular, the Josephson critical currents in single wires approach 0.5 microampere. The critical magnetic fields exceed 1.7 Tesla. The developed wires are also used in applications of quantum devices such as transmon qubit with coherence time T1 = 27 microseconds, which is state-of-the-art for hybrd transmons and in parametric amplifiers. These applications are beyond the scope of this project, but they benefit from nanowire characterization performed here.

1.c. ZnTe-InAs nanowires. For the ultimate Majorana devices we are interested in controlling the superconductor-semiconductor coupling and we intend to do this through the intermediate ZnTe shell which would act as a tunnel barrier. Towards this end, we have perfected the growth on ZnTe shells of various thickness, in situ, on InAs nanowires. The growth is carried out in the lab of collaborator Hocevar. Transport characterization is performed within this project. We demonstrate that the shell of ZnTe does not degrade the transport characteristics of the InAs core, which retains high mobility and low gate hysteresis. Transport measurement indirectly confirm DOE-supported DFT calculations that predict that ZnTe is a tunnel barrier based on the band alignment. Indeed, for thicker shells the nanowires do not conduct at low bias even after surface oxide cleaning. These results are in preparation for publication.

2. Tunneling signatures of Majorana Modes.

In this funding cycle, we maintained focus on false-positives in Majorana identification protocols. It remains as important as ever to have the ability to clearly delineate instances of trivial states from potential observations of topological superconductivity. In this context, our work on 'Smoking gun signatures of topological phenomena' has been further advanced, and is currently unofficially accepted to Science. The delay with publication is caused by the need to create a new article category to accommodate this new type of effort. Within the work, supercurrent signatures of triplet superconductivity are scrutinized for alternative explanations.

3. Chiral materials and phenomena.

Interested in triplet superconductivity more broadly, we are exploring combinations of both semiconductors and superconductors with layers of self-assembled molecules (SAM) of different chirality. This work is done in collaboration with Waldeck at the University of Pittsburgh. Within this effort, we have deposited SAM on InAs. SAM exhibit surface passivation, replacing the oxygen peak in XPS. The layers are uniform as revealed by AFM.

We have coated thin films of superconductor NbTiN with SAM. In 5nm thick films, we have observed a considerable reducing in superconductor critical temperature Tc in films coated with SAM. In thicker films, no effect on Tc is observed. We are investigating the origins of these effects and its potential relation with chirality which is premature to discuss at this stage. We have determined that superconductors such as Al and Sn may not be suitable for coating with SAM because of the oxide layers. We shall continue exploring the possibilities for selectively removing the oxide prior to SAM deposition.

Future Plans

In the next funding cycle, we shall develop two shell InAs-ZnTe-Sn nanowires, combining the knowledge we gained from developing the binary combinations. This is facilitated by the installation of the cryogenic evaporators in both Pittsburgh and Grenoble.

With two-sell nanowires, we shall perform two- and three-terminal tunneling experiments. An important element for tunneling experiments in the creatioin of a longer shadow in the Sn shell. Our wires are currently produced by nanowire shadows which are 100 nm in diameter. This works for Josephson junction devices, but for tunnel junctions we need 500 nm shadows. This will be accomplished by templated nanowire growth, as well as by shadow wall fabrication. Both techniques are already developed in Pittsburgh.

We shall explore the origins of the effect of SAM layers on the critical temperature of thin superconductor films. We shall experiment with chiral and non-chiral molecules and obtain additional information from XPS, AFM and EDS.

Publications

1. Amritesh Sharma, An-Hsi Chen, Connor P. Dempsey, Amrita Purkayastha, Mihir Pendharkar, Susheng Tan, Christopher J. Palmstrøm, Sergey M. Frolov, Moïra Hocevar *Sn-InAs nanowire shadow-defined Josephson junctions* arXiv:2503.13725 (Accepted to Nano Letters)

2. S.M. Frolov, P. Zhang, B. Zhang, Y. Jiang, S. Byard, S.R. Mudi, J. Chen, A.-H. Chen, M. Hocevar, M. Gupta, C. Riggert, V.S. Pribiag *"Smoking gun" signatures of topological milestones in trivial materials by measurement fine-tuning and data postselection* arXiv:2309.09368 (Submitted to Science)

$Ti_3C_2T_x$ MXene Composites for Electrochemical Applications

Bhoj Raj Gautam, Fayetteville State University (Principal Investigator)

Daniel Autrey, Fayetteville State University (Co- Investigator)

Chandra Mani Adhikari, Fayetteville State University (Co- Investigator)

Shubo Han, Fayetteville State University (Co- Investigator)

Bishnu Prasad Bastakoti, North Carolina Agricultural and Technical State University (Co-Investigator)

Binod Kumar Rai, Savannah River National Laboratory (Co- Investigator)

Keywords: Transition metal compounds, electrochemistry, optical spectroscopy**,** magnetism

Research Scope

MXenes, which are derived from selective etching of the A element in layered MAX phases ($M_{n+1}AX_n$, where M = early transition metal, A = group IIIA or IVA element, and X = C and/or N), offer a unique combination of metallic conductivity, hydrophilicity, magnetism, good dispersion ability in solvents, mechanical stability, and structural diversity, making them promising for applications in catalysis, sensing, electrochemical energy storage, spintronics, and optoelectronics[1-5]. In the last two years, we synthesized several MXenes with different synthetic routes and investigated their magnetic, optical, and electrochemical properties. Here, we report the intercalation of polyacrylonitrile (PAN) nanoparticles in $Ti_3C_2T_x$ MXene layers through simple sonication. In this work, a composite consisting of MXene and PAN was successfully synthesized and assessed for supercapacitor applications using electrochemical tests. We also developed bifunctional electrodes from the combination of rare earth metal selenides (Ce_2Se_3 and Er_2Se_3) with a $Ti_3C_2T_x$/S-doped graphitic carbon nitride (CN) heterostructure for bifunctional application in flexible supercapacitors and oxygen evolution reactions (OER).

Recent Progress

In this work, MXene ($Ti_3C_2T_x$) was derived from its parent MAX phase (Ti_3AlC_2) using LiF/HCl as an etchant to remove aluminum, while PAN was synthesized via radical polymerization. The MXene-PAN composite was subsequently produced using a straightforward sonication technique. Utilizing a solvent dimethyl sulfoxide (DMSO) that solubilizes PAN but disperses MXene, the PAN nanoparticles were effectively intercalated into the interlayer spaces of MXene sheets, causing subsequent delamination of the layers. X-ray diffraction analysis showed an increase in the c-lattice parameter from 22.31 Å for the pristine MXene to 37.73 Å for the MXene-PAN composite, indicating an expanded interlayer spacing between the multilayer MXene sheets. This

intercalation of PAN nanoparticles and the resulting increase in interlayer gaps proved beneficial in preventing MXene sheet restacking, thereby exposing more surface area, which is crucial for energy storage applications. The rising trend in the specific capacitance (C_s) among the samples ($C_{s,MAX} < C_{s,MXene} < C_{s,MXene\text{-}DMSO} < C_{s,MXene\text{-}PAN\text{-}DMSO}$) just mirrored the increasing trend in the c-lattice parameter ($c\text{-}LP_{MAX} < c\text{-}LP_{MXene} < c\text{-}LP_{MXene\text{-}DMSO} < c\text{-}LP_{MXene\text{-}PAN\text{-}DMSO}$). Electrochemical tests showed that the composite had the best performance in capacitance, resistance, and conductivity. These findings highlight the crucial role of PAN intercalation in MXene, providing new design strategies for high-performance, electrochemically active materials for energy storage and related applications.

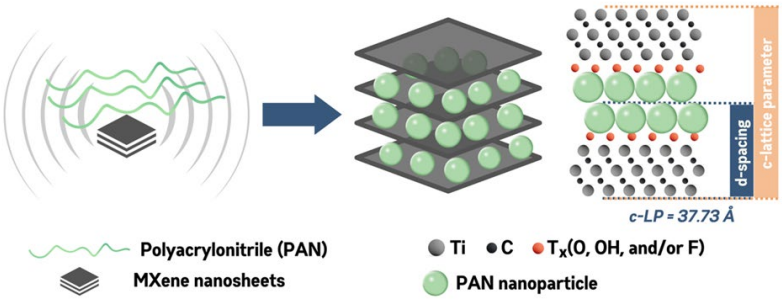


Figure. 1. Graphical illustration of the synthesis of PAN intercalation in MXene layers.

The ternary composite of MXene/S-CN (MCN) and cerium-erbium-selenide (MCN/CESe) was prepared via a facile hydrothermal method. The incorporation of S-doped graphitic carbon nitride in MXenes reduced the layer stacking tendency of both two-dimensional sheets and eliminated volume expansion by forming a heterostructure. Cerium and erbium rare earth metal centers induce reactive surface sites, whereas binary layers of $Ti_3C_2T_x$/S-doped graphitic carbon nitride provide a conducting matrix for the homogeneous growth of the metal selenides. This work is the first to investigate the bifunctional energy efficiency of rare earth metal selenides grown over MXene materials. This study reports the successful hydrothermal fabrication of Ce_2Se_3 and Er_2Se_3-grown MCN nanohybrids and the investigation of their bifunctional efficiency toward flexible All Solid-State Asymmetric Supercapacitor (ASSASC) as well as the OER. Among the fabricated nanohybrids, MCN/ CESe-5:1 delivered the optimum electrochemical performance for both flexible supercapacitors and the OER.

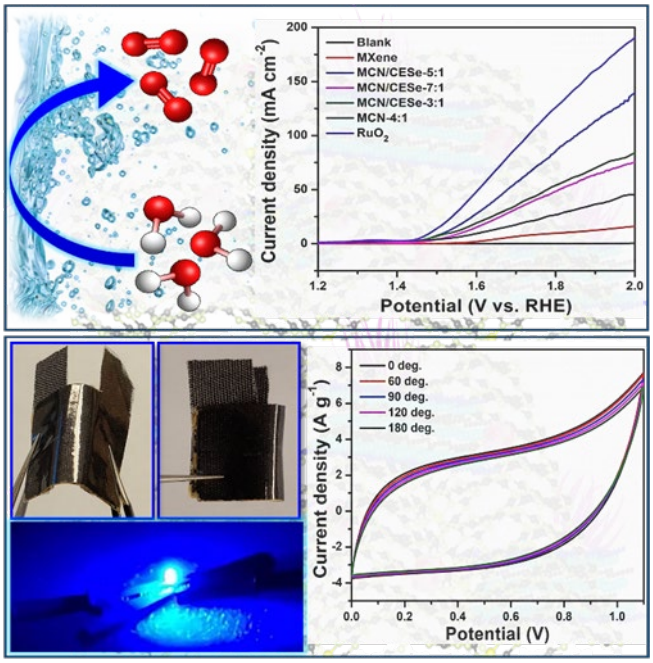


Figure 2. Combination of rare earth metal selenides (Ce_2Se_3 and Er_2Se_3) with a $Ti_3C_2T_x$/S-doped graphitic carbon nitride heterostructure for bifunctional application in flexible supercapacitors and oxygen evolution reactions.

Future Plans

We will complete the ongoing projects and disseminate results for publication. We will continue our study (both experimentally and computationally) in electronic, optical, magnetic, and electrochemical properties of functionalized MXenes. We will continue mentoring student researchers throughout the year and also train them through SRNL and NC A&T's intern programs.
For the coming year, we are planning to work on the following projects.

Plans for thrust 1 (Magnetic Properties of 2D MXenes):

(1) We will continue the study of pristine, and gamma irradiated rare earth i-MAX and MXene materials using resources at SRNL, DOE user facilities, and partner universities.
(2) Neutron diffraction beamtime will be submitted at DOE user's facilities to study microstructures and magnetic properties of pristine and gamma irradiated materials.
(3) We will continue magnetic measurements at SRNL on MAX and MXene samples obtained from FSU and NC A&T utilizing PPMS and Electronic Paramagnetic Resonance.

Plans for thrust 2 (MXenes for Electrochemical Energy Storage):

(1) We will explore other materials to combine with MXene, aiming to achieve a nanocomposite with high porosity, a large surface area, and high conductivity, and to test these materials for use in supercapacitors.
(2) Conductive polymer will be incorporated into MXene layers through in-situ polymerization to enhance the overall electrochemical performance of MXene.
(3) We will focus on MQD optimization, functionalization, biosensor stability, and method validation. We will optimize hydrothermal synthesis parameters to control MQD size, surface chemistry, and batch-to-batch reproducibility.
(4) We will further explore the incorporation of redox-active materials and conductive polymers into MXene to enhance its electrochemical performance.

Plans for thrust 3 (Optoelectronic Properties of 2D MXenes):

(1) We plan to investigate the impact of dimensionality and stoichiometry of functionalized MXenes in photon absorption and charge generation and charge transfer.
(2) Density functional theory (DFT) calculations will be used to study the optical and dielectric properties of functionalized MXenes.
(3) We plan to use thin films of MXenes as substrates for the sensing of analytes and study the effect of gamma radiation on SERS enhancement. DFT calculations will be performed for the optimization of SERS sensitivity in MXene-based substrates.
(4) We plan to study the energy transfer process between MXene quantum dots and conjugated polymers for ratiometric fluorescent detection.

References

1. J.-H. Han, J. Park, Y. H. Jin, Y. Chae, J. Han, J. Wang, S.-H. Seok, Y. Sim,S.-Y. Kwon, Ultrahigh Conductive MXene Films for Broadband Electromagnetic Interference Shielding, *Adv. Mater.*, **37**, 2502443 (2025).

2. J. Zhang, R. Muñoz-Mármol, S. Fu, X. Li, W. Zheng, A. Villa, G. Paterno, D. Pohl, A. Tahn, M. Hambsch, S. Mannsfeld, D. Li, H. Xu, Q. Guo, H. Wang, F. Scotognella, M. Yu, X. Feng, Interface-Tailored Secondary Excitation and Ultrafast Charge/ Energy Transfer in $Ti_3C_2T_x$-MoS_2 Heterostructure Films, *J. Am. Chem. Soc.*, **147**, 10012−10022 (2025).
3. W. Li, T. Zhou, Z. Zhang, L. Li, W. Lian, Y. Wang, J. Lu, J. Yan, H. Wang, L. Wei, Q. Cheng, Ultrastrong MXene Film Induced by Sequential Bridging with Liquid Metal, *Science* **385**, 62–68 (2024).
4. B. K. Rai, C. A. Mizzi, A. Bretaña, L. Breton, C. Housley, D. Ivy, J. Abbott, B. Maiorov, B. R. Gautam, M. Frontzek, R. C. Rai, S. Calder, Magnetic Properties of $(Mo_{2/3}Dy_{1/3})2AlC$ Arc Melted Polycrystalline Samples, *J. Magn. Magn. Mater.,* **624**, 172992 (2025).
5. S. M. M. Alonzo, S. De, V. Morris, D. E. Autrey, B. R. Gautam, G. Pathiraja, and B. P. Bastakoti, Intercalation of Polyacrylonitrile Nanoparticles in Ti_3C_2Tx MXene Layers for Improved Supercapacitance, *ACS Appl. Mater. Interfaces*, **16**, 47, 64784–64796 (2024).

Publications

1. N. H. Makani, A. Wilson, J. Abbott, and B. Gautam, Investigation of Structural and Thermal Properties of Nb_2CT_X MXenes at Elevated Temperature, *Microsc. Microanal*. **31** (7), 353–354 (2025).
2. N. H. Makani, J. Wu, J. Florentino, S. Han, and B. Gautam, Optical Properties of Hydrothermally Synthesized $Ti_3C_2T_X$ MXene Quantum Dots and Their Application in Biosensors, *Microsc. Microanal*., **31** (7), 916–917 (2025).
3. B. K. Rai, C. A. Mizzi, A. Bretaña, L. Breton, C. Housley, D. Ivy, J. Abbott, B. Maiorov, B. R. Gautam, M. Frontzek, R. C. Rai, S. Calder, Magnetic Properties of $(Mo_{2/3}Dy_{1/3})2AlC$ Arc Melted Polycrystalline Samples, *J. Magn. Magn. Mater.,* **624**, 172992 (2025).
4. C. M. Adhikari, D. Dahal, S. Kunwar, and B. R. Gautam, Ti_3C_2 and Ti_2C MXenes-Based Distributed Bragg Reflectors in Fabry Pérot Cavity's Resonance Tuning, *J. Electron. Mater.* **54**, 4309–4318 (2025).
5. S. De and B. P. Bastakoti, Doped and Functionalized Non-Ti-MXenes for Flexible and Wearable Electronic Devices, *J. Mater. Chem. A*, **13**, 855-888 (2025).
6. S. De, J. Florentino, G. Pathiraja, B. R. Gautam, B. P. Bastakoti, MXene/Graphitic Carbon Nitride-Supported Metal Selenide for All-Solid-State Flexible Supercapacitor and Oxygen Evolution Reaction, *J. Mater. Chem. A*, **13**, 11300-11313 (2025).
7. S. L. Lyles, S. Vattikuti, G. Kinney, A. Smith, B. R. Gautam, and C. M. Adhikari Structural Stability and Electronic Structure of $(Ti,Ta)_2C$ MXenes. *JNPS*, **10**(1), 8–14(2024).
8. S. M. M. Alonzo, S. De, V. Morris, D. E. Autrey, B. R. Gautam, G. Pathiraja, and B. P. Bastakoti, Intercalation of Polyacrylonitrile Nanoparticles in Ti_3C_2Tx MXene Layers for Improved Supercapacitance, *ACS Appl. Mater. Interfaces*, **16**, 47, 64784–64796 (2024).
9. S. Garcia, A. K. Locke, B. D. Core, B. R. Gautam, D. E. Autrey, and Shubo Han, Electrochemical Amyloid β Immunosensor Based on $Ti_3C_2T_x$ MXene Nanosheets, *Microsc. Microanal*. **30** (Suppl 1), 932–933 (2024).
10. J. Abbott, V. Morris, M. Adhikari, S. Balabhadra, A. Bretana, B. Rai, D. Autrey, and B. Gautam, Structural and Morphological Characteristics of Rare Earth Element based MAX Phase and MXene, *Microsc. Microanal*. **30** (Suppl 1), 1215–1216 (2024).

Science of 100 tesla: The reverse quantum limit and its implications for unconventional quantum oscillations in YbB_{12}

Neil Harrison, Mun Chan, Arkady Shekhter, John Singleton, Priscila Rosa, Scott Crooker, Marcelo Jaime

Keywords: Kondo insulator, quantum oscillations, strong magnetic fields, quantum limit

Research Scope

Achieving breakthroughs in materials essential to extending U.S. leadership in AI and quantum information science requires a fundamental understanding of new paradigms in electronic matter. This depends on discoveries at the frontier of condensed matter physics, where highly entangled correlated electron states, low dimensionality, and topological effects yield novel emergent phenomena, such as neutral quasiparticles, unconventional spin-triplet and/or high-temperature superconductivity, robust topological surface states, and composite excitons. Understanding these phenomena is critical as a foundation for future quantum computing, photovoltaics, resilient microelectronics for extreme environments, and high-field magnet technologies. High magnetic fields offer a uniquely powerful means to address this grand challenge. Our research program leverages the unparalleled capabilities of the Pulsed Field Facility to generate non-destructive pulsed magnetic fields (~100 T) aimed at three interrelated research thrusts: (one) Orbital Effects in Metals and Insulators: studying fundamental changes in electronic properties induced by orbital quantization in strongly interacting electron systems under high magnetic fields; (two) Magnetic Field-Tuned States in Correlated Matter: probing the suppression and emergence of novel electronic phases by coupling extreme magnetic fields to spin degrees of freedom; (three) Magnetic Field Effects on Quantum Critical Fluctuations in Strange Metals: examining the coupling of extreme magnetic fields to highly entangled quantum critical states hypothesized to underlie strange metallic behavior.

Recent Progress

Excitonic insulators [1], fractional quantum Hall states [2], and similar unconventional electronic phases are more than a curiosity. These phases are experimental platforms to critically examine our theoretical understanding of condensed-matter systems, making them instrumental in pushing the limits of our basic scientific knowledge. Such electronic phases are expected to readily arise in metals under large magnetic fields and should be more likely to occur if the electrons exhibit strong correlations. This is because large magnetic fields force electrons in metals into a single state, a highly unstable configuration often called the “quantum limit”. However, other competing effects tend to win out in metals with strongly correlated electrons making these phases difficult to experimentally realize.

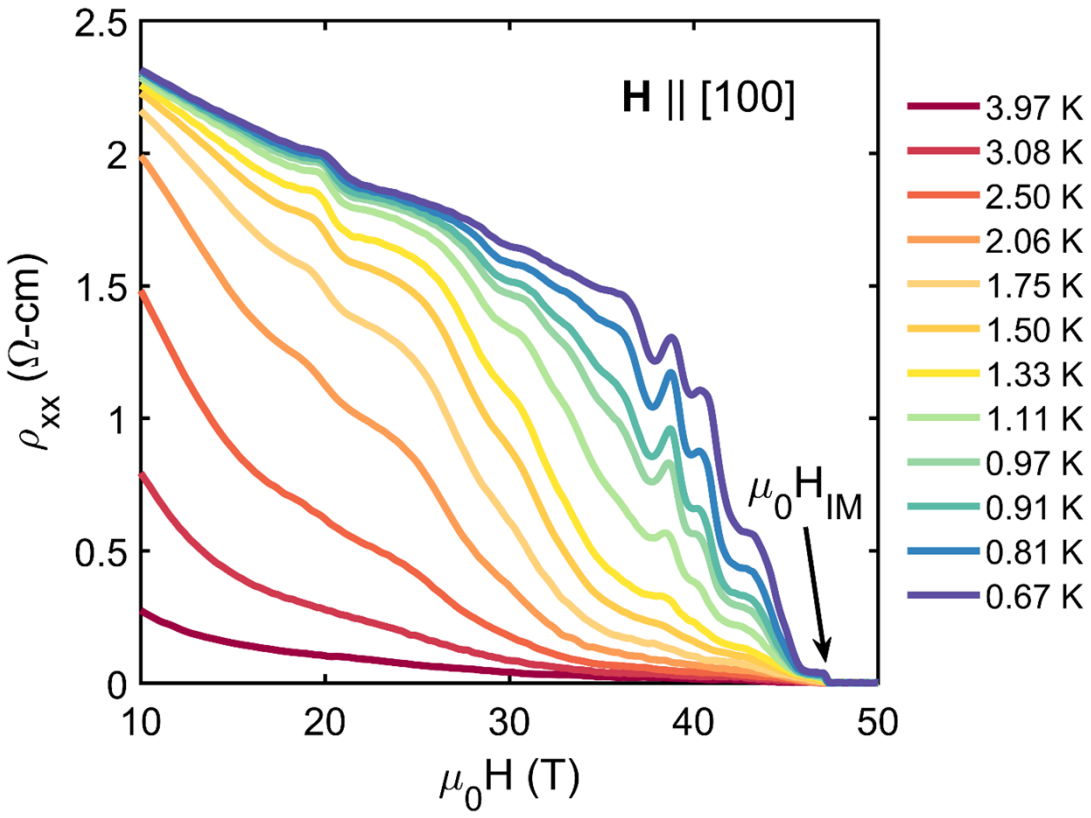


Fig 1. Quantum oscillations in the Kondo insulator YbB_{12} using high magnetic field measurements supported by the Science of 100T BES project.

We have discovered that the quantum-limit-physics expected to occur in strongly-correlated metals under high magnetic fields, can instead be realized in strongly-correlated insulators [3]. We call this phenomenon the "reverse quantum limit" because it is a direct analogue to the conventional quantum limit occurring in metals, with the important distinction that magnetic fields cause electronic states in insulators to move in a manner that is opposite to electronic states in metals. This suggests that strongly-correlated insulators are the foremost platform to explore the rich array of unconventional electronic phases expected to arise in the (reverse) quantum limit.

Beyond developing the concept of the reverse quantum limit, we show it explains many extraordinary observations in the strongly-correlated insulator YbB_{12}. In particular, our reverse quantum limit proposal suggests that the recent paradoxical observation of quantum oscillations in the insulating state of YbB_{12} (see Fig. 1), an observation which seems to challenge the most basic notions differentiating metals from insulators and represents one of the outstanding puzzles in condensed-matter physics, are possibly manifestations of electronic instabilities associated with the quantum limit.

This specific work utilized ultrahigh quality single crystals of the Kondo insulator YbB_{12} grown at Johns Hopkins University using the synthesis capabilities of the Platform for the Accelerated

Realization, Analysis, and Discovery of Interface Materials (PARADIM). The crystal structure of the material, as well as its physical properties, were characterized at Los Alamos National Laboratory.

Central to this work were the unique pulsed magnet capabilities at the National High Magnetic Field Laboratory's Pulsed Field Facility located within Los Alamos National Laboratory. High field data for this paper utilized two magnet systems: the 65T short-pulse magnet and 75T duplex magnet.

Future Plans

As Fig. 2 illustrates, the reverse quantum limit scenario occurs in insulators when the product of the effective mass enhancement and the effective *g*-factor is greater than 2. This also sets the conditions for an insulator-to-metal transition occurring in a Kondo insulator under a magnetic field. The large value of the effective mass in this scenario means that the electronic correlations are much stronger than in conventional quantum limit scenarios, which increases the likelihood of an instability to a broken symmetry phase, such as an excitonic insulator [1]. One of the aims of ongoing experiments will be to look for evidence for a transition into such a phase close to the boundary of the magnetic field-induced insulator-to-metal transition. Another implication of the above inequality is that the anisotropy of the insulator-to-metal transition is determined primarily by that of the *g*-factor and also that of the effective mass on the Fermi surface. This means that pockets of Fermi surface situated at lower symmetry positions on the Fermi surface can have different critical fields depending on the relative orientations with respect to the magnetic field, providing a novel opportunity to map out the Fermi surface geometry.

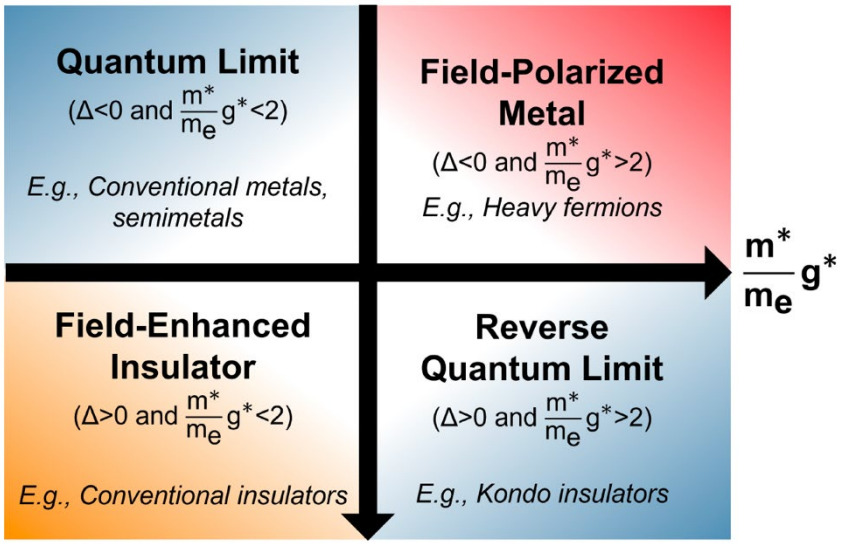


Fig. 2. Schematic of the conditions under which the quantum limit is realized in orbitally quantized system. The conventional quantum limit corresponds to the upper left-hand quadrant. The reverse quantum limit corresponds to the lower right-hand quadrant. Other scenarios include a magnetic field-polarized metal, or a magnetic field-enhanced insulator.

The finding that the reverse quantum limit scenario occurs in insulators when the product of the effective mass enhancement and the effective *g*-factor is greater than 2 implies that similar physics could potentially occur in other types of insulator, including topological insulators if the effective *g*-factor is strongly

renormalized by, for example, spin-orbit interactions. This is potentially the case in $ZrTe_5$ [4] and related systems. We are planning further experiments to determine whether this could be responsible for the apparent log *B* behavior of the reported quantum oscillations in this system [5].

References

[1] D. Jérome, T. M. Rice, and W. Kohn, *Excitonic Insulator*, Phys. Rev. B **158**, 462 (1967).

[2] B. Schwarzschild, *Physics Nobel Prize Goes to Tsui, Stormer and Laughlin for the Fractional Quantum Hall Effect*, Physics Today **51**, 17 (1998).

[3] C. A. Mizzi, S. K. Kushwaha, P. F. S. Rosa, W. A. Phelan, D. C. Arellano, L. A. Pressley, T. M. McQueen, M. K. Chan and N. Harrison, *The reverse quantum limit and its implications for unconventional quantum oscillations in YbB_{12}*, Nature Communications **15**, 1607 (2024).

[4] D. Xing, B. Tong, S. Pan, Z. Wang, J. Luo, J. Zhang & C.-L. Zhang, *Rashba-splitting-induced topological flat band detected by anomalous resistance oscillations beyond the quantum limit in $ZrTe_5$*, Nature Commun. **15**, 4407 (2024).

[5] H. Wang, H. Liu, Y. Li, Y. Liu, J. Wang, J. Liu, J.-Y. Dai, Y. Wang, L. Li, J. Yan, D. Mandrus, X. C. Xie and J. Wang, *Discovery of log-periodic oscillations in ultraquantum topological materials*, Science Advances **4**, DOI: 10.1126/sciadv.aau5096 (2018).

Publications

A. Shekhter, R. D. Mcdonald, B. J. Ramshaw and K. A. Modic, *Magnetotropic susceptibility*, Phys. Rev. B **108**, 035111 (JUL 2023).

M. O. Ajeesh, S. K. Kushwaha, S. M. Thomas, J. D. Thompson, M. K. Chan, N. Harrison, J. M. Tomczak and P. F. S. Rosa "Localized f-electron magnetism in the semimetal $Ce_3Bi_4Au_3$.", Phys. Rev. B **108**, 245125 (DEC 2023).

R. Schönemann, P. F. S. Rosa, S. M. Thomas, Y. Lai, D. N. Nguyen , J. Singleton, E. L. Brosha, R. D. McDonald, V. Zapf, B. Maiorov and M. Jaime, *Sudden adiabaticity signals reentrant bulk superconductivity in UTe_2*, PNAS Nexus 3, doi.org/10.1093/pnasnexus/pgad428 (DEC 2023).

J. Choi, J. Li, D. Van Tuan , H. Dery and S. A. Crooker, *Emergence of composite many-body exciton states in WS_2 and $MoSe_2$ monolayers*, Phys. Rev. B **109**, L041304 (JAN 2024).

C. A. Mizzi, S. K. Kushwaha, P. F. S. Rosa, W. A. Phelan, D. C. Arellano, L.A. Pressley, T. M. McQueen, M. K. Chan and Neil Harrison, *The reverse quantum limit and its implications for unconventional quantum oscillations in YbB_{12}*, Nature Commun. **15**, 1607 (FEB 2024).

N. Harrison, G. L. Chappell and P. H. Tobash, *Indications of flat bands driving the δ to a volume collapse of plutonium*, Proc. Natl. Acad. Sci. USA **121**, e2308729121 (FEB 2024).

C. E. Frank, S. K. Lewin, G. S. Salas, P. Czajka, I. M. Hayes, H. Yoon, T. Metz, J. Paglione, J. Singleton and N. P. Butch, *Orphan high field superconductivity in non-superconducting uranium ditelluride*, Nature Commun. **15**, 3378 (APR 2024).

K. Rubi, D. R. Candido, M. Dumen, S. Zeng, E. L.Q.N. Ammerlaan, F. Bangma, M. K. Chan, M. Goiran, A. Ariando, S. Chakraverty, W. Escoffier, U. Zeitler and N. Harrison, *Unconventional quantum oscillations and evidence of*

nonparabolic electronic states in quasi-two-dimensional electron system at complex oxide interfaces, Phys. Rev. Research **6**, 043231 (DEC 2024).

G. Zheng, Y. Zhu, K.-W. Chen, B. Kang, D. Zhang, K. Jenkins, A. Chan, Z. Zeng, A. Xu, O. A. Valenzuela, J. Blawat, J. Singleton, S. Li, P. A. Lee and L. Li, *Unconventional magnetic oscillations in a kagome Mott insulator*, Proc. Natl. Acad. Sci. USA **122**, e2421390122 (JAN 2025).

J. Wang, D. G. Rickel, C. F. C. Chang, Z. Zhang, P. Peng, Y. Huang, A. K. Azad, D. Jena, H. G. Xing and S. A. Crooker, *THz cyclotron resonance of a 2D hole gas in a GaN/AlN heterostructure.* Appl. Phys. Lett. **126**, 213102 (MAY 2025).

Prediction, Design, and Synthesis of New Magnetic Nitrides

Sage Bauers | National Renewable Energy Laboratory

Keywords: ferromagnets, polycrystalline materials, materials discovery, metastability

Research Scope: Magnetic Materials Discovery

This program seeks to discover new magnetic materials toward lanthanide-free permanent magnet applications. Inspired by examples of sub-nitrides with high magnetic performance, we elected to focus on similar chemical spaces. The underlying hypothesis is that nitrogen's intermediate electronegativity enables strong magnetic exchange and structural distortions that enhance magnetocrystalline anisotropy energy without driving metals into highly oxidized states. Over the period of this program, we have integrated high-throughput prediction, computationally guided synthesis, and advanced characterization to identify and realize several new magnetic nitrides.

Recent Progress

Materials discovery efforts often begin with prediction of candidate phases using ionic substitution-based strategies (the underlying assumption being two metals with the same preferred oxidation state are likely to substitute).[1,2] Such approaches often fail for intermetallic or anion-lean systems where oxidation states are ambiguous. To map the stability of *metal-rich* ternary nitrides, we instead developed and employed a new strategy where substitutions are performed based on the *number of shared structural prototypes* between metals. This approach generated 1800 new candidate nitrides, and follow-on thermochemical calculations revealed many of the candidate structures to be stable. In total, 70 new ternary chemical systems with no previously known nitride phases were identified. Of these new predictions, 49 contain two non-alkaline metals plus nitrogen, making many of them promising candidates for magnetic behavior. **Fig 1** shows some of the predicted materials containing ferrous 3d elements, where each colored swatch represents a unique ternary chemical space and swatches with a border are spaces where stable nitrides are predicted but none are currently known.

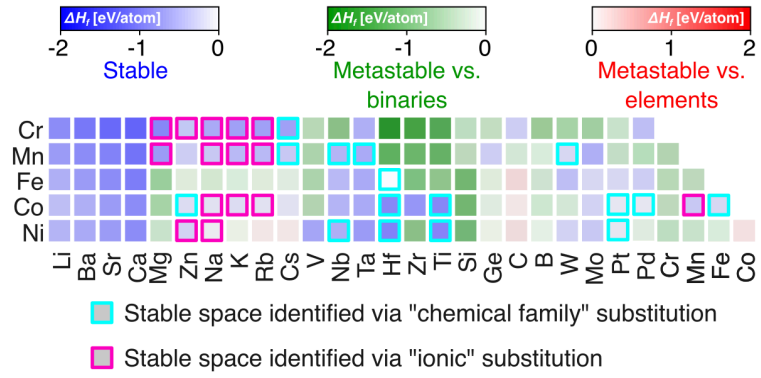


Fig 1: Snippet of a larger map of calculated ternary nitride stability. Chemical spaces with a cyan border were identified using our beyond-ionic substitution "chemical family" algorithm and are less likely to be anion rich than spaces identified using ionic substitution (magenta).

The row of Co-containing nitrides contains 5 compounds predicted to be stable using our updated prediction algorithm. From left to right these are: Co_3ZnN, Hf_4Co_2N, Ti_4Co_2N, Co_3PtN, Co_3PdN, and $CoFeN_2$. Previous ionic substitution efforts also identified new compositions, including $MnCoN_2$.[1] To demonstrate the efficacy of these predictions, several of the predicted nitrides were synthesized in the lab.

Antiperovskite Co_3PdN

Although Co_3PdN has been repeatedly flagged by computation[3,4]—including our novel beyond ionic algorithm—its synthesis and stability had never been experimentally verified. Using reactive sputtering, we achieved the first experimental realization of Co_3PdN[5] (**Fig 2a**), verifying its antiperovskite crystal structure through both laboratory and synchrotron x-ray scattering. Importantly, we established the compound's thermal stability to 600 K (persisting even to ~700 K under inert atmosphere), showing its practical viability in the use environment.

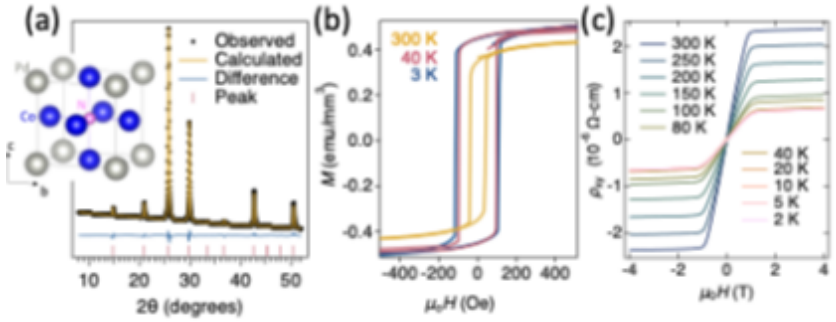


Fig 2: Characterization of Co_3PdN. (a) X-ray diffraction confirming antiperovskite structure. (b) Magnetic hysteresis loops from this ferromagnetic material. (c) Hall resistivity showing saturation of the anomalous signal.

Magnetometry demonstrated that Co_3PdN is a soft ferromagnet (**Fig 2b**) with a Curie temperature of $\mathbf{T_c = 560 \pm 5\ K}$, well above room temperature and squarely within the range needed for applications. The measured saturation magnetization (1.2 μ_B/Co) is close to—but slightly below—the theoretical expectation (1.7 μ_B/Co), reflecting subtle electronic effects. A narrow hysteresis loop with a coercive field of 100 Oe at low temperature highlights potential for **fast magnetic switching**, relevant to electronic and spintronic applications. A clear anomalous Hall effect (**Fig 2c**) further confirms Co_3PdN's ferromagnetism.

We also resolved conflicting reports on its electronic structure. Prior predictions suggested a gapped state, but we demonstrated that this arose from incomplete Brillouin-zone sampling. Our calculations and transport measurements confirm **metallic behavior with a sizable anomalous Hall effect**, reinforcing Co_3PdN as both a scientifically and technologically intriguing magnetic nitride.

Together, these results establish Co_3PdN as a **benchmark for predictive nitride discovery**, demonstrating the transition from theory to experiment while opening the door to a broader family of unexplored antiperovskites. A similar suite of experiments on other predicted antiperovskites, Co_3ZnN and Co_3PtN, including through epitaxial stabilization, showed that Co_3ZnN can be synthesized using very similar methods to Co_3PdN, but Co_3PtN cannot; an ongoing scientific question is why this is the case.

Disordered Rocksalt $MnCoN_2$

$MnCoN_2$ represents one of the few ternary nitrides composed exclusively of transition metals that were predicted by ionic substitution, making it a compelling discovery target. Although originally proposed in a zincblende-derived structure with tetrahedral coordination,[1] our follow-on calculations revealed a more stable rocksalt-derived polymorph with octahedral coordination (**Fig 3a, 3b**). We realized this phase experimentally as thin films synthesized by reactive sputtering within a narrow growth window just above ambient temperature, demonstrating that careful kinetic control can stabilize $MnCoN_2$ over competing binaries and amorphous products.[6]

Laboratory and synchrotron diffraction confirm that $MnCoN_2$ adopts a cation-disordered rocksalt structure (**Fig 3c**). X-ray absorption spectroscopy further verifies octahedral coordination of Mn^{3+} and Co^{3+}. Importantly, $MnCoN_2$ cannot be described as a simple mixture of binary nitrides but instead represents a genuinely new ternary phase space.

Magnetometry (**Fig 3d**) reveals a canted antiferromagnetic ground state below ~10 K, with a Weiss temperature of –50 K indicating strong AFM correlations. This contrasts sharply with the high-T_N antiferromagnetism of MnN and the paramagnetism of CoN, clear evidence that the ternary chemistry drives emergent magnetic behavior not present in the binaries. At the last ECMP program meeting we showed with Monte Carlo + DFT calculations that similar behavior in $MnSnN_2$ arises from cation disorder.[7] A small net moment and coercivity at 2 K suggest weak canting or ferrimagnetic clusters within the disordered rocksalt lattice.

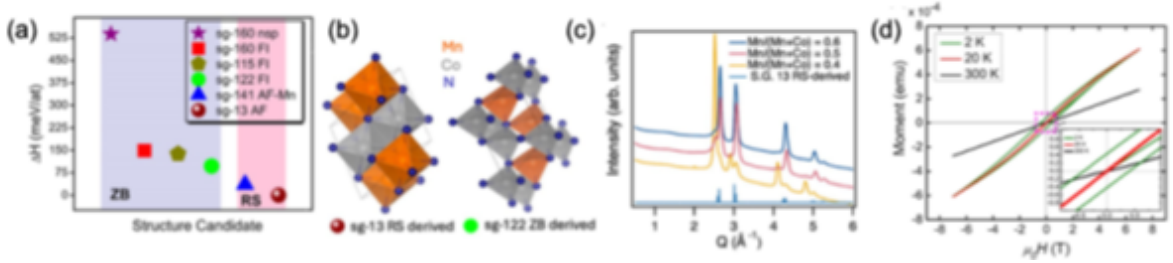


Fig 3: Discovery of $MnCoN_2$. (a) Calculated formation enthalpy of $MnCoN_2$ in various space groups and magnetic configurations. (b) Lowest-energy zincblende- and rocksalt-derived structures. (c) X-ray diffraction providing experimental confirmation of rocksalt $MnCoN_2$. (d) Small hysteresis at low temperature suggests canted antiferromagnetic order.

Altogether, $MnCoN_2$ expands the library of known ternary nitrides and establishes a blueprint for discovering other transition-metal–only compounds that may have structures that appear very similar to binary parent compounds when using global structure probes. It highlights how cation disorder, metastability, and multi-metal chemistries can combine to produce exotic magnetic ground states, offering fertile ground for both predictive design and future synthesis efforts.

η-nitride Hf_4Co_2N

An unexpected materials family identified by our substitution algorithm was compounds in the Fe_3W_3C prototype (space group 227), often associated with η-carbide superalloys. New Mn, Ni, Fe, and Co compositions were identified in subsets of this structure. To test the predictions, we elected to prepare Hf_4Co_2N, guiding our approach by also preparing Fe_4W_2N, which is known.

We found that direct growth of either phase was not possible because the requisite nitrogen chemical potential μ(N) is lower than can be supplied by a synthesis tool and an fcc phase forms at elevated deposition temperatures. However, we found that Fe_4W_2N can be prepared by post-annealing amorphous Fe-W-N thin films in a low μ(N) environment. Because of the very low μ(N) required for Hf_4Co_2N and strong competition from HfN (**Fig 4a**), even this approach was found intractable for Hf_4Co_2N. Instead, we designed a synthetic route consisting of depositing intermetallic Hf_2Co thin films, which have a very similar structure to Hf_4Co_2N, and then post-annealing in nitrogen-containing environments. This approach readily yields Hf_4Co_2N over HfN (**Fig 4b**), surprisingly even when μ(N) is high (NH_3 environment at 500 °C). We hypothesize that kinetic barriers to restructuring the Hf_2Co intermetallic lattice prevent conversion, enabling the stabilization of Hf_4Co_2N even at high μ(N).

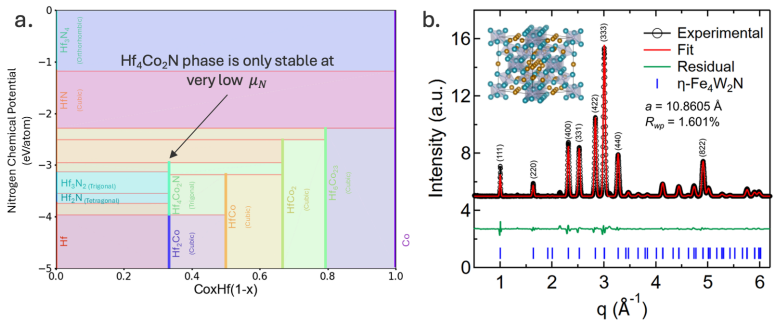


Fig 4: Synthesis of "η-nitride" Hf_4Co_2N. (a) Calculated phase diagram in mixed nitrogen chemical potential (y) and metal composition (x) axes, which was used to guide synthesis. (b) XRD of Hf_4Co_2N synthesized from Hf_4Co_2 intermetallic and nitrided in NH_3.

Future Plans

While we have demonstrated effective rational *discovery* of new magnetic compounds, there are currently no prescriptive *design* principles to navigate the structure-chemistry-bonding-property relationships of ferromagnets. For this reason, we lack a conceptual framework on how to navigate the bewilderingly high-dimensional "crystal chemistry" space for permanent magnet design.

However, we are now positioned to remedy this. Through our ECMP funding, we unveiled innovative new computational tools to extract real space bonding-magnetism relationships directly from spin-polarized electronic structure calculations,[8] and we have also refined our ability to selectively synthesize metastable magnetic sub-nitride powders[9] and thin films[5] with targeted structures and compositions. From this platform, our next stage will be to establish the first quantitative set of design principles to connect magnetic moment and magnetocrystalline anisotropy energies to the underlying bonding, structure, and stability of inorganic solids.

References

(1) Sun, W.; Bartel, C. J.; Arca, E.; Bauers, S. R.; Matthews, B.; Orvañanos, B.; Chen, B. R.; Toney, M. F.; Schelhas, L. T.; et al. *Nat. Mater. 2019 187* **2019**, *18* (7), 732–739.
(2) Hautier, G.; Fischer, C.; Ehrlacher, V.; Jain, A.; Ceder, G. *Inorg. Chem.* **2011**, *50* (2), 656–663.
(3) Singh, H. K.; Zhang, Z.; Opahle, I.; Ohmer, D.; Yao, Y.; Zhang, H. *Chem. Mater.* **2018**, *30* (20), 6983–6991.
(4) Ahmad Khandy, S.; Islam, I.; Kaur, K.; Laref, A.; Dhiman, S.; Rubab, S.; Gupta, D. C.; Khenata, R. *Results Phys.* **2020**, *17*, 103112.
(5) Dugu, S.; Mahatara, S.; Regier, C. E.; Leahy, I. A.; Zakutayev, A.; Neilson, J. R.; Lany, S.; Bauers, S. R. *Chem. Mater.* **2025**, *37* (5), 1906–1913.
(6) Dugu, S.; Smaha, R. W.; Quadir, S.; Treglia, A.; Martin, J.; O'Donnell, S.; Mahatara, S.; Teeter, G.; Lany, S.; Neilson, J. R.; Bauers, S. R. *Phys. Rev. Mater.* **2024**, *8* (10), 104411.
(7) Rom, C. L.; Smaha, R. W.; Melamed, C. L.; Schnepf, R. R.; Heinselman, K. N.; Mangum, J. S.; Lee, S.-J.; Lany, S.; Schelhas, L. T.; et al. *Chem. Mater.* **2023**, *35* (7), 2936–2946.
(8) Oliphant, E.; Mantena, V.; Brod, M.; Snyder, G. J.; Sun, W. *Mater. Horiz.* **2025**, *12* (9), 3073–3083.
(9) O'Donnell, S.; Mahatara, S.; Lany, S.; Bauers, S. R.; Smaha, R. W.; Neilson, J. R. *Inorg. Chem.* **2024**, *63* (34), 16075–16080.

Publication List (since last PI meeting)

Led by this FWP

(1) Oliphant, E.; Mantena, V.; Brod, M.; Snyder, G. J.; Sun, W. Why Does Silicon Have an Indirect Band Gap? *Mater. Horiz.* 2025, 12 (9), 3073–3083.

(2) Dugu, S.; Mahatara, S.; Regier, C. E.; Leahy, I. A.; Zakutayev, A.; Neilson, J. R.; Lany, S.; Bauers, S. R. Synthesis, Stability, and Magnetic Properties of Antiperovskite Co_3PdN. *Chem. Mater.* 2025, 37 (5), 1906–1913.

(3) O'Donnell, S.; Leahy, I. A.; Jana, S.; Gabilondo, E. A.; Halasyamani, P. S.; Maggard, P. A.; Smaha, R. W. Magnetic Properties and Large Second-Harmonic Generation Response of a Chiral Ternary Chalcogenide: Eu_2SiSe_4. *Chem. Mater.* 2025, 37 (14), 5036–5042.

(4) Bauers, S. R. Combinatorial investigation of the Mn-Ge-N chemical system containing ternary nitrides Mn_3GeN and $MnGeN_2$. Accepted at *MRS Commun.* for 2025 Distinguished Early Career Special Issue.

(5) Dugu, S.; Smaha, R. W.; Quadir, S.; Treglia, A.; Martin, J.; O'Donnell, S.; Mahatara, S.; Teeter, G.; Lany, S.; Neilson, J. R.; Bauers, S. R. Thin Film Synthesis, Structural Analysis, and Magnetic Properties of Novel Ternary Transition Metal Nitride $MnCoN_2$. *Phys. Rev. Mater.* 2024, 8 (10), 104411.

(6) O'Donnell, S.; Mahatara, S.; Lany, S.; Bauers, S. R.; Smaha, R. W.; Neilson, J. R. "Mn_3AlN" Is Really Mn_4N. *Inorg. Chem.* 2024, 63 (34), 16075–16080.

(7) Rom, C. L.; Smaha, R. W.; O'Donnell, S.; Dugu, S.; Bauers, S. R. Emerging Magnetic Materials for Electric Vehicle Drive Motors. *MRS Bull.* 2024, 49 (7), 738–750.

(8) Chen, J.; Powell-Palm, M. J.; Sun, W. The Geometry of High-Dimensional Phase Diagrams: III. Engineering Relative Stability in Four Dimensions. arXiv April 9, 2024.

(9) Regier, C. E.; O'Donnell, S.; Goyal, A.; Dzara, M. J.; Park, J. E.; Bell, R. T.; Kramer, M. J.; Paddison, J. A. M.; Shulda, S.; Ginley, D. S.; Yahne, D. R.; Lany, S.; Smaha, R. W.; Klein, R. A. Interlayer Ions Control Spin Canting in Low-Dimensional Manganese Trimers in 12R-$Ba_4MMn_3O_{12}$ (M = Ce, Pr) Layered Perovskites. *Inorg. Chem.* 2024, 63 (51), 24176–24186.

Acknowledging this FWP

(1) Lee, C.-W.; Smaha, R. W.; Brennecka, G. L.; Haegel, N. M.; Gorai, P.; Yazawa, K. From Prediction to Experimental Realization of Ferroelectric Wurtzite $Al_{1-x}Gd_xN$ Alloys. *APL Mater.* 2025, 13 (2), 021114.

(2) Brown, W. K.; Oyekunle, I. P.; Truong, E.; Chen, Y.; Ogbolu, B.; Schundelmier, B.; O'Donnell, S.; Smaha, R. W.; Hu, Y.-Y.; Wei, K.; McCandless, G. T.; Chan, J. Y. $Co_3Ga_2Ge_5$: Probing Site Mixing of the Ru_3Sn_7 Structure Type with Elements Difficult to Distinguish by Diffraction. *J. Alloys Compd.* 2025, 1010, 177828.

(3) Julien, B.; Leahy, I. A.; Smaha, R. W.; Mangum, J. S.; Perkins, C. L.; Bauers, S. R.; Zakutayev, A. Structural Stability, Elemental Ordering, and Transport Properties of Layered $ScTaN_2$. In revision at *Phys. Rev. Mater.* arXiv July 8, 2025.

(4) Smaha, R. W.; Mangum, J. S.; Yadav, N.; Rom, C. L.; Wieliczka, B. M.; Julien, B.; Treglia, A.; Perkins, C. L.; Gorai, P.; Bauers, S. R.; Zakutayev, A. $GdWN_3$ Is a Nitride Perovskite. *Appl. Phys. Lett.* 2024, 125 (11), 112902.

(5) Jana, S.; O'Donnell, S.; Leahy, I. A.; Koldemir, A.; Pöttgen, R.; Smaha, R. W.; Maggard, P. A. Synthesis, Crystal Structure, and Physical Properties of the Eu(II)-Based Selenide Semiconductor: $EuHfSe_3$. *J. Mater. Chem. C* 2024, 12 (31), 11769–11777.

Poster Session II

Controlled electronic coupling to graphene-based heterostructure materials: towards atomically precise two-probe STM transport

Marek Kolmer, *Ames National Laboratory, Ames, Iowa 50011*

Keywords: Scanning tunneling microscopy and spectroscopy, graphene heterostructures, edge states, transport, multi-probe STM

Research Scope

Recent scientific developments in synthesizing low-dimensional materials in hierarchical heterostructures enable the realization of emerging properties that derive from controlling their exact atomic-level architectures. Their transport characterization requires locally confined electronic states, i.e., one- or zero-dimensional edge states, to be coupled with mesoscale, multi-terminal averaging device interconnects. As these two aspects are typically performed in separate experimental setups, there exists an understanding gap between mesoscale transport information obtained from fabricated external contact leads and local, less-invasive electronic properties determined with techniques commonly based on scanning probe setups. This problem is particularly critical for atomically precise structures, where the external contact leads cannot be treated separately but are an integral part of the active nanoscale system and therefore influence its output.

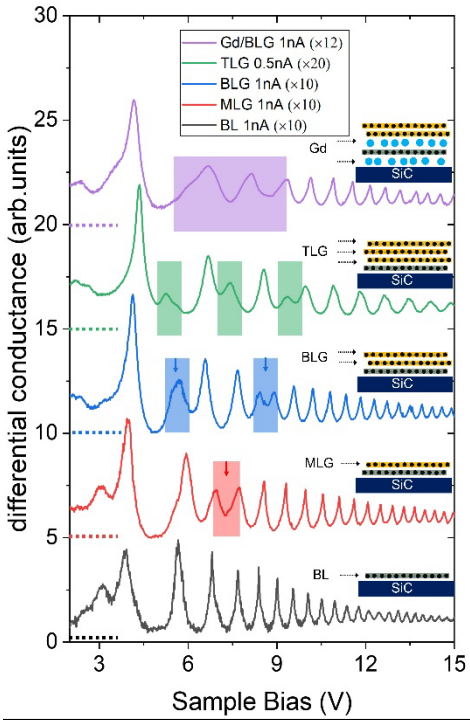


Fig.1. a) Constant-STS dI/dV data obtained at ~4.5 K for various graphene heterostructures on SiC(0001). Red, blue, and green color shaded regions reflect energy locations around the Γ point for interface resonance bands registered in the low energy electron microscopy reflectivity experiment [2] for MLG, BLG, and TLG, respectively. Dotted lines present corresponding dI/dV zero intensities. Insets present schematics of the heterostructures.

The program's overarching goal is to address this gap and propose a rational approach to understand functionality in low-dimensional graphene-based quantum materials. The program combines atomically precise on-surface synthesis strategies and in situ advanced scanning probe microscopy-based methods to reveal the origins of their mesoscale characteristics. These complementary activities are based on (1) atomically precise synthesis of graphene-based heterostructures, i.e., on substrates providing electronic decoupling, and (2) developing scanning tunneling microscopy (STM)-based techniques, including atomically precise multi-probe scanning tunneling microscopy and spectroscopy (MP-STM/S).

The primary two scientific aims of the project are: Aim I: Realizing the emergent designer magnetic and topologically non-trivial ground states in graphene-based

nanostructures, which is dedicated to experimental verification of the envisioned properties. Aim II: Establish novel, state-of-the-art techniques for non-local detection of quasiparticle excitations via their addressing with multi-probe scanning tunneling microscopy and spectroscopy operating in single-atom-contact, tunneling, or coherent field emission regimes. This approach will remove the limitations between probing of local properties and mesoscale transport characteristics in nanoscale devices by providing STM-based contacts to the low-dimensional quantum systems developed under the first aim.

Recent Progress

Addressing high-energy unoccupied interface states in graphene-based heterostructures. The low-temperature STM operating in the high-sample bias voltages reaching ~40 V was used to study the interaction between graphene interface states within the unoccupied electronic band regime and high-bias resonances formed within the triangular potential in the tip-sample gap. We developed the methodology of identifying the intrinsic electronic density of states of unoccupied bands located above the vacuum level as a function of graphene thickness and Gd intercalated phases from high-bias scanning tunneling spectroscopy (STS) experiments [1]. Due to the graphene heterostructures' two-dimensional (2D) nature, their high-bias STS spectra show pronounced features in the 5-15 eV range above the Fermi level, which strongly depend on the interlayer couplings within the heterostructure [2].

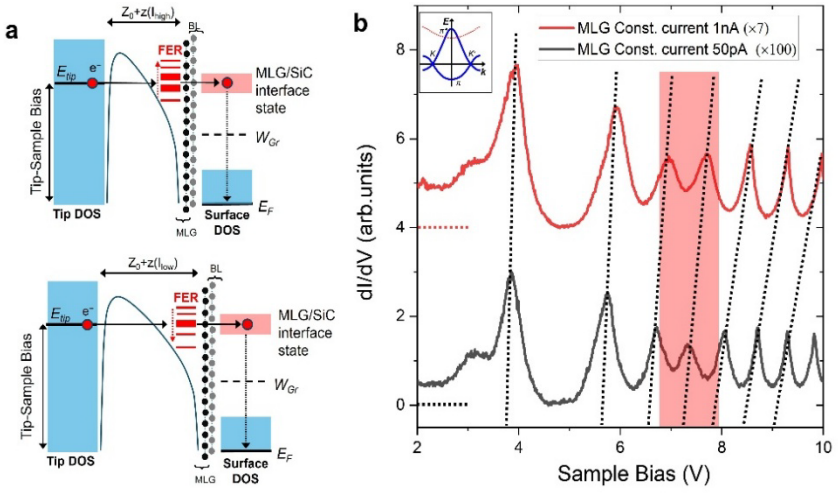


Fig.2. **a**) Schematics presenting tip-sample distance (z) control of coupling between FER and interface states. **b**) Constant-current STS dI/dV data obtained for two effective tip-sample distances demonstrating the concept. Once the energy of FERs and the interface state match, the dI/dV resonance broadens and its intensity drops. Inset: schematic presentation of the high-energy interface state parabolic band (red) on top of MLG band structure (blue). Vertical dotted lines mark the corresponding FER resonances.

We studied systematically how the 2D interface structure and related electronic states interact with the field emission resonances (FER). The systems studied involve buffer layer (BL), monolayer (MLG), bilayer (BLG), and trilayer (TLG) graphene prepared on silicon carbide SiC(0001) surface, as well as intercalated phases of gadolinium under graphene (Fig.1). With increasing tunneling current for the same tip-sample voltage, the potential well becomes progressively steeper and narrower, and the confined energy levels of the resonances shift (Fig.2). The alignment between the resonance's energy and the intrinsic interface electronic states is a unique way to map the unoccupied bands in the different types of heterostructures and selectively study specific

interface states. The work opens possibilities to access transport properties of high-energy electronic states in a MP-STM configuration as in ref. [3].

Controlling electronic properties of buried graphene-SiC interface. In the previous work [4], we showed that the covalent bonds between the first epitaxial graphene buffer layer (C_{buffer}) and the silicon carbide substrate may be reversibly broken and restored using the polarity of the electric field from the STM tip, generating protrusions at the interface of slightly higher amplitude. This buried interface manipulation allowed us to pattern the epitaxial graphene with lateral precision, reaching the dimension of a single 1.8 nm unit cell of the graphene-SiC interface moiré lattice. We propose to apply this local patterning of the epitaxial graphene heterostructures from the bottom interface for synthesizing metastable interface configurations, which affect the pristine or intercalated epitaxial graphene layer(s). The decoupled interface could be locally arranged in ordered superstructures of nanoprotrusions, creating a new 2D phase with a long-range periodic potential for the Dirac electrons, as currently done in the artificially arranged atomic or molecular adsorbates.

Now, we have extended these measurements by using low-temperature STM/S. We discovered direct evidence of silicon vacancies at the interface and provided their distribution at the topmost reconstructed SiC(0001) layer [5]. Bias-voltage and epitaxial graphene thickness dependent characterization of the collective C_{buffer}-SiC interface showed that 'Si' vacancy sites beneath C_{buffer} provide stable, non-switching behavior of the nanoprotrusions under STM electric fields. Moreover, the vacancies introduce localized electronic states below the Fermi level, thereby enhancing the n-type charge-transfer doping phenomenon across the interface. Our experimental results directly elucidate the atomic-scale interface, atomic and bonding configuration influence on the local density of states for different thicknesses of graphene on SiC(0001).

Future Plans

Electronic transport properties of bilayer graphene edge states determined by multiprobe scanning probe spectroscopy. Under symmetry-breaking conditions, the bilayer configuration of graphene (BLG) is expected to host chiral edge states within its Dirac bands' hybridization gap. However, creating such edge states is challenging. One strategy is to use a differing lattice stacking from regular AB Bernal stacked graphene bilayer to a BA stacking that produces an AA stacked domain wall, which is expected to host a topologically protected 1D electronic (edge) state in the gapped BLG electronic structure. Based on our initial measurements on a model system of epitaxial BLG on SiC(0001) and the observed formation of electronically different behavior of BLG domain walls, we plan to use this BLG-based system to directly probe the relation between the local signatures of the edge state, i.e., energy-dependent local density of states from the STM/S experiment, and its transport properties determined in the two-probe STM configuration. Part of the work will be performed as a user proposal at the Center for Nanophase Materials Sciences (Oak Ridge National Laboratory).

Novel electronic phases in rare-earth-graphene heterostructures. We plan to study metastable phases of rare-earth (Gd, Dy) intercalated epitaxial graphene on SiC(0001), which, in contrast to our previous works [6-8], are obtained at lower temperatures and for lower coverages of initial rare-earth metal deposition. This kinetically controlled processing stabilizes the rare earth elements in-between the graphene layers. Due to similar chemical activity given by the valence sp orbitals that controls their sub-surface bonding, we observe the same structural phases for both Gd and Dy after intercalation. However, the difference in their non-valence 4f electron configuration is expected to vary the magnetic anisotropy in their confined 2D phases significantly. Low-temperature STM/S will test this hypothesis, and if confirmed, further experiments will continue in the magnetic field STM facilities available at the DOE User Centers.

References

1. M. Kolmer, U. Thupakula, S. Chen, M. Mootz, H. Jeon, W. Ko, A.-P. Li., and M. C. Tringides, *Electronic coupling of field-emission resonances to high-energy unoccupied electronic bands in graphene-SiC heterostructures*, in preparation (2025)
2. J. Jobst, J. Kautz, D. Geelen, R. M. Tromp, and S. J. van der Molen, *Nanoscale measurements of unoccupied band dispersion in few-layer graphene*, Nature Communications, **6**, 8926 (2015)
3. M. Kolmer et al., *Electronic transport in planar atomic-scale structures measured by two-probe scanning tunneling spectroscopy*, Nature Communications, **10**, 1573 (2019)
4. M. Kolmer, J. Hall, S. Chen, S. Roberts, Z. Fei, Y. Han, and M. C. Tringides, *Atomic-scale manipulation of buried graphene–silicon carbide interface by local electric field*, Communications Physics, **7**, 16 (2024)
5. U. Thupakula, S. Chen, Y. Han, M. C. Tringides, and M. Kolmer, *Subsurface Interface Structure Controlling Local Electronic Properties of Epitaxial Graphene on SiC(0001)*, The Journal of Physical Chemistry Letters, after revision (2025)
6. M. Kolmer et al., *Highly Asymmetric Graphene Layer Doping and Band Structure Manipulation in Rare Earth–Graphene Heterostructure by Targeted Bonding of the Intercalated Gadolinium*, The Journal of Physical Chemistry C, **126(15)**, 6863–6873 (2022)
7. M. Kolmer et al., *Breaking of inversion symmetry and interlayer electronic coupling in bilayer graphene heterostructure by structural implementation of high electric displacement fields*, The Journal of Physical Chemistry Letters, **13(49)**, 11571–11580 (2022)
8. S. Chen, Y. Han, M. Kolmer, J. Hall, M. Hupalo, J. W. Evans, and M. C. Tringides, *Targeted Dy intercalation under graphene/SiC for tuning its electronic band structure*, Physical Review B, **107**, 045408 (2023)

Publications

1. M. Kolmer, U. Thupakula, S. Chen, M. Mootz, H. Jeon, W. Ko, A.-P. Li., and M. C. Tringides, *Electronic coupling of field-emission resonances to high-energy unoccupied electronic bands in graphene-SiC heterostructures*, in preparation (2025)
2. U. Thupakula, S. Chen, Y. Han, M. C. Tringides, and M. Kolmer, *Subsurface Interface Structure Controlling Local Electronic Properties of Epitaxial Graphene on SiC(0001)*, The Journal of Physical Chemistry Letters, after revision (2025)
3. Y. Han, M. Kolmer, J. W. Evans, and L.-L. Wang, *Plumbene: A Comprehensive Review of Theoretical and Experimental Advances*, Journal of Physics: Condensed Matter, accepted (2025)

Multidimensional Optical Probes of Quantum Materials

Albert Liu (Brookhaven National Laboratory)

Keywords: Nonlinear Spectroscopy, Coupling, Disorder

Research Scope

A complex interplay of electronic, lattice, and spin properties give rise to numerous novel and functional properties in quantum materials. Yet this very complexity that gives rise to the spectacular properties of quantum materials presents a formidable challenge to understand. This Early Career program exploits recent advances in optical analogues of nuclear magnetic resonance, termed multidimensional optical spectroscopy [1], to probe the many degrees of freedom of quantum materials at their intrinsic energy scales. These multidimensional optical probes will be implemented across the electromagnetic spectrum to probe the full gamut of quantum materials of interest to the Department of Energy, ranging from three-dimensional correlated electron systems (hosting collective excitations at terahertz frequencies) to defect centers in diamond (hosting electronic transitions at optical frequencies). The goal of the program is to address two outstanding challenges in quantum materials both in- and out-of-equilibrium, namely **interacting degrees of freedom** and **disorder** (shown in Figure 1). The understanding of such physics is a vital step towards the rational design of quantum material platforms for future quantum technologies and next-generation microelectronics.

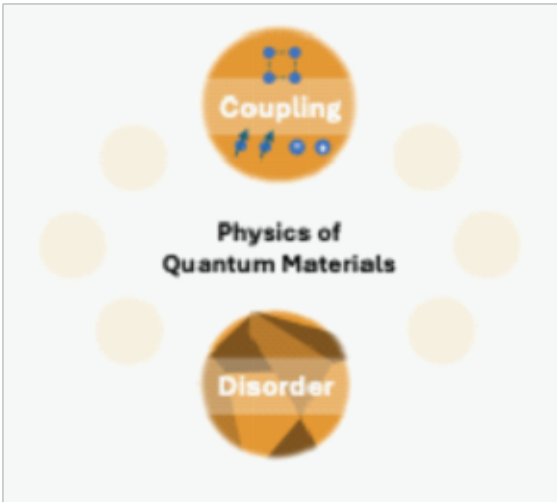


Figure 1: Among the numerous physics of quantum materials, this program focuses on the essential aspects of coupling between varied degrees of freedom and disorder.

Recent Progress

As this Early Career program has just been awarded, here we detail two recent studies that demonstrate the unique capabilities of multidimensional optical spectroscopy in resolving coupling and disorder in quantum materials.

While disorder is difficult to study using conventional spectroscopic techniques, a homogeneous and disordered optical resonance each result in a distinct multidimensional spectrum. As shown in Figure 2a, the degree of asymmetry in the two-dimensional lineshape can be used to directly infer the presence of disorder. In a recent experiment [2] we implemented

multidimensional spectroscopy at terahertz frequencies to study collective excitations in a high-temperature superconductor $La_{2-x}Sr_xCuO_4$ (LSCO). In particular, we implemented multidimensional terahertz spectroscopy (MDTS) [3] in a novel non-collinear excitation geometry (shown in Figure 2b) to probe *Josephson plasmons* in LSCO, collective excitations arising from Josephson tunneling between adjacent superconducting copper-oxygen planes. Two-dimensional spectra were acquired temperatures approaching the phase transition (shown in Figure 2c), which reveal lineshapes with different degrees of asymmetry. At temperatures well-below the transition temperature ($T = 0.15T_c$), an asymmetric lineshape is observed that reveals a disordered superconducting state. At temperatures approaching the phase transition ($T = 0.7T_c$), however, the peak broadens and becomes more symmetric, indicating that intrinsic scattering of the Josephson plasmons begins to dominate over the effects of disorder. We have since developed a complete theory for MDTS of a disordered many-body system [4], and have corroborated our optical measurements of superconducting disorder with previous local measurements of superconducting gap disorder. This confirms that MDTS is indeed a complementary method to conventional local probes of disorder and, due to its all-optical nature, may further be applied at far higher temperatures.

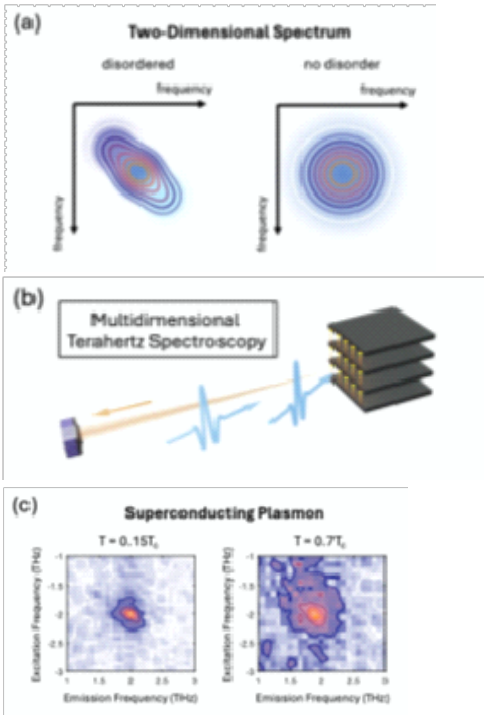


Figure 2: (a) Asymmetry in a two-dimensional spectrum indicates disorder. (b) Non-collinear MDTS probes Josephson plasmons in LSCO. (c) MDTS spectra of LSCO reveal a disordered superconducting state.

Coupling between different degrees of freedom gives rise to among the most intriguing properties of quantum materials, but often results in ambiguous signatures in conventional spectra. Multidimensional spectroscopy resolves these ambiguities, however, by correlating the frequencies of initial optical absorption and final optical emission in a two-dimensional spectrum. In a recent study [5] we applied multidimensional spectroscopy at optical frequencies to study coupling between exciton-polaritons in a semiconductor microcavity. A schematic of our device is shown in Figure 3a, which consists of distributed Bragg reflectors and a sub-wavelength grating (SWG) mirror that form the cavity. The lateral dimensions of the SWG are exceeded by the coherence length of the exciton-polaritons, which result in quantum-confined exciton-polariton wavefunctions that can be seen in their photoluminescence (Figure 3b).

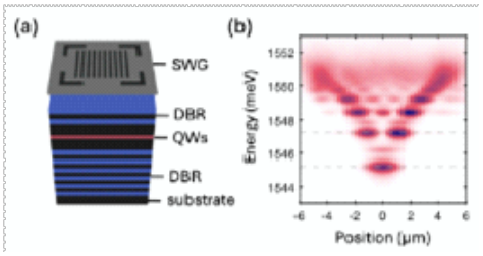


Figure 3: (a) Hybrid cavity device consisting of quantum wells (QWs) between distributed Bragg reflectors and a sub-wavelength grating (SWG) mirror. (b) Lateral dimensions of the SWG results in quantum-confined exciton-polariton wavefunctions visualized in photoluminescence.

To probe these confined exciton-polariton wavefunctions at their intrinsic length scales, we applied multidimensional optical spectroscopy (MDOS) in a collinear geometry (shown in Figure 4a), allowing us to perform these experiments near the optical diffraction limit (~1 um). We first performed experiments in which all three excitation pulses excite the same location on the sample (shown in Figure 4b). In this case, local nonlinearities are observed that correspond to absorption and emission from the same exciton-polariton state. Notably, only one of the two states was excited at once, indicating a locally-distinct nonlinear optical response. Subsequently, we performed measurements in which the different excitation pulses are displaced from each other and excite distinct spatial locations on the sample (shown in Figure 4c). In this case, the dominant features become 'off-diagonal' peaks in which absorption and emission occur from different exciton-polariton states. These spectra therefore represent a direct observation of nonlocal coupling between different confined exciton-polariton wavefunctions, in which excitation at one spatial location coherently modulates emission stimulated at a different location in space. We note that these nonlocal optical nonlinearities are distinctly quantum in nature, and differ from previous observations of nonlocal optical nonlinearities that have almost all derived from transport effects.

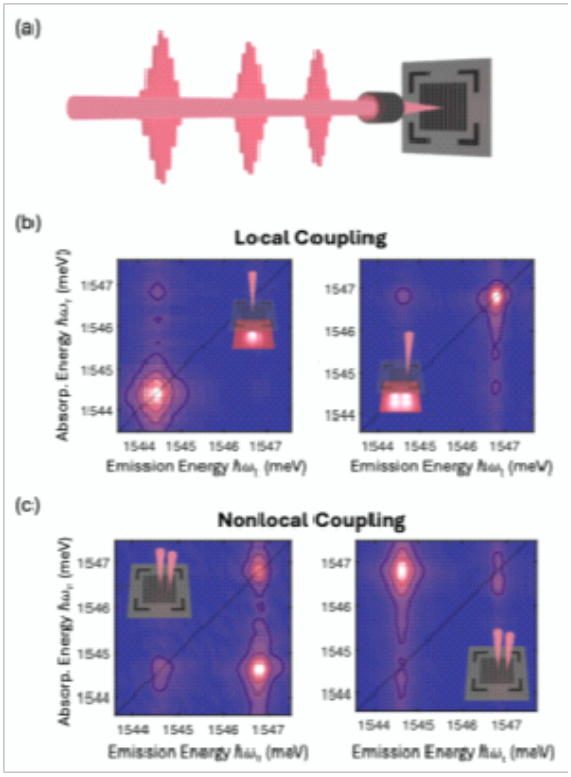


Figure 4: (a) Multidimensional optical spectroscopy in a collinear geometry. (b) When all excitation beams excite the same location on the sample, local nonlinearities are observed from the same exciton-polariton state. (c) When the excitation beams excite different locations, nonlocal nonlinearities are observed from coupling between different exciton-polariton states.

Future Plans

In the course of this Early Career program, we plan to apply MDTS and MDOS to study a variety of quantum materials in which disorder and coupling play primary roles. In particular, we will apply MDTS toward elucidating disordered quantum phases such as quantum paraelectricity and quantum spin liquidity, as well as coupling between lattice and magnetic degrees of freedom in complex oxides. We will also apply MDOS toward defect center systems in diamond and hBN toward elucidating their disorder across microscopic and macroscopic length scales as well as characterizing coupling between individual defect centers, both crucial steps toward realizing defect centers as scalable material platforms for quantum technologies.

References

1. S. T. Cundiff, S. Mukamel, *Optical Multidimensional Coherent Spectroscopy*, Phys. Today **66**, 7 (2013).

2. A. Liu et al., *Probing Inhomogeneous Cuprate Superconductivity by Terahertz Josephson Echo Spectroscopy*, Nat. Phys. **20**, 1751-1756 (2024).

3. A. Liu, *Multidimensional Terahertz Probes of Quantum Materials*, npj Quant. Mater. **10**, 18 (2025).

4. A. G. Salvador et al., *Two-Dimensional Spectroscopy of Bosonic Collective Excitations in Disordered Many-Body Systems*, arXiV:2501.16856.

5. A. Liu et al., *Nonlocal Coherent Optical Nonlinearities of a Macroscopic Quantum System*, arXiV:2504.13830.

Publications

n/a (project has not yet begun)

Light-driven proximity control of designer moiré nanomaterials

Kyle Seyler, *University of Arizona*

Keywords: moiré physics, magnetism, light-matter phenomena, 2D and layered crystals, optical spectroscopy

Research Scope

The overarching goal of this program is to develop and deploy novel ultrafast driving protocols to realize nonequilibrium electronic and magnetic phases in two-dimensional (2D) semiconductor moiré nanomaterials. Moiré nanomaterials host flat bands with a wide variety of strongly correlated states that have been heavily explored in equilibrium and are exquisitely sensitive to tuning parameters such as doping, dielectric screening, and magnetic field. We seek to demonstrate simultaneous equilibrium and nonequilibrium control over such parameters to study the dynamics of correlated states in moiré bilayer devices. In particular, we are developing strategies to modify moiré bilayers in a non-local fashion using light-induced phenomena in neighboring heterostructured 2D materials, leading to ultrafast control of carrier doping, Coulomb screening, and magnetic exchange fields.

Recent Progress

The semiconductor moiré bilayers WS_2/WSe_2 and twisted $MoTe_2$ have served as exemplary highly tunable systems for strongly correlated states including Mott insulators, frustrated magnetism, and fractional Chern insulators [1]. While most studies have been performed under equilibrium conditions, recent studies have begun to reveal interesting phenomena when these systems are driven out of equilibrium by optical excitation [2-4]. This program encompasses three distinct objectives that work towards generating ultrafast doping, ultrafast screening, and ultrafast magnetic exchange fields to dynamically control WS_2/WSe_2 and twisted $MoTe_2$ bilayer devices (Fig. 1). Recently, progress has been focused towards three ends: (1) establishing ultrafast pump-probe setups and instrument control routines; (2) fabricating and studying dual-gated WS_2/WSe_2 devices to better understand the transient magnetic properties of the light-induced ferromagnetic state; and (3) developing the ultrafast screening protocol.

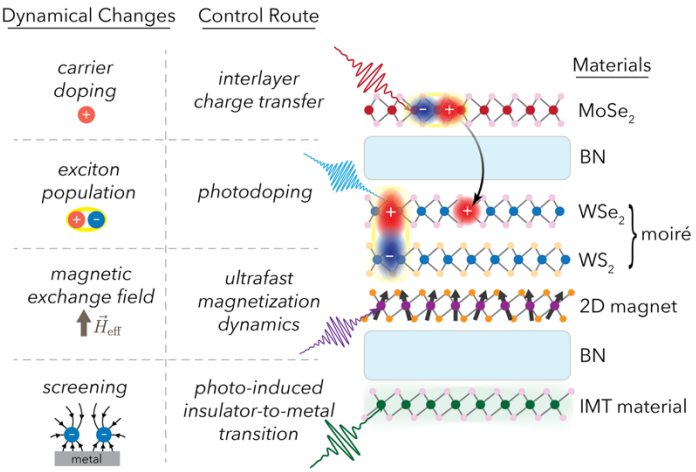


Fig. 1 | A semiconductor moiré heterostructure is modified through different ultrafast control routes. Tailored photoexcitation of proximitized 2D materials can generate unique changes in the moiré through ultrafast light-induced effects.

Systematic exploration over both the equilibrium and nonequilibrium moiré phase diagrams requires simultaneous control and scanning over a wide variety of experimental parameters including temperature, doping, electric field, magnetic field, pump intensity, pump/probe wavelengths, pump/probe polarizations, pump/probe positions, and pump-probe time delay. Developing robust data acquisition code is therefore crucial for these complex experiments. Most data acquisition code in smaller labs is custom-built for very specific experiments. Re-engineering code as project requirements evolve and new equipment is added therefore requires significant effort. To enable efficient and reproducible control in our experiments, we have adopted the Bluesky Project data acquisition and analysis framework, which provides a standardized, flexible, and extensible platform using open Python libraries that is successfully deployed in national labs [5]. We have developed an intuitive interface for benchtop Bluesky experiments and integrated all instruments into the Ophyd hardware abstraction layer, which then straightforwardly work together within Bluesky for experiment orchestration, including multi-dimensional scans over any number of instrument control variables with detailed metadata. We are currently working towards gate- and field-dependent, time-resolved magneto-optical measurements on WS_2/WSe_2 devices to study the formation, stability, melting, and switching of light-induced ferromagnetism. On a separate front, we have fabricated BN-separated 2L-$MoSe_2$/1L-WSe_2 samples for the ultrafast screening objective. We are using time-resolved excited exciton sensing spectroscopy to better understand ultrafast screening effects of the photoexcitations in bilayer $MoSe_2$ on the 2s exciton in monolayer WSe_2.

Future Plans

In the coming year, we will be focused on the first two objectives of the program, namely studying ultrafast doping in WS_2/WSe_2 heterostructures and ultrafast screening in twisted $MoTe_2$. For ultrafast photodoping, immediate goals include measuring the formation and relaxation timescale of the light-induced ferromagnetic state. We will extend these measurements using pump-push-probe measurements to pump transient ferromagnetism, perturb this transient ordered state with a push pulse, and probe the stability, melting dynamics, and possible ultrafast switching or coherent manipulation of the transient ferromagnetic state. In parallel, we will continue to develop our ultrafast screening protocol based on the ultrafast exciton Mott transition in bilayer $MoSe_2$ and $WSe_2/MoSe_2$. After calibrating the light-induced screening, we aim to integrate the screening layer into twisted $MoTe_2$ devices and systematically explore how Coulomb screening impacts the magnetic phases in both steady-state and nonequilibrium conditions, with an eye toward realizing metastable magnetic orders.

References

1. K. F. Mak and J. Shan, *Semiconductor moiré materials*, Nature Nanotechnology **17**, 686–695 (2022).
2. X. Wang et al. *Light-induced ferromagnetism in moiré superlattices*. Nature **604**, 468–473 (2022).
3. E. A. Arsenault, Y. Li, B. Yang, T. Taniguchi, K. Watanabe, J. C. Hone, C. R. Dean, X. Xu and X.-Y. Zhu. *Time-domain signatures of distinct correlated insulators in a moiré superlattice*. Nat. Commun. **16**, 549 (2025).

4. Y. Wang, J. Choe, E. Anderson, W. Li, J. Ingham, E. A. Arsenault, Y. Li, X. Hu, T. Taniguchi, K. Watanabe, X. Roy, D. Basov, D. Xiao, R. Queiroz, J. C. Hone, X. Xu and X.-Y. Zhu. *Hidden states and dynamics of fractional fillings in twisted $MoTe_2$ bilayers*. Nature **641** 1149-1155 (2025).
5. D. Allan, T. Caswell, S. Campbell, and M. Rakitin. *Bluesky's Ahead: A Multi-Facility Collaboration for an a la Carte Software Project for Data Acquisition and Management*. Synchrotron Radiation News **32**, 19–22 (2019).

Ultrafast Spin Torque Dynamics in van der Waals Magnetic Heterostructures

Yunqiu Kelly Luo, *University of Southern California*

Keywords: spin torque, van der Waals heterostructures, ultrafast dynamics, magneto-optics, spintronics

Research Scope

This project aims to visualize, understand, and control nonequilibrium spin, charge, and magnetic order in van der Waals (vdW) magnetic heterostructures with ultrafast spatial and temporal precision. Using advanced probes such as Sagnac interferometry, time-resolved Kerr rotation (TRKR) microscopy, and quantum spin-polarized low-energy electron microscopy (qSPLEEM), the program investigates the microscopic mechanisms of spin torque, magnon dynamics, and spin–charge coupling. These approaches enable femtosecond and nanometer resolution of spin transport and symmetry-breaking phenomena in engineered 2D magnets and topological interfaces.

As an extension of the original research plan, synchrotron-based scanning transmission X-ray microscopy (STXM) at the MAXYMUS beamline (BESSY II, Berlin, Germany) has been incorporated through collaboration with Ohio State and Max Planck Institute. This addition provides element-specific, real-space visualization of spin textures in epitaxial Bi_2Te_3/Fe_3GeTe_2 heterostructures, complementing in-lab optical and electron microscopy methods. By combining these complementary capabilities, the project establishes a comprehensive platform for probing spin and charge dynamics across multiple scales, with the long-term aim of developing design principles for energy-efficient spintronic devices, ultrafast magnetic memory, and scalable quantum materials platforms.

Recent Progress

During the first project year, the program successfully transitioned from laboratory build-out to early data acquisition. Key infrastructure was completed, including a helium-free cryogenic optical system with a 9–1–1 T vector magnet, a fiber-based Sagnac interferometer, and an automated glovebox-integrated exfoliation and stacking system. These tools now provide the foundation for ultrafast Kerr microscopy and high-sensitivity interferometric measurements.

Initial experiments demonstrated current-induced switching in Pt/Fe_3GeTe_2 [1], magnetic tilting in $TaIrTe_4/Fe_3GeTe_2$, and magnetization detection in $Pt/CrBr_3$, confirming the versatility of the Sagnac platform for both metallic and insulating vdW magnets. Complementary studies at

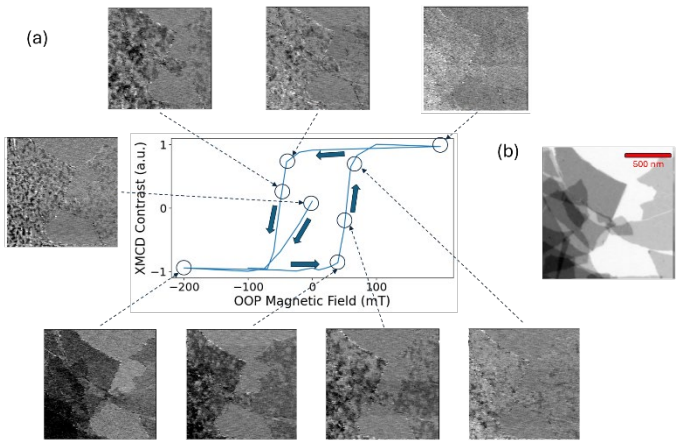


Figure 1: X-ray magnetic circular dichroism (XMCD) imaging of an MBE-grown Fe_3GeTe_2/Bi_2Te_3 heterostructure film transferred onto a SiN membrane. **(a)** Selected XMCD images acquired sequentially under varying out-of-plane magnetic fields after zero-field cooling to 165 K. Arrows and circles indicate the corresponding positions on the hysteresis loop, obtained by averaging pixel values across all XMCD images. **(b)** zero-field STXM image highlighting regions of varying film thickness.

national facilities advanced the imaging of nonequilibrium spin and charge textures. qSPLEEM measurements at LBNL captured temperature-dependent spin contrast in graphene/CrSBr and graphene/Fe_3GeTe_2. At the MAXYMUS beamline (BESSY II), synchrotron-based STXM uncovered highly fragmented "freckle-like" domain morphologies in epitaxial Bi_2Te_3/Fe_3GeTe_2 heterostructures, which were not previously reported in exfoliated Fe_3GeTe_2 systems (**Fig. 1**) [2]. These results highlight the unique ability of STXM to capture strain- and interface-driven magnetic states that remain invisible to purely optical probes.

The team also made significant progress in probing spin-filter tunneling and spin-torque-driven dynamics. As shown in **Fig. 2**, spin-filter tunneling magnetoresistance at 85 K and spin-torque antiferromagnetic resonance (ST-AFMR) spectra in $PtTe_2/CrSBr$ heterostructures demonstrate selective sensitivity to optical magnon modes while suppressing acoustic contributions. This work, carried out in collaboration with Cornell (lead) and Columbia and recently published in *Science*, establishes spin-torque-based detection as a powerful probe of dynamic order in antiferromagnets [3].

Altogether, nine interconnected projects were launched, spanning interferometric spin-torque detection, superconducting spintronics, Moiré magnetism, and micromagnetic simulations. Graduate and undergraduate researchers played central roles in these efforts, presenting their work at major conferences and preparing manuscripts. Two DOE-supported

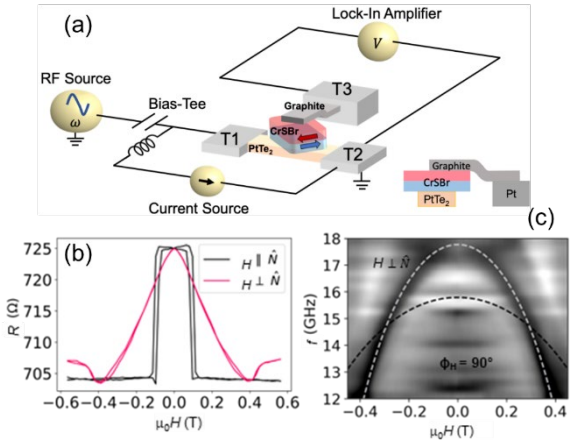


Figure 2: (a) Schematic of $PtTe_2/CrSBr$/graphite 3-terminal device and measurement configuration. **(b)** Spin-filter tunneling magnetoresistance at 85 K measured between the top and bottom contacts (T3–T2 in (a)) as a function of in-plane magnetic field H applied parallel to the CrSBr easy axis (H ∥ Ñ) and parallel to the intermediate axis (H ⊥ Ñ). **(c)** Spin-torque antiferromagnetic resonance (ST-AFMR) mixing voltage spectra for a magnetic field applied along the intermediate anisotropy axis (ϕ_H = 90°). Dashed gray line represents fit to the optical magnon field dependence based on a Landau-Lifshitz model for two antiferromagnetically-coupled sublattices.

papers are in preparation: one on fragmented domain formation in epitaxial magnet/topological insulator heterostructures [2] and another on Sagnac interferometry in Bi:YIG thin films [4]. In addition, DOE-supported publications from this period include a *Nature Materials* News & Views on anisotropic spin transport in proximitized graphene [5].

Future Plans

In the next period, the research will advance from infrastructure commissioning to time-resolved measurements of nonequilibrium spin and charge dynamics in vdW magnetic heterostructures. A key priority is the implementation of time-resolved Kerr rotation microscopy on exfoliated 2D magnets and topological insulator interfaces using the fully operational cryogenic vector-magnet optical setup and Sagnac interferometer. These experiments will provide high-sensitivity, ultrafast optical detection of dynamic spin phenomena.

Sample development will continue through glovebox-integrated, automated stacking of exfoliable epitaxial heterostructures and new air-stable 2D magnets, with designs optimized for ultrafast and variable-field experiments. This will allow correlation of static domain textures with dynamic responses under optical and electrical excitation.

Three emerging research directions will also be pursued:

1. **Spin torque in superconducting heterostructures** — extending optical probes of spin torque to vdW superconductor–magnet bilayers (e.g., $BaPb_{1-x}Bi_xO_3$) to examine dissipation, coherence, and spin-mixing conductance.

2. **Moiré magnetism and altermagnets** — applying time-resolved optical and transport probes to engineered Moiré superlattices and layered altermagnetic candidates, with emphasis on emergent chiral textures, symmetry breaking, and interlayer coupling.

3. **RF-driven spin dynamics in antiferromagnets** — developing opto-electronic probes of electrically driven antiferromagnetic resonance, combining GHz excitation with ultrafast and interferometric readout.

Parallel efforts will focus on completing and submitting manuscripts currently in preparation, including two experimental papers on Sagnac interferometry and magnetic domain formation, as well as two topical reviews on Moiré magnetism and magnon dynamics.

User-facility experiments will remain central, with scheduled or pending beamtime at LBNL (qSPLEEM), BESSY II (tr-STXM), and the NSF NeXUS facility (tr-ARPES). These campaigns will complement in-lab ultrafast optics by providing nanoscale, element-specific imaging of current-induced switching and emergent spin textures.

On the training front, the PI will continue one-on-one and group mentorship, with an emphasis on guiding student-led manuscripts, supporting graduate and fellowship applications,

and fostering leadership through proposal development and project ownership. Expanded collaborations with national labs and theory groups will support data interpretation and seed new efforts in THz magnetism, altermagnetic spintronics, and spin-based interconnects.

Together, these activities will drive progress toward the project's overarching goal: establishing the ability to resolve and control spin, charge, and magnetic order in quantum materials with ultrafast spatiotemporal precision, while training the next generation of scientists in frontier spintronics and quantum materials research.

References

1. Cham, T. M. J.; Dorrian, R.; Zhang, X.; Dismukes, A. H.; Chica, D. G.; Roy, X.; May, A. F.; Muller, D. A.; Ralph, D. C.; Luo, Y. K. *Exchange bias between van der Waals materials: tilted magnetic states and field-free spin–orbit–torque switching*. Advanced Materials **36**, 2305739 (2024).
2. Yu, X.; Khurana, B.; Jain, R.; Cham, T. M. J.; Smedley, O.; Ross, C. A.; Ralph, D. C.; Luo, Y. K. *Sagnac interferometry for high-sensitivity spin-orbit torque measurements in Bi:YIG*. In preparation.
3. T. M. J. Cham*, M. Zhao*, W. Zhou*, L. Powalla, A. Koerner, K. D. Le, E. Thareja, S. Wintz, D. Bergner, E. Youssef, Z. Li, M. Weigand, D. C. Ralph, J. Gayles, R. K. Kawakami, and Y. K. Luo*, *Highly fragmented magnetic domain formation in exfoliable epitaxial 2D magnet/topological insulator heterostructure*, in preparation.
4. Luo, Y. K. *Anisotropic spin transport in proximitized graphene*. *Nature Materials* **24**, 808–809 (2025).
5. Cham, T. M. J.; Chica, D. G.; Watanabe, K.; Taniguchi, T.; Roy, X.; Luo, Y. K.; Ralph, D. C. *Spin-filter tunneling detection of antiferromagnetic resonance with electrically tunable damping*. Science **389**, 479-482 (2025).

Publications

1. Luo, Y. K. *Anisotropic Spin Transport in Proximitized Graphene*. Nature Materials **24**, 808-809 (2025).
2. Cham, T. M. J.; Chica, D. G.; Watanabe, K.; Taniguchi, T.; Roy, X.; Luo, Y. K.; Ralph, D. C. *Spin-filter tunneling detection of antiferromagnetic resonance with electrically tunable damping*. Science **389**, 479-482 (2025).

Engineering Correlated Phases in Higher-Order Moiré Quantum Matter

Kenji Yasuda, *Cornell University*

Keywords: 2D materials, Moiré superlattice, Thin film growth, Quantum Transport, Scanning Probe Microscopy

Research Scope

Our project aims to expand the scope of moiré quantum matter by introducing higher-order moiré superlattices in van der Waals heterostructures. Moiré quantum matter formed by stacking 2D materials with a precisely controlled angle often exhibits unique electronic and optical properties. In conventional moiré systems, it is generally assumed that the two stacked layers must have nearly identical lattice constants to achieve long-period superlattices, which has constrained material choices. Our research challenges this limitation by creating a heterostructure between two 2D materials with significantly different lattice constants and different lattice symmetries while achieving higher-order commensurability through twist angle control, named higher-order moiré superlattices. This approach dramatically broadens the material palette of moiré quantum matter, enabling us to design new classes of topological flat bands.

We specifically explore two different types of higher-order moiré superlattices: $\sqrt{3}$-moiré graphene and 1D-moiré graphene. In the former, we employ an insulating 2D material with a lattice constant approximately $\sqrt{3}$ times larger than that of graphene as a substrate, such as CdI_2. By aligning the $\sqrt{3}$-substrate close to a 30° twist angle relative to monolayer graphene, the substrate and the $\sqrt{3} \times \sqrt{3}$ supercell of graphene become nearly commensurate, creating a long-period moiré superlattice, which we term $\sqrt{3}$-moiré graphene (Fig. 1a). Interestingly, theory predicts that the resulting $\sqrt{3}$-moiré graphene will exhibit flat band similar to that in magic-angle twisted bilayer graphene due to the coupling between the two Dirac points at K and K' [1]. Our project aims to establish a material system for the

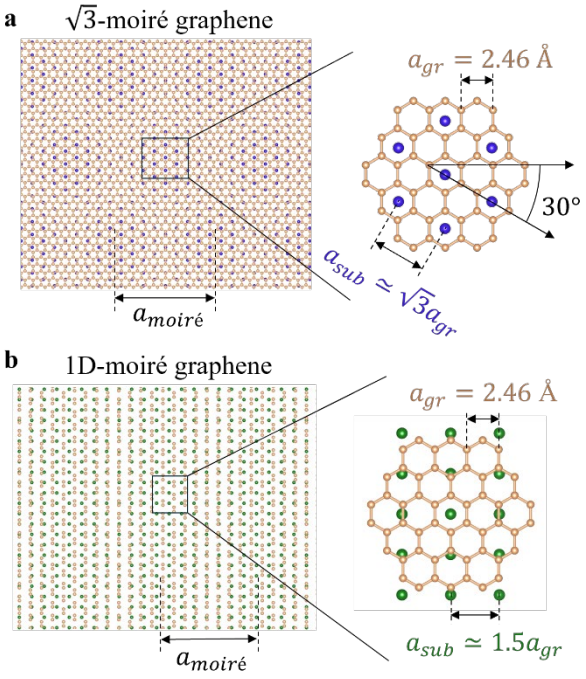


Fig. 1 **a**, Schematic of the moiré superlattice formed between graphene (orange) and a substrate (purple) with a lattice constant approximately $\sqrt{3}$ times larger than that of graphene. **b**, Schematic of the moiré superlattice formed between graphene (orange) and a rectangular lattice substrate (green) with one of the lattice constants being approximately 1.5 times larger than that of graphene.

realization of $\sqrt{3}$-moiré graphene, directly observe the band structure modulation, and explore correlated and topological phases at low temperatures through transport measurement.

In 1D-moiré graphene, we interface monolayer graphene with an insulating 2D material substrate that has a rectangular lattice, such as MoO_3. We choose the substrate so that one of its lattice constants is 1.5 times larger than that of graphene, while the other is significantly mismatched. This specific geometry results in a moiré interference pattern that is periodic along only one direction, effectively creating an array of one-dimensional electron channels (Fig. 1b). This platform allows electrons to move freely along one direction but confines them in the perpendicular direction, providing a clean and highly gate-tunable environment to study fundamental 1D physics. Our project aims to establish the unique 1D-moiré graphene and explore exotic physics, including phenomena like spin-charge separation and Tomonaga-Luttinger liquid behavior.

Recent Progress

Progress 1. Fabrication and AFM characterization of higher-order moiré superlattices

We first assembled CdI_2/graphene heterostructure using exfoliation and dry transfer method. We obtained single crystals of CdI_2 from Zdenek Sofer (University of Chemistry and Technology Prague), and then exfoliated and assembled the heterostructure inside a glovebox to prevent the degradation of CdI_2 due to moisture. We carefully aligned the flakes of CdI_2 and graphene by using Laue diffraction on the bulk crystals and exfoliating them while preserving their crystal orientations.

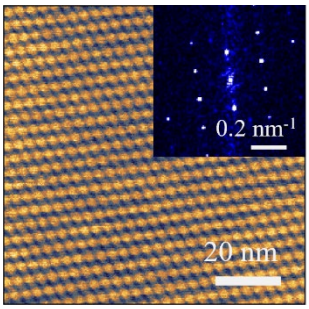


Fig. 2 Torsional force microscope image of $\sqrt{3}$-moiré graphene in CdI_2/graphene, and its Fourier transform (inset).

We then characterized the assembled heterostructure using a torsional force microscope, which is an atomic force microscopy (AFM)-based method known to be efficient for characterizing the moiré superlattices of 2D materials [2]. Figure 2 displays the torsional force microscope image of the $\sqrt{3}$-moiré superlattice of a CdI_2/graphene heterostructure taken in our lab. The image shows a moiré periodicity of around 6 nm with a clear hexagonal pattern in the Fourier transform, demonstrating the uniformity of the sample. This is the first experimental real-space imaging of a $\sqrt{3}$-moiré superlattice. This achievement lays the foundation for the future fabrication and characterization of higher-order moiré superlattices.

Progress 2. PVD growth and TEM characterization of higher-order moiré superlattices

Despite the success of assembling CdI_2/graphene through the dry transfer method, we found that the interface between them often contains a large number of bubbles originating from interlayer contamination. This is likely because of the weaker interlayer cleansing effect between CdI_2 and graphene compared to that of the graphene/graphene interface. To overcome this

challenge, we developed a method to grow monolayer CdI_2 directly on graphene using physical vapor deposition (PVD) [3]. We placed CdI_2 powders on a hotplate, positioned the substrate with exfoliated graphene upside down over them with a spacer, and grew the CdI_2 on graphene at 250 °C. This process yielded atomically flat CdI_2 on graphene (Fig. 3a).

We further collaborated with David Muller (Cornell University) to characterize the heterostructure with transmission electron microscopy (TEM). The electron diffraction pattern of the grown crystal (Fig. 3b) shows that the $CdI_2(110)$ diffraction spots coincide well with the Gr(100) spots, demonstrating that we successfully grew CdI_2 aligned with graphene. We also observed a 100 nm-scale moiré superlattice in the TEM image, originating from the slight lattice mismatch between CdI_2 and graphene and strain (Fig. 3c). Additionally, we applied this technique to grow MoO_3 on graphene [4], successfully yielding a MoO_3/graphene heterostructure via PVD (Fig. 3d). These studies establish PVD as an alternative method for creating heterostructures with pristine, contamination-free interfaces.

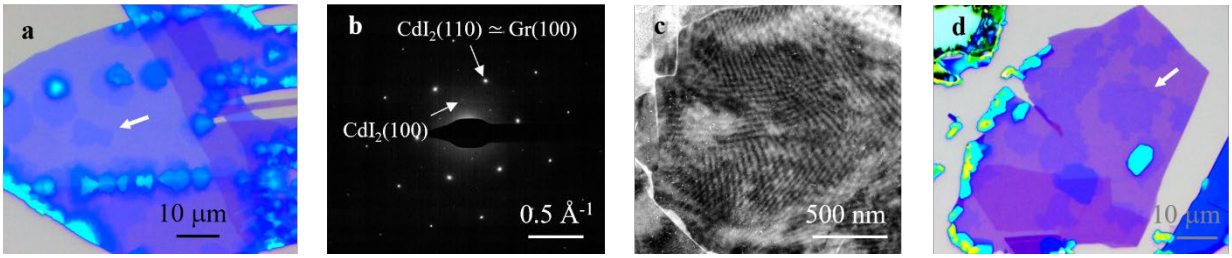


Fig. 3 **a**, Optical microscope image of PVD-grown CdI_2/graphene. The highlighted region by a white arrow corresponds to monolayer CdI_2 grown on graphene. **b**, Electron diffraction image. The overlap of $CdI_2(110)$ and graphene (100) spots demonstrates their crystallographic alignment. **c**, TEM image of CdI_2/graphene showing 100-nm-scale moiré superlattice. **d**, Optical microscope image of PVD-grown MoO_3/graphene. The highlighted region by a white arrow corresponds to monolayer MoO_3 grown on graphene.

Progress 3. Development of a quantum twisting microscope

To directly visualize the electronic band structure of our heterostructures, we built a quantum twisting microscope based on our existing AFM system. It uses a customized, blunt AFM tip coated with a layer of graphene. This tip is brought into physical contact with the sample heterostructure, which is mounted on a rotatable stage. By measuring the tunneling current between the tip and the sample while simultaneously varying the bias voltage and the twist angle, the microscope directly maps the sample's band structure in momentum space.

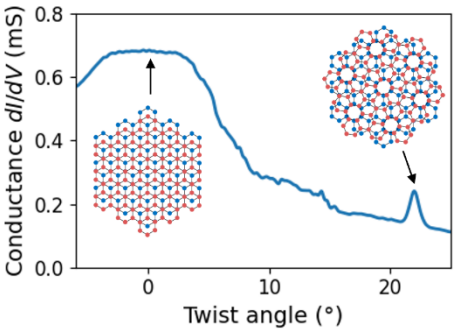


Fig. 4 Conductance between two graphite layers as a function of the twist angle as measured in quantum twisting microscope.

We have successfully demonstrated this technique by measuring the twist-angle-dependent conductance

between two layers of graphite (Fig. 4) [5]. This tool will be crucial for mapping the band structure of higher-order moiré superlattices to identify the ideal twist angles for achieving flat bands.

Future Plans

Plan 1. Measurement of higher-order moiré superlattices

Having established methods to create and characterize higher-order moiré heterostructures (CdI_2/graphene and MoO_3/graphene) via the dry transfer method and PVD, we will now investigate their electronic properties. We will fabricate dual-gated devices and perform low-temperature transport measurements using our variable temperature insert and dilution refrigerator. We will also measure the electronic band structures of these heterostructures with our quantum twisting microscope.

Plan 2. Growth of MoO_3/graphene with MBE

In collaboration with Darrell Schlom (Cornell University), we will grow MoO_3 on exfoliated graphene using the NSF-funded molecular beam epitaxy (MBE) user facility at PARADIM. We anticipate that the crystal quality of the MBE-grown MoO_3 will be much higher than that from our PVD growth, due to the ultrahigh vacuum and slow growth speed of MBE. This enhanced quality will facilitate the exploration of low-energy exotic physics.

Plan 3. Exploration of other materials

Through an extensive 2D materials database search, we have identified more than a dozen candidate materials that should exhibit higher-order moiré superlattices in combination with graphene. We will establish fabrication methods for heterostructures made from these materials to identify the best combinations for exploring exotic physics. In particular, we plan to focus on $BiSbTeSe_2$; we will obtain atomically thin flakes using the gold-assisted exfoliation method and then create heterostructures with graphene.

References

[1] V. Crépel, A. Dunbrack, D. Guerci, J. Bonini, and J. Cano, *Chiral model of twisted bilayer graphene realized in a monolayer*, Phys. Rev. B Condens. Matter **108**, 075126 (2023).

[2] M. Pendharkar, S.J. Tran, G. Zaborski Jr, J. Finney, A.L. Sharpe, R.V. Kamat, S.S. Kalantre, M. Hocking, N.J. Bittner, K. Watanabe, T. Taniguchi, B. Pittenger, C.J. Newcomb, M.A. Kastner, A.J. Mannix, and D. Goldhaber-Gordon, *Torsional force microscopy of van der Waals moirés and atomic lattices*, Proc. Natl. Acad. Sci. U. S. A. **121**, e2314083121 (2024).

[3] M. Zhao and L. Qiao, *Rapid fabrication of submillimeter ultrathin CdI_2 flakes via a facile hot plate-assisted vapor deposition method*, J. Phys.: Conf. Ser. **1907**, 012052 (2021).

[4] H. Kim, J.H. Kim, J. Kim, J. Park, K. Park, J.H. Baek, J.C. Shin, H. Lee, J. Son, S. Ryu, and Y.W. Son, *In-plane anisotropy of graphene by strong interlayer interactions with van der Waals epitaxially grown MoO_3*, Science Advances **9**, eadg6696 (2023).

[5] A. Inbar, J. Birkbeck, J. Xiao, T. Taniguchi, K. Watanabe, B. Yan, Y. Oreg, A. Stern, E. Berg, and S. Ilani, *The quantum twisting microscope*, Nature **614**, 682 (2023).

Publications

Not applicable. The funding period just started in August 2025.

Twisted oxide membrane interface by local atomic registry design

Chang-Beom Eom

University of Wisconsin-Madison

Keywords: Thin Film Synthesis, Quantum Heterostructures, Heterointerfaces, Superconductivity

Program Scope

Quantum materials such as unconventional superconductors, interfacial 2D electron gases (2DEGs), and multiferroics have been fertile ground for new discoveries. We develop novel synthesis routes to create a new generation of epitaxial quantum thin film and membrane heterostructures for study of fundamental science. These films can be of comparable or higher quality than available bulk single crystals, but more importantly film deposition conditions can be maintained far from equilibrium, so that metastable phases (nonexistent in nature) can be obtained through epitaxial stabilization. But these novel systems are sensitive to constraints of thin film heterostructures, including interaction with the substrate, the difficulty in controlling stoichiometry and point defects, and the challenge of forming atomically perfect interfaces.

Our goal is to design substrate interactions, control point defects and stoichiometry, and to fabricate atomically perfect interfaces and single crystal free standing membranes to reveal new phenomena and discover fundamental intrinsic properties of quantum materials by leveraging dimensionality, anisotropy, and electronic correlations. We have developed a unique free-standing oxide stacked membrane fabrication technique to address these challenges, which can also apply large dynamic strain through a piezoelectric layer. We control stoichiometry and point degects through a Hybrid Pulsed Laser Deposition (HPLD), and have begun to understand a route to new discoveries through control of highly perfect and defect free films and heterostructures.

The **thrusts** of the proposed new work expand into new materials systems:

Fabrication of Novel Quantum Material Platforms

Novel Hybrid PLD Synthesis Route – We continue to develop hybrid PLD, in particular for Nb doping of $KTaO_3$ (KTO). We have demonstrated that the ferroelectric quantum critical point can be controlled by Nb doping and strain, possible only with thin films. Hybrid PLD is seemingly the only approach to synthesize high-quality KTO thin film membranes.

Complex oxide membranes We are developing a registry design synthesis approach for twisted heterostructures expanding the landscape of quantum heteromaterials. This new approach assembles complex oxide and nitride membranes into twisted heterostructures.

Fundamental Science of Novel Quantum Materials Platform

$LaAlO_3/KTaO_3$ interface superconductivity – We propose to control the KTO carrier concentration with Nb doping and electrostatic gating to move the system toward the quantum critical point, enhancing superconductivity. We will also use dynamic strain of KTO membranes to understand the role of the quantum critical point in KTO superconductivity.

Strain controlled twisted oxide membranes heterostructures - building on our discovery of 2D charge configurations at $SrTiO_3$ (STO) moiré interfaces, we investigate structural, electronic, and magnetic phenomena in different types of complex oxide moiré heterostructures including 2D charge localization, structured 2D polarization-vortex crystals, and topological spin textures at twisted oxide interfaces in heterostructures assembled from freestanding membranes with a relative twist around their crystalline axes.

$Ba(Pb_xBi_{1-x})O_3$ superconducting films and membranes with strong spin-orbit coupling –We have shown that BPBO shows strong spintronic effects as well as high-temperature superconductivity.

Recent Progress

The interplay of lattice-orbital-charge in strongly correlated oxides has hosted a plethora of exotic quantum phases and physical properties. Even though stacked heterostructures of freestanding oxide twisted membranes can provide an extended pathway regarding moiré engineering with local lattice control, research on lattice-driven electronic structural modulations of twisted oxide bilayers remains unexplored. We have developed synthesis routes for epitaxial thin-film oxide freestanding membranes and their controlled-twist assembly into layered heterostructures and made atomic scale measurements of the atomically clean, high-quality interfaces necessary to establish exotic moiré phenomena[1].

$SrTiO_3$ twisted membrane heterostructures We constructed a twisted bilayer system using freestanding $SrTiO_3$ and adapt STEM and EELS as a proper toolset to investigate lattice-electron correlation at the moiré interface. We found theoretical and experimental

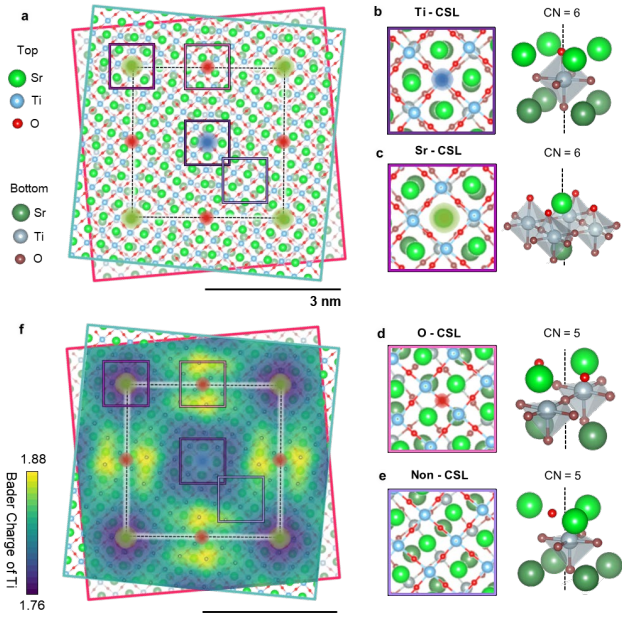


Figure 1 | Self-mediated moiré electronic lattice. a, Schematic representation of commensurate moiré lattice of 10.4° twisted STO bilayers under Σ 61 CSL boundary. The white dashed box represents a moiré supercell and CSL components are highlighted as violet (Sr), dark violet (Ti), red (O), pink (Non) color squares in **a**, **f**. **b-e**, Schematic of plan-view and interfacial atomic geometry for Sr-, Ti-, O-, and non-CSL region, respectively. **f**, Bader charge calculation corresponding to the same region.

evidence of locally and periodically reconstructed electronic structure under the coincidence site lattice (CSL) condition, as well as of directly coupled interfacial atomic geometries. The moiré charge localizations accompany the emergence of localized states, and bandwidths controlled by atomic reconstructions, determined by the twist angle relative to coincident lattice values. Our work gives a novel insight into interfacial phenomena at the twisted interface and opens pathways to discovering new moiré-electronic properties and functionalities.

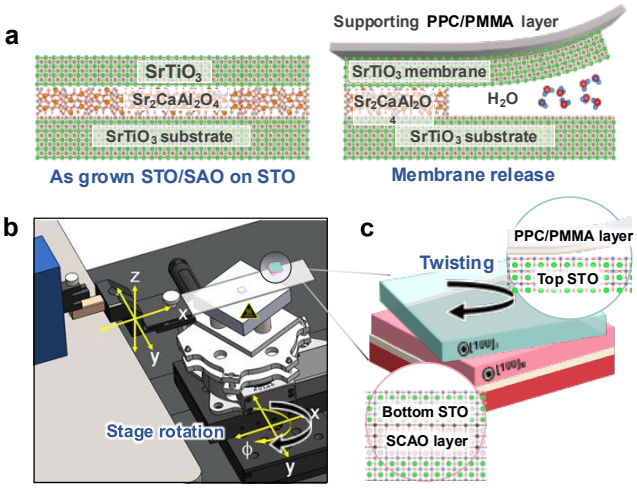


Fig. 2 (a) Fabrication of twisted moiré heterostructure of $SrTiO_3$ membranes using a water soluble $Sr_2CaAl_2O_6$. (b) Schematic of a manipulator for fabrication of twisted bilayers. (c) Schematic of a twisted $SrTiO_3$

For example, we designed a $SrTiO_3$ (STO) membrane bilayer with a twist angle of 10.4° (Σ 61) and a 3.04 nm periodic moiré supercell (Fig. 1a). The oxide bilayer has the stoichiometric interfacial geometry terminated by an SrO plane at top membrane and TiO_2 plane at the bottom membrane, respectively. The three non-equivalent atoms in STO form three unique CSLs, where Sr, Ti, and O align in columns at different commensurate points within the moiré cell, in addition to an incommensurate point (non-CSL), as shown in Fig. 1a.

At Ti-CSL points, four Sr atoms surround the Ti ion in the upper and lower layers, replicating the Ti-O octahedral structure characteristic of bulk STO at the interface (Fig. 1b). Similarly, the Ti-O polyhedral structure around Sr-CSL sites form octahedral structures where the Ti ion coordinates with six oxygen atoms (Fig. 1c). Since both types of cation-centered CSLs exhibit minimal structural differences at the interface, there is little change in Ti oxidation states. However atomic rearrangements at some local CSL structures can exceed the limits for octahedral coordination, leading to different properties. In our case, this leads to a lower coordination number (CN), changing the charge state of Ti. For instance, at the O-CSL point centered around a corner-sharing oxygen atom the oxygen atom at the interfacial Ti-O polyhedron remains 5-fold coordinated due to the absence of a structural connection with the SrO layer in the top STO (Fig. 1d). As a result, this O-CSL point exhibits a relatively low coordination number CN = 5, and the Ti-O polyhedron in non-CSL structure with atomically staggered distributions also coordinates with only five oxygen atoms (Fig. 1e).

We have the ability to create twisted (in-plane rotation) and tilted (different crystalline orientation) membrane heterostructures. The delicate balance in the couplings among structural symmetry, electronic properties, and spin configurations in modern complex materials positions

twist and tilt interactions across interfaces as a natural knob to dynamically control and design functional thin-film properties.

In addition, new properties can be strain-activated by utilizing an electrically controlled piezoelectric layer. However, the traditional growth techniques of such epitaxial thin-film heterostructures are challenged by the limited range of functional materials compatible with growth on piezoelectric layers, the in-plane strain-restricting clamping by growth substrates, and the limited accessible strain configurations in piezoelectric materials.

Our recent advances allow us to synthesize epitaxial thin film functional membranes free from substrate clamping and assemble them into piezoelectric activated membrane heterostructures, overcoming these limitations. This ability to synthesize heterostructures with incompatible structure and lattice constant, and generate new properties with designed dynamic strains provides pathways to new functionalities.

We employ a sacrificial layer method, to create membranes by releasing epitaxial films from their growth substrate (Fig. 2a). Fig. 2b shows a schematic of the instrument we have created to controllably assemble functional membranes into twisted heterostructures. One membrane is twisted with a controllable rotation, while the other is assembled into place with a micromanipulator creating a twisted heterostructure, as shown in Fig. 2c. We have demonstrated a precise twist angle control and successfully assembled twisted membranes of $SrTiO_3$, ferroelectric $BaTiO_3$, and ferromagnetic $SrRuO_3$ and $LaSrMnO_3$.

Our preliminary experimental results on twisted membrane assembled heterostructures are intriguing, showing their excellent structural quality and unexpected electronic properties.

Fig. 3 shows results of characterization for a fabricated 10.4°-twisted $SrTiO_3$ bilayer with a 5 nm thick $SrTiO_3$ membrane. Our depth sectioning-based TEM method, allowing selective imaging of depth-dependent $SrTiO_3$ atomic planes across the bilayer (Fig. 3a), clearly resolves the moiré periodic structure at the twisted interface (Fig. 3b).

The observed atomic structure is in excellent agreement with our model (Fig. 3c). Moreover, using depth-resolved electron energy loss spectroscopy (EELS), we observe a modulated e_g-t_{2g} energy peak difference in a Ti-L_3 edge spectrum indicating electronic reconstruction within the moiré cell.

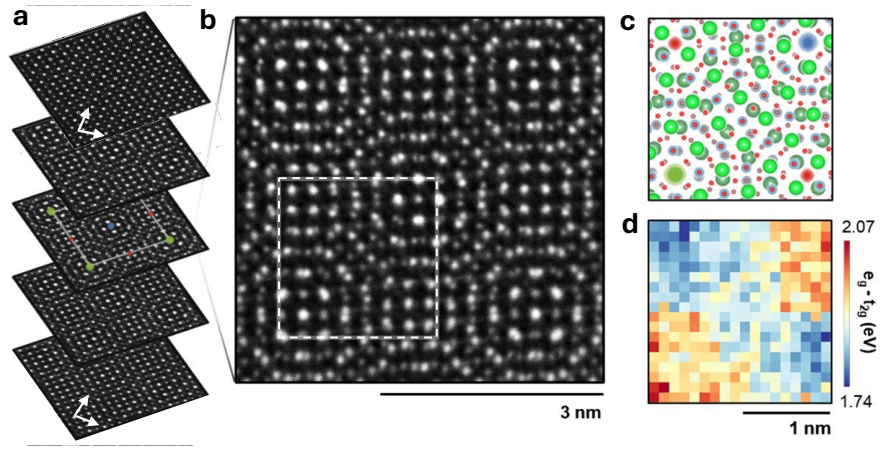


Fig. 3 (a) A focal series of HAADF-STEM images STO planes from top to bottom in a 10.4°-twisted STO bilayer. The white arrows indicate the in-plane orientations of the top and bottom STO layers. The components of moiré supercell are highlighted as green (Sr-), blue (Ti-), and red (O-) overlapped circles. (b) Atomic-scale HAADF image of moiré supercell for 10.4°-twisted STO bilayer. (c,d) Atomic structure (c) and mapping of the e_g-t_{2g} energy peak difference in a Ti-L_3 edge EEL spectrum for a region in (b) outlined by a dashed white square, reflecting valence charge modulation within the moiré supercell.

Our theoretical modeling signifies clear correlation of the EELS mapping with our calculated Bader charge, demonstrating that the electronic behavior at the twisted interface is controlled by the local atomic registry. This observation demonstrates how the strong interlayer bonding in oxide moiré heterostructures can lead to pronounced modulation of electronic properties through variations in atomic registry, potentially enabling new functionalities through enhanced coupling between structural and electronic degrees of freedom.

Future Plans

(1) Strain controlled twisted oxide membranes heterostructures,

The delicate balance in the couplings among structural symmetry, electronic properties, and spin configurations in modern complex materials positions twist and tilt interactions across interfaces as a natural knob to dynamically control and design functional thin-film properties. We plan to investigate structural, electronic, and magnetic phenomena in different types of complex oxide moiré heterostructures including 2D charge localization, structured 2D polarization-vortex crystals, topological spin textures at twisted oxide interfaces.

(2) $KTaO_3$ interface superconductivity

We plan to use Hybrid PLD for growth of electronic grade $KTaO_3$ thin films, $LaAlO_3/KTaO_3$ heterostructures of different crystallographic orientations, and $KTaO_3$ membrane films and heterostructures for fundamental explanations of the mechanism of recently observed superconductivity. We will use electrostatic gating layer to vary the carrier concentration and Nb doping to approach the ferroelectric quantum critical point of KTO. This task will be achieved by employing $Ba_{1-x}Sr_xRuO_3$ sacrificial layer, during the growth of $KTaO_3$ (001) and (111) heterostructures.

References

1. "Twisted oxide membrane interface by local atomic registry design" M.Kim, K. Lee, Ryo Ishikawa, K. Song, Naafis A. Shahed, K.T. Eom, M. S. Rzchowski, E. Y. Tsymbal, N. Shibata, T. Mizoguchi, C.B. Eom, and S.Y. Choi, *submitted* (2005) https://arxiv.org/abs/2502.20738

Publications (which acknowledge DOE support)

1. "Atomic lift-off of epitaxial membranes for cooling-free infrared detection" Xinyuan Zhang, Owen Ericksen, Sangho Lee, Marx Akl, Min-Kyu Song, Haihui Lan, Pratap Pal, Jun Min Suh, Shane Lindemann, Jung-El Ryu, Xudong Zheng, Bikram Bhatia, Frances Ross, Hyunseok Kim, Celesta S. Chang, Yunfeng Shi, Chang-Beom Eom, and Jeehwan Kim, *Nature* **641**, 98 (2025). https://doi.org/10.1038/s41586-025-08874-7
2. "Crystallographic Spin Torque Conductivity Tensor of Epitaxial IrO_2 Thin Films for Oxide Spintronics" Michael Patton, Daniel A. Pharis, Gautam Gurung, Xiaoxi Huang, Gahee Noh, Evgeny Y. Tsymbal, Si-Young Choi, Daniel C. Ralph, Mark S. Rzchowski, Chang-Beom Eom, *Advanced Materials*, 2414267 (2025) https://doi.org/10.1002/adma.202414267
3. "Feld-induced modulation of two-dimensional electron gas at $LaAlO_3/SrTiO_3$ interface by polar distortion of $LaAlO_3$" Jinsol Seo, Hyungwoo Lee, Kitae Eom, Jinho Byun, Taewon Min, Jaekwang Lee, Kyoungjun Lee, Chang-Beom Eom & Sang Ho Oh, *Nature Communications* **15**, 5268 (2024) https://doi.org/10.1038/s41467-024-48946-2
4. "Electronic-grade epitaxial (111) $KTaO_3$ heterostructures" Jieun Kim, Muqing Yu, Jung-Woo Lee, Shun-Li Shang, Gi-Yeop Kim, Pratap Pal, Jinsol Seo, Neil Campbell, Kitae Eom, Ranjani Ramachandran, Mark S. Rzchowski, Sang Ho Oh, Si-Young Choi, Zi-Kui Liu, Jeremy Levy, Chang-Beom Eom, *Science Advances,* **10**, eadk4288 (2024) (2024) https://doi.org/10.1126/sciadv.adk42
5. "Surface triggered stabilization of metastable charge-ordered phase in $SrTiO_3$" Kitae Eom, Bongwook Chung, Sehoon Oh, Hua Zhou, Jinsol Seo, Sang Ho Oh, Jinhyuk Jang, Si-Young Choi, Minsu Choi, Ilwan Seo, Yun Sang Lee, Youngmin Kim, Hyungwoo Lee, Jung-Woo Lee, Kyoungjun Lee, Mark Rzchowski, Chang-Beom Eom & Jaichan Lee, *Nature Communications,* **15**, 1180 (2024) https://doi-orgI10.1038/s41467-024-45342-8
6. "Large spin–orbit torque in bismuthate-based heterostructures" Anthony L. Edgeton, Isaac A. Harris, Neil G. Campbell, Yahong Chai, Marcel M. Mazur, Gautam Gurung, Xiaoxi Huang, Sandhya Susarla, Evgeny Y. Tsymbal, Daniel C. Ralph, Tianxiang Nan, Mark S. Rzchowski, Ramamoorthy Ramesh & Chang-Beom Eom, *Nature Electronics* **6**, 973 (2023). https://doi.org/10.1038/s41928-023-01080-1
7. "Electron pairing and nematicity in $LaAlO_3/SrTiO_3$ nanostructures" Aditi Nethwewala, Hyungwoo Lee, Jianan Li, Megan Briggeman, Yun-Yi Pai, Kitae Eom, Chang-Beom Eom, Patrick Irvin & Jeremy Levy, *Nature Communications* **14**, 7657 (2023). https://doi.org/10.1038/s41467-023-43539-x
8. "Symmetry Control of Unconventional Spin-Orbit Torques in IrO_2" Michael Patton, Gautam Gurung, Ding-Fu Shao, Gahee Noh, Joseph A. Mittelstaedt, Marcel Mazur, Jong-Woo Kim, Philip J. Ryan, Evgeny Y. Tsymbal, Si-Young Choi, Daniel C. Ralph, Mark S. Rzchowski, Tianxiang Nan, Chang-Beom Eom, *Adv. Mater.* **35**, 2301608 (2023) https://doi.org/10.1002/adma.202301608
9. "Engineered Chirality of One-Dimensional Nanowires" Megan Briggeman, Elliott Mansfield, Johannes Kombe, Franc¸ois Damanet, Hyungwoo Lee, Sayanwita Biswas, Jianan Li, Mengchen Huang, Chang-Beom Eom, Patrick Irvin, Andrew J. Daley, and Jeremy Levy, *Science Advances* **11**, eadx4761 (2024). https://doi.org/10.1126/sciadv.adx4761
10. "Prediction of polarization vortices, charge modulation, flat bands, and moiré magnetism in twisted oxide bilayers" Naafis Ahnaf Shahed, Kartik Samanta, Mohamed Elekhtiar, Kai Huang, Chang-Beom Eom, Mark S. Rzchowski, Kirill D. Belashchenko, and Evgeny Y. Tsymbal, Phys. Rev. B, **111**, 195420 (2025) https://doi.org/10.1103/PhysRevB.111.195420

Ultrafast Isospin Dynamics in Flatband Graphene

Chenhao Jin, *University of California, Santa Barbara*

Keywords: graphene, correlation and topology, isospin fluctuations, nonequilibrium dynamics, ultrafast pump probe

Research Scope

Flatband graphene systems recently emerged as an intriguing platform for engineering correlated and topological phenomena. A plethora of exotic ground states have been reported such as superconductivity, orbital ferromagnetism, integer and fractional Chern insulators. Nevertheless, available experimental tools typically only capture long-range orders in the ground state and have no access to the excitations. Such deficiency has limited our understanding of competing orders and quantum critical physics, as well as the opportunity for engineering non-equilibrium phenomena through driving the excitations. In this project, we develop a novel ultrafast pump-probe technique dubbed Time-Resolved Imaging of Isospin Orders (TRIO) that directly creates and monitors excitations in flatband graphene systems at femtosecond timescales; and leverage this unique experimental capability to access previously unavailable information such as strength and dynamics of isospin (i.e., spin and valley) fluctuations. Our results will offer key input to the understanding of correlated and topological phases in flatband graphene and help answer central questions in condensed matter physics such as the nature of competing orders, superconductivity and quantum critical points.

Recent Progress

We have successfully developed the first generation of TRIO, which allows us to optically probe isospin orders and excitations in flatband graphene systems. One major challenge behind optically probing graphene systems is their weak optical response as atomically thin semimetals. Worse still, the relevant energy scales of correlated phases typically fall in the milli electron-volt, or terahertz range, which is inconvenient for direct optical access. We have addressed these challenges through exciton sensing[1]: a monolayer semiconductor sensor, such as WSe2, is placed in direct contact with the target graphene system without a spacer in between, which encodes the correlated phases in graphene into exciton energy shift in WSe2. This new sensing scheme we developed not only paves the way for optically detecting correlated states in flatband graphene systems but also offers the unique capability to identify isospin orders and distinguish them from other mechanisms of Fermi surface change.

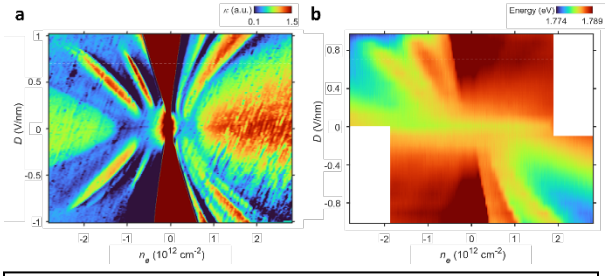


Fig. 1: Phase diagram of RTG from electrical capacitance (a) and TRIO (b).

As an example[1], Fig. 1, a and b compare the equilibrium phase diagram of a rhombohedral trilayer graphene device measured by electrical capacitance and TRIO. The horizontal and vertical axes are charge carrier density and displacement field, respectively. In capacitance measurement, isospin orders and transitions manifest as incompressible lobes on the hole-doping side and compressibility jumps on the electron side. TRIO fully captures these isospin order features in the top left and bottom right quadrants, while shows weak responses in the other two quadrants. Such asymmetry can be naturally understood from a short-range interaction between WSe2 and graphene such that WSe2 primarily interacts with charges in the top (closest) layer. TRIO therefore also provides a sensitive probe of layer polarization.

Going beyond measuring equilibrium isospin orders, TRIO allowed us to extract key properties of the isospin soft modes without directly coupling to the order parameter[2]. It has been conjectured that the isospin soft modes can provide the pairing glue for superconductivity. However, most isospin orders have exotic order parameters that are difficult to couple to, making experimental investigation challenging. Using TRIO, we record the first video of ultrafast melting and recovery of isospin orders in magic angle twisted bilayer graphene (Fig. 2). By inspecting the transition between isospin orders and the damping of collective excitations using TRIO, we uncover remarkably slow dynamics of isospin orders in MATBG in the filling range of -3< v < -2, indicating the existence of long-lived isospin soft modes and strong isospin fluctuations. Interestingly, both IVC orders and superconductivity also emerge in this carrier filling range. The weakly-damped isospin modes we observe could naturally originate from the IVC goldstone mode and provide the paring glue for superconductivity. Our results therefore provide a key missing piece of the complete picture.

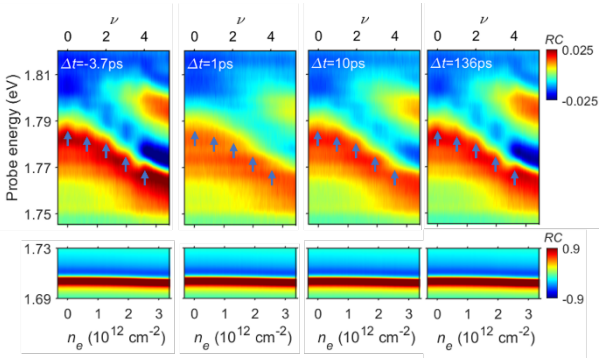


Fig. 2: Ultrafast melting and recovery of isospin orders (arrows) in magic-angle twisted bilayer graphene. Δt is the delay between the pump and probe lights.

Building upon these recent successes, we have further investigated isospin excitations and dynamics in RTG, a representative crystalline flatband graphene system, and obtained intriguing preliminary results. Fig. 3a shows the time-evolution of transient TRIO spectra at fixed displacement field and representative fillings on the hole-doped side. The signal remains zero before the pump arrives and rises sharply at time zero; then gradually diminishes as the system relaxes back to equilibrium. Interestingly, the relaxation dynamics show remarkable slowing-down in multiple filling ranges, separated by regions of fast decay (Fig. 3b). This indicates that weakly-damped isospin soft modes also exist in RTG with relaxation dynamics up to 1 ns, even slower than in MATBG. Since RTG is metallic throughout the phase diagram except for near charge neutrality, the observed weak damping does not originate from a large particle-hole excitation gap. It instead indicates a flat energy landscape and strong competition between different isospin orders.

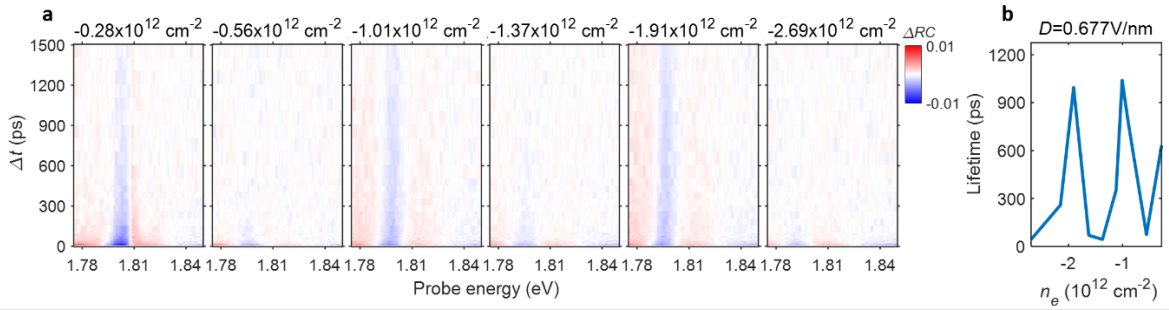


Fig. 3: Isospin dynamics in RTG. (a) Time-evolution of transient TRIO spectra at representative fillings and fixed displacement field. (b) Extracted isospin recovery time.

Future Plans

In the current supporting period, we plan to leverage TRIO to investigate both equilibrium isospin orders and nonequilibrium isospin dynamics and excitations in flatband graphene. On the equilibrium order side, we plan to apply TRIO to probe isospin orders inside superconducting domes. This has remained an experimental challenge since most techniques probe isospin orders and superconductivity through the same measurement channel, resulting in disruption and conflict between the two. For example, electrical transport is short-circuited by superconductivity inside the superconducting domes and cannot provide information about isospin orders anymore. We will bypass such issues using TRIO, which detects isospin orders through a distinct and independent optical channel. We will start with MATTG, which has the highest superconducting critical temperature among all flatband graphene systems that approaches 2 Kelvin. This allows us to achieve the superconducting regime with our Opticool cryostat, which has a base temperature of 1.65 K. In collaboration with Prof. John Harter, we are also constructing a new TRIO setup around a Janis He-3 cryostat with a base temperature of 300 mK (Fig. 6a). We will simultaneously monitor superconductivity and isospin orders from electrical transport and TRIO, respectively, while navigating the phase diagram. We will also examine the behaviors of isospin orders when superconductivity is suppressed by magnetic field and/or temperature. We aim to establish a coherent picture of the interplay between isospin orders and superconductivity under all relevant tuning parameters and answer key questions regarding the nature of superconductivity.

On the excitations and dynamics side, we will apply TRIO systematically to flatband graphene systems, both moiré and non-moiré, to further establish the connection between nonequilibrium dynamics, collective excitations and correlated orders. We will focus on RTG, where we have already observed long-lived isospin modes in specific regions of the phase diagram. Compared to moiré graphene, RTG provides several unique advantages, such as tunability through electric field and no complication from moiré superlattice. We will systematically investigate the evolution of isospin soft modes and fluctuations with tuning parameters such as carrier density, displacement field, magnetic field and temperature; and combine this information about

excitations with the ground state properties obtained from electrical measurements. Doing so will allow us to elucidate the correspondence between equilibrium isospin orders and the nonequilibrium collective excitations, as well as their interplay with superconductivity; thereby significantly advancing our understanding of correlated physics.

References

1. Tian Xie, Tobias M. Wolf, Siyuan Xu, Zhiyuan Cui, Richen Xiong, Yunbo Ou, Patrick Hays, Ludwig F. Holleis, Yi Guo, Owen I. Sheekey, Caitlin Patterson, Trevor Arp, Kenji Watanabe, Takashi Taniguchi, Seth Ariel Tongay, Andrea F. Young, Allan H. MacDonald, Chenhao Jin, "*Optical imaging of flavor order in flat band graphene*", Nature Communications **16**, 5555 (2025)

2. Tian Xie, Siyuan Xu, Zhiyu Dong, Zhiyuan Cui, Yunbo Ou, Melike Erdi, Kenji Watanabe, Takashi Taniguchi, Seth A. Tongay, Leonid S. Levitov, Chenhao Jin, "*Long-Lived Isospin Excitations in Magic-Angle Twisted Bilayer Graphene*". Nature **633**, 77-82 (2024)

Selective Area Epitaxial Growth of Superconducting MgB_2 Nanowires and MgB_2/graphene hybrid structures on SiC

Qi Li

Department of Physics, Pennsylvania State University, University Park, PA 16802

Keywords: superconductivity, Superconducting nanowires, graphene, proximity effect, selective area epitaxy

Research Scope

The goal of the project is to study proximity-induced superconductivity in two-dimensional quantum materials, graphene, and unconventional superconductivity. The focus of the research is on the interplay between superconductivity, Rashba spin orbit coupling, topological bands, and low filling Landau level states. The systems to be studied include 2D electron systems at transition metal oxides interfaces in (111) orientation with large Rashba spin-orbit coupling (SOC) and graphene. The superconductor to be used is MgB_2 which has the highest T_c ~40 K for an s-wave superconductor in a solid in comparison with the commonly used Nb compound which has a T_c ~10 K. Furthermore, MgB_2 has very high upper critical field H_{c2} (above 60 T in slightly carbon doped thin films in a magnetic field parallel to the C-plane) which can create low Landau level quantum Hall states in the 2D systems while MgB_2 is still superconducting. This provides a possibility that chiral superconductivity can be induced in low Landau level states. The goal of the project is (1) to achieve a high temperature platform for inducing topological superconducting states, and (2) to induce chiral superconductivity in low Landau level states utilizing the high T_c and high upper critical field of MgB_2 thin films. In addition, Dirac nodal line has been predicted and observed by ARPES on MgB_2 *M*-plane (10-10), which supports the prospect of an intrinsic topological superconductor.[1] The overall goal of this project is to explore the unconventional superconductivity in topological or quantum limit states in graphene and metal oxide (111) orientation based 2D electron systems.

Recent Progress

1. Selective Area Epitaxy of MgB_2 on Epitaxial Graphene-SiC

Hybrid structures of superconductors with graphene and 2D electron gas systems are extensively studied recently due to the prospect of achieving Majorana Fermions for fault-tolerant quantum computing. However, current studies have been largely based on low temperature superconductors, such as Nb (T_c~9 K). Higher operation temperature is extremely desirable for both fundamental research and potential applications. MgB_2 has a bulk transition temperature (T_c) of 39 K, the highest T_c BCS s-wave superconductor at ambient pressure, and it has also been shown to be able to achieve an upper critical field (H_{c2}) larger than 60 T. Furthermore, MgB_2 possesses

two superconducting energy gaps, a small gap of ~2.3 meV due to the π band and a larger gap of ~7.1 meV due to the two-dimensional σ band which contributes to its high T_c, but also has Fermi nodal lines along *ab* directions, making it a potential topological superconductor. We have discovered a selective area epitaxy on both epitaxial graphene on SiC and transferred graphene, where areas with graphene prohibit the growth of MgB_2. This is possibly due to the low surface energy of epitaxial graphene and van der Waals bonds which inhibit MgB_2 deposition to allow for selective area growth onto SiC. Selective area epitaxial growth of *C*-plane films would allow not only direct growth of superconducting devices, but it also offers the opportunity to fabricate high quality thin film-based lateral hybrid MgB_2-graphene superconducting devices for unconventional Josephson devices and chiral superconductivity in Landau level states. Fig. 1 shows the schematic

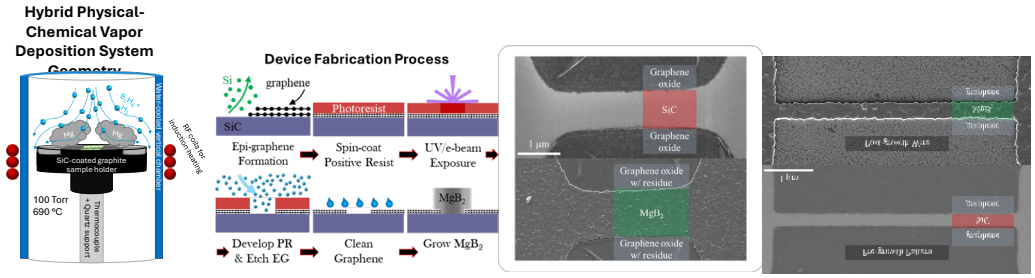


Fig. 1. (from left to right) Schematic diagram of HPCVD growth technique. Process to pattern epitaxial grown graphene and expose the SiC substrate for selective area growth of MgB_2 films. Nanobridge pattern on a transferred graphene for both before and after MgB_2 growth. Nanowire pattern using e-beam lithography for both before and after MgB_2 growth.

diagram of Hybrid Physical-Chemical Vapor Deposition System (HPCVD) for fabricating high quality epitaxial MgB_2-thin films and the process of making MgB_2 devices with a patterned graphene template.

The significance of the selective area epitaxy is that it can allow a high T_c and high H_{c2} superconductor platform to form hybrid devices with graphene to study unconventional superconductivity such as Josephson effect, proximity effect and predicted chiral superconductivity in low filled Landau level states, topological superconductivity along Fermi nodal lines, and nanostructured superconducting devices.

2. Superconducting epitaxial MgB_2 nanowires grown via selective area epitaxy

Superconducting nanowires are useful in many areas of studies, especially for single photon detection. We have patterned the epitaxial graphene on SiC (which was formed by vacuum annealing of SiC) with the nanowire area removed using electron beam lithography. The subsequent growth of MgB_2 films was only on the area of nanowires, forming well defined epitaxial nanowires with high T_c, H_{c2}, and critical current density. Fig. 2 shows a SEM image of two nanowires of 300 nm and 500 nm wide and nominal ~60 nm thick. The superconducting transitions in magnetic fields up to 10 T in both parallel and perpendicular fields are also shown. The extrapolated H_{c2} at T =0 are 8.5 T and 25.2 T for perpendicular and parallel field, respectively.

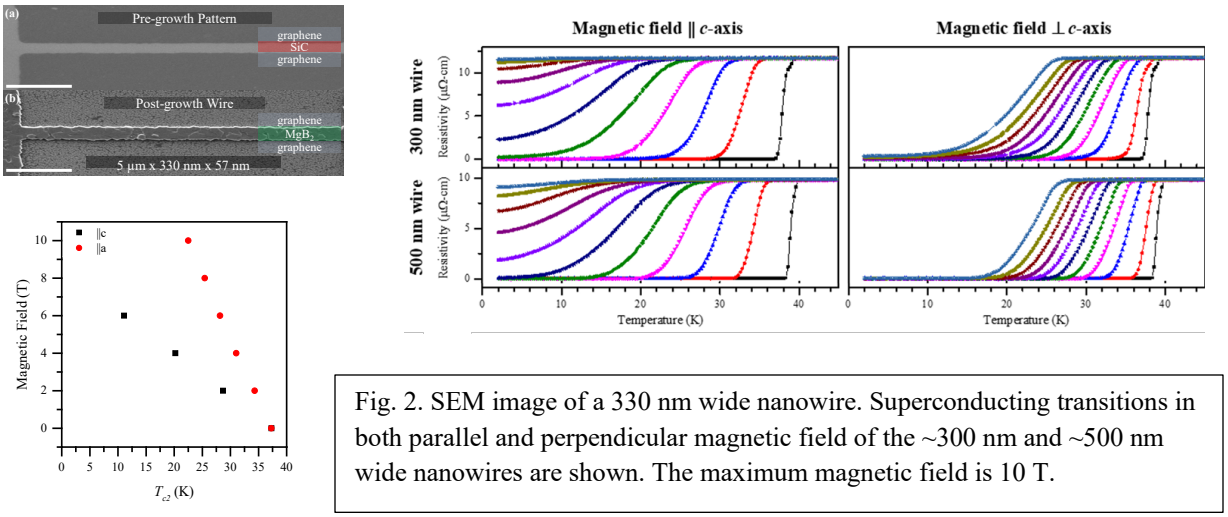


Fig. 2. SEM image of a 330 nm wide nanowire. Superconducting transitions in both parallel and perpendicular magnetic field of the ~300 nm and ~500 nm wide nanowires are shown. The maximum magnetic field is 10 T.

The critical current density of the 300 nm and 500 nm wires shows very high values at J_c(2 K, 0 T) = 6.1 x 10^7 A/cm^2 and 4.6 x 10^7 A/cm^2, respectively, similar to that of the normal wider and thicker films. The critical current density decreases faster in magnetic field in the nanowires than that of the thicker films.

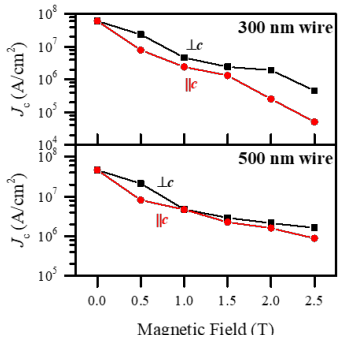


Fig. 3. Critical current density of the 300 nm and 500 nm nanowires as a function of magnetic field.

3. Ultrathin and tilted *ab*-axis MgB_2 films

Ultrathin superconducting films with high transition temperature and high critical magnetic field are desirable for many potential applications, such as hybrid superconductor-topological material structure for quantum computing, and single photon detectors. We have studied the superconducting transition of ultrathin MgB_2 film with film thickness down to nominal 3 nm. The T_c of the nominal 3 nm- thick film is still above 30 K. Separately, the *ab*-axis MgB_2 thin films have been very desirable due to that it exposes the 2D σ band and Fermi nodal line normal to the surface direction for probing those properties. In addition, the H_{c2} is large when the magnetic field is parallel to the *ab* axis direction due to the intrinsic layered structures, which can be used for studying the proximity effect to quantum Hall states. Toward this effort, we have grown MgB_2 films on *M*-plane sapphire which produced bi-directional grains that tilt the MgB_2 *C*-plane 37° relative to the substrate surface and significantly expose the MgB_2 *M*-plane.

4. Shubnikov-de Haas Oscillations reaching the quantum limit in Two-Dimensional electron Systems at $SrTiO_3$ (111) Interfaces

Transition metal oxides in the (111) orientation have been predicted to harbor topological phases and unconventional quantum states because of their hexagonal crystal symmetry and strong interactions between charge, spin, and orbital degrees of freedom. We report Shubnikov-de Haas oscillations into the quantum limit at magnetic fields up to 35 T in high mobility (>20,000 $cm^2V^{-1}s^{-1}$) two-dimensional electron liquids at (111) oriented $SrTiO_3$ interfaces with controllable carrier densities. Spin splitting is observed at low Landau levels which is attributed to the interplay between the Zeeman splitting and Rashba spin-orbit coupling according to our theoretical modeling, yielding Landé factor $g = 0.29$ and Rashba coefficient $\alpha = 0.6\ \mathrm{meV \cdot nm}$. At high magnetic field after the system reaches the lowest Landau level, the temperature dependence of the resistance shows a metallic to insulating state transition with the magnetoresistance changing significantly from a primarily quadratic to a large linear field dependence.

Future Plans

The future plan will focus on proximity induced superconductivity in hybrid structures of MgB_2/graphene and MgB_2/2D electron gas systems. The selective area epitaxy method will be utilized as a template for fabricating hybrid structures of MgB_2 and graphene. Transferred graphene sandwiched between hBN will be explored due to the much higher mobility of the transferred graphene than that of the epitaxial graphene. The base template of graphene on SiC will still be used even for transferred graphene for the reason that it can be used as a mask for the MgB_2 growth. There are two major goals of this study: (1). Josephson junction type of devices through graphene to have a high operating temperature to study the unconventional Josephson effect due to Dirac band. (2) Induced superconductivity in Landau level states in graphene utilizing both the high T_c, H_{c2}. It is possible to also study induced superconductivity in fractional Quantum Hall regime. All are predicted to display chiral (p-wave) superconductivity. P-wave superconductors are important for fault tolerant quantum computing.

In addition to the hybrid structure with graphene, we will also follow the proposal on studying the proximity induced superconductivity in the transition metal oxide 2D electron gas systems with high mobility. These interface electron gases contain topological band, large Rashba spin orbit coupling, and other quantum states where single layer graphene does not have. With using reasonably low magnetic field to reach the quantum limit in the STO (111) systems, we also expect that the proximity effect can be reached when the system reaches low Landau levels. In addition, we will also be looking at the possible topological superconducting state in MgB_2 along the ab directions through tunneling measurements on the side junctions.

References

1. Zhou, X. *et al.* Observation of topological surface states in the high-temperature superconductor MgB2. *Phys. Rev. B* **100**, 184511 (2019).

Publications and submitted manuscripts

1. Z. Wang, W. Yang, K. Chen, X.X. Xi, and Qi Li. “Anisotropic high upper critical field in ultrathin MgB2 films”. *IEEE Trans. Appl. Supercond.* 33, (2023). DOI: 10.1109/TASC.2023.3264173
2. Rondomanski, P. A., Bansal, A. J., Dong, C. J., Wang, K. J., Gray, J. I., Shallenberger, J. R., Robinson, J. A., Li, Q., & Redwing, J. M. (2023). Comparison of physical and chemical vapor deposition for magnesium intercalation underneath epitaxial graphene. *Journal of Crystal Growth, 627*, 127521 (2024). DOI: 10.1016/j.jcrysgro.2023.127521
3. Rondomanski, P. A., Heltman, A. B., Glaser, J. J., Redwing, J. M., & Li, Q. “Tilted ab-axes MgB2 films with high Tc and anomalous upper critical field anisotropy”. *IEEE Trans. Appl. Superconductivity*. 34, (2024) on-line DOI:10.1109/TASC.2024.3369573
4. Ziqiao Wang, Autumn Heltman, Shalini Kumari, Lunhui Hu, Zhu Lin, Rojin Taheri, Nasim Alem, Lin Jiao, Shalinee Chikara, Alexey Suslov, John Singleton, Fedor Balakirev, Chaoxing Liu, and Qi Li “Shubnikov-de Haas Oscillations into the Quantum Limit in Two-Dimensional Electron Systems at $SrTiO_3$ (111) Interfaces” Phys. Rev. B 112, 035153 (2025) DOI: https://doi.org/10.1103/why6-1fl8
5. P. A. Rondomanski, A. Heltman, C. Chen, A. R. Richardella, J. L. Gray, J. M. Redwing, and Q. Li, *Exposure of the MgB2 M-plane via HPCVD Grown Tilted C-plane Films*, Appl.Phys. Lett., submitted (2025)
6. Shaoqing Ding, Jinyuan Yao, Zhen Bi, Quyen Tran, Bangzhi Liu, Qi Li, Susan Trolier-McKinstry, Thomas N. Jackson, and Ying Liu “Indirect Tunneling Enabled Spontaneous Time-Reversal Symmetry Breaking and Josephson Diode Effect in TiN/AlOHf0.8Zr0.2O /Nb tunnel junctions” submitted to Science Advance (2025).
7. *Patrick A. Rondomanski, Chengye Dong, Joshua Robinson*, *Joan M. Redwing,* and *Qi Li* “Fabrication of Magnesium Diboride epitaxial Nanowires via Selective Area Epitaxy on graphene-SiC substrate” to be submitted to Nano Lett. (2025)

Tunable Exciton and Spin Dynamics in 2D Materials: Role of Thickness, Defects, Synthesis Method and Substrates

Dr. Birol Ozturk, Department of Physics and Engineering Physics, Morgan State University, Baltimore, 21251, MD

Keywords: Defect engineering, 2D materials, Excitonic behavior, ODMR

Research Scope

This project aims to advance quantum photonic platforms based on two-dimensional (2D) materials by tuning their excitonic and spin-related properties through strain engineering, controlled defect formation, and substrate selection. Special focus is given to monolayer WSe_2 and multilayer GaSe systems, owing to their favorable optical and electronic properties. Our approach combines cryogenic photoluminescence (PL), optically detected magnetic resonance (ODMR), and first-principles defect simulations to build a comprehensive understanding of how mechanical strain, defect type, and synthesis method influence emission behavior, spin coherence, and localization.

Recent Progress

A. Strain-Modulated Exciton Dynamics in Monolayer WSe_2

Localized mechanical strain was introduced into monolayer WSe_2 using atomic force microscopy (AFM) indentation patterns with spacing of 3, 4, and 5 μm (Figure 1). PL spectroscopy performed between 5 and 50 K revealed significant spectral changes between indented and unindented regions. Multiple excitonic peaks were observed: neutral exciton (X_0), trion (X_T), dark exciton (X_D), and dark trion (X_{DT}) [1-3]. Indentation resulted in redshifts and broadened linewidths, particularly for X_D and X_T. A power-dependent blue shift of emission peaks followed the form $E(P) = E_0 - mP^n$, with extracted parameters indicating that trions and dark excitons are more sensitive to strain-induced carrier screening than bright excitons. Global fitting of logI–logP intensity plots revealed superlinear α values for dark and trion states in indented regions (Figure 1), confirming many-body recombination effects enhanced by mechanical strain.

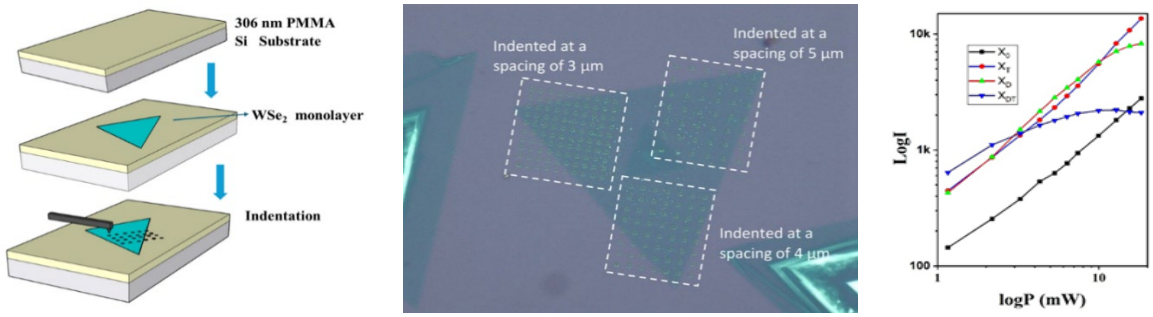


Figure 1 Schematic illustration of transferring the WSe_2 monolayer to PMMA/Si and formation of defects by AFM tip (left) optical image of WSe_2 monolayer with different indentation spacing (middle) and logI–logP intensity plots

B. Influence of Growth and Substrate on Exciton Behavior

To decouple the effects of material synthesis and substrate type, we performed a comparative PL study on exfoliated WSe_2 (placed on SiO_2/Si) and MOCVD-grown monolayers transferred onto quartz substrates. Both power- and temperature-dependent PL measurements were analyzed via global pseudo-Voigt profile fitting. MOCVD-grown WSe_2 exhibited higher-energy excitonic features (X_0 at 1.774 eV vs. 1.732 eV in exfoliated samples) and more stable peak positions across power and temperature ranges. Exfoliated samples showed broader features and more pronounced defect-bound states. Varshni analysis [4] revealed that MOCVD samples had lower thermal broadening coefficients (α_V) and more consistent β values, indicating reduced disorder due to quartz support and controlled synthesis conditions. These findings support the use of CVD methods for scalable fabrication of quantum-optical-grade 2D materials.

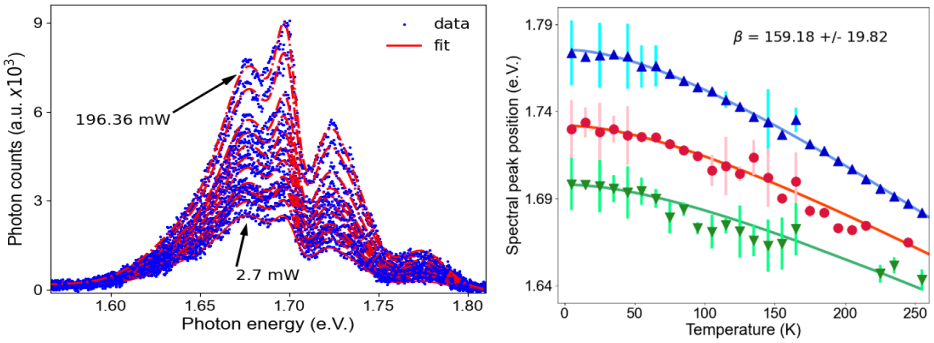


Figure 2 Excitation laser power dependent PL data and their global fits (left) and Varshni plots of 3 main peaks (right) of MOCVD grown WSe_2 monolayer transferred on quartz.

C. Thickness and Substrate Dependence in GaSe Multilayers

We extended our study to gallium selenide (GaSe) flakes, mechanically exfoliated onto SiO_2 and TEM grids, with thicknesses ranging from 4.6 to 38.1 nm. AFM and Raman spectroscopy were used for structural characterization. The A_1' mode in Raman spectra redshifted systematically with decreasing thickness, consistent with reduced interlayer coupling [5]. Photoluminescence measurements performed at cryogenic temperatures revealed enhanced emission on TEM grids, likely due to reduced non-radiative quenching and fewer surface traps compared to SiO_2. Power-dependent PL spectra showed the emergence of sub-bandgap localized excitons at higher excitation levels, indicating that structural disorder and thickness significantly modulate exciton dynamics in GaSe.

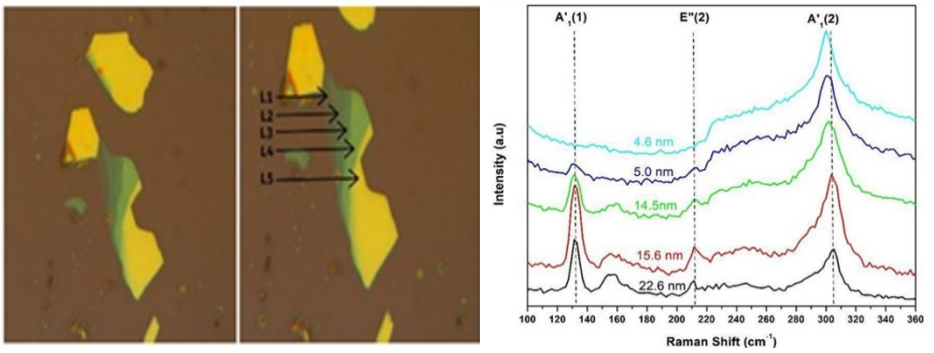


Figure 3 (left) Optical images showing layer thickness variation and (right) Raman analysis at different thicknesses of exfoliated GaSe flakes.

D. Observation of Spin Resonance via ODMR in Strained WSe_2

One of the key achievements was the detection of optically addressable spin transitions using ODMR method. WSe_2 samples patterned with 5 μm AFM indentations were cooled to 20 K, and PL signals were monitored while sweeping microwave frequencies. A clear, repeatable resonance was observed near 1890 MHz (Figure 4), with a clear ODMR contrast. The signal broadened and shifted under an external magnetic field, consistent with Zeeman splitting, verifying the spin nature of the transition. Notably, this effect was achieved without chemical doping, suggesting that strain-engineered native or extended defects can act as spin-active quantum centers. This establishes WSe_2 as a promising 2D host for coherent spin manipulation.

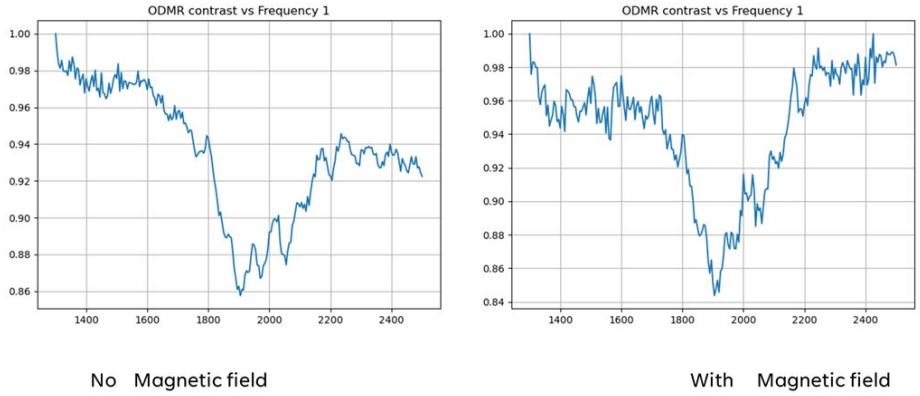


Figure 4 ODMR results of WSe_2 monolayer obtained from AFM indented region with 5 μm spacing.

E. First-Principles Defect Modeling

To better understand the experimental spin signals, we performed density functional theory (DFT) simulations of both point and edge defects in WSe_2 using the SCAN meta-GGA functional. While point defects (e.g., W or Se vacancies) produced limited zero-field splitting (ZFS) frequencies, zigzag edge terminations generated ZFS values near 1860 MHz—closely matching experimental ODMR resonances as shown in Table 1. These calculations confirm that extended edge-like structures, particularly those created through indentation-induced strain gradients, can produce magnetic transitions in the GHz range. This insight bridges the gap between ODMR observation and atomic-level modeling, guiding defect engineering strategies for future spintronic devices.

Table 1. Zero-field splitting parameters (D and E) of zigzag edge configurations in monolayer WSe_2 calculated via density functional theory (DFT). Different atomic terminations (e.g., 2Se+W, W+W, and hydrogenated W+W[H]) exhibit a wide range of splitting values, highlighting their potential contribution to the observed ODMR signal.

Shape of the edge	Atoms at the edge	Width Å	D (MHz)	E (MHz)
Zigzag	Se + W	15.3567	1762.5	454.0205
Zigzag	Se + W	21	1860	484.6595
Zigzag	W+ W	7.632	2443.473	430.074
Zigzag	W+ W	13.26912	2630.571	337.401

Zigzag	W+ W	18.934	3091.18	394.658
Zigzag	W+ W[H]	7.58747	9897.576	1800.213
Zigzag	W+ W[H]	13.14417	8246.712	1412.6455
Zigzag	W+ W[H]	18.74264	7067.658	1138.066

Future Plans

We will continue our ODMR experiments on WSe_2 monolayers, extending the frequency range up to 20 GHz to identify potential zero-field splitting features from various defects. In addition, MoS_2 and GaSe monolayers will be studied using similar low-temperature PL and ODMR techniques to examine the universality of observed spin-dependent signals. Following ODMR detection, quantum sensing tests for small magnetic field detection will be conducted.

To achieve zigzag-oriented edge defects, directional scratching is being applied to newly prepared WSe_2 samples, replacing previous AFM indentation methods. This approach enables more controlled orientation of cracks and better alignment with theoretical predictions.

A custom-built maskless laser lithography setup will be employed to deposit micron-scale electrodes on exfoliated flakes, facilitating measurements of photoconductance and gated exciton modulations.

On the theoretical side, DFT calculations will be extended to MoS_2 and GaSe to determine their defect-related ZFS properties. Concurrently, a graduate student is being trained in machine learning-based interatomic potential generation and will perform molecular dynamics simulations at both nano- and mesoscales, using GPU-accelerated tools for large-scale modeling of defect dynamics.

References

1. J. Kim, Y. Yu, A. Bergman, X. Lu, J. Pan, X. Xu, and C. Jin, Correlation-driven nonequilibrium exciton site transition in a WSe_2/WS_2 moiré supercell, Nat. Commun. **15**, 3312 (2024).
2. X.-X. Zhang, T. Cao, Z. Lu, Y.-C. Lin, F. Zhang, Y. Wang, Z. Li, J. Hone, J. A. Robinson, D. Smirnov, S. G. Louie, and T. F. Heinz, Magnetic brightening and control of dark excitons in monolayer WSe_2, Nat. Nanotechnol. **12**, 883 (2017).
3. Z. Zhang, P. Chen, X. Li, C. T. Koch, and Z. Ren, Direct observation of gate-tunable dark trions in monolayer WSe_2, Nano Lett. **19**, 6886 (2019).
4. Varshni, Y.P., "Temperature dependence of the energy gap in semiconductors," *Physica*, **34**, 149–154 (1967)
5. S. Lei, L. Ge, W. Najmaei, A. George, R. Kappera, J. Lou, M. Chhowalla, H. Yamaguchi, and P. M. Ajayan, *Evolution of the electronic band structure and efficient photo-detection in atomic layers of GaSe*, ACS Nano, 8, 1263–1272 (2014).

Publications

1. Y. S. Ocak, S. Mahtab, P. Milas, S. Lee, H.-J. Chuang, K. M. McCreary, B. Jonker, and B. Ozturk, Strain-driven modulation of excitonic states in AFM-engineered WSe_2 monolayer, To be submitted to *npj 2D Mater. Appl* .
2. P. Milas, Y. S. Ocak, P. Shrestha, M. Merritt, A. Aybar, J. Pellegrino, S. Krylyuk, A. V. Davydov, C. Chen, S. Kumari, N. Trainor, and B. Ozturk, A comparative study on excitonic dynamics in WSe_2 monolayers using a high-fidelity global fitting method, *To be submitted*.
3. M. Salami, Y. S. Ocak, M. Spencer, and B. Ozturk, Thickness-dependent excitonic behavior of GaSe flakes, *in preparation*.
4. D. Wines, A. Ibrahim, N. Gudibandla, T. Adel, F. M. Abel, S. Jois, K. Saritas, J. T. Krogel, L. Yin, T. Berlijn, A. T. Hanbicki, G. M. Stephen, A. L. Friedman, S. Krylyuk, A. V. Davydov, B. Donovan, M. E. Jamer, A. R. Hight Walker, K. Choudhary, F. Tavazza, and C. Ataca, Quantum Monte Carlo and density functional theory study of strain and magnetism in 2D 1T-VSe_2 with charge density wave states, *ACS Nano* **19**, 9925–9935 (2025).
5. D. Wines, J. Ahn, A. Benali, P. R. C. Kent, J. T. Krogel, Y. Kwon, L. Mitas, F. A. Reboredo, B. Rubenstein, K. Saritas, H. Shin, I. Štich, and C. Ataca, Towards improved property prediction of two-dimensional (2D) materials using many-body quantum Monte Carlo methods, *Appl. Phys. Rev.*, accepted (2025).
6. A. Ibrahim, A. M. Hagez, M. Sultana, and C. Ataca, Data-driven molecular dynamics and TEM analysis of platinum crystal growth on graphene and reactive hydrogen-sensing dynamics, *submitted to ACS Nano* (2025).
7. A. Ibrahim, C. Ataca, Prediction of frequency-dependent optical spectrum for solid materials: A multioutput and multifidelity machine learning approach, *ACS Appl. Mater. Interfaces* **16**, 41145–41156 (2024).

Probing Chirality-Dependent Magnetotransport in 2D $(MBA)_2PbI_4$ Hall Devices

Dr. Meenakshi Singhs, Colorado School of Mines

Collaborators: Matt Beard, CHOISE EFRC, National Renewable Energy Laboratory (NREL)

DOE Award Number: DE-SC0024115

Keywords: Chirality-Induced Spin Selectivity (CISS), hybrid organic-inorganic perovskites, Hall effect, magneto-transport, spin–orbit coupling

Research Scope

Understanding how chirality interacts with electronic spin is a fundamental challenge in condensed matter physics, with implications for spintronics, quantum information, and energy-efficient electronics. The chirality-induced spin selectivity (CISS) effect—where electrons become spin-polarized when transmitted through a chiral medium, even in the absence of ferromagnetism [1]—offers a powerful pathway to harness chirality for spin control. Strong evidence of CISS has been reported in DNA, peptides, and helicenes, but the microscopic origin of the effect remains elusive. Theoretical frameworks invoke helicity, interfacial spin–orbit coupling, or many-body interactions, yet rigorous experimental tests have been limited because molecular systems are fragile and difficult to integrate into multi-terminal device architectures required for quantitative transport studies.

To address this limitation, we turn to the two-dimensional, chiral, hybrid perovskite, Methylbenzylammonium Lead Iodide $(MBA)_2PbI_4$, discovered at the CHOISE EFRC at NREL [2]. In this material, chirality is introduced by the (MBA) cation, while the layered inorganic lattice provides strong spin–orbit coupling (SOC). Crucially, unlike conventional molecular assemblies, $(MBA)_2PbI_4$ combines several advantages that make it uniquely suited for CISS investigations and device integration: it is semiconducting, it can be processed into uniform thin films, and it can be patterned into Hall-bar geometries for controlled magnetotransport measurements. Together, these features enable systematic studies that were previously inaccessible. Here, we report the first comprehensive Hall-effect study of chiral $(MBA)_2PbI_4$ devices across a broad temperature range (290–50 K). By probing how chirality and SOC influence charge transport in a semiconducting platform compatible with scalable device architectures, this work lays the foundation for advancing both the fundamental understanding of CISS and its translation into practical spintronic technologies.

Research Progress

We have (1) developed fabrication process that can ensure high-quality devices with reliable performance, (2) performed structural and morphological characterization, and (3) performed transport measurements.

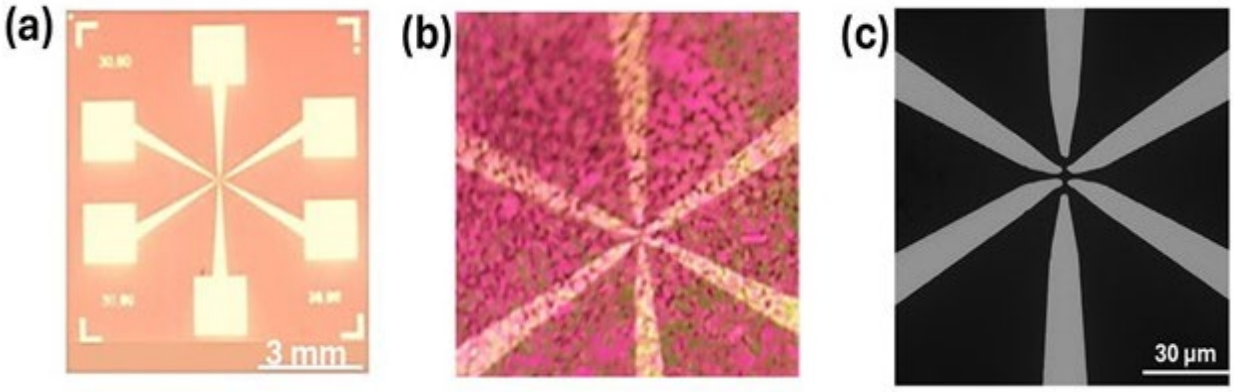


Fig 1: (a) Optical microscope image of a symmetric Hall bar structure. **(b)** Zoomed-in view of the Hall bar after coating with the CISS-active $(MBA)_2PbI_4$ film. **(c)** SEM image of the Hall bar device, highlighting the electrode geometry.

1.Fabrication

We have selected Si/SiO_2 substrates for their compatibility with thin-film deposition and spin-coating processes. To enhance the adhesion of the CISS film, the substrates were treated in a UV ozone chamber at 50°C for 10 minutes. A bilayer of Titanium (Ti) and Gold (Au) was deposited using DC sputtering. The Ti layer (4 nm) served as an adhesion layer, while the Au layer (40 nm) functioned as the primary conductive electrode. This combination ensures robust electrode-substrate bonding and stable electronic transport characteristics. An 80 nm thick Aluminum (Al) back gate was evaporated on the back of the silicon substrate. Laser lithography was utilized to define the electrode pattern with precise alignment (10 µm separation between current probes, 2 µm separation between voltage probes) (Fig.1). The small size of the device was necessary to mitigate gigaohm-level resistances encountered in early long-channel devices. A precursor solution of $(MBA)_2PbI_4$ was prepared by dissolving the crystalline material in DMF solvent. The spin-coating parameters—rotations per minute, duration, and solution concentration—were carefully optimized to achieve uniform film coverage. The films were annealed at 100°C for 5 minutes to promote crystallization and enhance their structural integrity. After the successful fabrication of the devices, we conducted transport measurements using a 1.8 K cryostat over a wide temperature range (290 K down to 50 K) under perpendicular magnetic fields up to 12 T.

2. Structural and Morphological Characterization

The structure and morphology of the spin-coated $(MBA)_2PbI_4$ thin films were checked before device fabrication. XRD patterns reflect a set of sharp diffraction peaks (00l), indicating the layered Ruddlesden-Popper crystal structure with preferred out-of-plane orientation. The presence of higher-order peaks such as (002), (004), and (006) implies good crystallinity and uniform vertical stacking (Fig. 2a). Scanning Electron microscopy (SEM) displays uniform film coverage with micron-scale grains with distinct grain boundaries, along with cracks that are likely introduced during the annealing process (Fig. 2b).

3. Transport Measurements

3(a). Longitudinal Resistance measurements

The temperature dependence of the longitudinal resistance (R_{xx}) (Fig. 3) reveals two distinct transport regimes. From 290–70 K, R_{xx} remains in the megaohm range and shows only a weak variation with temperature, consistent with thermally activated transport dominated by electron–phonon scattering. At room temperature, the effective resistivity is 1.7×10^3 Ω·cm (film thickness = 100 nm) whereas out-of-plane devices typically exhibit orders-of-magnitude higher resistivity. Below ~70 K, however, the resistance increases sharply by several orders of magnitude, reaching the gigaohm range. This dramatic upturn signals carrier freeze-out and the onset of localized hopping transport. A similar low-temperature upturn is also observed in bulk $MAPbI_3$, reflecting the crossover to hopping transport [3].

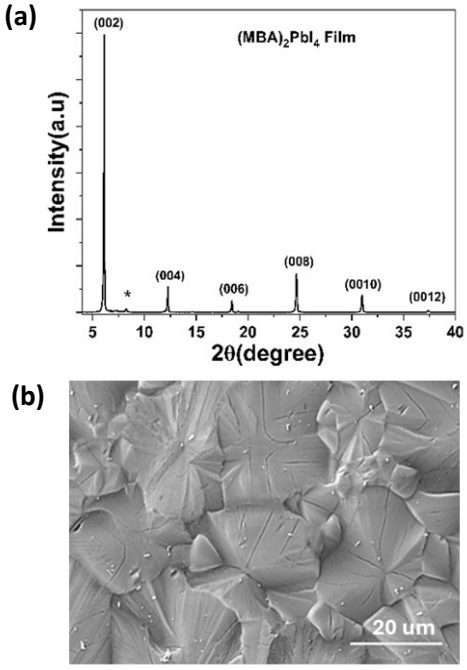


Fig 2: (a) XRD Pattern of $(MBA)_2PbI_4$ thin film. (b) SEM Image showing surface morphology with large grains.

3(b). Hall measurements

Hall measurements (Fig. 4) show nonlinear field dependence behavior. This nonlinearity suggests the possible involvement of multiple charge carriers contributing to transport [4]. A sign reversal in Hall slope is observed near 100 K, marking a distinct crossover in transport behavior. At lower temperatures, at 50 K, the negative Hall slope persists, indicating that the initial carrier population freezes out while another charge carrier dominates.

During Hall measurements, we observed an anomalously large Hall voltage, unexpected for a material with such low mobility. This suggests that non-ideal effects—arising from device geometry and current spreading—complicate the reliable extraction of intrinsic carrier density and mobility. To address this, we propose a two-step corrective strategy. First, a symmetry-based decomposition using the α-model with polynomial fitting will be applied to separate the odd (Hall) and even (longitudinal) voltage components. Second, finite-element device modeling with COMSOL will be used to simulate current pathways in the Hall-bar geometry, clarifying how factors such as film coverage on the leads and electrode spacing influence the measured response. Together, these methods will disentangle inhomogeneous

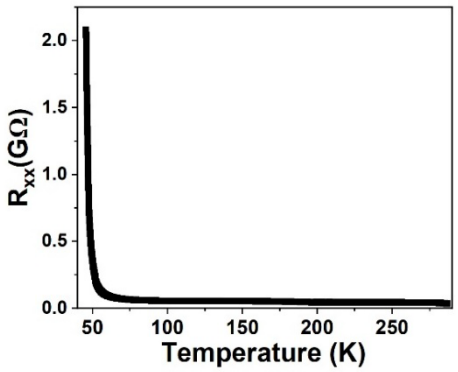


Fig 3: Temperature dependent longitudinal resistance.

contributions to the Hall signal and provide a more robust assessment of charge transport in chiral 2D perovskites.

3(c). Non-Local Device strategy

In parallel, we have fabricated non-local Hall bar devices incorporating Pt electrodes. Initial observations showed very large non-local voltage signals indicating pure spin transport behavior in $(MBA)_2PbI_4$, comparable to those observed in low spin dissipation systems such as YIG. We are continuing to explore this.

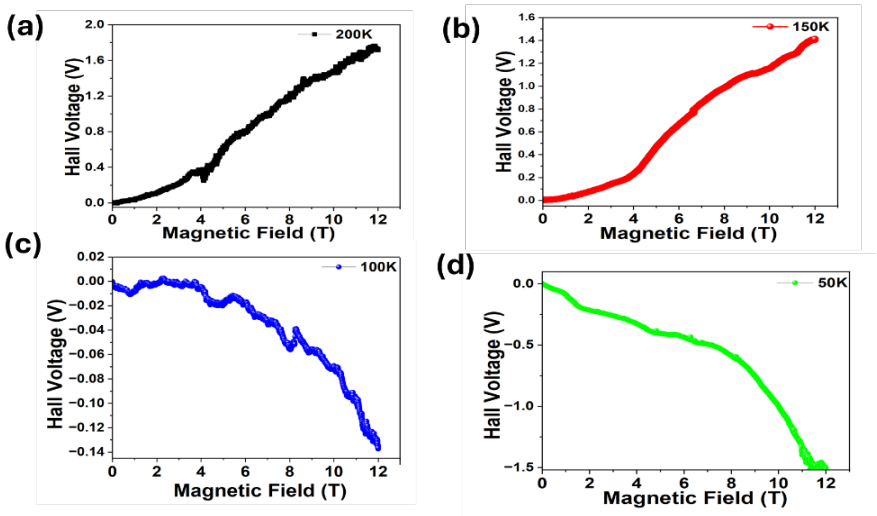


Fig 4: (a-d) Temperature dependent Hall measurements.

Future Plans

Our first priority is to use our measured Hall data to understand various transport regimes in the material. As described in the 'research progress' section, this will involve modeling. We also have plans to modify device geometry with an additional layer of lithography to minimize current crowding effects. Second, now that we have demonstrated that we can consistently make and measure Hall devices, we plan to fabricate asymmetric devices with ferromagnetic contacts of different coercive fields to extract spin diffusion length. Our initial measurements on non-local devices with Pt electrodes have yielded surprising results with implications for the CISS material's spin properties. We plan to pursue this direction further. Finally, depending on the outcomes from the asymmetric devices, it may be necessary to investigate Sn-rich compositions with enhanced transport properties. If so, we will implement the optimized hybrid encapsulation strategies that we have developed and carry out comparable measurements on these compositions to benchmark their performance.

References

1. Naaman, Ron, et al. "Chiral molecules and the electron spin." *Nature Reviews Chemistry* 3.4 (2019): 250-260.

2. Lu, Haipeng, et al. "Spin-dependent charge transport through 2D chiral hybrid lead-iodide perovskites." *Science advances* 5.12 (2019): eaay0571.

3. Keshavarz, Masoumeh, et al. "Light-and temperature-modulated magneto-transport in organic–inorganic lead halide perovskites." *ACS Energy Letters* 3.1 (2017): 39-45.

4. Bansal, Namrata, et al. "Thickness-independent transport channels in topological insulator Bi 2 Se 3 thin films." *Physical review letters* 109.11 (2012): 116804.

Publications and Presentations

1. PI presented the work at the APS March Meeting (2025), Anaheim, CA, in a presentation titled. “Hall Transport in Chirality Induced Spin Selective $(MBA)_2PbI4$”.
2. Post Doc attended the Gordon Research conference (2025), Manchester, NH, and presented a poster titled “Probing Chirality-Dependent Magnetotransport in 2D $(MBA)_2PbI_4$ Hall Devices”.
3. Manuscript in Preparation – “Probing Chirality-Dependent Magnetotransport in 2D $(MBA)_2PbI_4$ Hall Devices” by Shehreen Aslam, Sam Saiter, Matt Hautzinger, Matthew Beard, and Meenakshi Singh, is currently being finalized.

Heteroepitaxial growth and surface investigation of Weyl semimetals Mn3Ga and Mn3Sn on hexagonal wurtzite GaN substrates

PI: *Arthur R. Smith*

Address: Ohio University
Nanoscale & Quantum Phenomena Institute
Department of Physics & Astronomy
Athens, OH 45701

E-mail: smitha2@ohio.edu

Keywords: spintronics, Weyl semimetals, antiferromagnets, scanning tunneling microscopy, molecular beam epitaxy

1. Research Scope

The scope of the project is to utilize a combination of molecular beam epitaxial growth and in-situ scanning tunneling microscopy to investigate the surfaces of selected Weyl semimetal systems including Mn_3Ga and Mn_3Sn. These materials are known for their fascinating electronic and magnetic properties and effects including anomalous Hall effect, topological Hall effect, giant piezospintronic effect, large exchange bias, full electronic switching, and more [1, 2, 3, 4, 5, 6, 7, 8, 9] Both Mn_3Ga and Mn_3Sn are non-collinear antiferromagnetic having the Kagome inverse triangular spin structure. This project aims to produce high quality, mirror-like surfaces and to study the structural, electronic, and magnetic properties of the surfaces using ultimately, spin-polarized STM and tunneling spectroscopy. The project makes use of two independently operating laboratories, each including an MBE-STM system. Lab 1 includes a variable low-temperature STM with a small permanent magnet allowing applied fields up to 1 Tesla and having a 2-spring + air-leg vibration isolation system connected to a 5-source MBE system. Lab 2 includes a variable low-temperature STM system with a variable 4.5 Tesla superconducting magnet on a 2-stage air-leg vibration isolation system combined with a 7-source MBE system. Both STM systems operate with liquid helium cooling and are home-built.

2. Recent Progress

Completion of low-temperature STM systems and initial testing

Both Lab 1 and Lab 2 underwent extensive modifications over the past 6 years. For Lab 1, the previously operating microscope was a room-temperature STM. Finally, the variable LT-STM system was completed in 2025 and is now in the testing phase. Modifications over summer 2025 are resulting in cooling tests demonstrating good efficiency in cooling and in temperature stability tests. The scanning capability of the STM was previously demonstrated, with initial table-top results showing atomic resolution on a graphite surface. Some challenges with the course approach are currently being sorted out, but initial tests on Weyl semimetal surfaces in UHV are imminent. For Lab 2, the variable low-temperature STM was completed and has already undergone temperature testing. The ultimate temperature for the microscope as currently configured appears to be 13 K, and it can operate over a range of temperatures up to 100 K or higher while under variable magnetic field, a true variable T/variable B system. Scanning tests look promising with noise

levels as good as 600 f$A/\sqrt{Hz}$. Both Lab 1 and Lab 2 MBE/STM systems allow for tip and sample exchange, magnetic STM tip coating, variable temperatures, and variable *B* fields.

Growth and Analysis of Weyl Semimetal Mn_3Sn and Mn_3Ga films on GaN substrates

We previously reported Mn_3Sn films grown successfully on sapphire (0001) substrates [10, 11], but we have achieved much higher quality films using GaN substrates. We grew Mn_3Sn on N-polar wurtzite GaN (000$\underline{1}$) substrates, and Mn_3Ga films on Ga-polar wurtzite GaN (0001) substrates. Publications on these results are close to submission [12, 13].

In the case of Mn_3Sn, we grew extremely high-quality films on GaN which was grown on sapphire (0001). Reflection high energy electron diffraction and x-ray diffraction were used to determine the *in-plane* and *out-of-plane* lattice constants, respectively. The final determined values were a = 5.670 Å, c = 4.526 Å which are in excellent agreement with ideal expected values (differences from expected are +0.0833% for a and -0.1104% for c, respectively). Furthermore, the RHEED azimuthal map reveals high crystallinity from all directions (see **Fig. 1**). RHEED shows very streaky streaks with spacings very closely matching expected values. Streaky streaks indicate highly (atomically) smooth surfaces.

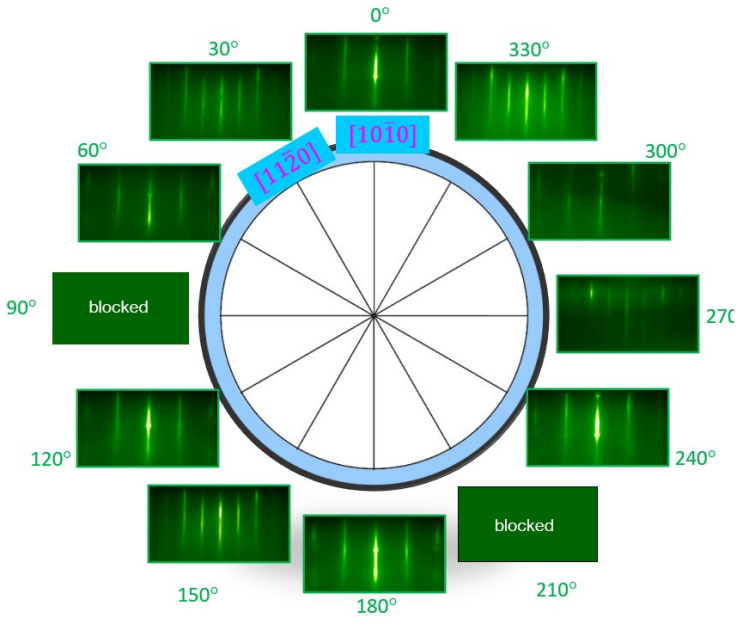


Fig. 1 360° RHEED azimuthal map for Mn_3Sn(0001). The patterns exhibit well-defined streaks, indicative of a well-ordered crystalline surface. A clear sixfold rotational symmetry is observed, consistent with the hexagonal crystal structure of Mn_3Sn. The primary crystallographic orientations, [10$\underline{1}$0] and [11$\underline{2}$0], are marked for reference. Specific azimuths are obscured due to experimental constraints.

In the case of Mn_3Ga, we have successfully performed MBE growth and room-temperature STM investigations of the surface, finding smooth spiral growth mounds and a spattering of pinholes on the surface (see **Fig. 2**). The surface step edges indicate that the structure is hexagonal given the 120° step angles. Atomic resolution images also reveal the hexagonal structural motif of the surface with a surface spacing *a = 5.60 +/- 0.10 Å* (reported a = 5.4037 Å [4]). Therefore, the spacing matches a 1×1 unit cell. The existence of pinholes could be related to the presence of lattice mismatch between the film and substrate, or it might indicate the presence of some type of defects. The heights of the atomic steps are consistent with c/2 (~2.20 Å) where c = 4.350 +/- 0.023 Å as measured by X-ray diffraction (reported c = 4.3603 Å). The *dI/dV* spectra reveals the presence of an LDOS peak near the Fermi level.

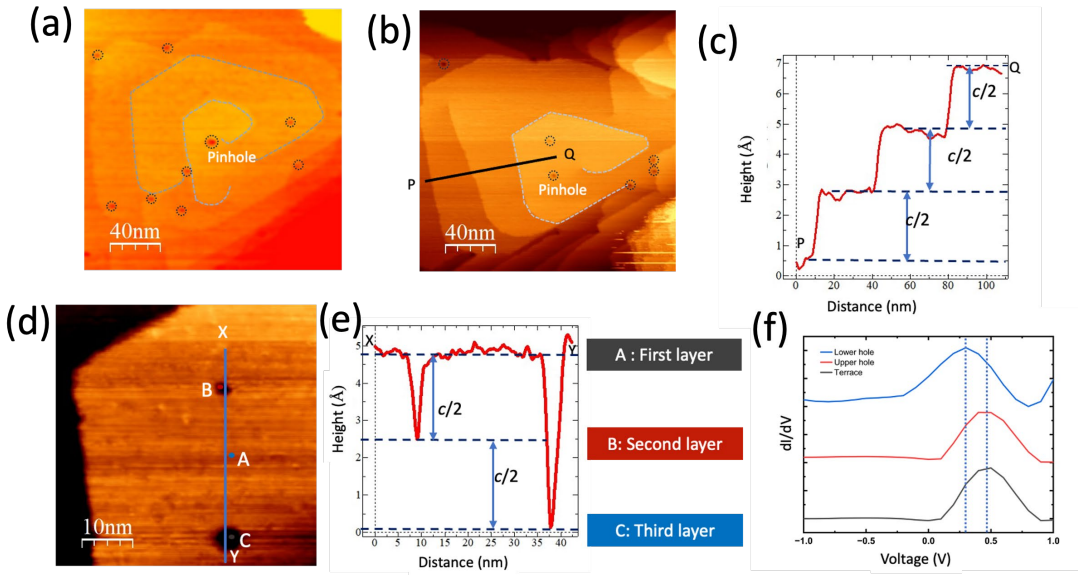


Fig. 2 200 nm × 200 nm STM topographic image showing spiral growth on the surface with several pinholes in a) region 1 (V_s = -0.2 V, I_t = 90 pA) and b) region 2 (V_s = 2 V, I_t = 90 pA), and inset shows an atomic resolution image with V_s = 1 V, I_t = 183 pA; c) line profile along line PQ showing the step height of terraces in (b); d) zoom-in view of top terrace of (b); e) line profile along line XY in (d)

In some other areas of the surface, some different structures are also seen. This includes triangular wells and some surface periodicities which are different from the *a*-value noted in the atomic resolution image. These other regions may correspond to either different reconstructions or else minority grains with alternative crystalline orientations. In any case, overall, the surface is of very high quality and suitable for spin-polarized STM measurements.

3. Future Plans

In the case of Mn_3Sn, next steps for this project are to a) grow GaN/sapphire and perform atomic resolution scanning tests in Lab 2 with a GaN (000$\underline{1}$) surface; then b) grow Mn_3Sn (0001) on GaN (000$\underline{1}$); and then c) begin STM measurements on the *in-situ* grown Weyl semimetal surface. We also plan to investigate the density of states of the surface and to probe the surface using magnetic-coated STM tips for doing spin-polarized measurements to hopefully resolve the Kagome inverse triangular spin structure.

In the case of Mn_3Ga, we plan similarly to continue with the STM investigations of Mn_3Ga/GaN (0001) and to use spin-polarized STM to explore the spin properties of this surface also. Such high-resolution measurements are challenging, but we think it is possible to do this and to perform *dI/dV* measurements to reveal and verify the electronic LDOS around the Fermi level, and also with spin-polarization.

Such investigations are just the beginning of what we can explore in these systems using the combined power of MBE/STM. For example, by varying the strain in these layers using different growth conditions, it is possible to observe how strain can be used to control the spin structure and electronic and magnetic properties of the surface in general. We can also investigate the temperature dependence and the effects of applied magnetic fields on these properties.

4. References

[1] Liu, Z.H., Zhang, Y.J., Liu, G.D. *et al.*, "Transition from Anomalous Hall Effect to Topological Hall Effect in Hexagonal Non-Collinear Magnet Mn_3Ga," *Sci Rep* **7**, 515 (2017).
[2] Song, L., Ding, B., Li, H., Lv, S., Yao, Y., Zhao, D., ... & Wang, W. (2021). Observation of structural distortion and topological Hall effect in noncollinear antiferromagnetic hexagonal Mn3Ga magnets. *Applied Physics Letters*, *119*(15).
[3] Guo, H., Feng, Z., Yan, H., Liu, J., Zhang, J., Zhou, X., ... & Liu, Z. (2020). Giant piezospintronic effect in a noncollinear antiferromagnetic metal. *Advanced Materials*, *32*(26), 2002300.
[4] Song, L., Ding, B., Li, H., Lv, S., Yao, Y., Zhao, D., ... & Wang, W. (2021). Observation of large exchange bias above room temperature in antiferromagnetic hexagonal Mn3Ga. *Journal of Magnetism and Magnetic Materials*, *536*, 168109.
[5] Liu, J., Zhang, Z., Fu, M., Zhao, X., Xie, R., Cao, Q., ... & Liu, G. (2023). The anomalous Hall effect controlled by residual epitaxial strain in antiferromagnetic Weyl semimetal Mn3Sn thin films grown by molecular beam epitaxy. *Results in Physics*, *52*, 106803.
[6] Zhou, X. F., Chen, X. Z., You, Y. F., Liao, L. Y., Bai, H., Zhang, R. Q., ... & Pan, F. (2020). Exchange Bias in Antiferromagnetic Mn3Sn Monolayer Films. *Physical Review Applied*, *14*(5), 054037.
[7] Nakatsuji, S., Kiyohara, N., & Higo, T. (2015). Large anomalous Hall effect in a non-collinear antiferromagnet at room temperature. *Nature*, *527*(7577), 212-215.
[8] Cheng, Y., Yu, S., Zhu, M., Hwang, J., & Yang, F. (2021). Tunable topological Hall effects in noncollinear antiferromagnet Mn3Sn/Pt bilayers. *APL Materials*, *9*(5).
[9] Higo, T., Kondou, K., Nomoto, T., Shiga, M., Sakamoto, S., Chen, X., ... & Nakatsuji, S. (2022). Perpendicular full switching of chiral antiferromagnetic order by current. *Nature*, *607*(7919), 474-479.
[10] Upadhyay, S., Erickson, T., Hall, H., Shrestha, A., Ingram, D. C., Sun, K., ... & Smith, A. R. (2023). Molecular beam epitaxy and crystal structure of majority a-plane-oriented and substrate-strained Mn3Sn thin films grown directly on sapphire (0001). *Journal of Vacuum Science & Technology A*, *41*(4).
[11] Upadhyay, S., Erickson, T., Hall, H., Shrestha, A., Ingram, D. C., Sun, K., ... & Smith, A. R. (2023). Exploring the interfacial structure and crystallinity for direct growth of Mn3Sn (0001) on sapphire (0001) by molecular beam epitaxy. *Surfaces and Interfaces*, *42*, 103379.
[12] Ashok Shrestha, Daniel Russell, Fengyuan Yang, David C. Ingram and Arthur R. Smith, manuscript in preparation (2025).
[13] Hannah Hall, Sunil Timilsina, Sneha Upadhyay, Tyler Erickson, and Arthur R. Smith, manuscript in preparation (2025).

5. Publications of DOE sponsored research (2023-2025)

Papers listed below are shown in reverse chronological order, with the numbering defined based on paper #1 = A.R. Smith's first paper. Full publication list can be seen at: http://www.phy.ohiou.edu/~asmith/publist.html.

2025

110. Experimental and theoretical investigation of the crystalline surface, film, and interface properties of antiperovskite Mn_3GaN grown by molecular beam epitaxy on MgO(001), Ali Abbas, Juan Carlos Moreno Hernandez, Ashok Shrestha, Daniel Russell, Tyler Erickson, Kai Sun, Gregorio Hernandez Cocoletzi, Fengyuan Yang, and Arthur R. Smith, *Surfaces and Interfaces* **64**, 106201 (2025).

2024

109. Accommodating a hexagonal z- phase Mn2N film on a cubic MgO (001) substrate, Ashok Shrestha, Juan Carlos Moreno Hernandez, Ali Abbas, Gregorio Hernandez Cocoletzi, Noboru Takeuchi, David C. Ingram, and Arthur R. Smith, *Applied Surface Science* **664**, 160152 (2024).

108. Co-deposition of bismuth-nitrogen films on MgO (001) by molecular beam epitaxy, Ashok Shrestha, Ali Abbas, David C. Ingram, and Arthur R. Smith, *Journal of Vacuum Science & Technology A* **42**, 023407 (2024).

2023

107. Exploring the interfacial structure and crystallinity for direct growth of Mn_3Sn(0001) on sapphire (0001) by molecular beam epitaxy, S. Upadhyay, T. Erickson, H. Hall, A. Shrestha, D. C. Ingram, K. Sun, J. C. M. Hernandez, G. H. Cocoletzi, N. Takeuchi, and A. R. Smith, *Surfaces and Interfaces* **42**, 103379 (2023).

106. A Study of the Structure, Structural Transition, Interface Model, and Magnetic Moments of CrN Grown on

MgO(001) by Molecular Beam Epitaxy, Khan Alam, Rodrigo Ponce-Pérez, Kai Sun, Andrew Foley, Noboru Takeuchi, and Arthur R. Smith, *Journal of Vacuum Science & Technology A* **41**, 053411 (2023).

105. Molecular beam epitaxy and crystal structure of majority a-plane-oriented and substrate-strained Mn_3Sn thin films grown directly on sapphire (0001), Sneha Upadhyay, Tyler Erickson, Hannah Hall, Ashok Shrestha, David C. Ingram, Kai Sun, Juan Carlos Moreno Hernandez, Gregorio Hernandez Cocoletzi, Noboru Takeuchi, and Arthur R. Smith, *Journal of Vacuum Science & Technology A* **41**, 042710 (2023).

Abelian and Non-Abelian Quantum Entanglement in Landau Flatbands

PI: *Gabor Csathy*, **affiliation:** *Purdue University*

Keywords: topological materials, abelian anyons, non-abelian anyons, topology - quantum Hall, magnetotransport

Research Scope

The study of the quantum phases with topological order has permeated contemporary condensed matter physics. Most of the topological phases are single-particle in origin. There is, however, a second group of topological phases that form because of strong electron-electron interactions. Materials with flat electronic bands naturally support abelian and non-abelian quasiparticles, candidates for quantum resources. These flatband systems are currently under intense scrutiny, partly because of their rich physics and partly because of the hope that the interaction supported quantum entanglement stabilizes more intricate topological order. Topological phases in flatband systems hold the promise for applications in quantum memories and qubits, especially the ones that will be immune to noise.

Landau bands in the two-dimensional electron gas exposed to static magnetic fields are naturally flat and support an astonishingly large number of phases, many of which are predicted to host non-abelian quasiparticles. We seek to understand and control various aspects of flatband physics in the two-dimensional electron gas in GaAs/AlGaAs heterostructures in phases realized in the fractional quantum Hall regime. All the notable fractional quantum Hall states were discovered in this material system and material growth was significantly improved recently [a]. As a result, this system continues to exhibit new physics, even when it is compared to graphene; the flat bands and high quality assure that the electron gas in GaAs/AlGaAs continues to exhibit novel phenomena.

Recent Progress

Several of our results make use of the most recent advance in molecular beam epitaxy technology [a]. The mobility of the two-dimensional electron gas in these new GaAs/AlGaAs heterostructures increased by more than a factor of 4 at densities less than $1x10^{11}/cm^2$ as compared to that of earlier generation of samples. In addition, we employ state of the art cryogenic techniques to cool this system to temperatures as low as 5 mK.

Topological Protection due to Six-Flux Composite Fermions.

The fractional quantum Hall states (FQHS) are a prototypical example of a strongly correlated topological phase that hosts quasiparticles with fractional charge and fractional statistics. FQHSs are elegantly explained by the composite fermion theory. Furthermore, foundational ideas of the composite fermion theory can be extended to explain other recently observed correlated states, such as the Fractional Chern Insulators. Composite fermions are a resource for topological protection that arise from the correlated motion of flux tubes, or vortices, and the electrons themselves.

The success of the composite fermion theory is rooted in the ability to describe the complex correlations of the system with analytical many-body wavefunctions. The construction of these trial wavefunctions relies on the introduction of Jastrow factors which may be interpreted as

electrons capturing magnetic flux quanta. FQHSs are then understood as integer quantum Hall states of CFs moving in a magnetic field modified by the Berry phases associated with the attached fluxes and having a spectrum of quantized and degenerate energy levels.

So far there are more than 100 FQHSs observed in single layer systems and their number is steadily increasing due to advances in materials and cryogenic technology. Interestingly, to explain all observed FQHSs, only two types of composite fermions need to be invoked: the two-flux and 4-flux composite fermions – see Fig.1. These composite fermions and the associated FQHSs were discovered in GaAs/AlGaAs and were reported in other high quality host materials, such as graphene ZnO/MgZnO, and AlAs. While over the years the number of experimentally detected FQHSs is steadily increasing,



Fig.1 Schematic representation of two-flux, four-flux, and six-flux composite fermions.

Flux-six composite fermions and topological protection associated with them were predicted early on by theory but were not observed until our recent work. Over the years, there was an intense search for these flux-six composite fermions in the predicted region, at and near n=1/7. However, these searches failed in spite for significant progress with the quality of all host materials over the years.

In our work [1], we found evidence of six-flux composite fermions in a high-quality GaAs/AlGaAs sample that belongs to the newest generation of samples of the highest quality. This FQHS is at filling factor n =9/11. The intriguing aspect of our discovery is that the FQHS develops not at a filling factor of the form n =n/6n+1, but at n =1-n/6n+1. This indicates a not-yet-understood stabilizing effect of the particle-hole symmetry in the two-dimensional electron gas.

Our result provides evidence for a composite fermion of a new type. This composite fermion with six fluxes attached is the most intricate composite fermion known and expands the already diverse family of highly correlated topological phases with a new member that cannot be characterized by correlations present in other known members. Our observations pave the way towards the study of higher order correlations in the fractional quantum Hall regime. To our knowledge, topological protection associated with such intricate composite fermions was not reported in any other high-quality hosts such as graphene, ZnO/MgZnO, or AlAs.

A New Incarnation of a Non-Abelian Candidate State.

One of the most exciting and challenging endeavors in the study of correlated matter is the discovery of states with fundamentally new types of correlations. In the fractional quantum Hall regime such novel states are referred to as unconventional FQHSs. Unconventional FQHSs thus have more intricate electronic correlations than those of the Jain states. Because of highly non-trivial properties and potential uses in topological quantum computation among the unconventional FQHSs the non-abelian candidate states have generated the most interest. There are only a handful of unconventional FQHSs; examples are the Moore-Read Pfaffian and the Read-Rezayi parafermionic candidate states and there are a handful of experimental work with evidence for unconventional behavior.

Since the n =4/11 FQHS is not part of the n =n/2n+1 or n =n/4n+1 Jain sequences, it motivated numerous theoretical studies. It is believed that a partially spin polarized v=4/11 FQHS can be described by a conventional mixed-flavor composite fermion description. However, a fully spin polarized n =4/11 FQHS has unconventional correlations described by the Wójs, Yi, and

Quinn (WYQ) model. The unconventional topological order of the WYQ state stems from the unusual form of the inter-composite fermion interactions. We are unaware of an analytical construction for the WYQ wavefunction, hence attempts to schematically present the distinction between mixed flavor CF Jain state and WYQ state at n =4/11 are challenging. Instead, the WYQ wavefunction can be calculated using numerical methods. The hallmark property of the WYQ wavefunction is the clustering of composite fermions that suppresses the number of CF pairs with a relative angular momentum of three quantum units. The onset of this unusual topological order is quantified by a shift invariant distinct from that of a conventional Jain state. The WYQ state may support abelian or non-abelian quasiparticle excitations. For now, spin polarization and the nature of the topological order of the experimentally realized n =4/11 FQHSs remain unknown and can only be determined by further investigations. However, this FQHS remains a candidate for unconventional topological order and for hosting non-abelian anyons.

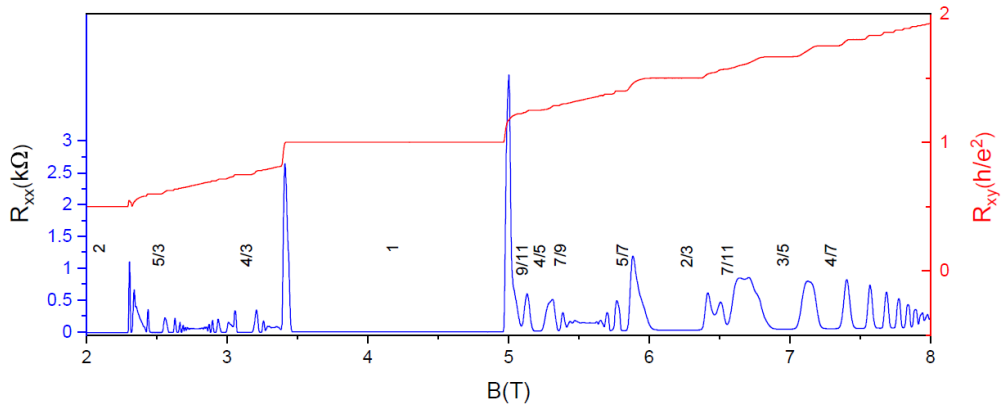


Fig.2 Evidence of a new FQHS at ν=7/11. There are several candidate states for this filling factor, one of which supports unusual non-abelian excitations. This exotic state is stable when this state is fully spin polarized.

As shown in Fig2, we report hallmarks of topological protection at the Landau level filling factor n =7/11 in a two-dimensional electron system [6]. The n =7/11 filling factor is the particle-hole conjugate of n =4/11, a filling factor intensely studied for the possibility of realizing unconventional electronic correlations. Our data establishes a new instance for an unusual fractional quantum Hall state and opens up possibilities for the study of unconventional correlations in an enlarged parameter space. We also report and discuss transport signatures developing at other filling factors of interest n =11/17, 5/8, and 8/13, which however in our sample do not exhibit topological protection.

Interplay of Andeson localization and of collective localization in the topological regime.

Magnetotransport measurements in low-disorder electron systems confined to GaAs/AlGaAs samples revealed that the n =1 integer quantum Hall plateau is broken into three distinct regions. These three regions were associated with two phases with different types of bulk localization: the Anderson insulator is due to random quasiparticle localization, and the integer quantum Hall Wigner solid is due to pinning of a stiff quasiparticle lattice [a].

The transition from the Anderson insulator to the charge ordered phase, the so-called integer quantum Hall Wigner solid, is not currently understood. We undertook a series of work to inquire new information on this transition via a detailed study of their temperature dependence [2] and by investigating the electrical breakdown of the n=1 plateau in the two different localization

regimes [3]. We found that the magnetoresistance is activated in both localization regimes. As shown in Fig.3, the activation energy E_a has local maxima in the center of the Anderson insulator and

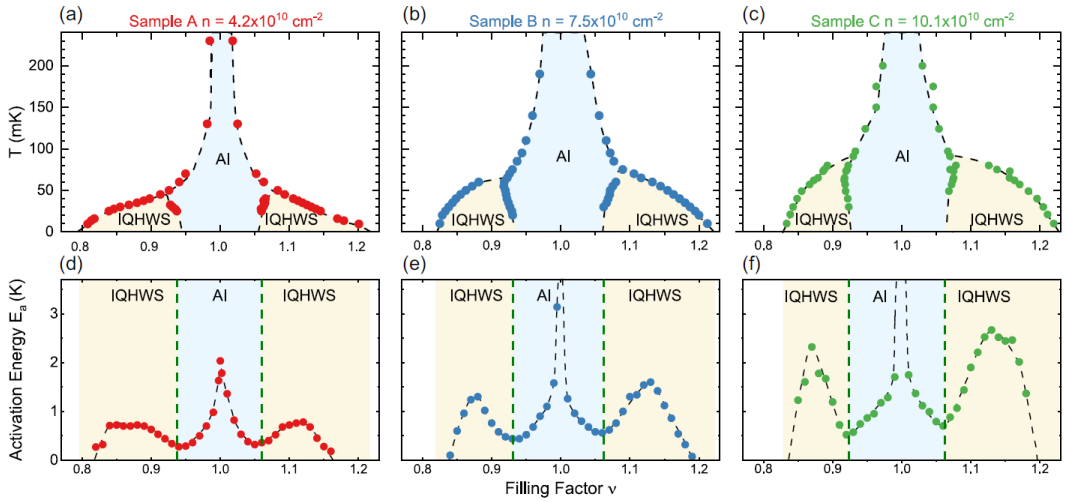


Fig.3 An unusual phase diagram and dependence of the activation energy E_a on the filling factor ν near filling factor ν=1.

Wigner solid, but it has conspicuous minima at the boundary between the two phases.

Our most recent work [4] highlights the universal properties of the n =1 plateau: the structure of the stability diagram, the non-monotonic dependence of the activation energy on the filling factor, and the alignment of features of the activation energy with features of the stability regions of the different phases are found to be similar in three samples spanning a wide range of electron densities. We also discuss quantitative differences between the samples, such as the dependence of the onset temperature and the activation energy of the integer quantum Hall Wigner solid on the electron density. Our findings provide insights into the localization behavior along the n =1 integer quantum Hall plateau in the low disorder regime.

Future Plans

In order to incisively probe the elusive non-abelian entanglement, we need to develop novel probing techniques. We are developing novel low noise circuitry and sample architectures suitable for thermoelectrical measurement techniques at millikelvin temperatures. These circuits will enable thermoelectric measurements of unprecedented resolution as they will be limited by fundamental properties of the sample and temperature, rather than amplifier noise.

References

a. Yoon Jang Chung, K. A. Villegas Rosales, K. W. Baldwin, P. T. Madathil, K. W. West, M. Shayegan, and L. N. Pfeiffer, "*Ultra-high-quality two-dimensional electron systems*", Nature Materials 20, 632–637 (2021)

b. S. Myers, H. Huang, L.N. Pfeiffer, K.W. Baldwin, and G.A. Csathy, "*Magnetotransport patterns of collective localization near ν = 1 in a high-mobility two-dimensional electron gas*", Phys. Rev. B **104**, 045311 (2021).

Publications

1. Haoyun Huang, Waseem Hussain, S.A. Myers, L.N. Pfeiffer, K.W. West, K.W. Baldwin, and G.A. Csathy, "*Evidence for Topological Protection Derived from Six-Flux Composite Fermions*", Nature Communications **15**, 1461 (2024)

2. S.A. Myers, Haoyun Huang, W. Hussain, L.N. Pfeiffer, K.W. West, and G.A. Csathy, "*Anomalous thermal activation in the Breakdown of the $\nu = 1$ integer quantum Hall effect in the single electron and collective localization regimes of the integer quantum Hall plateau*", Physica Status Solidi Rapid Research Letters 2400376 (2024)

3. S.A. Myers, Haoyun Huang, Waseem Hussain, L.N. Pfeiffer, K.W. West, and G.A. Csathy, "*Thermal Activation Signatures of the Anderson Insulator and the Wigner Solid forming near n=1*", Physical Review Research **6**, L022056 (2024)

4. Haoyun Huang, Waseem Hussain, S.A. Myers, L.N. Pfeiffer, K.W. West, and G.A. Csathy, "*Density Dependence of the Phases of the n=1 Integer Quantum Hall Plateau in Low Disorder Electron Gases*", Physica Status Solidi Rapid Research Letters 2400376 (2024)

5. Haoyun Huang, "*Collective Insulators in the Integer and Fractional Quantum Hall Regimes in the Limit of Low Disorder*", PhD Thesis (2025)

6. Waseem Hussain, Haoyun Huang, L.N. Pfeiffer, K.W. West, and G.A. Csathy, "*Topological Protection in a Landau Flat Band at n=7/11, a Candidate Filling Factor for Unconventional Correlations*", PNAS Nexus pgaf254, https://doi.org/10.1093/pnasnexus/pgaf254 (2025)

Generalizing Quantum Geometry to many-body wavefunctions

N. Peter Armitage, *The Johns Hopkins University*

Keywords: quantum geometry, THz spectroscopy, many-body physics, localization

Research Scope

Quantum geometry has recently been shown to play a key role in many areas of condensed matter physics, ranging from flat band superconductivity (1), optical response (2), and the fractional quantum anomalous Hall effect. The fundamental quantity in band theory – the quantum geometric tensor – naturally decomposes into two parts: an imaginary part that is the well known *Berry curvature* (3), central to topological physics, while its real component describes the *quantum metric*, a measure of the distinguishability between nearby quantum states. The QG has mostly been discussed in the context of band theory, but QG is believed to apply more broadly and is expected to survive its generalization to a many-body description of interacting and disordered systems. Recently it has been noted that the first negative moment sum rule of the conductivity - known since 1990s (4,5) to be related to the quantum fluctuations of the polarization - is related to the quantum geometry. In a band picture this sum rule provides a gauge-invariant part of the Wannier function spread. This sum rule has been used in a different context to quantify the quantum Fisher information. In a many body system this sum rule plays the role of a localization length.

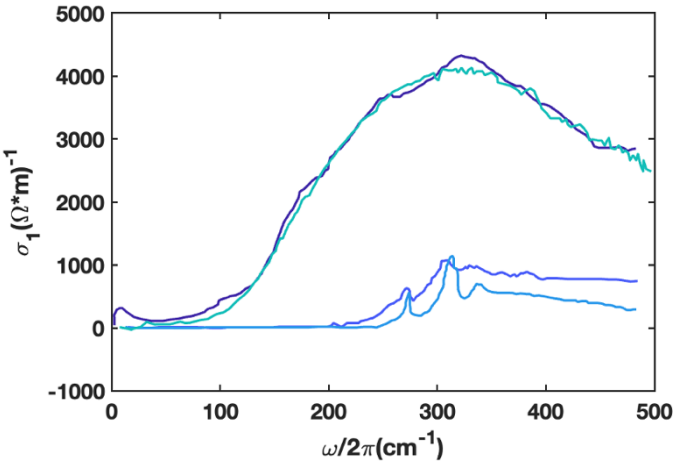


Figure 8, Optical conductivity of P doped Si samples on the approach to the 3D metal-insulator transition

Recent Progress

We apply these ideas to silicon samples doped with phosphorus across the 3D metal-insulator transition (MIT). Due to the disordered landscape of P doped randomly into Si we call such a state of matter an electronic glass. On the insulating side far the MIT, where dopants are well separated, the sum rule returns – to surprisingly high precision – the value produced from modern calculations for the Bohr radius of the hydrogenic like orbital for P into Si. As the system approaches the MIT from the insulating side, the extracted localization length grows rapidly and ultimately diverges. Notably, the rate of divergence differs from that found by conventional single-particle measures of localization.

Future Plans

This part of the project is an entre into investigating these materials with 2D THz spectroscopy. Here technique development is ongoing and we will commence measurements on such electron glass systems like this one and to spin liquids shortly.

References

[1] Peotta, S. & Torma, P. Superfluidity in topologically nontrivial flat bands. *Nature Communications* **6**, 8944 (2015).

[2] Morimoto, T. & Nagaosa, N. Topological nature of nonlinear optical effects in solids. *Science Advances* **2**, e1501524 (2016).

[3] Berry, M. V. Quantal phase factors accompanying adiabatic changes. *Proceedings of the Royal Society of London. Series A, Mathematical and Physical Sciences* **392**, 45–57 (1984).

[4] E.K.Kudinov. Difference between insulating and conducting states. *Sov.Phys. Solid State* **33**, 1299 (1991).

[5] Souza, I., Wilkens, T. & Martin, R. M. Polarization and localization in insulators: Generating function approach. *Physical Review B* **62**, 1666 (2000).

Publications

1. J. Yan, T.F. Rosenbaum, N.P. Armitage, In preparation (2025).

Understanding and Harvesting Topological Transport in Centrosymmetric Layered Ferromagnets and Their Heterostructures

Luis Balicas, *Florida State University and National High Magnetic Field Laboratory*

Keywords: anomalous and topological Hall effects, skyrmions and other topological spin textures, neutrons, electronic and thermal transport, Lorentz transmission electron microscopy.

Research Scope

This program aims at unveiling the physical mechanism(s) leading to the observation of topological Hall, topological Nernst, and topological thermal Hall like responses in layered, and a priori centrosymmetric ferromagnets in occasions in an experimental configuration that is usually understood to preclude their observation. Such effects should be observed in structures that lack inversion or mirror symmetries, and only for certain magnetic field orientations relative to the crystallographic axes. We propose clarifying this point through systematic structural analysis combined with transport experiments as a function of field orientation. Furthermore, these materials display topological spin textures that influence the described behavior, but their evolution as a function of thickness and field orientation is poorly characterized and understood. We are studying this aspect through a combination of powerful imaging techniques, associated to detailed structural analysis, via collaborations and the use of national facilities. The observation of a very sizeable remnant Hall response (under zero magnetic field) with preliminary imaging techniques revealing the presence of remnant spin textures, suggests an ability to "write" field-induced chiral spin textures that are detectable via an electrical signal. We aim at exposing their presence and manipulating their properties, as well as extracting their lifetimes. Since the remnant signal is observed in certain compounds at room temperature and above, our program will unveil their usefulness for technological applications. Finally, we are studying the stacking of these

ferromagnetic layers with superconductors in heterostructures, in a quest for detecting and exposing topological superconductivity.

Recent Progress

The layered compound Fe_3GaTe_2 is attracting attention due to its high Curie temperature, low dimensionality, and the presence of topological spin textures above room temperature, making Fe_3GaTe_2 a good candidate for applications in spintronics. Here, we show, through transmission electron microscopy (TEM) techniques, that Fe_3GaTe_2 single crystals break local inversion symmetry (**Fig. 1**) while maintaining global inversion symmetry according to X-ray diffraction. Coupled to the observation of Néel skyrmions via Lorentz-TEM, our structural analysis provides a convincing explanation for their presence in centrosymmetric materials[1]. Magnetization measurements as a function of the temperature displays a sharp first-order thermodynamic phase-transition leading to a reduction in the magnetic moment (see, **Fig. 1**). This implies that the ground state of Fe_3GaTe_2 is globally ferrimagnetic and not a glassy magnetic state composed of ferrimagnetic, and ferromagnetic domains as previously claimed. Neutron diffraction studies indicate that the ferromagnetic to ferrimagnetic transition upon reducing the external magnetic field is associated with a change in the magnetic configuration/coupling between Fe1 and Fe2 moments. We observe a clear correlation between the hysteresis observed in both the skyrmion density and the magnetization of Fe_3GaTe_2. This indicates that its topological spin

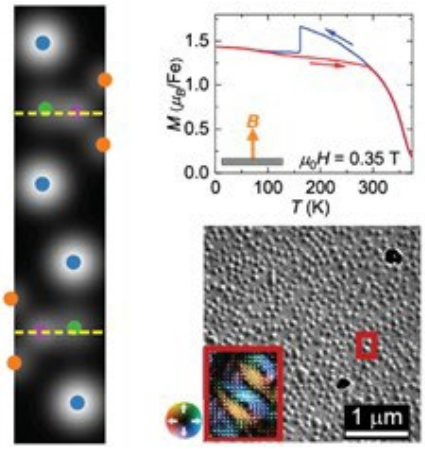


Fig. 1. Left: Average atomic positions for Fe1 (orange dot), Te (blue), Ga (purple) and Fe2 (green) as extracted from a transmission electron microscopy image containing ~ 1000 atoms. Notice that the Fe2 is displaced with respect to the mirror position between Te atoms. Top right: phase transition towards ferrimagnetism as observed in the magnetization. Bottom right: L-TEM image revealing Neel skyrmions at room T.

textures are affected by the development of ferrimagnetism upon cooling. Observation, via magnetic force microscopy, of magnetic bubbles at the magnetic phase boundary suggests skyrmions stabilized by the competition among magnetic phases and distinct exchange interactions. Our study provides an explanation for the observation of Néel skyrmions in centrosymmetric systems, while exposing a correlation between the distinct magnetic phases of Fe_3GaTe_2 and topological spin textures.

We have also exposed[2] the intrinsic nature of the anomalous Hall conductivity (AHC) in Fe_3GaTe_2 crystals characterized by high conductivities, which show disorder-independent AHC with a pronounced value $\sigma_{xy}^{c} \approx 420\ \Omega^{-1}\text{cm}^{-1}$. In the low-conductivity regime, we observe the scaling relation $\sigma_{xy} \propto \sigma_{xx}^{1.6}$, which crosses over to $\sigma_{xy} \cong \sigma_{xy}^{c}$ as σ_{xx} increases. Disorder in low-conductivity crystals is confirmed by the broadening of a first-order transition between ferromagnetism and the ferrimagnetic ground state. Through density functional theory (DFT) calculations, we reveal that the dominant sources of Berry curvature are located a few hundred meV below the Fermi energy around the Γ-point. Therefore, Fe_3GaTe_2 clearly exposes the disorder-induced crossover among distinct AHC regimes, previously inferred from measurements on different ferromagnets located on either side of the crossover region.

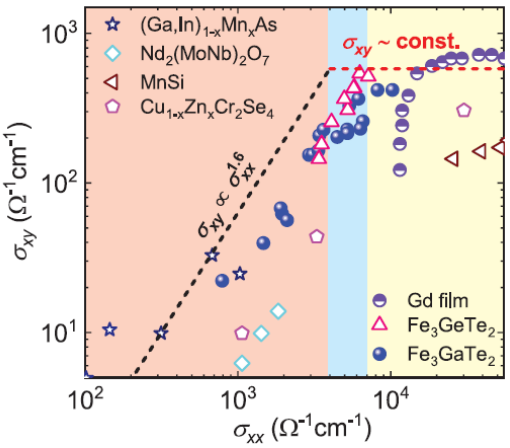


Fig. 2. Hall conductivity σ_{xy} as a function of the conductivity σ_{xx} in a magnified scale focusing on the dirty to moderately dirty and crossover regimes. Red, yellow, and blue shaded areas represent the dirty regime below $\sigma_{xy} = 4 \times 10^3\ \Omega^{-1}\text{cm}^{-1}$, the moderately dirty regime above $\sigma_{xy} = 7 \times 10^3\ \Omega^{-1}\text{cm}^{-1}$, and the intermediate or crossover regime between them, respectively.

Future Plans

We have synthesized the Co doped Fe_3GaTe_2 revealing an evolution from ferrimagnetism to antiferromagnetism as a function of Co concentration. This was already reported by other groups as we were collecting the data in our crystals. However, we found a pronounced anomalous Hall response when the system is driven to the spin polarized state. More importantly, the data also reveals behavior consistent with a pronounced topological Hall response occurring at remarkably large magnetic fields. Preliminary magnetic force microscopy measurements reveal the presence of complex magnetic domains as antiferromagnetism is suppressed by the external field, while revealing structures that seemingly are skyrmions under magnetic fields in the order of the tesla. Currently, we are transferring samples onto transmission electron microscopy (TEM) grids for subsequent Lorentz transmission electron microscopy studies under fields as high as 1 T in collaboration with Argonne. Our goal is to verify and confirm the presence of topological spin textures in the antiferromagnetic phase.

On the same token we are also preparing exfoliated samples of Fe_3GaTe_2 and $Fe_{5-x}GeTe_2$ to be transferred onto TEM grids containing pre-patterned electrical contacts for simultaneous transport and imaging. Our goal is multifold, study the evolution of the spin textures as functions of the crystal thickness, electrical currents, and perpendicular electrical field.

References

1. Sang-Eon Lee, Yue Li, Yeonkyu Lee, W. Kice Brown, Pei Yu, Gregory T. McCandless, Alex Moon, Lingrui Mei, Jaeyong Kim, Yan Xin, Julia Y. Chan, Elton J. G. Santos, Jeehoon Kim, Charudatta M. Phatak, Vadym Kulichenko, Luis Balicas, Ferrimagnetism, *Local Absence of Inversion Symmetry, and Distinct Topological Spin Textures in Fe_3GaTe_2*, ACS Nano (in press). DOI: 10.1021/acsnano.5c08312.
2. Sang-Eon Lee, Minkyu Park, W. Kice Brown, Vadym Kulichenko, Yan Xin, S. H. Rhim, Chanyong Hwang, Jaeyong Kim, Gregory T. McCandless, Julia Y. Chan, and Luis Balicas, *Disorder driven crossover between anomalous Hall regimes in $Fe_{3-x}GaTe_2$*, Phys. Rev. B **111**, 184438 (2025).

Publications

Put the list of publications in the recent 2-years SUPPORTED BY BES here. **If more than 10 publications, list only the 10 most relevant.**

1. A. Flessa-Savvidou, A. Ptok, G. Sharma, B. Casas, J. K. Clark, V. M. Li, M. Shatruk, S. Tewari and L. Balicas, *Anisotropic positive linear and sub-linear magnetoresistivity in the cubic type-II Dirac metal Pd_3In_7*, npj Quantum Mater. **8**, 68 (2023).
2. Mason Klemm, Shirin Mazaffari, Rui Zhang, Brian W. Casas, Alexei E. Koshelev, Ming Yi, Luis Balicas*, and Pengcheng Dai*, *Nematic superconductivity from selective orbital pairing in $Ba(Fe_{1-x}M_x)_2As_2$ (M = Co, Ni) single crystals*, Cell Rep. Phys. Sci **5**, 101816 (2024).
3. Alex Moon, Yue Li, Conor McKeever, Brian W. Casas, Moises Bravo, Wenkai Zheng, Juan Macy, Amanda K. Petford-Long, Gregory T. McCandless, Julia Y. Chan, Charudatta Phatak, Elton J. G. Santos, and Luis Balicas, *Writing and detecting topological charges in exfoliated $Fe_{5-x}GeTe_2$,* ACS Nano **18**, 4216–4228 (2024).
4. Md Shafayat Hossain, Qi Zhang, Eun Sang Choi, Danilo Ratkovski, Bernhard Lüscher, Yongkai Li, Yu-Xiao Jiang, Maksim Litskevich, Zi-Jia Cheng, Jia-Xin Yin, Tyler A. Cochran, Brian Casas, Byunghoon Kim, Xian Yang, Jinjin Liu, Yugui Yao, Alimamy F. Bangura, Zhiwei Wang, Mark H. Fischer, Titus Neupert, Luis Balicas, and M. Zahid Hasan, *Unconventional gapping behaviour in a kagome superconductor*, Nat. Phys. **21**, 556–563 (2025)
5. Sang-Eon Lee, Minkyu Park, W. Kice Brown, Vadym Kulichenko, Yan Xin, S. H. Rhim, Chanyong Hwang, Jaeyong Kim, Gregory T. McCandless, Julia Y. Chan, and Luis Balicas, *Disorder driven crossover between anomalous Hall regimes in $Fe_{3-x}GaTe_2$*, Phys. Rev. B **111**, 184438 (2025).
6. Shyam Raj Karullithod, Vadym Kulichenko, Mario A. Plata, Andrzej Ptok, Sang-Eon Lee, Gregory T. McCandless, Julia Y. Chan, and Luis Balicas, *Type-II Weyl nodes, flat bands, and evidence for a topological Hall-effect in the new ferromagnet $FeCr_3Te_6$*, Phys. Rev. Mater. **9**, 044203 (2025).
7. Y. Y. Wu, L. Balicas, R. Cheng, X.-X. Zhang, *Spin excitations and dynamics in 2D magnets: an overview on magnons and magnetic skyrmions*, Prog. in Quantum Electron. **100–101**, 100564 (2025).
8. Md Shafayat Hossain, Qi Zhang, David Graf, Mikel Iraola, Tobias Müller, Sougata Mardanya, Yi-Hsin Tu, Zhuangchai Lai, Martina O. Soldini, Siyuan Li, Yao Yao, Yu-Xiao Jiang, Zi-Jia Cheng, Maksim Litskevich, Brian Casas, Tyler A. Cochran, Xian P. Yang, Byunghoon Kim, Kenji Watanabe, Takashi Taniguchi, Sugata Chowdhury, Arun Bansil, Hua Zhang, Tay-Rong Chang, Mark H. Fischer, Titus Neupert, Luis Balicas, and M. Zahid Hasan, *Tunable superconductivity coexisting with the anomalous Hall effect in a transition metal dichalcogenide*, Nat. Commun. **16**, 2399 (2025).
9. Md Shafayat Hossain, Rajibul Islam, Zi-Jia Cheng, Zahir Muhammad, Qi Zhang, Zurab Guguchia, Jonas A. Krieger, Brian Casas, Yu-Xiao Jiang, Maksim Litskevich, Xian P. Yang, Byunghoon Kim, Tyler A. Cochran, Ilias E. Perakis, Thomas Hicken, Hubertus Luetkens, Fei Xue, Mehdi Kargarian, Weisheng Zhao, Luis Balicas, and M. Zahid Hasan, Superconductivity and a van Hove singularity confined to the surface of a topological semimetal, Nat. Commun. **16**, 3998 (2025).
10. Sang-Eon Lee, Yue Li, Yeonkyu Lee, W. Kice Brown, Pei Yu, Gregory T. McCandless, Alex Moon, Lingrui Mei, Jaeyong Kim, Yan Xin, Julia Y. Chan, Elton J. G. Santos, Jeehoon Kim, Charudatta M. Phatak, Vadym Kulichenko, Luis Balicas, *Ferrimagnetism, Local Absence of Inversion Symmetry, and Distinct Topological Spin Textures in Fe_3GaTe_2*, ACS Nano (in press). DOI: 10.1021/acsnano.5c08312.

Heterogeneous Integration of 2D-3D Materials for Energy Efficient Electronics

Nihar R. Pradhan1, Anirudha V. Sumant2, Jerzy Leszczynski1, Dinesh Kumar Sengottuvelu3, Mohammed Majdoub3, Sasan Nouranian3 and Ahmed Al-Ostaz[3]

[1] Jackson State University, Jackson, Mississippi, 39217, USA
[2] Argonne National Laboratory, 9700 South Cass Avenue, Lemont, Illinois 60439, USA
[3] University of Mississippi, Mississippi 38677, USA

Keywords: 2D and layered crystals, thin film heterostructures, Metal-Insulator transition, Phototransistor and 2D assembly

Research Scope

The integration of 0D, 2D and 3D materials has emerged as a promising avenue to develop innovative technological solutions with enhanced performance and reduced energy consumption in the semiconductor industry. Our objective in this project is to explore the understanding of interface science in hetero-integrated devices using multi-dimensional materials systems and how these interfaces work to develop design rules that governs the different functionality of the devices with unprecedented properties.

Recent Progress:

We explored the efficient charge transfer mechanism in 0D WS_2 QDs/2D MoS_2 heterostructure using photoconductivity measurements by fabricating the heterostructure of 0D WS_2 QDs/2D MoS_2 phototransistor[1,2]. Theoretical DFT study explained physics of enhanced photoresponse. The 0D WS_2 QDs/2D MoS_2 heterostructure shows extremely high charge transfer capability compared to the 2D pristine materials under the influence of white light source. Metal-to-insulator phase transition was explored on few layered of $MoSe_2$ FETs with Co and Cr contacts. Co-contact $MoSe_2$ shows 2D percolative phase transition at extended temperature range while Cr-contact $MoSe_2$ devices deviate below 100K[3]. We explored the high current density and high temperature P-N junction devices using 2D/3D heterostructure of single layer MoS_2-diamond P-N junction heterostructure devices[4]. The measurement shows extremely high current density without degrading till 250°C. We explored the Photoluminescence and Raman Enhancement by Edge Plasmons in 2D $MnPS_3$ 2D flakes[5]. In addition, we explored the 2D/2D integration of polymer and 2D materials such as MXene and Mica to develop high energy density dielectric capacitor materials[6,8].

<u>Metal-to-Insulator Percolative Phase Transition in 2D $MoSe_2$ FETs and the effect of Contacts (*Nanoscale*, (2025),17, 3160-3169):</u>

The metal-to-insulator phase transition (MIT) in two-dimensional (2D) materials under the influence of a electric field has been studied as a function of metal contacts to understand the MIT through temperature-dependent electronic transport measurements by tuning the carrier density in $MoSe_2$ channel. We have examined this phenomenon using the conventional chromium (Cr) and ferromagnetic cobalt (Co) as two metal contacts. For both Cr and Co, our devices demonstrated an *n*-type behavior with a room-temperature field-effect mobility of 16 $cm^2V^{-1}s^{-1}$ for the device with Cr contacts and 92 $cm^2V^{-1}s^{-1}$, for Co contact. At low temperature measurements of 50K, the mobilities increased significantly to 65 $cm^2V^{-1}s^{-1}$ for Cr and 394 $cm^2V^{-1}s^{-1}$ for the device with Co contacts. By fitting our experimental data to the percolative phase transition theory, the temperature-dependent conductivity data shows a transition from an insulating-to-metallic

behavior at a bias of ~28 V for Cr contacts and ~20 V for Co contacts. By extracting the critical exponents, we find that the transport behavior in Co-$MoSe_2$ devices aligns closely with the 2D percolation theory throughout the temperature measured from room to 2K. In contrast, the devices with Cr-contacted $MoSe_2$ deviates significantly from the 2D limit at low temperatures

We measure four-terminal temperature dependent conductivity at several applied gate bias, using back gate geometry to tune the carrier density in the channel. The extracted field-effect mobilities as a function of temperature for Cr- and Co- contacted devices which shows Co-$MoSe_2$ has higher mobility than Co-$MoSe_2$ devices. Such a difference in mobility for the Co-contacted $MoSe_2$ device demonstrates the significance of using a suitable contact with a high charge injection capacity. Furthermore, cobalt is ferromagnetic and spin current injection could be another factor that could potentially lead to a reduction in scattering mechanisms through spin-orbit coupling, thereby indirectly enhancing mobility by mitigating certain types of electrons scattering events in the Co-$MoSe_2$ device. Figure 1 displays a temperature-dependent conductivities of the Cr- and Co-contacted $MoSe_2$ devices. The quantized conductivity (σ) was calculated from the temperature dependent I_{ds} vs V_{bg} data using the relation, $\sigma = \frac{WI_{ds}}{lV_{ds}} \times \frac{e^2}{h}$, where e is the charge of the electron and h is Planck's constant. This device showed typically semiconducting behavior below $V_g = 27.5$ V, i.e., s decreased with decreasing temperature. Conversely, above the applied gate voltage of 27.5 V, the device showed metallic behavior, i.e., s increased with decreasing temperature. This infers that, upon injecting a high carrier density, the metallic phase emerged from the insulating phase at low temperature. We also performed the similar T-dependent conductivity analysis for the Co-contacted device at different gate voltages (5.1 V to 45 V) as depicted in Figure 1(b). In this case, the transition from metallic to insulating behavior was observed at a comparatively lower back gate voltage of 20.1 V. According to the Fermi-liquid model of conductors, the resistivity ($\rho = \sigma^{-1}$) is related to temperature through the relation $\rho = \rho_0 + AT^2$, where ρ_0 is the resistivity at 0 K. To verify the metallic behavior at higher gate voltages, we evaluated the resistivity of the channel as a function of temperature. Figure 1(c & d) shows the resistivity of Cr- and Co-contacted $MoSe_2$ at an applied backgated voltage, $V_{bg} = 45$ V, and $V_{bg} = 65$ V respectively. In both cases, the data fits the fermi-liquid equation well, as indicated by the red-line of the plot. This theoretical fitting shows the benchmark of metallic behavior of the $MoSe_2$.

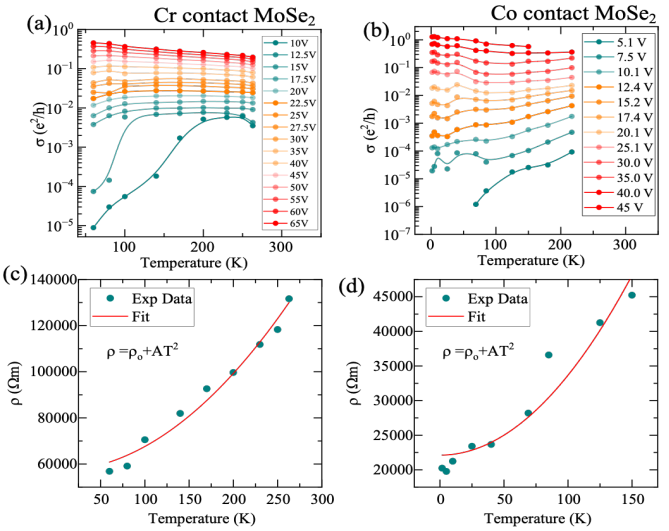


Figure. 1 (a-b) T-dependent conductivity at different back-gate voltage for Cr contacts and Co contacts, (c-d) Fermi-liquid model fitting of resistivity at a back-gate voltage of 20V, for Cr contacts and Co contacts.

We analyzed the temperature-dependent conductivities with the percolation model. The temperature-scaled percolation model formulates the relation between conductivity (s) and the carrier density (n) as $\sigma = A(n - n_c)^{\delta}$, where, n_c is the critical carrier density beyond which the carriers can form a percolating path in the random network of charged carriers between the source and the drain. From the theoretical predictions, $\delta = 1.33$ for 2D percolation. The induced carriers was obtained from the relation $n = C_{ox} \times V_{bg}/e$, hence the percolation prediction for the conductivity can be written in terms of V_{bg} as $\sigma = (A \times C_{ox}/e)(V_{bg} - V_c)^{\delta}$, where V_c is the critical back gate voltage. For Cr contacts, the critical exponent almost lies between 1.33 to 1.4, which is the theoretical predicted value of 2D percolation phase transition, δ = 1.33. The δ value deviated from the theoretical prediction when the device was cooled below 100 K reaching 1.63 at 61 K. For Co-contact device, δ = 1.33-1.4 almost all the temperature measured. For Cr-contacts, the critical carrier density (n_c) showed a slight increase with decreasing temperature while the Co-contacted device showed almost temperature independent carrier density. For Cr contacts we obtained the average critical carrier density n_c ~1×10^{12} cm^{-2} (dashed line in Fig 2a). In contrast, a higher n_c of ~2×10^{12} cm^{-2} was achieved in the Co-contacted $MoSe_2$ FET.

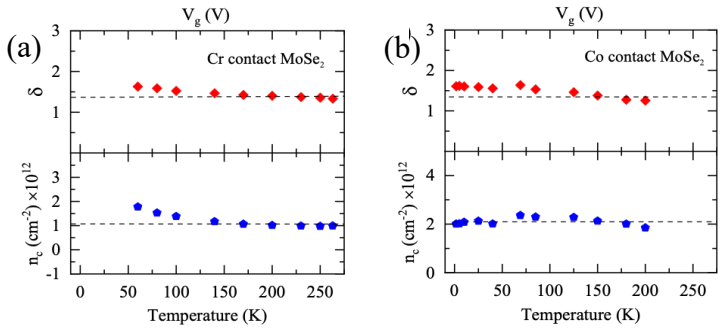


Figure. 2 Extracted critical exponent and carrier density from Percolation type phase transition model

<u>A 2D/3D Heterostructure Diode Based On n-type MoS_2 Integrated with p-type Diamond (*Nano Letter,* (in review, 2025)</u>

Diamond is a highly promising semiconductor material for power electronics due to its exceptional properties, including high breakdown strength, excellent carrier mobility, and superior thermal conductivity. In this context, n-type two-dimensional (2D) materials can offer interesting solutions. Here, we have demonstrated an ultra-thin *PN* junction device by combining monolayer molybdenum disulfide (MoS_2) with three-dimensional (3D) Boron doped single crystal diamond (SCD) and polycrystalline diamond (PCD) substrates. The choice of utilizing MoS_2 as the *n*-type material is attributed to its superior maturity amongst 2D materials. We find that the as fabricated diodes show excellent room temperature rectification and achieve an impressive current density (J_D) of 1132 A/cm^2, a high rectification ratio (RR) of ~7×10^5 and an ideality factor (η) value of 4.8 at room temperature (RT). An annealing step at 250℃ under high vacuum was found to improve the diode performance and yielded a $J_D \sim 4000\ A/cm^2$, a $RR \sim 10^6$ and $\eta \sim$ 3.7. **Figure 3(c-d)** illustrate the current voltage $(I - V)$ characteristics of the diode where the diode current (I_D) is plotted against applied voltage bias (V_A) in logarithmic and linear scale, respectively.

On examining the $I-V$ curves, the diode clearly exhibits excellent rectification at room temperature, as indicated by the strong current modulation between negative (reverse bias) and positive (forward bias) voltage values. To confirm that the rectification truly arises due to 2D/3D heterointegration, we fabricated contacts on the *p*-SCD prior to the MoS_2 transfer. The turn on voltage (V_T), determined by finding the x-intercept of the slope of the line fitted to I_D values in the linear regime was found to be $\sim 3.6\,V$. The maximum forward current density $\left(J_D = {}^{I_D}/_{A}\right)$, extracted for I_D of $0.32\,mA$ at V_A of $6\,V$ with the junction area $(A = 2.82 \times 10^{-7}\,cm^2)$ was found to be $\sim\ 1132\,A/cm^2$, which exceeds the values obtained for other 2D/3D heterojunction diodes. In addition, the diode demonstrated low reverse current of $1.23 \times 10^{-9}\,A$ at a reverse V_A of $-6\,V$. The rectification ratio (RR), defined as the ratio of I_D values at similar forward $(6\,V)$ and reverse voltage $(-6\,V)$ value was found to be $\sim 7 \times 10^5$. Finally, the ideality factor (η), extracted from the logarithmic scale plots for a small forward bias range $(0.9\,V - 1.5\,V)$ was found to be ~ 4.8 by fitting the experimental data to the Schottky diode equation.

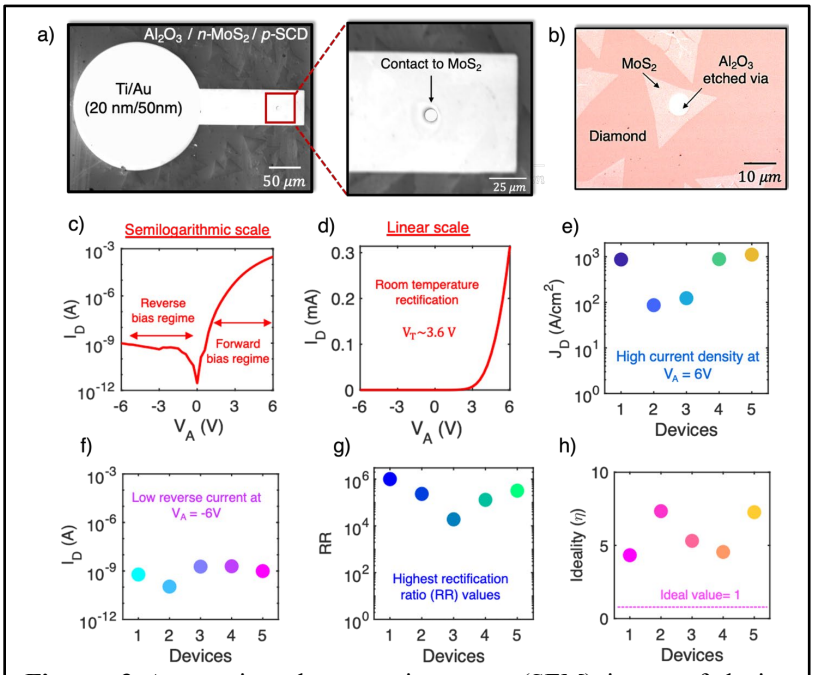


Figure. 3 A scanning electron microscopy (SEM) image of device features with top electrode which has point of contact to the monolayer n-MoS_2 flake through the Al_2O_3 etched vias. b) An optical image of a representative monolayer MoS_2 flake. Current voltage $(I - V)$ characteristics in c) logarithmic and d) linear scale measured at room temperature. e) Current density (J_D), f) Reverse current, g) Rectification ratio (RR), and h) Ideality factor (η) extracted for a total of five diodes of our MoS2/SCD heterostructure diode.

Future Plans:

We have plan to explore MIT properties using 2D metal contacts such as low band gap $PdSe_2$ or $PtSe_2$ contacts on n-$MoSe_2$ and p-WSe_2 to explored phase transition properties. This will extend to magnetic field assisted Phase transition and how it plays to define the critical exponents and whether this can explore the Quantum Hall Phase transition. Planned to explore 2D/Diamond heterostructure P-N junction in elevated temperature. We will extend our 0D WS_2 QDs/MoS_2 ultra high phototransistor to different 2D materials and QDs to understand the charge transfer mechanism. We recently explored high IR photoconductivity in low bandgap materials $PdSe_2$ which shows R~1mA/W at λ=1650 nm. Our aim to explore the IR photoconductivity to deep IR region with suitable heterostructure using $PdSe_2$,

A DFT and phonon transport studies will be carried out simultaneously to understand the thermal transport behavior of these hetero integrated systems, which is one of the crucial parameters to develop energy efficient electronics.

Publications

1. Dineshkumar Sengottuvelu, Mohammed Majdoub, Pabitra Narayan Samanta, Roshan Padhan, Akshay Wali, Anirudha V. Sumant, Nihar R. Pradhan, Shan Yang, Devashis Majumdar, Jerzy Leszczynski, Sasan Nouranian, Ahmed Al-Ostaz, "*Unraveling the Mechanism of Interfacial Charge Transfer and Photoresponsivity of WS_2 Quantum Dots/MoS_2 (0D-2D) Heterostructure-Based Transistor*", *ACS Applied Materials and Interfaces,* 2025 (Accepted)
2. Pabitra Narayan Samanta, Devashis Majumdar, and Jerzy Leszczynski, Rationalizing Linear and Nonlinear Optical Properties of Few-Layer Graphene−WSe_2 Heterostructures, ***ACS Appl. Electron. Mater.*** (2025), 7, 9, 3810–3827, https://doi.org/10.1021/acsaelm.5c00102
3. Roshan Padhan, Carlos Garcia, Ralu Divan, Anirudha V. Sumant, Daniel Rosenmann, Sujit A. Kadam, Akshay Wali, Suzanne Miller, Stephen McGill and Nihar R Pradhan, Percolation phase transition in few layered MoSe2 Field effect transistors using Co and Cr contacts. ***Nanoscale*** (**2025**),17, 3160-3169. https://doi.org/10.1039/D4NR03986F
4. A. Wali et al. A 2D/3D Heterostructure Diode Based On N-Type MoS2 Integrated with P-Type Diamond (Submitted2025) (In 2nd Review, Nano Letter, 2025)
5. Arup Barua, Matthew Cothrine, Sean Knapp, Shirin Mozaffari, Nihar Pradhan, David Mandrus, Denis Karaiskaj, and Dmitri V. Voronine, "Photoluminescence and Raman Enhancement by Edge Plasmons in 2D MnPS3", ***Journal of Physical Chemistry C*** (**2024**) (https://doi.org/10.1021/acs.jpcc.4c00810)
6. James FitzPatrick, Sumit Bera, Alex Inman, Alessandra Cabrera, Teng Zhang, Tetiana Parker, Bita Soltan Mohammadlou, Iryna Roslyk, Stefano Ippolito, Kateryna Shevchuk, Sujit A. Kadam, Nihar R. Pradhan*, Yury Gogotsi*, Record Efficiency of β-Phase PVDF-MXene Composites in Thin Film Dielectric Capacitors, ***Advanced Materials*** (**2025**) https://doi.org/10.1002/adma.202419088
7. Sujit Anil Kadam, Dhayanantha Prabu Jaihindh, Yan-Ruei Chen, Komal Prakash Kadam, Hao-Wei Hsieh, Sumit Bera, Santosh KC, Anirudha V. Sumant, Yen-Pei Fu, Chien-Chih Lai, Yuan-Ron Ma, Nihar Ranjan Pradhan, Ferromagnetic hybrid 2D FeS/FeS2 nanostructures as effective electrocatalysts for next generation electrochemical hydrogen evolution reaction, ***ACS Appl. Nano Mater.*** (**2024**), 7, 23, 27566–27578
8. Sumit Bera, Rukshan M. Thantirige, Sujit A Kadam, Anirudha V. Sumant and Nihar R. Pradhan, High Density Capacitive Energy Storage in Low Dielectric constant Polymer PMMA-2D Mica Nanofillers Heterostructure Composite, ***Molecules*** (**2024**) (doi.org/10.3390/molecules29194671)
9. Mohammed Majdoub, Dineshkumar Sengottuvelu, Sasan Nouranian, Ahmed Al-Ostaz, "Graphitic Carbon Nitride Quantum Dots (g-C 3 N 4 QDs): From Chemistry to Applications", ***ChemSusChem***,(**2024**). (DOI:https://doi.org/10.1002/cssc.202301462)
10. Sujit Kadam, Komal Prakash Kadam and Nihar Ranjan Pradhan, "Advancements in 2D MXene-Based Supercapacitor Electrodes: Synthesis, Mechanisms, Electronic Structure Engineering, Flexible Wearable Energy Storage for Real-World Applications, and Future Prospects", ***Journal of Materials Chemistry A.*** (**2024**) https://doi.org/10.1039/D4TA00328D

Influence of Dimensional Confinement at the Metal-Layered Crystal Interface

Andrew Stollenwerk (PI), Paul Shand (co-PI), Pavel Lukashev (co-PI)

University of Northern Iowa

Rui He (sub-award PI)

Texas Tech University

Keywords: layered crystal, metal thin film deposition, electrical transport, Raman spectroscopy, 2D magnetism

Research Scope

In this project, the PIs at the University of Northern Iowa (UNI) lead the fabrication efforts of samples as well as characterization of their physical and electronic properties. The subaward PI at Texas Tech University (TTU) focuses on optical studies of the physical properties of the samples made by the UNI team.

Our first goal is to explore magnetic features in the Ni/MoS_2 heterostructure system. Unlike noble metals, reactive species like Ni or Co form nanometer scale clusters with no evidence of quantization. At low temperatures, films of these magnetic metals deposited onto MoS_2 behave like standard disordered ferromagnets. However, at room temperature and above, the behavior is quite different. Spin glass effects can be seen in magnetization and magnetoresistance measurements which show memory and relaxation effects spanning several hours. Room temperature magnetoresistance measurements show an astonishingly large asymmetry, exceeding 9T. As with the magnetization measurements, magnetoresistance measurements at low temperature are quite normal and appear typical for a film with nanometer scale grains. Given the fact that we find no evidence for such behavior in bulk or thin Ni films, and that bulk MoS_2 has no significant magnetic features, we believe these behaviors arise from interactions at the interface. We believe that these effects are not unique to Ni on MoS_2 and could serve in the development and understanding of spin valves or other spintronic applications such as emergent topological spin textures.

Our second goal is to probe the interface effect at metal thin film-van der Waals magnet interfaces to explore the possibility of using metal thin films to tune the magnetic states of van der Waals magnets, which are potential candidates for ultracompact data storage and spintronic applications. In the large family of van der Waals magnets, chromium triiodide (CrI_3) is the first that has been shown to display ferromagnetic (FM) order in its monolayer limit. In the few-layer form, CrI_3 exhibits intralayer FM and interlayer antiferromagnetism (AFM), which makes it especially interesting for studies of fundamental properties and spintronic device applications. In this project,

we explore the possibility of using a thin film of Ni to tune the magnetic properties of CrI_3. A thin layer of Ni is deposited on a freshly cleaved CrI_3 surface to form a high-quality Ni/CrI_3 heterointerface. Magneto-Raman spectroscopy at low temperature is used to probe the magnetic properties of the heterostructure. This study not only helps in understanding the fundamental properties of van der Waals magnet-metal contacts but also investigates a new venue for modulating the spin degree of freedom in van der Waals magnets.

Recent Progress

We investigated the magnetic properties of Ni/MoS_2 interfaces to explore their potential for use in spintronic devices.[1] The relaxation rate was greater in samples where MoS_2 was annealed at 300°C before Ni deposition compared to unannealed samples (Fig. 1(a)). Annealed samples showed highly ordered interfaces as seen in Figs. 1(b) and (c), while unannealed ones exhibited a mix of ordered and disordered regions. This suggests that glassy behavior may arise from the effects of disorder at both the interface and within the Ni film.

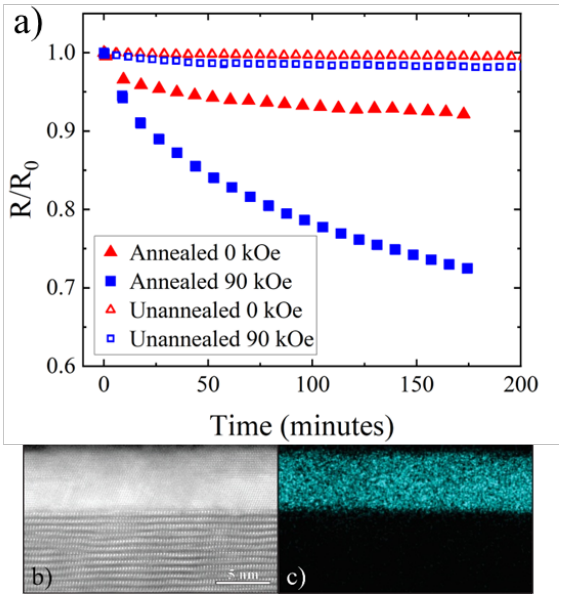


Figure 9. a) Magnetoresistance at 330 K as a function of time at the interface of thin film Ni on annealed and unannealed MoS_2; b) Cross-sectional TEM image of the Ni film on annealed MoS_2; c) The corresponding EDX mapping of the Ni film on annealed MoS_2.

We conducted STM studies of Cu on MoS_2 and found strong evidence of quantum growth.[2] Three preferred heights were observed with an average spacing of approximately 0.7 nm. These results were compared to nesting vectors in bulk Cu. The nesting vectors found in the Fermi surface of bulk Cu suggest we should observe preferred heights with a periodic spacing of approximately 1.0 nm. This is close to our experimental results. We believe that the differences are due to that fact the Fermi surface of our Cu films is slightly different from that of bulk Cu. DFT calculations of Cu slabs a few atomic layers thick were performed. These results were expected to be closer than the bulk analysis. These calculations showed an oscillation in the DOS at the Fermi level that was approximately 0.8 nm, significantly closer to our experimental results.

We performed DFT calculations on Au, Ag, Cu, and Ni on MoS_2.[3] Among these elements, Ni exhibits the strongest binding and lowest mobility on the surface of MoS_2. On the other hand, Au and Ag bond very weakly to the surface and have very high mobilities. High mobilities in this case are synonymous with the adatoms having multiple lowest energy configurations at room temperature. Our calculations for Cu show that its bonding and surface mobility are between these two groups. We are still in the process of exploring other materials such as platinum.

We probed the spin wave properties of Ni on bulk CrI_3 using magneto-Raman spectroscopy. Using ultralow frequency (Raman shift down to ~2.5 cm^{-1} or ~0.3 meV) magneto-Raman spectroscopy, we demonstrated that the AFM coupled surface layers of bulk CrI_3 transit into FM coupled layers after Ni deposition.[4] This is revealed by the absence of AFM spin wave branches in Raman spectra (Fig. 2(a)-(d)) from Ni/CrI_3. The spin wave mode from the FM state in Ni/CrI_3 displays a Zeeman shift as a function of an applied out-of-plane magnetic field, and the spin wave frequency is softened as compared to that in pristine CrI_3 (Fig. 2(d)).

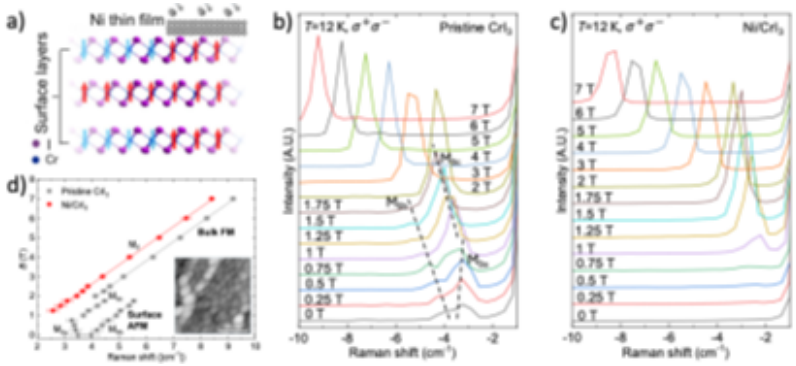


Figure 2. a) Schematic diagram of Ni thin film on CrI_3 crystal surface. b) Ultralow frequency Raman spectra from pristine CrI_3 crystal. The M_{0a} and M_{0b} branches are from surface AFM, and the M_{0c} branch is from bulk FM. c) Ultralow frequency Raman spectra of spin wave from CrI_3 crystal with a Ni thin film on surface. A single spin wave branch is observed. d) Zeeman shifts of spin wave modes from pristine CrI_3 and Ni/CrI_3. The inset shows an STM image of Ni deposited on CrI_3. Taken from the PIs' work, Ref. [4].

We studied Ni thin film on monolayer MoS_2. The deposition of Ni thin film (4-nm-thick) tuned the electronic structure of pristine MoS_2 so that the *A* exciton perfectly overlapped with the 633 nm laser photon energy. The optimization of resonance excitation led to pronounced tunability of the orbital-phonon hybridized states. As a result, the orbital transition mode is enhanced by a factor of 12 and shifts toward low frequency by about 6 cm^{-1} compared with that in pristine MoS_2 without Ni deposition. Both the Raman intensity enhancement and the frequency shift of the orbital transition Raman mode indicate that the Ni thin film has modified the electronic properties of MoS_2. Concurrently, the circularly polarized phonon (chiral phonon) mode red-shifts by nearly the same amount, confirming that the orbital transition and circularly polarized phonon are indeed coupled to each other.[5]

Future Plans

The discovery of spin glass behavior at the interface of the Ni/MoS_2 system was unexpected but also an excellent opportunity to study disordered magnetism in a 2D system. We plan to further investigate the role of the interface on the spin glass behavior. To do this, we plan to cover the MoS_2 with Au and Ni, each covering roughly 50% of the surface. Any chances to the spin glass effect would then be due to the reduced interaction between Ni and MoS_2. The interesting properties of thin metal films on MoS_2 have provided us with interesting data in a 2D disordered magnetic system. We hope to expand on our understanding by exploring other thin films such as Co and Fe beginning in the fall semester of 2025.

We plan to use magneto-Raman spectroscopy to probe the magnetic properties of bulk CrSBr with a thin layer of Ni on surface in a similar way as we did for Ni/CrI_3. CrSBr is a new van der Waals

magnet material and is air-stable and easier to handle compared to CrI_3. CrSBr crystal is highly anisotropic with its physical properties mainly of quasi-1D character. We will use ultralow frequency Raman techniques to study the spin wave properties when the magnetic field is applied along the *a*, *b*, and *c* crystalline axes. Our preliminary data have shown that by applying a moderate magnetic field of about 3 T along the *b* axis, we can stabilize the spin waves even at room temperature in pristine CrSBr which has a T_c of about 160 K. We intend to perform the same measurements on Ni/CrSBr to see if the Ni thin film would change the spin wave behaviors. The fact that CrSBr is stable and forms long-range magnetic order in the ambient condition, evidenced by the presence of spin wave modes at room temperature, makes it a very promising material for spintronic device applications.

Using optical emission and Raman spectroscopy, we plan to study the changes of the exciton photoluminescence band and circularly polarized phonon mode in monolayer MoS_2 after deposition of a thin layer of Fe on the surface. We will compare the results from Fe thin film on monolayer MoS_2 with those from two similar systems: 1) Ni/monolayer MoS_2 that we have studied; 2) Fe-doped monolayer MoS_2 in which the Fe atoms are in the lattice of MoS_2. Our preliminary data and theoretical calculations have shown that Fe-doping introduces a localized Fe band underneath the conduction band of MoS_2. As a result, an additional orbital transition between the Mo 4d and Fe 3d states emerges, producing a new orbital-phonon hybridized mode at 283 cm^{-1} in our Raman spectra. Under an external magnetic field, this new mode exhibits a large Zeeman splitting, which corresponds to an effective magnetic moment of ~2.8 μ_B. We intend to perform similar measurements on monolayer MoS_2 with an Fe thin film overlayer. This study will help us understand how the electronic structure of metallic and magnetic overlayers/dopants affect the orbital-lattice coupling in transition metal dichalcogenides.

References

1. P.M. Shand, Y. Moua, H. Harms, C. Cunningham, P.V. Lukashev, T.E. Kidd, and A.J. Stollenwerk, *Hopping crossover and high-temperature superspin glass behavior in Ni films deposited on MoS_2,* Physical Review B **109** 245432 (2024).

2. H. A. Harms, C. J. Cunningham, T. E. Kidd, and A. J. Stollenwerk, *Surface dependence of electronic growth of Cu(111) on MoS_2,* Applied Physics Letters **125** 081604 (2024).

3. H. A. Harms, A. J. Stollenwerk, C. J. Cunningham, E. O'Leary, T. E. Kidd, and P.V. Lukashev, *Adsorption of Ag, Au, Cu, and Ni on MoS_2: theory and experiment*, Journal of Physics: Condensed Matter **37** 015001 (2024).

4. C. Nnokwe, C. J. Cunningham, W. Liu, G. Ye, T. Nguyen, K. Wu, C. M. Hemesath, C. Sadler, P. V. Lukashev, Z. Zhai, B. Lv, J. Yan, P. M. Shand, A. J. Stollenwerk, and R. He, *Tuning the Magnetic Properties of CrI_3 Using Ni Thin Film Deposition for Applications in Spintronic Devices*, ACS Applied Nano Materials **8** 2412 (2025).

5. H. Mustafa, C. Nnokwe, G. Ye, M. Fang, S. Chaudhary, J. Yan, K. Wu, C. J. Cunningham, C. M. Hemesath*, A. J. Stollenwerk, P. M. Shand, E.Yang, G. A. Fiete. R. He, and W. Jin, *Origin of Large Effective Phonon Magnetic Moments in Monolayer MoS_2*, ACS Nano **19** 11241 (2025).

Publications

1. H. Mustafa, G. Ye, C. Nnokwe, M. Fang, M. Kandil, A. Al-Mahboob, K. Wu, A. J. Stollenwerk, T.E. Kidd, P. M. Shand, J. T. Sadowski, E.-H. Yang, Y. Zhou, R. He, and W. Jin, *Dilute Magnetic Impurity-Induced Effective Phonon Magnetic Moment in Fe-Doped Monolayer MoS_2*, 2D Materials (under review) (2025).

2. J. Choe, D. Lujan, G. Ye, C. Nnokwe, B. Ma, J. He, F.Y. Gao, T. N. Nunley, A. Leonardo, M. Arruabarrena, A. Ayuela, J. Zhou, M. Rodriguez-Vega, G.A. Fiete, R. He., and X. Li, *Long-lived zone-boundary magnons in an antiferromagnet*, Nature Communications **16**, 5486 (2025).

3. L. Chen, G. Ye, C. Nnokwe, X.-C. Pan, K. Tanigaki, G. Chen, Y. P. Chen, J. Yan, D.G. Mandrus, A.E. Llacsahuanga Allcca, N. Giles-Donovan, R.J. Birgeneau, and R. He, *Spontaneously formed phonon frequency combs in van der Waals solid $CrGeTe_3$ and $CrSiTe_3$*, Nature Communications **16**, 5795 (2025).

4. C. Sadler, J. Yan, A. J. Stollenwerk, P. M. Shand, R. He, and P.V. Lukashev, *Effect of Ni deposition on CrI_3 monolayer: First-principles study*, Journal of Magnetism and Magnetic Materials **628**, 173176 (2025).

5. H. Mustafa, C. Nnokwe, G. Ye, M. Fang, S. Chaudhary, J.-A. Yan, K. Wu, C. J. Cunningham, C. M. Hemesath, A. J. Stollenwerk, P. M. Shand, E.-H.Yang, G. A. Fiete. R. He, and W. Jin, *Origin of Large Effective Phonon Magnetic Moments in Monolayer MoS_2*, ACS Nano **19,** 11241 (2025).

6. C. Nnokwe, C. J. Cunningham, W. Liu, G. Ye, T. Nguyen, K. Wu, C. Hemesath, C. Sadler, P. Lukashev, Z. Zhai, B. Lv, J.-A. Yan, P. M. Shand, A. J. Stollenwerk, and R. He, *Tuning the Magnetic Properties of CrI_3 Using Ni Thin Film Deposition for Applications in Spintronic Devices*, ACS Applied Nano Materials **8,** 2412 (2025).

7. H. Harms, A. J. Stollenwerk, C. Cunningham, C. Sadler, E. O'Leary, T. E. Kidd, and P.V. Lukashev, *Adsorption of Ag, Au, Cu, and Ni on MoS_2: theory and experiment*, Journal of Physics: Condensed Matter **37,** 015001 (2025).

8. H. A. Harms, C. J. Cunningham, T. E. Kidd, and A. J. Stollenwerk, *Surface dependence of electronic growth of Cu(111) on MoS_2*, Applied Physics Letters **125**, 081604 (2024).

9. P. M. Shand, Y. Moua, H. Harms, C. Gorgen, C. J. Cunningham, P.V. Lukashev, T.E. Kidd, and A.J. Stollenwerk, *Hopping crossover and high-temperature superspin glass behavior in Ni film deposited on MoS_2*, Physical Review B **109,** 245432 (2024).

10. P. V. Lukashev, T. E. Kidd, H. A. Harms, C. Gorgen, and A. J. Stollenwerk, *Natural formation of linear defect structures in MoS_2*, Applied Physics Letters **124,** 083103 (2024).

Electrical Switching and Antiferromagnetic Domain Imaging of $LaFeO_3$ Epitaxial Thin Films

Principle Investigator: *Fengyuan Yang*
Affiliation: Department of Physics, The Ohio State University, Columbus, OH 43210

Keywords: antiferromagnetic perovskite, epitaxial $LaFeO_3$ thin films, electrical switching, XMLD-PEEM domain imaging, biaxial anisotropy

Research Scope:

The goal of this DOE project is to control antiferromagnetic (AFM) spins using a multipronged approach including spin-orbit torques, magneto-elastic and magneto-electric effects in AFM and multiferroic epitaxial films. AFMs offer intrinsic advantages over their ferromagnetic (FM) counterparts with low damping, ultrafast speed, terahertz dynamics, and abundancy of materials. In this project, we investigate electrical switching of AFM insulator films at both quasi-DC and fast timescales. The AFM materials of interest to this project include simple binary oxides, such as NiO and α-Fe_2O_3, as well we complex oxides, in particular, AFM perovskites such as $LaFeO_3$ and other *RE*FeO_3 (*RE*: rare earth) antiferromagnets. Most of these AFMs have high Néel temperatures (T_N) and can be grown into high quality epitaxial thin films. In addition, some of these AFMs, such as α-Fe_2O_3 and $LaFeO_3$, have been predicted to be altermagnets, which due to a unique combination of spin and crystal symmetries, can generate orientation-dependent spin polarization. Exploration of altermagnetism in the predicted AFMs will be part of this research project for the coming year.

Recent Progress

The demonstration of electrical switching of the Néel vector in AFMs in recent years has been a major breakthrough in the field of spintronics. Practical AFM applications prefer AFMs with high T_N's and well-defined bi-stable states (e.g., two easy axes of Néel vector representing "0" and "1") separated by a robust hard axis, which should be strong enough for long-term information storage, but not too high for information writing. To date, electrical switching of AFM insulators has been mostly focused on a few binary oxides, which have their limitations, such as AFM anisotropy being too weak/strong or low T_N's. Thus, AFMs with moderate biaxial anisotropy and high T_N's are desired for AFM-based devices. In this regard, the large family of AFM perovskites are attractive but much less explored for AFM spintronics.

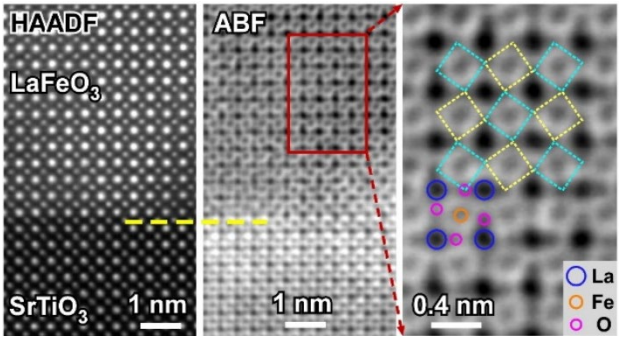


Figure 1. High-angle annular dark-field (HAADF) and annular bright-field (ABF) STEM images of a $LaFeO_3$ epitaxial film on $SrTiO_3$(001) viewed along the [100] direction with pristine ordering. The right panel shows the oxygen octahedra tilting in $LaFeO_3$.

Robust Biaxial AFM Anisotropy: Under primary support of this DOE grant, we have grown $LaFeO_3$ epitaxial thin films with pristine crystalline quality as shown in the scanning transmission electron microscopy (STEM) images in Fig. 1. Due to the fully strained epitaxy of $LaFeO_3$ on cubic $SrTiO_3$ (001) substrate, we observe a clear biaxial anisotropy in the $LaFeO_3$ films with a spin-flop field of 2-4 T, corresponding to a desired AFM anisotropy, which is stable at room temperature, but can be readily switched by an electrical pulse or magnetic field.

Figure 2 shows the angular dependence of transverse (ΔR_{xy}) and longitudinal (ΔR_{xx}) spin Hall magnetoresistance (SMR) for a Pt(3 nm)/$LaFeO_3$(3 nm) Hall bar at T = 25 K in an in-plane magnetic field ($\boldsymbol{H}$) of 0 to 14 T, where α is the angle between $\boldsymbol{H}$ and $SrTiO_3$ [100], with several notable features. First, ΔR_{xy} is flat at 0 and 1 T, indicating that the AFM spins are essentially unperturbed up to 1 T. In contrast, at 2 T, ΔR_{xy} becomes step-like with ~90°-wide plateaus, indicating a spin-flop transition.

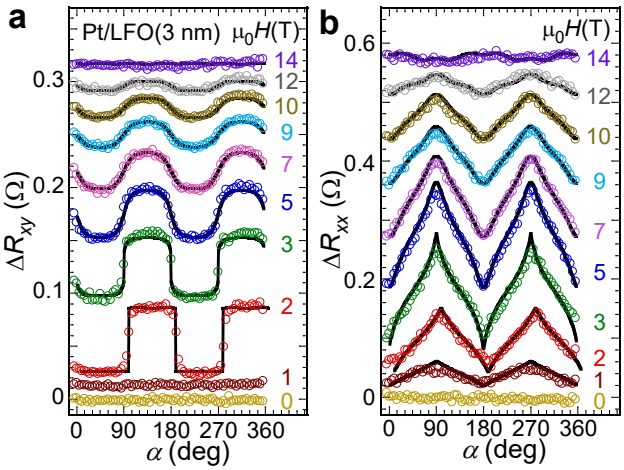


Figure 2. Angular dependencies of SMR. **a**, ΔR_{xy} and **b**, ΔR_{xx} for a Pt(3 nm)/$LaFeO_3$(3 nm) Hall bar at 25 K in an in-plane field of 0 to 14 T with the current channel along $SrTiO_3$ [100]. The solid curves are simulations which agree well with the experimental data.

Second, the square ΔR_{xy} in Fig. 2a at 2-3 T is uncommon for SMR in AFMs, which are mostly sinusoidal above the spin-flop transition. The square ΔR_{xy} indicates that the Néel vector ($\boldsymbol{n}$) strongly prefers to align along two orthogonal orientations: $\boldsymbol{n}$ || 45°/225° and -45°/135°, which correspond to two easy axes along $SrTiO_3$ [110] and [1$\bar{1}$0], respectively. These two preferred orientations can be detected by ΔR_{xy} with two discrete values with sharp switching near α = 90°, 180°, 270°, and 360°. At higher fields, ΔR_{xy} gradually evolves from square to sinusoidal shape with decreasing magnitude.

Third, ΔR_{xx} in Fig. 2b exhibits primarily a saw-tooth shape with fine features that evolve with field. The clear contrast of the ΔR_{xy} and ΔR_{xx} shapes arises from their dependencies on the Néel vector orientation: $\Delta R_{xy} \propto n_x n_y$ and $\Delta R_{xx} \propto n_y^2$ in a monodomain, which can be modeled by macrospin simulations. The free energy density for a two-sublattice AFM is,

$$\frac{E(\hat{m}_1,\hat{m}_2)}{M} = H_{ex}(\hat{m}_1 \cdot \hat{m}_2) - \boldsymbol{H} \cdot (\hat{m}_1 + \hat{m}_2) - D\hat{z} \cdot (\hat{m}_1 \times \hat{m}_2) + \frac{E_{an}}{M}, \quad (1)$$

where M is the sublattice magnetization, H_{ex} and D are the exchange and Dzyaloshinskii-moriya (DM) field, respectively. $\hat{m}_1$ and $\hat{m}_2$ are the normalized sublattice moments ($\boldsymbol{n} = (\hat{m}_1 - \hat{m}_2)/2$), which make an angle of φ_1 and φ_2, respectively, relative to $SrTiO_3$ [100] (Fig. 3a). E_{an} is the AFM anisotropy energy density. Assuming $\hat{m}_1$ and $\hat{m}_2$ lie in the xy plane, Eq. (1) can be rewritten,

$$\frac{E}{M} = H_{ex}\cos(\varphi_1 - \varphi_2) - H[\cos(\alpha - \varphi_1) + \cos(\alpha - \varphi_2)] - D\sin(\varphi_1 - \varphi_2) + \frac{H_a}{2}[\cos(4\varphi_1) + \cos(4\varphi_2)], \quad (2)$$

where H_a is the biaxial anisotropy field. $E(\varphi_1, \varphi_2)$ is then minimized to find the equilibrium φ_1 and φ_2, which are used to calculate the Néel vector orientation, $\varphi_n = (\varphi_1 + \varphi_2)/2 + \pi/2$. Finally, the SMR with current along $SrTiO_3$ [100] can be calculated by,

$$\Delta R_{xx} = A\frac{l}{w}[\cos(2\varphi_n) + (bH)\cos(2\alpha)],\ \Delta R_{xy} = A[\sin(2\varphi_n) + (bH)\sin(2\alpha)], \quad (3)$$

where A is a constant and $\frac{l}{w} = 4$ is the length/width aspect ratio of the Hall bar. The $(bH)\sin(2\alpha)$ term, where b is a constant, is introduced to account for the decreasing magnitude. For the simulations in Fig. 2, we use H_{ex} = 1,000 T, D = 2 T, H_a = 10 Oe, A = 0.035 Ω and b = 0.073 T^{-1}, which not only describe the shape and magnitude of ΔR_{xx} and ΔR_{xy} with excellent agreement, but

also reproduce the fine features and subtle curvatures, indicating that the model captures all the important mechanisms in Pt/$LaFeO_3$.

We pattern another Hall bar along $SrTiO_3$ [110] (easy axis) near the one along $SrTiO_3$[100] on the same bilayer (Fig. 3a). Figures 3b and 3c compare the SMR of the two Hall bars at 3 T, where the shapes of ΔR_{xy} and ΔR_{xx} for the two samples are switched, *i.e.*, Sample #[100] (blue) has *square* $\Delta R_{xy}^{\#[100]}$ and *saw-tooth* $\Delta R_{xx}^{\#[100]}$, while #[110] (red) has *saw-tooth* $\Delta R_{xy}^{\#[110]}$ and *square* $\Delta R_{xx}^{\#[110]}$. The SMR results for #[110] can also be accurately simulated by the same model by factoring in the 45° rotation, which explains the shape switch of ΔR_{xy} and ΔR_{xx} for the two samples.

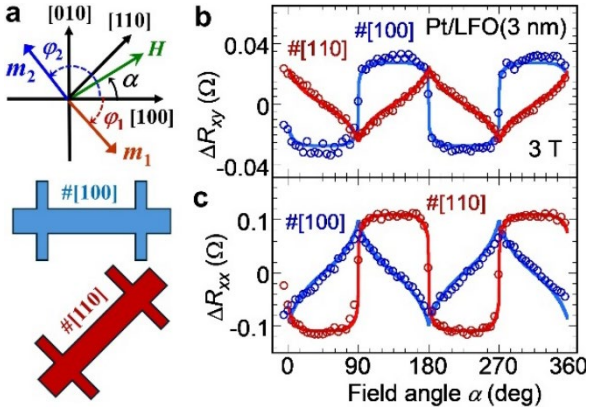


Figure 3. SMR with Hall channels along $SrTiO_3$ [100] and [110]. **a**, Schematic of Hall bars along [100] (hard axis) and [110] (easy axis). **b**, ΔR_{xy} and **c**, ΔR_{xx} for two Hall bars of a Pt(3 nm)/$LaFeO_3$(3 nm) bilayer in a 3 T field at 25 K with distinct square and triangular shapes. The simulations (solid curves) match well with the experimental data.

We also measured SMR for a Hall bar of a Pt(3 nm)/$LaFeO_3$(10 nm) bilayer, which exhibits robust biaxial anisotropy at room temperature. In addition, we performed the same measurement for Pt/$LaFeO_3$(t_{LFO}) bilayers with t_{LFO} = 1, and 2 nm at 25 K and 2 T. The 2-nm $LaFeO_3$ maintains a square shape, evidence of a robust biaxial anisotropy, while the 1-nm $LaFeO_3$ exhibits a small but clear negative SMR, indicating AFM ordering persists down to 1 nm $LaFeO_3$. This work was recently published in Nano Letters.[1]

Electrical Switching and Imaging: Under primary support of this DOE grant, we used the $LaFeO_3$ films with biaxial anisotropy for electrical pulse switching and AFM domain imaging. Figure 4a illustrates a Hall cross of a Pt(2 nm)/$LaFeO_3$(3 nm) bilayer with a channel width of 5.5 μm, which is rotated by 22.5° from the $SrTiO_3$ [100] axis for both electrical switching and SMR detection.[2]

We send electrical current pulses ($\mathbf{I_P}$) of 1-ms width and various current amplitude along Ch1 or Ch2 and detect ΔR_{xy} at 300 K (Fig. 4b). At a current density, $J_c = 6.82 \times 10^{11}$ A/m^2, we observe visible but inconsistent switching signals. The switching becomes much clearer, step-like plateaus at $J_c = 7.40 \times 10^{11}$ A/m^2 with a high SMR state along $\mathbf{I_P}$ || Ch1 and a low SMR state along $\mathbf{I_P}$ || Ch2. The reproducible step-like switching persists at higher current densities until 8.18×10^{11} A/m^2, where ΔR_{xy} becomes more sloped, which can be attributed to nonmagnetic changes in the Pt overlayer caused by the large current density. From the high/low SMR states, we note that the Néel vector tends to align perpendicular to the current pulse direction, which is opposite to the behavior observed in Pt/α-Fe_2O_3 and Pt/NiO.

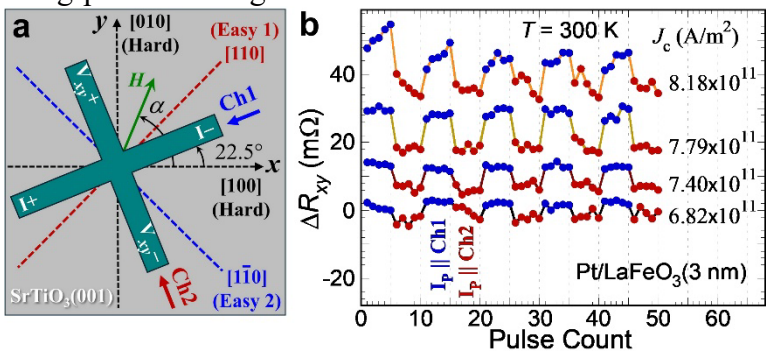


Figure 4. Electrical switching of Néel vectors. **a**, Schematic of a Hall cross oriented at 22.5° from both $SrTiO_3$ [100] (hard axis) and [110] (easy axis) to allow for AFM switching and AMR detection. **b**, Electrical pulse switching of a Pt(2 nm)/$LaFeO_3$(3 nm) device at various current densities sent alternatively along Ch1 or Ch2.

We image AFM domains in the $LaFeO_3$ films using X-ray Magnetic Linear Dichroism Photoemission

Electron Microscopy (XMLD-PEEM). Figure 5 shows room-temperature AFM domains of 3-nm and 10-nm $LaFeO_3$ films, where the AFM domain sizes of the 3-nm film are quite large (several to >10 μm), as compared to the sub-micron to a few μm domains for the 10-nm $LaFeO_3$. For electrical switching of a Pt(2 nm)/$LaFeO_3$(3 nm) bilayer, domain switching is visible at 5.0 mA, but only in some small areas (Fig. 6). As the current amplitude increases, larger and more domains are switched. In addition, current pulses along Ch1 result in more bright domains with the Néel vector along Easy 2 axis (see Fig. 4a), while current pulses along Ch2 yield more dark domains with the Néel vector along Easy 1 axis. This is consistent with the SMR result that the Néel vector tends to align perpendicular to the current pulse direction.

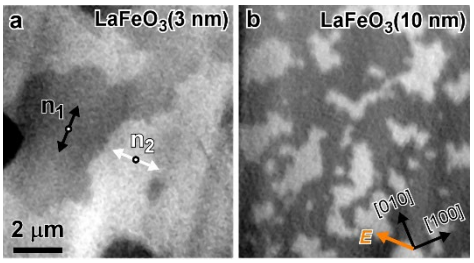


Figure 5. XMLD-PEEM images of AFM domains of **a**, Pt(2 nm)/$LaFeO_3$(3 nm) and **b**, Pt(2 nm)/$LaFeO_3$(10 nm) films.

This work offers the opportunity for electrical manipulation of epitaxial thin films of AFM perovskites with a large selection of AFM materials and highly tunable magnetic properties. In addition, this work provides a new materials platform for the exploration of the predicted insulating altermagnets such as $LaFeO_3$ and other AFM perovskites with spin-split bands. A manuscript[2] about this work will be submitted in August 2025.

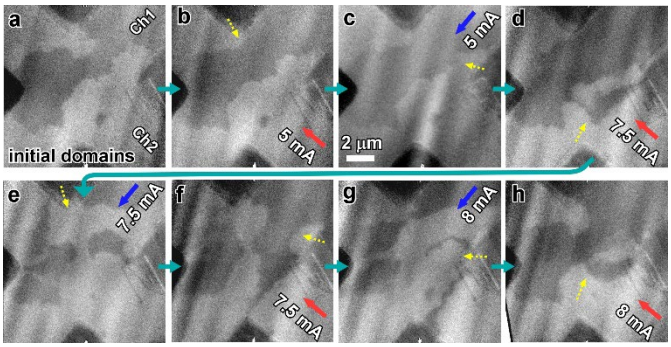


Figure 6. XMLD-PEEM images of electrical switching of AFM domains. **a**, Initial AFM domains of a Pt(2 nm)/$LaFeO_3$(3 nm) Hall cross, and AFM domains after an electrical pulse is sent along Ch1 or with a current of **b**, **c**, 5.0 mA (J_c = 4.5 × 10^{11} A/m^2), **d**, **e**, **f**, 7.5 mA (J_c = 6.8 × 10^{11} A/m^2), and **g**, **h**, 8.0 mA (J_c = 7.3 × 10^{11} A/m^2) at 300 K. Yellow arrows indicate domain changes.

Future Plans

In the coming year, we will investigate the microscopic origin and gain better control of the observed biaxial anisotropy in the $LaFeO_3$ epitaxial thin films (as compared to the uniaxial anisotropy in the bulk orthorhombic structure). Of particular interest is the nature and degrees of the pseudo-cubic lattice of the $LaFeO_3$ epitaxial thin films and their octahedral tilting and bond bending, which are essential for the emergence of the predicted altermagnetism in perovskite AFMs[3] such as $LaFeO_3$. Altermagnetism is an exciting new frontier[3] in condensed matter physics. While most of the research community is focused on conducting altermagnets because of the convenience of electrical detection, we will carry out an experimental investigation of the predicted altermagnetism in insulating AFMs, such as $LaFeO_3$ with sizable spin splitting of the electronic bands.[3] We will leverage our high-quality $LaFeO_3$ epitaxial films of a few nm thicknesses to explore novel heterostructures, in particular, all-perovskite tunnel junctions, to detect potential evidence of altermagnetism in AFM perovskites.

References

1. J. Lanier, J. Michel, J. Flores, and F. Y. Yang, *Robust Biaxial Anisotropy and Switchable Néel Vectors in $LaFeO_3$ Epitaxial Films*, Nano Lett. **25**, 4667 (2025).
2. J. Lanier, J. Michel, D. Russel, B. Liu, F. Kronast, B. Achinuq, J. Hwang, F. Yang, *Electrical Switching and Imaging of Antiferromagnetic Spins in Perovskite Epitaxial Thin Films*, to be submitted.
3. L. Šmejkal, J. Sinova and T. Jungwirth, *Emerging Research Landscape of Altermagnetism*, Phys. Rev. X **12**, 040501 (2022).

Publications (2023-2025)

1. J. Lanier, J. Michel, D. Russel, B. Liu, F. Kronast, B. Achinuq, J. Hwang, F. Yang, *Electrical Switching and Imaging of Antiferromagnetic Spins in Perovskite Epitaxial Thin Films*, to be submitted.
2. J. Michel, J. Flores, and F. Y. Yang, *Sub-Nanosecond Electrical Pulse Switching of an Easy Plane Antiferromagnetic Insulator*, to be submitted.
3. G. Fritjofson, A. Regmi, J. Hanson-Flores, J. Michel, F. Y. Yang, R. Cheng, E. Del Barco, *Coherent Spin Pumping Originated from Sub-Terahertz Néel Vector Dynamics in Easy Plane α-Fe_2O_3/Pt*, submitted to Phys. Rev. Lett. Under review.
4. J. Lanier, J. Michel, J. Flores, and F. Y. Yang, *Robust Biaxial Anisotropy and Switchable Néel Vectors in $LaFeO_3$ Epitaxial Films*, Nano Lett. **25**, 4667 (2025).
5. G. Fritjofson, A. Regmi, J. Hanson-Flores, J. Michel, J. Y. Tang, F. Y. Yang, R. Cheng, E. Del Barco, *Sub-terahertz bimodal spin pumping in canted antiferromagnetic heterostructure α-Fe_2O_3/Pt at room temperature*, npj Spintronics **3**, 24 (2025).
6. A. Abbas, J. C. M. Hernande, A. Shrestha, D. Russell, T. Erickson, K. Sun, G. H. Cocoletzi, F. Y. Yang, A. R. Smith, *Experimental and theoretical investigation of the crystalline surface, film, and interface properties of antiperovskite Mn_3GaN grown by molecular beam epitaxy on MgO(001)*, Surfaces and Interfaces **64**, 106201 (2025).
7. I. Lyalin, H. T. Zhang, J. Michel, D. Russell, F. Y. Yang, R. Cheng, and R. K. Kawakami, *Large Spin-Orbit Torque in α-Plane α−Fe_2O_3/Pt Bilayers*, Phys. Rev. Lett. **134**, 066701 (2025).
8. Y. Cheng, J. Y. Tang, J. J. Michel, S. K. Chong, F. Y. Yang, R. Cheng, and K. L. Wang, *Unidirectional Spin Hall Magnetoresistance in Antiferromagnetic Heterostructures*, Phys. Rev. Lett. **130**, 086703 (2023).
9. Q. C. Guo, A. D'Addario, Y. Cheng, J. Kline, I. Gray, H. F. H. Cheung, F. Y. Yang, K. C. Nowack, and G. D Fuchs, *Current-induced switching of thin film devices imaged using a scanning single-spin microscope*, Phys. Rev. Mater. **7**, 064402 (2023).
10. J. M. Li, Y. H. Gu, Y. Takahashi, K. Higashi, T. Kim, Y. Cheng, F. Y. Yang, J. Kuneš, J. Pelliciari, A. Hariki, and V. Bisogni, *Single- and Multimagnon Dynamics in Antiferromagnetic α-Fe_2O_3 Thin Films*, Phys. Rev. X **13**, 011012 (2023).

Discovery of novel layered multiferroics

Nasim Alem[1], Zhiqiang Mao[1,2], Weiwei Xie[3]

[1] Department of Materials Science and Engineering, The Pennsylvania State University, University Park, PA 16802, USA

[2] Department of Physics, The Pennsylvania State University, University Park, PA 16802, USA

[3] Department of Chemistry, Michigan State University, East Lansing, MI 48824, USA

Keywords: multiferroics, chalcogenides, magnetism, ferroelectricity, non-centrosymmetric

Research Scope

The research project is aimed at discovering novel multiferroic materials which have the coexistence of magnetic and ferroelectric ordering. Simultaneous coexistence of magnetism and ferroelectricity can induce novel properties that are not present in either state alone. These multiferroic materials open a route to control magnetism by electric field and vice versa. The electric field control of magnetism is of significant interest because using the electric field to tune magnetization requires much less power and is more energy efficient [1]. The recent discovery of 2D ferroelectricity in layered or van der Waals (vdW) crystals has provided a promising route to overcome the challenge of losing ferroelectric properties at reduced thicknesses [2]. These findings in turn have motivated the search for new layered or vdW multiferroics, particularly among the transition metal chalcogenides [3]. The goal of this project is to synthesize transition metal chalcogenides, investigate their tunability through chemical substitution to understand the structural nuances and the underlying physics of multiferroicity using advanced characterization.

Recent Progress

In the past year, we have successfully synthesized chalcogenide multiferroic systems, including $Mn_{1+x}Cu_{1-x}SiTe_3$, Cu_2MnSiS_4, and $AgCrSe_{2-x}S_x$ (x = 1, 1.5). $Mn_{1+x}Cu_{1-x}SiTe_3$ system is one of the first systems that was synthesized and fully investigated. While this crystal shows multiferroic properties, variation in the Cu concentration affects its structure and properties. We have observed that altering the Cu-to-Mn ratio leads to significant changes in the electronic properties of $Mn_{1+x}Cu_{1-x}SiTe_3$ [4]. Our studies have further focused on the local structure and defects in the $Mn_{1+x}Cu_{1-x}SiTe_3$ systems to understand how Cu concentration affects the defects and the atomic structure as well as the properties of this crystal. Specifically, Cu-deficient crystals ($Cu_{0.82}Mn_{1.08}SiTe_{2.99}$) exhibit semiconducting behavior, while Cu-rich crystals ($Cu_{1.14}Mn_{0.77}SiTe_{2.9}$) display semi-metallic behavior [4].

In a recent effort, our team also demonstrated the synthesis of Cu_2MnSiS_4, AgCrSeS, $AgCrSe_{0.5}S_{1.5}$, single crystals with possible evidence of multiferroicity through preliminary ferroelectric and magnetic measurements. Currently Our team is further investigating the

multiferroic properties and the atomic structure of Cu_2MnSiS_4, AgCrSeS, and $AgCrSe_{0.5}S_{1.5}$ crystals to further determine how the structural nuances affect multiferroicity in these systems using single-crystal X-ray diffraction (XRD) and advanced electron microscopy, in combination with theoretical predictions through collaborations. Besides these investigations, our team successfully synthesized a multiferroic oxide system, $BiMn_{7-x}Cu_xO_{12}$, using high pressure and high temperature synthesis technique. Below is a more detailed description of the work in progress:

a) Successful synthesis and characterization of $Mn_{1+x}Cu_{1-x}SiTe_3$

$Mn_{1+x}Cu_{1-x}SiTe_3$ is one of our originally proposed compositions grown as a seed for this grant. However, through this program we have been studying how the multiferroicity is affected by the structure and defects. We have published the multiferroic behavior observed in the Cu deficient ($Cu_{0.82}Mn_{1.08}SiTe_{2.99}$) crystals in a recent publication in 2025 [4]. More investigation has been carried out ever since to uncover the atomic structure of this sample and its defects using advanced electron microscopy imaging and spectroscopy. Stacking faults are observed as one prominent defect in Cu deficient crystals. We have also investigated how changing the Cu content from Cu-deficient to Cu-rich alters the structure, as we have already observed changes in their electronic properties [4]. Figure 1 shows the structural investigation using S/TEM overlaid with the structure obtained from single crystal XRD studies and the magnetodielectric and magentocurrent measurements of the Cu deficient $Cu_{0.82}Mn_{1.08}SiTe_{2.99}$ crystals. We observed that the ΔP reaches ~ 0.8 μC/cm^2 at 10 K and 9 T, as reported in our recent work [4], and this value is comparable to the record magnetic field-induced polarization in oxide multiferroics. We observe that both Cu-deficient and Cu-rich samples share the same space group but differ in the number of sites per unit cell. From our S/TEM studies, we observe several types of defects present in the Cu-rich ($Mn_{0.77}Cu_{1.14}SiTe_{2.9}$) crystals, including stacking faults, dislocations, and tweed-shaped

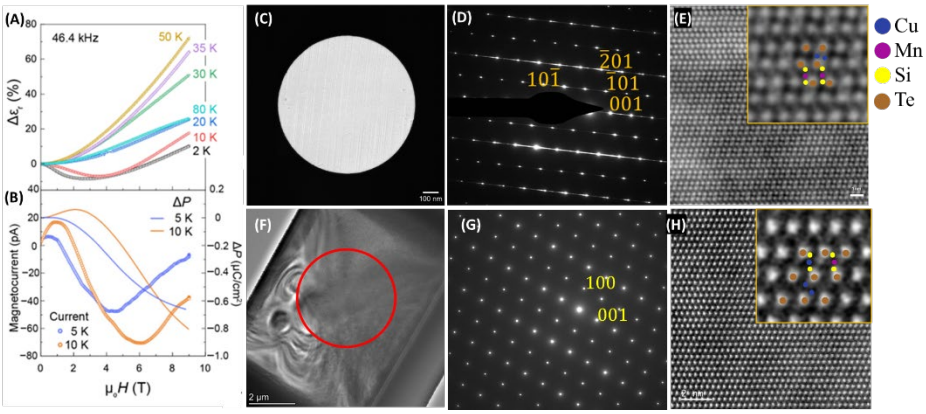


Fig.1. Investigation of $Mn_{1+x}Cu_{1-x}SiTe_3$ crystals using S/TEM: (A) Magnetodielectric constant, $\Delta\varepsilon/\varepsilon=[\varepsilon(H)-\varepsilon(0)]/\varepsilon(0)$, as a function of magnetic field at 20 various temperatures. (B) Magnetocurrent recorded by sweeping the magnetic field at 5 and 10 K (left axis), change in the electric polarization (ΔP) induced by applying a magnetic field at 5 and 10 K in Cu deficient $Cu_{0.82}Mn_{1.08}SiTe_{2.99}$. (C) TEM image of Cu deficient $Cu_{0.82}Mn_{1.08}SiTe_{2.99}$ cross-section specimen along [010] zone axis. (D) SAED pattern from region in (C). (E) Atomic STEM imaging from [010] zone axis. Similarly, a cross-section specimen along [010] zone axis is made of Cu rich $Mn_{0.77}Cu_{1.14}SiTe_{2.9}$ and (F) TEM image is shown. (G) SAED pattern from the red circle region in (F). (H) Atomic STEM imaging from [010] zone axis.

precipitates. Our future work will focus on further examining these defect structures, their formation origin, and understanding their influence on the material's properties.

b) Successful synthesis and characterization of Cu_2MnSiS_4 and Cu_2FeSiS_4:

In our most recent study, upon searching the database, we identified Cu_2MnSiS_4 as new promising material, since it shows possible evidence of multiferroic behavior. Single crystals of Cu_2MnSiS_4 and Cu_2FeSiS_4 were synthesized via chemical vapor transport (CVT) using iodine as a transport agent. The magnetic behavior of Cu_2MnSiS_4 single crystals was measured using SQUID (Fig. 2A) and shows the temperature dependence of magnetic susceptibility under zero field cooling (ZFC) as well as the field-cooling (FC) with a magnetic field of 0.1T applied in the out-of-plane and in-plane directions. The susceptibility measurement reveals an antiferromagnetic behavior with Neel temperature $T_N \sim 8K$. The Curie-Weiss fitting ($\chi = \frac{C}{T-\theta}$) of the inverse magnetic susceptibility gives a negative Weiss constant of $\theta = -15.44$ K, indicating AFM coupling between the Mn^{2+} moments. The field-dependence of magnetization at 3K shows a linear behavior which also confirms antiferromagnetic coupling in Cu_2MnSiS_4 (Fig. 2B). To verify if this material exhibits magneto-dielectric and magnetoelectric effects, we performed temperature dependent and magnetic field dependent capacitance measurements (Fig. 2C). From the measurements, we observed that ε_r shows an anomaly at the AFM transition temperature T_N. Between T_N up to 10K we see a variation in $\Delta\varepsilon_r$ across the magnetic field, which vanishes at 10K (Fig. 2D). These results suggest that Cu_2MnSiS_4 is a possible multiferroic material. We plan to perform P-E loop as well as magnetoelectric measurements and thorough structural analysis to find further evidence for its multiferroicity and the role of the atomic structure.

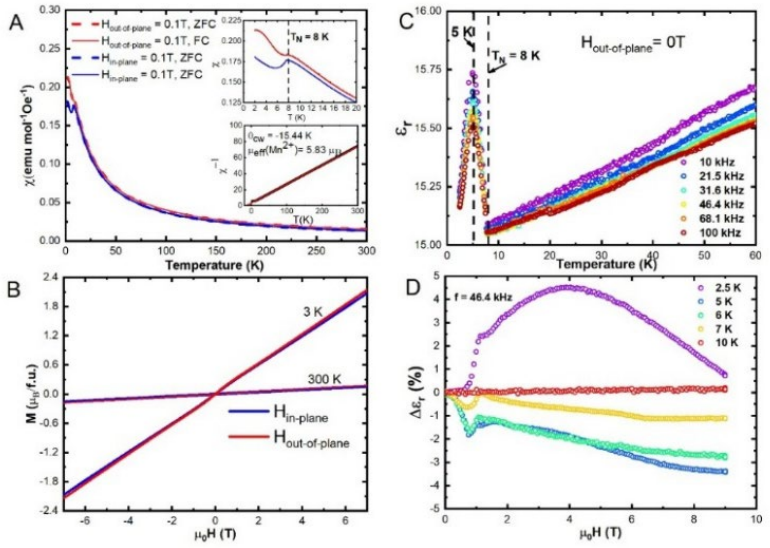


Fig.2. Magnetic and Dielectric Measurements on Cu_2MnSiS_4 single crystals (A) Temperature dependent susceptibility (χ) measurement under ZFC and FC with a magnetic field (0.1T) applied out-of-plane and in-plane. B) Magnetic field sweep of magnetization with applied field out-of-plane and in-plane at temperatures 3K and 10K. (C) Temperature dependence of dielectric constant ε_r under 0T and at different frequencies. (D) Magnetodielectric constant $\Delta\varepsilon_r = \frac{\varepsilon_r(H)-\varepsilon_r(0)}{\varepsilon_r(0)}$, as a function of magnetic field at different temperatures.

c) Synthesis of $AgCrSe_{2-x}S_x$ (x = 1, 1.5) single crystals and their Magnetic properties

$AgCrS_2$ and $AgCrSe_2$ are among our originally proposed materials for synthesis since they both have polar space group and show magnetic ordering. $AgCrS_2$ has indeed been reported to a be multiferroic material [5]. We have synthesized single crystals of $AgCrSe_2$, AgCrSeS and $AgCrSe_{0.5}S_{1.5}$ using a two-step process, where polycrystalline powders were initially made via melt growth technique, followed by single crystal preparation using CVT method. The synthesized single crystals are plate-like, suggestive of their layered structure. Following the synthesis, we performed magnetization measurements on these single crystals using SQUID and have observed multiferroic behavior in $AgCrS_2$. Our preliminary measurements show AgCrSeS and $AgCrSe_{0.5}S_{1.5}$ exhibiting magnetic properties distinct from $AgCrS_2$. We are at the nascent stage of this investigation and plan to perform further systematic measurements to determine if the mixed Se/S compounds indicate multiferroicity and the role of their atomic structure and composition.

Future Plans

We will continue studies on Cu_2MnSiS_4, AgCrSeS and $AgCrSe_{0.5}S_{1.5}$ and perform systematic magnetodielectric and magnetoelectric measurements to find evidence of multiferroic properties. High-pressure and high-temperature synthesis methods will be employed as needed to stabilize metastable phases and obtain high-quality crystals. To uncover the atomic structure and defects, we will continue to use advanced S/TEM imaging and spectroscopy in addition to in-situ heating or cooling experiments inside the TEM to investigate the structural transformation from the ferroelectric to the paraelectric phase. These experiments enable real-time observation of ferroelectric and magnetic domain dynamics as well as defect transformation under applied stimuli. Furthermore, low-temperature Lorentz Transmission Electron Microscopy (LTEM) will be employed to reveal and study the magnetic domain behaviour at reduced temperatures.

References

1. Spaldin, N. A., Cheong, S. W. & Ramesh, R., *Multiferroics: Past, present, and future*. Phys. Today **63**, 38–43 (2010).
2. Yuan, S., Luo, X., Chan, H.L., Xiao C., Dai, Y., Xie, M., Hao, J., *Room-temperature ferroelectricity in MoTe2 down to the atomic monolayer limit,* Nat. Comm. **10**, 1–6 (2019).
3. Huang C., Du, Y., Wu, H., Xiang, H., Deng, K., Kan, E., *Prediction of Intrinsic Ferromagnetic Ferroelectricity in a Transition-Metal Halide Monolayer*, Phys. Rev. Lett. **120**, 147601 (2018).
4. De, C., Liu, Y., Ayyagari, S.V.G., Zheng, B., Kelley, K.P., Hazra, S., He, J., Pawledzio, S., Mali, S., Guchhait,S., Yoshida, S., Guan, Y., Lee, S.H., Sretenovic, M., Ke, X., Wang, L., Engelhard, M.H., Du, Y., Xie, W., Wang, X., Crespi, V.H., Alem, N., Gopalan, V., Zhang, Q., Mao, Z., *Discovery of a layered multiferroic compound Cu1−xMn1+ySiTe3 with strong magnetoelectric coupling*, Sci. Adv. **11**,eadp9379 (2025).
5. Singh, K., Maignan, A., Martin, C. & Simon, C., *AgCrS2: A spin driven ferroelectric*, Chem. Mat. **21**, 5007–5009 (2009).

Publications

1. De, C., Liu, Y., Ayyagari, S.V.G., Zheng, B., Kelley, K.P., Hazra, S., He, J., Pawledzio, S., Mali, S., Guchhait,S., Yoshida, S., Guan, Y., Lee, S.H., Sretenovic, M., Ke, X., Wang, L., Engelhard, M.H., Du, Y., Xie, W., Wang, X., Crespi, V.H., Alem, N., Gopalan, V., Zhang, Q., Mao, Z., *Discovery of a layered multiferroic compound Cu1−xMn1+ySiTe3 with strong magnetoelectric coupling*, *Sci. Adv.* **11**,eadp9379 (2025).
2. Ayyagari, S.V.G., De,C., Liu, Y., Zheng, B., Anil, S., Crespi, V.H., Mao, Z., Alem, N., *Exploring the Structure and Defects in MnCuSiTe, a Multiferroic System using Electron Microscopy*, Microsc. Microanal. **31**, Issue Supplement_1, ozaf048.579 (2025).
3. Anil, S., Ayyagari, S.V.G., Zhang, Y., Liu, Y., Zheng, B., Crespi, V.H., Mao, Z., Alem, N., *Probing the Structure of a Novel Chalcogenide Multiferroic Crystal* $Cu_{1.14}Mn_{0.77}SiTe_{2.9}$, Microsc. Microanal. **31**, Issue Supplement_1, ozaf048.585 (2025).

Program Title: Non-Equilibrium Magnetism: Materials and Phenomena

Principle Investigator: Frances Hellman; ***Co-PIs*** Peter Fischer, Sinéad Griffin, Sujoy Roy, Inna Vishik (Materials Sciences Division, LBNL); Josh Turner (SLAC)

Keywords: magnetism, spintronics, thin film heterostructures, magnetotransport, magnetic imaging and spectroscopy

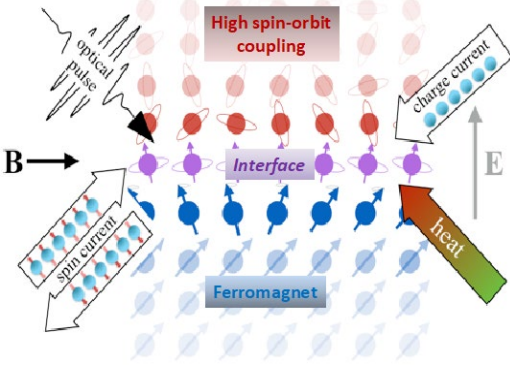


Fig. 1 Interface between ferromagnet (or other magnet) and high spin orbit coupling material, subject to optical, electrical, or heat pulses, and E or B fields.[1]

Research Scope: The NEMM program investigates the fundamental science of non-equilibrium magnetic materials and phenomena in amorphous thin film materials with strong spin-orbit interactions in the presence of interfacially-induced or other local inversion symmetry breaking. It integrates design, fabrication, measurement, and modeling of static and dynamic magnetic properties, emphasizing the thermodynamic and dynamic control of magnetization and topological spin textures. Future research addresses two strongly interrelated thrusts: (i) understanding and controlling the free energy landscape of two- and three-dimensional chiral spin textures in amorphous films; and (ii) studying the dynamic response of these textures, including thermally induced fluctuations. Advanced optical, electron, and x-ray techniques with nanoscale resolution and across time scales from seconds to femtoseconds combining lab-based tools with capabilites at large scale facilities, and theoretical modeling are used to explore these phenomena. By advancing the understanding and control of amorphous quantum materials, using AI/ML to assist this process, the NEMM program aims to enable stable emergent magnetic phases, understand their dynamical properties and novel functionalities essential for future technologies.

Recent Progress (select results, grouped by thrust)

Thrust 1 ***Static and quasi-static novel thin film spin structures in amorphous alloys***

a) *Goal: Understand and control the free energy landscape of chiral spin textures, enabling stability and tunability of novel topological and complex spin textures and phases*

We previously discovered and developed a theory for enhanced magnetization, large intrinsic anomalous Hall effect and Hall angle, and high spin polarization in amorphous *a*-Fe_xSi_{1-x} and *a*-Fe_xGe_{1-x}, along with non-collinear spin structures driven by local SOC and DMI.[2] Lorentz TEM and X-ray scattering of *a*-Fe_xGe_{1-x} revealed a rich *x*–*H*–*T* phase diagram with helical and skyrmion phases and a low-T transition to rapidly fluctuating domains [2,A4]. Recent coherent X-ray scattering showed that spatial heterogeneity (pinning, domain walls, defects) drives temporal heterogeneity and complex transition pathways with a universal power law, as well as a novel nematic phase and non-ergodic behavior. Fluctuations expand with T or x and collapse onto a universal power-law. Speckle analysis revealed multiple spin texture classes. [A4,A10].

Additional accomplishments:

- 3D skyrmion mapped by magnetic soft X-ray laminography in Ir/Co/Pt nanodisks; observed depth-dependent variations in winding number and exchange parameters.
- Participated in commissioning of Timepix detectors using *a*-Fe–Ge test films.
- Curvature-driven spin textures found in *a*-Fe–Ge, Si and multilayers via X-ray tomography.

b) *Amorphous topological insulators (a-TIs)*

Highlight: Discovered spin-momentum locked surface states in *a*-Bi_2Se_3, both theoretically and experimentally—a milestone toward realizing topological states in amorphous systems.[3]

Additional accomplishments:

- Experimentally investigated disorder effects in Bi_xTeI films (x = 1–3), a material we predicted would transition from trivial to topological insulator with increasing disorder. Low growth temperature caused strong localization and electron–electron interactions, producing disorder- and composition-dependent metal–insulator transitions [A5].
- **Theory of amorphous topology:** Proposed "structural spillage" as a new indicator to diagnose nontrivial topology in amorphous systems relative to a crystalline reference [4]

Thrust 2 ***Spin accumulation, spin currents, magnetization control via interfaces and SOC***

Understand and control magneto-transport, spin accumulation, and spin-orbit torque (SOT) in amorphous heterostructures; the impact on these of topology, disorder, and thermal fluctuations.

- Amorphous *a*-Fe_xSi_{1-x} and *a*-Fe_xGe_{1-x} films show large AHE, AHA, and spin polarization, suggesting strong SHE from enhanced SOC, spin-split scattering and short mean free paths. In $\{Fe,Co\}_x$–$\{Ge,Si\}_{1-x}$ alloys, resistivity scales with *x*, while magnetization differs, enabling separation of their effects. In *a*-Co_xGe_{1-x}, we achieved large SHA ≈ 0.25 with low switching currents (2×10^6 A/cm²). MOKE confirmed SOT-driven domain nucleation and motion.[5]
- Amorphous Pt_xGe_{1-x} and Pt_xSi_{1-x} show enhanced SHA; current work aims to disentangle the roles of amorphization, carrier density, and short mean free path on SOT efficiency.[5]

Thrust 3 ***Highly non-equilibrium magnetic states and ultrafast spin dynamics; magnetization dynamics following ultrafast optical or electrical pulse***

a) *Ultrafast helicity-independent all-optical switching in ferrimagnet alloys and multilayers*

- Achieved direct electrical detection of single-shot optical switching in 20 nm Tb/Co multilayer cells with high anisotropy, creating opportunities for ultrafast nanoscale switching.
- Published invited review: *"A perspective on ultrafast magnetization switching in ferromagnets using helicity-independent optical pulses"* [A6].

b) *Fluctuations in a non-equilibrium magnetic state*

- X-ray studies of *a*-Fe_xGe1-x films revealed fluctuation hot-spots and skewed distributions that destabilize the helical phase and mark a transition to non-ergodic behavior [A4, A10].
- Ultrafast X-ray pump–probe and single-shot XPCS revealed how light-induced fluctuations drive entropy changes, topological dynamics, and Weyl-fermion coupling control. [B1].
- Ultrafast spin dynamics: awarded five LCLS beamtimes; measured μsec skyrmion fluctuations at European XFEL; completed design of new LCLS-II fluctuation instrument.
- Invited review for Adv. Phys. X: *"On Ultrafast X-ray Methods for Magnetism"* [B1].

Future Plans: two interrelated Thrusts with complementary topics and foci (interfaces, disorder, local and global symmetry breaking effects, spin-orbit coupling, non-relativistic spin-splitting).

Thrust 1: Novel spin structures in amorphous magnetic and topological films

a) Understanding and controlling complex spin textures

We hypothesize that amorphous materials and heterostructures can be used to create chiral spin textures and through their tunability, control their stability, dynamics, and size. We focus on the role of disorder, the importance of local symmetry breaking, and their contributions to emergent topological phenomena, including how chirality impacts the topological properties and behavior.

- **Amorphous Mn–Ge alloys:** Building on our *a*-Fe_xGe_{1-x} work, we now turn to *a*-Mn_xGe_{1-x}. Crystalline B20 MnGe and FeGe exhibit very different skyrmion length scales (3 vs. 90 nm),

lattice types, and internal structures, suggesting different exchange and DMI interactions. *a*-Mn_xGe_{1-x} should similarly yield distinct textures, and pseudo-binary a-$(Mn_yFe_{1-y})_xGe_{1-x}$ will allow us to tune the spin texture length scale, from the short length of the Mn alloy, where the amorphous structure may couple directly to the spin texture, to the Fe alloy, where the averaging over DMI disorder may limits its impact.

- **Heterostructure design:** We are developing amorphous heterostructures (e.g., *a*-Fe_xGe_{1-x} or *a*-Mn_xGe_{1-x} with high-SOC over/underlayers *a*-Pt_xGe_{1-x} or *a*-Ir_xGe_{1-x}). By varying layer thicknesses and alloy compositions, we separately control magnetization, carrier density, and magnetic anisotropy to stabilize new textures.
- **Spin texture dynamics in *a*-Fe_xGe_{1-x}:** Continuing studies of ergodic–nonergodic transitions, helical and skyrmion clusters, and the effects of randomized DMI on phase stability and fluctuations, leveraging tunability in magnetization and carrier density.
- **ARPES probes (new co-PI Vishik):** Photoemission studies will enable understanding of the electronic structure of the proposed novel amorphous alloy systems.
- *Ab initio* theory and mesoscopic modeling in a multi-scale framework incorporates spin–orbit coupling, disorder, and non-equilibrium effects to predict spin textures without translational symmetry. AI/ML and materials informatics will accelerate discovery of new amorphous alloys and identify controllable routes (alloying, strain, disorder)
- **Curvature and strain control:** Exploring how these shape the magnetic energy landscape. Depositing amorphous films on curved substrates will allow deliberate creation and tuning of 3D topological textures, studied with advanced vector X-ray imaging methods.

b) Amorphous magnetic topological insulators and kagome-like materials: Quantum Anomalous Hall Effect (QAHE), novel spin textures, and spin-momentum locking effects

We hypothesize that emergent spin-orbit phenomena (spin-momentum locking, Rashba splitting, and topological band inversions) are driven by local environment, not global crystal symmetries. Amorphous materials therefore provide a promising platform to create and study magnetic topological insulators and the QAHE: *disorder localizes bulk carriers while preserving metallic surface states including chiral edge states.*

- **Magnetic a-TIs:** We will combine experiment and theory (first-principles, tight-binding) to explore Mn-doped *a*-Bi_2Se_3 as a first candidate, followed by *a*-$MnBi_2Te_4$ and Mn-doped (Si,Ge,Sn,Sb)-(Se,Te). Heterostructures such as *a*-Fe–Ge/*a*-Bi_2Se_3 will also be grown. Using DFT, ARPES, spin-ARPES, and magnetotransport, we will probe exchange gaps, spin–momentum locking, and gating-tuned QAHE, with soft X-ray ARPES enabling access to buried amorphous TI layers.
- *Amorphous Kagome-like Materials:* Synthesize *a*-Fe_xSn_{1-x} and *a*-$R_xT_6X_6$ alloys (R = rare earth, T = V/Mn, X = Ge/Sn) to extend kagome physics—Dirac fermions, flat bands, frustrated magnetism—into the amorphous regime, targeting disorder-enabled topological spin phases.
- **Controlling disorder:** Growth conditions will be used to tune the amorphous structure and rapid scanning nanocalorimetry to quantify the disorder via depth in the energy landscape, enabling systematic control of spin textures and topological states.

c) Amorphous Non-Relativistic Spin Splitting (NRSS): Compensated collinear magnetic order, altermagnetism, intrinsic anomalous Hall effect

We hypothesize that it is possible to control local structure in an amorphous material such that true antiferromagnetism and even non-relativistic spin split (NRSS) states exist via bipartite networks, and orbital ordering achieved via strain or growth-induced structural texturing.

- Starting with *a*-Mn–Ge–Te and *a*-Cr–Ge–Sb, we will investigate how atomic disorder governs the balance between spin-glass and antiferromagnetic phases, including NRSS. Magnetometry and nanocalorimetry will distinguish true AFM transitions from glassy freezing, while spin-ARPES will probe anisotropic spin-splitting and polarization. Theory will link atomic structure to magnetism, showing how alloying, strain, and disorder stabilize NRSS or altermagnetic states. This work lays the foundation for compensated magnetism in amorphous systems, advancing spintronic applications.

Thrust 2 Dynamics of spin textures and magnetic domains in amorphous films

Goal: *To understand and model dynamic phenomena—including equilibrium fluctuations, non-equilibrium properties, and driven responses of spin textures in amorphous systems—through advanced experiments and theory, advancing our understanding of magnetic phase transitions.*

a) Fluctuations at equilibrium

We hypothesize that the spin textures and magnetic/topological states identified in Thrust 1 will exhibit unconventional dynamics near phase transitions. By tuning materials parameters, we will probe fluctuations that test theoretical models and may uncover hidden phases.

Within the Gibbs free energy framework, fluctuations in order parameters stabilize phases and drive universal critical behavior, but spontaneous or intrinsic heterogeneities (domain walls, pinning centers, competing interactions) break equilibrium assumptions, producing speckle in coherent X-ray diffraction and dynamic heterogeneity over multiple timescales [A10]. We will exploit speckle analysis to connect spatial and temporal heterogeneity and extend this to non-thermal transitions dominated by quantum fluctuations.

b) Non-equilibrium and Near-Equilibrium Fluctuations

We will focus on non- and near-equilibrium phases accessible through excitation mechanisms such as THz or optical laser pulses. We hypothesize that the fluctuations and transition pathways observed in these states—particularly in amorphous materials—will reveal fundamental links between metastable phases and non-equilibrium thermodynamics.

Using THz and optical excitation, we will probe metastable and transient phases where disorder strongly impacts dynamics. Recent studies (Turner, Roy) in a-Fe/Gd revealed broad distributions of dynamical behavior. We aim to combine traditional pump-probe methods with correlation spectroscopy to track domain formation and transition pathways across timescales inaccessible to conventional probes, clarifying the role of disorder in non-equilibrium thermodynamics.

c) Driven Systems: Multi-scale behavior and dynamic heterogeneity

We will study amorphous systems driven by currents or RF fields, using speckle correlations to link dissipation and damping to spin textures. Our discovery of an ergodicity transition in *a*-Fe–Ge suggests the fluctuation–dissipation theorem (FDT) holds only above this transition, enabling tests of FDT breakdown. Competing inter- and intra-cluster interactions drive multi-scale spatio-temporal dynamics, which we will image with X-ray, Lorentz, photoelectron, and magnetic force microscopies to advance understanding of dynamic heterogeneity in marginally ordered phases.

References (limit of 5 papers).

1. F. Hellman, A. Hoffmann, Y. Tserkovnyak, G.S.D. Beach, E.E. Fullerton, C. Leighton, A.H. MacDonald, D.C. Ralph, D.A. Arena, H.A. Durr, P. Fischer, J. Grollier, J.P. Heremans, T. Jungwirth, A.V. Kimmel, B. Koopmans, I.N. Krivorotov, S.J. May, A. K. Petford-Long, J.M. Rondinelli, N. Samarth, I.K. Schuller, A.N. Slavin, M.D. Stiles, O. Tchernyshyov, A. Thiaville, B.L. Zink, *"Interface-Induced Phenomena in Magnetism"*, invited review article, Rev. Mod. Phys. **89**, 025006 (2017).
2. R. Streubel, D.S. Bouma, F. Bruni, X. Chen, P. Ercius, J. Ciston, A.T. N'Diaye, S. Roy, S.D. Kevan, P. Fischer, F. Hellman,*"Chiral Spin Textures in Amorphous Iron–Germanium Films",* Adv. Mat. Comm. 2004830 (2021).

3. P. Corbae, S. Ciocys, D. Varjas, E. Kennedy, S. Zeltmann, M. Molina-Ruiz, S. M. Griffin, C. Jozwiak, Z. Chen, L.-W. Wang, A. M. Minor, M. Scott, A. G. Grushin, A. Lanzara and F. Hellman, *"Observation of spin-momentum locked surface states in amorphous Bi2Se3"*, Nature Materials **22**, 200 (2023). 10.1038/s41563-022-01458-0
4. D. Muñoz-Segovia*, P. Corbae*, D. Varjas, F. Hellman, S. M. Griffin^{+} and A. G. Grushin^{+}, *"Structural spillage: An efficient method to identify noncrystalline topological materials"*, Physical Review Research **5** (4), L042011 (2023). 10.1103/PhysRevResearch.5.L042011
5. R. Ozgur, PhD thesis, UC Berkeley Aug 2025.

Publications since last ECMP (Oct 2023-Sept 2025): limited to 10 publications in A & B

A. Publications primarily funded and intellectually led by this FWP:

A1. P. Corbae, J. D. Hannukainen, Q. Marsal, D. Muñoz-Segovia and A. G. Grushin, *"Amorphous topological matter: Theory and experiment"*, Europhysics Letters 142 (1), 16001 (2023). 10.1209/0295-5075/acc2e2
A2. D. Raftrey, S. Finizio, R.V. Chopdekar, S. Dhuey, T. Bayaraa, P. Ashby, J. Raabe, T. Santos, S. Griffin, P. Fischer, Sci Adv 10, eadp8615 (2024). "*Quantifying the topology of magnetic Skyrmions in three dimensions"*, Sci. Adv. 10 eadp8615 (2024). https://doi.org/10.1126/sciadv.adp8615
A3. C.-H. Hsu, M. J. Gross, H. C. Kleidermacher, S. Sayed and S. Salahuddin, "*Tunable multistate field-free switching and ratchet effect by spin-orbit torque in canted ferrimagnetic alloy*", Nat. Comm. 15 (1), 8713 (2024). 10.1038/s41467-024-52834-0]
A4. A. Singh, E. Hollingworth, S. A. Morley, A. Us Salaheen, Z. Tumbleson, D. Raftrey, M. R. McCarter, P. Fischer, F. Hellman, S. D. Kevan. S. Roy, "*Ergodicity transitions in spin spiral domains in amorphous FeGe thin films"*, Phys. Rev. B 110, L220406 (2024). 10.1103/PhysRevB.110.L220406
A5. P. Corbae, N. Taufertshöfer, E. Kennedy, M. Scott and F. Hellman, *"Disorder-driven localization and electron interactions in Bi_xTeI thin films"*, Phys. Rev. Mat. 8 (4), 044204 (2024). 10.1103/PhysRevMaterials.8.044204
A6. D. Polley and J. Bokor, *"A perspective on ultrafast magnetization switching in ferromagnets using helicity-independent optical pulses"*, Invited review article J. Physics D*:* App. Phys. 58, 102001 (2025). https://doi.org/10.1088/1361-6463/ada1e0
A7. D. Polley, J. Chatterjee, H. Jang and J. Bokor, *"Analysis of ultrafast magnetization switching dynamics in exchange-coupled ferromagnet–ferrimagnet heterostructures"*, Journal of Magnetism and Magnetic Materials 574, 170680 (2023). https://doi.org/10.1016/j.jmmm.2023.170680
A8. D. Polley, A. Pattabi, A. Rastogi, K. Jhuria, E. Diaz, H. Singh, A. Lemaitre, M. Hehn, J. Gorchon and J. Bokor, *"Picosecond spin-orbit torque–induced coherent magnetization switching in a ferromagnet"*, Science Advances 9 (36), eadh5562 (2023). doi:10.1126/sciadv.adh5562
A9. T. Bayaraa, V. Ivanov, L. Z. Tan and S. M. Griffin, *"Intrinsic origin and enhancement of topological responses in ferrimagnetic antiperovskite Mn_4N"*, Physical Review B 109 (1), 014430 (2024). 10.1103/PhysRevB.109.014430
A10. Z. Tumbleson, S. A. Morley, E. Hollingworth, A. Singh, T. Bayaraa, N. G. Burdet, A. Us Salaheen, M. R. McCarter, D. Raftrey, R. J. Pandolfi, V. Esposito, G. L. Dakpovski, F.-J. Decker, A. H. Reid, T. A. Assefa, P. Fischer, S. M. Griffin, S. D. Kevan, F. Hellman, J. Turner, S. Roy, *Thermodynamic phase transitions of nematic order in magnetic helices, Sci. Adv. 11, eadt5680 (2025) 20 June 2025, https://doi.org/10.1126/sciadv.adt5680*

B. Collaborative publications:

B1. R. Plumley, S. R. Chitturi, C. Peng, T. A. Assefa, N. Burdet, L. Shen, Z. Chen, A.H. Reid, G.L. Dakowvski, M. H. Seaberg, F. O'Dowd, S. A. Montoya, H. Chen. A. Okullo, S. Mardanya, S. D. Kevan. P. Fischer, E. E. Fullerton, S. K. Sinha, W. Colocho, A. Lutman. F.-J. Decker, S. Roy, J. Fujioka, S. K. Sinha, Y. Tokura, M. P. Minitti, J. A. Johnson, M. Hoffmann, M. E. Amoo, A. Feiguin, C. Yoon, J. Thayer, Y. Nahed, C. Jia, A. Bansil, S. Chowdhury, A, M. Lindenberg, M. Dunne, E. Blackburn, J. J. Turner, "On ultrafast x-ray scattering methods for magnetism", *Adv. Phys. X* 9(1), 2423935 (2024), doi: 10.1080/23746149.2024.2423935.
B2. A. Mangu, V. A. Stoica, H. Zheng, T. Yang, M. Zhang, H. Wang, R. Zu, Q. L. Nguyen, S. Song, S. Das, P. Meisenheimer, E. Donoway, M. Chollet, Y. Sun, J. J. Turner, J. W. Freeland, H. Wen, L. W. Martin, L.-Q. Chen, V. Gopalan, D. Zhu, Y. Cao and A. M. Lindenberg, "Hidden domain boundary dynamics toward crystalline perfection", *Proc. Natl. Acad. Sci.* 122(2), e2407772122 (2025), doi: 10.1073/pnas.2407772122.
B3. S. T. Ciocys, Q. Marsal, P. Corbae, D. Varjas, E. Kennedy, M. Scott, F. Hellman, A. G. Grushin and A. Lanzara, "Establishing coherent momentum-space electronic states in locally ordered materials", *Nat. Commun.* 15(1), 8141 (2024), doi: 10.1038/s41467-024-51953-y.
B4. S. Mondal, D. Polley, A. Pattabi, J. Chatterjee, D. Salomoni, L. Aviles-Felix, A. Olivier, M. Rubio-Roy, B. Diény, L. D. B. Prejbeanu, R. Sousa, I. L. Prejbeanu, and J. Bokor, "Single-shot switching in Tb/Co-multilayer based nanoscale magnetic tunnel junctions", *J. Magn. Magn. Mater.* 581, 170960 (2023), doi:

10.1016/j.jmmm.2023.170960.
B5. A. U. Saleheen, A. Singh, D. Raftrey, M. A. Broziu, M. R. McCarter, Z. Tumbleson, M.-Y. Im, S. A. Montoyo, E. E. Fullerton, P. Fischer, S. D. Kevan, S. Roy, S. A. Morley, "Multimodal correlative study of Hall transport and magnetic phases in Fe/Gd multilayer systems", *Appl. Phys. Lett.* 126(14), 142401 (2025), doi: 10.1063/5.0239472.
B6. R. M. Harton, A. Ceballos-Sanchez, V. Unikandanunni, A. X. Gray, S. Bonetti, P. Krüger, and F. Hellman, "Characterizing the nonequilibrium response of FeRh thin films using time-domain thermoreflectance", *Phys. Rev. B* 110(9), 094417 (2024), doi: 10.1103/PhysRevB.110.094417.
B7. E. Harding, T. Araki, J. Askey, M. Hunt, A. Van Den Berg, D. Raftrey, L. Aballe, B. Kaulich, E. MacDonald, P. Fischer, and S. Ladak, "Imaging the magnetic nanowire cross section and magnetic ordering within a suspended 3D artificial spin-ice", *APL Mater.* 12(2), 021116 (2024), doi: 10.1063/5.0176907.
B8. A. Singh, J. Li, S. A. Montoya, S. Morley, P. Fischer, S. D. Kevan, E. E. Fullerton, D.-X. Yao, T. Datta, and S. Roy, "Periodicity staircase in a centrosymmetric Fe/Gd magnetic thin film system", *Npj Quantum Mater.* 9(1), 1–9 (2024), doi: 10.1038/s41535-023-00613-3.
B9. Ellis Kennedy, Emily Hollingworth, Alejandro Ceballos, Daisy O'Mahoney, Colin Ophus, F. Hellman, and M.C. Scott, "Exploring Structural Anisotropy in Amorphous Tb-Co via Changes in Medium-Range Ordering", *Microsc. Microanal.* 31(1), ozae113 (2025), doi: 10.1093/mam/ozae113.
B10. R. Plumley, S. Mardanya, C. Peng, J. Nokelainen, T. A. Assefa, L. Shen, N. Burdet, Z. Porter, A. Petsch, A. Israelski, H. Chen, J. S. Lee, S. Morley, S. Roy, G. Fabbris, E. Blackburn, A. Feiguin, A. Bansil, W. S. Lee, A. Lindenberg, S. Chowdhury, M. Dunne, and J. J. Turner, "3D Heisenberg universality in the van der Waals antiferromagnet NiPS3", *Npj Quantum Mater.* 9(1), 1–7 (2024), doi: 10.1038/s41535-024-00696-6.

Digital Synthesis: A pathway to novel states of condensed matter

A. Bhattacharya, Dillon D. Fong, J. S. Jiang, Ulrich Welp **(Argonne National Laboratory)**

Self-identify keywords to describe your project: superconductivity, magnetism, spintronics, thin film heterostructures, transition metal compounds, molecular beam epitaxy, x-ray scattering.

Research Scope: In our program, we seek to create, explore and understand novel electronic and magnetic states with new functionalities that emerge at interfaces between different materials. These include collective states like interfacial magnetism and superconductivity, as well as topological states of matter, that may have relevance for spintronics and quantum information science. We seek to realize these states in materials synthesized with atomic layer-by-layer control using molecular beam epitaxy and related techniques. A significant part of our research is devoted to understanding growth processes that lead to these interfacial states, and to refine our synthesis conditions. In the research presented here, we focus on the synthesis and emergent properties of two recently discovered oxide superconductors. In the first class of materials, the superconducting nickelates, we use in-situ x-ray diffraction during synthesis with molecular beam epitaxy to understand the processes underlying the growth of the infinite layer perovskite and $n = 5$ Ruddlesden-Popper phases in epitaxial thin films, and their subsequent topotactic reduction to the square-planar phase to realize superconductivity. Next, we will present our results from ongoing efforts to explore and understand the superconducting state found at interfaces of $KTaO_3$ (KTO). We will describe how we probe the inversion breaking transverse optical TO1 phonons found near the surface of KTO using a unique 'spintronic' THz spectroscopic technique. These are the same phonons that soften to give rise to the 'quantum paraelectric' nature of KTO at low temperatures and may also mediate pairing in the two-dimensional superconducting gas at KTO interfaces. We have also fabricated superconducting coplanar waveguide resonators using the electron gas formed at interfaces of KTO (111), where we find very large sheet kinetic inductance, and as a result also very low phase velocities or 'slow light', which sheds light on the nature of the superfluid in this two-dimensional superconductor.

Recent Progress

Understanding topotactic reduction in superconducting nickelates: Topotactic reduction is critical to a wealth of phase transitions of current interest, including synthesis of the superconducting nickelate $Nd_{0.8}Sr_{0.2}NiO_2$, reduced from the initial $Nd_{0.8}Sr_{0.2}NiO_3/SrTiO_3$ heterostructure[1]. Due to the highly sensitive and often damaging nature of the topotactic reduction, however, only a handful of research groups have been able to reproduce the superconductivity results. A series of in-situ synchrotron-based investigations by our team (Y. Li et al., *Adv. Mater*. 2024) reveal that this is due to the necessary formation of an initial, ultrathin layer at the $Nd_{0.8}Sr_{0.2}NiO_3$ surface that helps to mediate the introduction of hydrogen into the film such that apical oxygens are first removed from the $Nd_{0.8}Sr_{0.2}NiO_3/SrTiO_3$ (001) interface and delivered into the reducing environment. This

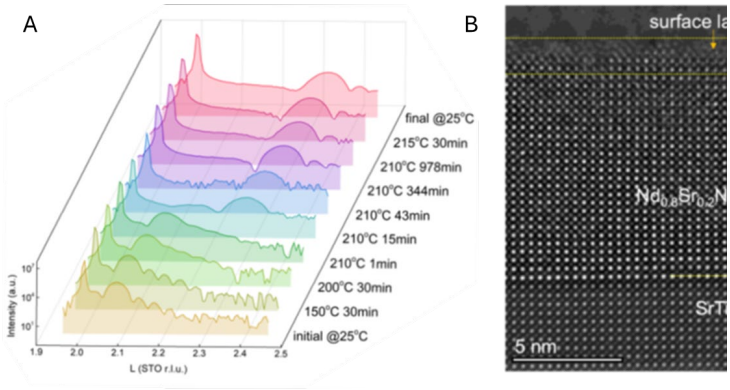


Fig. 1 (A) *In situ* synchrotron X-ray results on the reduction of 11-nm-thick $Nd_{0.8}Sr_{0.2}NiO_3$ / $SrTiO_3$ (001) during reduction with CaH_2 (solid curves). The sharp peak at L = 2 rlu is from the $SrTiO_3$ substrate. (B) Cross-sectional high-angle annular dark-field imaging (HAADF) scanning transmission electron microscopy (STEM) image of the reduced infinite-layer nickelate $Nd_{0.8}Sr_{0.2}NiO_2$, illustrating the allows the square-planar / perovskite interface to stabilize and propagate from the bottom to the top of the film without the formation of interphase defects. Importantly, neither geometric rotations in the square planar structure nor significant incorporation of hydrogen within the films is detected, obviating its need for superconductivity. These findings unveil the structural basis underlying the transformation pathway and provide important guidance on achieving the superconducting phase in reduced nickelate systems.

Superconductivity in an ultrathin multilayer nickelate: We report the appearance of superconductivity in a single unit-cell thick film of $Nd_6Ni_5O_{12}$ (X. Yan et al., *Adv. Mater.* (2024)), exhibiting a transition temperature similar to that of thicker films[2]. In-situ synchrotron x-ray scattering performed during growth of the parent phase, $Nd_6Ni_5O_{16}$, shows that the necessary layer-by-layer deposition sequence does not follow the sequence of the formula unit but an alternate order due to the relative stability of the perovskite unit cell (Fig. 2). We exploit this insight to grow ultrathin $Nd_6Ni_5O_{16}$ heterostructures and conduct in-situ studies of topotactic reduction, finding that formation of the square-planar phase occurs rapidly and is highly sensitive to reduction temperature, with small deviations from the optimum condition leading to inhomogeneity and the loss of superconductivity. The fluorite layer within the unit cell facilitates reduction by initially stabilizing the square-planar phase in the upper half of the unit cell. Our findings provide insight into the growth of the Ruddlesden-Popper nickelates, highlighting the need for in-situ studies of the metastable phases key to superconductivity.

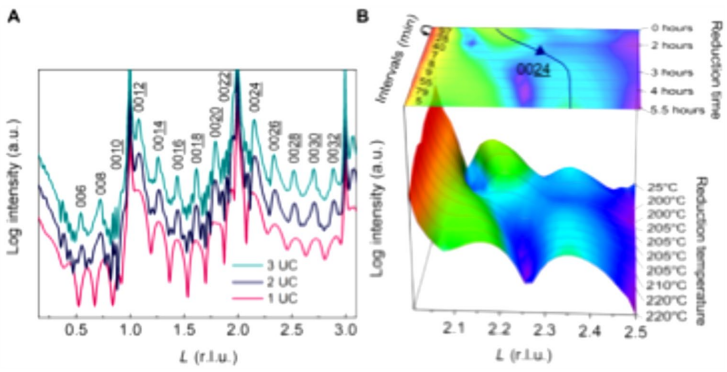


Fig. 2 (A) Measurements of the specular rod for 1-, 2-, and 3-UC-thick $Nd_6Ni_5O_{16}$ films grown on $NdGaO_3$ substrates. (B) Map of specular rods measured for the 1-UC-thick film at different temperatures in the CaH_2 reducing environment. the arrowed profile at the top shows the shift of the 00<u>24</u> reflection.

Tunable 'giant' kinetic inductance of superconducting $KTaO_3$ (111) interfacial 2DEGs: Superconductivity in the electron gas found at $KTaO_3$ (KTO) interfaces[2] is characterized by an unusually low superfluid stiffness J_s, inferred from both transport[2] and microwave measurements[2]. The reason for the low value of superfluid stiffness J_s and the resulting large sheet kinetic inductance $L_{K/\square} \sim 1/J_s$ is not well understood. If we assume that J_s is probing the superfluid density, that would imply that less than 1% of the carriers in the band are participating in the superfluid. This is highly unusual, even in a disordered superconductor where J_s is reduced by scattering. The resultant large kinetic inductance can be potentially useful in device applications. We fabricated coplanar waveguide resonators (Fig. 3) from the two-dimensional superconductor formed at KTO_3 (111) interfaces to characterize the superconductor's $L_{K/\square}$ as a function of carrier density (J. Yang et al., *Nano Letters* 2025). Upon varying the carrier density, in samples with T_c ranging from 0.62 to 1.81 K, we can tune $L_{K/\square}$ between 1.88 and 7.42 nH/□ at the lowest temperatures, exceeding the highest values reported for granular aluminum films. The temperature dependence of $L_{K/\square}$ is consistent with a superconducting gap without nodes. The high $L_{K/\square}$ of superconducting KTO (111) interfacial electron gases combined with the high dielectric constant of KTO results in resonators with exceedingly low phase velocities ("slow light") and small mode volumes. In addition, superconducting KTO (111) interfacial electron gases are robust in magnetic fields well above a Tesla. These features can enable unique device applications in superconducting electronics and quantum information science.

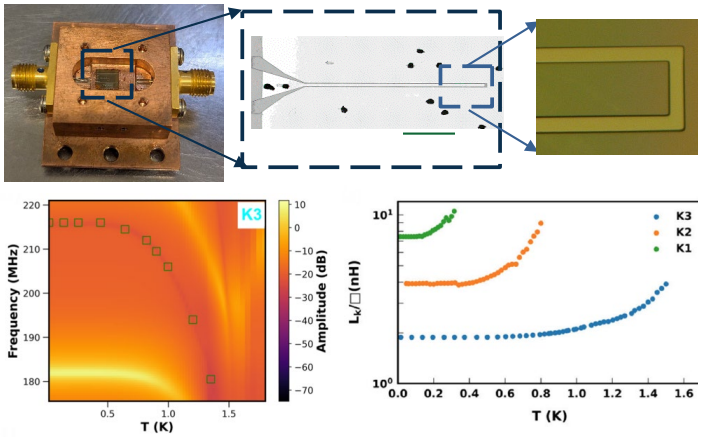


Fig. 3 (Top) Superconducting coplanar waveguide patterned from a $AlO_x/KTaO_3$ (111) 2DEG. (Bottom Left) Temperature evolution of its microwave resonant frequency, which is governed by the kinetic inductance of the resonator. The resonance signal disappears above T_C. (Bottom Right) Temperature evolution of sheet kinetic inductance $L_{K/\square}$of superconducting $KTaO_3$(111) 2DEGs at different doping levels, where higher doping levels lead to higher T_C and lower values of $L_{K/\square}$.

Spintronic THz spectroscopy of surface phonons in $KTaO_3$. With the discovery[Error! Bookmark not defined.] of superconductivity at interfaces of KTO, there has been intense interest in its underlying pairing mechanism. A unique property of the superconductivity at KTO interfaces is its orientation selectivity. For KTO (111) interfaces, the transition temperature can be as high as 2.2 K, for the (110) interface, the maximum T_c is ~ 1.1 K, whereas on the KTO (001) interface, superconductivity was found in ionic liquid gated samples with a $T_c < 0.047$ K (K. Ueno et al., *Nat. Nanotech*. 2011). Since then, other groups have failed to find superconductivity in chemically doped or ionic liquid gated KTO (001) 2DEGs with similar carrier densities down to ~ 20 mK. In a recent paper[Error!

Bookmark not defined., we proposed a theory of superconductivity involving inter-orbital interactions that explains this striking orientation selectivity of superconductivity. The proposal relies upon the inversion-breaking TO1 phonon as the 'superconducting glue'. This is the same phonon that softens as $KTaO_3$ is cooled to low temperatures causing it to behave as a 'quantum paraelectric', which is an incipient ferroelectric thwarted by quantum fluctuations. However, phonons at surfaces can differ from the bulk. With this in mind, we devised a spectroscopic technique – 'spintronic THz spectroscopy' – where THz generated from a magnetic overlayer interacts with the surface phonons, which in turn leaves a signature in the emitted THz spectrum (Z. Chu et al., *Sci. Adv*. 2024). With this technique, we are able to probe the near-surface TO1 phonons in two different quantum paraelectric materials – $SrTiO_3$ and $KTaO_3$, where we find that the surface phonons are distinct from the bulk. These findings are useful for our understanding of ferroelectric fluctuations and their role in superconductivity in these materials.

Future Plans

1. In-situ studies of MBE and PLD growth of nickelates, using coherent x-rays and dynamics of resulting speckle patterns (x-ray photo correlation spectroscopy or XPCS) to track defect dynamics and phase formation during synthesis and topotactic reduction.
2. Explore pathways to tune superconductivity in the nickelates, including strain, interfacial doping and dimensional confinement.
3. Develop new giant spin-Hall effect A15 compounds by tuning the Fermi level via stoichiometry or creating pseudobinary alloys. Many of these are superconducting, and several are predicted to have topological surface states.
4. Carry out high resolution spectroscopy of the superconducting electron gas at KTO interfaces to determine the nature of the superconducting gap.
5. Explore the interaction between magnetism and superconductivity in the KTO interfacial electron gas.

References

1. Danfeng Li, Kyuho Lee, Bai Yang Wang, Motoki Osada, Samuel Crossley, Hye Ryoung Lee, Yi Cui, Yasuyuki Hikita, and Harold Y. Hwang, Superconductivity in an infinite-layer nickelate. Nature 572, 624-627 (2019)
2. Grace A. Pan, Dan Ferenc Segedin, Harrison LaBollita, Qi Song, Emilian M. Nica, Berit H. Goodge, Andrew T. Pierce et al. "Superconductivity in a quintuple-layer square-planar nickelate." Nature Materials 21, 160-164 (2022)
3. Changjiang Liu, Xi Yan, Dafei Jin, Yang Ma, Haw-Wen Hsiao, Yulin Lin, Terence M. Bretz-Sullivan et al. "Two-dimensional superconductivity and anisotropic transport at KTaO3 (111) interfaces." Science 371, 716-721 (2021).
4. Changjiang Liu, Xianjing Zhou, Deshun Hong, Brandon Fisher, Hong Zheng, John Pearson, Jidong Samuel Jiang, Dafei Jin, Michael R. Norman, and Anand Bhattacharya. "Tunable superconductivity and its origin at KTaO3 interfaces." Nature Communications 14, 951 (2023).

5. Mallik, S., G. C. Ménard, G. Saïz, H. Witt, J. Lesueur, Alexandre Gloter, L. Benfatto, Manuel Bibes, and Nicolas Bergeal. "Superfluid stiffness of a KTaO3-based two-dimensional electron gas." Nature Communications 13, 4625 (2022).

Publications

1. Y. Li, C. Liu, H. Zheng, Z. Zhu, X. Yan, H. Cao, K. V. L. V. Narayanachari, B. Paudel, Z. Zhang, B. Fisher, H. Wang, E. Karapetrova, C. Sun, S. Kelly, D. Phelan, Y. Du, B. Buchholz, J. F. Mitchell, A. Bhattacharya, D. D. Fong, H. Zhou, "On the topotactic phase transition in the infinite-layer nickelates", *Adv. Mater.* 2402484 (2024).

2. X. Yan, H. Zheng, Y. Li, H. Cao, D. P. Phelan, H. Zheng, Z. Zhang, H. Hong, A. Bhattacharya, H. Zhou, D. D. Fong, "Superconductivity in an ultrathin multilayer nickelate", *Sci. Adv.* **11,** eado4572 (2025).

3. Z. Chu, J. Yang, Y. Li, K. Hwangbo, J. Wen, Q.i Zhang, S. Hruszkewycz, D. D. Fong, X. Xu, M. R. Norman, A. Bhattacharya, H. Wen, "Revealing subterahertz atomic vibrations in quantum paraelectrics by surface-sensitive spintronic terahertz spectroscopy", *Sci. Adv.* **10,** eads8601 (2024).

4. Junyi Yang, Adem Imamovic, Xinhao Li, Xianjing Zhou, John Pearson, Changjiang Liu, Ulrich Welp, Andrew Higginbotham, Jidong S. Jiang, Dafei Jin, Michael R. Norman, and Anand Bhattacharya, "Tuning Kinetic Inductance with Doping in Superconducting Electron Gases at the $KTaO_3$ (111) Interface", *Nano Letters* (2025). https://doi.org/10.1021/acs.nanolett.4c06029

5. R. Chapai, G. Peterson, M. Smylie, X. Chen, J. S. Jiang, D. Graf, J. F. Mitchell, and U. Welp, "Fermi surface topology and magnetotransport properties of superconducting $Pd_3Bi_2Se_2$", *Physical Review* B, 110, 075152 (2024).

6. Q. Zhang, G. Wan, V. Starchenko, G. Hu, E. M. Dufresne, H. Zhou, H.Jeen, I. C. Almazan, Y. Dong, H. Liu, A. R. Sandy, G. E. Sterbinsky, H. N. Lee, P. Ganesh, D. D. Fong, "Intermittent Defect Fluctuations in Oxide Heterostructures"*, Adv. Mater.* 2305383 (2023).

7. L. Zhang, C. Liu, H. Cao, A. J. Erwin, D. D. Fong, A. Bhattacharya, L. Yu, L. Stan, C. Zou, M. V. Tirrell, H. Zhou, W. Chen, "Redox gating for colossal carrier modulation and unique phase control", *Adv. Mater.* 2308871 (2024).

8. A. Vasdev, G. Sheet, R. Chapai, T. Polakovic, V. Novosad, J. S. Jiang, A. Bhattacharya, J. F. Mitchell, D. Y. Chung, and U. Welp, "Superconducting and spin-wave orders in $Ba_{0.6}K_{0.4}Fe_2As_2$ probed by point contact spectroscopy", *Physical Review B* 110, 094518 (2024).

9. Y. Li, Y. Liu, I.-C. Tung. H. Hong, J. W. Freeland, H. Zhou, H. Wang, and D. D. Fong, "On the Emergence of Ferromagnetism in $LaCoO_3$ Ultrathin Films", *Adv. Funct. Mater.* 2406037 (2024).

10. H. Cao, C. Liu, X. Zhai, D. D. Fong, A. Bhattacharya, M. V. Tirrell, H. Zhou, and W. Chen, "Redox Gating-Induced Modulation of Charge Carrier Density and Lattice Expansion in $LaNiO_3$ Thin Films", *Appl. Phys. Lett.* **125,** 074101 (2024).

Author
Index

Adhikari, Chandra Mani 276
Ahn, Charles H..... 93
Alem, Nasim 368
Al-Ostaz, Ahmed 353
Andrei, Eva Y. 28
Armitage, N. Peter 346
Ashoori, Raymond 183
Assaf, Badih A. 157
Autrey, Daniel..... 276
Balicas, Luis..... 348
Basov, D.N. 161
Bastakoti, Bishnu Prasad 276
Bauer, Eric 223
Bauers, Sage..... 84, 285
Bhattacharya, A..... 379
Bian, Guang 138
Bockrath, Marc 24
Bozhko, Dmytro..... 178
Brahlek, Matt 268
Brahlek, Matthew..... 132
Bud'ko, Sergey 228
Butov, Leonid 165
Canfield, Paul..... 228
Cao, Huibo 232
Celinski, Zbigniew..... 178
Cha, Judy J. 79
Chakhalian, Jak 136
Chan, Mun..... 280
Chang, Cui-Zu..... 169
Christianson, Andrew 232
Crommie, Michael 193
Crooker, Scott 280
Csathy, Gabor 341
Dessau, Dan 108
Dhital, Chetan 232
Eom, Chang-Beom..... 311
Eres, Gyula..... 268
Finkelstein, Gleb 41
Fischer, Peter 373
Fisher, I. R..... 103
Fong, Dillon D. 379
Frolov, Sergey..... 273
Furukawa, Yuji 228
Gautam, Bhoj Raj..... 276
Ghimire, Nirmal..... 98
Goldhaber-Gordon, David 18
Griffin, Sinéad..... 373
Hadjipanayis, George..... 251
Han, Shubo..... 276
Harrison, Neil..... 280
He, Rui 358
Hellman, Frances 373
Hirata, Michihiro..... 223
Hong, Xia..... 122
Hsu, Yi-Ting 157
Hu, Jin 212
Jaime, Marcelo..... 280
Jiang, J. S. 379
Jiang, Zhigang..... 113
Jin, Chenhao..... 317
Ju, Long..... 11
Kaminski, Adam 228
Kapitulnik, A..... 103
Kastner, Marc..... 18
Ke, L. 69
Kim, Eun-Ah..... 79
Kivelson, S. A. 103
Kolmer, Marek..... 291
Kong, Tai 89
Lanzara, Alessandra..... 193
Lau, Chun Ning (Jeanie)..... 24
Lee, Ho Nyung..... 268
Lee, Minhyea 242
Leonard, Brian M. 153
Leszczynski, Jerzy 353
Lewis, Laura H..... 251
Li, Qi 321
Liu, Albert..... 295
Liu, Jian..... 125
Liu, Xiaolong 157
Liu, Xinyu 157
Louie, Steven 193
Lukashev, Pavel 358
Luo, Yunqiu Kelly 302
Madhavan, Vidya..... 256
Majdoub, Mohammed..... 353
Mandrus, David..... 64
Mannix, Andrew 18
Mao, Zhiqiang..... 368
Maple, M. Brian..... 259
Marshall, Madalynn 232
May, Andrew F. 64

McGuire. Michael A. 64
McIver, James 173
McQueeney, R. J. 69
Menon, Vinod 208
Miao, Hu 268
Mitchell, John F. 98
Natelson, Douglas 36
Ni, Chaoying 251
Ni, Ni 140
Nouranian, Sasan 353
Novosad, Valentine 178
Ojeda-Aristizabal, Claudia 187
Ong, N. P. 34
Ortiz, Brenden R. 64, 246
Ozturk, Birol 326
Paglione, Johnpierre 264
Pasupath, Abhay 74
Paudel, Tula 122
Phelan, Daniel 98
Pradhan, Nihar R. 353
Prozorov, Ruslan 228
Qian, Xiaofeng 148
Qiu, Zi Q. 193
Quirk, Nicholas P. 34
Rai, Binod Kumar 276
Raja, Archana 193
Ralph, Daniel C. 49
Ramirez, Arthur P. 130
Ran, Sheng 217
Rhodes, Daniel 148
Ronning, Filip 223
Rosa, Priscila 223, 280
Roy, Sujoy 373
Roy, Xavier 74
Sapkota, A. 69
Sapkota, Aashish 228
Scheie, Allen 223
Schiffer, Peter 235
Schuller, Ivan K. 117
Sengottuvelu, Dinesh Kumar 353
Seyler, Kyle 299
Shand, Paul 358
Sharpe, Aaron 18
Shekhter, Arkady 280
Sim, Sangwoo 34
Singh, Meenakshi 331
Singleton, John 280
Slade, T. J. 69
Slade, Tyler 228
Smirnov, Dmitry 113
Smith, Arthur R. 336
Staunton, Julie B. 251
Stollenwerk, Andrew 358
Sumant, Anirudha V. 353
Tanatar, Makariy 228
Tang, Yue 34
Thomas, Sean 223
Tian, Jifa 153
Turner, Josh 373
Ueland, B. G. 69
Vaknin, D. 69
Vishik, Inna 373
Wang, Feng 193
Wang, Linlin 228
Wang, Xiaoling 246
Ward, T. Zac 268
Weitering, Hanno H. 239
Welp, Ulrich 98, 379
Wu, Mingzhong 145
Wu, Sanfeng 34
Xie, Weiwei 368
Yan, Jiaqiang 64
Yang, Fengyuan 363
Yasuda, Kenji 306
Ye, Linda 220
Young, Andrea 16
Zaletel, Mike 193
Zhang, Ruixing 239
Zhang, Xiao-Xiao 46
Zhao, Liuyan 203
Zhou, Haidong 125
Zhou, You 198
Zhu, Jun 22

Participant

List

Name	Institution
Abhay Narayan	Columbia University
Albert Liu	Broohaven National Laboratory
Ali Sayir	Air Force Office of Scientific Research
Anand Bhattacharya	Argonne National Laboratory
Andrea Young	University of California, Santa Barbara
Andrew Mannix	SLAC National Accelerator Laboratory/Stanford University
Andrew Schwartz	U.S. Department of Energy
Arthur Ramirez	University of California Santa Cruz
Arthur Smith	Ohio University
Badih Assaf	University of Notre Dame
Benjamin Ueland	Ames National Laboratory
Bhoj Gautam	Fayetteville State University
Birol Ozturk	Morgan State University
Brenden Ortiz	Oak Ridge National Laboratory
Brian Leonard	University of Wyoming
Chang-Beom Eom	University of Wisconsin-Madison
Charles Ahn	Yale University
Chenhao Jin	University of California, Santa Barbara
Chetan Dhital	Kennesaw State University
Christopher Jones	National Academies of Sciences, Engineering, and Medicine
Chun Ning Lau	U.S. Department of Energy
Claudia Cantoni	U.S. Department of Energy
Claudia Mewes	U.S. Department of Energy
Claudia Ojeda-Aristizabal	California State University Long Beach
Cui-Zu Chang	The Pennsylvania State University
Dan Dessau	University of Colorado
Daniel Phelan	Argonne National Laboratory
Daniel Ralph	Cornell University
Daniel Rhodes	University of Wisconsin-Madison
David Goldhaber-Gordon	SLAC National Accelerator Laboratory
David Tennant	University of Tennessee
Dillon Fong	Argonne National Laboratory
Dmitri Basov	Columbia University
Dmitry Smirnov	National High Magnetic Field Laboratory, Florida State University
Dmytro Bozhko	University of Colorado Colorado Springs
Douglas Natelson	Rice University
Eric Bauer	Los Alamos National Laboratory
Eva Andreu	Rutgers
Feng Wang	University of California, Berkeley and Lawrence Berkeley National Laboratory

Fengyuan Yang	The Ohio State University
Filip Ronning	Los Alamos National Laboratory
Frances Hellman	University of California, Berkeley and Lawrence Berkeley National Laboratory
Gabor Csathy	Purdue University
Gleb Finkelstein	Duke University
Guang Bian	University of Missouri
Haidong Zhou	University of Tennessee
Hanno Weitering	University of Tennessee-Physics
Harold Hwang	SLAC
Ho Nyung Lee	Oak Ridge National Laboratory
Hu Miao	Oak Ridge National Laboratory
Ian Fisher	SLAC and Stanford University
Ivan Schuller	University of California San Diego
Jak Chakhalian	Rutgers University
James Analytis	Lawrence Berkeley National Laboratory
James McIver	Columbia University
Jane Zhu	U.S. Department of Energy
Jifa Tian	University of Wyoming
Jin Hu	University of Arkansas
Johnpierre Paglione	University of Maryland
Judy Cha	Cornell University
Jun Zhu	Penn State University
Kenji Yasuda	Cornell University
Kyle Seyler	University of Arizona
Laura Lewis	Northeastern University
Leonid Butov	University of California San Diego
Linda Ye	California Institute of Technology
Liuyan Zhao	University of Michigan
Long Ju	Massachusetts Institute of Technology
Lu Li	University of Michigan
Luis Balicas	Florida State University
M. Brian Maple	University of California, San Diego
Marek Kolmer	Ames National Laboratory
Matthew Brahlek	Oak Ridge National Laboratory
Matthias Graf	U.S. Department of Energy
Meenakshi Singh	Colorado School of Mines
Michael McGuire	Oak Ridge National Laboratory
Mingzhong Wu	Northeastern University
Minhyea Lee	University of Colorado Boulder
N. Peter Armitage	Johns Hopkins

N. Phuan Ong	Princeton University
Nasim Alem	Penn State University
Neil Harrison	Los Alamos National Laboratory
Ni Ni	University of California, Los Angeles
Nihar Pradhan	Jackson State University
Patrick El Khoury	U.S. Department of Energy
Paul Canfield	Ames National Laboratory
Peter Schiffer	Princeton University
Philip Kim	Harvard University
Qi Li	Penn State University
Qiang Li	Brookhaven National Laboratory
Raymond Ashoori	Massachusetts Institute of Technology
Robert McQueeney	Ames National Laboratory
Rui He	Texas Tech University
Ruixing Zhang	University of Tennessee
Sage Bauers	National Renewable Energy Laboratory
Sergey Frolov	University of Pittsburgh
Sheng Ran	Washington University
T. Arul Mozhi	National Academies of Sciences, Engineering, and Medicine
Tai Kong	University of Arizona
Tim Mewes	U.S. Department of Energy
Timothy Kidd	U.S. Department of Energy
Tula Paudel	South Dakota School of Mines and Technology
Tyler Slade	Ames National Laboratory
Ulrich Welp	Argonne National Laboratory
Vidya Madhavan	University of Illinois at Urbana Champaign
Vinod Menon	City College & Grad Center of CUNY
Xavier Roy	Columbia University
Xia Hong	University of Nebraska-Lincoln
Xiao-Xiao Zhang	University of Florida
Xiaofeng Qian	Texas A&M University
Xiaoling Wang	California State University, East Bay
Yi-Ting Hsu	University of Notre Dame
You Zhou	University of Maryland College Park
Yunqiu Kelly Luo	University of Southern California
Zhigang Jiang	Georgia Institute of Technology